

H 24/3097

**MONASH UNIVERSITY**  
**THESIS ACCEPTED IN SATISFACTION OF THE**  
**REQUIREMENTS FOR THE DEGREE OF**  
**DOCTOR OF PHILOSOPHY**

ON..... 7 December 2001 .....

.....  
for Sec. Research Graduate School Committee

Under the copyright Act 1968, this thesis must be used only under the normal conditions of scholarly fair dealing for the purposes of research, criticism or review. In particular no results or conclusions should be extracted from it, nor should it be copied or closely paraphrased in whole or in part without the written consent of the author. Proper written acknowledgement should be made for any assistance obtained from this thesis.

*Diverse Lanthanoid and Lithium  
Complexes with Pendant Donor Amide  
Ligands*

by

Natalie M. Scott

B.Sc.(Hons)

A thesis submitted for the degree of  
Doctor of Philosophy

School of Chemistry  
Monash University

August, 2001

'Without the darkness of the tunnel,  
The light at the end wouldn't seem so bright'

*J.A. Davis*

*For my family and the people, who have directly and indirectly helped and inspired me along the way*

## Contents

ABSTRACT .....	vi
STATEMENT.....	ix
ACKNOWLEDGEMENTS.....	x
ABBREVIATIONS .....	xi

### Chapter 1

#### Introduction

1.1 Introduction .....	1
1.1.1 General Properties of the Lanthanoid Series .....	1
1.1.2 Lanthanoid Cyclopentadienyl Chemistry .....	3
1.1.3 Lanthanoid(III) Monodentate Amide Complexes .....	5
1.1.4 Lanthanoid(III) Bidentate Amide Complexes .....	8
1.1.5 Lanthanoid(III) Multidentate Amide Complexes .....	14
1.1.6 Current Study.....	17
1.2 References .....	19

### Chapter 2

#### *Heteroleptic Lanthanoid(III) Complexes of the Chelating N,N-dimethyl-N'-trimethylsilylethane-1,2-diamine Ligand*

2.1 Introduction .....	24
2.2 Results and Discussion.....	25
2.2.1 Preparation of Ln(L <sup>1</sup> ) <sub>2</sub> Cl Complexes .....	25
2.2.2 Derivatisation of [Ln(L <sup>1</sup> ) <sub>2</sub> (μ-Cl)] <sub>2</sub> Complexes .....	26
2.3 Conclusion .....	32
2.4 References .....	33

### Chapter 3

#### *Homoleptic Ether Functionalised (Diorganoamido)lanthanoid(III) Complexes*

3.1	Introduction .....	34
3.1.1	Preparation of Target Bidentate Amine Ligands .....	34
3.2	Results and Discussion.....	41
3.2.1	Synthesis and Characterisation of $[\text{Ln}(\text{L}^2)_3]$ Complexes .....	41
3.2.2	Synthesis and Characterisation of $[\text{Ln}(\text{L}^3)_3]$ Complexes .....	49
3.3	Conclusion .....	59
3.4	References .....	61

### Chapter 4

#### *Solvent-free Heteroleptic Lanthanoid(III) Complexes Stabilised by Mixed N,O Ligands*

4.1	Introduction .....	62
4.2	Results and Discussion.....	63
4.2.1	Preparation of $[\text{Ln}(\text{L})_2(\mu\text{-Cl})]_2$ Complexes ( $\text{L} = \text{L}^2, \text{L}^3$ ) .....	63
4.2.1.1	Structures of $[\text{Ln}(\text{L}^2)_2(\mu\text{-Cl})]_2$ ( $\text{Ln} = \text{Tb}, \text{Er}$ and $\text{Yb}$ ) .....	66
4.2.1.2	Structure of $[\text{Nd}(\text{L}^3)_2(\mu\text{-Cl})]_2(\text{PhMe})_2$ .....	74
4.2.1.3	General Remarks on $[\text{Ln}(\text{L})_2(\mu\text{-Cl})]_2$ ( $\text{L} = \text{L}^2$ or $\text{L}^3$ ) Complexes .....	79
4.2.2	Alternative Routes to Heteroleptic Lanthanoid Complexes.....	80
4.2.3	Bridging the Gap in Heteroleptic Chemistry.....	85
4.3	Conclusions .....	95
4.4	References .....	96

### Chapter 5

#### *Lanthanoid(II) Complexes of Mixed N,O Ligands and Their Oxidation Chemistry*

5.1	Introduction .....	98
5.1.1	Lanthanoid(II) Monodentate Amide Complexes.....	99

5.1.2 Lanthanoid(II) Bidentate Amide Complexes .....	106
5.1.3 Oxidation of Lanthanoid(II) Organoamide Complexes .....	107
5.2 Results and Discussion .....	109
5.2.1 Transmetallation / Ligand Exchange Reactions using $L^2$ and $L^3$ .....	109
5.2.1.1 Proposed Reaction Pathway .....	118
5.2.2 Ligand Exchange Reactions using $L^2$ and $L^3$ .....	121
5.2.3 Oxidation Chemistry of $[Yb(L^2)_2(THF)_2]$ .....	129
5.2.3.1 Syntheses .....	129
5.2.3.2 Characterisation of $[Yb(C_5R_5)_2(L)]$ ( $R = H, Me, L = L^2; R = Me, L = L^3$ ) .....	132
5.3 Conclusion .....	140
5.4 The Bigger Picture-'edge-on' versus 'face-on' .....	141
5.5 References .....	143

## Chapter 6

### *Structural Characterisation of Some Lanthanoid Trihalide Complexes*

6.1 Introduction .....	148
6.1.1 Formation of Ether Solvated Lanthanoid Trihalide Complexes .....	150
6.1.1.1 $[LnCl_3(S)_n]$ Compounds .....	150
6.1.1.2 $[LnX_3(S)_n]$ ( $X = Br, I$ ) .....	151
6.1.2 Structural Properties of Lanthanoid Trihalide Ether Adducts .....	152
6.1.2.1 The Trichlorides .....	152
6.1.2.2 The Tribromides and Triiodides .....	154
6.1.3 Current Study .....	156
6.2 Results and Discussion .....	157
6.2.1 $[LnCl_3(DME)_x]$ Complexes .....	157
6.2.2 $[YbBr_3(S)_x]$ Complexes ( $S = THF, DME$ ) .....	161
6.2.3 Alternative $[LnCl_3(L)_xL'_y]$ Complexes ( $L = MeCN, L' =$ chelating diamine) .....	167
6.2.3.1 Synthesis .....	167
6.2.3.2 Characterisation .....	170
6.2.3.3 Thermal Evaluation of $LnCl_3(L)_xL'_y$ Complexes ( $L = MeCN, L' =$ chelating diamine) .....	173
6.3 Conclusions .....	175

6.4	References .....	176
-----	------------------	-----

## Chapter 7

### *Diorganoamidolithium Complexes – Preparation, Properties and Crystal Structures*

7.1	Introduction .....	179
7.1.1	Uncomplexed Lithium Amides (RR'NLi) <sub>n</sub> .....	180
7.1.2	Complexed Lithium Amides [RR'NLi(L) <sub>x</sub> ] <sub>n</sub> .....	183
7.1.3	Lithium Complexes Containing Multidentate Amide Ligands .....	186
7.1.4	Current Study.....	189
7.2	Results and Discussion.....	190
7.2.1	Reaction of L <sup>2</sup> H with LiBu <sup>n</sup> .....	190
7.2.2	Reaction of L <sup>3</sup> H with LiBu <sup>n</sup> .....	195
7.2.3	Reaction of L <sup>3</sup> H with excess LiBu <sup>n</sup> .....	203
7.2.4	Attempted Reactions of Li <sub>2</sub> (L <sup>1</sup> ) with Lanthanoid Chlorides.....	221
7.3	Conclusions .....	231
7.4	References .....	232

## Chapter 8 Experimental Section

8.1	General Experimental.....	235
8.2	Analysis.....	235
8.2.1	Elemental Analyses.....	235
8.2.2	IR-, FIR-, UV-, VIS-, NIR- Spectroscopy .....	236
8.2.3	Mass Spectroscopy, TGA/DSC/DTA/MS and GC/MS .....	236
8.2.4	<sup>1</sup> H and heteronuclear NMR spectroscopy .....	237
8.2.5	X-ray Crystallography.....	237
8.3	Reagents and Solvents.....	237
8.3.1	Preparation of starting materials.....	238
8.3.1.1	Synthesis and Characterisation of [Yb(MeCp)Cl <sub>2</sub> (THF)] .....	238
8.4	Experimental Procedures for Chapter 2 .....	239
8.4.1	Synthesis of [Ln(L <sup>1</sup> ) <sub>2</sub> (μ-Cl) <sub>2</sub> Complexes (Ln = Yb, Er, Nd, Sm, La).....	239
8.4.2	Synthesis of of [Nd(L <sup>1</sup> )(Ph <sub>2</sub> pz) <sub>3</sub> ][Li(DME) <sub>3</sub> ] .....	241

8.5	Experimental Procedures for Chapter 3 .....	242
8.5.1	Synthesis of $L^2H$ .....	242
8.5.2	Synthesis of $L^3H$ .....	243
8.5.3	Synthesis of Homoleptic Lanthanoid Complexes Containing $L^2$ .....	244
8.5.4	Synthesis of Homoleptic Lanthanoid Complexes Containing $L^3$ .....	247
8.6	Experimental Procedures for Chapter 4 .....	252
8.6.1	Synthesis of $[Ln(L^2)_2(\mu-Cl)]_2$ Complexes ( $Ln = Yb, Er$ and $Tb$ ) .....	252
8.6.2	Synthesis of $[Ln(L^3)_2(\mu-Cl)]_2$ .....	254
8.6.3	Synthesis of $[Yb(L^3)_2(OAr)]$ ( $OAr = 2,6-(Bu^t)_2C_6H_3O$ ) .....	255
8.6.4	Synthesis of $[Yb(MeCp)(L)(\mu-Cl)]_2$ Complexes ( $L = L^2, L^3$ ) .....	255
8.7	Experimental Procedures of Chapter 5 .....	257
8.7.1	Oxidation / Transmetallation Reactions .....	257
8.7.2	Synthesis of Diorganoamidolanthanoid(II) Complexes by Ligand Exchange Reactions .....	260
8.7.3	Oxidations of $Ln(II)$ Species .....	261
8.8	Experimental Procedures for Chapter 6 .....	265
8.8.1	Synthesis of $[LnCl_3(DME)_x]$ Complexes ( $Ln = La, Nd, Yb$ ) .....	265
8.8.2	Synthesis of $[YbBr_3(L)]$ Complexes ( $L = THF_3$ or $DME_2$ ) .....	266
8.8.3	Synthesis of Diorganoaminolanthanoid Halide Complexes .....	267
8.8.3.1	Attempted preparations of $LnCl_3(HL)$ ( $Ln = Sm, Yb; HL = A, L^1H, C, D$ ) .....	267
8.8.3.2	Lanthanoid Trichloride Complexes Containing $L^1H$ .....	268
8.8.3.3	Lanthanoid Trichloride Complexes Containing $[HN(SiMe_3)CH_2]_2 (C)$ .....	269
8.9	Experimental Procedures of Chapter 7 .....	270
8.9.1	Reaction of $L^2H$ with $LiBu^n$ .....	270
8.9.2	Reaction of $L^3H$ with $LiBu^n$ .....	272
8.9.3	Reaction of $L^3H$ with excess $LiBu^n$ .....	274
8.9.4	Reaction of $Li_2(L^*)$ with $LnCl_3$ .....	277
8.9.5	Attempted Reactions of $Li_2(L^*)$ with $[Yb(C_5Me_5)_2Cl(THF)]$ .....	279
8.10	References .....	280
	PUBLICATIONS .....	281



## Abstract

The general theme of this thesis entails the potential stabilisation of metal environments through ligands having pendant donor arms supporting a primary metal amide interaction. A brief review on organoamidolanthanoid(III) complexes is given in Chapter 1. The synthesis and characterisation of some heteroleptic lanthanoid organoamide complexes with the bidentate amide ligand,  $L^1$  ( $L^1 = N(\text{SiMe}_3)\text{CH}_2\text{CH}_2\text{NMe}_2$ ) is discussed in Chapter 2. The homoleptic and heteroleptic lanthanoid(III) chemistry incorporating the new mixed N,O-donor ligands  $L^2$  and  $L^3$  ( $L^2 = N(2\text{-MeOC}_6\text{H}_4)(\text{SiMe}_3)$  and  $L^3 = N(2\text{-PhOC}_6\text{H}_4)(\text{SiMe}_3)$ ) is presented in Chapters 3 and 4, while their divalent lanthanoid chemistry is examined in Chapter 5. Since many lanthanoid preparations in this thesis utilize metathesis reactions and require strict stoichiometric control, aspects of the chemistry of the reagents were also explored. Structural features of ether-ligated lanthanoid trihalide complexes are described in Chapter 6. The coordination of  $L^2$  and  $L^3$  to lithium, which unexpectedly opened new chemistry for the  $L^3$  ligand, is described in Chapter 7.

Treatment of two equivalents of  $\text{LiL}^1$  with  $\text{LnCl}_3$  in THF gave the solvent-free dimeric heteroleptic lanthanoid complexes  $[\text{Ln}(\text{L}^1)_2(\mu\text{-Cl})_2]$  ( $\text{Ln} = \text{Sm, Nd, La, Er, Yb}$ ). Reaction of  $[\text{Nd}(\text{L}^1)_2(\mu\text{-Cl})_2]$  (generated *in situ*) with  $\text{Li}(\text{Ph}_2\text{pz})$  ( $\text{Ph}_2\text{pz} = 3,5\text{-diphenylpyrazolate}$ ) in THF afforded a mixture of products, one of which was identified as the charge separated ionic complex  $[\text{Nd}(\text{L}^1)(\text{Ph}_2\text{pz})_3][\text{Li}(\text{DME})_3]$  by X-ray crystallography.

The new ligands *N*-(2-methoxyphenyl)-*N*-trimethylsilylamine ( $L^2\text{H}$ ) and *N*-(2-phenoxyphenyl)-*N*-trimethylsilylamine ( $L^3\text{H}$ ) were synthesised from 2-methoxyaniline and 2-phenoxyaniline respectively, by successive treatment with  $\text{LiBu}^n$  and  $\text{ClSiMe}_3$  in  $\text{Et}_2\text{O}$ . Treatment of  $\text{LnCl}_3$  with three equivalents of  $\text{LiL}$  ( $\text{L} = L^2, L^3$ ), generated *in situ* from  $L^2\text{H}$  or  $L^3\text{H}$  with  $\text{LiBu}^n$ , yielded the homoleptic lanthanoid(III) complexes  $[\text{Ln}(\text{L})_3]$  ( $\text{Ln} = \text{Nd, Pr, Sm, Er, L} = L^2$ ;  $\text{Ln} = \text{Y, Yb, Sm, Nd, La, L} = L^3$ ). Reaction of the isolated lithium salt  $[\text{Li}(L^2)(\text{OEt})_2]_2$  with  $\text{YbCl}_3$  (3 : 1 Li to Ln molar ratio) also afforded  $[\text{Yb}(L^2)_3]$  in high yield. The homoleptic complexes  $[\text{Ln}(\text{L})_3]$  ( $\text{Ln} = \text{Nd, Yb, L} = L^2$ ;  $\text{Ln} = \text{La, Nd, Yb, L} = L^3$ ) were also isolated from an *in situ* reaction between two equivalents of pre-isolated  $\text{LiL}$  ( $\text{L} = L^2, L^3$ ) in THF and  $\text{LnCl}_3$ . However, treatment of two equivalents of  $[\text{Li}(L^2)(\text{OEt})_2]_2$  with  $\text{LnCl}_3$  in THF gave, for the heavier lanthanoids, the solvent free

heteroleptic complexes  $[\text{Ln}(\text{L}^2)_2(\mu\text{-Cl})]_2$  ( $\text{Ln} = \text{Tb}, \text{Er}, \text{Yb}$ ) but for Nd the homoleptic complex  $[\text{Nd}(\text{L}^3)_3]$  was obtained. In contrast, similar reactions of  $[\text{Li}(\text{L}^3)(\text{DME})]$  with  $\text{LnCl}_3$  yielded the heteroleptic species  $[\text{Ln}(\text{L}^3)_2(\mu\text{-Cl})]_2$  only for  $\text{Ln} = \text{Nd}$  and, at either end of the Ln series, the homoleptic  $[\text{Ln}(\text{L}^3)_3]$  ( $\text{Ln} = \text{La}, \text{Yb}$ ) were isolated. Single crystal X-ray analyses of  $[\text{Nd}(\text{L}^3)_3]$ ,  $[\text{La}(\text{L}^3)_3]$ ,  $[\text{Nd}(\text{L}^3)_3]$ ,  $[\text{Y}(\text{L}^3)_3](\text{C}_5\text{H}_9\text{Me})$ ,  $[\text{Yb}(\text{L}^3)_3](\text{C}_5\text{H}_9\text{Me})$  and  $[\text{Yb}(\text{L}^3)_3](\text{PhMe})$  showed these complexes to be monomeric and six-coordinate (*mer* isomer) whereas the heteroleptic complexes  $[\text{Ln}(\text{L}^2)_2(\mu\text{-Cl})]_2$  ( $\text{Ln} = \text{Tb}, \text{Er}, \text{Yb}$ ) and  $[\text{Nd}(\text{L}^3)_2(\mu\text{-Cl})]_2$  were found to be dimeric with bridging chloride atoms. Reaction of  $[\text{Yb}(\text{OAr})_3]$  ( $\text{OAr} = 2,6\text{-}(\text{Bu}^t)_2\text{C}_6\text{H}_3\text{O}$ ) with two equivalents of  $[\text{Li}(\text{L}^3)(\text{DME})]$  afforded the five-coordinate monomeric amide/aryloxide complex  $[\text{Yb}(\text{L}^3)_2(\text{OAr})]$ . Mixed cyclopentadienyl/amide ytterbium complexes were prepared by reaction of  $[\text{Yb}(\text{MeCp})\text{Cl}_2(\text{THF})]$  with  $[\text{Li}(\text{L}^2)(\text{OEt}_2)]_2$  or  $[\text{Li}(\text{L}^3)(\text{DME})]$  (1 : 1 Li to Yb mole ratio) which gave the heteroleptic chloride complexes  $[\text{Yb}(\text{MeCp})(\text{L})(\mu\text{-Cl})]_2$  ( $\text{L} = \text{L}^2, \text{L}^3$ ).

The redox transmetallation / ligand exchange reaction of Yb metal,  $\text{HgPh}_2$  and  $\text{L}^2\text{H}$  or  $\text{L}^3\text{H}$  in THF afforded the ytterbium(III) complexes  $[\text{Yb}(\text{L}^2)_2(\mu\text{-OMe})]_2$  and  $[\text{Yb}(\text{L}^3)_2(\text{OPh})(\text{THF})]$ , the structures of which were established by X-ray crystallography. Aryl ether C—O bond activation by the initially formed  $\text{Yb}(\text{L}^2)_2$  species (detected for  $\text{L}^2$  via this reaction route) is considered to produce these complexes. Ligand exchange reactions of  $[\text{Ln}\{\text{N}(\text{SiMe}_3)_2\}_2(\text{S})]$  ( $\text{Ln} = \text{Eu}$  or  $\text{Yb}$ ;  $\text{S} = (\text{THF})_2$  or  $\text{DME}$ ) with  $\text{L}^2\text{H}$  in toluene at low temperatures yielded thermally unstable  $[\text{Ln}(\text{L}^2)_2(\text{S})]$  ( $\text{Ln} = \text{Eu}$  or  $\text{Yb}$ ;  $\text{S} = (\text{THF})_2$  or  $\text{DME}$ ), but still afforded the lanthanoid(III) complex  $[\text{Yb}(\text{L}^3)_2(\text{OPh})(\text{THF})]$ . Oxidation of  $[\text{Yb}(\text{L}^2)_2(\text{THF})_2]$  with  $\text{Tl}(\text{C}_5\text{H}_5)$  yielded thallium metal and  $[\text{Yb}(\text{C}_5\text{H}_5)_2(\text{L}^2)]$ , presumably formed by ligand redistribution of the initially formed, but not detected,  $\text{Yb}(\text{L}^2)_2(\text{C}_5\text{H}_5)$  species. Treatment of  $[\text{Yb}(\text{C}_5\text{Me}_5)_2(\text{THF})]$  with one equivalent of  $\text{Hg}(\text{L}^2)_2$  or  $\text{Hg}(\text{L}^3)_2$  gave mercury metal and the ytterbium(III) complexes  $[\text{Yb}(\text{C}_5\text{Me}_5)_2(\text{L}^2)]$  and  $[\text{Yb}(\text{C}_5\text{Me}_5)_2(\text{L}^3)]$ .

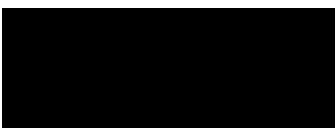
Treatment of Ln metal ( $\text{Ln} = \text{La}, \text{Nd},$  or  $\text{Yb}$ ) with hexachloroethane in DME under ultrasound conditions yielded  $[\text{LnCl}_3(\text{DME})_n]$  ( $\text{Ln} = \text{La}, n = 1$ ;  $\text{Ln} = \text{Nd}, \text{Yb}, n = 2$ ) in good yield. Reaction of ytterbium metal with  $\text{CH}_2\text{Br}_2$  in THF or DME afforded  $[\text{YbBr}_3(\text{THF})_3]$  and  $[\text{YbBr}_3(\text{DME})_2]$  respectively. The X-ray crystal structures of  $[\text{YbCl}_3(\text{DME})_2]$ , and  $[\text{YbBr}_3(\text{DME})_2]$  revealed a monomeric seven-coordinate metal environment while  $[\text{YbBr}_3(\text{THF})_3]$  is a six-coordinate monomer. Refluxing  $\text{LnCl}_3$  in acetonitrile with excess

diamine yields the lanthanoid trichloride amine adducts,  $\text{LnCl}_3(\text{MeCN})_x(\text{L}^1\text{H})_y$  (where  $\text{Ln} = \text{Yb}$ ,  $x = 2$ ,  $y = 2/3$ ;  $\text{Ln} = \text{Sm}$ ,  $x = 0$ ,  $y = 1/2$ ), and  $\text{LnCl}_3(\text{MeCN})_x(\text{C})_y$  (where  $\text{C} = \{\text{NH}(\text{SiMe}_3)\text{CH}_2\}_2$ ,  $\text{Ln} = \text{Yb}$ ,  $x = 2$ ,  $y = 1/2$  or  $\text{Sm}$ ,  $x = 0$ ,  $y = 1/3$ ).

Deprotonation of  $\text{L}^2\text{H}$  and  $\text{L}^3\text{H}$  with  $\text{LiBu}^n$  in a variety of solvents gave the expected monodeprotonated lithium amides,  $[\text{Li}(\text{L}^2)(\text{OEt}_2)]_2$ ,  $[\text{Li}(\text{L}^2)(\text{DME})_{0.5}]$ ,  $[\text{Li}(\text{L}^3)(\text{THF})]$ ,  $[\text{Li}(\text{L}^3)(\text{DME})]$  and  $[\text{Li}(\text{L}^3)]_n$  in good yields. Treatment of  $\text{L}^3\text{H}$  with a slight excess of  $\text{LiBu}^n$  in  $\text{Et}_2\text{O}$ , followed by work up in hexane containing trace amounts of diglyme, afforded a low yield of  $[\{\text{Li}(\text{OEt}_2)(\text{L}^3)\text{Li}_2(\text{L}^*)\}_2(\text{diglyme})]$  ( $\text{L}^* = \text{N}(2-(2'-\text{C}_6\text{H}_4\text{O})\text{C}_6\text{H}_4)(\text{SiMe}_3)$ ), a hexalithium aggregate containing  $\text{LiL}^3$  units and also a doubly-deprotonated  $\text{L}^3\text{H}$  (designated  $\text{L}^*$ ) with an *ortho*-hydrogen of the phenoxy group removed. This is presumably derived from reaction of  $\text{LiL}^3$  with  $\text{LiBu}^n$ . Deliberate attempts to prepare a pure sample of  $\text{Li}_2\text{L}^*$  by reaction of  $\text{L}^3\text{H}$  with two equivalents of  $\text{LiBu}^n$  in  $\text{Et}_2\text{O}$  gave two different complexes depending on the crystallisation solvent. A hexalithium aggregate  $[\text{Li}_2(\text{L}^*)(\text{OEt}_2)(\text{LiBu}^n)]_2$  was obtained from hexane, while the trapped molecule of  $\text{LiBu}^n$  was removed by a DME/hexane mixture giving  $[\text{Li}(\text{L}^*)_2(\text{DME})]_2$  in good yield. The reaction of  $\text{LaCl}_3$  with  $\text{Li}_2\text{L}^*$ , formed *in situ* from  $\text{LiBu}^n$  with  $\text{L}^3\text{H}$  in  $\text{Et}_2\text{O}$ , gave the remarkable multi-faceted decalithium complex  $[\{\text{Li}_2(\text{L}^*)\}_2(\text{LiOEt})(\text{OEt}_2)]_2(\text{hexane})$ , which contains three different superbases anions, amide, carbanion and alkoxide, all of which are bound to one lithium.

## *Statement*

To the best of my knowledge and belief, this thesis contains no material which has been presented for any other degree or diploma at any University, and contains no material previously published or written by any other person except where due reference is made.



**Natalie Maree Scott**  
School of Chemistry  
Monash University  
August, 2001

## *Acknowledgments*

I wish to express my gratitude to Professor Glen B. Deacon for his guidance and endless enthusiasm throughout my studies at Monash University. I am also indebted to Dr. C. Forsyth, Dr. P. Junk and Prof. A.H. White for the crystal structure determinations in this thesis. A special thank you must be given to Dr. Craig Forsyth for not only the many hours of helpful discussions and structure solutions, but also to be being a good friend - thanks for putting up with me! I also convey my deepest appreciation to Dr. Joanna Cosgriff and Dr. Mike Devery for their excellent and prompt proof reading.

I acknowledge the helpful assistance of the technical staff of the School of Chemistry at Monash, in particular, Dr. Jo Weigold for teaching me to run my NMR spectra and for running variable temperature and multinuclear spectra for me. Thanks also to Sally Duck for training me to run my own mass spectra. I must thank the general office administration staff, in particular, Maureen Walmsley and Birute Hanlon, for advice and friendship. I am indebted to Prof. Gerd Meyer for a five-month stay at the Universität zu Köln, Köln, Deutschland, and for many helpful discussions and more than a few laughs. I would like to acknowledge Prof. J. Harrowfield and his group for an enjoyable short stay at the University of Western Australia, Nedlands. A special thankyou to Imogen Schwarz, Catharina Quitmann, Andrea Fehren, Claudia Scarabis, Anna Peatt and Klaus Mueller-Buschbaum (in no particular order) for making life less serious and a lot more fun. I am also appreciative of the members of 128N, past and present, for their support and encouragement in a pleasant and enjoyable work environment.

Financial assistance in the forms of a Postgraduate Research Award from the Australian Government, a Departmental Scholarship from the School of Chemistry, Monash, a Qantas Travel Award and a DAAD Scholarship are acknowledged.

Finally, I would like to thank Dad, Leanne and Nanny, for their unfailing love and support.

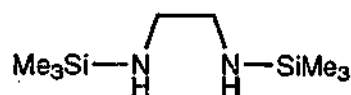
## Abbreviations

i.r. = ionic radius

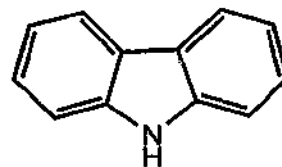
CN = coordination number

C =

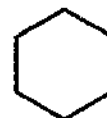
N,N'-bis(trimethylsilyl)ethylene-1,2-diamine



cbzH = carbazole



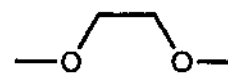
CyH = cyclohexane = c-C<sub>6</sub>H<sub>12</sub>



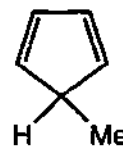
diglyme = bis(2-methoxyethyl) ether



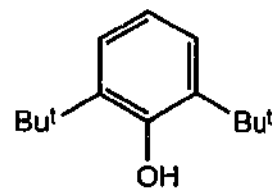
DME = 1,2-dimethoxyether



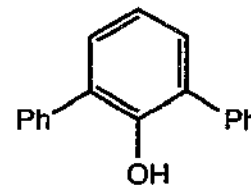
MeCpH = methylcyclopentadiene



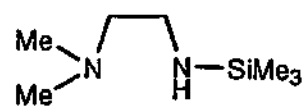
HOAr = 2,6-di-*tert*-butylphenol



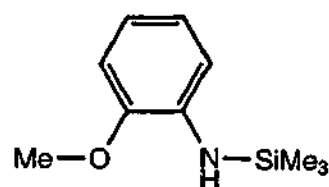
HOdpp = 2,6-diphenylphenol



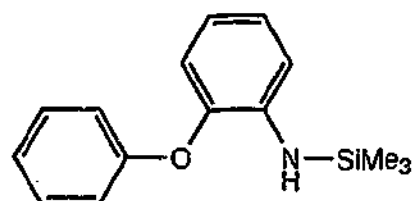
$L^1H =$   
*N,N*-dimethyl-*N'*-trimethylsilylethane-1,2-diamine



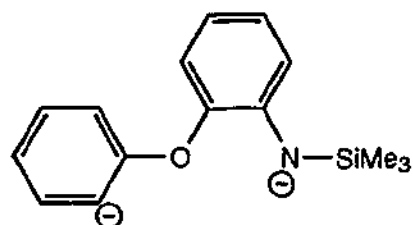
$L^2H =$   
*N*-(2-methoxyphenyl)-*N*-(trimethylsilyl)amine



$L^3H =$   
*N*-(2-phenoxyphenyl)-*N*-(trimethylsilyl)amine



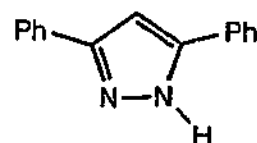
$(L^*)^{2-} = N(C_6H_4(OC_6H_4-2')-2)(SiMe_3)$



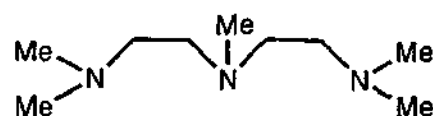
$C_5H_9Me =$  methylcyclopentane



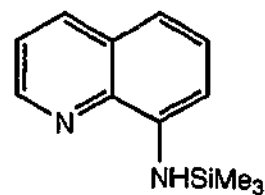
$Ph_2pzH =$  3,5-diphenylpyrazole



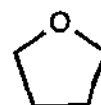
PMDETA =  
*N,N,N',N',N''*-pentamethyldiethylenetriamine



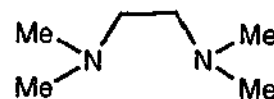
qsta = 8-(trimethylsilylamino)quinoline



THF = tetrahydrofuran



TMEDA = *N,N,N',N'*-tetramethylethylenediamine



## Chapter 1

# Introduction

In the last decade an increasing number of investigators have turned their attention away from organometallic chemistry to find alternative systems to stabilise the metal-carbon bond for catalytic work.<sup>[1]</sup> The 6e<sup>-</sup> donor cyclopentadienyl ligand (Cp) has been extensively used as a coligand with early transition metals for various types of catalytic transformations. Important applications include highly active group 4 and 5 metal and lanthanoid organometallic compounds in homogeneous Ziegler-Natta alkene polymerisation.<sup>[2-7]</sup> Alternative systems, using alkoxy and amide ligands in place of Cp (*Figure 1.1*) have shown similar reaction chemistry with the stabilisation of early, electron deficient transition metals in medium to high oxidation states.<sup>[8, 9]</sup> Of these two alternatives, greater opportunities exist for the amide ligand since the specific electron configuration of the nitrogen allows more ligand variation i.e., double substitution (see *Figure 1.1 (c)*). In the work described in this thesis, the synthesis of novel amide ligands and their chemistry with the *f*-block elements is explored.

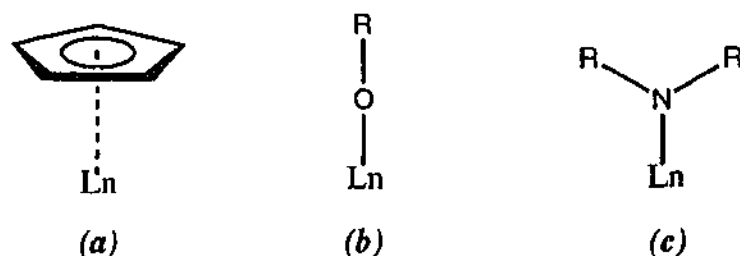


*Figure 1.1*

### 1.1.1 General Properties of the Lanthanoid Series

The lanthanoid series is a family of 15 elements more alike in their properties than any other group of elements. Headed by lanthanum ( $Z = 57$ ), the lanthanoid series is collectively the 15 elements from cerium ( $Z = 58$ ) to lutetium ( $Z = 71$ ).<sup>[10, 11]</sup> These elements are similar as their differences in electronic structure chiefly involve the filling of the inner 4f<sup>n</sup> subshell across the series. Although lanthanum contains no 4f electrons,<sup>[10]</sup> it closely resembles the lanthanoids and is included in the series. Scandium ( $Z=21$ ) and



yttrium ( $Z=39$ ), which lie above lanthanum in the periodic table, are also often discussed in conjunction with the lanthanoid series. These elements have similar electronic structures but fewer filled shells and exhibit close chemical behaviour to the series. The larger yttrium atom has a comparable ionic radius to the heavier members of the series due to the lanthanoid contraction. This contraction in ionic radii across the series is the result of an increase in effective nucleophilicity to inadequately screen each other by  $f$  electrons hence the  $4f$  subshell is pulled closer to the nucleus. Thus, the ionic radius of yttrium is comparable to erbium and as a result shows similar properties. However, scandium with its smaller ionic radius has chemical properties intermediate between the lanthanoids and aluminium.[10, 12, 13]

All of the lanthanoid elements have a characteristic oxidation state of  $\text{Ln}^{3+}$  though others are possible.[7, 10] In molecular chemistry, divalent derivatives are known for all the lanthanoids, with only three elements being stable under normal laboratory conditions, namely samarium, europium and ytterbium, and two of these require an inert atmosphere environment. However, more recent work has isolated from solution divalent species of lanthanum[14] and thulium.[15] Only cerium is stable in the tetravalent oxidation state, though terbium(IV) and praseodymium(IV) can be prepared under more extreme conditions. The coordination number of lanthanoid ions can vary from 2-12 as a result of their high ionic radius. They are essentially ionic and form strong bonds with hard Lewis bases such as  $\text{F}^-$  ions or O and N donors.[12] The first authentic organometallic lanthanoid compound incorporated the cyclopentadienyl ligand[16, 17] which stabilised the highly oxophilic lanthanoid centre. For a long time these cyclopentadienyl species remained the only organometallic compounds known for the lanthanoids (for reviews see [4, 18]). More recent work has focused on other ligand systems, in particular amido-, aryloxy- and alkoxy- lanthanoid complexes (for reviews see [9, 19-21]). The coordination of these hard donor ligands[22] to the lanthanoid metals should produce compounds of higher thermodynamic stability when compared to alkyl derivatives. This has already been shown for the early transition metals where the N-metal bond produces well-defined reaction centres.[8] As there have been a number of recent comprehensive reviews (see [7, 19, 20, 23]) on organoamidolanthanoid compounds a complete review is not needed here. A selection of lanthanoid amide chemistry, with emphasis on compounds containing the

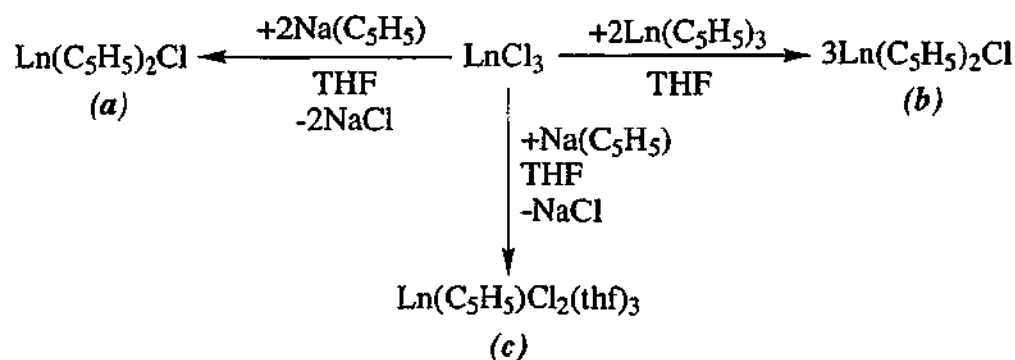
bulky silyl amide group follows. The synthetic methods used to prepare lanthanoid(III) organoamides as well as some of their significant structural features are highlighted.

### 1.1.2 Lanthanoid Cyclopentadienyl Chemistry

The original preparation of lanthanoid cyclopentadienyl complexes by a salt elimination reaction (metathesis reaction) (*Equation 1.1*) [16, 17] began over 40 years ago. This reaction produced a range of homoleptic complexes of the type,  $\text{Ln}(\text{C}_5\text{H}_5)_3$  (*Equation 1.1*), as well as a series of heteroleptic lanthanoid compounds by simple modification of the reagents (*Scheme 1.1 (a)-(c)*). [4]



*Equation 1.1*



*Scheme 1.1*

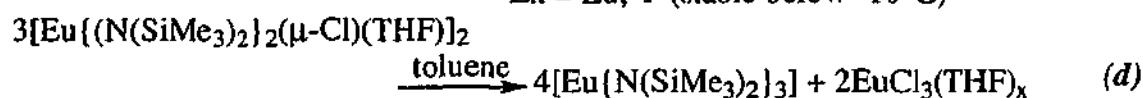
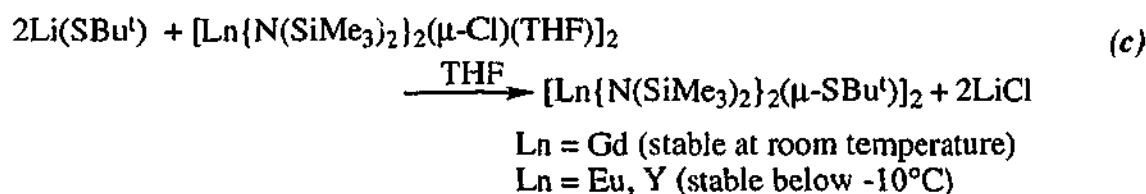
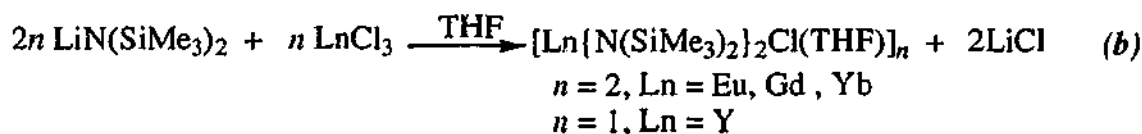
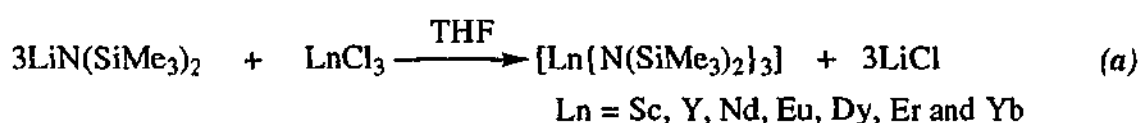
Lanthanoid chemistry of the unsubstituted cyclopentadienyl ligand has been inhibited by the low solubility of many compounds in hydrocarbon solvents. [4] Replacement of the hydrogen atoms with bulky substituents, such as alkyl or silyl groups, resulted in the preparation of lanthanoid compounds that had greater volatility and a higher solubility in non-coordinating solvents. [4, 12, 18] The most studied bulky Cp ligand in lanthanoid chemistry is the pentamethylcyclopentadienyl ligand. Due to the size of the ligand the homoleptic complexes  $\text{Ln}(\text{C}_5\text{Me}_5)_3$  are relatively difficult to prepare. [24] As a result, the disubstituted pentamethylcyclopentadienyllanthanoid(III) complexes are stable toward ligand redistribution and have had a major impact on organolanthanoid chemistry. [5, 25] There has been a plethora of lanthanoid complexes of the type,

$\text{Ln}(\text{C}_5\text{Me}_5)_2\text{X}$  ( $\text{X}$  = anionic ligand),<sup>[4]</sup> and some of these (e.g.  $\text{X}$  = alkyl, H) are highly active homogeneous catalysts for olefin transformations including ethylene polymerisation and hydrogenation reactions.<sup>[4, 26]</sup> Important precursors to such active compounds are the halide derivatives of the type  $[\text{Ln}(\text{C}_5\text{Me}_5)_2\text{X}]$  ( $\text{X}$  = halide) as they contain a reactive halide site that can be replaced by various substituents such as hydride, alkyl or alkoxide ligands.<sup>[4, 5]</sup> These precursors do not exist as monomeric species but as halide bridged dimers. Bridge cleavage can occur through the coordination of neutral donors to form  $[(\text{C}_5\text{Me}_5)_2\text{LnCl}(\text{L})]$  ( $\text{L}$  = typically THF) or the formation of 'ate' complexes, e.g.  $[(\text{C}_5\text{Me}_5)_2\text{Ln}(\mu\text{-X})_2\text{Li}(\text{S})_2]$  ( $\text{X}$  = Cl, Br, I;  $(\text{S})_2$  =  $(\text{Et}_2\text{O})_2$ ,  $(\text{THF})_2$ , DME, TMEDA) by incorporation of an alkali metal halide. Steric saturation through the use of large  $\text{X}$  anions, e.g. OAr ( $\text{Ar}$  = 2,6-( $\text{Bu}^t$ ) $_2\text{C}_6\text{H}_3\text{O}$ , 2,6- $\text{Me}_2\text{C}_6\text{H}_3\text{O}$ ) and  $\text{N}(\text{SiMe}_3)_2$  can overcome this coordination behaviour resulting in solvent and alkali metal free species.<sup>[4]</sup>

Despite the advantages of the  $\text{C}_5\text{Me}_5$  ligand, it is important to find other ancillary ligands that can stabilise highly reactive organolanthanoid species. The size, basicity and functionalisation of the alternative ligands should stabilise the large lanthanoid atom to produce a well-defined precatalyst system that ultimately is mononuclear, chemically robust and rigid. The organoamide ligand system (see *Figure 1.1 (c)*) offers a wide range of opportunities for such ligands. The incorporation of bulky substituents, such as trimethylsilyl or isopropyl, at the nitrogen increases the steric bulk of the ligand and assures a high degree of solubility of the lanthanoid products in non-coordinating solvents. Features such as bidentate nitrogen donors improve the stability of the resulting complexes compared with monodentate amides due to chelation and increased electron donation to the metal centre. Although a number of lanthanoid complexes containing amide N-ligands have been synthesized in comparison to work with the transition metals, it still remains a relatively under developed area of research.

### 1.1.3 Lanthanoid(III) Monodentate Amide Complexes

In the mid 1970's Bradley and co-workers produced the first homoleptic, donor-free lanthanoid amide complexes. These lanthanoid amide complexes contained either the bulky bis(trimethylsilyl)amide[27-29] or the bis(isopropyl)amide ligand,[30] which resulted in complexes of low coordination number. Of these two ligands the bis(trimethylsilyl)amide ligand has been by far the most widely applied in lanthanoid amide chemistry. The first three-coordinate monomeric lanthanoid complex of the type  $[\text{Ln}\{\text{N}(\text{SiMe}_3)_2\}_3]$ [27-29] was prepared from dehydrated lanthanoid halides and  $\text{LiN}(\text{SiMe}_3)_2$  in THF at room temperature (*Scheme 1.2 (a)*). The resulting complex can withstand sublimation under vacuum to yield the donor-free compound,  $[\text{Ln}\{\text{N}(\text{SiMe}_3)_2\}_3]$ . Due to their high solubility in non-coordinating solvents,  $[\text{Ln}\{\text{N}(\text{SiMe}_3)_2\}_3]$  complexes are used as key synthetic precursors to prepare pure compounds in a halide-free ligand exchange reaction,[7, 20] and have recently been shown to catalyze hydroamination or tischenko reactions in their own right.[31] The formation of a number of heteroleptic lanthanoid silylamide complexes has been reported[32-35] and a selection is given in *Scheme 1.2*. However, only a small number of Ln metals can be used which is due to the steric bulk of this ligand insufficiently stabilising the larger lanthanoids (*Scheme 1.2 (b)*[32], *(c)*[33]). As a consequence of the steric unsaturation, rearrangement to yield the homoleptic derivatives is commonly observed (*Scheme 1.2 (d)*).[36]



*Scheme 1.2*

The chemistry of the less spacially demanding bis(dimethylsilyl)amide ligand with lanthanoid metals has also been investigated. The solvated complexes,  $[\text{Ln}\{\text{N}(\text{SiMe}_2\text{H})_2\}_3(\text{THF})_n]$  ( $\text{Ln} = \text{Y, La-Lu, } n = 2$ ;  $\text{Ln} = \text{Sc, } n = 1$ ) were obtained by a metathesis reaction of  $\text{LiN}(\text{SiMe}_2\text{H})_3$  with  $\text{LnCl}_3(\text{THF})_x$  (3:1 ratio) in hexane.[37, 38] In the molecular structure of five-coordinate  $[\text{Ln}\{\text{N}(\text{SiMe}_2\text{H})_2\}_3(\text{THF})_2]$  the THF molecules occupy the axial positions of a distorted trigonal bipyramidal coordination polyhedron, whereas in four-coordinate  $[\text{Sc}\{\text{N}(\text{SiMe}_2\text{H})_2\}_3(\text{THF})]$  (distorted tetrahedral geometry) only one coordinated THF is present which reflects the significantly smaller ionic radius of scandium. The THF ligands in  $[\text{Ln}\{\text{N}(\text{SiMe}_2\text{H})_2\}_3(\text{THF})_n]$  ( $n = 1, 2$ ) can be replaced by stronger donor molecules such as 1,3-dimethylimidazol-2-ylidene (carbene) to form adducts of the type  $[\text{Y}\{\text{N}(\text{SiMe}_2\text{H})_2\}_3(\text{carbene})_x]$  ( $x = 1, 2$ ).[38]

The sublimation to yield the solvent-free species  $[\text{Ln}\{\text{N}(\text{SiMe}_2\text{H})_2\}_3]$  requires higher temperatures than for  $[\text{Ln}\{\text{N}(\text{SiMe}_3)_2\}_3]$ . This unusual thermal behaviour is possibly due to the strong agostic  $\text{Ln}\cdots(\text{SiH})$  interactions which help to sterically saturate the metal centre in  $[\text{Ln}\{\text{N}(\text{SiMe}_2\text{H})_2\}_3(\text{THF})_x]$  ( $x = 1, 2$ ) complexes. On heating the complex to the temperatures needed to release THF a rearrangement to a dimeric species was detected which reflects the steric unsaturation of the metal centre.[20] This enhanced thermal stability of the bis(dimethylsilyl)amide complexes enables exchange reactions to be performed at high temperatures.[38, 39]

Whilst steric variation of the  $\text{N}(\text{SiR}_3)_2$  ligands, through use of bulkier R groups (e.g.  $\text{Bu}^t$ , Ph) has yet to be explored in *f*-element chemistry (c.f. transition and main group metals)[40-42], modification of ligand bulk by replacement of one of the  $\text{SiMe}_3$  groups with an aryl group has yielded interesting results. The aryl group can be readily modified by substitution in the 2,6-positions and this has been shown to have significant effects on the structures of the derived lanthanoid amide complexes (see *Figure 1.2 (a)-(c)*).[43] Metathesis reactions involving the lithiated unsubstituted phenyl ligand with  $\text{LnCl}_3$  in a 3:1 mole ratio yields solvated homoleptic complexes of the type  $[\text{Ln}\{\text{N}(\text{Ph})(\text{SiMe}_3)\}_3(\text{THF})_x]$  ( $x = 2, \text{Ln} = \text{La}$ ;  $x = 1, \text{Ln} = \text{Y, Nd - Lu}$ ). For the larger lanthanum ion two THF groups are present which is comparable to the structure of  $[\text{Ln}\{\text{N}(\text{SiMe}_3)_2\}_3(\text{THF})_2]$ . However, for the smaller lanthanoid elements only one THF molecule is coordinated to the metal

centre as well as weak interactions from the *ortho*-phenyl and the *ipso*-carbon atoms of the amide ligands (*Figure 1.2 (a)*).

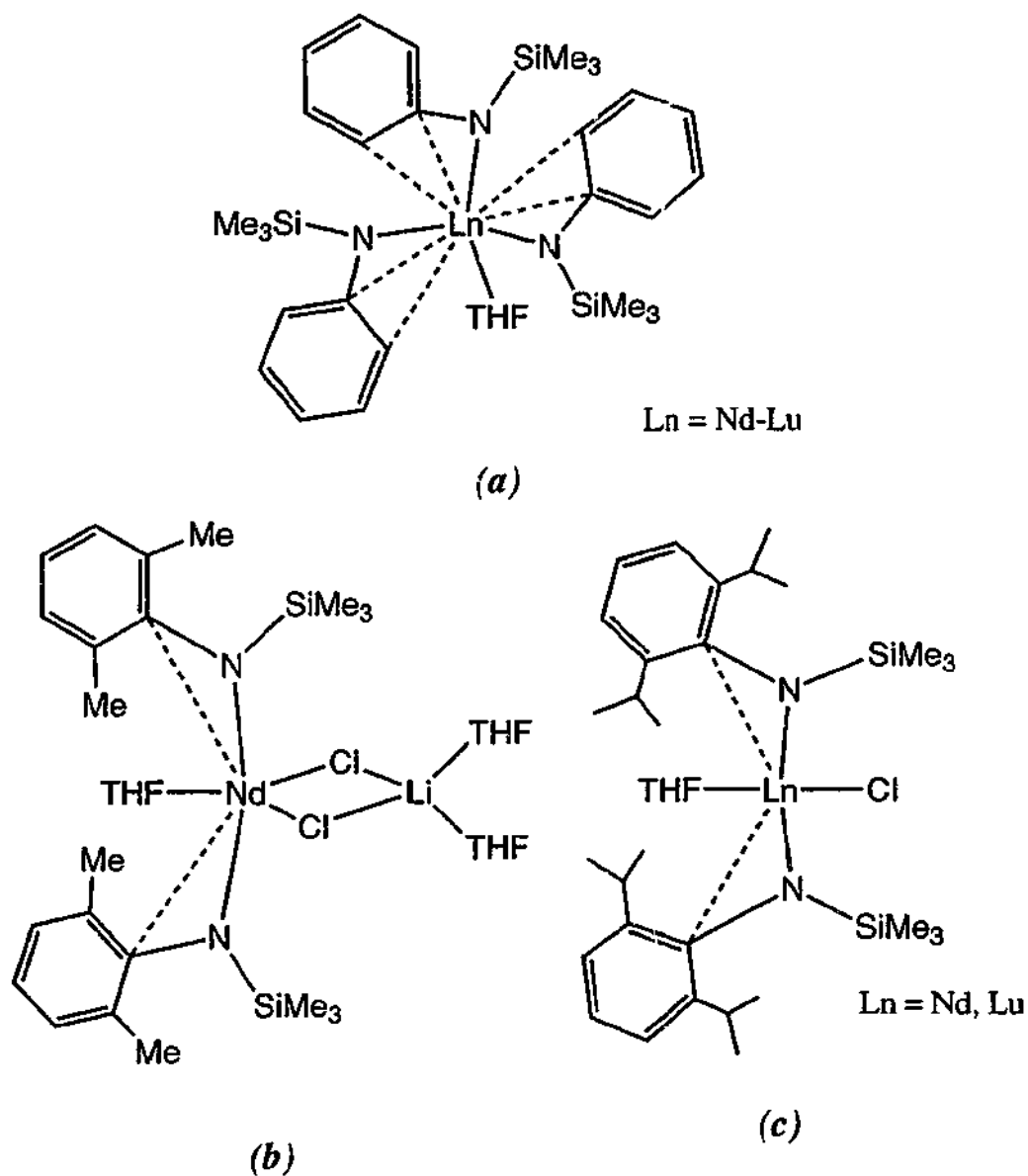


*Figure 1.2*

In the 2,6-dimethylphenyl case a five-coordinate 'ate' complex was formed (*Figure 1.2 (b)*) whereas for the 2,6-isopropylphenylsilylamide ligand, a four-coordinate monomeric complex was isolated (*Figure 1.2 (c)*). This complex has two amide ligands, a terminal chloride bond, and a THF ligand. As was seen for  $[\text{Ln}\{\text{N}(\text{Ph})(\text{SiMe}_3)\}_3(\text{THF})]$  complexes, weak interactions involving the  $\text{Ln}\dots\text{C}(\textit{ipso})$  were also observed in the heteroleptic and 'ate' complexes.

In a similar manner, the reaction of the silyl-free derivative  $\text{KHNAr}$  ( $\text{Ar} = 2,6\text{-Me}_2\text{C}_6\text{H}_3$ ,  $2,6\text{-(Pr}^i)_2\text{C}_6\text{H}_3$ ) with lanthanoid halides was examined by Evans *et al.*[44] As above, structural dependence on the size of the ligand and the lanthanoid metal was observed with a variety of structural types isolated. With the smaller 2,6-dimethyl-substituted ligand and a larger lanthanoid ion the formation of a bimetallic anionic complex of the type  $[\text{K}(\text{THF})_6][\text{Ln}\{\mu\text{-HN}(2,6\text{-Me}_2\text{C}_6\text{H}_3)\}\{\text{HN}(2,6\text{-Me}_2\text{C}_6\text{H}_3)\}_3]$  ( $\text{Ln} = \text{Sm}$  or  $\text{Nd}$ ) resulted. For the smaller lanthanoid metals the isolation of a mixed bridged chloride and amide anionic species,  $[\text{K}(\text{DME})_2(\text{THF})_2][\text{Y}_2(\mu\text{-Cl})\{\mu\text{-HN}(2,6\text{-Me}_2\text{C}_6\text{H}_3)\}\{\text{HN}(2,6\text{-Me}_2\text{C}_6\text{H}_3)\}_4(\text{THF})_2]$  was observed. In contrast to the 2,6-dimethylphenyltrimethylsilyl amide ligand where 'ate' complexation occurs, the 2,6-diisopropylphenylamide ligand forms neutral complexes of both solvated  $[\text{Ln}\{\mu\text{-HN}(2,6\text{-(Pr}^i)_2\text{C}_6\text{H}_3)\}_3(\text{THF})_x]$  (where  $\text{Ln} = \text{Nd}$ ,  $x = 3$ ;  $\text{Ln} = \text{Y}$  or  $\text{Yb}$ ,  $x = 2$ ) and unsolvated  $[\text{Ln}\{\mu\text{-HN}(2,6\text{-(Pr}^i)_2\text{C}_6\text{H}_3)\}\{\text{HN}(2,6\text{-(Pr}^i)_2\text{C}_6\text{H}_3)\}_2]_2$  types depending on the reaction pathway. Attempts to prepare the anionic analogues with the 2,6-diisopropylphenylamide ligand were unsuccessful. Overall, variation of the steric bulk in the 2,6-position of the phenyl ring causes different structural chemistry, providing a detailed structural insight into steric saturation about the lanthanoid centre. So far, the catalytic activity of these complexes has not been evaluated.

### 1.1.4 Lanthanoid(III) Bidentate Amide Complexes

The next generation of organoamidolanthanoid(III) complexes concentrated on ligands having a similar steric equivalence to the cyclopentadienyl ligand to increase stability of the lanthanoid centre for catalytic work. Earlier work done by Dehnicke[45] and Roesky[46] showed that the chelating silyl-substituted *N,N'*-bis(trimethylsilyl)benzamidinate ligand is very useful in stabilising a variety of coordinatively unsaturated main group and transition metal centres. The benzamidinate ligand was found to act either as a monodentate[47, 48] (*Figure 1.3 (a)*) or a bidentate ligand[45, 46, 49-51] (*Figure 1.3 (b)*) depending on the reaction conditions and metal character. Later, lanthanoid complexes containing this ligand were prepared by the metathesis route and are discussed in a review by Edlmann.[23] A range of homoleptic and heteroleptic lanthanoid benzamidinate complexes has been synthesised (for examples, see *Table 1.1*) in which the benzamidinate ligand coordinates in a bidentate mode (*Figure*

1.3 (b)). The resultant lanthanoid complexes show high thermal stability, with no disproportionation or ligand transfer at elevated temperatures, presumably owing to the formation of the four-membered ring.

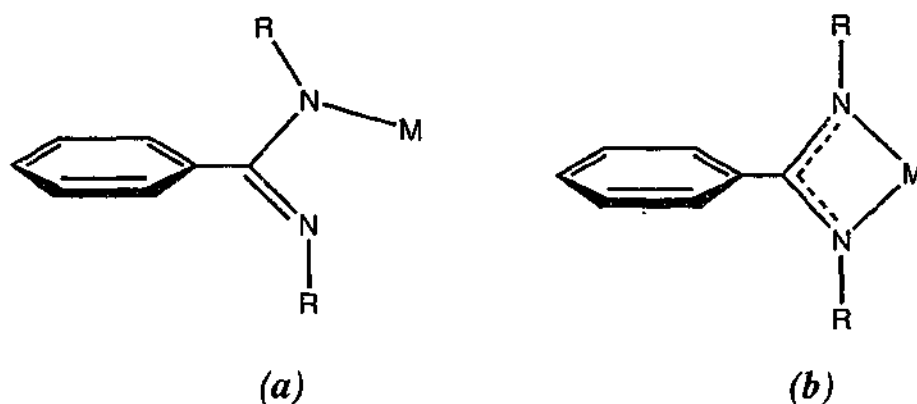


Figure 1.3

Table 1.1 Homoleptic and Heteroleptic Lanthanoid(III) Benzamidinate Complexes

Compound	Ref.
<i>Homoleptic complexes</i>	
$[\text{Ln}\{4\text{-RC}_6\text{H}_4\text{C}(\text{NSiMe}_3)_2\}_3]$	[52]
Where R = H, Me, OMe, CF <sub>3</sub> , Ph	
$[\text{Ln}\{\text{C}_6\text{H}_4\text{S}(\text{NSiMe}_3)_2\}_3]$ (Ln = Sc, Nd)	[53]
<i>Heteroleptic complexes</i>	
$[\text{Ln}\{\text{Ph}_2\text{P}(\text{NSiMe}_3)_2\}_2\text{Cl}(\text{THF})]$ (Ln = Pr, Nd)	[54]
$[\text{Nd}\{(\text{CF}_3)_3\text{C}_6\text{H}_2\text{C}(\text{NSiMe}_3)_2\}_2(\mu\text{-Cl})_2\text{Li}(\text{THF})_2]$	[49]
$[\text{Y}\{\text{PhC}(\text{NSiMe}_3)_2\}_2\text{Cl}(\text{THF})]$	[55]
$[\text{Y}\{\text{PhC}(\text{NSiMe}_3)_2\}_2\text{R}]$ (R = (CH <sub>2</sub> Ph).THF, CH(SiMe <sub>3</sub> ) <sub>2</sub> )	[56]
$[\text{Y}\{\text{PhC}(\text{NSiMe}_3)_2\}_2(\mu\text{-R})_2]$ (R = H, C≡CH)	[57]
$[\text{Y}\{4\text{-MeOC}_6\text{H}_4\text{C}(\text{NSiMe}_3)_2\}_2(\mu\text{-H})_2]$	[55]



The molecular structure of  $[\text{Pr}\{4\text{-MeOC}_6\text{H}_4\text{C}(\text{NSiMe}_3)_2\}_3]$ ,<sup>[52]</sup> which was prepared using a metathesis route, shows a monomeric six-coordinate praseodymium atom with three bidentate ligands. The ligands are coordinated to the lanthanoid in a distorted octahedral arrangement. Despite measurements on this complex confirming that this benzamidinate ligand has steric requirements similar to those of  $\text{C}_5\text{H}_5$ , it is quite clear that it does not behave in a similar manner to Cp. In the complex  $[\text{Pr}\{4\text{-MeOC}_6\text{H}_4\text{C}(\text{NSiMe}_3)_2\}_3]$ ,<sup>[52]</sup> the benzamidinate ligand provides sufficient steric saturation around the metal centre to form a six-coordinate monomeric, solvent-free species, unlike the unsolvated eleven-coordinate polymeric tris(cyclopentadienyl) lanthanoid complexes.<sup>[4]</sup>

Reaction of  $\text{YCl}_3$  with two equivalents of  $\text{LiPhC}(\text{NSiMe}_3)_2$  affords the crystallographically characterised monomeric complex  $[\text{Y}\{\text{PhC}(\text{NSiMe}_3)_2\}_2(\text{Cl})(\text{THF})]$ . This has two chelating ligands, a terminal chloride molecule and a coordinated THF in a distorted octahedral array. The steric saturation about the lanthanoid centre is similar to that of the complex  $[\text{Ln}(\text{C}_5\text{Me}_5)_2\text{Cl}(\text{THF})]$ , and therefore the benzamidinate ligand for heteroleptic derivatives can be considered to be a steric analogue of  $\text{C}_5\text{Me}_5$ , having a steric coordination number of approximately 2.5.<sup>[58]</sup> The stabilising ability of the benzamidinate ligand is apparent from the fact that alkyl and hydrido species are obtainable.<sup>[55-57]</sup> Catalytic use of these complexes has been examined and the results showed that this system has a poorer catalytic activity when compared to the corresponding pentamethylcyclopentadienyl lanthanoid system. A reason given for the low activity is the higher ionicity of the bis(benzamidinate) system. The larger negative charge on the spectator ligand leads to a more strongly positively charged lanthanoid ion. As a result, a highly stable dimeric precursor species (e.g.  $[\text{LnL}_2\text{R}]_2$ ) is formed which lowers the potential ability of the catalytic site to complex substrates.<sup>[55]</sup> Recently, alternative amidinate-type ligands have been synthesised in an attempt to prepare lanthanoid complexes of unusual structure and reactivity. The use of a terphenyl substituent at the amidine carbon to increase the steric bulk resulted in the isolation of the first mono-amidinate lanthanoid halide species (see *Figure 1.4*).<sup>[59]</sup>

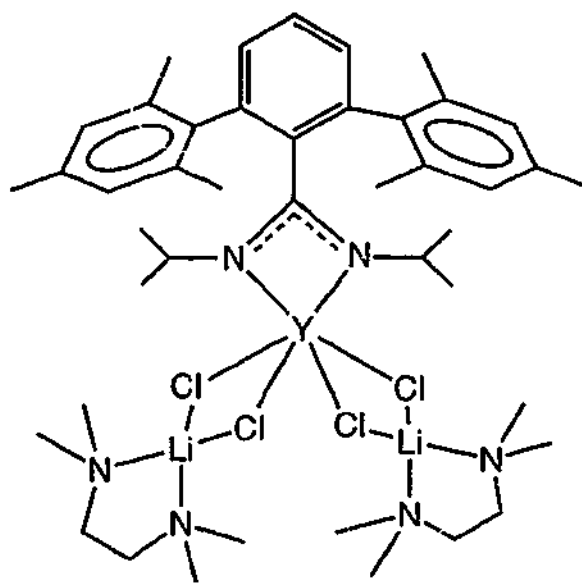


Figure 1.4

Coordination of the bidentate aminopyridinate ligands results in a more highly strained  $\eta^2$ -ligation compared with amidinate ligand systems.[60-63] Two of the aminopyridinate ligands can be linked using a siloxane-bridge resulting in the formation of a biligand.[64] The synthesis of lanthanoid biligand aminopyridinate complexes results in the formation of an 'ate' compound (see Figure 1.5) due to steric unsaturation of the metal centre.[64]

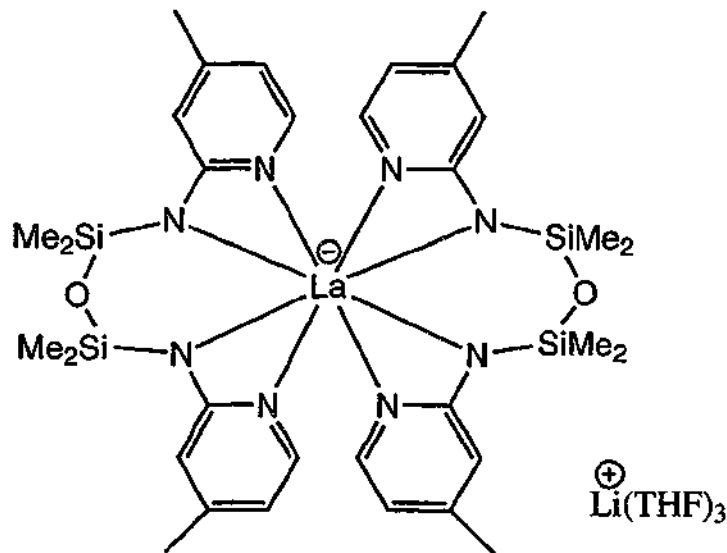
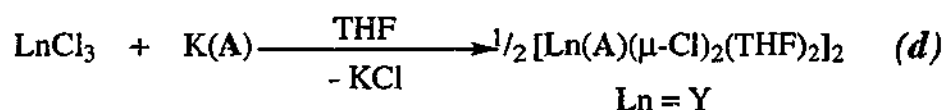
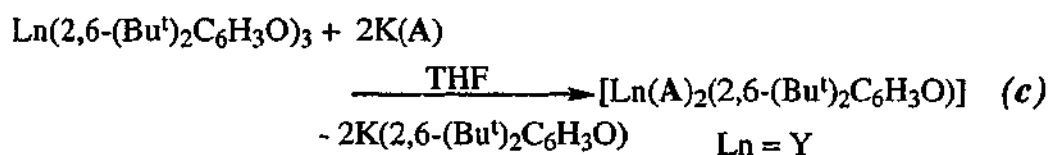
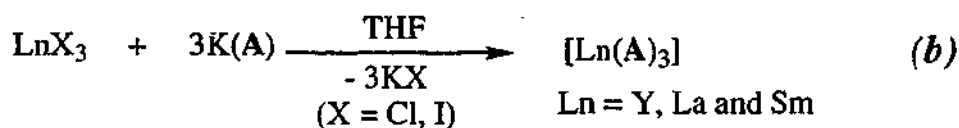
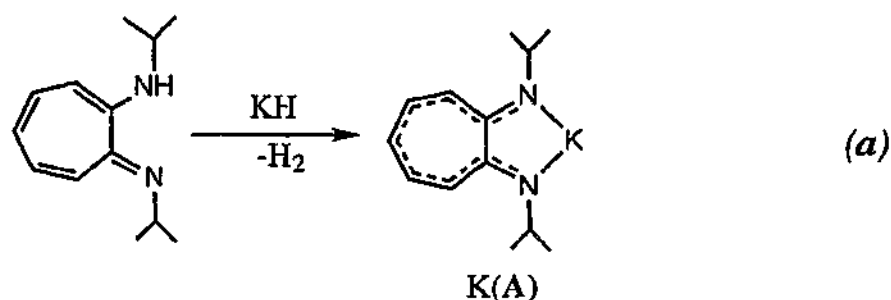


Figure 1.5

Alternatives to benzamidinates are ligands such as *N,O*-bis(*tert*-butyl)-(alkoxydimethylsilyl)amides.[65] This ligand system was found to have a much higher tendency to undergo ligand redistribution to form tris(alkoxysilylamido)lanthanoid

complexes. In addition, the ligand can react with the substrate ( $H_2$ ) in hydrogenation reactions and loss of alkoxysilylamine is observed.

Another N-based ligand system, the aminotroponimines, has recently been introduced into early transition metal chemistry as a cyclopentadienyl analogue.[66-69] This ligand is a bidentate monoanionic donor containing a  $10\pi$  electron backbone. The synthesis of a range of aminotroponiminatolanthanoid(III) complexes has been developed by Roesky where the potassium salt (see *Equation 1.2 (a)*) was used in metathesis reactions (see *Equation 1.2 (b)-(d)*).[70]



*Equation 1.2*

The aminotroponimine ligand provides adequate steric shielding of the lanthanoid centre to form solvent-free, monomeric homoleptic lanthanoid complexes. These complexes contain three ligands in a six-coordinate octahedral array around the lanthanoid centre. NMR studies have confirmed this geometry but crystallographic studies on these homoleptic complexes have so far been unsuccessful.

Interestingly, the transmetallation of lanthanoid halides with potassium aminotroponimate in a 2:1 ratio did not lead selectively to a pure complex of composition  $\text{Ln}(\text{A})_2\text{Cl}$ , and there was no indication of a rearrangement to the homoleptic product. In an alternative approach to obtaining a pure disubstituted product, the reaction of two equivalents of **A** with tris(2,6-( $\text{Bu}^t$ ) $_2\text{C}_6\text{H}_3\text{O}$ )yttrium (see *Equation 1.2 (c)*) yielded the required product  $[\text{Y}(\text{A})_2(2,6-(\text{Bu}^t)_2\text{C}_6\text{H}_3\text{O})]$ . Crystallographic analysis of the unusual five-coordinate species has not been successful, but NMR and other spectroscopic measurements indicated a monomeric, solvent-free five-coordinate complex. The 1:1 mole ratio reaction of **A** with  $\text{YCl}_3$  (see *Equation 1.2 (d)*) resulted in the formation of a dinuclear species,  $[\text{Y}(\mu\text{-Cl})_2(\text{A})(\text{THF})_2]_2$ . The formation of this dimer presumably results from steric unsaturation around the yttrium atom in which the coordination of two THF molecules and bridging chloride groups leads to seven-coordination. The ligand is attached asymmetrically to the metal centre with one isopropyl group pointing down and the other up. The aminotroponimate ligand has a similar steric demand to the cyclopentadienyl and benzamidinate ligands.<sup>[70]</sup> The bis(aminotroponimate)yttrium complexes were found to be active catalysts for hydroamination / cyclization.<sup>[71]</sup>

Two aminotroponimine units linked by a trimethylene bridge have also been coordinated onto various lanthanoid metals.<sup>[72]</sup> The metathesis reaction of two equivalents of the biligand potassium salt with lanthanum chloride results in a *homoleptic* lanthanoid species with chelating and bridging coordination modes (*Figure 1.6 (a)*). Addition of one equivalent of the biligand potassium salt to  $\text{LnCl}_3$  affords a *heteroleptic* dimeric lanthanoid complex that contains a chelating biligand and two bridging chloride atoms per metal (*Figure 1.6 (b)*). These heteroleptic complexes either form a six-fold (Er, Yb) or a seven-fold coordination sphere (La, Nd) around the central atom. The larger lanthanoid ions also coordinate a molecule of THF in order to reach steric saturation. The catalytic potential of these complexes as linked cyclopentadienyl alternatives is yet to be determined.

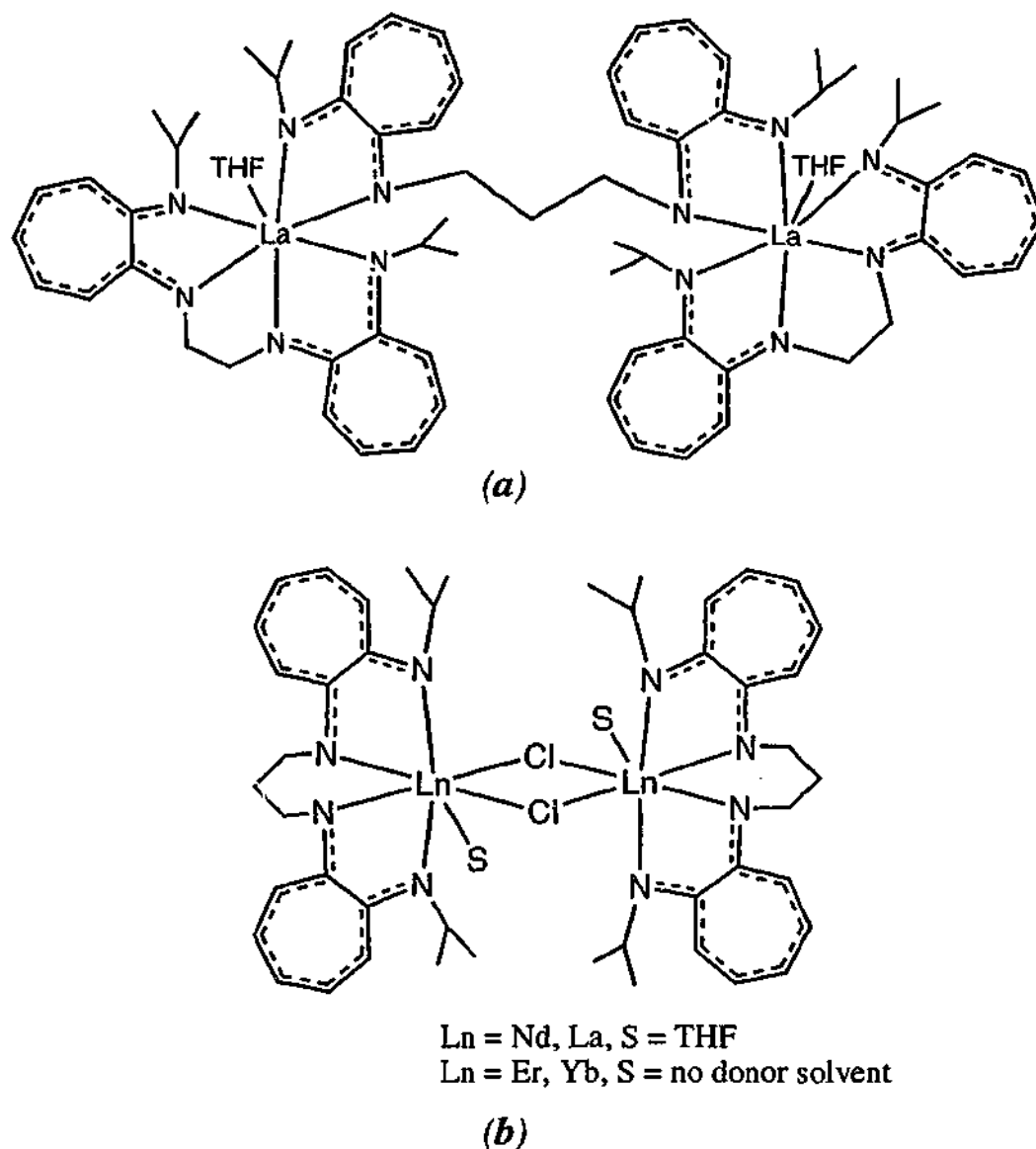


Figure 1.6

### 1.1.5 Lanthanoid(III) Multidentate Amide Complexes

A dipyrrolide dianion (see *Figure 1.7*) has recently been reacted with the lanthanoids by Gambarotta *et al.*[73, 74] Whilst simple pyrrole ligands in heteroleptic lanthanoid(III) complexes form  $\sigma$ -bonds,[75] placing more sterically demanding groups, such as *tert*-butyl, in the 2,5-positions of the pyrrole increases the steric shielding of the nitrogen and results in  $\eta^5$ -coordination to the lanthanoid centre.[76]

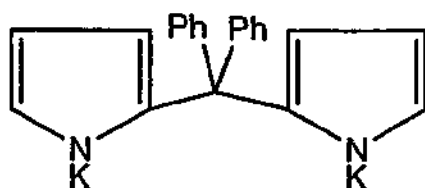


Figure 1.7

A metathesis reaction involving the divalent diphenylmethyldipyrrolyl dianion (either disodium or dipotassium salt) with samarium trichloride in THF resulted in the isolation of an unusual 'ate' complex,  $[[[\mu\text{-Ph}_2\text{C}(\eta^1:\eta^5\text{-C}_4\text{H}_5\text{N})_2\text{Sm}]_4(\mu_4\text{-Cl})\{\text{K}(\text{THF})_2\}]]$ .<sup>[73]</sup> The samarium complex featured both  $\sigma$  and  $\eta^5\text{-}\pi\text{-Sm}$  coordination modes in a tetranuclear arrangement with one potassium  $\pi$ -bonded to a pyrrole ring which already bonds with two samarium centres in a  $\sigma$  and  $\pi$ - arrangement (see *Figure 1.8*).

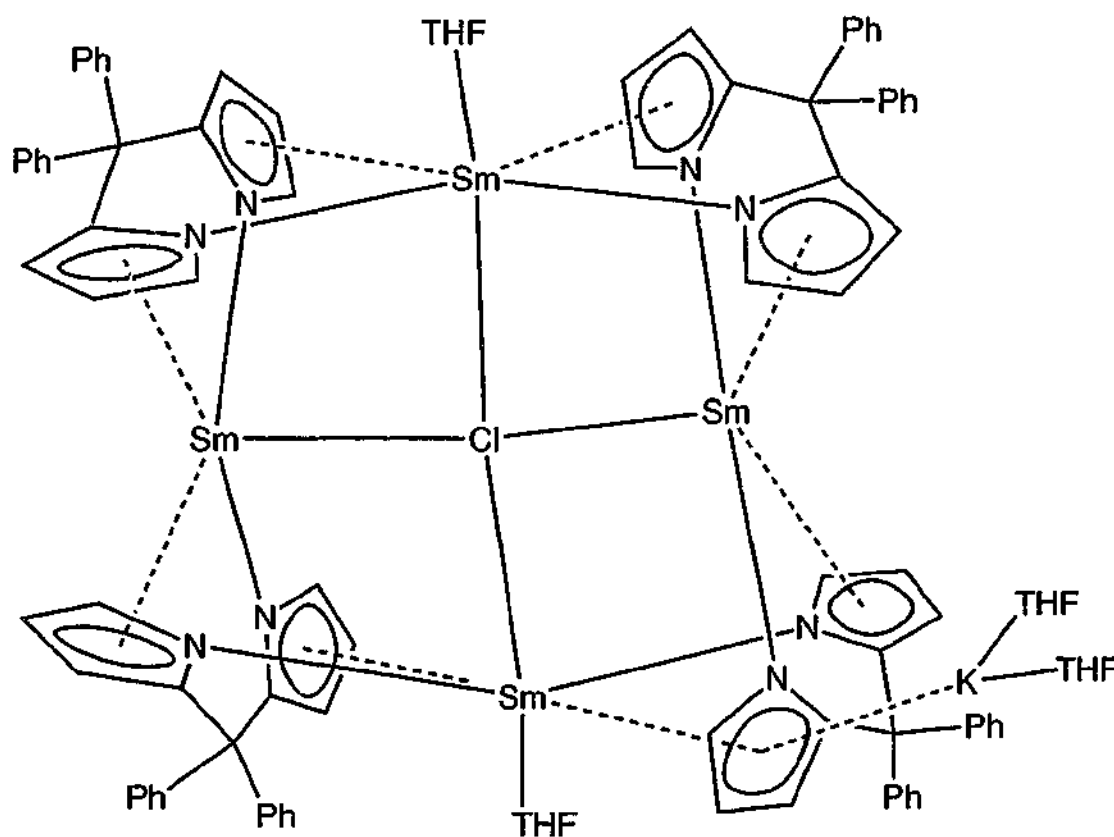


Figure 1.8

This unusual lanthanoid structural architecture is also exhibited by other substituted dipyrrolyl dianion ligand complexes e.g. methylphenyldipyrrole,<sup>[77]</sup> cyclohexyldipyrrole (see *Figure 1.9 (a)* and *(b)* respectively),<sup>[74, 77]</sup>  $[(-\text{CH}_2-)_5]_4$ -calix-tetrapyrrole (*Equation 1.3*)<sup>[78]</sup> and  $[\text{Et}_6]$ -calix-tetrapyrrole.<sup>[79-81]</sup>

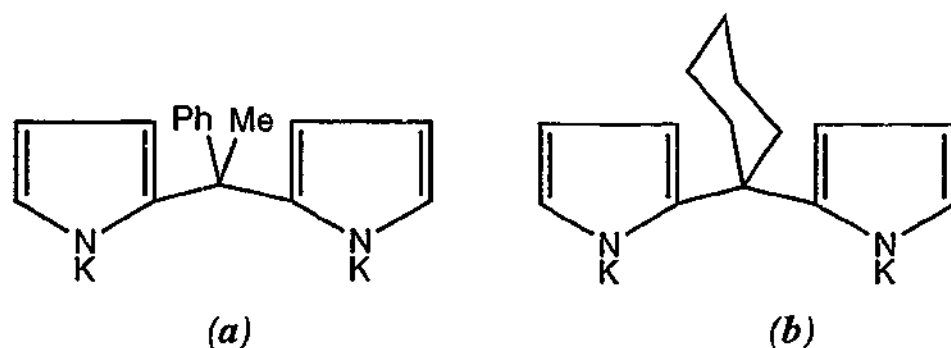
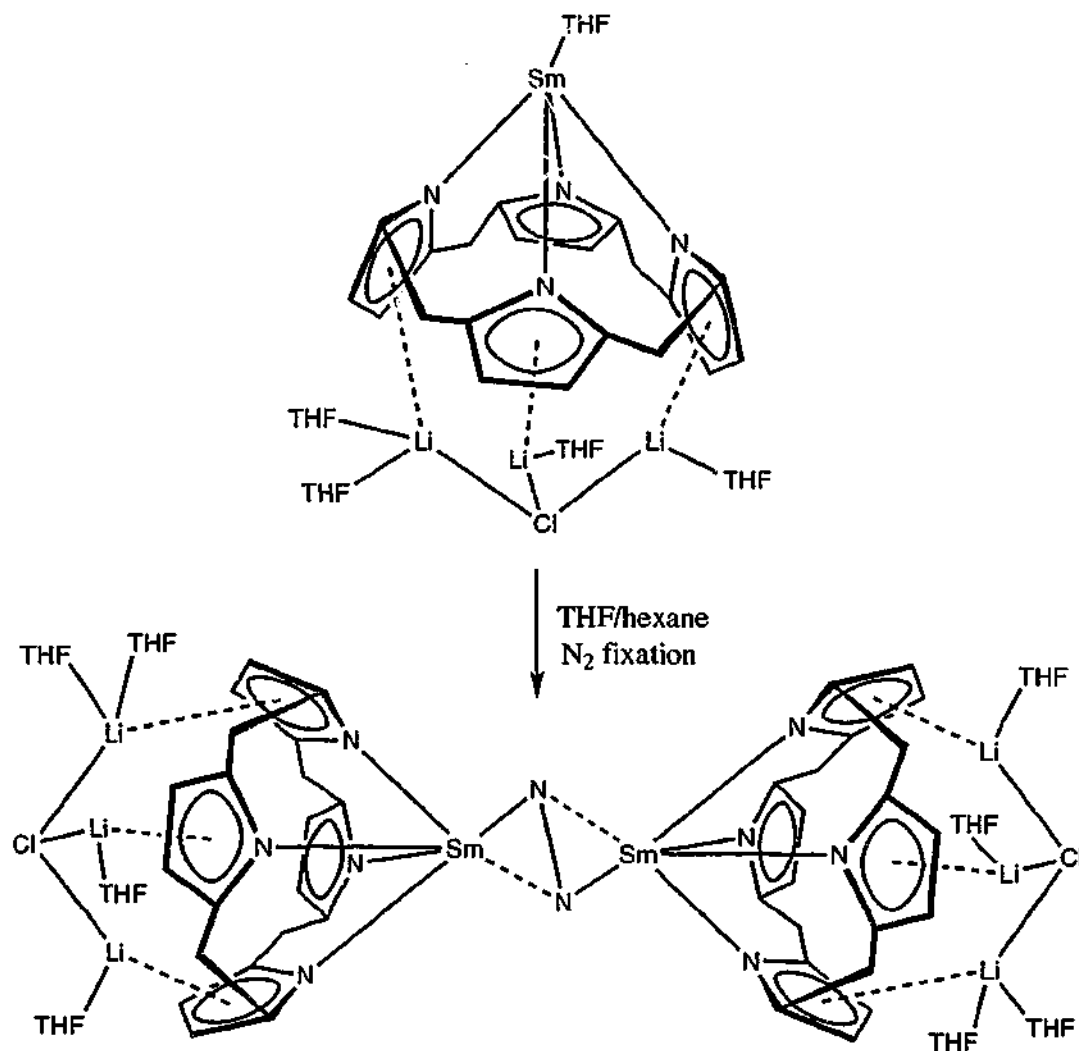


Figure 1.9

To date, successful fixation of dinitrogen and other small molecules using the samarium(II) (calix-tetrapyrrole) complexes e.g.  $\{[(-\text{CH}_2)_5]_4\text{-calix-tetrapyrrole}\}\text{Sm}(\text{THF})[\text{Li}(\text{THF})]_2[\text{Li}(\text{THF})]_2(\mu_3\text{-Cl})$  [78] has been achieved (see *Equation 1.3*). In all these compounds the pyrrole rings have a pseudo cyclopentadienyl character rather than an amide interaction with both  $\sigma$  and  $\pi$ -bonding modes around the metal centre.



Equation 1.3

### 1.1.6 Current Study

As can be seen above, there are numerous N-containing ligands that can stabilise highly reactive organolanthanoid complexes. Below is a list of some other N-ligands (*Figure 1.10*) that have been investigated with the lanthanoid metals though in comparison to the stability offered by the cyclopentadienyl ligand still behave poorly.[82-85]

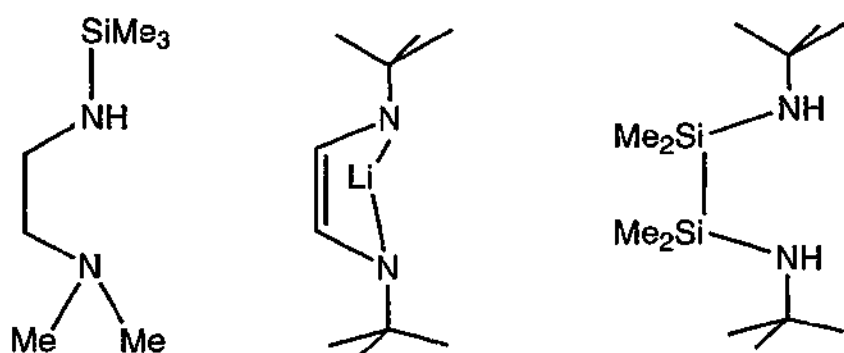


*Figure 1.10*

The aim of the research reported here is to investigate the use of sterically demanding amide ligands in preparing derivatives of the lanthanoids. Bulky ligands that can block coordination sites around the metal centre should lead to monomeric, hydrocarbon soluble, electron poor species that might display unique chemical properties. Of particular interest is the formation of heteroleptic lanthanoid compounds that can undergo further derivatisation.

A new ligand system has been developed in this research. Modification of the monodentate ligand  $\text{NH}(\text{SiMe}_3)\text{R}$  with the addition of an aromatic *ortho*-aryl or alkyl ether substituent produces a new class of mixed N, O-donor ligand (*Figure 1.11*). The bulky trimethylsilyl group increases the hydrocarbon solubility, as well as helping to delocalise the lone pair on the nitrogen, to produce more stable lanthanoid compounds. This is the first time that this ligand system (**B**) has been applied to any metals.



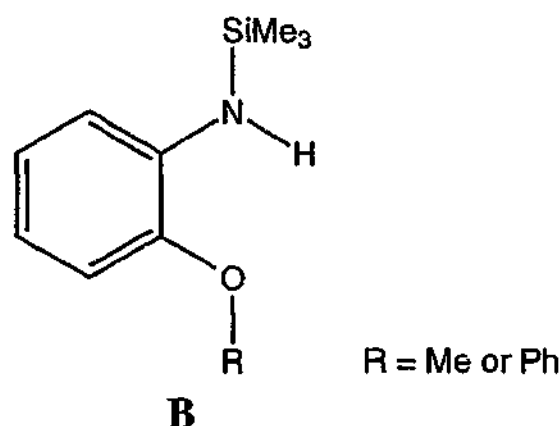


Figure 1.11

The target molecules are heteroleptic  $\text{LnL}_2\text{X}$  species that may parallel the chemistry exhibited by the classical  $\text{LnCp}_2\text{X}$  derivatives. Synthetic routes primarily involve metathesis but also oxidation and ligand exchange reactions. This was initially investigated using the known *N,N*-dimethyl-*N'*-trimethylsilylethane-1,2-diamine ( $\text{L}^1\text{H}$ ) ligand system<sup>[82]</sup> and a series of heteroleptic derivatives were prepared (Chapter 2). Subsequently, using a metathetical approach with the new ligand systems (**B**) and an appropriate lanthanoid trihalide, a range of homoleptic (Chapter 3) and heteroleptic derivatives (Chapter 4) were synthesised and fully characterised. Further reaction chemistry to fully explore the synthetic regime with this new ligand system employed other methods such as ligand exchange/transmetallation reactions and oxidation that resulted in unique reaction chemistry (Chapter 5).

As the chemistry of lanthanoid metals is relatively undeveloped compared with other elements of the periodic table, even simple synthetic precursors such as lanthanoid trihalides have unique coordination behaviour and often display unusual structures. Since both these aspects may influence their reactivity, the continued exploration of their properties is of considerable interest (Chapter 6). The other reagents required for metathesis reactions are typically alkali metal salts and in particular lithium amides that have already demonstrated a wide structural diversity. The proposed bidentate amide ligand offers the potential for new and unusual structural architecture in lithium chemistry. Furthermore, unexpected chemistry was found for the aryl ether substituted bidentate ligand in which a double deprotonation occurred at the *ortho*-carbon site. As a consequence, a unique series of structural aggregates containing mixed donor functionalities were isolated (Chapter 7).

## 1.2 References

- 1 A. Togni and L. M. Venanzi, *Angew. Chem. Int. Ed. Engl.*, 1994, **33**, 497.
- 2 J. Jubb, J. Song, D. Richeson, and S. Gambarotta, in *Comprehensive Organometallic Chemistry*, 2nd edn, eds. E. W. Abel, F. G. A. Stone, and G. Wilkinson, Pergamon, Oxford, 1995, vol. 4, ch. 11.
- 3 A. N. Guram and R. F. Jordan, in *Comprehensive Organometallic Chemistry*, 2nd edn, eds. E. W. Abel, F. G. A. Stone, and G. Wilkinson, Pergamon, Oxford, 1995, vol. 4, ch. 12.
- 4 H. Schumann, J.-A. Meese-Markscheffel, and L. Esser, *Chem. Rev.*, 1995, **95**, 865.
- 5 F. T. Edelmann, in *Comprehensive Organometallic Chemistry*, 2nd edn, eds. E. W. Abel, F. G. A. Stone, and G. Wilkinson, Pergamon, Oxford, 1995, vol. 4, ch. 2, p. 11.
- 6 M. N. Bochkarev, L. N. Zakharov, and G. S. Kalinina, *Organoderivatives of Rare Earth Elements*, Kluwer Academic, Dordrecht, 1995.
- 7 R. Anwander, *Top. Organomet. Chem.*, 1999, **2**, 1.
- 8 M. F. Lappert, P. P. Power, A. R. Sanger, and R. C. Srivastava, *Metal and Metalloid Amides*, Ellis Norwood, Chichester, 1980.
- 9 R. C. Mehrotra, A. Singh, and U. M. Tripathi, *Chem. Rev.*, 1991, **91**, 1287.
- 10 W. A. Cotton and G. Wilkinson, *Advanced Inorganic Chemistry*, 5th edn, Wiley-Interscience, New York, 1988, ch. 23.
- 11 National Measurement Laboratory, *Rare Earth Horizons 1987*, Department of Industry, Technology and Commerce, Canberra, 1987, p. 237.
- 12 F. A. Hart, in *Comprehensive Organometallic Chemistry*, eds. G. A. Wilkinson, R. D. Gillard, and J. A. McLverty, Pergamon, Oxford, 1987, vol. 3, ch. 39.
- 13 T. J. Marks and R. D. Ernst, in *Comprehensive Organometallic Chemistry*, eds. E. W. Abel, F. G. A. Stone, and G. Wilkinson, Pergamon, Oxford, 1982, vol. 3, ch. 21, p. 173.
- 14 M. C. Cassani, D. J. Duncalf, and M. F. Lappert, *J. Am. Chem. Soc.*, 1998, **120**, 12958.

- 15 M. N. Bochkarev, I. L. Fedushkin, A. A. Fagin, T. V. Petrovskaya, J. W. Ziller, R. N. R. Broomhall-Dillard, and W. J. Evans, *Angew. Chem. Int. Ed. Engl.*, 1997, **36**, 133.
- 16 G. Wilkinson and J. M. Birmingham, *J. Am. Chem. Soc.*, 1954, **76**, 6210.
- 17 J. M. Birmingham and G. Wilkinson, *J. Am. Chem. Soc.*, 1956, **78**, 42.
- 18 S. A. Cotton, *Coord. Chem. Rev.*, 1997, **160**, 93.
- 19 R. Kempe, *Angew. Chem. Int. Ed.*, 2000, **39**, 468.
- 20 R. Anwander, *Top. Curr. Chem.*, 1996, **179**, 33.
- 21 D. C. Bradley, R. C. Mehrotra, and C. P. Gaur, *Metal Alkoxides*, Academic Press, London, 1978.
- 22 R. G. Pearson, in *Hard and Soft Acids and Bases*, eds. Dowden, Hutchinson, and Ross, Stroudsburg, 1973.
- 23 F. T. Edelmann, *J. Alloys and Compounds*, 1994, **207/208**, 182.
- 24 W. J. Evans, S. L. Gonzales, and J. W. Ziller, *J. Am. Chem. Soc.*, 1991, **113**, 7423.
- 25 W. J. Evans, *Coord. Chem. Rev.*, 2000, **206/207**, 263.
- 26 F. T. Edelmann, *Top. Curr. Chem.*, 1996, **179**, 247-276.
- 27 D. C. Bradley, J. S. Ghortra, and F. A. Hart, *J. Chem. Soc. Chem. Commun.*, 1972, 349.
- 28 D. C. Bradley, E. C. Alyea, and R. G. Copperthwaite, *J. Chem. Soc. Dalton Trans.*, 1972, 1580.
- 29 D. C. Bradley, J. S. Ghortra, and F. A. Hart, *J. Chem. Soc., Dalton Trans.*, 1973, 1021.
- 30 D. C. Bradley, J. S. Ghortra, and F. A. Hart, *Inorg. Nucl. Chem. Letters*, 1976, **12**, 735.
- 31 M. R. Bürgstein, H. Berberich, and P. W. Roesky, *Chem. Eur. J.*, 2001, **7**, 3078.
- 32 D. C. Bradley, M. B. Hursthouse, H. C. Aspinall, K. D. Sales, N. P. C. Walker, and B. Hussian, *J. Chem. Soc., Chem. Comm.*, 1989, 623.
- 33 D. C. Bradley, M. B. Hursthouse, H. C. Aspinall, K. D. Sales, and N. P. C. Walker, *J. Chem. Soc., Chem. Comm.*, 1985, 1585.
- 34 M. Karl, G. Seybert, W. Massa, S. Agarwal, A. Greiner, and K. Dehnicke, *Z. Anorg. Allg. Chem.*, 1999, **625**, 1405.

- 35 J. Collin, N. Giuseppone, N. Jaber, A. Domingos, L. Maria, and I. Santos, *J. Organomet. Chem.*, 2001, **628**, 271.
- 36 D. C. Bradley, M. B. Hursthouse, H. C. Aspinall, K. D. Sales, N. P. C. Walker, and B. Hussian, *J. Chem. Soc., Dalton Trans.*, 1989, 623.
- 37 W. A. Herrmann, R. Anwander, F. C. Munck, W. Scherer, V. Dufaud, N. W. Huber, and G. R. J. Artus, *Z. Naturforsch.*, 1994, **49b**, 1789.
- 38 R. Anwander, O. Runte, J. Eppinger, G. Gerstberger, E. Herdtweck, and M. Spiegler, *J. Chem. Soc., Dalton Trans.*, 1998, 847.
- 39 J. Eppinger, M. Spiegler, W. Hieringer, W. A. Herrmann, and R. Anwander, *J. Chem. Soc. Chem.*, 2000, **122**, 3080.
- 40 H. Chen, M. M. Olmstead, S. C. Shoner, and P. P. Power, *J. Chem. Soc., Dalton Trans.*, 1994, 451.
- 41 R. A. Bartlett, M. M. Olmstead, and P. P. Power, *Inorg. Chem.*, 1994, **33**, 4800.
- 42 M. A. Petrie, K. Ruhlandt-Senge, and P. P. Power, *Inorg. Chem.*, 1993, **32**, 1135.
- 43 H. Schumann, J. Winterfeld, E. C. E. Rosenthal, H. Hemling, and L. Esser, *Z. Anorg. Allg. Chem.*, 1995, **621**, 122.
- 44 W. J. Evans, M. A. Ansari, J. W. Ziller, and S. I. Khan, *Inorg. Chem.*, 1996, **35**, 5435.
- 45 D. Fenske, E. Hartmann, and K. Dehnicke, *Z. Naturforsch.*, 1988, **43b**, 1611.
- 46 H. W. Roesky, B. Meller, M. Noltemeyer, H.-G. Schmidt, U. Scholz, and G. M. Sheldrick, *Chem. Ber.*, 1988, **121**, 1403.
- 47 A. Zinn, K. Dehnicke, D. Fenske, and G. Baum, *Z. Anorg. Allg. Chem.*, 1991, **596**, 47.
- 48 C. Ergezinger, F. Weller, and K. Dehnicke, *Z. Naturforsch.*, 1988, **43b**, 1119.
- 49 A. Rechnagel, F. Knoesel, H. Gornitzka, M. Noltemeyer, F. T. Edelman, and U. Behrens, *J. Organomet. Chem.*, 1991, **417**, 363.
- 50 M. Wedler, F. Knoesel, and F. T. Edelman, *Chem. Ber.*, 1992, **125**, 1313.
- 51 K. Dehnicke, C. Ergezinger, E. Hartmann, A. Zinn, and K. Hoesler, *J. Organomet. Chem.*, 1988, 352, C1.
- 52 M. Wedler, F. Knoesel, U. Pieper, D. Stalke, and F. T. Edelman, *Chem. Ber.*, 1992, **125**, 2171.

- 53 F. Knoesel, N. Noltemeyer, and F. T. Edelmann, *Z. Naturforsch.*, 1989, **44b**, 1171.
- 54 A. Rechnagel, M. Witt, and F. T. Edelmann, *J. Organomet. Chem.*, 1989, **371**.
- 55 R. Duchateau, C. T. van Wee, A. Meetsma, P. T. van Duijen, and J. H. Teuben, *Organometallics*, 1996, **15**, 2279.
- 56 R. Duchateau and C. T. van Wee, *Organometallics*, 1996, **15**, 2291.
- 57 R. Duchateau, C. T. van Wee, A. Meetsma, and J. H. Teuben, *J. Am. Chem. Soc.*, 1993, **115**, 4931.
- 58 M. Wedler, A. Rechnagel, J. W. Gilje, M. Noltemeyer, and F. T. Edelmann, *J. Organomet. Chem.*, 1992, **426**, 295.
- 59 J. A. R. Schmidt and J. Arnold, *J. Chem. Soc., Chem. Commun.*, 1999, 2149.
- 60 A. Spannenberg, P. Arndt, and R. Kempe, *Angew. Chem. Int. Ed.*, 1998, **110**, 824.
- 61 A. Spannenberg, P. Arndt, and R. Kempe, *Angew. Chem. Int. Ed.*, 1998, **37**, 832.
- 62 A. Spannerberg, M. Oberthur, H. Noss, A. Tillack, P. Arndt, and R. Kempe, *Angew. Chem. Int. Ed.*, 1998, **110**, 2190.
- 63 A. Spannerberg, M. Oberthur, H. Noss, A. Tillack, P. Arndt, and R. Kempe, *Angew. Chem. Int. Ed.*, 1998, **37**, 2079.
- 64 H. Noss, M. Oberthür, C. Fischer, W. P. Kretschmer, and R. Kempe, *Eur. J. Inorg. Chem.*, 1999, 2283.
- 65 R. Duchateau, T. Tuinstra, E. A. C. Brussee, A. Meetsma, and P. T. van Duijnen, *Organometallics*, 1997, **16**, 3511.
- 66 H. V. R. Dias, W. Jin, and Z. Wang, *Inorg. Chem.*, 1996, **35**, 6074.
- 67 H. V. R. Dias, W. Jin, and R. E. Ratcliff, *Inorg. Chem.*, 1995, **34**, 6100.
- 68 H. V. R. Dias and W. Jin, *J. Am. Chem. Soc.*, 1996, **118**, 9123.
- 69 H. V. R. Dias and W. Jin, *Inorg. Chem.*, 1996, **35**, 6546.
- 70 P. W. Roesky, *Chem. Ber.*, 1997, **130**, 859.
- 71 M. R. Bürgstein, H. Berberich, and P. W. Roesky, *Organometallics*, 1998, **17**, 1452.
- 72 P. W. Roesky and M. R. Bürgstein, *Inorg. Chem.*, 1999, **38**, 5629.
- 73 T. Dubé, S. Conoci, S. Gambarotta, G. P. A. Yap, and G. Vasapollo, *Angew. Chem. Int. Ed.*, 1999, **38**, 3657.

- 74 M. Ganesan, S. Gambarotta, and P. A. G. Yap, *Angew. Chem. Int. Ed.*, 2001, **40**, 766.
- 75 H. Schumann, P. R. Lee, and A. Dietrich, *Chem. Ber.*, 1990, **123**, 1331.
- 76 H. Schumann, J. Winterfeld, H. Hemling, and N. Kuhn, *Chem. Ber.*, 1993, **126**, 2657.
- 77 T. Dubé, S. Conoci, S. Gambarotta, and G. P. A. Yap, *Organometallics*, 2000, **19**, 1182.
- 78 J. Guan, T. Dubé, S. Gambarotta, and G. P. A. Yap, *Organometallics*, 2000, **19**, 4820.
- 79 T. Dubé, S. Gambarotta, and G. P. A. Yap, *Angew. Chem. Int. Ed.*, 1999, **38**, 1432.
- 80 T. Dubé, S. Gambarotta, and G. P. A. Yap, *Organometallics*, 2000, **19**, 121.
- 81 T. Dubé, S. Gambarotta, and G. P. A. Yap, *Organometallics*, 2000, **19**, 817.
- 82 G. B. Deacon, C. M. Forsyth, P. C. Junk, B. W. Skelton, and A. H. White, *J. Chem. Soc., Dalton Trans.*, 1998, 1381.
- 83 H. Görls, B. Neumüller, A. Scholz, and J. Scholz, *Angew. Chem. Int. Ed. Engl.*, 1995, **34**, 673.
- 84 S. A. A. Shah, H. Dorn, H. W. Roesky, P. Lubini, and H. G. Schmidt, *Inorg. Chem.*, 1997, 1102.
- 85 L. Lee, D. J. Berg, F. W. Einstein, and R. J. Batchelor, *Organometallics*, 1997, **16**, 1819.

## Chapter 2

# *Heteroleptic Lanthanoid(III) Complexes of the Chelating $N,N$ -dimethyl- $N'$ -trimethylsilylethane-1,2-diamine Ligand*

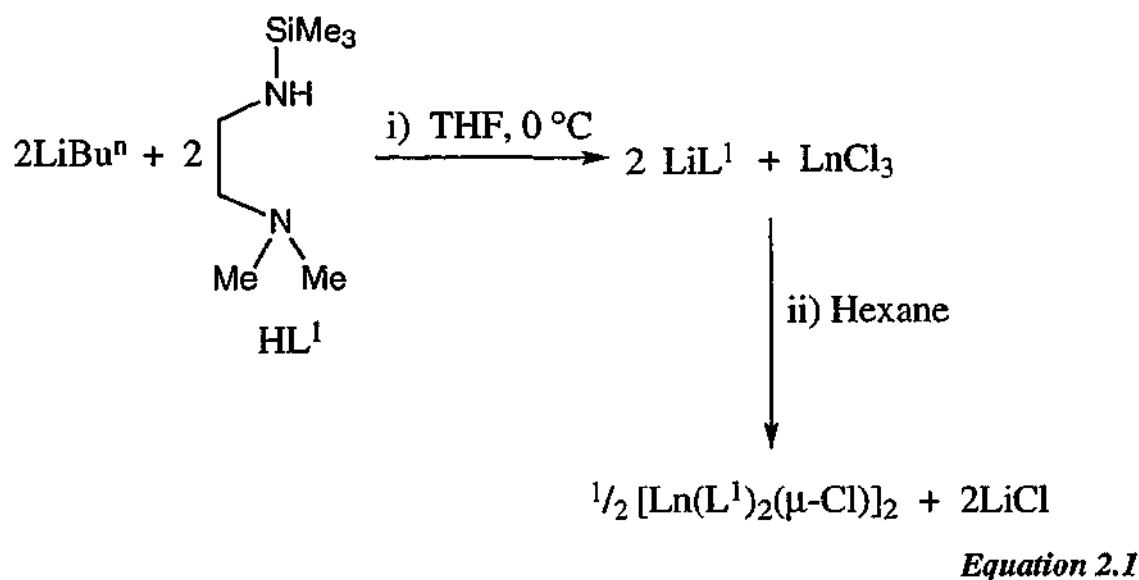
### 2.1 Introduction

The labile nature of organoamide ligands has often caused problems in the stabilisation of coordinatively unsaturated heteroleptic complexes of the type  $\text{Ln}(\text{L})_2\text{X}$  ( $\text{X}$ = anionic ligand) (see Chapter 1). Typically, ligand redistribution is sterically preferred resulting in isolation of only the homoleptic derivatives. Utilising the premise that incorporation of at least a bidentate amide ligand may improve the stability of the heteroleptic complexes,  $N,N$ -dimethyl- $N'$ -trimethylsilylethane-1,2-diamine ( $\text{L}^1\text{H}$ ) has recently been applied to this area.<sup>[1]</sup> A range of hydrocarbon soluble homoleptic complexes  $[\text{Ln}(\text{L}^1)_3]$  ( $\text{Ln} = \text{Lu}, \text{Er}, \text{Eu}, \text{Sm}, \text{Nd}, \text{La}$ ) were prepared but significantly also *one* example of a heteroleptic derivative  $[\text{Er}(\text{L}^1)_2\text{Cl}]$  was isolated. Although not verified by a crystal structure, a monomeric complex was indicated spectroscopically. The commencement of work in this thesis was therefore to extend this new important class of compounds to other members of the lanthanoid series and obtain structural details by X-ray crystallography. Furthermore the subsequent derivatisation by replacement of the remaining halide was also to be pursued.

## 2.2 Results and Discussion

### 2.2.1 Preparation of $\text{Ln}(\text{L}^1)_2\text{Cl}$ Complexes

The preparation of heteroleptic diorganoamidolanthanoid complexes  $[\text{Ln}(\text{L}^1)_2(\mu\text{-Cl})]_2$  ( $\text{Ln} = \text{Yb, Er, Sm, Nd}$  and  $\text{La}$ ) involved the reaction of two equivalents of  $\text{LiL}^1$ , which was generated *in situ* in THF, with suitable lanthanoid trihalides (Equation 2.1). The lanthanoid products were very soluble in hydrocarbon solvents and were crystallised with difficulty from concentrated solutions at  $-20^\circ\text{C}$ . Furthermore, the removal of  $\text{LiCl}$  from the reaction mixture was tedious with numerous low temperature extractions required in order to obtain pure  $[\text{Ln}(\text{L}^1)_2(\mu\text{-Cl})]_2$  derivatives which were subsequently isolated in low to moderate yields.



The difficulty in removing  $\text{LiCl}$  from  $\text{L}^1$  systems has previously been observed in the isolation of homoleptic  $[\text{Ln}(\text{L}^1)_3]$  complexes.<sup>[1]</sup> A structural investigation on crystals of the mother liquor from the low yielding synthesis of  $[\text{Lu}(\text{L}^1)_3]$  showed that a  $\text{LiCl}$  was encapsulated by two  $\text{LiL}^1$  units forming a mixed lithium aggregate  $[\{\text{LiL}^1\text{LiClLiL}^1(\text{THF})\}_2]$ . This aggregate has a higher solubility than  $\text{LiCl}$  and hence is more difficult to remove in hydrocarbon solutions. As a similar procedure was used in the preparation of  $[\text{Ln}(\text{L}^1)_2(\mu\text{-Cl})]_2$  complexes, it is likely that such a mixed aggregate between  $\text{LiCl}$  and  $\text{LiL}^1$  is formed, thereby explaining the work up difficulties.



Concentration of the extracted reaction mixture from hexane yielded crystals of  $[\text{Ln}(\text{L}^1)_2(\mu\text{-Cl})]_2$  ( $\text{Ln} = \text{Yb, Er, Sm, Nd, La}$ ). Elemental analysis (C, H, N) for  $[\text{Yb}(\text{L}^1)_2(\mu\text{-Cl})]_2$  and lanthanoid analyses on  $[\text{Nd}(\text{L}^1)_2(\mu\text{-Cl})]_2$  and  $[\text{La}(\text{L}^1)_2(\mu\text{-Cl})]_2$  confirmed the ligand to metal ratios which were similar to that for the reported  $[\text{Er}(\text{L}^1)_2\text{Cl}]$  complex.<sup>[1]</sup> The infrared spectra of  $[\text{Ln}(\text{L}^1)_2(\mu\text{-Cl})]_2$  ( $\text{Ln} = \text{Yb, Er, Sm, Nd, La}$ ) were almost identical showing peaks attributable to  $\text{L}^1$  with no evidence of coordinated THF at 900-850  $\text{cm}^{-1}$ . Mass spectra identified a bimolecular species to be present in each case with the highest-mass fragment, except for ytterbium, giving an ion  $[\text{Ln}_2(\text{L}^1)_3\text{Cl}_2]^+$ . For the heavier ytterbium metal only the fragment  $[\text{Yb}_2(\text{L}^1)_2\text{Cl}_2]^+$  was detected due to limitations in the mass spectrum range. These data imply that a dimeric structure is formed resulting in complexes of the type  $[\text{Ln}(\text{L}^1)_2(\mu\text{-Cl})]_2$ . Numerous attempts to prepare crystals suitable for X-ray diffraction studies were unsuccessful due to the highly soluble nature of  $[\text{Ln}(\text{L}^1)_2(\mu\text{-Cl})]_2$ . Whilst each complex was isolated as a crystalline solid, the crystals were not single and therefore were unsuitable for crystallographic studies. Similar isolation difficulties were encountered in  $[\text{Ln}(\text{L}^1)_3]$ ,<sup>[1]</sup> with sufficient crystallographic data only obtained for three lanthanoid species.

### 2.2.2 Derivatisation of $[\text{Ln}(\text{L}^1)_2(\mu\text{-Cl})]_2$ Complexes

The reaction of  $\text{NdCl}_3$  with 2 equivalents of  $\text{LiL}^1$  in THF gives  $[\text{Nd}(\text{L}^1)_2(\mu\text{-Cl})]_2$  (see above). This precursor reacts further with one equivalent of  $\text{Li}(\text{Ph}_2\text{Pz})$  ( $\text{Ph}_2\text{pz} = 3,5$ -diphenylpyrazolate) in THF, hexane and DME affording blue crystals of the unexpected stoichiometry  $[\text{Nd}(\text{L}^1)(\text{Ph}_2\text{pz})_3][\text{Li}(\text{DME})_3]$  in low yield. The structure of  $[\text{Nd}(\text{L}^1)(\text{Ph}_2\text{pz})_3][\text{Li}(\text{DME})_3]$  was established by an X-ray diffraction study (see below). The infrared spectrum of the blue crystalline material showed peaks attributable to  $\text{L}^1$  and  $\text{Ph}_2\text{pz}$  ligands as well as a strong band at 1026  $\text{cm}^{-1}$  from the antisymmetric C—O—C stretching absorption of the DME ligand. The highest mass fragment detected in the mass spectrum was the ion  $[\text{Nd}(\text{L}^1)(\text{Ph}_2\text{pz})_3\text{Li}]^+$  although the intensity was very weak. In a similar manner low intensity isotope patterns could be assigned to  $[\text{Nd}(\text{L}^1)_3]^+$  and  $[\text{Nd}(\text{Ph}_2\text{pz})_3]^+$  ions as well as their subsequent breakdown fragments. An elemental analysis (C, H, N) indicated that the blue crystalline material was not pure having a much lower (8%) carbon content than expected with  $\text{LiCl}$  being a likely source of contamination. The molecular structure of  $[\text{Nd}(\text{L}^1)(\text{Ph}_2\text{pz})_3][\text{Li}(\text{DME})_3]$  is shown in *Figure 2.1*. Crystallographic refinement details and selected bond lengths and angles are listed in

**Table 2.1** and **Table 2.2** respectively. The complex consists of discrete ion pairs  $[\text{Li}(\text{DME})_3]^+$  and  $[\text{Nd}(\text{L}^1)(\text{Ph}_2\text{pz})_3]^-$ . In  $[\text{Li}(\text{DME})_3]^+$ , the six-coordinate lithium adopts an octahedral geometry with three molecules of DME chelating to the central Li atom. The Li—O bond distances and the O—Li—O bite angles are typical<sup>[2, 3]</sup> and lie in the range, 2.08(1)—2.20(1) Å and 76.8(4)—78.9(5)°, respectively. The anion consists of a central eight-coordinate neodymium atom that is surrounded by one chelating  $\text{L}^1$  group and three  $\eta^2$ - $\text{Ph}_2\text{pz}$  ligands. The centres of the N(11)—N(12) (cen(1)) and N(31)—N(32) (cen(3)) bonds together with N(42) are approximately in the equatorial positions of a triangular bipyramid with the apical positions occupied by the amide nitrogen N(41) on  $\text{L}^1$  and the centre of the N(21)—N(22) bond (cen(2)). The geometry is distorted toward a square based pyramid as a result of the chelation of the  $\text{L}^1$  ligand. The average Nd(1)—N( $\text{Ph}_2\text{pz}$ ) distance is 2.49 Å and subtraction of the ionic radius (i.r.)<sup>[4]</sup> of eight-coordinate  $\text{Nd}^{3+}$  (1.11 Å) gives 1.38 Å which is comparable with those values observed for eight-coordinate lanthanoid complexes  $[\text{Er}(\eta^2\text{-}(\text{Bu}^i)_2\text{pz})_4][\text{K}(18\text{-crown-}6)(\text{DME})(\text{PhMe})]$ <sup>[5]</sup> (subtraction of i.r. = 1.35 Å) and  $[\text{Yb}(\text{Ph}_2\text{pz})_3(\text{DME})].0.5(\text{DME})$ <sup>[6]</sup> (subtraction of i.r. = 1.32 Å). The bidentate  $\text{L}^1$  amide ligand is unsymmetrically coordinated to the metal centre with the weaker amine bond length (Nd(1)—N(41)) significantly longer (0.30 Å) than the amide (Nd(1)—N(42)) distance. A similar lengthening of the amine nitrogen of  $\text{L}^1$  was observed in homoleptic  $[\text{Ln}(\text{L}^1)_3]$  ( $\text{Ln} = \text{Eu}, \text{Er}, \text{Lu}$ )<sup>[1]</sup> although a much greater difference (0.50 Å) was observed reflecting the greater steric repulsion of the three bulky  $\text{SiMe}_3$  groups. The bite angles of  $\text{L}^1$  (N(41)—Nd(1)—N(42)) and  $\text{Ph}_2\text{pz}$  (N(x1)—Nd(1)—N(x2) (x = 1,3)) ligands to the metal centre in  $[\text{Nd}(\text{L}^1)(\text{Ph}_2\text{pz})_3]^-$  are similar to those values in  $[\text{Ln}(\text{L}^1)_3]$  ( $\text{Ln} = \text{Eu}, \text{Er}, \text{Lu}$ ) and  $[\text{Yb}(\text{Ph}_2\text{pz})_3(\text{DME})].0.5(\text{DME})$  respectively. In contrast to the eight-coordinate anions  $[\text{Nd}(\text{L}^1)(\text{Ph}_2\text{pz})_3]^-$ ,  $[\text{Er}(\eta^2\text{-tBu}_2\text{pz})_4]^-$  and the  $[\text{Yb}(\text{Ph}_2\text{pz})_3(\text{DME})].0.5(\text{DME})$  complex are nine-coordinate  $[\text{Nd}(\text{Ph}_2\text{pz})_3(\text{DME})_2]$  and  $[\text{Er}(\text{Ph}_2\text{pz})_3(\text{DME})_2]$  where one DME ligand is chelating while the other binds in a  $\eta^1$ -fashion to the lanthanoid metal. This unusual bonding indicates that the lanthanoid centre is unable to accommodate two chelating DME ligands. Hence the steric demand of  $\text{L}^1$  in  $[\text{Nd}(\text{L}^1)(\text{Ph}_2\text{pz})_3]^-$  must be less than two DME molecules but greater than one and as a result adequately saturates the lanthanoid centre from further coordination.

Table 2.1 Summary of Crystallographic data for  $[\text{Nd}(\text{L}^1)(\text{Ph}_2\text{pz})_3][\text{Li}(\text{DME})_3]$ 

Compound	$[\text{Nd}(\text{L}^1)(\text{Ph}_2\text{pz})_3][\text{Li}(\text{DME})_3]$
Formula	$\text{C}_{64}\text{H}_{82}\text{LiN}_6\text{O}_6\text{Si}$
<i>M</i>	1238.65
<i>a</i> (Å)	14.543(3)
<i>b</i> (Å)	18.381(4)
<i>c</i> (Å)	24.091(5)
$\alpha$ (°)	90
$\beta$ (°)	90.08(3)
$\gamma$ (°)	90
<i>V</i> (Å <sup>3</sup> )	6440(2)
Crystal system	Monoclinic
Space Group	<i>P2<sub>1</sub>/c</i>
<i>Z</i>	4
Diffractometer	Enraf Nonius Kappa CCD
$\rho_{\text{calcd}}$ (g cm <sup>-3</sup> )	1.278
$\mu(\text{MoK}\alpha)$ (mm <sup>-1</sup> )	0.879
$2\theta_{\text{max}}$ (°)	56.5
$N^a N_o^b$	14565, 4633
<i>R, R<sub>w</sub></i> (observed data)	0.0682, 0.0707
<i>R, R<sub>w</sub></i> (all data)	0.2997, 0.1022

<sup>a</sup> *N* = number of unique reflections<sup>b</sup> *N<sub>o</sub>* = number of observed reflections [*I* > 2σ(*I*)]

## Chapter 2

# Heteroleptic Lanthanoid(III) Complexes of the Chelating *N,N*-dimethyl-*N'*-trimethylsilylethane-1,2-diamine Ligand

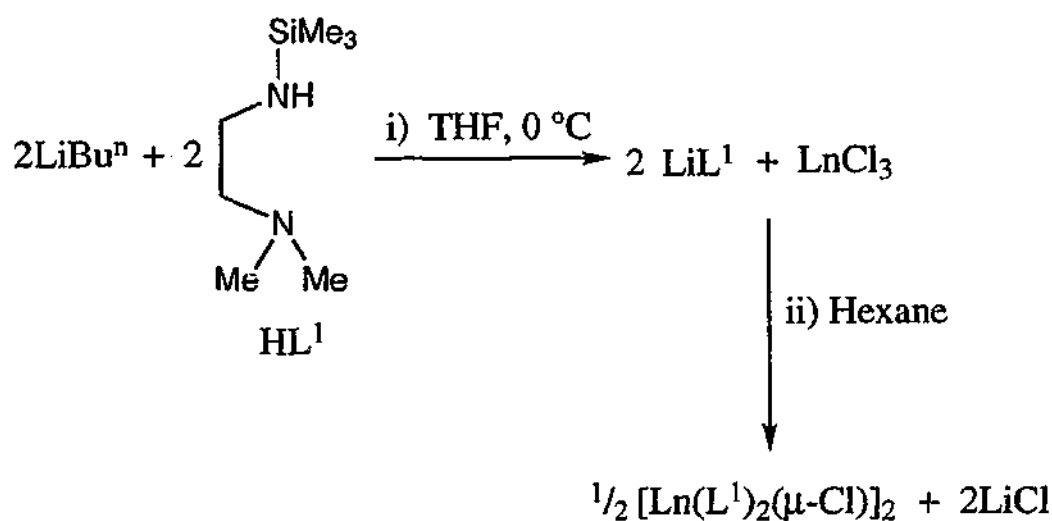
### 2.1 Introduction

The labile nature of organoamide ligands has often caused problems in the stabilisation of coordinatively unsaturated heteroleptic complexes of the type  $\text{Ln}(\text{L})_2\text{X}$  ( $\text{X}$ = anionic ligand) (see Chapter 1). Typically, ligand redistribution is sterically preferred resulting in isolation of only the homoleptic derivatives. Utilising the premise that incorporation of at least a bidentate amide ligand may improve the stability of the heteroleptic complexes, *N,N*-dimethyl-*N'*-trimethylsilylethane-1,2-diamine ( $\text{L}^1\text{H}$ ) has recently been applied to this area.<sup>[1]</sup> A range of hydrocarbon soluble homoleptic complexes  $[\text{Ln}(\text{L}^1)_3]$  ( $\text{Ln} = \text{Lu}, \text{Er}, \text{Eu}, \text{Sm}, \text{Nd}, \text{La}$ ) were prepared but significantly also *one* example of a heteroleptic derivative  $[\text{Er}(\text{L}^1)_2\text{Cl}]$  was isolated. Although not verified by a crystal structure, a monomeric complex was indicated spectroscopically. The commencement of work in this thesis was therefore to extend this new important class of compounds to other members of the lanthanoid series and obtain structural details by X-ray crystallography. Furthermore the subsequent derivatisation by replacement of the remaining halide was also to be pursued.

## 2.2 Results and Discussion

### 2.2.1 Preparation of $\text{Ln}(\text{L}^1)_2\text{Cl}$ Complexes

The preparation of heteroleptic diorganoamidolanthanoid complexes  $[\text{Ln}(\text{L}^1)_2(\mu\text{-Cl})]_2$  ( $\text{Ln} = \text{Yb}, \text{Er}, \text{Sm}, \text{Nd}$  and  $\text{La}$ ) involved the reaction of two equivalents of  $\text{LiL}^1$ , which was generated *in situ* in THF, with suitable lanthanoid trihalides (*Equation 2.1*). The lanthanoid products were very soluble in hydrocarbon solvents and were crystallised with difficulty from concentrated solutions at  $-20^\circ\text{C}$ . Furthermore, the removal of  $\text{LiCl}$  from the reaction mixture was tedious with numerous low temperature extractions required in order to obtain pure  $[\text{Ln}(\text{L}^1)_2(\mu\text{-Cl})]_2$  derivatives which were subsequently isolated in low to moderate yields.



*Equation 2.1*

The difficulty in removing  $\text{LiCl}$  from  $\text{L}^1$  systems has previously been observed in the isolation of homoleptic  $[\text{Ln}(\text{L}^1)_3]$  complexes.<sup>[1]</sup> A structural investigation on crystals of the mother liquor from the low yielding synthesis of  $[\text{Lu}(\text{L}^1)_3]$  showed that a  $\text{LiCl}$  was encapsulated by two  $\text{LiL}^1$  units forming a mixed lithium aggregate  $\{[\text{LiL}^1\text{LiClLiL}^1(\text{THF})]_2\}$ . This aggregate has a higher solubility than  $\text{LiCl}$  and hence is more difficult to remove in hydrocarbon solutions. As a similar procedure was used in the preparation of  $[\text{Ln}(\text{L}^1)_2(\mu\text{-Cl})]_2$  complexes, it is likely that such a mixed aggregate between  $\text{LiCl}$  and  $\text{LiL}^1$  is formed, thereby explaining the work up difficulties.

Concentration of the extracted reaction mixture from hexane yielded crystals of  $[\text{Ln}(\text{L}^1)_2(\mu\text{-Cl})]_2$  ( $\text{Ln} = \text{Yb, Er, Sm, Nd, La}$ ). Elemental analysis (C, H, N) for  $[\text{Yb}(\text{L}^1)_2(\mu\text{-Cl})]_2$  and lanthanoid analyses on  $[\text{Nd}(\text{L}^1)_2(\mu\text{-Cl})]_2$  and  $[\text{La}(\text{L}^1)_2(\mu\text{-Cl})]_2$  confirmed the ligand to metal ratios which were similar to that for the reported  $[\text{Er}(\text{L}^1)_2\text{Cl}]$  complex.<sup>[1]</sup> The infrared spectra of  $[\text{Ln}(\text{L}^1)_2(\mu\text{-Cl})]_2$  ( $\text{Ln} = \text{Yb, Er, Sm, Nd, La}$ ) were almost identical showing peaks attributable to  $\text{L}^1$  with no evidence of coordinated THF at 900-850  $\text{cm}^{-1}$ . Mass spectra identified a bimolecular species to be present in each case with the highest-mass fragment, except for ytterbium, giving an ion  $[\text{Ln}_2(\text{L}^1)_3\text{Cl}_2]^+$ . For the heavier ytterbium metal only the fragment  $[\text{Yb}_2(\text{L}^1)_2\text{Cl}_2]^+$  was detected due to limitations in the mass spectrum range. These data imply that a dimeric structure is formed resulting in complexes of the type  $[\text{Ln}(\text{L}^1)_2(\mu\text{-Cl})]_2$ . Numerous attempts to prepare crystals suitable for X-ray diffraction studies were unsuccessful due to the highly soluble nature of  $[\text{Ln}(\text{L}^1)_2(\mu\text{-Cl})]_2$ . Whilst each complex was isolated as a crystalline solid, the crystals were not single and therefore were unsuitable for crystallographic studies. Similar isolation difficulties were encountered in  $[\text{Ln}(\text{L}^1)_3]$ ,<sup>[1]</sup> with sufficient crystallographic data only obtained for three lanthanoid species.

### 2.2.2 Derivatisation of $[\text{Ln}(\text{L}^1)_2(\mu\text{-Cl})]_2$ Complexes

The reaction of  $\text{NdCl}_3$  with 2 equivalents of  $\text{LiL}^1$  in THF gives  $[\text{Nd}(\text{L}^1)_2(\mu\text{-Cl})]_2$  (see above). This precursor reacts further with one equivalent of  $\text{Li}(\text{Ph}_2\text{Pz})$  ( $\text{Ph}_2\text{pz} = 3,5$ -diphenylpyrazolate) in THF, hexane and DME affording blue crystals of the unexpected stoichiometry  $[\text{Nd}(\text{L}^1)(\text{Ph}_2\text{pz})_3][\text{Li}(\text{DME})_3]$  in low yield. The structure of  $[\text{Nd}(\text{L}^1)(\text{Ph}_2\text{pz})_3][\text{Li}(\text{DME})_3]$  was established by an X-ray diffraction study (see below). The infrared spectrum of the blue crystalline material showed peaks attributable to  $\text{L}^1$  and  $\text{Ph}_2\text{pz}$  ligands as well as a strong band at 1026  $\text{cm}^{-1}$  from the antisymmetric C—O—C stretching absorption of the DME ligand. The highest mass fragment detected in the mass spectrum was the ion  $[\text{Nd}(\text{L}^1)(\text{Ph}_2\text{pz})_3\text{Li}]^+$  although the intensity was very weak. In a similar manner low intensity isotope patterns could be assigned to  $[\text{Nd}(\text{L}^1)_3]^+$  and  $[\text{Nd}(\text{Ph}_2\text{pz})_3]^+$  ions as well as their subsequent breakdown fragments. An elemental analysis (C, H, N) indicated that the blue crystalline material was not pure having a much lower (8%) carbon content than expected with  $\text{LiCl}$  being a likely source of contamination. The molecular structure of  $[\text{Nd}(\text{L}^1)(\text{Ph}_2\text{pz})_3][\text{Li}(\text{DME})_3]$  is shown in *Figure 2.1*. Crystallographic refinement details and selected bond lengths and angles are listed in

*Table 2.1* and *Table 2.2* respectively. The complex consists of discrete ion pairs  $[\text{Li}(\text{DME})_3]^+$  and  $[\text{Nd}(\text{L}^1)(\text{Ph}_2\text{pz})_3]^-$ . In  $[\text{Li}(\text{DME})_3]^+$ , the six-coordinate lithium adopts an octahedral geometry with three molecules of DME chelating to the central Li atom. The Li—O bond distances and the O—Li—O bite angles are typical<sup>[2, 3]</sup> and lie in the range, 2.08(1)—2.20(1) Å and 76.8(4)—78.9(5)°, respectively. The anion consists of a central eight-coordinate neodymium atom that is surrounded by one chelating  $\text{L}^1$  group and three  $\eta^2$ - $\text{Ph}_2\text{pz}$  ligands. The centres of the N(11)—N(12) (cen(1)) and N(31)—N(32) (cen(3)) bonds together with N(42) are approximately in the equatorial positions of a triangular bipyramid with the apical positions occupied by the amide nitrogen N(41) on  $\text{L}^1$  and the centre of the N(21)—N(22) bond (cen(2)). The geometry is distorted toward a square based pyramid as a result of the chelation of the  $\text{L}^1$  ligand. The average Nd(1)—N( $\text{Ph}_2\text{pz}$ ) distance is 2.49 Å and subtraction of the ionic radius (i.r.)<sup>[4]</sup> of eight-coordinate  $\text{Nd}^{3+}$  (1.11 Å) gives 1.38 Å which is comparable with those values observed for eight-coordinate lanthanoid complexes  $[\text{Er}(\eta^2\text{-}(\text{Bu}^i)_2\text{pz})_4][\text{K}(18\text{-crown-}6)(\text{DME})(\text{PhMe})]$ <sup>[5]</sup> (subtraction of i.r. = 1.35 Å) and  $[\text{Yb}(\text{Ph}_2\text{pz})_3(\text{DME})].0.5(\text{DME})$ <sup>[6]</sup> (subtraction of i.r. = 1.32 Å). The bidentate  $\text{L}^1$  amide ligand is unsymmetrically coordinated to the metal centre with the weaker amine bond length (Nd(1)—N(41)) significantly longer (0.30 Å) than the amide (Nd(1)—N(42)) distance. A similar lengthening of the amine nitrogen of  $\text{L}^1$  was observed in homoleptic  $[\text{Ln}(\text{L}^1)_3]$  (Ln = Eu, Er, Lu)<sup>[1]</sup> although a much greater difference (0.50 Å) was observed reflecting the greater steric repulsion of the three bulky  $\text{SiMe}_3$  groups. The bite angles of  $\text{L}^1$  (N(41)—Nd(1)—N(42)) and  $\text{Ph}_2\text{pz}$  (N(x1)—Nd(1)—N(x2) (x = 1,3)) ligands to the metal centre in  $[\text{Nd}(\text{L}^1)(\text{Ph}_2\text{pz})_3]^-$  are similar to those values in  $[\text{Ln}(\text{L}^1)_3]$  (Ln = Eu, Er, Lu) and  $[\text{Yb}(\text{Ph}_2\text{pz})_3(\text{DME})].0.5(\text{DME})$  respectively. In contrast to the eight-coordinate anions  $[\text{Nd}(\text{L}^1)(\text{Ph}_2\text{pz})_3]^-$ ,  $[\text{Er}(\eta^2\text{-tBu}_2\text{pz})_4]^-$  and the  $[\text{Yb}(\text{Ph}_2\text{pz})_3(\text{DME})].0.5(\text{DME})$  complex are nine-coordinate  $[\text{Nd}(\text{Ph}_2\text{pz})_3(\text{DME})_2]$  and  $[\text{Er}(\text{Ph}_2\text{pz})_3(\text{DME})_2]$  where one DME ligand is chelating while the other binds in a  $\eta^1$ -fashion to the lanthanoid metal. This unusual bonding indicates that the lanthanoid centre is unable to accommodate two chelating DME ligands. Hence the steric demand of  $\text{L}^1$  in  $[\text{Nd}(\text{L}^1)(\text{Ph}_2\text{pz})_3]^-$  must be less than two DME molecules but greater than one and as a result adequately saturates the lanthanoid centre from further coordination.

Table 2.1 Summary of Crystallographic data for  $[\text{Nd}(\text{L}^1)(\text{Ph}_2\text{pz})_3][\text{Li}(\text{DME})_3]$ 

Compound	$[\text{Nd}(\text{L}^1)(\text{Ph}_2\text{pz})_3][\text{Li}(\text{DME})_3]$
Formula	$\text{C}_{64}\text{H}_{82}\text{LiN}_8\text{O}_6\text{Si}$
<i>M</i>	1238.65
<i>a</i> (Å)	14.543(3)
<i>b</i> (Å)	18.381(4)
<i>c</i> (Å)	24.091(5)
$\alpha$ (°)	90
$\beta$ (°)	90.08(3)
$\gamma$ (°)	90
<i>V</i> (Å <sup>3</sup> )	6440(2)
Crystal system	Monoclinic
Space Group	$P2_1/c$
<i>Z</i>	4
Diffractometer	Enraf Nonius Kappa CCD
$\rho_{\text{calc}}$ (g cm <sup>-3</sup> )	1.278
$\mu(\text{MoK}\alpha)$ (mm <sup>-1</sup> )	0.879
$2\theta_{\text{max}}$ (°)	56.5
$N^a, N_o^b$	14565, 4633
<i>R, R<sub>w</sub></i> (observed data)	0.0682, 0.0707
<i>R, R<sub>w</sub></i> (all data)	0.2997, 0.1022

<sup>a</sup> *N* = number of unique reflections

<sup>b</sup> *N<sub>o</sub>* = number of observed reflections [*I* > 2σ(*I*)]



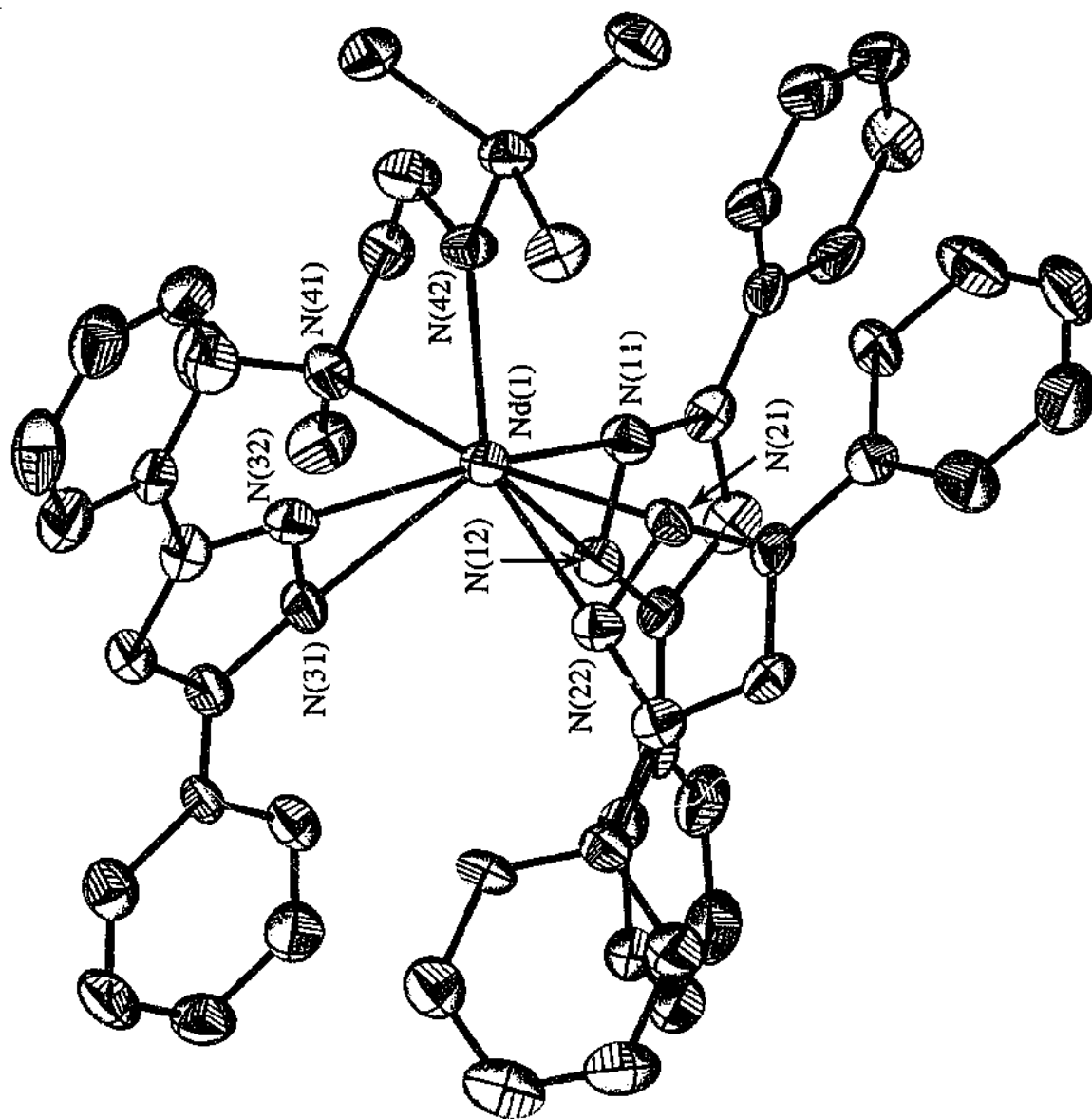


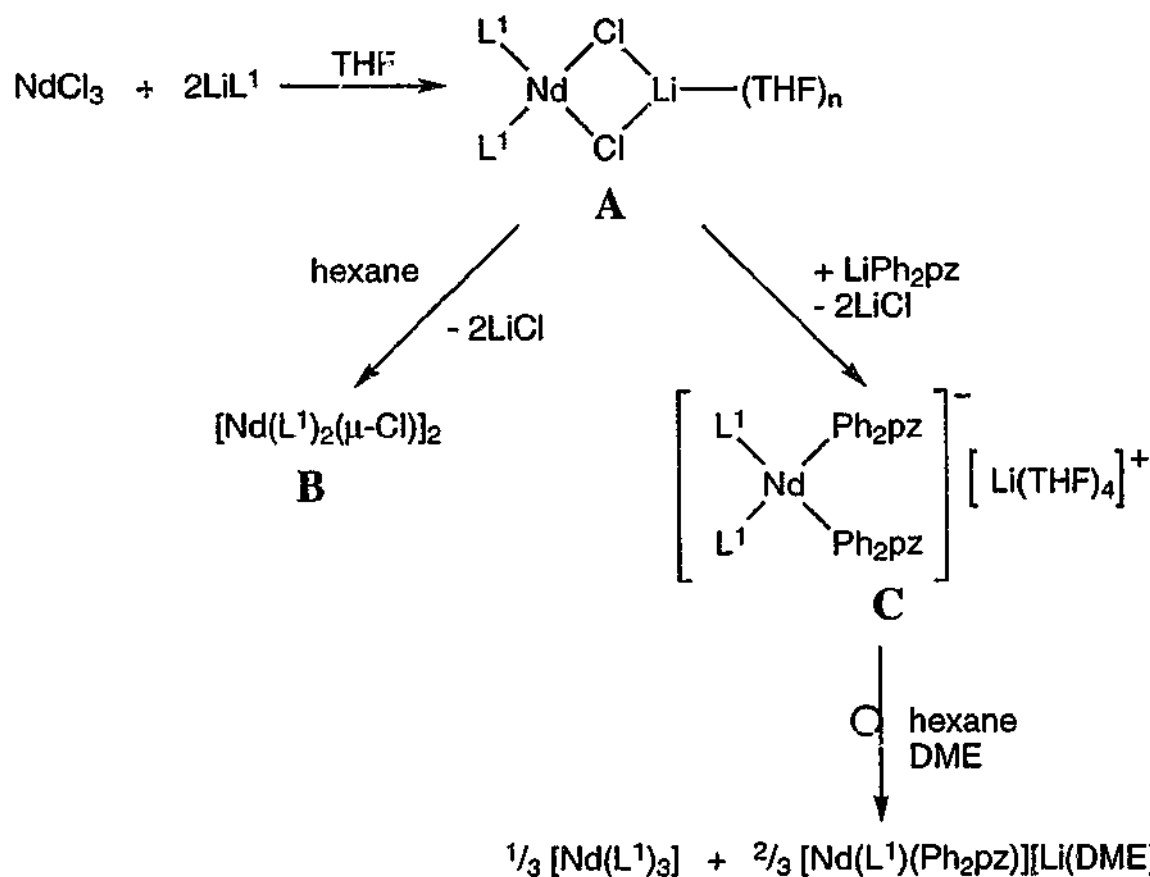
Figure 2.1 Molecular structure of  $[\text{Nd}(\text{L}')(\text{Ph}_2\text{pz})_3][\text{Li}(\text{DME})_3]^+$   
(Hydrogen atoms and  $[\text{Li}(\text{DME})_3]^+$  have been omitted for clarity)

Table 2.2 Selected distances (Å) and angles (°) with estimated standard deviations in parentheses for  $[Nd(L')(Ph_2pz)_3][Li(DME)_3]$ .

Nd(1)—N(11)	2.447(5)	N(12)—Nd(1)—N(22)	82.79(15)
Nd(1)—N(12)	2.522(5)	N(12)—Nd(1)—N(31)	100.84(17)
		N(12)—Nd(1)—N(32)	132.43(17)
Nd(1)—N(21)	2.496(5)	N(12)—Nd(1)—N(41)	85.97(15)
Nd(1)—N(22)	2.485(5)	N(12)—Nd(1)—N(42)	122.71(17)
		N(21)—Nd(1)—N(22)	31.74(13)
Nd(1)—N(31)	2.482(5)	N(21)—Nd(1)—N(31)	113.50(16)
Nd(1)—N(32)	2.484(5)	N(21)—Nd(1)—N(32)	107.86(16)
		N(21)—Nd(1)—N(41)	166.87(16)
Nd(1)—N(41)	2.652(5)	N(21)—Nd(1)—N(42)	103.92(16)
Nd(1)—N(42)	2.351(4)	N(22)—Nd(1)—N(31)	83.50(16)
		N(22)—Nd(1)—N(32)	87.94(15)
Li(1)—O(11)	2.08(1)	N(22)—Nd(1)—N(41)	156.96(16)
Li(1)—O(12)	2.20(1)	N(22)—Nd(1)—N(42)	132.29(17)
Li(1)—O(21)	2.17(1)	N(31)—Nd(1)—N(32)	31.61(14)
Li(1)—O(22)	2.11(1)	N(31)—Nd(1)—N(41)	78.95(16)
Li(1)—O(31)	2.05(1)	N(31)—Nd(1)—N(42)	123.10(15)
Li(1)—O(32)	2.16(1)	N(32)—Nd(1)—N(41)	84.91(17)
		N(32)—Nd(1)—N(42)	97.56(15)
N(11)—Nd(1)—N(12)	31.67(14)	N(41)—Nd(1)—N(42)	70.49(16)
N(11)—Nd(1)—N(21)	88.43(16)		
N(11)—Nd(1)—N(22)	100.04(16)	cen(1) <sup>a</sup> —Nd(1)—cen(2) <sup>b</sup>	89.56
N(11)—Nd(1)—N(31)	128.98(17)	cen(1) <sup>a</sup> —Nd(1)—cen(3) <sup>c</sup>	130.65
N(11)—Nd(1)—N(32)	158.51(17)	cen(2) <sup>b</sup> —Nd(1)—cen(3) <sup>c</sup>	98.67
N(11)—Nd(1)—N(41)	80.02(16)	N(42)—Nd(1)—cen(1) <sup>a</sup>	107.51
N(11)—Nd(1)—N(42)	91.77(16)	N(42)—Nd(1)—cen(2) <sup>b</sup>	118.32
N(12)—Nd(1)—N(21)	87.45(15)	N(42)—Nd(1)—cen(3) <sup>c</sup>	110.61

<sup>a</sup> cen(1) = midpoint of N(11)—N(12) bond; <sup>b</sup> cen(2) = midpoint of N(21)—N(22) bond; <sup>c</sup> cen(3) = midpoint of N(31)—N(32) bond.

The complex  $[\text{Nd}(\text{L}^1)(\text{Ph}_2\text{pz})_3][\text{Li}(\text{DME})_3]$  was obtained in low yield and this suggests that it was only a minor product in the reaction mixture. Since  $[\text{Nd}(\text{L}^1)_2(\mu\text{-Cl})_2]$  was isolated contaminated with  $\text{LiCl}$ , despite numerous extractions with hexane, it is postulated that the clear reaction mixture in THF contains an 'ate' complex (*Scheme 1.2 (A)*) which in non-polar solvents collapses to the dimer (*Scheme 1.2 (B)*). Whilst amide ligated 'ate' complexes of the type  $\text{L}_2\text{LnX}_2\text{Li}$  ( $\text{L}$  = amide ligand,  $\text{X}$  = anion) are known (e.g.  $[\text{Nd}\{\text{N}(2,6\text{-Me}_2\text{C}_6\text{H}_3)(\text{SiMe}_3)_2(\text{THF})(\mu\text{-Cl})_2(\text{Li})(\text{THF})_2\}]^{\text{7}}$  and  $[\text{Ln}\{\text{Me}_2\text{Si}(\text{OtBu})(\text{NtBu})\}_2(\mu\text{-Cl})_2\text{Li}(\text{THF})_2]$  ( $\text{Ln} = \text{Yb}$ [8] and  $\text{Y}$ [9]) they are very dependent on the ligand and lanthanoid combination. Substitution of both chlorides in **A** by  $\text{Ph}_2\text{pz}$  anions would yield the ionic complex **C** (*Scheme 1.2*). Subsequent rearrangement in hexane and replacement of THF by DME would generate the observed product in addition to the homoleptic  $[\text{Nd}(\text{L}^1)_3]$  complex. The latter species was detected in the mass spectrum of the isolated blue crystals of  $[\text{Nd}(\text{L}^1)(\text{Ph}_2\text{pz})_3][\text{Li}(\text{DME})_3]$ .



Scheme 2.1

### 2.3 Conclusion

The stabilisation of solvent-free heteroleptic lanthanoid complexes of the type  $[\text{Ln}(\text{L}^1)_2(\mu\text{-Cl})]_2$  was achieved utilising the bidentate amide ligand  $\text{L}^1$ . Whilst previous work indicated a monomeric complex to be present for erbium, further investigation by mass spectroscopy revealed that it may be dimeric, however single crystals were elusive. Analogous reactions with lighter ( $\text{Ln} = \text{Sm}, \text{Nd}, \text{La}$ ) and heavier ( $\text{Ln} = \text{Yb}$ ) lanthanoid elements were investigated with the products having similar spectroscopic data to  $[\text{Er}(\text{L}^1)_2(\mu\text{-Cl})]_2$  therefore indicating a solvent-free dimeric arrangement is formed throughout the lanthanoid series. Whilst salt contamination was a major problem in the isolation of  $[\text{Ln}(\text{L}^1)_2(\mu\text{-Cl})]_2$  complexes, pure samples could be obtained by extracting the reaction mixture with hexane numerous times.

In order to avoid the tedious separation procedure required to obtain a clean sample of  $[\text{Nd}(\text{L}^1)_2(\mu\text{-Cl})]_2$  a substitution reaction with  $\text{Li}(\text{Ph}_2\text{pz})$  was investigated *in situ* in THF. Whilst this method was unsuccessful in obtaining the expected compound  $\text{Nd}(\text{L}^1)_2(\text{Ph}_2\text{pz})$ , it did result in an interesting charge separated ionic complex,  $[\text{Nd}(\text{L}^1)(\text{Ph}_2\text{pz})_3][\text{Li}(\text{DME})_3]$  in low yield. A single crystal X-ray determination identified the complex to be  $[\text{Nd}(\text{L}^1)(\text{Ph}_2\text{pz})_3][\text{Li}(\text{DME})_3]$  although spectroscopic data indicated this product was not the only metal-containing species present within the isolated material.

## 2.4 References

- 1 G. B. Deacon, C. M. Forsyth, P. C. Junk, B. W. Skelton, and A. H. White, *J. Chem. Soc., Dalton Trans.*, 1998, 1381.
- 2 H. Schumann, S. Nickel, J. Loebel, and J. Pickardt, *Organometallics*, 1988, **7**, 2004.
- 3 J. Guan, S. Jin, Y. Lin, and Q. Shen, *Organometallics*, 1992, **11**, 2483.
- 4 R. D. Shannon, *Acta. Crystallogr., Sect. A*, 1976, **32**, 751.
- 5 G. B. Deacon, E. E. Delbridge, and C. M. Forsyth, *Angew. Chem. Int. Ed.*, 1999, **38**, 1766.
- 6 E. E. Delbridge, PhD Thesis, Monash University, Melbourne, 1999.
- 7 H. Schumann, J. Winterfeld, E. C. E. Rosenthal, H. Hemling, and L. Esser, *Z. Anorg. Allg. Chem.*, 1995, **621**, 122.
- 8 A. Recknagel, A. Steiner, S. Brooker, D. Stalke, and E. T. Edelman, *J. Organomet. Chem.*, 1991, **415**, 315.
- 9 R. Duchateau, T. Tuinstra, E. A. C. Brussee, A. Meetsma, and P. T. van Duijnen, *Organometallics*, 1997, **16**, 3511.

## Chapter 3

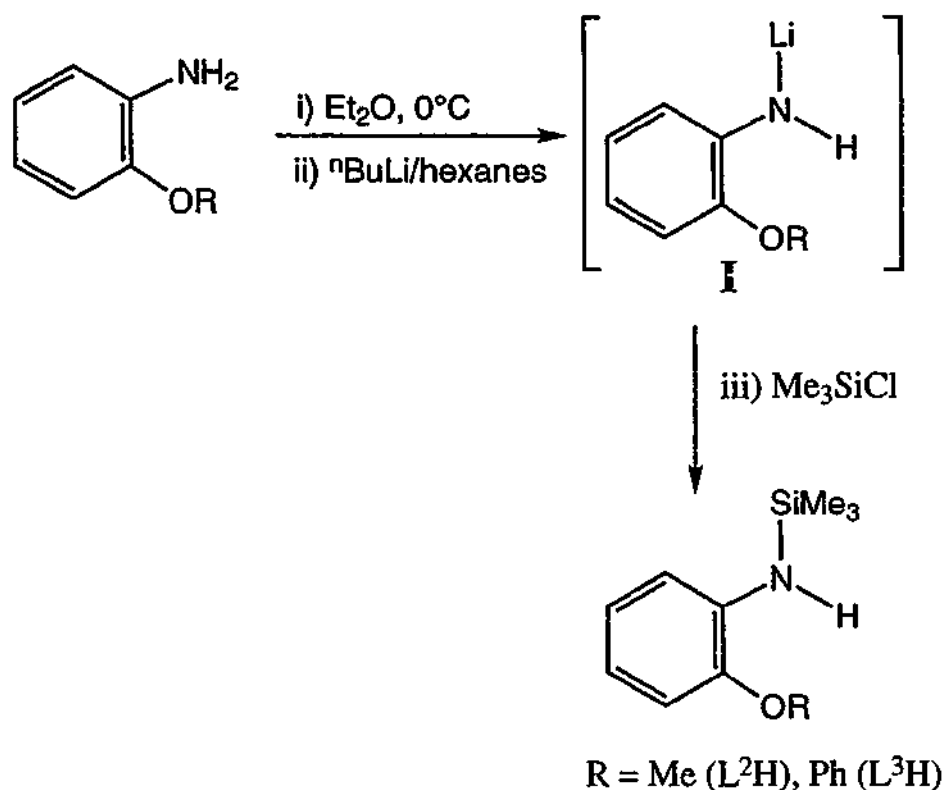
# Homoleptic Ether Functionalised (Diorganoamido)lanthanoid(III) Complexes

### 3.1 Introduction

The heteroleptic lanthanoid complexes of the chelating  $L^1$  ligand prepared in Chapter 2 exposed several disadvantages of this ligand system. These included (i) the very high solubility in hexane (leading to difficulties with crystal growth) (ii) the tendency to retain LiCl and (iii) ligand redistribution upon further substitution. As a consequence new amide ligand systems were pursued. The oxophilic nature of lanthanoid elements encourages the incorporation of a pendant ether donor arm on the amide functionality. A mixed N, O- donor bidentate ligand system was investigated to examine the effect on stability of both homoleptic and heteroleptic complexes. Hence the new amine ligands 2-MeOC<sub>6</sub>H<sub>4</sub>NHSiMe<sub>3</sub> ( $L^2H$ ) and 2-PhOC<sub>6</sub>H<sub>4</sub>NHSiMe<sub>3</sub> ( $L^3H$ ) were synthesised from their primary amines and were fully characterised in this study. These have a rigid arene backbone that may reduce the solubility of the resulting lanthanoid complexes in hexane and also limit the number of conformational isomers, relative to the  $L^1$  ethylene backbone ligand.

#### 3.1.1 Preparation of Target Bidentate Amine Ligands

The secondary amine ligands, 2-MeOC<sub>6</sub>H<sub>4</sub>NHSiMe<sub>3</sub> ( $L^2H$ ) and 2-PhOC<sub>6</sub>H<sub>4</sub>NHSiMe<sub>3</sub> ( $L^3H$ ), were prepared in high yield from 2-methoxyaniline and 2-phenoxyaniline respectively, by successive treatment with LiBu<sup>n</sup> and ClSiMe<sub>3</sub> in diethyl ether (Equation 3.1). This method is similar to that used by Schumann *et al.* for the preparation of HN(Ph)(SiMe<sub>3</sub>).<sup>[1]</sup>



Equation 3.1

The amine ligands,  $L^2H$  and  $L^3H$  are air- and moisture-sensitive colourless crystalline solids, and were unequivocally characterised by elemental analyses, IR,  $^1H$  NMR and X-ray structure determinations. The key features of the spectra of  $L^2H$  and  $L^3H$  were single  $\nu(N-H)$  bands at 3403 and 3401  $cm^{-1}$  respectively, as well as  $\delta(CH_3)$  frequencies attributable to a  $SiMe_3$  group observed in the regions 1480-1504  $cm^{-1}$  (asymmetric deformation) and 1238-1240  $cm^{-1}$  (symmetric deformation).<sup>[2]</sup> Whilst the spectrum of  $L^3H$  shows two very intense aromatic  $\nu(C-C)$  bands at 1606 and 1589  $cm^{-1}$ ,  $L^2H$  has only one intense peak at 1600  $cm^{-1}$  with the second band being very weak at 1589  $cm^{-1}$ . Two aromatic C-H out of plane bending vibrations are observed for  $L^2H$  at 738 and 751  $cm^{-1}$  and for  $L^3H$  at 732 and 750  $cm^{-1}$  whereas a greater number of bands would be expected in the spectrum of  $L^3H$  due to the presence of the phenoxy substituent. An overlap of the symmetric C—O—C stretching absorptions from the ether substituents  $MeOAr$  and  $PhOAr$  with another  $SiMe_3$  band is also apparent with a very strong broad absorption near 840  $cm^{-1}$  being the result. Absorptions near 1030  $cm^{-1}$ , possibly due to antisymmetric C—O—C stretching vibrations, can easily differentiate  $L^2H$  and  $L^3H$ . For  $L^2H$  one set of two bands (of equal intensity) was found in this region while for  $L^3H$  two sets of two bands of unequal intensity were observed.  $^1H$  NMR spectra of  $L^2H$  and  $L^3H$  also showed the presence of NH and  $SiMe_3$  groups and confirmed the ratios of the various

substituents present on the amine ligand. The  $^1\text{H}$  NMR data for  $\text{C}_6\text{D}_6$  solutions of  $\text{L}^2\text{H}$  and  $\text{L}^3\text{H}$  show distinct aromatic patterns attributable to the backbone protons in addition to characteristic methyl or phenyl ether signals. The analyses were confirmed by single crystal X-ray determination of the structures of  $\text{L}^2\text{H}$  and  $\text{L}^3\text{H}$ , which were crystallised by cooling the fractionally distilled products. The molecular structures of  $\text{L}^2\text{H}$  and  $\text{L}^3\text{H}$  are shown in *Figure 3.1* and *Figure 3.2* respectively. Crystallographic details for both structures are given in *Table 3.1* with selected bond distances and angles presented in *Table 3.2* and *Table 3.3* for  $\text{L}^2\text{H}$  and  $\text{L}^3\text{H}$  respectively.

The solid state structure of  $\text{L}^2\text{H}$  (illustrated in *Figure 3.1*) comprises two, essentially identical but independent functionalised molecules in the asymmetric unit with a (trimethylsilyl)amine group *ortho* to a methoxy ether moiety. The  $\text{N}(1)\text{—C}(11)$  and  $\text{O}(1)\text{—C}(12)$  bonds have partial double bond character (*Table 3.2*) which indicates conjugation of the lone pairs of the nitrogen and oxygen atoms with the aromatic ring. The planar environment ( $\Sigma(\circ) 358^\circ$ ) of the nitrogen is consistent with delocalisation into the surrounding  $\text{N}(1)\text{—C}(11)$  and  $\text{N}(1)\text{—Si}(1)$  bonds. The methoxy group is positioned in approximately the same plane as the arene backbone (torsion angles;  $\text{C}(13)\text{—C}(12)\text{—O}(1)\text{—C}(10)$   $2.2(2)^\circ$ ,  $\text{C}(23)\text{—C}(22)\text{—O}(2)\text{—C}(20)$   $10.9(2)^\circ$ ) and exhibits no unusual features.



Table 3.1 Summary of Crystallographic Data for L<sup>2</sup>H and L<sup>3</sup>H.

Compound	L <sup>2</sup> H	L <sup>3</sup> H
Formula	C <sub>10</sub> H <sub>17</sub> NOSi	C <sub>15</sub> H <sub>19</sub> NOSi
<i>M</i>	195.34	257.41
<i>a</i> (Å)	25.5964(5)	21.4777(4)
<i>b</i> (Å)	25.5964(5)	7.9215(2)
<i>c</i> (Å)	7.06844(2)	16.9555(2)
$\alpha$ (°)	90	90
$\beta$ (°)	90	90
$\gamma$ (°)	90	90
<i>V</i> (Å <sup>3</sup> )	4631.0(13)	2884.7(10)
Crystal system	tetragonal	orthorhombic
Space Group	<i>P</i> 4/ <i>n</i>	<i>Pbcn</i>
<i>Z</i>	16	8
Diffractometer	Nonius Kappa CCD	Nonius Kappa CCD
$\rho_{\text{calcd}}$ (g cm <sup>-3</sup> )	1.121	1.185
$\mu$ (MoK $\alpha$ ) (mm <sup>-1</sup> )	0.169	0.152
$2\theta_{\text{max}}$ (°)	55.8	55.7
<i>N</i> , <i>N</i> <sub>o</sub>	5455, 4207	3414, 2851
<i>R</i> , <i>R</i> <sub>w</sub> (observed data)	0.041, 0.098	0.045, 0.090
<i>R</i> , <i>R</i> <sub>w</sub> (all data)	0.062, 0.107	0.060, 0.095

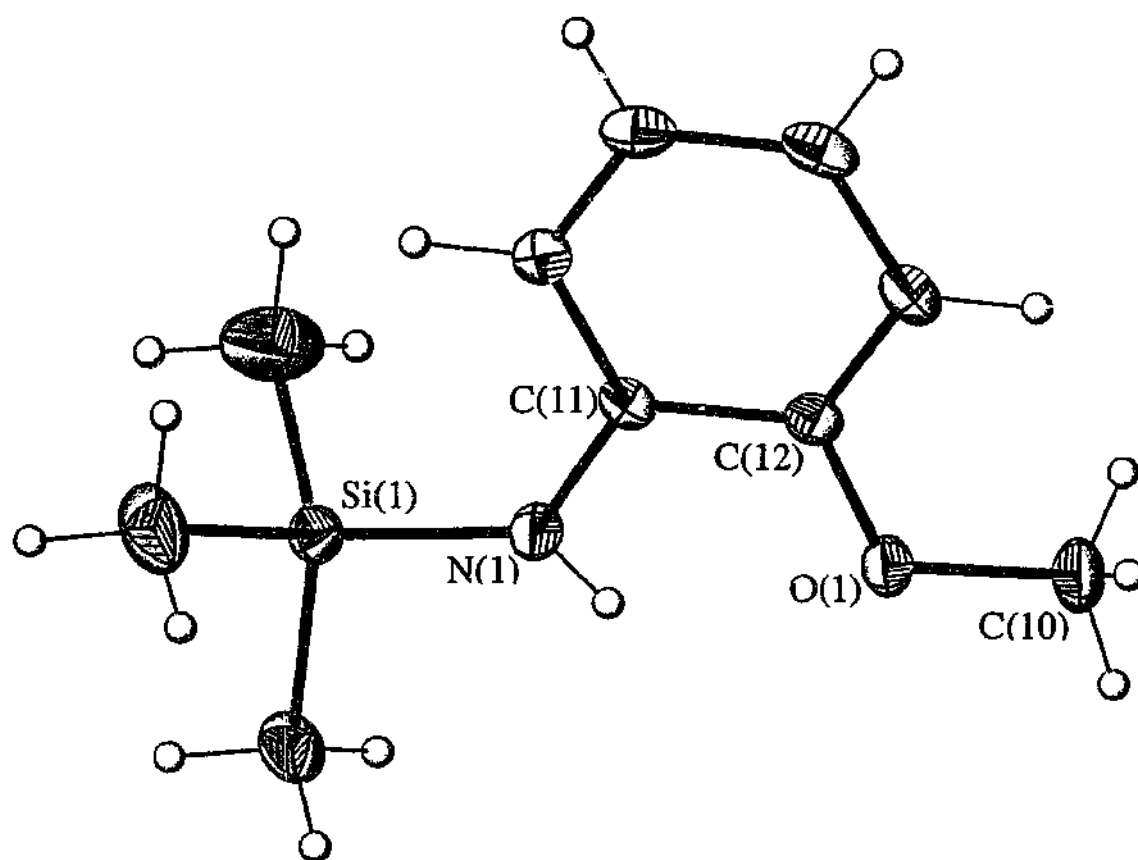
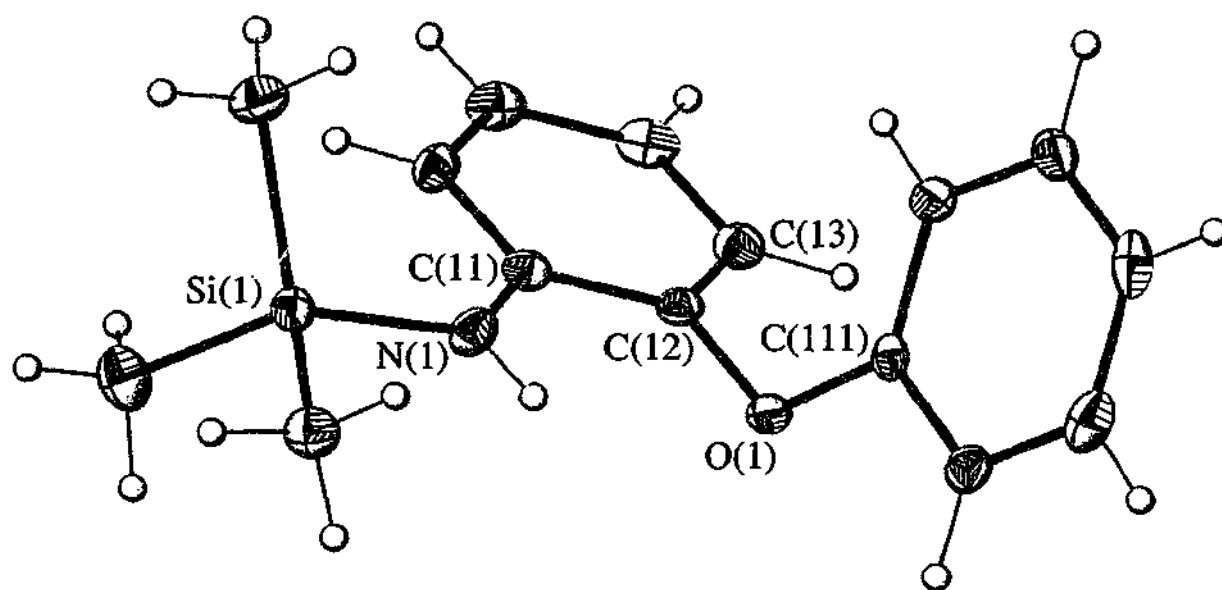


Figure 3.1 Molecular structure of  $L^2H$ .

Table 3.2 Selected bond lengths ( $\text{\AA}$ ) and angles ( $^\circ$ ) with estimated standard deviations in parentheses for  $L^2H$ .

Si(1)—N(1)	1.737(1)	C(11)—N(1)—Si(1)	130.2(1)
C(11)—N(1)	1.393(2)	C(11)—N(1)—H(1)	111.44(5)
C(12)—O(1)	1.372(2)	Si(1)—N(1)—H(1)	116.24(5)
C(10)—O(1)	1.428(2)	C(12)—O(1)—C(10)	117.4(1)
Si(1)—C(Me) av.	1.858(2)		

The structure of  $L^3H$ , pictured in *Figure 3.2*, is similar to  $L^2H$  although the alkyl ether moiety is replaced by a phenoxy group. The N(1)—C(11) bond also has a partial double bond character (*Table 3.3*) which indicates the conjugation of the nitrogen atom with the aromatic ring. Again, the planar environment ( $\Sigma(\circ) 357^\circ$ ) of the nitrogen atom is consistent with delocalisation of the lone pair into the N(1)—Si(1) and N(1)—C(11) bonds (*Table 3.3*). Unlike the methyl ether substituent in  $L^2H$  which is in the same plane as the arene backbone, the phenyl ether group of  $L^3H$  is bent away (torsion angle C(13)—C(12)—O(1)—C(11)  $78.5(2)^\circ$ ) and rotated near perpendicular to the  $C_6H_4N(O)$  ring (interplanar angle  $76.64(4)^\circ$ ). Furthermore the O(1)—C(11) bond is considerably shorter than the O(1)—C(12) distance which may indicate partial delocalisation of the oxygen lone pair with the phenyl substituent rather than the aromatic backbone. For both  $L^2H$  and  $L^3H$  ligands no close interactions (e.g. hydrogen bonding) to other molecules were observed in the unit cell.



*Figure 3.2* Molecular structure of  $L^3H$

**Table 3.3** Selected bond lengths (Å) and angles (°) with estimated standard deviations in parentheses for  $L^3H$ .

Si(1)—N(1)	1.745(1)	C(11)—N(1)—Si(1)	130.9(1)
C(11)—N(1)	1.389(2)	C(11)—N(1)—H(1)	113.1(1)
C(12)—O(1)	1.402(2)	Si(1)—N(1)—H(1)	115.6(1)
C(111)—O(1)	1.388(2)	C(12)—O(1)—C(111)	118.2(1)
Si(1)—C(Me) av.	1.862(5)		

With these new ligands in hand their coordination to lanthanoid centres was investigated. Initial work focussed on preparing homoleptic complexes of both the trivalent ( $LnL_3$ ) (this Chapter) and divalent ( $LnL_2$ ) (see Chapter 5) lanthanoid oxidation states. These complexes are important for assessing the steric requirements and possible structural characteristics of  $L^2$  and  $L^3$  when bound to a lanthanoid centre. Subsequently the heteroleptic derivatives were explored and these are discussed in Chapter 4. Generally the lithium salts of  $L^2H$  and  $L^3H$  were used *in situ*. For isolated lithium complexes see Chapter 7.

## 3.2 Results and Discussion

### 3.2.1 Synthesis and Characterisation of $[Ln(L^2)_3]$ Complexes

The reaction of  $LnCl_3$  ( $Ln = Er, Sm, Pr, Nd$ ) with three equivalents of  $LiL^2$ , which was generated *in situ* from a reaction of  $L^2H$  with  $LiBu^n$  in THF, affords the homoleptic complex  $[Ln(L^2)_3]$  in good yield (*Scheme 3.1 (a)*). The compounds could be isolated from hexane as crystals after removal of the precipitated  $LiCl$  (*Table 3.4*). The ytterbium derivative was synthesised from the reaction using a 3:1 Li to Ln molar ratio of the isolated lithium salt,  $[Li(L^2)(OEt_2)]_2$  (see Chapter 7) with  $YbCl_3$  in THF (*Scheme 3.1 (b)*). A similar work up procedure in hexane gave red crystalline  $[Yb(L^2)_3]$ . This preparation gave a slightly higher yield than is generally observed with the *in situ* generated lithium salts (*Table 3.4*) consistent with the general view that isolated crystalline alkali metal starting materials give cleaner reactions. The  $[Ln(L^2)_3]$  complexes ( $Ln = Nd$  and  $Yb$ ) were also isolated from an *in situ* reaction between two equivalents of  $LiL^2$  with  $LnCl_3$  (*Scheme 3.1 (c)*) instead of the anticipated heteroleptic complex  $Ln(L)_2Cl$  (see also Chapter 4). The infrared spectra of these complexes were identical to  $[Nd(L^2)_3]$  and  $[Yb(L^2)_3]$ . A unit cell determination on crystals obtained from the reaction (*Scheme 3.1 (c)*) of  $LiL^2$  with  $NdCl_3$  established the product to be  $[Nd(L^2)_3]$ .

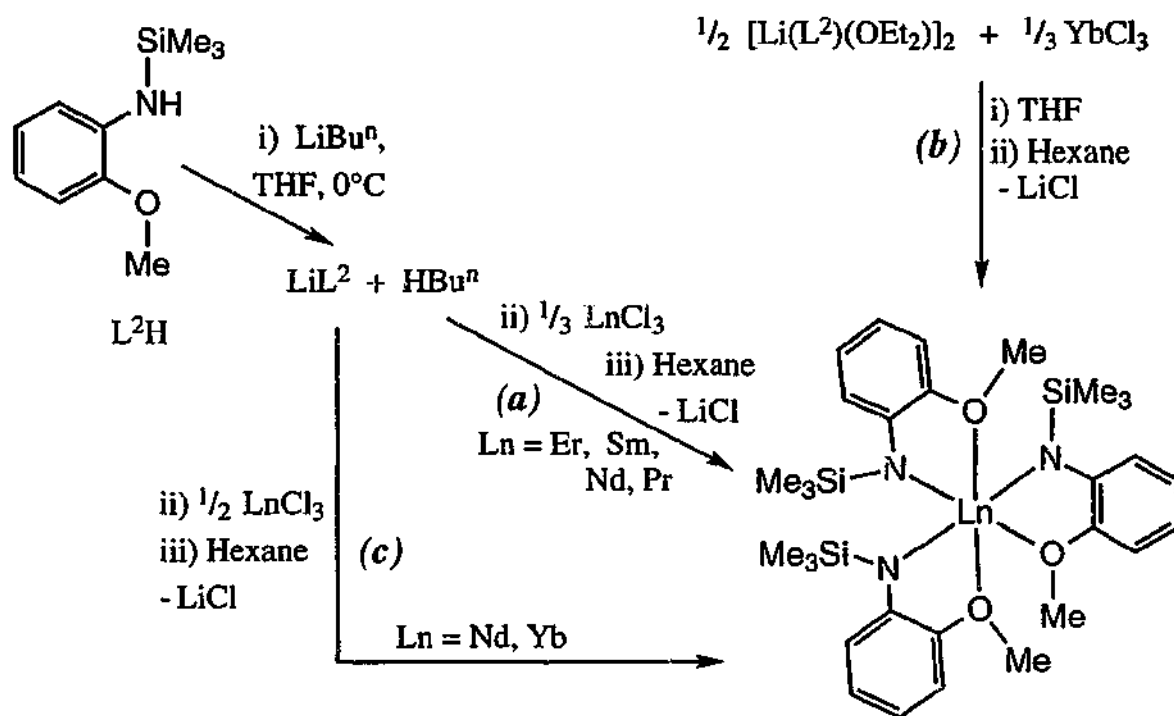
*Table 3.4 Preparations of  $[Ln(L^2)_3]$  complexes*

Complex	Yield (%)		Colour
$[Nd(L^2)_3]$	65	(36) <sup>a</sup> (55) <sup>b</sup>	Blue
$[Pr(L^2)_3]$	57		Green
$[Sm(L^2)_3]$	41		Yellow
$[Er(L^2)_3]$	48		Pink
$[Yb(L^2)_3]$	72 <sup>c</sup>	(29) <sup>a</sup>	Red

<sup>a</sup> from a 2:1 Li:Ln mole ratio *in situ* reaction.

<sup>b</sup> by a 2:1 ratio of isolated lithium salt  $[Li(L^2)(OEt_2)]_2$  with  $NdCl_3$ .

<sup>c</sup> using a 3:1 Li:Ln mole ratio of isolated lithium salt  $[Li(L^2)(OEt_2)]_2$  with  $YbCl_3$ .



Scheme 3.1

All complexes were very sensitive to air and moisture and their compositions were confirmed by elemental analysis (C, H, N). Their infrared spectra were almost identical and showed peaks characteristic of  $\text{L}^2$  with no evidence of coordinated THF at  $900\text{--}850\text{ cm}^{-1}$ . This suggests that for each  $[\text{Ln}(\text{L}^2)_3]$  complex a similar structural arrangement occurs. The C—O—C stretching absorptions (antisymmetric) near  $1030\text{ cm}^{-1}$  have two sets of two bands in this region while for  $\text{L}^2\text{H}$  only one set is observed. This may suggest two ligand environments reflecting the *cis* and *trans*  $(\text{Me})\text{O—Ln—O}(\text{Me})$  arrangement around the metal centre (see below). In the mass spectra of  $[\text{Nd}(\text{L}^2)_3]$  and  $[\text{Sm}(\text{L}^2)_3]$  the highest metal-containing fragment was attributable to the parent ion  $[\text{Ln}(\text{L}^2)_3]^+$  while for  $[\text{Er}(\text{L}^2)_3]$  the loss of the groups  $\text{SiMe}_3$  and  $\text{OCH}_3$  from the molecular ion was observed. The mass fragment  $[\text{Ln}(\text{L}^2)_2]^+$  was displayed in the spectra of all three complexes as well as the metal-free fragment  $[\text{L}^2\text{H}]^+$ . The UV/VIS/NIR spectrum of a solution of  $[\text{Yb}(\text{L}^2)_3]$  in DME exhibited absorptions which are characteristic of  $f \leftarrow f$  transitions of the  $\text{Yb}^{3+}$  cation<sup>[3]</sup> near  $1000\text{ nm}$ . The room temperature  $^1\text{H}$  NMR spectrum of the paramagnetic  $[\text{Nd}(\text{L}^2)_3]$  in  $\text{C}_6\text{D}_6$  shows peaks characteristic of  $\text{L}^2$  paramagnetically shifted from the region for a diamagnetic sample. In  $[\text{Nd}(\text{L}^2)_3]$  single peaks attributable to the  $\text{SiMe}_3$  and  $\text{OMe}$  moieties on  $\text{L}^2$  were broad and were shifted to a significantly lower frequency from those of  $\text{L}^2\text{H}$ . Four proton resonances on the aromatic backbone were observed and these have been tentatively assigned on the basis of the distance of the proton nuclei from the paramagnetic

centre. Two of these resonances were shifted to a higher frequency (14.18 (H3 or H6) and 23.60 (H3 or H6) ppm), one to a lower frequency at 1.14 ppm (H4 or H5) and one was near unchanged at 7.88 ppm (H4 or H5) compared with a diamagnetic species. These data are consistent with a single  $L^2$  environment present in solution, where the at least two different ligand environments observed in the solid state are presumably averaged by an exchange process on the NMR time scale.

Single crystals of  $[\text{Nd}(L^2)_3]$  suitable for a structure determination were obtained from a hexane solution, but attempts to prepare crystals of other  $[\text{Ln}(L^2)_3]$  ( $\text{Ln} = \text{Yb}, \text{Er}, \text{Sm}, \text{Pr}$ ) complexes were unsuccessful. Three views of the molecular structure of  $[\text{Nd}(L^2)_3]$  are displayed in *Figure 3.3*. The central neodymium atom is six-coordinate, comprising three bidentate  $L^2$  ligands in a *mer* configuration. Two enantiomers are possible for *mer*- $[\text{Nd}(L^2)_3]$  ( $\Delta$  and  $\Lambda$ ) with only one occupying the asymmetric unit, the other being generated by the inversion centre present in the centrosymmetric space group. Crystallographic refinement data for the crystal structure are presented in *Table 3.5* and selected bond lengths and angles are collected in *Table 3.6*. The geometry is best described as a distorted octahedron (best fit polyhedron<sup>[4]</sup>) with the oxygen atoms (O(1) and O(3)), nitrogen atoms (N(1) and N(2)), and the other pair O(2) and N(3) occupying *transoid* sites. The *mer* arrangement of  $L^2$  differs from that of the closely related  $[\text{Ln}(L^1)_3]$ <sup>[5]</sup> which has a *fac* orientation of the bidentate  $L^1$  amide ligands. The latter was unexpected since the very bulky  $\text{NSiMe}_3$  groups are all in a *cis* disposition. Thus in  $[\text{Ln}(L^1)_3]$  the N—Ln—N angles lie in the range (104.8(5)—109.0(1)°) whereas  $[\text{Nd}(L^2)_3]$  has two similar but one larger *transoid* angle (*Table 3.6*). Even with the *mer* configuration, two of the  $\text{NSiMe}_3$  groups are pushed above and below the equatorial plane presumably to reduce steric repulsion from the otherwise closely proximate bulky amides. The less sterically dominating OMe groups occupy the *trans* sites with O(1)—Nd(1)—O(3) verging on linear but the angles between the remaining *transoid* donors N(1)—Nd—N(2) and N(3)—Nd—O(2) are significantly less than 180°. This is presumably due to the combination of the small bite angle of the chelated  $L^2$  ligand and the proximity of the *cis* amide groups.

The Nd(1)—N(amide) bond distances in  $[\text{Nd}(L^2)_3]$  are not equivalent with one shorter (2.349(3) Å) and two longer Nd(1)—N(X) (X = 2, 3) distances (2.385(3), 2.376(3) Å respectively) in contrast to the three Nd—O(ether) distances which are nearly identical

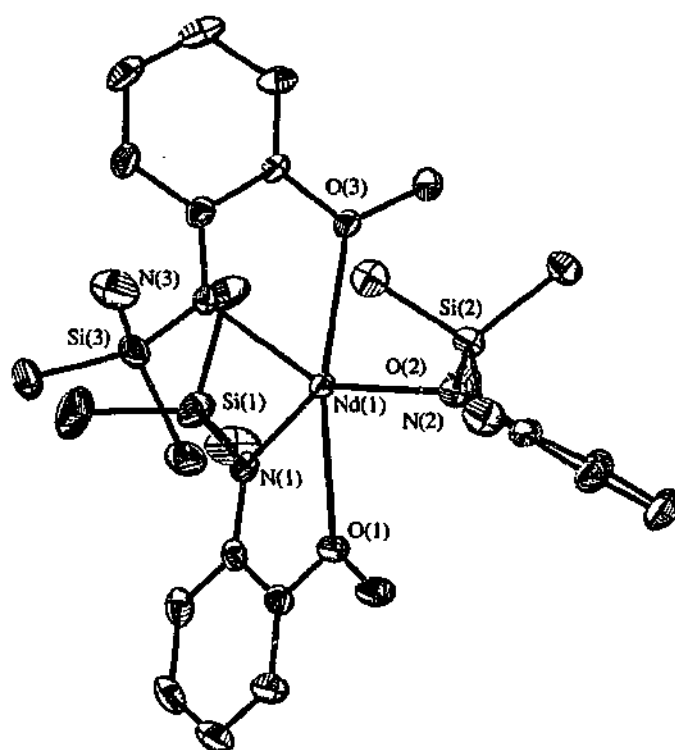
(see *Table 3.6*). Comparison of the metal—nitrogen distances with those of other lanthanoid organoamides can be made by subtraction of the appropriate metal ionic radius (*Table 3.7*).<sup>[6]</sup> Selected examples from the literature are listed in *Table 3.7* and the values derived for  $[\text{Nd}(\text{L}^2)_3]$  (1.37—1.40 Å) lie near the middle of this range (1.34 — 1.49 Å). In general for the monodentate amides the length of the Ln—N bond appears to be dependent on the substituents present at the nitrogen atom ( $\text{N}(\text{RR}')$ ) (e.g.  $\text{R}, \text{R}' = \text{Ar}, \text{H} < \text{Me}_3\text{Si}, \text{CH}_2\text{R} < \text{R}_2\text{CH}, \text{CHR}_2 < \text{Me}_3\text{SiAr} < \text{Me}_3\text{Si}, \text{SiMe}_3$ ). For example a decrease in steric demand by incorporating a small H and electron withdrawing phenyl substituent (e.g.  $\text{R} = \text{C}_6\text{H}_5, \text{R}' = \text{H}$ ) results in a shortening of the Ln—N(amide) bond. Alternatively for bulky substituents ( $\text{R}$  and  $\text{R}' = \text{SiMe}_3$ ) the distance is considerably lengthened. The current values fit into this regime being slightly smaller than those of  $[\text{Nd}\{\text{N}(\text{Ph})(\text{SiMe}_3)\}_3(\text{THF})]$  (*Table 3.7*).<sup>[11]</sup> Some shortening may be associated with the formation of a chelate as is also shown by the bulky  $\text{Bu}^t\text{NSiMe}_2\text{OBu}^t$  ligand<sup>[7]</sup> which has Ln—N distances smaller than for other bulky amides. The exception to this chelate effect is the benzamidinates<sup>[8]</sup> that have the longest observed Ln—N bonds. This is possibly due to the delocalisation of the negative charge across the N—C—N backbone leading to a weaker Coulombic interaction with the lanthanoid cation in addition to strain associated with the formation of the small four-membered chelate ring.

Similar treatment of the Nd—O(methyl) distances gives a value of 1.56 Å which is significantly longer than subtraction values derived from organolanthanoid or halolanthanoid ether complexes ( $\text{LnR}_3(\text{ether})_n, 1.34$ ; <sup>[13]</sup>  $\text{LnX}_3(\text{THF})_n, 1.39-1.44$  Å)<sup>[14]</sup> but the Nd—O distances are shorter than those (2.614(4)—2.740(4) Å) in the related neodymium bidentate amide complex  $[\text{Nd}\{\text{Me}_2\text{Si}(\text{OBu}^t)(\text{NBu}^t)\}_3]$ .<sup>[7]</sup> The ether fragments of  $[\text{Nd}(\text{Me}_2\text{Si}(\text{OBu}^t)(\text{NBu}^t))_3]$  and  $[\text{Nd}(\text{L}^2)_3]$  are bulkier than a simple ether ligand, e.g. THF, and this may account for the long Ln—O distances, however the bond lengthening may also be an indication of general steric crowding in these complexes.

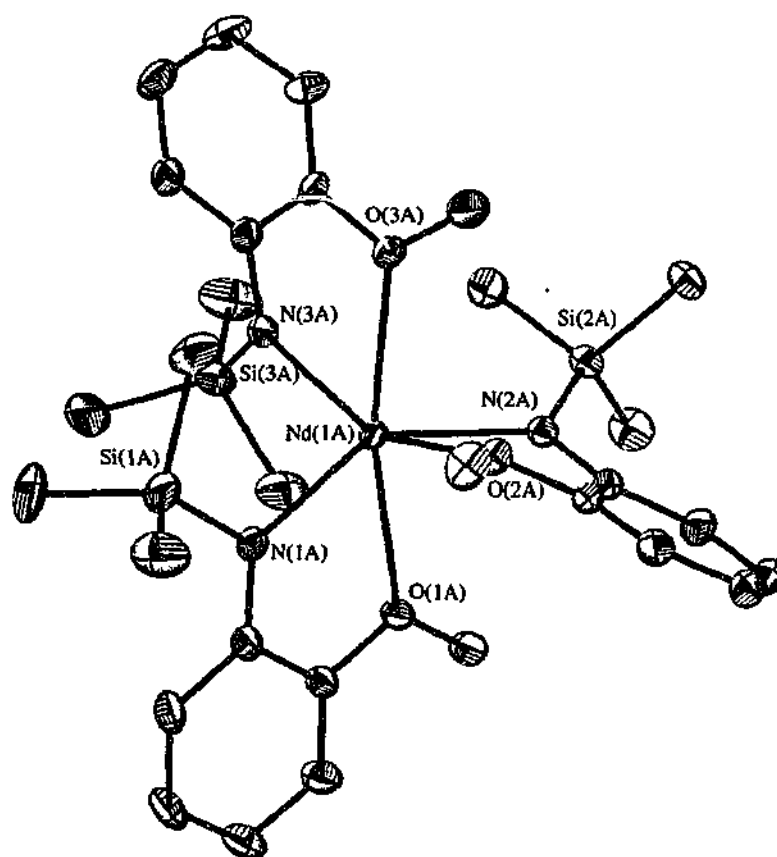


Table 3.5. Summary of Crystallographic Data for  $[\text{Nd}(\text{L}^2)_3]$ .

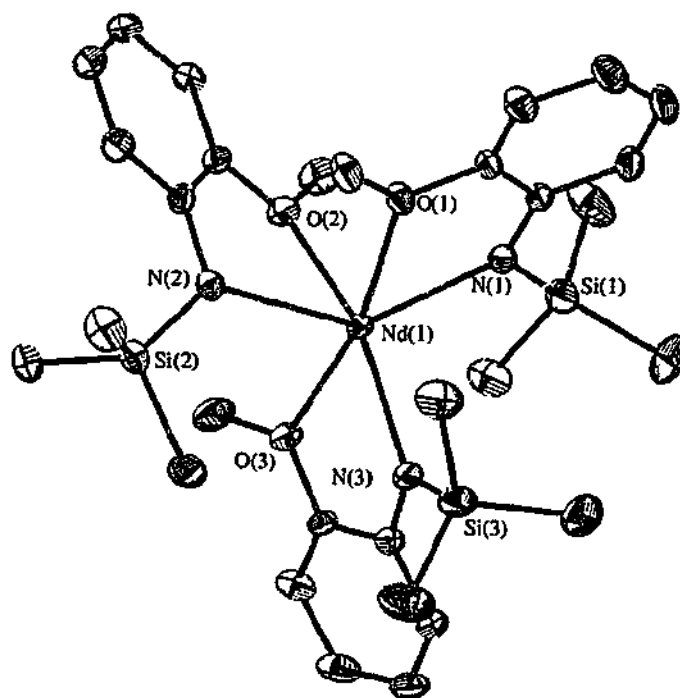
Compound	$[\text{Nd}(\text{L}^2)_3]$
Formula	$\text{C}_{30}\text{H}_{48}\text{N}_3\text{NdO}_3\text{Si}_3$
$M$	727.22
$a$ (Å)	10.1207(3)
$b$ (Å)	18.9788(6)
$c$ (Å)	18.8243(2)
$\alpha$ (°)	90
$\beta$ (°)	104.376(1)
$\gamma$ (°)	90
$V$ (Å <sup>3</sup> )	3502.5(12)
Crystal system	monoclinic
Space Group	$P2_1/c$
$Z$	4
Diffractometer	Nonius Kappa CCD
$\rho_{\text{calcd}}$ (g cm <sup>-3</sup> )	1.379
$\mu(\text{MoK}\alpha)$ (mm <sup>-1</sup> )	1.617
$2\theta_{\text{max}}$ (°)	56.6
$N, N_o$	8539, 5881
$R, R_w$ (observed data)	0.0343, 0.0612
$R, R_w$ (all data)	0.0673, 0.0729



(a) View perpendicular to the equatorial plane ( $\Delta$  enantiomer)



(b) View perpendicular to the equatorial plane ( $\Lambda$  enantiomer)

(c) General view ( $\Delta$  enantiomer)Figure 3.3 Three views of the molecular structure of  $[\text{Nd}(\text{L}^2)_3]$ Table 3.6 Metal environment in  $[\text{Nd}(\text{L}^2)_3]$  (distances in Å, angles $^\circ$ ) with estimated standard deviations in parentheses

Nd(1)—N(1)	2.385(3)	N(1)—Nd(1)—O(1)	65.62(8)
Nd(1)—N(2)	2.376(3)	N(2)—Nd(1)—O(2)	66.12(8)
Nd(1)—N(3)	2.349(3)	N(3)—Nd(1)—O(3)	65.38(8)
Average	2.37		
Nd(1)—O(1)	2.534(2)	O(1)—Nd(1)—O(2)	88.48(7)
Nd(1)—O(2)	2.535(2)	O(1)—Nd(1)—O(3)	167.65(7)
Nd(1)—O(3)	2.536(2)	O(2)—Nd(1)—O(3)	82.42(7)
Average	2.54		
		O(1)—Nd(1)—N(2)	80.87(8)
N(1)—Nd(1)—N(2)	139.63(9)	O(1)—Nd(1)—N(3)	124.75(8)
N(1)—Nd(1)—N(3)	98.82(9)	O(2)—Nd(1)—N(1)	90.19(8)
N(2)—Nd(1)—N(3)	119.23(9)	O(2)—Nd(1)—N(3)	146.38(8)
		O(3)—Nd(1)—N(1)	122.48(8)
		O(3)—Nd(1)—N(2)	87.79(8)

**Table 3.7 Lanthanoid—nitrogen distances of a selection of organoamidolanthanoid complexes**

Compound	Ref.	Av. Ln—N distance (d(N)) Å	Ionic Radii of Ln <sup>3+</sup> (i.r.) <sup>[6]</sup> Å	d(N)—i.r. Å
[Nd(L <sup>2</sup> ) <sub>3</sub> ]	this section	2.37	0.98	1.39
[La(L <sup>3</sup> ) <sub>3</sub> ]	section 3.3.2	2.45	1.03	1.42
[Nd(L <sup>3</sup> ) <sub>3</sub> ]	section 3.3.2	2.39	0.98	1.41
[Y(L <sup>3</sup> ) <sub>3</sub> ].(C <sub>5</sub> H <sub>9</sub> Me)	section 3.3.2	2.30	0.90	1.40
[Yb(L <sup>3</sup> ) <sub>3</sub> ].(MePh)	section 3.3.2	2.26	0.87	1.39
[Yb(L <sup>3</sup> ) <sub>3</sub> ].(C <sub>5</sub> H <sub>9</sub> Me)	section 3.3.2	2.27	0.87	1.40
[Nd{N(SiMe <sub>3</sub> ) <sub>2</sub> }] <sub>3</sub>	[9]	2.29	0.82 <sup>a</sup>	1.47
[Eu{N(SiMe <sub>3</sub> ) <sub>2</sub> }] <sub>3</sub>	[10]	2.26	0.78 <sup>a</sup>	1.48
[Yb{N(SiMe <sub>3</sub> ) <sub>2</sub> }] <sub>3</sub>	[10]	2.16	0.71 <sup>a</sup>	1.45
[Nd{N(Ph)(SiMe <sub>3</sub> ) <sub>2</sub> }(THF)]	[1]	2.31	0.88 <sup>a</sup>	1.43
[Yb{NH(2,6-(Pr <sup>i</sup> ) <sub>2</sub> C <sub>6</sub> H <sub>3</sub> ) <sub>3</sub> (THF) <sub>2</sub> }]	[11]	2.17	0.82 <sup>a</sup>	1.35
[Sm{N(Cy) <sub>2</sub> }] <sub>3</sub> (THF) <sup>b</sup>	[12]	2.28	0.90 <sup>a</sup>	1.38
[Eu(L <sup>1</sup> ) <sub>3</sub> ]	[5]	2.29	0.95	1.34
[Er(L <sup>1</sup> ) <sub>3</sub> ]	[5]	2.24	0.89	1.35
[Lu(L <sup>1</sup> ) <sub>3</sub> ]	[5]	2.19	0.86	1.33
[Nd{Me <sub>2</sub> Si(OBu <sup>t</sup> )(NBu <sup>t</sup> )}] <sub>3</sub>	[7]	2.40	0.98	1.42
[Pr{4-MeOC <sub>6</sub> H <sub>4</sub> C(NSiMe <sub>3</sub> ) <sub>2</sub> }] <sub>3</sub>	[8]	2.48	0.99	1.49

<sup>a</sup> values extrapolated from values of higher coordination number; <sup>b</sup> Cy = cyclohexyl

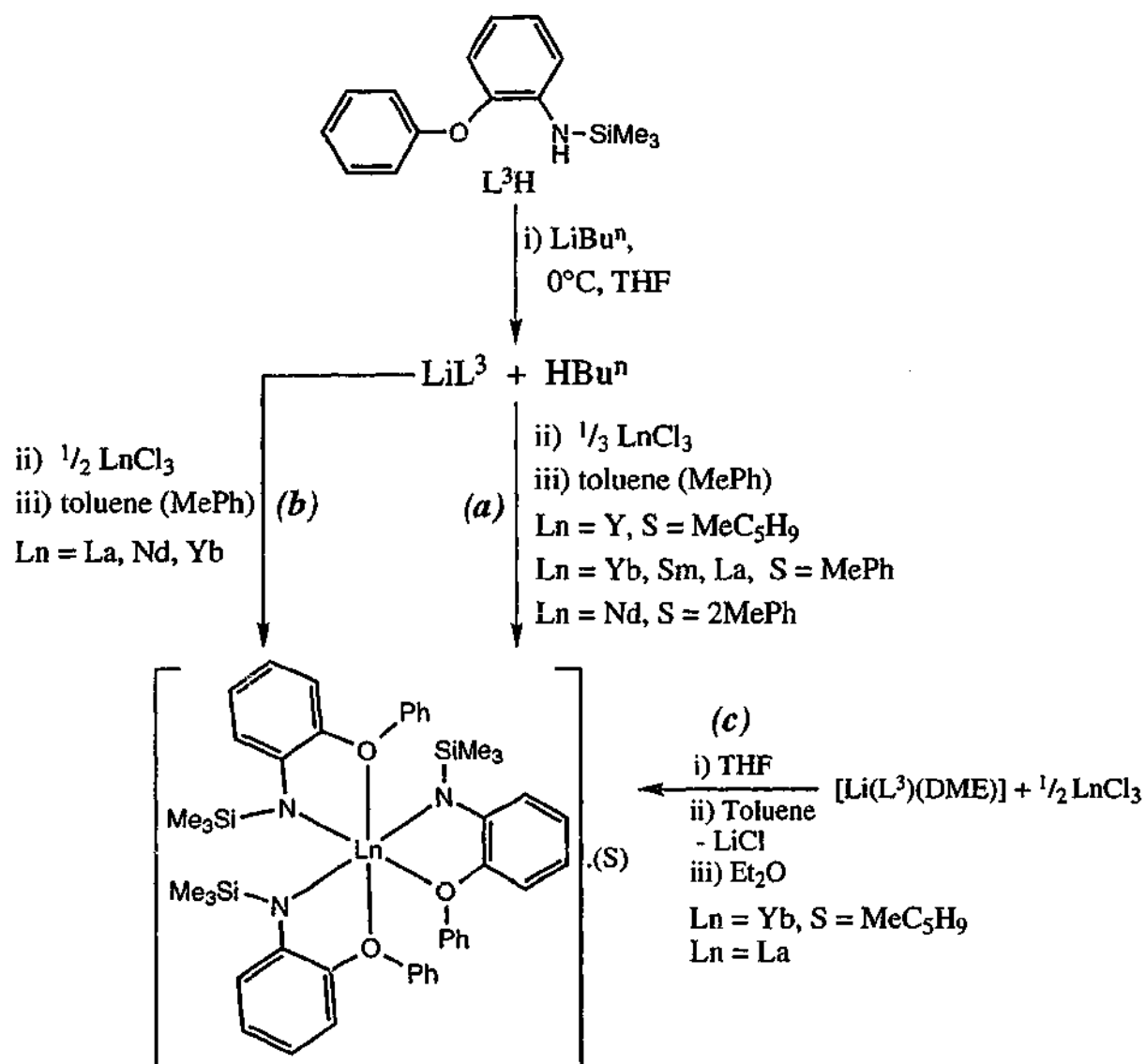
### 3.2.2 Synthesis and Characterisation of $[\text{Ln}(\text{L}^3)_3]$ Complexes

A range of  $[\text{Ln}(\text{L}^3)_3]$  ( $\text{Ln} = \text{Y}, \text{Yb}, \text{Sm}, \text{Nd}, \text{La}$ ) complexes (see *Table 3.8*) were synthesised using a procedure analogous to that for the preparation of the closely related  $[\text{Ln}(\text{L}^2)_3]$  complexes (see above). The initial metathesis reaction was carried out in THF where  $\text{LnCl}_3$  was added to 3 equivalents of  $\text{LiL}^3$ , which was formed *in situ* from  $\text{L}^3\text{H}$  and  $\text{LiBu}^n$  (*Scheme 3.2 (a)*). Isolation of the homoleptic products  $[\text{Ln}(\text{L}^3)_3]$  ( $\text{Ln} = \text{La}, \text{Nd}$  and  $\text{Yb}$ ) from either an *in situ* reaction between two equivalents of  $\text{LiL}^3$  with  $\text{LnCl}_3$  (*Scheme 3.2 (b)*) or from reactions of  $\text{LnCl}_3$  ( $\text{Ln} = \text{La}, \text{Yb}$ ) with two equivalents of  $[\text{Li}(\text{L}^3)(\text{DME})]$  (*Scheme 3.2 (c)*) was observed instead of the expected heteroleptic chloro complexes  $\text{Ln}(\text{L}^3)_2\text{Cl}$  (see also Chapter 4). The products obtained from reactions of  $\text{LiL}^3$  and  $\text{LnCl}_3$  (2:1 mole ratio) (*Scheme 3.2 (b), (c)*) had identical infrared spectra to  $[\text{Ln}(\text{L}^3)_3]$  (from the 1:3 Li to Ln reactions) (*Scheme 3.2 (a)*) and a unit cell determination on crystals obtained from reaction of  $\text{LiL}^3$  with  $\text{NdCl}_3$  (2:1 mole ratio (*Scheme 3.2 (b)*)) confirmed the product to be  $[\text{Nd}(\text{L}^3)_3]$ .

The bulk products were crystallised from toluene owing to the low solubility of the homoleptic complexes  $[\text{Ln}(\text{L}^3)_3]$  in hexane. The final homoleptic complexes were isolated as solvates, either with toluene or methylcyclopentane in the lattice (see *Table 3.8*). The latter is presumed to be an impurity in one of the solvents used and its presence was accidental. For  $\text{Ln} = \text{La}$ , the lattice toluene was lost upon recrystallisation from diethyl ether giving  $[\text{La}(\text{L}^3)_3]$  (see *Table 3.8*) which was used for X-ray determination, whilst single crystals of solvent-free  $[\text{Nd}(\text{L}^3)_3]$  were obtained from hexane.

Table 3.8 General Properties of  $[Ln(L^3)_3]$  complexes

Complex	Yield (%)	Colour	X-ray Structure determination
$[La(L^3)] \cdot (MePh)$ $[La(L^3)]$	68	Pale yellow	✓
$[Nd(L^3)_3] \cdot (MePh)_2$	62	Blue	✓
$[Sm(L^3)_3] \cdot (MePh)$	56	Yellow	
$[Y(L^3)_3] \cdot (MeC_5H_9)$	71	Pale yellow	✓
$[Yb(L^3)_3] \cdot (MePh)$	68	Orange/Red	✓
$[Yb(L^3)_3] \cdot (MeC_5H_9)$	68	Orange/Red	✓



Scheme 3.2

Satisfactory elemental analyses (C, H, N) were obtained for all of the homoleptic complexes except for unsolvated  $[\text{La}(\text{L}^3)_3]$ , which was not examined since the crystal structure was determined and the corresponding toluene solvate was obtained analytically pure. In the case of  $[\text{Yb}(\text{L}^3)_3] \cdot (\text{C}_5\text{H}_9\text{Me})$  the analysis fitted for solvent-free  $[\text{Yb}(\text{L}^3)_3]$  and the methylcyclopentane was evidently removed from the lattice on drying the sample under vacuum, but the corresponding yttrium complex analysed as the solvate. The infrared spectra of the complexes were virtually identical and indicated the presence of coordinated  $\text{L}^3$  in accordance with the proposed structures. The presence of toluene could not be detected by IR due to the large number of bands below  $1000\text{ cm}^{-1}$ . The C—O—C stretching region (asymmetric) shows three sets of two absorptions for the homoleptic complexes and is different from  $\text{L}^3\text{H}$  that displays only two sets of two absorptions in this region.  $^1\text{H}$  NMR spectra of the diamagnetic complexes,  $[\text{La}(\text{L}^3)_3]$  and  $[\text{La}(\text{L}^3)_3] \cdot (\text{PhMe})$  exhibited single  $\text{SiMe}_3$  resonances and aromatic peaks attributable to coordinated  $\text{L}^3$ . Characteristic toluene resonances were observed for the latter and confirmed the presence of one toluene molecule of crystallisation. In a similar manner to the  $^1\text{H}$  NMR spectrum of  $[\text{Nd}(\text{L}^2)_3]$  (see Section 3.2.1), the 'paramagnetic shift' in the spectrum of  $[\text{Nd}(\text{L}^3)_3] \cdot (\text{PhMe})_2$  causes the backbone aromatic protons on  $\text{L}^3$  to shift considerably, however these are in similar positions to those of  $[\text{Nd}(\text{L}^2)_3]$ . The protons on the phenyl substituent are observed as three broad singlets at  $-8.05$  ( $\text{H}2'$ ,  $\text{H}6'$ ),  $0.48$  ( $\text{H}3'$ ,  $\text{H}5'$ ), and  $1.20$  ppm ( $\text{H}4'$ ). A single broad resonance attributable to  $\text{SiMe}_3$  is observed at  $-1.22$  ppm which is closer to the diamagnetic region than was observed for  $[\text{Nd}(\text{L}^2)_3]$  ( $-4.22$  ppm). For diamagnetic  $[\text{Y}(\text{L}^3)_3] \cdot (\text{C}_5\text{H}_9\text{Me})$  the presence of methylcyclopentane was confirmed in the  $^1\text{H}$  NMR spectrum although the integration showed only half a methylcyclopentane molecule per  $[\text{Y}(\text{L}^3)_3]$ ,<sup>[15]</sup> whereas the X-ray structure determination and elemental analyses indicated one  $\text{C}_5\text{H}_9\text{Me}$  per yttrium. There was no evidence of toluene thus excluding the possibility that the solvent of crystallisation was toluene. Overall the  $^1\text{H}$  NMR data for the  $[\text{Ln}(\text{L}^3)_3]$  complexes indicate that one  $\text{L}^3$  environment is present in solution which contrasts the at least two  $\text{L}^3$  environments observed in the solid state. Presumably the ligands are rapidly exchanging under these conditions. The mass spectra obtained for  $[\text{Ln}(\text{L}^3)_3] \cdot (\text{S})$  ( $\text{Ln} = \text{La}, \text{Sm}, \text{Y}$ ) showed a weak molecular ion,  $[\text{Ln}(\text{L}^3)_3]^+$  and associated fragment ions (notably  $[\text{Ln}(\text{L}^3)_2]^+$  and  $[\text{Ln}(\text{L}^3)]^+$ ) as well as an intense  $[\text{L}^3\text{H}]^+$  ion. However for  $[\text{La}(\text{L}^3)_3] \cdot (\text{MePh})$  the highest mass ion observed was  $[\text{La}(\text{L}^3)_2]^+$ .

Single crystal X-ray diffraction data were collected for  $[\text{La}(\text{L}^3)_3]$  (Figure 3.4),  $[\text{Nd}(\text{L}^3)_3]$ ,  $[\text{Y}(\text{L}^3)_3] \cdot (\text{C}_5\text{H}_9\text{Me})$ ,  $[\text{Yb}(\text{L}^3)_3] \cdot (\text{MePh})$  (Figure 3.5) and  $[\text{Yb}(\text{L}^3)_3] \cdot (\text{C}_5\text{H}_9\text{Me})$  which encompass both extremes of the lanthanoid ionic radius. Crystallographic data and parameters are listed in Table 3.9 and selected bond distances and angles are given in Table 3.10. Although the lattice symmetry differs between the solvent-free complexes  $[\text{La}(\text{L}^3)_3]$ ,  $[\text{Nd}(\text{L}^3)_3]$  and the solvates  $[\text{Y}(\text{L}^3)_3] \cdot (\text{C}_5\text{H}_9\text{Me})$ ,  $[\text{Yb}(\text{L}^3)_3] \cdot (\text{MePh})$  and  $[\text{Yb}(\text{L}^3)_3] \cdot (\text{C}_5\text{H}_9\text{Me})$  (see Table 3.9), the lanthanoid environments are similar but differences exist between the two complex types (see below). Each of the molecules is monomeric with a six-coordinate metal centre surrounded by three bidentate  $\text{L}^3$  ligands with a very distorted octahedral coordination geometry. As with  $[\text{Nd}(\text{L}^2)_3]$  the bulky amido groups are in a *meridinal* configuration. In general, the *mer*-configuration has one chelating  $\text{L}^3$  ligand in the equatorial plane along with two nitrogen atoms from the remaining  $\text{L}^3$  ligands. However these nitrogen atoms lie above and below the equatorial plane in a similar manner to the arrangement in  $[\text{Nd}(\text{L}^2)_3]$  (see Section 3.2.1). The remaining two oxygen atoms from the two  $\text{L}^3$  ligands occupy the axial sites. Throughout the  $[\text{Ln}(\text{L}^3)_3]$  series the orientations of the  $\text{L}^3$  ligand are similar with the C—O(Ph) bond in the same plane as the arene backbone (see Table 3.11 for torsion angles) but the phenyl ring plane is rotated near perpendicular (see Table 3.11 for interplanar angles). This differs from the arrangement of  $\text{L}^3\text{H}$  (see above).

The geometry of  $[\text{Nd}(\text{L}^3)_3]$  is almost identical to that of  $[\text{Nd}(\text{L}^2)_3]$ . The angles defining the coordinated atoms deviate by less than  $10^\circ$  between the two structures (Table 3.6, Table 3.10). Whilst the general appearance of the  $[\text{Ln}(\text{L}^3)_3]$  complexes is the same, significant differences are apparent between the solvates and solvent-free structures. The *trans* N—Ln—N angles for unsolvated La and Nd derivatives are approximately  $15^\circ$  smaller than those for the Yb and Y solvates and a similar trend is also observed for the *cis* N—Ln—N angles, but to a lesser extent (Table 3.10). Due to the restrictions of the bite angles of the bidentate  $\text{L}^3$ , similar patterns are also apparent in the inter-ligand O—Ln—N angles. Thus the solvates are much closer to a regular octahedral structure. These differences are clearly not due to the gradual change in ionic radii from La (1.03 Å) to Yb (0.87 Å).<sup>[6]</sup> For example the smaller elements would be expected to be more sterically crowded which would presumably cause a widening of the *cis* N—Ln—N angles, through greater repulsion between the bulky  $\text{SiMe}_3$  groups, and in fact the opposite is observed (Table 3.10). However the *cis* N—Ln—N angles are not unreasonably narrow and still



compare well with those of *fac*-[Ln(L<sup>1</sup>)<sub>3</sub>].<sup>[5]</sup> Therefore the variation in angles is possibly associated with differences in the crystal packing required to accommodate solvent molecules.

Subtraction of the appropriate metal ionic radii<sup>[6]</sup> from the Ln—N and Ln—O lengths gives values of 1.36—1.43 Å and 1.48—1.60 Å respectively. These ranges encompass the values observed for [Nd(L<sup>2</sup>)<sub>3</sub>] in which the distances were found to be consistent with related compounds (see *Table 3.7*). However there are values both above and below the L<sup>2</sup> data contrary to the anticipated general increase associated with the greater steric demand of L<sup>3</sup>. Furthermore, there are some variations in the subtraction values across the series that deserve further comment. The values derived from the Ln—O distances show, for the smaller elements, a broadening of the observed range and a distinct decrease in the values. For the Yb and Y structures, the three Ln—N distances differ by approximately 0.06 Å whereas the Ln—O bond lengths show two shorter and one longer distance. The subtraction values for the shorter Ln—O bonds are significantly less than those of [Nd(L<sup>2</sup>)<sub>3</sub>] (1.56 Å) despite the bulkier O(Ph) substituent of the L<sup>3</sup> ligand. The contraction of the Ln—O radius adjusted distances from La to Yb is contrary to the expected trend since the increase in steric crowding associated with the smaller size of the metal centre may result in longer metal-oxygen bond lengths. Since there are two distinct groups of data corresponding to the presence or absence of a solvent of crystallisation, these variations in bond distances and angles may be a result of a packing effect resulting from the presence or absence of the solvent.

Table 3.9 X-ray crystal data and refinement parameters for  $[\text{La}(\text{L}^3)_3]$ ,  $[\text{Nd}(\text{L}^3)_3]$ ,  $[\text{Y}(\text{L}^3)_3] \cdot (\text{C}_5\text{H}_9\text{Me})$  and  $[\text{Yb}(\text{L}^3)_3] \cdot (\text{MePh})$ ,  $[\text{Yb}(\text{L}^3)_3] \cdot (\text{C}_5\text{H}_9\text{Me})$ .

Compound	$[\text{La}(\text{L}^3)_3]$	$[\text{Nd}(\text{L}^3)_3]$	$[\text{Y}(\text{L}^3)_3] \cdot (\text{C}_5\text{H}_9\text{Me})$	$[\text{Yb}(\text{L}^3)_3] \cdot (\text{MePh})$	$[\text{Yb}(\text{L}^3)_3] \cdot (\text{C}_5\text{H}_9\text{Me})$
Formula	$\text{C}_{45}\text{H}_{54}\text{LaN}_3\text{O}_3\text{Si}_3$	$\text{C}_{45}\text{H}_{54}\text{NdN}_3\text{O}_3\text{Si}_3$	$\text{C}_{51}\text{H}_{66}\text{N}_3\text{O}_3\text{Si}_3\text{Y}$	$\text{C}_{52}\text{H}_{62}\text{N}_3\text{O}_3\text{Si}_3\text{Yb}$	$\text{C}_{51}\text{H}_{66}\text{N}_3\text{O}_3\text{Si}_3\text{Yb}$
$M$	908.09	913.42	942.25	1034.36	1026.38
$a$ (Å)	16.2330(1)	16.1450(2)	13.3738(2)	13.4071(3)	13.2868(1)
$b$ (Å)	15.4788(1)	15.4738(2)	13.3789(3)	13.4511(3)	13.3693(1)
$c$ (Å)	18.0579(2)	18.0246(2)	14.8419(3)	14.7899(2)	14.7962(2)
$\alpha$ (°)	90	90	92.605(1)	100.240(1)	92.976(1)
$\beta$ (°)	103.313(1)	103.032(1)	100.502(1)	92.274(1)	100.536(1)
$\gamma$ (°)	90	90	109.447(1)	110.243(1)	108.856(1)
$V$ (Å <sup>3</sup> )	4415.4(15)	4387.0(15)	2446.0(9)	2447.8(9)	2427.9(9)
Crystal system	monoclinic	monoclinic	triclinic	triclinic	triclinic
Space Group	$P2_1/n$	$P2_1/n$	$P(-1)$	$P(-1)$	$P(-1)$
$Z$	4	4	2	2	2
Diffractometer	Nonius Kappa CCD	Nonius Kappa CCD	Nonius Kappa CCD	Nonius Kappa CCD	Nonius Kappa CCD
$\rho_{\text{calcd}}$ (g cm <sup>-3</sup> )	1.366	1.383	1.279	1.403	1.404
$\mu(\text{MoK}\alpha)$ (mm <sup>-1</sup> )	1.090	1.307	1.309	2.028	2.044
$2\theta_{\text{max}}$ (°)	56.6	56.6	56.6	61.0	56.6
$N, N_o$	10885, 8914	10849, 9244	11730, 7014	13093, 10634	11666, 9838
$R, R_w$ (observed data)	0.0277, 0.0607	0.0271, 0.0588	0.0624, 0.1259	0.0394, 0.0744	0.0305, 0.0621
$R, R_w$ (all data)	0.0417, 0.0672	0.0378, 0.0631	0.1289, 0.1460	0.0678, 0.1172	0.0440, 0.0655

Table 3.10 Metal Atom environment for  $[Ln(L^3)_3]$  complexes

	$[La(L^3)_3]$	$[Nd(L^3)_3]$	$[Y(L^3)_3] \cdot (C_3H_9Me)$	$[Yb(L^3)_3] \cdot (MePh)$	$[Yb(L^3)_3] \cdot (C_3H_9Me)$
<i>Bond distance (Å)</i>					
Ln(1)—N(1)	2.454(2)	2.396(2)	2.306(3)	2.272(2)	2.271(2)
Ln(1)—N(2)	2.447(2)	2.387(2)	2.331(3)	2.289(3)	2.290(2)
Ln(1)—N(3)	2.446(2)	2.386(2)	2.270(3)	2.231(3)	2.233(2)
Average	2.45	2.39	2.30	2.26	2.27
<i>Angles (°)</i>					
Ln(1)—O(1)	2.609(1)	2.550(2)	2.381(2)	2.350(3)	2.348(2)
Ln(1)—O(2)	2.606(2)	2.543(2)	2.441(2)	2.359(3)	2.409(2)
Ln(1)—O(3)	2.633(1)	2.575(1)	2.386(2)	2.405(3)	2.361(2)
Average	2.62	2.56	2.40	2.37	2.373
N(1)—Ln(1)—N(2)	134.17(5)	136.05(6)	148.15(10)	150.10(10)	149.09(3)
N(1)—Ln(1)—N(3)	109.22(5)	107.77(6)	105.71(10)	104.40(10)	104.64(8)
N(2)—Ln(1)—N(3)	116.09(5)	115.47(6)	106.01(10)	105.298(10)	106.10(8)
N(1)—Ln(1)—O(1)	64.65(5)	66.32(5)	70.33(9)	71.37(8)	71.47(7)
N(2)—Ln(1)—O(2)	64.19(5)	65.95(5)	68.37(9)	69.39(9)	69.25(7)
N(3)—Ln(1)—O(3)	63.82(5)	65.51(5)	71.02(9)	72.16(8)	72.24(7)
O(1)—Ln(1)—O(2)	85.43(5)	86.02(5)	85.63(8)	86.56(8)	85.81(7)
O(1)—Ln(1)—O(3)	168.26(4)	168.08(5)	174.28(7)	174.55(7)	174.87(6)
O(2)—Ln(1)—O(3)	83.78(5)	83.28(5)	89.97(8)	90.06(8)	90.46(7)
O(1)—Ln(1)—N(2)	82.32(5)	82.08(6)	94.23(9)	94.39(9)	94.14(7)
O(1)—Ln(1)—N(3)	127.19(5)	125.49(6)	113.58(9)	111.47(9)	111.65(7)
O(2)—Ln(1)—N(1)	81.56(5)	81.51(5)	82.44(9)	83.30(9)	82.23(7)
O(2)—Ln(1)—N(3)	147.35(5)	148.44(5)	160.63(9)	161.78(8)	162.43(7)
O(3)—Ln(1)—N(1)	118.06(5)	116.96(5)	105.48(9)	104.00(8)	104.56(7)
O(3)—Ln(1)—N(2)	88.81(5)	88.75(5)	87.53(9)	88.41(9)	87.81(7)

Table 3.11 Torsion Angles of  $L^3$  in  $[Ln(L^3)_3]$  complexes

	$[La(L^3)_3]$	$[Nd(L^3)_3]$	$[Y(L^3)_3] \cdot (C_5H_9Me)$	$[Yb(L^3)_3] \cdot (PhMe)$	$[Yb(L^3)_3] \cdot (C_5H_9Me)$
<i>Torsion angle (°)</i>					
C(13)—C(12)—O(1)—C(111)	13.4(3)	12.9(3)	-3.6(4)	3.7(4)	3.7(4)
C(23)—C(22)—O(2)—C(211)	-6.8(3)	-6.7(3)	26.5(5)	-26.8(4)	-24.9(4)
C(33)—C(32)—O(3)—C(311)	3.4(3)	2.1(3)	-5.2(5)	5.6(4)	4.1(3)
<i>Planar angles (°)</i>					
P(1A) <sup>a</sup> —P(1B) <sup>b</sup>	14.7(1)	15.0(1)	21.4(1)	22.8(1)	23.7(4)
P(2A) <sup>c</sup> —P(2B) <sup>d</sup>	5.4(1)	4.9(1)	23.1(2)	23.5(2)	-24.9(4)
P(3A) <sup>e</sup> —P(3B) <sup>f</sup>	6.5(1)	7.2(1)	26.4(7)	28.0(1)	24.1(3)
P(1B) <sup>b</sup> —P(1C) <sup>g</sup>	84.0(1)	84.4(1)	89.8(1)	90.0(1)	88.6(1)
P(2B) <sup>d</sup> —P(2C) <sup>h</sup>	83.3(1)	83.3(1)	88.2(1)	88.0(1)	88.1(1)
P(3B) <sup>f</sup> —P(3C) <sup>i</sup>	74.6(1)	76.7(1)	75.5(1)	76.2(1)	75.4(1)

<sup>a</sup>P(1A) = the plane defined by Ln-N(1)-O(1) atoms; <sup>b</sup>P(1B) = plane defined by the arene backbone (C(11)-C(16)); <sup>c</sup>P(2A) = the plane defined by Ln-N(2)-O(2) atoms; <sup>d</sup>P(2B) = plane defined by the arene backbone (C(21)-C(26)); <sup>e</sup>P(3A) = the plane defined by Ln-N(3)-O(3) atoms; <sup>f</sup>P(3B) = plane defined by the arene backbone (C(31)-C(36)); <sup>g</sup>P(1C) = plane defined by the phenyl ring carbon atoms C(111)-C(116); <sup>h</sup>P(2C) = plane defined by the phenyl ring carbon atoms C(211)-C(216); <sup>i</sup>P(3C) = plane defined by the phenyl ring carbon atoms C(311)-C(316).

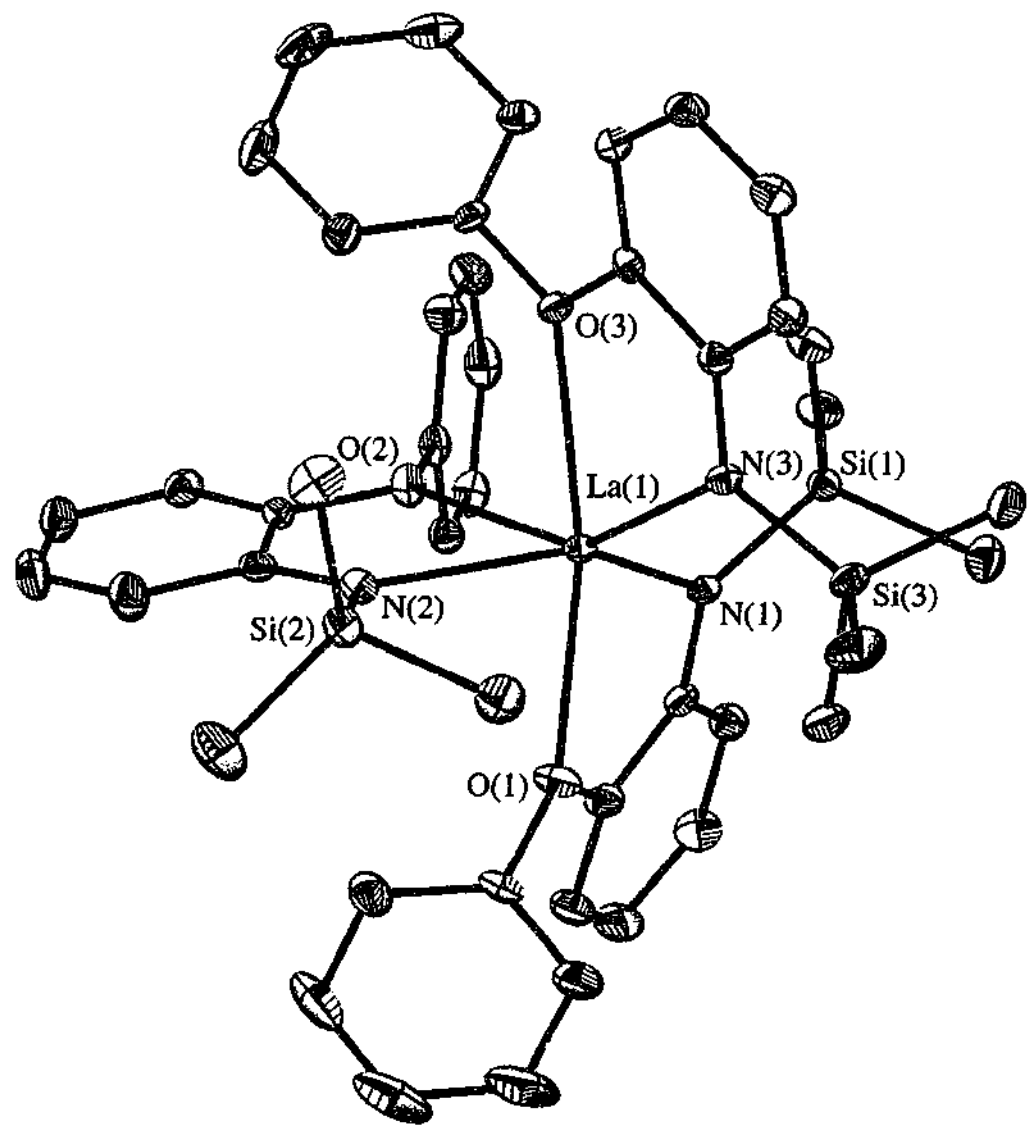


Figure 3.4 Molecular Structure of  $[La(L^3)]_3$  ( $\Lambda$  enantiomer)

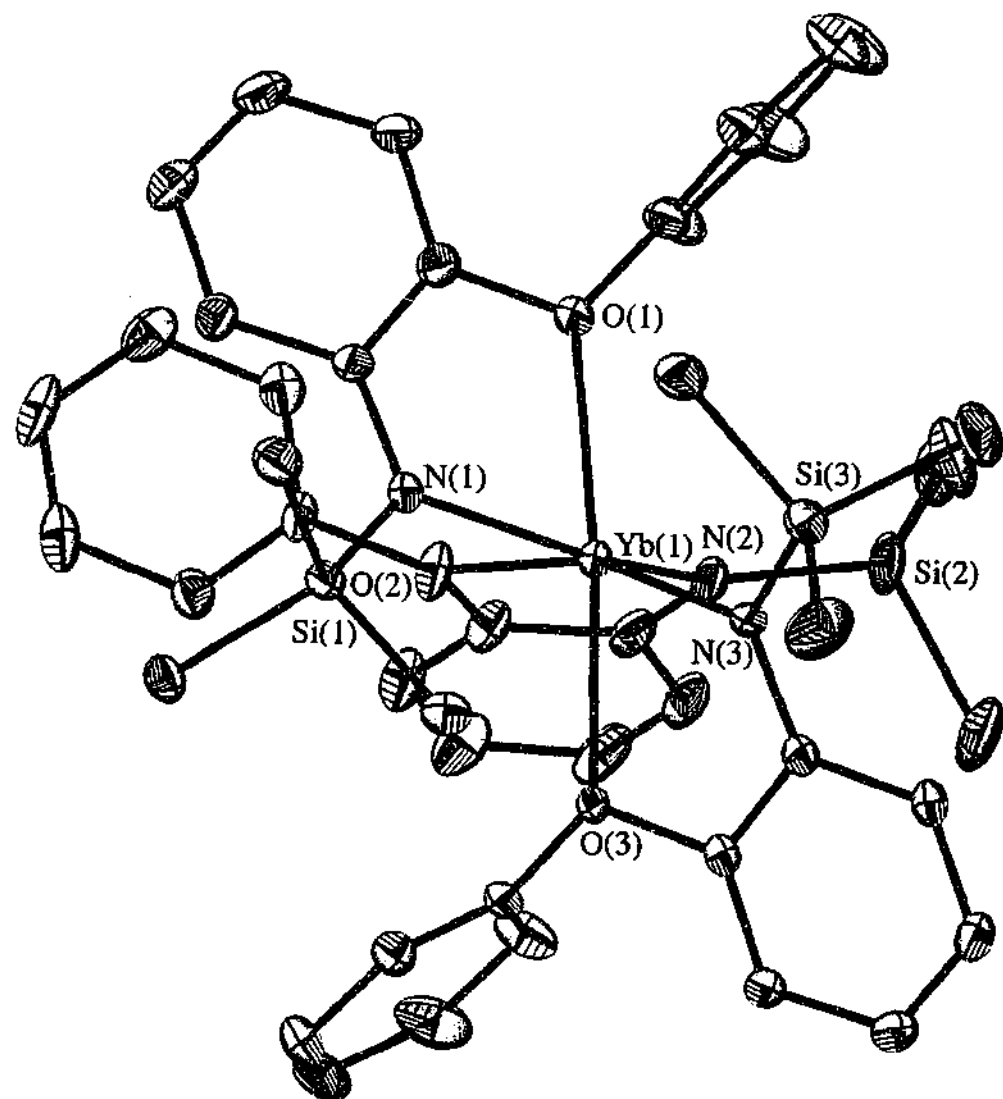


Figure 3.5 Molecular Structure of  $[Yb(L^3)]_3 \cdot (MePh)$  ( $\Delta$  enantiomer)

### 3.3 Conclusion

For the first time, homoleptic (diorganoamido)lanthanoid(III) complexes containing either 2-MeOC<sub>6</sub>H<sub>4</sub>NSiMe<sub>3</sub> (L<sup>2</sup>) or 2-PhOC<sub>6</sub>H<sub>4</sub>NSiMe<sub>3</sub> (L<sup>3</sup>) ligands have been prepared. They were synthesised by a metathesis reaction between lanthanoid trihalide and the lithiated ligand in a 1 to 3 mole ratio. The method of isolation of the pure homoleptic complexes from the reaction mixture was slightly different for each ligand system. In general the [Ln(L<sup>2</sup>)<sub>3</sub>] complexes have a greater solubility in hexane than the [Ln(L<sup>3</sup>)<sub>3</sub>] series.

The solid state structures of [Nd(L<sup>2</sup>)<sub>3</sub>], [La(L<sup>3</sup>)<sub>3</sub>], [Nd(L<sup>3</sup>)<sub>3</sub>], [Y(L<sup>3</sup>)<sub>3</sub>](C<sub>5</sub>H<sub>9</sub>Me), [Yb(L<sup>3</sup>)<sub>3</sub>](C<sub>5</sub>H<sub>9</sub>Me) and [Yb(L<sup>3</sup>)<sub>3</sub>](PhMe) were investigated by X-ray crystallography. Clearly the steric influence of L<sup>2</sup> and L<sup>3</sup> is sufficient to block all coordination sites available on the lanthanoid atom. A six-coordinate, distorted octahedral lanthanoid centre in a *mer*-configuration was found for each homoleptic arrangement suggesting similar steric demand between L<sup>2</sup> and L<sup>3</sup>. This arrangement does however differ from the *facial* configuration in [Ln(L<sup>1</sup>)<sub>3</sub>] which suggests that the steric and electronic demands of L<sup>2</sup> and L<sup>3</sup> are different from L<sup>1</sup>.

The proposed stronger binding of the pendent ether arms of the L<sup>2</sup> and L<sup>3</sup> ligands to the oxophilic lanthanoids, compared to the amine substituent of L<sup>1</sup>, is supported by the current structural data. Thus comparison of the Ln—O and Ln—N(Me)<sub>2</sub> distances by subtraction of the anchoring Ln—N(SiMe<sub>3</sub>) distance clearly shows weaker coordination of the amine (*Table 3.12*). This is despite the presence of the bulky O(Ph) of L<sup>3</sup> which has Ln—O(ether) distances comparable to those for very crowded Ln(OAr)<sub>3</sub>(S) systems (range 1.48 — 1.60 Å).<sup>[16]</sup> Thus it may be possible to generate a range of more stable heteroleptic derivatives incorporating L<sup>2</sup> or L<sup>3</sup> ligands, and investigations of such are discussed in Chapter 4.

Table 3.12 Subtraction of lanthanoid amide distances from lanthanoid donor distances.

Complex	Av. Ln—O (Å)	Av. Ln—NR <sub>2</sub> (Å)	Av. Ln—N(SiMe <sub>3</sub> ) (Å)	Subtraction (Å)
[Nd(L <sup>2</sup> ) <sub>3</sub> ]	2.54		2.37	0.17
[La(L <sup>3</sup> ) <sub>3</sub> ]	2.62		2.45	0.17
[Nd(L <sup>3</sup> ) <sub>3</sub> ]	2.56		2.39	0.17
[Y(L <sup>3</sup> ) <sub>3</sub> ].(C <sub>5</sub> H <sub>9</sub> Me)	2.40		2.30	0.10
[Yb(L <sup>3</sup> ) <sub>3</sub> ].(PhMe)	2.37		2.26	0.11
[Yb(L <sup>3</sup> ) <sub>3</sub> ].(C <sub>5</sub> H <sub>9</sub> Me)	2.37		2.27	0.10
[Eu(L <sup>1</sup> ) <sub>3</sub> ] <sup>a</sup>		2.81	2.29	0.52
[Er(L <sup>1</sup> ) <sub>3</sub> ] <sup>a</sup>		2.72	2.24	0.48
[Lu(L <sup>1</sup> ) <sub>3</sub> ] <sup>a</sup>		2.69	2.19	0.50

<sup>a</sup> see ref[5]



### 3.4 References

- 1 H. Schumann, J. Winterfeld, E. C. E. Rosenthal, H. Hemling, and L. Esser, *Z. Anorg. Allg. Chem.*, 1995, **621**, 122.
- 2 D. H. Williams and I. Fleming, in *Spectroscopic Methods in Organic Chemistry*, McGraw-Hill, 5th edn, 1995, ch. 2, p. 28.
- 3 W. T. Carnall, in *The Absorption and Fluorescence Spectra of Rare Earth Ions in Solution*, in *Handbook on the Physics and Chemistry of Rare Earths*, eds. K.A. Gschneider and L. Eyring, North-Holland, Amsterdam, 1979, vol. 3, ch. 24, p. 171.
- 4 M. Johnson, J. C. Taylor, and G. W. Cox, *J. Appl. Crystallogr.*, 1980, **13**, 188.
- 5 G. B. Deacon, C. M. Forsyth, P. C. Junk, B. W. Skelton, and A. H. White, *J. Chem. Soc., Dalton Trans.*, 1998, 1381.
- 6 R. D. Shannon, *Acta. Crystallogr., Sect. A*, 1976, **32**, 751.
- 7 A. Recknagel, A. Steiner, S. Brooker, D. Stalke, and E. T. Edelman, *J. Organomet. Chem.*, 1991, **415**, 315.
- 8 M. Wedler, F. Knosel, U. Pieper, S. Dietmar, F. T. Edelman, and H.-D. Amberger, *Chem. Ber.*, 1992, **125**, 2171.
- 9 R. A. Anderson, D. H. Templeton, and A. Zalkin, *Inorg. Chem.*, 1978, **17**, 2317.
- 10 P. G. Eller, D. C. Bradley, M. B. Hursthouse, and D. W. Meek, *Coord. Chem. Rev.*, 1977, **24**, 1.
- 11 W. J. Evans, M. A. Ansari, J. W. Ziller, and S. I. Khan, *Inorg. Chem.*, 1996, **35**, 5435.
- 12 R. K. Minhas, Y. Ma, J.-I. Song, and S. Gambarotta, *Inorg. Chem.*, 1996, **35**, 1866.
- 13 G. B. Deacon, P. I. MacKinnon, T. W. Hambley, and J. C. Taylor, *Organomet. Chem.*, 1983, **259**, 91.
- 14 G. B. Deacon, T. Feng, P. C. Junk, B. W. Skelton, A. N. Sobolev, and A. H. White, *Aust. J. Chem.*, 1998, **51**, 75.
- 15 C. J. Pouchert and J. R. Campbell, in *Aldrich Library of NMR Spectra*, Aldrich Chemical Company, Milwaukee, Wisconsin, 1974, vol. 1, p. 32C.
- 16 D. C. Bradley, R. C. Mehrotra, I. P. Rothwell, and A. Singh, in *Alkoxo and Aryloxo Derivatives of Metals*, Academic Press, London, 2001.

## Chapter 4

# *Solvent-free Heteroleptic Lanthanoid(III) Complexes Stabilised by Mixed N,O Ligands*

### 4.1 Introduction

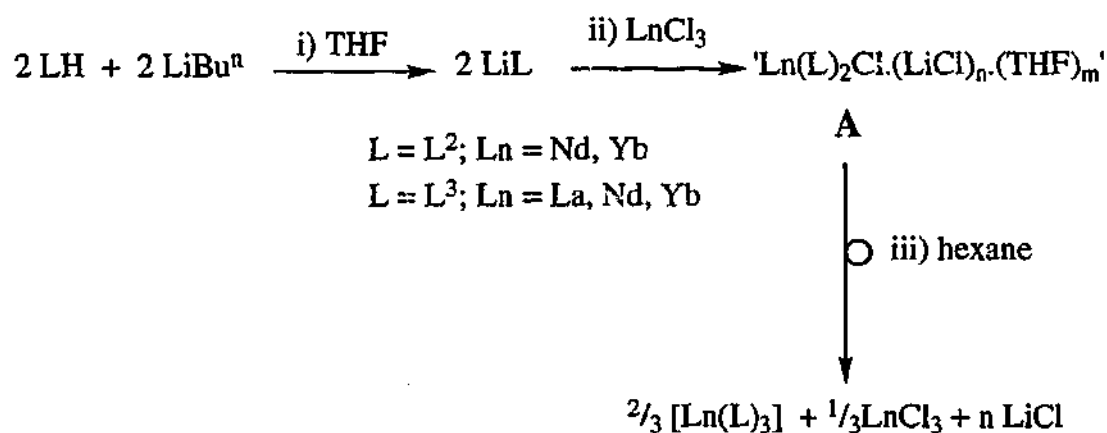
The mixed N, O-donor ligands  $L^2$  and  $L^3$  have been successfully coordinated to lanthanoid metals to form complexes of the type,  $[Ln(L)_3]$ . Whilst  $L^1$ ,  $L^2$  and  $L^3$  gave solvent-free six-coordinate complexes, there are significant differences in the binding of the two ligand types (see Chapter 3). Notably stronger binding of the ether (OR) group of  $L^2$  and  $L^3$  as compared with the amine substituent ( $NMe_2$ ) of  $L^1$  was evident, even with the bulky O(Ph) group of  $L^3$ . This confirmed the initial premise that a mixed nitrogen oxygen organoamide ligand would have better binding properties for lanthanoid cations. Therefore utilisation of these ligands would be expected to improve the stability of the heteroleptic derivatives and consequently the syntheses and structures of these are pursued in this Chapter. Initially the heteroleptic complexes of the type  $[Ln(L)_2Cl]$  were investigated since these are pivotal complexes for the preparation of the general class  $[Ln(L)_2X]$  ( $X = \text{anion}$ ) by subsequent derivatisation with MR ( $M = \text{alkali metal, Tl}$ ). Alternatively a direct route to one example of  $[Ln(L)_2X]$  was explored, viz. synthesis of  $[Ln(L^3)_2(OAr)]$  ( $OAr = \text{aryloxide}$ ) from  $[Ln(OAr)_3]$ . The next section takes a step back towards cyclopentadienyl chemistry and bridges the gap between the  $[Ln(Cp)_2X]$  and  $[Ln(L)_2X]$  compounds through the preparation of  $[Ln(Cp)(L)Cl]$  derivatives. This should provide a better understanding of the overall steric and electronic properties of the mixed N, O-donor organoamide ligand system.

## 4.2 Results and Discussion

### 4.2.1 Preparation of $[\text{Ln}(\text{L})_2(\mu\text{-Cl})]_2$ Complexes ( $\text{L} = \text{L}^2, \text{L}^3$ )

A 'one pot' reaction was initially adopted for the synthesis of heteroleptic lanthanoid complexes  $[\text{Ln}(\text{L})_2(\mu\text{-Cl})]$  containing the  $\text{L}^2$  and  $\text{L}^3$  ligands. The addition of  $\text{LnCl}_3$  to 2 equivalents of  $\text{LiL}$  ( $\text{L} = \text{L}^2, \text{L}^3$ ), which was generated *in situ* in THF, resulted in an immediate colour change depending on the lanthanoid element (see also Chapter 3), and complete dissolution of the starting materials. Neodymium and ytterbium metals were examined for both  $\text{L}^2$  and  $\text{L}^3$  systems, and in the case of  $\text{L}^3$  lanthanum was also investigated. Extraction of the evaporated reaction mixtures with hexane removed the lanthanoid-containing product leaving insoluble  $\text{LiCl}$  and the compounds deposited as crystalline materials from hexane on standing.

The IR spectra (to  $650\text{ cm}^{-1}$ ) of all these products were identical with those of the homoleptic complexes  $[\text{Ln}(\text{L})_3]$  (Chapter 3) and the unit cell data for the Nd product agreed with those of  $[\text{Nd}(\text{L})_3]$  confirming that ligand redistribution had taken place.

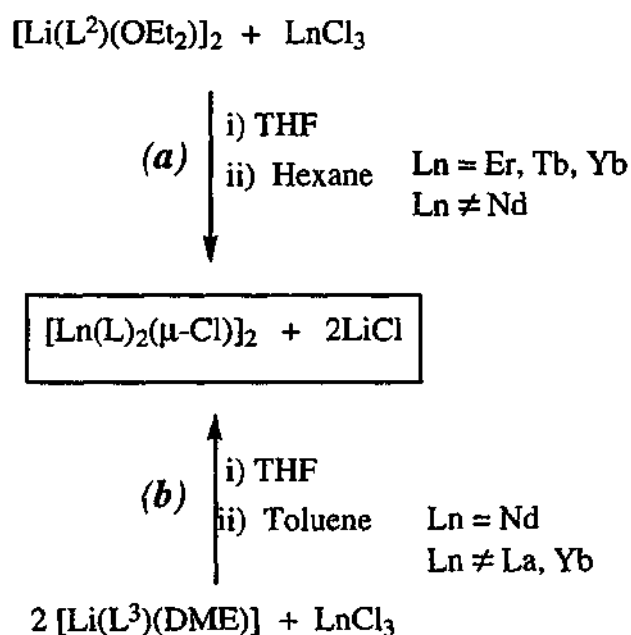


Scheme 4.1

Direct formation of  $[\text{Ln}(\text{L})_3]_3$  in THF would leave 0.33 equivalents of  $\text{LnCl}_3$  unreacted, and lanthanoid halides have low solubility in THF. Since all the  $\text{LnCl}_3$  dissolved, it suggests that the heteroleptic species is first formed, possibly stabilised as an 'ate' complex e.g. (A) *Scheme 4.1*. The formation of 'ate' complexes has previously been observed for other bulky organoamidolanthanoids, for example  $[\text{Yb}(\text{Me}_2\text{Si}(\text{OBu}^t)(\text{NBu}^t))_2(\mu\text{-Cl})_2\text{Li}(\text{THF})_2]$  [1] and  $[\text{Nd}\{(\text{CF}_3)_3\text{C}_6\text{H}_2\text{C}(\text{NSiMe}_3)_2\}(\mu\text{-Cl})_2\text{Li}(\text{THF})_2]$  [2]. Therefore the rearrangement

presumably occurs on addition of hexane with precipitation of LiCl and  $\text{LnCl}_3$  or even  $\text{LiLnCl}_4$ . This is contrary to the findings of the *in situ*  $[\text{Ln}(\text{L}^1)_2(\mu\text{-Cl})]_2$  preparation (see Chapter 2) where the heteroleptic derivatives were obtained from hexane. Isolation of the 'ate' complex (A) (Scheme 4.1) was unsuccessful due to the very high solubility of the reaction products in  $\text{Et}_2\text{O}$ .

Subsequently, reactions using isolated crystalline lithium salts of  $\text{L}^2$  and  $\text{L}^3$  viz. dimeric  $[\text{Li}(\text{L}^2)(\text{OEt}_2)]_2$  and monomeric  $[\text{Li}(\text{L}^3)(\text{DME})]$  from reaction of  $\text{LiBu}^n$  with the secondary amines, with a variety of  $\text{LnCl}_3$  compounds in a 1:2 Li to  $\text{LnCl}_3$  mole ratio were found to give  $\text{LnL}_2\text{Cl}$  complexes ( $\text{L} = \text{L}^2$ ,  $\text{Ln} = \text{Tb, Er, Yb}$ ;  $\text{L} = \text{L}^3$ ,  $\text{Ln} = \text{Nd}$ ) (Scheme 4.2 (a)). Typically hexane extraction was employed for the isolation of  $[\text{Ln}(\text{L}^2)_2(\mu\text{-Cl})]_2$  species whilst toluene was required for  $[\text{Nd}(\text{L}^3)_2(\mu\text{-Cl})]_2$  (Scheme 4.2 (b)). Analogous reactions of  $\text{Li}(\text{L}^2)$  with  $\text{NdCl}_3$  and  $\text{Li}(\text{L}^3)$  with  $\text{LaCl}_3$  or  $\text{YbCl}_3$  gave homoleptic  $[\text{Ln}(\text{L})_3]$  complexes. A similar outcome using *in situ* generated lithium salts was observed but isolation of  $[\text{Nd}(\text{L}^3)_2(\mu\text{-Cl})]_2$  contrasts the failure to obtain this compound by the *in situ* route (Scheme 4.1).



Scheme 4.2

Thus these results show that for  $\text{L}^2$  and  $\text{L}^3$  there is only a narrow window to the heteroleptic chlorides. Access to the smaller lanthanoid elements Tb, Er and Yb is available using  $\text{L}^2$  whilst  $\text{L}^3$  gives the derivative for the larger Nd but not La. In the case of  $\text{L}^2$  the larger neodymium gave  $[\text{Nd}(\text{L}^2)_3]$ . However for  $\text{L}^3$  this was the only element

yielding a heteroleptic complex with both the lighter (La) and heavier (Yb) extremes of the lanthanoid series yielding  $[\text{Ln}(\text{L}^3)_3]$ . Heteroleptic complexes of the other intermediate lanthanoids e.g. Pr, Sm, may be possible but these were not attempted.

Infrared spectra and elemental analyses (C, H, N) for  $[\text{Ln}(\text{L}^2)_2(\mu\text{-Cl})]_2$  (Ln = Tb, Er, Yb) and  $[\text{Nd}(\text{L}^3)_2(\mu\text{-Cl})]_2(\text{PhMe})$  were consistent with the presence of two ligand molecules ( $\text{L}^2$  or  $\text{L}^3$ ) and no coordinated THF. For both heteroleptic systems the majority of bands were similar to those of the corresponding homoleptic  $[\text{Ln}(\text{L})_3]$  complexes. However intense infrared absorptions of  $[\text{Ln}(\text{L}^2)_2(\mu\text{-Cl})]_2$  (Ln = Tb, Er, Yb) attributable to C—O—C stretching of the MeOAr substituent were observed as single bands near 1000 (antisymmetric) and 843  $\text{cm}^{-1}$  (symmetric). For *mer*- $[\text{Nd}(\text{L}^2)_3]$ , two bands were observed in each region perhaps owing to the *cis* and *trans* (Me)O—Yb—O(Me) arrangement around the metal centre. The presence of single bands in  $[\text{Ln}(\text{L}^2)_2(\mu\text{-Cl})]_2$  (Ln = Tb, Er, Yb) is consistent with solely *trans* ether groups in these structures (see below). Bands at 1266 and 859  $\text{cm}^{-1}$  were observed for  $[\text{Nd}(\text{L}^3)_2(\mu\text{-Cl})]_2(\text{PhMe})_2$  but not in  $[\text{Nd}(\text{L}^3)_3](\text{PhMe})_2$ , and a band of the latter at 802  $\text{cm}^{-1}$  was absent in the former, thereby distinguishing the spectra of the two complexes.

Despite the paramagnetism of  $[\text{Nd}(\text{L}^3)_2(\mu\text{-Cl})]_2(\text{PhMe})_2$ ,  $^1\text{H}$  NMR resonances attributable to the  $\text{L}^3$  ligand could be assigned (Chapter 8) whilst those of toluene were in the usual diamagnetic region and integrations confirmed the proposed composition. Only a single  $\text{L}^3$  environment was detected and this is consistent with the single type of  $\text{L}^3$  coordination in the solid state structure. Whilst the features of this NMR spectrum were similar to those of  $[\text{Nd}(\text{L}^3)_3]$ , small changes in the chemical shift values were observed. These changes may be due to differences in the concentrations of the two samples and therefore this method is not a reliable indicator of the identity of the complex at present. With  $[\text{Nd}(\text{L}^3)_3]$ , the single set of resonances are indicative of exchange in solution between the two coordination environments (*cis* / *trans*) of the  $\text{L}^3$  ligands in the solid state. The visible/near infrared spectrum of  $[\text{Nd}(\text{L}^3)_2(\mu\text{-Cl})]_2(\text{PhMe})_2$  showed absorptions characteristic of  $\text{Nd}^{3+}$ .<sup>[3]</sup> Mass spectra were not obtained due to instrumental difficulties. Single crystal X-ray diffraction studies on each of the heteroleptic complexes confirmed compositions from the spectroscopic and analytical data.

#### 4.2.1.1 Structures of $[\text{Ln}(\text{L}^2)_2(\mu\text{-Cl})_2]$ , ( $\text{Ln} = \text{Tb}, \text{Er}$ and $\text{Yb}$ )

Each  $[\text{Ln}(\text{L}^2)_2(\mu\text{-Cl})_2]$  ( $\text{Ln} = \text{Tb}, \text{Er}, \text{Yb}$ ) complex crystallises from hot hexane as large prisms. They all have the monoclinic centrosymmetric space group  $P2_1/n$  with one dimer comprising the asymmetric unit. Data collection parameters are listed in *Table 4.1*. Selected bond lengths and angles for each  $[\text{Ln}(\text{L}^2)_2(\mu\text{-Cl})_2]$  ( $\text{Ln} = \text{Tb}, \text{Er}, \text{Yb}$ ) molecule are given in *Table 4.2* and *Table 4.3* respectively. The molecular structures of  $[\text{Ln}(\text{L}^2)_2(\mu\text{-Cl})_2]$  ( $\text{Ln} = \text{Tb}, \text{Er}, \text{Yb}$ ) are dimeric with two lanthanoid atoms bridged by two chlorine atoms (*Figure 4.1*,  $\text{Ln} = \text{Yb}$ ). Two chelating  $[\text{L}^2]$  units are bound to each lanthanoid centre completing a six-coordination environment with a very distorted octahedral geometry. Clearly, the steric demand of two  $\text{L}^2$  ligands and one chloride is not sufficient to saturate all coordination sites on the lanthanoid metal since dimerisation takes place. Alternatively coordination of a molecule of THF generating monomeric  $\text{Ln}(\text{L})_2\text{Cl}(\text{THF})$  may occur in THF solution prior to workup in hexane. The chloride bridged dimer is presumably less crowded than  $\text{Ln}(\text{L})_2\text{Cl}(\text{THF})$  with the steric coordination number<sup>[4]</sup> for THF (1.2) larger than that for chloride (1.0) in addition to longer  $\text{Ln}-\mu\text{-Cl}$  than  $\text{Ln}-\text{Cl}_{\text{ter}}$  distances which will also reduce crowding. Thus in the absence of an excess of THF, steric oversaturation of  $\text{Ln}(\text{L})_2\text{Cl}(\text{THF})$  causes elimination of THF from the lanthanoid coordination sphere and subsequent dimerisation. The axial positions are occupied by the O(Me) group on  $\text{L}^2$  with  $\text{O}(1)-\text{Ln}(1)-\text{O}(2)$  angles close to the expected  $180^\circ$ . The remaining  $\text{NSiMe}_3$  units and chloride atoms are located at the equatorial sites. Deviations from ideal octahedral geometry result from the bulky  $\text{NSiMe}_3$  groups lying above and below the equatorial plane. This presumably is a result of steric repulsion between the *cis*  $\text{NSiMe}_3$  groups as is also observed for the homoleptic complex  $[\text{Nd}(\text{L}^2)_3]$  (Chapter 3). The distortion is evident in the very large intra-ligand *cis*  $\text{N}(1)-\text{Ln}(1)-\text{O}(2)$  and *cis*  $\text{N}(3)-\text{Ln}(2)-\text{O}(4)$  angles which range from  $119-130^\circ$  instead of the expected  $90^\circ$ . The two  $\text{L}^2$  ligands on each metal centre are not equivalent. Thus the  $\text{O}(2)-\text{Ln}(1)-\text{Cl}$  and  $\text{O}(4)-\text{Ln}(2)-\text{Cl}$  angles are similar for both chlorides and are in the range  $80-90^\circ$ , whilst the corresponding  $\text{O}(1)-\text{Ln}(1)-\text{Cl}(1)/\text{O}(1)-\text{Ln}(1)-\text{Cl}(2)$  and  $\text{O}(3)-\text{Ln}(2)-\text{Cl}(1)/\text{O}(3)-\text{Ln}(2)-\text{Cl}(2)$  angles are different with the angle to one chloride  $30^\circ$  larger than to the other. Furthermore, the central  $\text{Ln}_2\text{Cl}_2$  core is not planar (*Table 4.3*) as there is a variation in the *cis*- $\text{Cl}-\text{Ln}-\text{O}$  angles ( $79.30(7)-108.44(19)^\circ$ ) from the expected  $90^\circ$ . The distance between the lanthanoid centres is non-bonding and varies in line with the ionic radii of the

respective metals (*Table 4.2*).

The coordination geometry of the metal centre in  $[\text{Ln}(\text{L}^2)_2(\mu\text{-Cl})]_2$  is similar to that of the homoleptic derivative  $[\text{Nd}(\text{L}^2)_3]$  (Chapter 3). In the former the two bridging chloride atoms replace the equatorial  $\text{L}^2$  ligand in  $[\text{Nd}(\text{L}^2)_3]$ . Considerably larger N—Ln—N angles for the heteroleptic derivative is observed and this suggests that the  $\text{L}^2$  ligands are rotating about the axial axis toward the two chloride atoms. This presumably is a result of the lower steric demand of two chlorides versus one  $\text{L}^2$  ligand. The Ln—N and Ln—O bond lengths in  $[\text{Ln}(\text{L}^2)_2(\mu\text{-Cl})]_2$  (Ln = Tb, Er and Yb) are slightly shorter than those of  $[\text{Nd}(\text{L}^2)_3]$  after accounting for the differences in ionic radii and this further emphasises the lower steric crowding of the heteroleptic complexes.

A list of structurally characterised  $[\text{Ln}\{\text{N}(\text{RR}')\}\text{Cl}]$  complexes is compiled in *Table 4.4* with values derived from the subtraction of appropriate  $\text{Ln}^{3+}$  ionic radii from the Ln—N and Ln—Cl distances. These data show that the values for the current structures are in the middle of the observed ranges and therefore are considered to be not unusual. Indeed the closely related 'ate' complex  $[\text{Yb}\{\text{Me}_2\text{Si}(\text{O}^-\text{Bu}')(\text{N}^+\text{Bu}')\}_2(\mu\text{-Cl})_2\text{Li}(\text{THF})_2]$ <sup>[1]</sup> has marginally longer Yb—N distances but shorter Yb—Cl bond lengths consistent with the bulky substituents on the amido ligand. These values of the Ln—Cl bonds are similar with  $[\text{Yb}(\text{Cl})_2(\mu\text{-Cl})(\text{THF})_2]_2$  (which has an analogous donor array to  $[\text{Yb}(\text{L}^2)_2(\mu\text{-Cl})]_2$  i.e. two *cis*  $\mu$ -chlorides, two *cis* anion donors and two *trans* neutral oxygens)<sup>[5]</sup> and are longer than the Yb—Cl distances of  $[\text{Yb}(\text{C}_5\text{H}_5)_2(\mu\text{-Cl})]_2$ .<sup>[6]</sup> The steric coordination number summations<sup>[4]</sup> for  $[\text{Yb}(\text{Cl})_2(\mu\text{-Cl})(\text{THF})_2]_2$  (6.42) and  $[\text{Yb}(\text{C}_5\text{H}_5)_2(\mu\text{-Cl})]_2$  (6.08) suggest that the difference between their Ln—Cl distances is not a result of steric effects. In the complex  $[\text{Yb}(\text{Cl})_2(\mu\text{-Cl})(\text{THF})_2]_2$  each chloride is *trans* to another chloride which may cause lengthening of the Yb—Cl distances. The bent metallocene structure of  $\text{Cp}_2\text{LnX}$  complexes allows the ligand (X) to more closely approach the metal centre in the wedge formed by the tilted planes of the Cp ligands. However, for dimeric complexes such as  $[\text{Yb}(\text{C}_5\text{H}_5)_2(\mu\text{-Cl})]_2$  replacing the simple  $\text{C}_5\text{H}_5$  with the larger  $\text{C}_5\text{Me}_5$  ligand results in steric repulsion between the two  $\text{Ln}(\text{C}_5\text{Me}_5)_2$  units. This causes lengthening of the Ln—Cl distance and ultimately structural changes occur. For example  $[\text{Sm}(\text{C}_5\text{Me}_5)_2(\mu\text{-Cl})]_3$  is trimeric and in  $[\text{Sm}(\text{C}_5\text{Me}_5)_2\text{Cl}]_2(\mu\text{-Cl})$  there is only a single chloride bridge and the two  $\text{Sm}(\text{C}_5\text{Me}_5)_2$  units are rotated by  $90^\circ$ .<sup>[7]</sup> Subtraction of the appropriate ionic radii<sup>[8]</sup> from

the Ln—Cl bonds in  $[\text{Ln}(\text{L}^2)_2(\mu\text{-Cl})]_2$  gives values that are similar to  $[\text{Sm}(\text{C}_5\text{Me}_5)_2(\mu\text{-Cl})]_2$  (Table 4.4) suggesting steric similarity between  $\text{L}^2$  and  $\text{C}_5\text{Me}_5$ , but the current structures are more like those of the unsubstituted cyclopentadienyl complex  $[\text{Yb}(\text{C}_5\text{H}_5)_2(\mu\text{-Cl})]_2$ . This may reflect both the more adaptable coordination environment of the 'edge-on' bound bidentate organoamide ligands compared with the 'face-on' cyclopentadienyl ligand and a possible lengthening of the Ln—Cl bond due to the *trans* influence of the amide nitrogens.

The  $\text{L}^2$  ligand environment is planar for each of the  $[\text{Ln}(\text{L}^2)_2(\mu\text{-Cl})]_2$  complexes with the O(Me) substituent in line with the aromatic backbone (see Table 4.5 for C(X0)—O(X)—C(X2)—C(X3) (X = 1-4) angles). There is little variation in the coordination architecture of the  $\text{L}^2$  ligands between the three complexes. However, the interplanar angles between the Ln-N-O plane and the arene backbone are slightly larger than the corresponding angles in  $[\text{Nd}(\text{L}^2)_3]$  complex (see Chapter 3).

Table 4.1 Summary of Crystallographic Data for  $[\text{Ln}(\text{L}^2)_2(\mu\text{-Cl})]_2$

Compound	$[\text{Tb}(\text{L}^2)_2(\mu\text{-Cl})]_2$	$[\text{Er}(\text{L}^2)_2(\mu\text{-Cl})]_2$	$[\text{Yb}(\text{L}^2)_2(\mu\text{-Cl})]_2$
Formula	$\text{C}_{40}\text{H}_{64}\text{Cl}_2\text{N}_4\text{O}_4\text{Si}_4\text{Tb}_2$	$\text{C}_{40}\text{H}_{64}\text{Er}_2\text{Cl}_2\text{N}_4\text{O}_4\text{Si}_4$	$\text{C}_{40}\text{H}_{64}\text{Cl}_2\text{N}_4\text{O}_4\text{Si}_4\text{Yb}_2$
M	1166.06	1182.73	1194.3
<i>a</i> (Å)	14.5575(1)	14.6389(1)	14.6143(3)
<i>b</i> (Å)	18.2621(2)	18.1148(1)	18.0518(4)
<i>c</i> (Å)	19.0461(2)	19.0169(2)	19.0058(5)
$\alpha$ (°)	90	90	90
$\beta$ (°)	92.653(1)	92.875(1)	92.327(1)
$\gamma$ (°)	90	90	90
V (Å <sup>3</sup> )	5058.0(18)	5036.6(17)	5009.9(17)
Crystal system	monoclinic	monoclinic	Monoclinic
Space group	<i>P</i> 2 <sub>1</sub> / <i>n</i>	<i>P</i> 2 <sub>1</sub> / <i>n</i>	<i>P</i> 2 <sub>1</sub> / <i>n</i>
Z	4	4	4
Diffractometer	Nonius Kappa CCD	Nonius Kappa CCD	Nonius Kappa CCD
$\rho_{\text{calc}}$ (g cm <sup>-3</sup> )	1.531	1.560	1.583
$\mu$ (MoK $\alpha$ ) (mm <sup>-1</sup> )	3.013	3.550	3.953
$2\theta_{\text{max}}$ (°)	56.6	56.6	56.6
<i>N</i> , <i>N</i> <sub>o</sub>	12457, 9175	12025, 8910	12341, 6357
<i>R</i> , <i>R</i> <sub>w</sub> (observed data)	0.0369, 0.0728	0.0307, 0.0667	0.0686, 0.1023
<i>R</i> , <i>R</i> <sub>w</sub> (all data)	0.0639, 0.0809	0.0545, 0.0737	0.1795, 0.1272



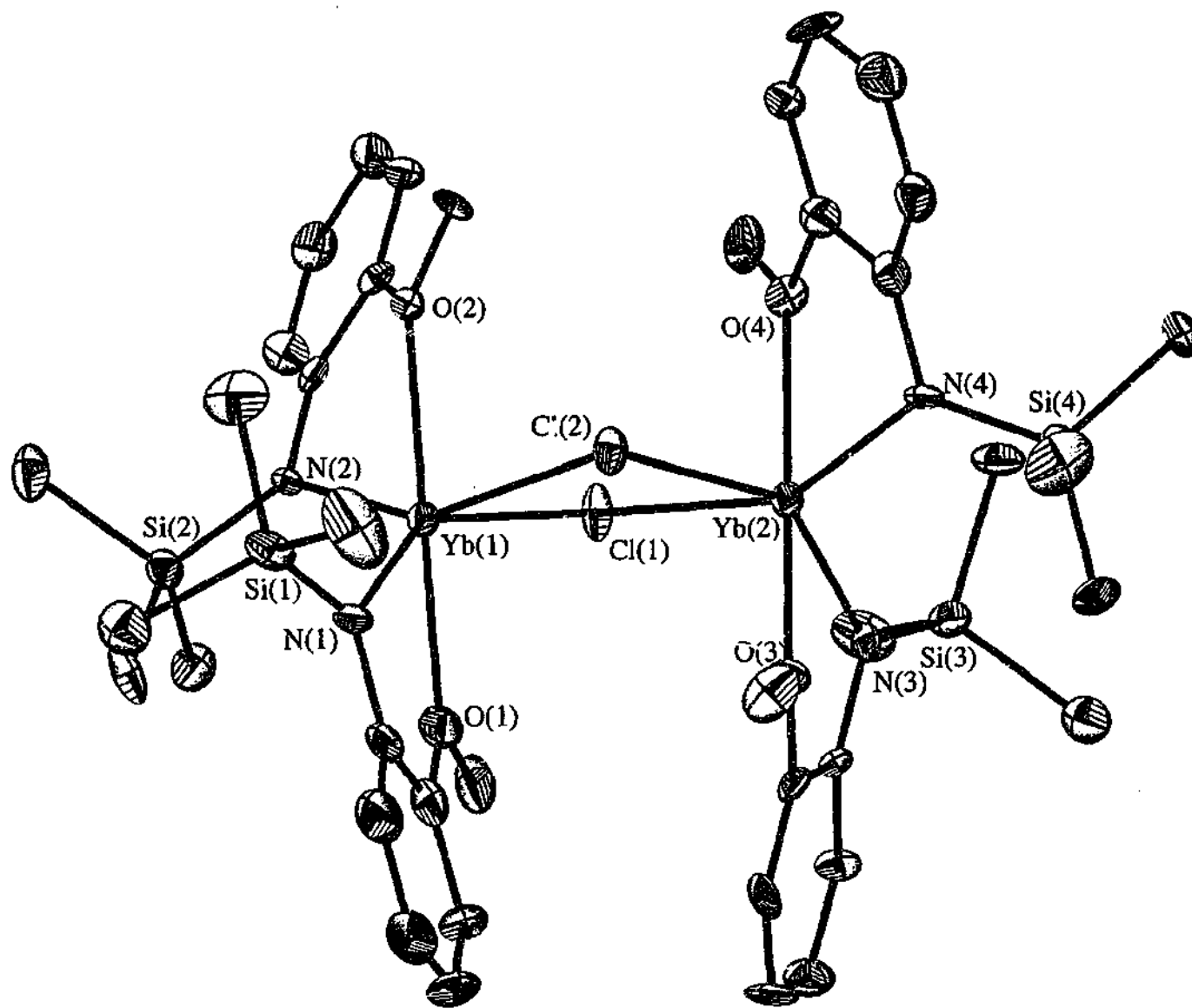


Figure 4.1 Molecular Structure of  $[Yb(L^2)_2(\mu\text{-Cl})]_2$

**Table 4.2** Metal atom distances (Å) in  $[\text{Ln}(\text{L}^2)_2(\mu\text{-Cl})_2]$  with estimated standard deviations in parentheses

Complex	$[\text{Tb}(\text{L}^2)_2(\mu\text{-Cl})_2]$	$[\text{Er}(\text{L}^2)_2(\mu\text{-Cl})_2]$	$[\text{Yb}(\text{L}^2)_2(\mu\text{-Cl})_2]$
<i>Bond distance (Å)</i>			
Ln(1)—N(1)	2.266(3)	2.233(3)	2.184(8)
Ln(1)—N(2)	2.265(3)	2.221(3)	2.190(7)
Ln(2)—N(3)	2.257(3)	2.225(3)	2.188(8)
Ln(2)—N(4)	2.257(3)	2.223(3)	2.202(8)
<i>Average</i>	2.26	2.23	2.19
Ln(1)—O(1)	2.416(3)	2.354(2)	2.350(7)
Ln(1)—O(2)	2.437(3)	2.383(2)	2.370(6)
Ln(2)—O(3)	2.414(3)	2.353(2)	2.337(7)
Ln(2)—O(4)	2.414(3)	2.363(2)	2.354(6)
<i>Average</i>	2.42	2.36	2.35
Ln(1)—Cl(1)	2.748(1)	2.713(1)	2.680(2)
Ln(1)—Cl(2)	2.727(1)	2.683(1)	2.668(3)
Ln(2)—Cl(1)	2.740(1)	2.701(1)	2.678(2)
Ln(2)—Cl(2)	2.734(1)	2.703(1)	2.675(2)
<i>Average</i>	2.74	2.70	2.68
Ln(1)—Ln(2)	4.1545(9)	4.1048(8)	4.066(1)

Table 4.3 Metal atom angles ( $^{\circ}$ ) in  $[\text{Ln}(\text{L}^2)_2(\mu\text{-Cl})]_2$ 

Complex	$[\text{Tb}(\text{L}^2)_2(\mu\text{-Cl})]_2$	$[\text{Er}(\text{L}^2)_2(\mu\text{-Cl})]_2$	$[\text{Yb}(\text{L}^2)_2(\mu\text{-Cl})]_2$
<i>Angles (<math>^{\circ}</math>)</i>			
N(1)—Ln(1)—N(2)	116.34(11)	113.80(10)	113.5(3)
N(3)—Ln(2)—N(4)	117.06(11)	113.21(10)	112.7(3)
O(1)—Ln(1)—O(2)	161.28(9)	162.54(8)	162.2(3)
O(3)—Ln(2)—O(4)	166.85(9)	168.31(7)	166.6(2)
Cl(1)—Ln(1)—Cl(2)	79.38(3)	79.57(3)	79.55(7)
Cl(1)—Ln(2)—Cl(2)	79.38(3)	79.42(3)	79.47(7)
Ln(1)—Cl(1)—Ln(2)	98.41(3)	98.62(3)	98.72(8)
Ln(1)—Cl(2)—Ln(2)	99.05(4)	99.31(3)	99.12(8)
N(1)—Ln(1)—O(1)	68.23(11)	69.83(9)	71.5(3)
N(2)—Ln(1)—O(2)	69.45(10)	70.84(9)	71.1(2)
N(3)—Ln(2)—O(3)	69.01(10)	70.72(9)	71.8(3)
N(4)—Ln(2)—O(4)	69.82(10)	71.47(9)	72.0(3)
N(1)—Ln(1)—O(2)	129.52(10)	126.23(9)	124.7(3)
N(3)—Ln(2)—O(4)	123.66(10)	119.63(9)	120.0(3)
N(1)—Ln(1)—Cl(1)	88.71(9)	88.85(7)	88.5(2)
N(2)—Ln(1)—Cl(2)	89.51(8)	90.89(7)	91.0(2)
N(1)—Ln(1)—Cl(2)	141.33(9)	143.13(7)	144.3(2)
N(2)—Ln(1)—Cl(1)	149.43(8)	150.89(7)	151.2(2)
N(3)—Ln(2)—Cl(1)	140.26(8)	142.32(7)	143.3(2)
N(4)—Ln(2)—Cl(2)	149.06(8)	151.24(7)	152.3(2)
N(3)—Ln(2)—Cl(2)	86.33(9)	86.64(7)	86.7(2)
N(4)—Ln(2)—Cl(1)	92.06(8)	94.36(7)	93.8(2)
O(1)—Ln(1)—Cl(1)	107.56(7)	108.02(7)	108.49(19)
O(2)—Ln(1)—Cl(2)	85.10(7)	86.65(6)	86.81(16)
O(1)—Ln(1)—Cl(2)	80.48(8)	80.64(7)	80.6(2)
O(2)—Ln(1)—Cl(1)	81.19(7)	81.12(6)	81.17(16)
O(3)—Ln(2)—Cl(1)	79.30(7)	79.89(6)	79.92(18)
O(4)—Ln(2)—Cl(2)	80.48(7)	80.72(6)	81.31(17)
O(3)—Ln(2)—Cl(2)	105.33(7)	106.38(6)	106.82(18)
O(4)—Ln(2)—Cl(1)	90.41(7)	92.58(6)	91.37(17)
N(1)—Ln(1)—O(2)	129.52(10)	126.23(9)	124.7(3)
N(2)—Ln(1)—O(1)	98.40(11)	92.29(9)	96.5(3)
N(3)—Ln(2)—O(4)	123.66(10)	119.63(9)	120.0(3)
N(4)—Ln(2)—O(3)	102.11(10)	100.00(9)	98.2(3)

Table 4.4 Metal-nitrogen distances of a selection of organoamide lanthanoid complexes

Compound	Ref	Coordination number	Av. Ln—N distance (d(N)) Å	Av. Ln—Cl distance (d(Cl)) Å	Ionic Radii of Ln <sup>3+</sup> (ir) Å <sup>a</sup>	d(N)—ir (Å)	d(Cl)—ir (Å)
[Ln(L <sup>2</sup> ) <sub>2</sub> (μ-Cl)] <sub>2</sub> (Ln = Tb, Er, Yb)	this work	6	see Table 4.2		0.92, 0.89, 0.87	1.32—1.34	1.79—1.83
[Nd(L <sup>3</sup> ) <sub>2</sub> (μ-Cl)] <sub>2</sub> (PhMe) <sub>2</sub>	this work	6	see Table 4.6		0.98	1.32—1.34	1.80—1.87
[Nd{N(2,6-(Pr <sup>i</sup> ) <sub>2</sub> C <sub>6</sub> H <sub>3</sub> )(SiMe <sub>3</sub> ) <sub>2</sub> (THF)(μ-Cl) <sub>2</sub> Li(THF) <sub>2</sub> }]	[9]	5	2.30	2.76	0.92 <sup>b</sup>	1.38	1.84
[Sm{N(SiMe <sub>3</sub> ) <sub>2</sub> (μ-Cl)(THF)} <sub>2</sub> ]	[10]	5	2.27	2.78	0.90 <sup>b</sup>	1.37	1.86
[Gd{N(SiMe <sub>3</sub> ) <sub>2</sub> (μ-Cl)(THF)} <sub>2</sub> ]	[11]	5	2.25	2.75	0.89 <sup>b</sup>	1.36	1.86
[Yb{N(SiMe <sub>3</sub> ) <sub>2</sub> (μ-Cl)(THF)} <sub>2</sub> ]	[11]	5	2.19	2.68	0.82 <sup>b</sup>	1.37	1.86
[Sm{N(Cy) <sub>2</sub> (μ-Cl)(THF)} <sub>2</sub> ] <sup>c</sup>	[12]	5	2.21	2.80	0.90 <sup>b</sup>	1.31	1.90
[Nd{(CF <sub>3</sub> ) <sub>3</sub> C <sub>6</sub> H <sub>2</sub> C(NSiMe <sub>3</sub> ) <sub>2</sub> (μ-Cl) <sub>2</sub> Li(THF) <sub>2</sub> }]	[2]	6	2.53	2.71	0.98	1.55	1.73
[Sm{LiBu'DAB) <sub>2</sub> (THF)}(μ-Cl) <sub>2</sub> Li(THF) <sub>2</sub> ] <sup>d</sup>	[13]	8	2.45	2.88	1.08	1.37	1.80
[Yb{Me <sub>2</sub> Si(OBu <sup>i</sup> )(NBu <sup>i</sup> ) <sub>2</sub> (μ-Cl) <sub>2</sub> Li(THF) <sub>2</sub> }]	[1]	6	2.24	2.64	0.87	1.37	1.77
[Er{(Pr <sup>i</sup> )TP}(μ-Cl)] <sub>2</sub> <sup>e</sup>	[14]	6	2.32	2.73	0.89	1.44	1.84
[Yb{(Pr <sup>i</sup> )TP}(μ-Cl)] <sub>2</sub> <sup>e</sup>	[14]	6	2.30	2.71	0.87	1.43	1.84
[Y(η <sup>5</sup> ;η <sup>1</sup> -C <sub>5</sub> Me <sub>4</sub> SiMe <sub>2</sub> NCMe <sub>2</sub> Et)(THF)(μ-Cl)] <sub>2</sub>	[15]	7	2.24	2.74	0.96	1.28	1.78
[Yb(η <sup>5</sup> -C <sub>5</sub> H <sub>5</sub> ) <sub>2</sub> (μ-Cl)] <sub>2</sub>	[6]	8	—	2.64	0.98	—	1.66
[Lu(η <sup>5</sup> -C <sub>5</sub> H <sub>4</sub> SiMe <sub>3</sub> ) <sub>2</sub> (μ-Cl)] <sub>2</sub>	[16]	8	—	2.62	0.98	—	1.64
[Sm(η <sup>5</sup> -C <sub>5</sub> Me <sub>5</sub> ) <sub>2</sub> (μ-Cl)] <sub>3</sub>	[7]	8	—	2.88	1.08	—	1.80
[Yb(Cl) <sub>2</sub> (μ-Cl)(THF) <sub>2</sub> ] <sub>2</sub> <sup>f</sup>	[5]	6	—	2.68	0.87	—	1.81

<sup>a</sup> Values derived from R.D. Shannon<sup>[8]</sup>; <sup>b</sup> numbers extrapolated from values of higher coordination number from <sup>a</sup>; <sup>c</sup> Cy = cyclohexyl; <sup>d</sup> Bu'DAB = 1,4-diazabutadiene; <sup>e</sup> [(Pr<sup>i</sup>)TP]<sub>2</sub><sup>2-</sup> = 1,3-bis(2-(isopropylamino)troponimate)propane; <sup>f</sup> value of the Yb—μ-Cl distance only.

Table 4.5 Torsion and interplanar angles in  $[\text{Ln}(\text{L}^2)_2(\mu\text{-Cl})]_2$ 

Compounds	$[\text{Tb}(\text{L}^2)_2(\mu\text{-Cl})]_2$	$[\text{Er}(\text{L}^2)_2(\mu\text{-Cl})]_2$	$[\text{Yb}(\text{L}^2)_2(\mu\text{-Cl})]_2$
<i>Torsion angles (°)</i>			
C(10)—O(1)—C(12)—C(13)	5.91(6)	7.59(5)	6.6(1)
C(20)—O(2)—C(22)—C(23)	9.50(5)	10.30(4)	11.9(1)
C(30)—O(3)—C(32)—C(33)	9.86(5)	11.49(5)	10.7(1)
C(40)—O(4)—C(42)—C(43)	14.24(5)	15.97(5)	17.1(1)
<i>Interplanar angles (°)</i>			
P(1A) <sup>a</sup> —P(1B) <sup>b</sup>	13.55(2)	15.91(1)	18.04(4)
P(2A) <sup>c</sup> —P(2B) <sup>d</sup>	33.87(2)	34.90(1)	33.82(4)
P(3A) <sup>e</sup> —P(3B) <sup>f</sup>	20.09(1)	23.49(1)	22.64(3)
P(4A) <sup>g</sup> —P(4B) <sup>h</sup>	33.25(2)	34.04(1)	34.02(4)

<sup>a</sup> P(1A) = the plane defined by Ln—N(1)—O(1) atoms; <sup>b</sup> P(1B) = plane defined by the arene backbone (C(11)—C(16)); <sup>c</sup> P(2A) = the plane defined by Ln—N(2)—O(2) atoms; <sup>d</sup> P(2B) = plane defined by the arene backbone (C(21)—C(26)); <sup>e</sup> P(3A) = the plane defined by Ln—N(3)—O(3) atoms; <sup>f</sup> P(3B) = plane defined by the arene backbone (C(31)—C(36)); <sup>g</sup> P(4A) = the plane defined by Ln—N(4)—O(4) atoms; <sup>h</sup> P(4B) = plane defined by the arene backbone (C(41)—C(46)).

#### 4.2.1.2 Structure of $[\text{Nd}(\text{L}^3)_2(\mu\text{-Cl})_2](\text{PhMe})_2$

Single crystals of  $[\text{Nd}(\text{L}^3)_2(\mu\text{-Cl})_2](\text{PhMe})_2$  suitable for structure determination were obtained from a concentrated toluene solution. The complex  $[\text{Nd}(\text{L}^3)_2(\mu\text{-Cl})_2](\text{PhMe})_2$  is dimeric with bridging chloride atoms and two  $\text{L}^3$  units positioned in a similar fashion to that of  $\text{L}^2$  in  $[\text{Nd}(\text{L}^2)_2(\mu\text{-Cl})_2]$ . A toluene of crystallisation is present in each asymmetric unit that comprises half the dimer. A molecular projection of  $[\text{Nd}(\text{L}^3)_2(\mu\text{-Cl})_2]$  is pictured in *Figure 4.2*. Data collection parameters and selected bond distances and angles are listed in *Table 4.6* and *Table 4.7* respectively. A crystallographic inversion centre is located in the middle of the  $\text{Nd}_2\text{Cl}_2$  plane. The neodymium atoms are six-coordinate having two chelating  $\text{L}^3$  units in addition to two  $\mu_2\text{-Cl}$  atoms in a distorted octahedral environment. This distortion from regular octahedral is slightly greater than for  $[\text{Ln}(\text{L}^2)_2(\mu\text{-Cl})_2]$  complexes as evidenced by narrower *trans*  $\text{O—Ln—O}$  and *trans*  $\text{N—Ln—Cl}$  angles. The *trans*  $\text{O}(1)\text{—Nd}(1)\text{—O}(2)$  angle is also smaller than the corresponding angle in the homoleptic derivative  $[\text{Nd}(\text{L}^3)_3]$  (see Chapter 3). The  $\text{Nd—N}$  and  $\text{Nd—O}$  distances are similar to those found in  $[\text{Nd}(\text{L}^3)_3]$  (2.386(2)—2.396 and 2.543(2)—2.575(1) Å) (*Table 3.6*, Chapter 3). The chlorine atoms are somewhat unsymmetrically bound between the neodymium atoms with the bond lengths differing by 0.07 Å, i.e. much more than for the corresponding  $\text{L}^2$  complex (*Table 4.2*).

Subtraction of the appropriate ionic radii from the  $\text{Nd—N}$  and  $\text{Nd—O}$  distances (*Table 4.4*) shows similar bonding of the amide unit but marginally longer coordination of the ether substituent than for  $[\text{Ln}(\text{L}^2)_2(\mu\text{-Cl})_2]$ . This is consistent with the larger phenyl ether on  $\text{L}^3$  versus the methyl ether on  $\text{L}^2$ . Similar treatment of the  $\text{Nd—Cl}$  bond lengths in  $[\text{Nd}(\text{L}^3)_2(\mu\text{-Cl})_2]$  gives one value within the range observed for those in  $[\text{Ln}(\text{L}^2)_2(\mu\text{-Cl})_2]$  but also has one slightly longer. This may be a result of greater steric crowding present in the former case and is similar to the changes in the  $\text{Ln—Cl}$  distances found for increased substitution of the cyclopentadienyl ligands in  $\text{Ln}(\text{Cp})_2(\mu\text{-Cl})$  systems (*Table 4.4*).

The phenyl ether group of  $\text{L}^3$  is bent away from the arene backbone (torsion angle  $\text{C}(13)\text{—C}(12)\text{—O}(1)\text{—C}(111)$  50.87(3)°,  $\text{C}(23)\text{—C}(22)\text{—O}(2)\text{—C}(211)$  62.85(3)°) and rotated near perpendicular to it (interplanar angle 71.41(4), 78.95(7)°). This  $\text{L}^3$  arrangement is similar to that of  $\text{L}^3\text{H}$ . A remarkable feature of the coordination of the two  $\text{L}^3$  ligands to neodymium is the noticeable tilt in one of the aromatic backbones

(C(21)—C(26)). Thus the interplanar angle to the Nd-N-O plane is  $61.41(7)^\circ$  which is almost double that of the other  $L^3$  ligand ( $31.49(6)^\circ$ ) and the maximum observed for the homoleptic  $[\text{Ln}(L^3)_3]$  derivatives. As a result two of the carbon atoms (C(21) and C(22)) approach the metal centre with distances of 2.911(2) and 3.035(2) Å which are only marginally longer than  $\pi$ -arene lanthanoid interactions e.g.  $[\text{Nd}(\eta^6\text{-PhH})(\text{AlCl}_4)_3]$ <sup>[17]</sup> with Nd—C distances of 2.93(2) to 2.94(2) Å. Examples of secondary arene coordination from phenyl substituted ligands has been observed in neodymium aryloxide complexes, e.g.  $[\text{Nd}(\text{Odpp})_3]$  (Odpp' = 2,6-diphenylphenolate) with one  $\eta^6$ - and one  $\eta^1$ -Ph...Nd interaction and  $[\text{Nd}(\text{Odpp})_3(\text{THF})]$  with one  $\eta^3$ -contact. Subtracting the metal ionic radii<sup>[8]</sup> from the Nd—C distances gives values for  $[\text{Nd}(\text{Odpp})_3]$  of 2.16—2.37 Å for formal CN = 3 or 1.92—2.12 Å for CN = 7 and for  $[\text{Nd}(\text{Odpp})_3(\text{THF})]$  of 2.23—2.27 Å for CN = 4 or 2.17 and 2.21 for CN = 5<sup>[18]</sup> which are longer than values derived from the current structure (1.93 and 2.05 Å). The lanthanoid  $\pi$ -arene interactions exclusively have the Ln—C bonds approaching a perpendicular geometry to the plane of the arene ring (Nd(1)—centre of C(21)—C(22) bond—centroid of C(21)—C(26) ring angle is  $139.4^\circ$ ). This contrasts the more 'edge-on' binding of the other unique  $L^3$  ligand in  $[\text{Nd}(L^3)_2(\mu\text{-Cl})]_2$  and the  $L^2$  ligands in both the  $[\text{Ln}(L)_3]$  ( $L = L^2, L^3$ ) and  $[\text{Ln}(L^3)_2(\mu\text{-Cl})]_2$  complexes. Even though the last two have metal carbon separations only slightly larger (greater than 2.25 Å) than the close contacts in  $[\text{Nd}(L^3)_2(\mu\text{-Cl})]_2$  these presumably do not represent an interaction of this type. The tilted  $L^3$  ligand shows a resemblance to the bonding of the  $\eta^4$ -diazabutadiene ligand system in for example  $[\text{Sm}\{\text{Li}(\text{Bu}^t\text{DAB})_2(\text{THF})\}(\mu\text{-Cl})_2\text{Li}(\text{THF})_2]$ <sup>[13]</sup> The samarium nitrogen distances are comparable with those of the current structure (*Table 4.4*) but the Sm centre interacts very strongly with the  $\pi$ -electron system of the C=C bond leading to a much shorter average Sm—C distance of 2.67 Å (subtraction value for eight-coordinate  $\text{Sm}^{3+}$  is 1.59 Å) which is typical of a Sm—C(Cp) separation.

Table 4.6. Summary of Crystallographic Data for  $[\text{Nd}(\text{L}^3)_2(\mu\text{-Cl})]_2 \cdot (\text{PhMe})_2$ 

Compound	$[\text{Nd}(\text{L}^3)_2(\mu\text{-Cl})]_2 \cdot (\text{PhMe})_2$
Formula	$\text{C}_{74}\text{H}_{88}\text{Cl}_2\text{N}_4\text{Nd}_2\text{O}_4\text{Si}_4$
$M$	1569.22
$a$ (Å)	10.1897(1)
$b$ (Å)	13.3375(2)
$c$ (Å)	15.5566(2)
$\alpha$ (°)	74.48(3)
$\beta$ (°)	77.36(3)
$\gamma$ (°)	67.38(3)
$V$ (Å <sup>3</sup> )	1848.0(6)
Crystal system	Triclinic
Space Group	$P(-1)$
$Z$	1
Diffractometer	Nonius Kappa CCD
$\rho_{\text{calcd}}$ (g cm <sup>-3</sup> )	1.410
$\mu(\text{MoK}\alpha)$ (mm <sup>-1</sup> )	1.575
$2\theta_{\text{max}}$ (°)	56.6
$N, N_o$	8040, 7457
$R, R_w$ (observed data)	0.0250, 0.0552
$R, R_w$ (all data)	0.0292, 0.0567



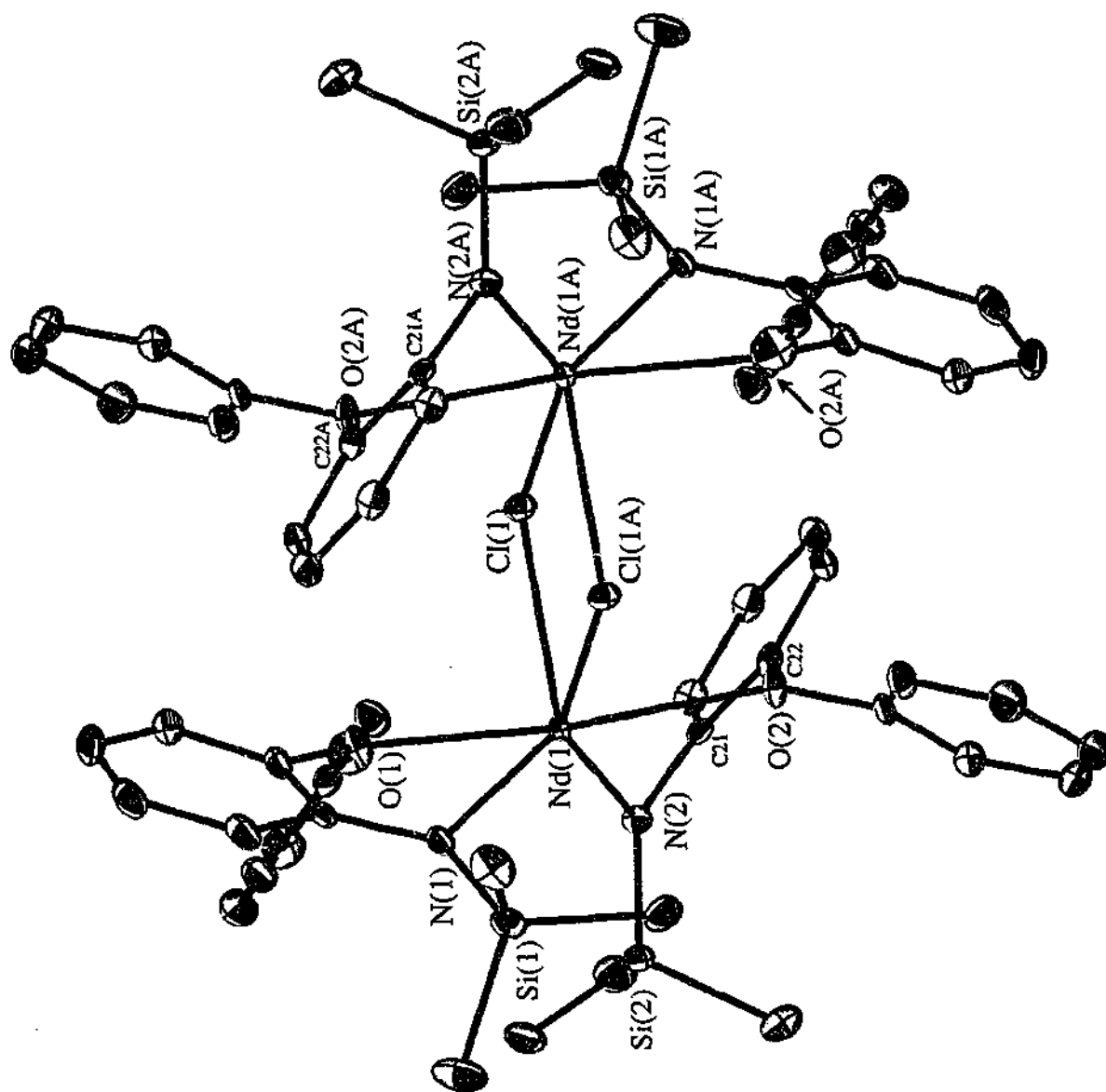


Figure 4.2 Solid State Structure of  $[Nd(L')_2(\mu-Cl)]_2 \cdot (PhMe)_2$

**Table 4.7** Selected distances (Å) and angles (°) with estimated standard deviations in parentheses for  $[Nd(L^3)_2(\mu-Cl)]_2(PhMe)_2$ .

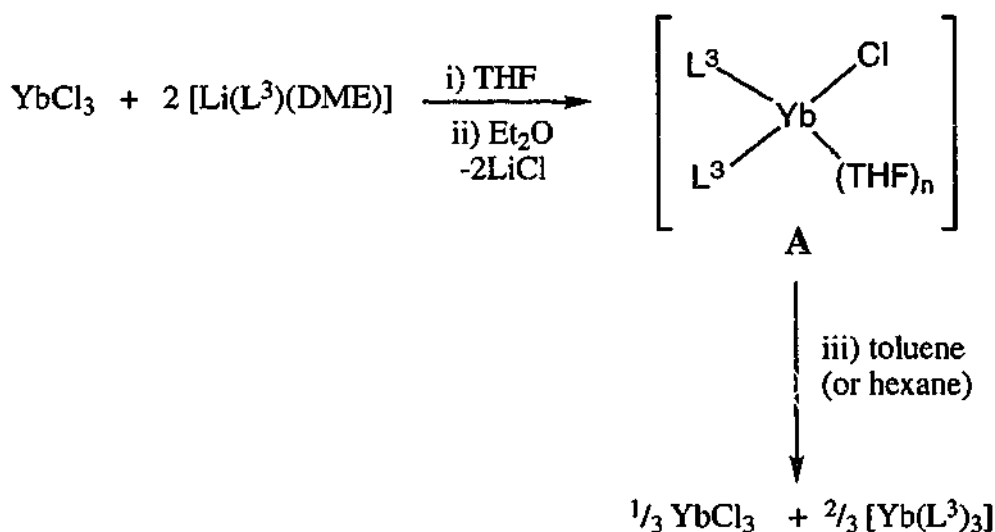
Nd(1)—N(1)	2.319(2)	N(1)—Nd(1)—Cl(1)	128.17(5)
Nd(1)—N(2)	2.299(2)	N(1)—Nd(1)—Cl(1A)	87.21(6)
Nd(1)—O(1)	2.519(2)	N(2)—Nd(1)—Cl(1)	104.20(5)
Nd(1)—O(2)	2.567(2)	N(2)—Nd(1)—Cl(1A)	145.91(5)
Nd(1)—Cl(1)	2.785(1)	O(1)—Nd(1)—Cl(1)	78.61(5)
Nd(1)—Cl(1A) <sup>a</sup>	2.856(1)	O(1)—Nd(1)—Cl(1A)	121.30(5)
Nd(1)—C(21)	2.911(2)	O(2)—Nd(1)—Cl(1)	87.60(5)
Nd(1)—C(22)	3.035(2)	O(2)—Nd(1)—Cl(1A)	77.73(5)
N(1)—Nd(1)—N(2)	114.69(7)	Cl(1)—Nd(1)—Cl(1A)	77.96(2)
N(1)—Nd(1)—O(1)	67.53(6)	Nd(1)—Cl(1)—Nd(1A)	102.04(2)
N(1)—Nd(1)—O(2)	137.36(6)		
N(2)—Nd(1)—O(2)	68.47(7)	<i>Torsion angles</i>	
N(2)—Nd(1)—O(1)	91.99(7)	C(13)—C(12)—O(1)—C(111)	-50.87(3)
O(1)—Nd(1)—O(2)	152.65(5)	C(23)—C(22)—O(2)—C(211)	-62.85(3)

Symmetry transformations used to generate equivalent atoms:

<sup>a</sup>  $-x+2, -y+2, -z+1$

### 4.2.1.3 General Remarks on $[\text{Ln}(\text{L})_2(\mu\text{-Cl})_2]$ ( $\text{L} = \text{L}^2$ or $\text{L}^3$ ) Complexes

The smaller steric demand of  $\text{L}^2$  can stabilise the heteroleptic chloro complexes only for the lighter lanthanoid elements, namely Tb, Er and Yb, with the larger neodymium undergoing rearrangement to  $[\text{Nd}(\text{L}^2)_3]$ . However for  $\text{L}^3$ , the neodymium derivative was the only heteroleptic complex isolated, with rearrangement observed for both larger (La) and smaller (Yb) lanthanoid elements. Whilst the results for the  $\text{L}^2$  system are consistent with insufficient steric bulk to support analogues of larger metals (yet possibly also too crowded to allow further coordination of THF e.g. as in  $\{\text{Ln}(\text{L}^2)_2(\mu\text{-Cl})(\text{THF})_2\}$ ), the presumably bulkier  $\text{L}^3$  ligand did not stabilise the chloride complexes of the smaller metals. In the case of ytterbium a monomeric complex may exist (*Scheme 4.3* (A)) but is unstable in the absence of a donor solvent. Indeed work up of the 2:1 reaction mixture in  $\text{Et}_2\text{O}$  gave an oily residue and the infrared spectrum was different from those of  $[\text{Yb}(\text{L}^3)_3]$  and  $[\text{Nd}(\text{L}^3)_2(\mu\text{-Cl})_2]$ . On recrystallisation of the oil from non-polar solvents, two compounds were apparent, one of which was identified as  $[\text{Yb}(\text{L}^3)_3]$  (*Scheme 4.3*). Thus there appears to be a delicate balance of ligand size, lanthanoid size and solvent which determines the outcome of the reactions of  $\text{LiL}$  ( $\text{L} = \text{L}^2, \text{L}^3$ ) with  $\text{LnCl}_3$ .

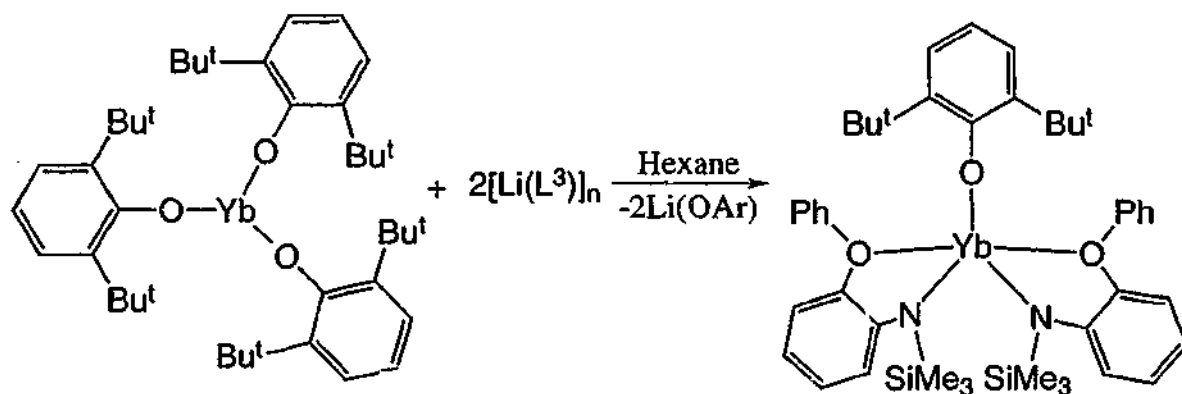


*Scheme 4.3*

### 4.2.2 Alternative Routes to Heteroleptic Lanthanoid Complexes

Substitution of a bulkier X anion in the heteroleptic complexes  $\text{Ln}(\text{L})_2\text{X}$  may stabilise a monomeric species rather than the dimer  $([\text{Ln}(\text{L})_2(\mu\text{-Cl})]_2)$  observed with the chlorides. Bulky aryloxy ligands (OAr, where  $\text{Ar} = 2,6\text{-}(\text{Bu}^t)_2\text{-4-R-C}_6\text{H}_3$ ) have been extensively utilised as ligands for lanthanoids and can also be potential precursors to organometallics by subsequent elimination of  $\text{Li}(\text{OAr})$  upon reaction with  $\text{LiR}$ . [19, 20] Consequently the preparation of  $\text{Ln}(\text{L})_2\text{OAr}$  was investigated using a combination of ytterbium and the larger  $\text{L}^3$  ligand which should provide the best opportunity for obtaining a monomeric product. The isolation and characterisation of an example of this compound class would enable further comparisons with the classical  $\text{Ln}(\text{C}_5\text{Me}_5)_2$  moieties since  $[\text{Ln}(\text{C}_5\text{Me}_5)_2(\text{OAr})]$  species have been well characterised.

A different synthetic approach was utilised for the preparation of  $[\text{Yb}(\text{L}^3)_2(\text{OAr})]$  ( $\text{OAr} = 2,6\text{-}(\text{Bu}^t)_2\text{C}_6\text{H}_3\text{O}$ ). The reaction between the solvent-free  $[\text{Li}(\text{L}^3)]_n$  (see Chapter 7) with tris(2,6-di-*tert*-butylphenolato)ytterbium(III) in a 2:1 mole ratio in hexane (Equation 4.1) afforded the product in high yield. The product  $\text{Li}(\text{OAr})$  was easily separated from  $[\text{Yb}(\text{L}^3)_2(\text{OAr})]$  due to the low solubility of the lithium salt in hexane.



Equation 4.1

The complex  $[\text{Yb}(\text{L}^3)_2(\text{OAr})]$  was characterised by IR and elemental analysis (C, H, N). The major distinction between the infrared spectrum of  $[\text{Yb}(\text{L}^3)_2(\text{OAr})]$  and that of the related  $[\text{Nd}(\text{L}^3)_2(\mu\text{-Cl})]_2(\text{PhMe})_2$  was the presence in the former of very strong bands at 1411, 845 and  $801\text{ cm}^{-1}$ . One of the latter bands may be a  $\gamma(\text{CH})$  vibration of an aromatic ring with three adjacent hydrogens e.g. 2,6-di-*tert*-butylphenolate. Spectra of  $[\text{Ln}(\text{OAr})_2(\text{S})]$  also exhibit these bands. [21, 22] The monomeric formula was confirmed

by an X-ray crystallographic study of orange crystals of the bulk product obtained from the reaction filtrate after removal of the precipitated lithium 2,6-di-*tert*-butylphenolate.

The  $[\text{Yb}(\text{L}^3)_2(\text{OAr})]$  molecule crystallises as discrete monomers, two of which comprise the asymmetric unit. A diagram of one of the monomers is shown in *Figure 4.3*. Crystal refinement parameters and selected bond distances and angles are listed in *Table 4.8* and *Table 4.9* respectively. The central ytterbium atom is five-coordinate and is surrounded by an oxygen-bound aryloxide group and two chelating  $\text{L}^3$  ligands in a distorted trigonal bipyramidal geometry. The *transoid* oxygen atoms (O(1) and O(2)) occupy the axial sites while the trigonal plane comprises the aryloxide oxygen (O(3)) and the two amide nitrogen atoms (N(1) and N(2)) (sum of the equatorial angles around Yb(1) is  $360^\circ$ ). As expected for this geometry, the *trans* O—Yb—O angle is virtually linear and the *cis* O—Yb—O angles are close to  $90^\circ$ . However the structure is distorted by the narrow bite angles of the  $\text{L}^3$  ligands leading to large inter-ligand *cis* N(1, 2)—Yb—O(2, 1) angles. Thus the equatorial plane is tilted about the O(3)—Yb(1) axis to accommodate the chelating nature of the  $\text{L}^3$  ligands. The central Yb atom and the two arene backbones are approximately coplanar. The  $\text{NSiMe}_3$  groups project below this plane and the OAr ligand is above, with the 2,6-(Bu')<sub>2</sub> substituents positioned directly above the  $\text{NSiMe}_3$  groups. The phenyl substituents protrude above the plane and occupy the space on either side of the flat faces of the OAr ligand. The C—O(phenoxy) bonds (C(111)—O(1), C(211)—O(2)) are in the plane (see *Table 4.9* for torsion angles) of the arene rings with the phenyl groups twisted by approximately  $80^\circ$  (see *Table 4.9* for interplanar angles). The tilt angles of the arene backbone to the Yb-N-O planes for each  $\text{L}^3$  ligand do not show the extreme leaning observed in the  $[\text{Nd}(\text{L}^3)_2(\mu\text{-Cl})]_2$  structure and are more like the normal 'edge-on' bonding mode (*Table 4.9*).

Subtraction of the five-coordinate ionic radius (extrapolated from values for higher coordination numbers)[8] from the Yb—N distances gives values (1.23, 1.39 Å) comparable to or shorter than the range (1.36—1.42 Å) observed for six-coordinate  $[\text{Nd}(\text{L}^3)_2(\mu\text{-Cl})]_2(\text{PhMe})_2$  and  $[\text{Ln}(\text{L}^3)_3](\text{S})$  (S = MePh, C<sub>5</sub>H<sub>9</sub>Me) (*Table 4.4* and *Table 3.10* respectively). In addition Yb—O(Ph) bond lengths (subtraction values 1.49—1.54 Å) are marginally longer than those observed in the homoleptic  $[\text{Ln}(\text{L}^3)_3]$  (Chapter 3) or heteroleptic  $[\text{Nd}(\text{L}^3)_2(\mu\text{-Cl})]_2(\text{PhMe})_2$  (*Table 4.7*). The bond lengthening of the coordinated phenyl ether substituents presumably results from the repulsion between the

phenyl rings and the 2,6-di-*tert*-butylphenolate ligand as can be seen in a space filling projection (*Figure 4.4*). In contrast the NSiMe<sub>3</sub> groups project away from the aryloxide (*Figure 4.3*) and are thus unaffected. The Yb(1)—O(3) distance is short as expected for an anionic oxygen. Subtraction of the ionic radii<sup>[8]</sup> gives a value (1.16 Å) which is much shorter than for crowded [Ln(OAr)<sub>3</sub>(THF)]<sup>[22]</sup> or [Ln(OAr)<sub>2</sub>(S)]<sup>[21, 22]</sup> complexes. However, for heteroleptic lanthanoid aryloxides e.g. [Sm(C<sub>5</sub>Me<sub>5</sub>)<sub>2</sub>(OAr)] (subtraction value 1.12 Å)<sup>[23]</sup> or [YbCl<sub>2</sub>(OAr)(THF)<sub>3</sub>] (1.22 Å),<sup>[24]</sup> generally shorter distances are observed than for the [Ln(OAr)<sub>3</sub>(THF)] or [Ln(OAr)<sub>2</sub>(S)] complexes. It may be possible that in [Yb(L<sup>3</sup>)<sub>2</sub>(OAr)], [Sm(C<sub>5</sub>Me<sub>5</sub>)<sub>2</sub>(OAr)] and [YbCl<sub>2</sub>(OAr)(THF)<sub>3</sub>] that the steric bulk of the 2,6-(Bu<sup>t</sup>)<sub>2</sub> groups is sufficiently removed from the metal centre to not interfere with binding of the other ligands to the lanthanoid.

**Table 4.8** Summary of Crystallographic Data for [Yb(L<sup>3</sup>)<sub>2</sub>(OAr)]

Compound	[Yb(L <sup>3</sup> ) <sub>2</sub> (OAr)]
Formula	C <sub>44</sub> H <sub>57</sub> N <sub>2</sub> O <sub>3</sub> Si <sub>2</sub> Yb
<i>M</i>	891.14
<i>a</i> (Å)	13.848(3)
<i>b</i> (Å)	15.656(3)
<i>c</i> (Å)	20.143(4)
$\alpha$ (°)	70.70(3)
$\beta$ (°)	82.81(3)
$\gamma$ (°)	88.25(3)
<i>V</i> (Å <sup>3</sup> )	4089.0(14)
Crystal system	Triclinic
Space Group	<i>P</i> (-1)
<i>Z</i>	4
Diffractometer	Nonius Kappa CCD
$\rho_{\text{calcd}}$ (g cm <sup>-3</sup> )	1.448
$\mu$ (MoK $\alpha$ ) (mm <sup>-1</sup> )	2.387
$2\theta_{\text{max}}$ (°)	60.6
<i>N</i> , <i>N<sub>p</sub></i>	19743, 15003
<i>R</i> , <i>R<sub>w</sub></i> (observed data)	0.0330, 0.0658
<i>R</i> , <i>R<sub>w</sub></i> (all data)	0.0564, 0.0725

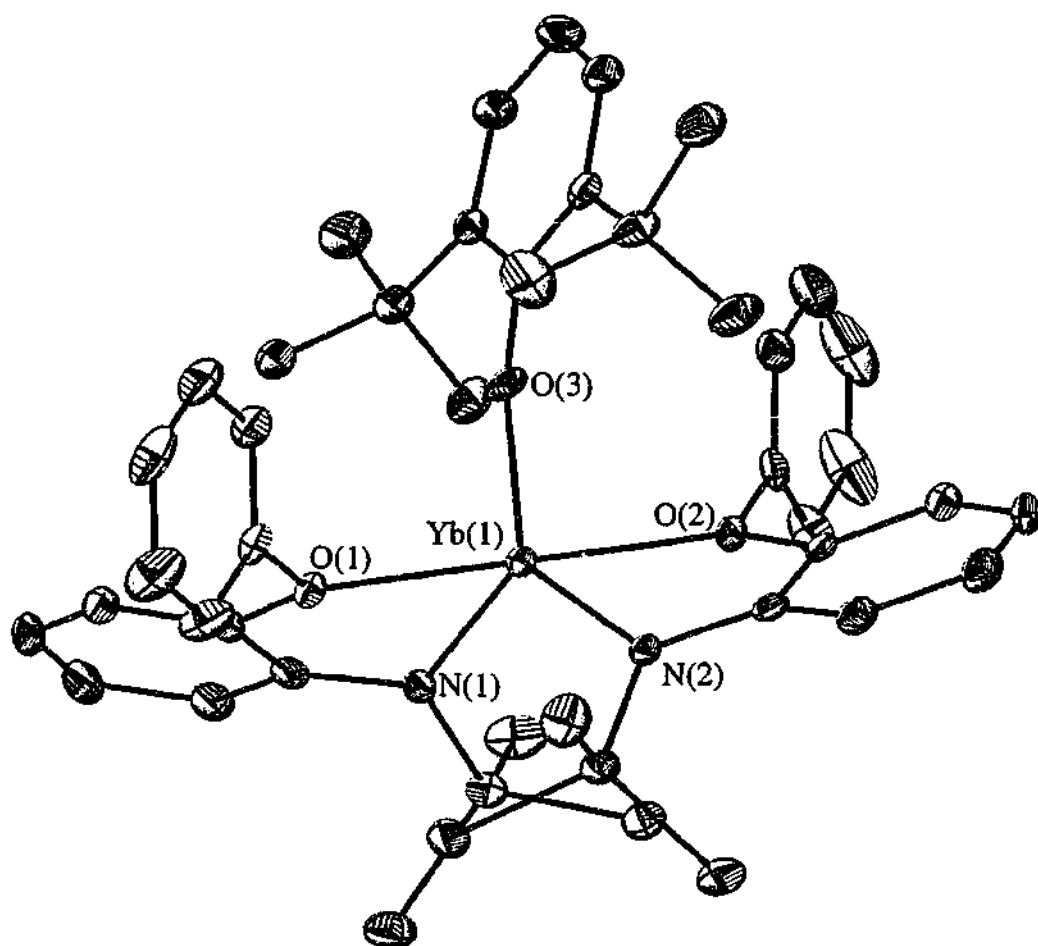


Figure 4.3 The X-ray structure of  $[Yb(L^3)_2(OAr)]$

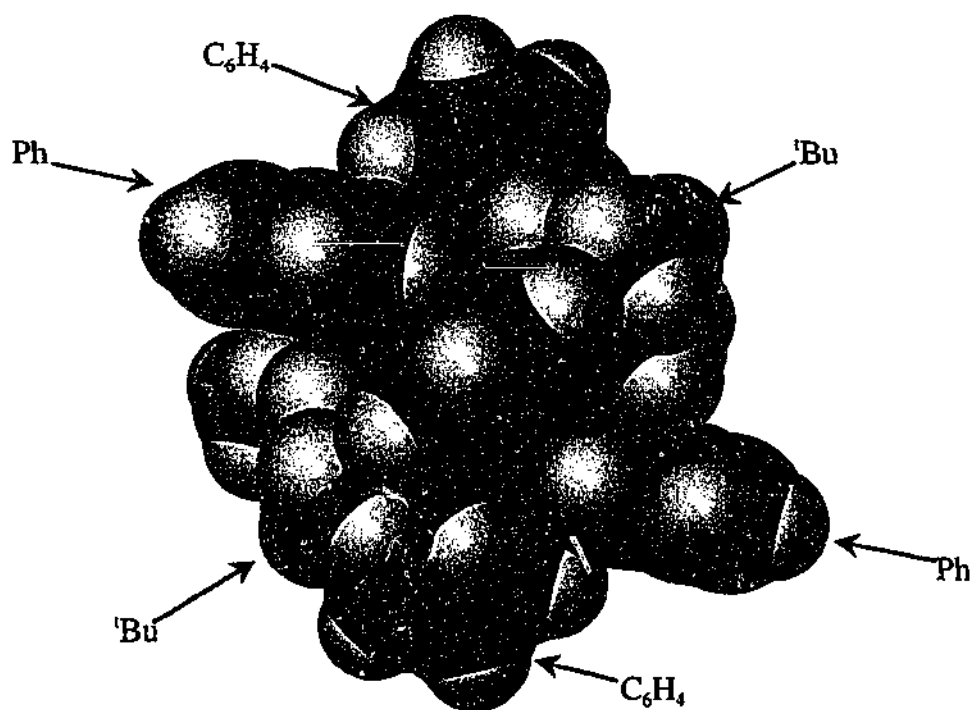


Figure 4.4 Space filling projection of  $[Yb(L^3)_2(OAr)]$

Table 4.9 Ytterbium environment in  $[Yb(L^3)_2(OAr)]^a$ .

Distances (Å)		Angles (°)	
Yb(1)—N(1)	2.050(2)	O(1)—Yb(1)—O(2)	178.72(7)
Yb(1)—N(2)	2.212(3)	O(1)—Yb(1)—O(3)	87.24(9)
		O(2)—Yb(1)—O(3)	92.92(9)
Yb(1)—O(1)	2.442(2)		
Yb(1)—O(2)	2.429(2)	N(1)—Yb(1)—N(2)	112.29(10)
Yb(1)—O(3)	1.979(2)	N(1)—Yb(1)—O(2)	106.32(9)
		N(1)—Yb(1)—O(3)	120.69(10)
		N(2)—Yb(1)—O(3)	127.01(9)
		N(1)—Yb(1)—O(1)	74.66(9)
		N(2)—Yb(1)—O(1)	106.06(9)
		N(2)—Yb(1)—O(2)	72.84(9)
Torsion Angles (°)			
C(13)—C(12)—O(1)—C(111)	-0.3(1)		
C(23)—C(22)—O(2)—C(211)	5.9(1)		
Interplanar Angles (°)			
P(1A) <sup>b</sup> —P(1B) <sup>c</sup>	25.8(1)		
P(2A) <sup>d</sup> —P(2B) <sup>e</sup>	29.0(1)		
P(1B) <sup>c</sup> —P(1C) <sup>f</sup>	79.4(1)		
P(2B) <sup>e</sup> —P(2C) <sup>g</sup>	84.5(1)		

<sup>a</sup> for one of the independent molecules only. <sup>b</sup> P(1A) = plane defined by Ln—N(1)—O(1) atoms; <sup>c</sup> P(1B) = plane defined by the arene backbone (C(11)—C(16)); <sup>d</sup> P(2A) = plane defined by Ln—N(2)—O(2) atoms; <sup>e</sup> P(2B) = plane defined by the arene backbone (C(21)—C(26)); <sup>f</sup> P(1C) = plane defined by the phenyl ring carbon atoms C(111)—C(116); <sup>g</sup> P(2C) = plane defined by the phenyl ring carbon atoms C(211)—C(216).

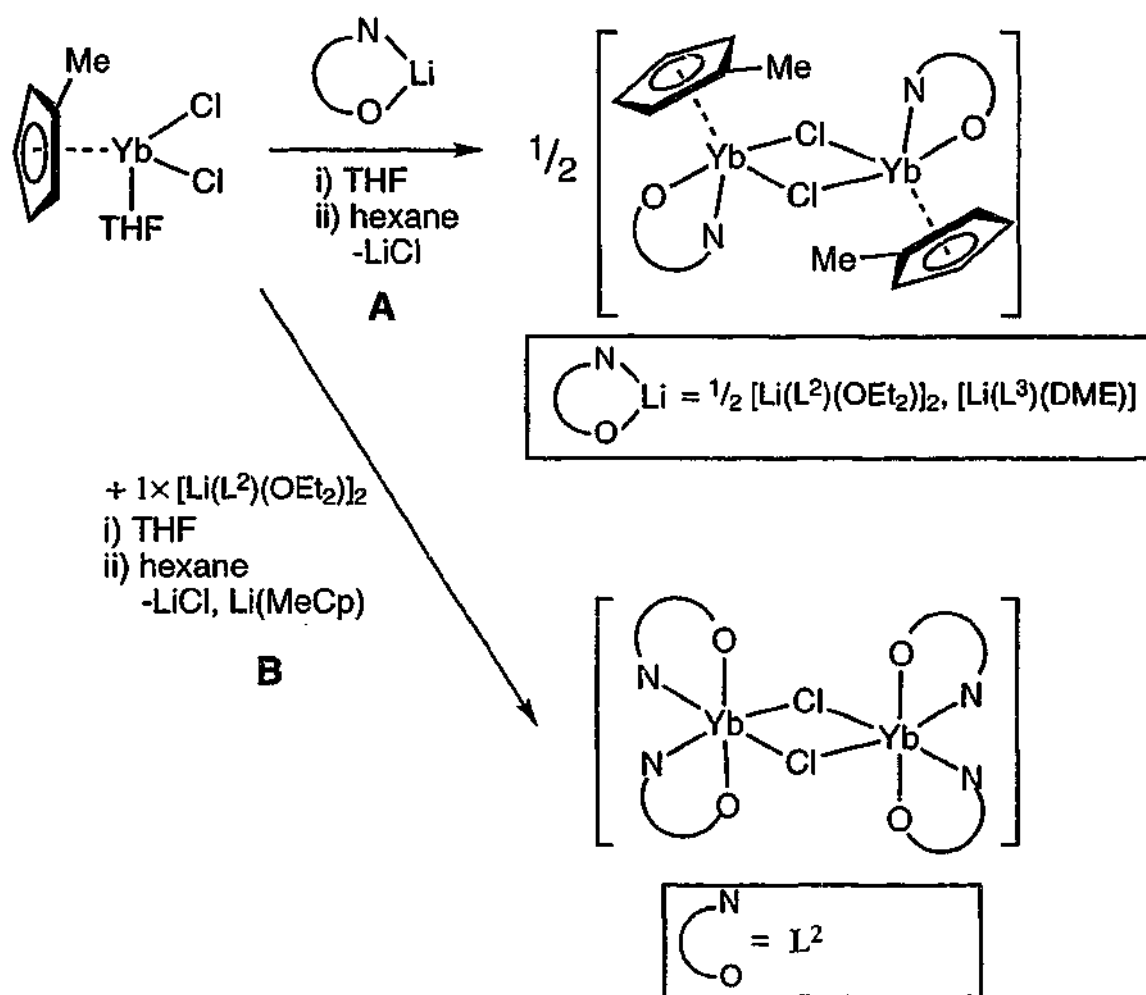


### 4.2.3 Bridging the Gap in Heteroleptic Chemistry

The further development of heteroleptic lanthanoid chemistry is challenged by the need to find suitable alternatives to the classical, highly stabilised  $[\text{LnCp}_2\text{X}]$  ( $\text{X} = \text{anion}$ ) system. Only a limited number of other ligand systems, incorporating groups such as amides, have played a role in obtaining complexes of the type  $[\text{Ln}(\text{L})_2(\text{X})]$  and these are less stable to rearrangement. A linked amido-cyclopentadienyl ligand has been introduced recently into lanthanoid chemistry where the stabilisation of small molecules was achieved affording complexes of the type  $[\text{Ln}(\eta^5\text{:}\eta^1\text{-C}_5\text{Me}_4\text{SiMe}_2\text{NCMe}_2\text{R})(\text{L})(\mu\text{-X})_2]$  ( $\text{Ln} = \text{Lu, Yb, Y}$ ;  $\text{R} = \text{Me, Et}$ ;  $\text{L} = \text{THF, PMe}_3$ ;  $\text{X} = \text{H}$ :[15]  $\text{Ln} = \text{Sc, R} = \text{Me, L} = \text{PMe}_3$ :[25-27]  $\text{Ln} = \text{Y}$ [15],  $\text{R} = \text{Me, Et}$ ;  $\text{L} = \text{THF}$ ). Furthermore solvent-free derivatives of the alkyl and amido complexes  $[\text{Ln}(\eta^5\text{:}\eta^1\text{-C}_5\text{Me}_4\text{SiMe}_2\text{NCMe}_2\text{R})(\text{X})_2]$  ( $\text{X} = \text{N}(\text{SiMe}_3)_2$ ,  $\text{Ln} = \text{Y, Nd, Sm, Lu}$ ;  $\text{X} = \text{CH}(\text{SiMe}_3)_2$ ,  $\text{Ln} = \text{Yb, Lu}$ ) have been prepared and some exhibit high catalytic activity in intramolecular hydroamination reactions.[28, 29, 30, 31] However the synthesis of other mono cyclopentadienyl complexes has attracted little attention despite their relevance to polymerisation catalysis.[15] (and references therein)

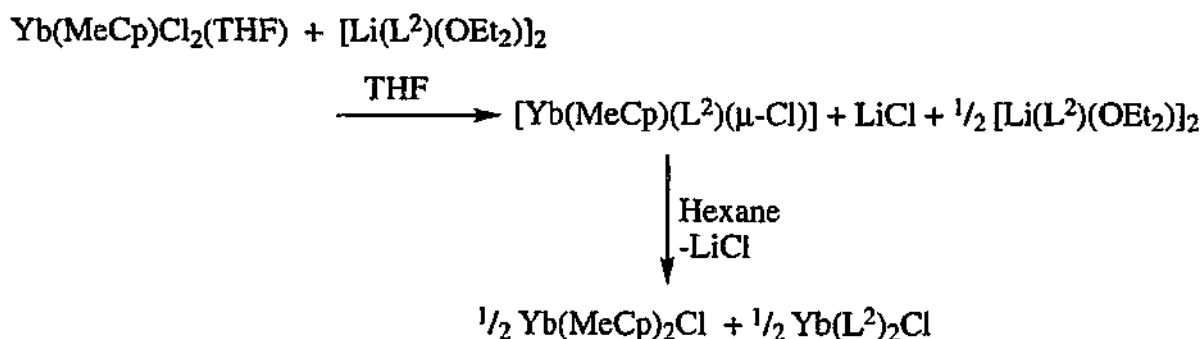
The benefit of mono(cyclopentadienyl) lanthanoid systems is that they are less sterically crowded than the bis(cyclopentadienyl) derivatives, but a kinetically stable, well defined configuration is more difficult to achieve. It is surprising that little attention has been paid to preparing complexes of the type  $[\text{Ln}(\text{Cp})(\text{NR}_2)\text{Cl}]$ . A search of the literature revealed only one complex of this type to have been reported.[32] This complex  $[\text{Y}(\text{C}_5\text{Me}_5)\{\text{PhC}(\text{NSiMe}_3)_2\}\text{Cl}(\text{THF})]$  contained a bidentate benzamidinate ligand but was not structurally characterised. Since the choice of metal is crucial for the stabilisation of the heteroleptic complexes  $[\text{Ln}(\text{L})_2(\mu\text{-Cl})_2]$  ( $\text{L} = \text{L}^2$ ,  $\text{Ln} = \text{Tb, Er, Yb}$ ;  $\text{L} = \text{L}^3$ ,  $\text{Ln} = \text{Nd}$ ) there is the possibility that a small structural modification might increase stability. Accordingly replacement of one L group by Cp was investigated.

The reaction of  $[\text{Yb}(\text{MeCp})\text{Cl}_2(\text{THF})]$  ( $\text{MeCp} = \text{MeC}_5\text{H}_4$ ) with  $[\text{Li}(\text{L}^2)_2(\text{OEt}_2)]_2$  or  $[\text{Li}(\text{L}^3)(\text{DME})]$  in a Li : Ln ratio of 1:1 in THF affords  $[\text{Yb}(\text{MeCp})(\text{L}^2)(\mu\text{-Cl})_2]$  and  $[\text{Yb}(\text{MeCp})(\text{L}^3)(\mu\text{-Cl})_2]$  respectively after extraction with hexane (*Scheme 4.4 (A)*).



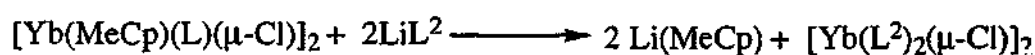
Scheme 4.4

The reaction of  $[\text{Yb}(\text{MeCp})\text{Cl}_2(\text{THF})]$  with  $[\text{Li}(\text{L}^2)(\text{OEt}_2)_2]$  in a Li:Ln ratio of 2:1 in THF afforded the heteroleptic complex  $[\text{Yb}(\text{L}^2)_2(\mu\text{-Cl})_2]$  in high yield (Scheme 4.4 (B)) rather than the target product  $\text{Yb}(\text{L}^2)_2(\text{MeCp})$ . Extraction with hexane separated the by-products  $\text{LiCl}$  and  $\text{LiMeCp}$  from the reaction mixture. A red crystalline material deposited from the reaction mixture which gave an identical infrared spectrum and similar unit cell parameters to those of the complex  $[\text{Yb}(\text{L}^2)_2(\mu\text{-Cl})_2]$  (see above). The high yield (74%) of  $[\text{Yb}(\text{L}^2)_2(\mu\text{-Cl})_2]$  from the reaction (Equation 4.2) excludes formation of this product from rearrangement of an intermediate 1:1 product  $[\text{Yb}(\text{MeCp})(\text{L}^2)(\mu\text{-Cl})_2]$  (maximum possible yield 50%) which has in any case been successfully isolated in good yield under similar reaction conditions using a 1:1 ratio of Li:Ln, and appears stable to rearrangement.



Equation 4.2

Furthermore, an attempt to prepare an analogous complex  $\text{Yb(L}^2)_2(\text{Cp})$  by an oxidation reaction from  $\text{Yb(L}^2)_2$  (see Chapter 5) instead gave  $[\text{Yb(Cp)}_2(\text{L}^2)]$ . This suggests that the target complex  $\text{Yb(MeCp)(L}^2)_2$  may be of low stability. Viewing the structure of  $[\text{Yb(MeCp)(L}^2)(\mu\text{-Cl)}]_2$  (Figure 4.5) it is evident that the one of the methyl groups on the  $\text{SiMe}_3$  and the OMe substituent on  $\text{L}^2$  block the lateral approaches to the  $\text{Ln}_2(\mu\text{-Cl)}_2$  bridge whereas the cyclopentadienyl ligands are relatively accessible to the large incoming  $\text{LiL}^2$ . Thus MeCp is removed rather than a chloride. Presumably the initial reaction sequence in THF forms  $[\text{Yb(MeCp)(L}^2)(\mu\text{-Cl)}]_2$  with  $\text{LiL}^2$  (1:1 ratio of Li:Ln) remaining unreacted (Equation 4.2). Upon extraction with hexane, the  $\text{Li(MeCp)}$  precipitates in this solvent. This scenario was independently confirmed by a small scale reaction of isolated  $[\text{Yb(MeCp)(L}^2)(\mu\text{-Cl)}]_2$  with  $\text{LiL}^2$  in a 1:1 ratio of Li:Ln in hexane which gave  $[\text{Yb(L}^2)_2(\mu\text{-Cl)}]_2$  in moderate yield (Equation 4.3).



Equation 4.3

The compositions of  $[\text{Yb(MeCp)(L}^2)(\mu\text{-Cl)}]_2$  and  $[\text{Yb(MeCp)(L}^3)(\mu\text{-Cl)}]_2$  were established by elemental analyses (C, H, N) and the presence of trivalent ytterbium was confirmed by characteristic<sup>[33]</sup>  $f \leftarrow f$  transitions near 1000 nm in the near infrared spectrum. A charge-transfer absorption in the visible region at 426 nm for  $\text{L}^2$  and 428 nm for  $\text{L}^3$  accounts for their intense red colour. The IR spectra showed characteristic absorptions of  $\text{L}^2$  or  $\text{L}^3$  but unequivocal indications of the methylcyclopentadienyl ligand were masked by the  $\text{L}^2$  or  $\text{L}^3$  absorptions. Only in the case of  $[\text{Yb(MeCp)(L}^3)(\mu\text{-Cl)}]_2$  was extra intensity apparent in the aromatic C-H bending region ( $700 - 800\text{cm}^{-1}$ ) possibly attributable to the MeCp.<sup>[34]</sup> In the mass spectrum of  $[\text{Yb(MeCp)(L}^3)(\mu\text{-Cl)}]_2$  no metal-

containing ions attributable to dinuclear species were detected. However the mononuclear ion  $[\text{Yb}(\text{MeCp})(\text{L}^3)(\mu\text{-Cl})]^+$  was observed in addition to the organic fragments  $[\text{L}^3]^+$  and  $[\text{MeCp}]^+$ . The monocyclopentadienyl ytterbium derivatives  $[\text{Yb}(\text{MeCp})(\text{L}^2)(\mu\text{-Cl})]_2$  and  $[\text{Yb}(\text{MeCp})(\text{L}^3)(\mu\text{-Cl})]_2$  were further characterised by single crystal X-ray structure studies.

$[\text{Yb}(\text{MeCp})(\text{L}^2)(\mu\text{-Cl})]_2$  and  $[\text{Yb}(\text{MeCp})(\text{L}^3)(\mu\text{-Cl})]_2$  are the first examples of this type of chloro(mono(cyclopentadienyl))organoamidolanthanoid complex to be structurally characterised. Despite the greater steric demand of  $\text{L}^3$  compared with  $\text{L}^2$ , the X-ray structures of  $[\text{Yb}(\text{MeCp})(\text{L}^2)(\mu\text{-Cl})]_2$  and  $[\text{Yb}(\text{MeCp})(\text{L}^3)(\mu\text{-Cl})]_2$  are almost identical and are displayed in *Figure 4.5* and *Figure 4.6* respectively. *Table 4.10* summarises the crystal refinement parameters and the important bond lengths and angles are listed in *Table 4.11*. The structures clearly show the contrasting coordination modes of 'face-on' cyclopentadienyl and 'edge-on' amide ligands. Both complexes are dimeric with two  $\text{Yb}(\text{MeCp})(\text{L})$  ( $\text{L} = \text{L}^2, \text{L}^3$ ) units bridged by two chloride atoms. The central four-membered  $\text{Yb}_2\text{Cl}_2$  core is exactly planar as the molecules lie on an inversion centre. The metal environment in each complex is seven-coordinate arranged in a pseudo square based pyramid with the centroid of the  $\eta^5$ -methylcyclopentadienyl ligand occupying the apical position. The amide nitrogen is pushed out of the plane away from the MeCp group presumably due to the angular restraints imposed by the five-membered chelate ring and the steric repulsion of the bulky  $\text{NSiMe}_3$  group and the cyclopentadienyl ligand. In both cases the methyl carbon (C(6)) is positioned in line with the  $\text{Yb}\dots\text{Yb}$  vector and blocks access to the chloride bridges. The substituents on N and O lie either side of the central  $\text{Yb}_2\text{Cl}_2$  core of the molecule in a *transoid* disposition. The backbones of the chelating  $\text{L}^2$  and  $\text{L}^3$  ligands are virtually planar (for torsion angles see *Table 4.11*) with the phenyl ring of  $\text{L}^3$  rotated  $69.42(1)^\circ$  to the arene backbone.

Subtraction of the  $\text{Yb}^{3+}$  ionic radius from the  $\text{Yb}\text{---}\text{N}$  and  $\text{Yb}\text{---}\text{O}$  distances in  $[\text{Yb}(\text{MeCp})(\text{L}^2)(\mu\text{-Cl})]_2$  and  $[\text{Yb}(\text{MeCp})(\text{L}^3)(\mu\text{-Cl})]_2$  gives values (*Table 4.12*) which can be directly compared with those of other related lanthanoid complexes and a selection these are given in *Table 4.12*. Whilst the bonding of the amide unit in the two complexes  $[\text{Yb}(\text{MeCp})(\text{L}^2)(\mu\text{-Cl})]_2$  and  $[\text{Yb}(\text{MeCp})(\text{L}^3)(\mu\text{-Cl})]_2$  is similar, the latter complex has a marginally longer coordination of the ether substituent. This is consistent with the larger phenyl ether group on  $\text{L}^3$  compared to the methyl ether on  $\text{L}^2$ . The  $\text{Yb}\text{---}\text{N}$  and  $\text{Yb}\text{---}\text{O}$

values are shorter than the corresponding lengths found for the respective heteroleptic complexes  $[\text{Yb}(\text{L}^2)_2(\mu\text{-Cl})]_2$  and  $[\text{Nd}(\text{L}^3)_2(\mu\text{-Cl})]_2(\text{PhMe})_2$  but are similar to those found in  $[\text{Y}(\eta^5:\eta^1\text{-SiMe}_2\text{C}_5\text{Me}_4\text{NCMe}_2\text{Et})(\text{THF})(\mu\text{-Cl})]_2$ <sup>[15]</sup> even though the ether ligand is not tethered to the amide in this case. An evaluation of the metal chloride distances in  $[\text{Yb}(\text{MeCp})(\text{L}^2)(\mu\text{-Cl})]_2$  and  $[\text{Yb}(\text{MeCp})_2(\mu\text{-Cl})]_2$  shows that these bonds (*Table 4.12*) are also significantly shorter than the corresponding heteroleptic derivative but are marginally longer than those in the linked cyclopentadienyl amide complex  $[\text{Y}(\eta^5:\eta^1\text{-SiMe}_2\text{C}_5\text{Me}_4\text{NCMe}_2\text{Et})(\text{THF})(\mu\text{-Cl})]_2$ . This latter complex parallels the current structures with the coordinated THF occupying a similar position to that of the ether substituent on  $\text{L}^2$  or  $\text{L}^3$ . From these considerations it can be clearly seen that the series of complexes  $[\text{Ln}(\text{MeCp})_2(\mu\text{-Cl})]_2$ ,  $[\text{Ln}(\text{MeCp})(\text{L})(\mu\text{-Cl})]_2$  and  $[\text{Ln}(\text{L})_2(\mu\text{-Cl})]_2$  display the anticipated graduation in not only the  $\text{Ln}\text{—Cl}$  distances, which decrease with increased substitution by cyclopentadienyl ligands, but also in the bonding of the supporting amide ligands. From this it can be concluded that the  $\text{L}^2$  and  $\text{L}^3$  ligands are of greater steric bulk than a MeCp ligand.

Minor variation in the  $\text{Yb}(1)\text{—carbon}$  bond lengths attributable to a slight ring tilt were observed for both complexes with the longest  $\text{Yb}\text{—C}$  bond corresponding to the methyl-substituted carbon ( $\text{C}(1)$ ), reflecting steric repulsion. The values obtained by subtraction of the ionic radius from the average  $\text{Yb}(1)\text{—C}$  distances in  $[\text{Yb}(\text{MeCp})(\text{L}^2)(\mu\text{-Cl})]_2$  and  $[\text{Yb}(\text{MeCp})(\text{L}^3)(\mu\text{-Cl})]_2$  (*Table 4.12*) are slightly above the usual upper limit for cyclopentadienyllanthanoid(III) complexes ( $1.64 \pm 0.04 \text{ \AA}$ ).<sup>[35]</sup>

Table 4.10. Summary of Crystallographic Data for  $[\text{Yb}(\text{MeCp})(\text{L})(\mu\text{-Cl})]_2$  ( $\text{L} = \text{L}^2$  and  $\text{L}^3$ )

Compound	$[\text{Yb}(\text{MeCp})(\text{L}^2)(\mu\text{-Cl})]_2$	$[\text{Yb}(\text{MeCp})(\text{L}^3)(\mu\text{-Cl})]_2$
Formula	$\text{C}_{32}\text{H}_{46}\text{Cl}_2\text{N}_2\text{O}_2\text{Si}_2\text{Yb}_2$	$\text{C}_{42}\text{H}_{50}\text{Cl}_2\text{N}_2\text{O}_2\text{Si}_2\text{Yb}_2$
<i>M</i>	963.86	1088.00
<i>a</i> (Å)	8.5538(3)	9.6568(1)
<i>b</i> (Å)	9.7537(2)	8.7267(1)
<i>c</i> (Å)	12.0433(2)	25.3241(3)
$\alpha$ (°)	76.953(1)	90
$\beta$ (°)	78.027(1)	98.997(1)
$\gamma$ (°)	64.868(1)	90
<i>V</i> (Å <sup>3</sup> )	879.1(3)	2107.9(7)
Crystal system	Triclinic	Monoclinic
Space Group	<i>P</i> (-1)	<i>P</i> 2 <sub>1</sub> / <i>c</i>
<i>Z</i>	1	2
Diffractometer	Nonius Kappa CCD	Nonius Kappa CCD
$\rho_{\text{calc}}$ (g cm <sup>-3</sup> )	1.821	1.714
$\mu(\text{MoK}\alpha)$ (mm <sup>-1</sup> )	5.537	4.630
$2\theta_{\text{max}}$ (°)	56.6	56.6
<i>N</i> , <i>N</i> <sub>o</sub>	4293, 3835	5202, 4877
<i>R</i> , <i>R</i> <sub>w</sub> (observed data)	0.0385, 0.0896	0.0224, 0.0539
<i>R</i> , <i>R</i> <sub>w</sub> (all data)	0.0456, 0.0926	0.0251, 0.0550

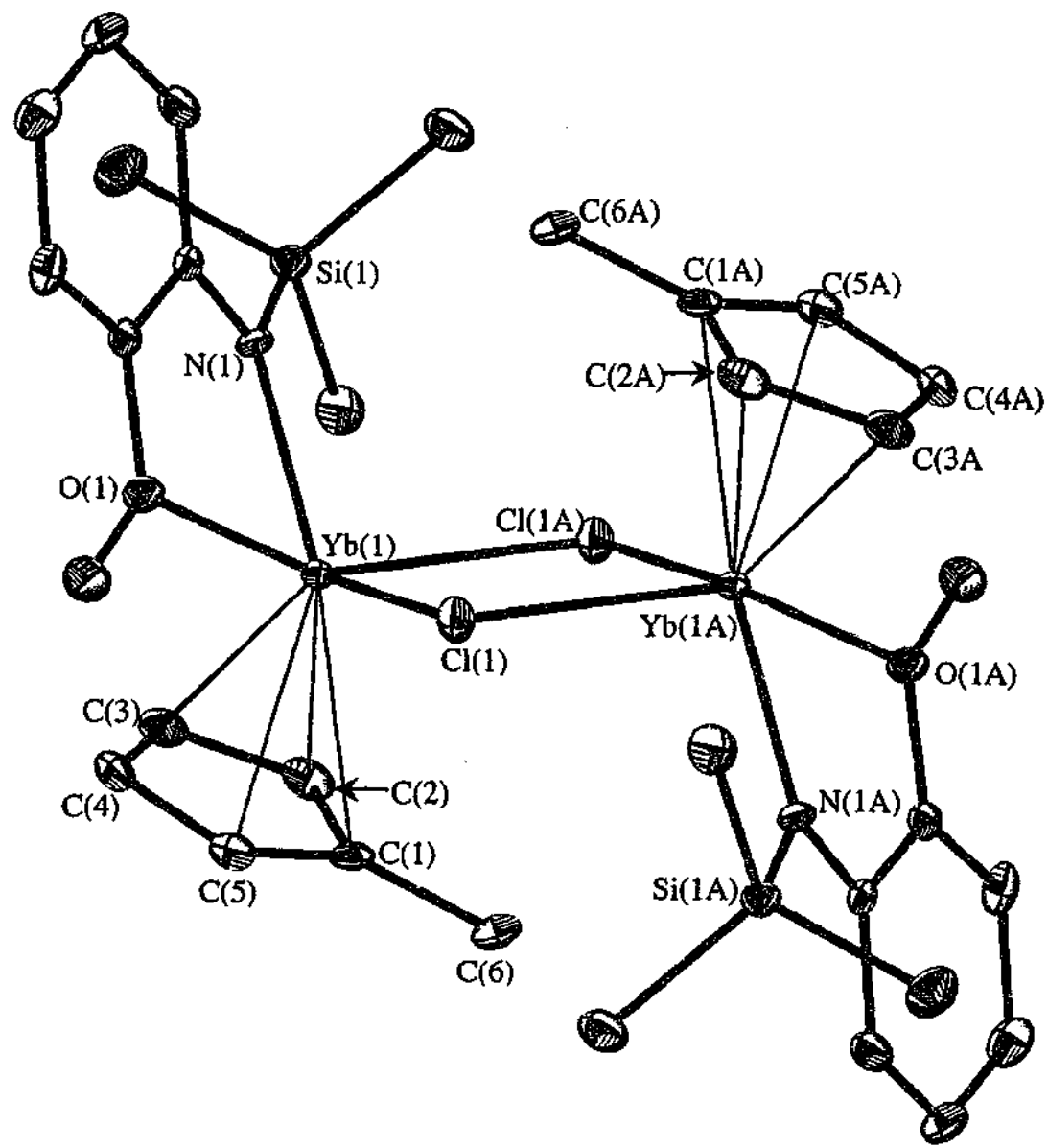


Figure 4.5 The X-ray Structure of  $[Yb(MeCp)(L^2)(\mu-Cl)]_2$

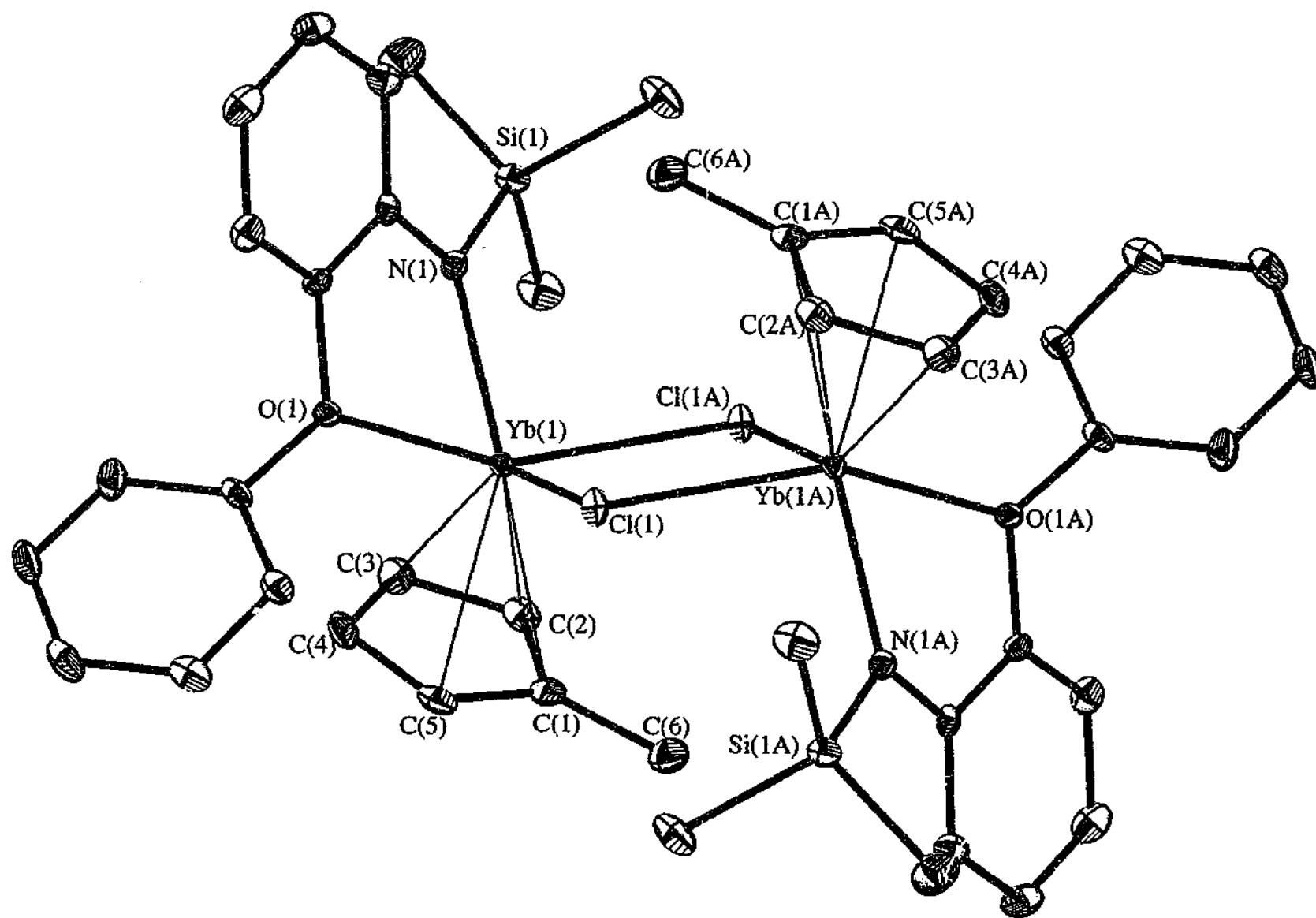


Figure 4.6 The X-ray Structure of  $[Yb(MeCp)(L^3)(\mu-Cl)_2]$



Table 4.11 Ytterbium environment in  $[\text{Yb}(\text{MeCp})(\text{L})(\mu\text{-Cl})]_2$  ( $\text{L} = \text{L}^2, \text{L}^3$ )

Compound	$[\text{Yb}(\text{MeCp})(\text{L}^2)(\mu\text{-Cl})]_2$	$[\text{Yb}(\text{MeCp})(\text{L}^3)(\mu\text{-Cl})]_2$
<i>Distances (Å)</i>		
Yb(1)—N(1)	2.212(4)	2.205(2)
Yb(1)—O(1)	2.334(3)	2.359(2)
Yb(1)—Cl(1)	2.646(2)	2.641(1)
Yb(1)—Cl(1A) <sup>a</sup>	2.655(2)	2.647(1)
Yb(1)—C(1C) <sup>b</sup>	2.307	2.301
Yb(1)—C(1)	2.635(5)	2.631(3)
Yb(1)—C(2)	2.587(5)	2.609(3)
Yb(1)—C(3)	2.567(5)	2.586(3)
Yb(1)—C(4)	2.593(5)	2.565(3)
Yb(1)—C(5)	2.626(5)	2.588(3)
<i>Angles (°)</i>		
N(1)—Yb(1)—O(1)	71.09(14)	72.09(8)
N(1)—Yb(1)—Cl(1)	117.47(11)	114.29(6)
N(1)—Yb(1)—Cl(1A) <sup>a</sup>	94.19(11)	92.33(6)
O(1)—Yb(1)—Cl(1)	78.21(9)	80.51(5)
O(1)—Yb(1)—Cl(1A) <sup>a</sup>	143.26(9)	145.68(5)
Yb(1)—Cl(1)—Yb(1A) <sup>a</sup>	100.04(5)	101.49(2)
N(1)—Yb(1)—C(1C) <sup>b</sup>	130.94	130.41
O(1)—Yb(1)—C(1C) <sup>b</sup>	106.71	105.90
Cl(1)—Yb(1)—C(1C) <sup>b</sup>	109.38	114.05
Cl(1A)—Yb(1)—C(1C) <sup>b</sup>	108.12	107.36
<i>Torsion Angles (°)</i>		
C(13)—C(12)—O(1)—C(10)	-4.15(6)	—
C(13)—C(12)—O(1)—C(111)	—	17.98(4)

<sup>a</sup> Symmetry transformations used to generate equivalent atoms:  $-x+2, -y+2, -z+1$  in  $[\text{Yb}(\text{MeCp})(\text{L}^2)(\mu\text{-Cl})]_2$  and  $-x+1, -y, -z$  in  $[\text{Yb}(\text{MeCp})(\text{L}^3)(\mu\text{-Cl})]_2$

<sup>b</sup> C(1C) = centroid of C(1)—C(5).

Table 4.12 A selection of metal distances of organometallic and / or organoamidolanthanoid(III) complexes.

Compound	Ref	Average Ln—Cl distance (d(Cl)) (Å)	Average Ln—C distance (d(C)) (Å)	Average Ln—N distance (d(N)) (Å)	Average Ln—O distance (d(O)) (Å)	Ionic Radii of Ln <sup>3+</sup> (ir) (Å) <sup>a</sup>	d(Cl)—i.r. (Å)	d(C)—i.r. (Å)	d(N)—i.r. (Å)	d(O)—i.r. (Å)
[Yb(MeCp) <sub>2</sub> (μ-Cl)] <sub>2</sub>	[36]	2.64	2.58	—	—	0.98	1.66	1.60	—	—
[Yb(MeCp)(L <sup>2</sup> )(μ-Cl)] <sub>2</sub>	this work	2.65	2.60	2.21	2.33	0.93	1.72	1.67	1.28	1.40
[Yb(MeCp)(L <sup>3</sup> )(μ-Cl)] <sub>2</sub>	this work	2.64	2.60	2.21	2.36	0.93	1.71	1.67	1.28	1.43
[Yb(L <sup>2</sup> ) <sub>2</sub> (μ-Cl)] <sub>2</sub>	Section 4.2.1	2.68	—	2.19	2.35	0.87	1.81	—	1.32	1.48
[Nd(L <sup>3</sup> ) <sub>2</sub> (μ-Cl)] <sub>2</sub> (PhMe) <sub>2</sub>	Section 4.2.1	2.82	—	2.31	2.54	0.98	1.84	—	1.33	1.56
[Nd(L <sup>2</sup> ) <sub>2</sub> ]	Chapter 3	—	—	2.37	2.54	0.98	—	—	1.39	1.56
[Yb(L <sup>3</sup> ) <sub>3</sub> ].(S)	Chapter 3	—	—	2.26	2.37	0.87	—	—	1.40	1.50
(S = MePh, C <sub>5</sub> H <sub>9</sub> Me)										
[Y(η <sup>5</sup> :η <sup>1</sup> -C <sub>3</sub> Me <sub>4</sub> SiMe <sub>2</sub> -NCMe <sub>2</sub> Et)(THF)(μ-Cl)] <sub>2</sub>	[15]	2.74	2.63	2.24	2.41	0.96	1.67	1.67	1.28	1.45

<sup>a</sup> Values derived from R.D. Shannon.[8]

### 4.3 Conclusions

In this Chapter, the synthesis and characterisation of several heteroleptic complexes of the type  $[\text{Ln}(\text{L})_2(\mu\text{-Cl})]_2$  with the organoamide ligands  $\text{L}^2$  and  $\text{L}^3$  were carried out. The stabilisation of these complexes involved a delicate balance between the size of the ligand and metal centre. Thus the increased bulkiness of  $\text{L}^3$  stabilised the complexes of the bigger Nd and  $\text{L}^2$  complexes of the smaller Tb – Yb. It may also be that  $[\text{Nd}(\text{L}^3)_2(\mu\text{-Cl})]_2(\text{PhMe})_2$  has a good solubility balance so that rearrangement is disfavoured since the larger  $\text{La}(\text{L}^3)_2\text{Cl}$  could not be isolated. The range of chloro complexes obtained was not as extensive as for the  $\text{L}^1$  system (Chapter 2) but the products did not suffer from LiCl contamination and were amenable to characterisation by X-ray crystallography. The sensitivity to the steric parameters of the ligands  $\text{L}^2$  and  $\text{L}^3$  appears not to be evident when one of the L ligands is replaced by cyclopentadienyl. Thus for the small ytterbium metal the closely similar heteroleptic complexes containing three different ligands, L, cyclopentadienyl and chloride can be readily prepared for both  $\text{L}^2$  and  $\text{L}^3$  ( $[\text{Ln}(\text{MeCp})(\text{L}^2)(\mu\text{-Cl})]_2$  and  $[\text{Ln}(\text{MeCp})(\text{L}^3)(\mu\text{-Cl})]_2$ ). These complexes complete the series  $[\text{Ln}(\text{MeCp})_2\text{Cl}]$ ,  $[\text{Ln}(\text{MeCp})(\text{L})\text{Cl}]$  and  $[\text{Ln}(\text{L})_2\text{Cl}]$ .

The current results indicate that the reactivity of the  $\text{Ln}_2(\mu\text{-Cl})_2$  bridge is restricted due to the steric protection provided by the bulky substituents on the  $\text{L}^2$  and  $\text{L}^3$  ligands. This is clearly disadvantageous for subsequent derivatisation to form active catalysts containing these ligand systems. However by utilising a bulky aryloxy monomeric complexes were obtained (e.g.  $[\text{Yb}(\text{L}^3)_2(\text{OAr})]$  and these also have the potential to be further substituted by an alkyl group. For example Lappert and co-workers have been successful in replacing OAr groups with the bulky alkyl  $\text{CH}(\text{SiMe}_3)_2$  group.<sup>[19]</sup> The preparation of  $\text{Ln}(\text{L})_2\text{R}$  species was beyond the scope of this thesis but, once obtained, these complexes may potentially be active in catalytic transformations.

#### 4.4 References

- 1 A. Recknagel, A. Steiner, S. Brooker, D. Stalke, and E. T. Edelman, *J. Organomet. Chem.*, 1991, **415**, 315.
- 2 A. Recknagel, F. Knoesel, H. Gornitzka, M. Noltemeyer, F. T. Edelman, and U. Behrens, *J. Organomet. Chem.*, 1991, **417**, 363.
- 3 W. T. Carnall, in *The Absorption and Fluorescence Spectra of Rare Earth Ions in Solution*, in *Handbook on the Physics and Chemistry of Rare Earths*, ed. K. A. Gschneider and L. Eyring, North-Holland, Amsterdam, 1979, vol. 3, ch. 24, p. 171.
- 4 J. Marcalo and A. P. De Matos, *Polyhedron*, 1989, **8**, 2431.
- 5 G. B. Deacon, T. Feng, S. Nickel, B. W. Skelton, and A. H. White, *J. Chem. Soc., Chem. Comm.*, 1993, 1328.
- 6 H. Lueken, J. Schmitz, W. Lamberts, P. Hannibal, and K. Handrick, *Inorg. Chim. Acta.*, 1989, **156**, 119.
- 7 W. J. Evans, D. K. Drummond, J. Grate, H. Zhang, and J. L. Atwood, *J. Am. Chem. Soc.*, 1987, **109**, 3928.
- 8 R. D. Shannon, *Acta. Crystallogr., Sect. A*, 1976, **32**, 751.
- 9 H. Schumann, J. Winterfeld, E. C. E. Rosenthal, H. Hemling, and L. Esser, *Z. Anorg. Allg. Chem.*, 1995, **621**, 122.
- 10 M. Karl, G. Seybert, W. Massa, S. Agarwal, A. Greiner, and K. Dehnicke, *Z. Anorg. Allg. Chem.*, 1999, **625**, 1405.
- 11 D. C. Bradley, M. B. Hursthouse, H. C. Aspinall, K. D. Sales, N. P. C. Walker, and B. Hussian, *J. Chem. Soc., Chem. Comm.*, 1989, 623.
- 12 R. K. Minhas, Y. Ma, J.-J. Song, and S. Gambarotta, *Inorg. Chem.*, 1996, **35**, 1866.
- 13 H. Görls, B. Neumüller, A. Scholz, and J. Scholz, *Angew. Chem. Int. Ed. Engl.*, 1995, **34**, 673.
- 14 P. W. Roesky and M. R. Bürgstein, *Inorg. Chem.*, 1999, **38**, 5629.
- 15 S. Arndt, P. Voth, T. P. Spaniol, and J. Okuda, *Organometallics*, 2000, **19**, 4690.
- 16 H. Schumann, M. R. Keitsch, J. Demtschuk, and G. A. Molander, *J. Organomet. Chem.*, 1999, **582**, 70.
- 17 B. Fan, Q. Shen, and Y. Lin, *J. Organomet. Chem.*, 1989, **377**, 51.

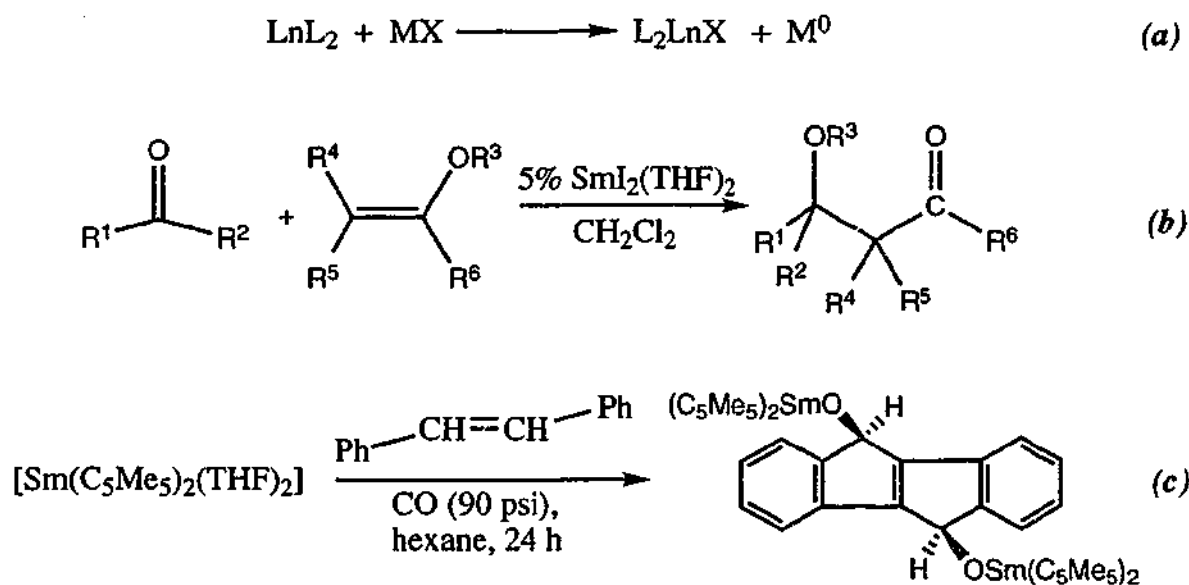
- 18 G. B. Deacon, T. Feng, B. W. Skelton, and A. H. White, *Aust. J. Chem.*, 1995, **48**, 741.
- 19 P. B. Hitchcock, M. F. Lappert, R. G. Smith, R. A. Bartlett, and P. P. Power, *J. Chem. Soc., Chem. Commun.*, 1988, 1007.
- 20 R. Anwender, *Top. Organomet. Chem.*, 1999, **2**, 1.
- 21 G. B. Deacon, P. B. Hitchcock, M. F. Lappert, P. MacKinnon, and R. H. Newnham, *J. Chem. Soc., Chem. Commun.*, 1989, 935.
- 22 G. B. Deacon, T. Feng, P. MacKinnon, R. H. Newnham, N. Siegbert, B. W. Skelton, and A. H. White, *Aust. J. Chem.*, 1993, **46**, 387.
- 23 Z. Hou, Y. Zhang, T. Yoshimura, and Y. Wakatsuki, *Organometallics*, 1997, **16**, 2963.
- 24 Y. Yao, Q. Shen, and J. Sun, *Polyhedron*, 1998, **17**, 519.
- 25 P. J. Shapiro, E. E. Bunel, W. P. Schaefer, and J. E. Bercaw, *Organometallics*, 1990, **9**, 867.
- 26 W. E. Piers, P. J. Shapiro, E. E. Bunel, and J. E. Bercaw, *Synlett*, 1990, 74.
- 27 P. J. Shapiro, W. D. Cotter, W. P. Schaefer, J. A. Labinger, and J. E. Bercaw, *J. Am. Chem. Soc.*, 1994, **116**, 4623.
- 28 S. Tian, V. M. Arrendondo, C. L. Stern, and T. J. Marks, *Organometallics*, 1999, **18**, 2568.
- 29 V. M. Arrendondo, S. Tian, F. E. MacDonald, and T. J. Marks, *J. Am. Chem. Soc.*, 1999, **121**, 3633.
- 30 Y. Mu, W. E. Piers, M.-A. MacDonald, and M. J. Zaworotko, *Can. J. Chem.*, 1995, **73**, 2233.
- 31 Y. Mu, W. E. Piers, D. C. MacQuarrie, M. J. Zaworotko, and V. G. J. Young, *Organometallics*, 1996, **15**, 2720.
- 32 R. Duchateau, A. Meetsma, and J. H. Teuben, *Organometallics*, 1996, **15**, 1656.
- 33 F. Calderazzo, R. Pappalardo, and S. Losi, *Inorg. Nucl. Chem.*, 1966, **28**, 987.
- 34 G. B. Deacon, A. J. Koplick, and T. D. Tuong, *Aust. J. Chem.*, 1984, **37**, 517 and references therein.
- 35 K. N. Raymond and W. Eigenbrot, *Acc. Chem. Res.*, 1980, **13**, 276.
- 36 E. C. Baker, L. D. Brown, and K. N. Raymond, *Inorg. Chem.*, 1975, **14**, 1376.

## Chapter 5

# Lanthanoid(II) Complexes of Mixed N,O Ligands and Their Oxidation Chemistry

### 5.1 Introduction

Divalent lanthanoid complexes offer alternative synthetic pathways to heteroleptic lanthanoid(III) complexes by oxidation reactions (e.g. *Equation 5.1 (a)*) and are also catalytic precursors through oxidation of organic substrates.[1, 2] For example  $\text{SmI}_2(\text{THF})_x$ [3, 4] has proven to be a one-electron reductant for selective transformations of organic substrates (e.g. *Equation 5.1 (b)*),[1, 5-7] while  $[\text{Sm}(\text{C}_5\text{Me}_5)_2(\text{THF})_2]$ [8] and its unsolvated analog,  $\text{Sm}(\text{C}_5\text{Me}_5)_2$ [9, 10] have shown unique reductive potential[2, 11] including the functionalisation of unsaturated hydrocarbon substrates (e.g. *Equation 5.1 (c)*) with carbon monoxide.[12-14]



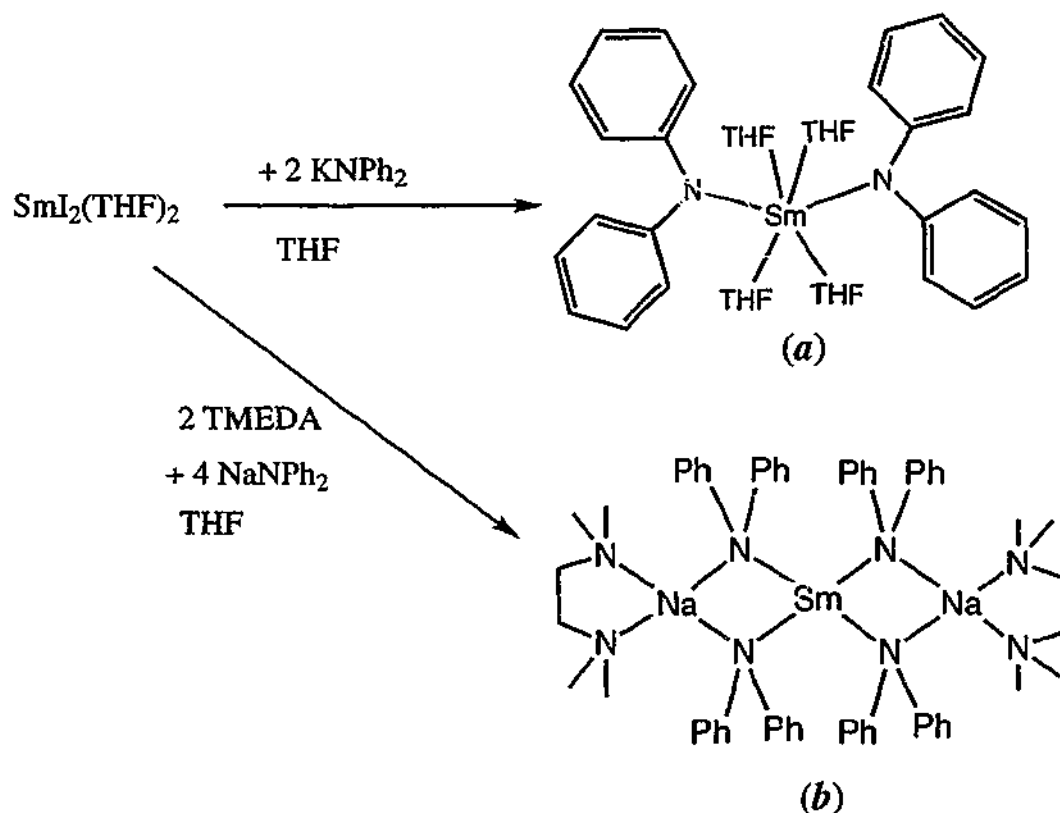
*Equation 5.1*

The divalent state is normally limited to the lanthanoids  $\text{Sm}^{2+}$  ( $4f^6$ ),  $\text{Eu}^{2+}$  ( $4f^7$ ) and  $\text{Yb}^{2+}$  ( $4f^{14}$ ) for molecular compounds[2, 11] but more recently this has been expanded to include  $\text{La}$  ( $4f^0$ )[15] and  $\text{Tm}$  ( $4f^{12}$ ).[16] With the new bidentate mixed N, O-donor ligands at hand,

the preparation and oxidation chemistry of Ln(II) derivatives is explored in this chapter. Since the discussions to date relate to the trivalent state a short overview of the current state of Ln(II) organoamide chemistry is included.

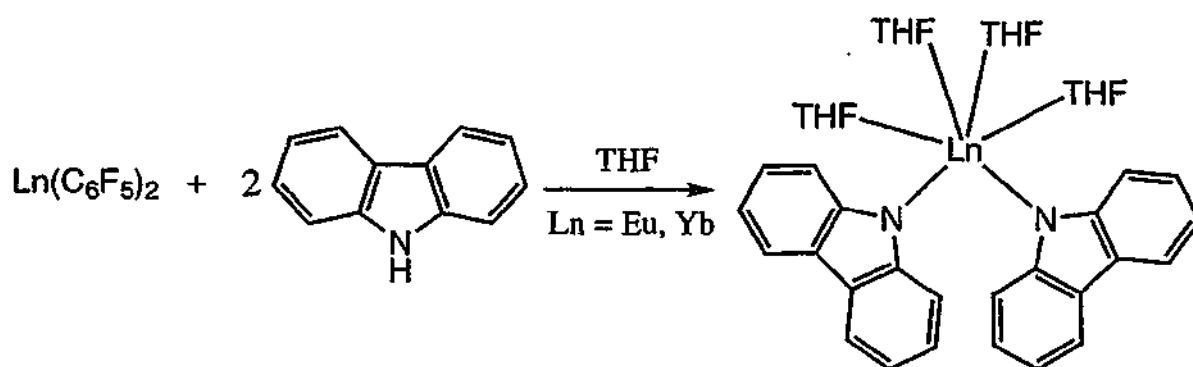
### 5.1.1 Lanthanoid(II) Monodentate Amide Complexes

As with lanthanoid(III) organoamide chemistry in general (see Chapter 1), the large cations require bulky ligands to stabilise monomeric species. This becomes even more critical with the much larger Ln(II) cations (e.g. coordination number 6; i.r.  $\text{Yb}^{2+} = 1.02 \text{ \AA}$ ;  $\text{Yb}^{3+} = 0.87 \text{ \AA}$ )<sup>[17]</sup> and the availability of only two anionic ligands per metal instead of three. The smallest organoamide ligand to be utilised in divalent lanthanoid chemistry has been the diphenyl amine ligand ( $\text{Ph}_2\text{N}^-$ ). A metathesis reaction involving the potassium diphenyl amide salt with  $\text{SmI}_2$  in THF resulted in the isolation of the monomeric complex,  $[\text{Sm}(\text{NPh}_2)_2(\text{THF})_4]$  (Equation 5.2 (a)).<sup>[18]</sup> The X-ray structure of this complex shows a trigonal prismatic geometry around the large samarium with the nitrogen atoms located in a *cisoid* arrangement. Using a 4:1 molar ratio of  $\text{NaNPh}_2$  with  $\text{SmI}_2(\text{TMEDA})_2$  in THF (Equation 5.2 (b)) yielded the 'ate' complex  $[\text{Sm}(\text{NPh}_2)_4\text{Na}_2(\text{TMEDA})_2]$ .<sup>[18]</sup>



Equation 5.2

Directly linking the phenyl substituents at the *ortho* position on  $\text{NPh}_2$  forms the carbazole ligand (Hcbz) which has been found to give similar monomeric lanthanoid(III) complexes (e.g.  $[\text{Ln}(\text{cbz})_2(\text{THF})_4]$   $\text{Ln} = \text{Sm}$ , [19]  $\text{Eu}$  [20] and  $\text{Yb}$  [20]). The samarium complex  $[\text{Sm}(\text{cbz})_2(\text{THF})_4]$  was prepared using a similar metathesis route where  $\text{SmI}_2(\text{THF})_2$  was treated with two equivalents of potassium carbazolate in THF. [19] For the ytterbium and europium derivatives  $[\text{Ln}(\text{cbz})_2(\text{THF})_4]$  ( $\text{Ln} = \text{Eu}$  and  $\text{Yb}$ ) an alternative protolytic ligand exchange between carbazole and bis(pentafluorophenyl)ytterbium or europium (2:1 molar ratio) in THF was successful (Equation 5.3). [20]

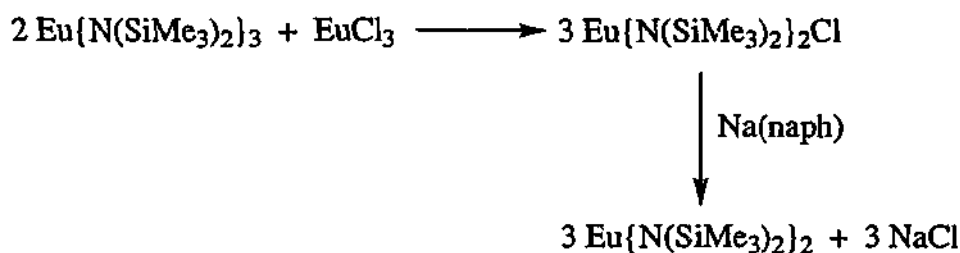


Equation 5.3

The complexes  $[\text{Ln}(\text{cbz})_2(\text{THF})_4]$  ( $\text{Ln} = \text{Sm}$ , [19]  $\text{Eu}$  [20]) are isostructural with the monomeric metal centre in an octahedral environment with a *cis* configuration of the organoamide ligands. Whilst a similar structural arrangement could be anticipated for  $[\text{Yb}(\text{cbz})_2(\text{THF})_4]$  [20] a *trans* isomer was observed for  $[\text{Sm}(\text{cbz})_2(\text{N-MeIm})_4]$  ( $\text{N-MeIm} = \text{N-methylimidazole}$ ) indicating that both *cis* and *trans* isomerisation is possible for  $[\text{Ln}(\text{cbz})_2(\text{L})_4]$  complexes.

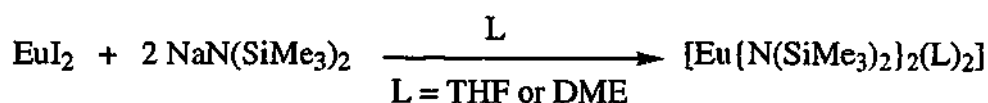
Increasing the steric demand of the organoamide ligand by substituting both sites on the nitrogen atom with the trimethylsilyl group gives  $\text{N}(\text{SiMe}_3)_2$ , which has been by far the most popular amide ligand in divalent lanthanoid chemistry. The europium complexes  $[\text{Eu}\{\text{N}(\text{SiMe}_3)_2\}_2(\text{THF})_2]$  and  $[\text{Eu}\{\text{N}(\text{SiMe}_3)_2\}_2(\text{DME})_2]$  are monomeric and were prepared in low yield by Anderson and co-workers from reduction of  $\text{Eu}\{\text{N}(\text{SiMe}_3)_2\}_2\text{Cl}$  with sodium naphthalene in the appropriate ether (Equation 5.4). [21]





Equation 5.4

A much improved synthesis of this europium(II) complex utilised the reaction of the corresponding lanthanoid diiodide with two equivalents of sodium bis(trimethylsilyl)amide in the appropriate ether (*Equation 5.5*).[22-24]



Equation 5.5

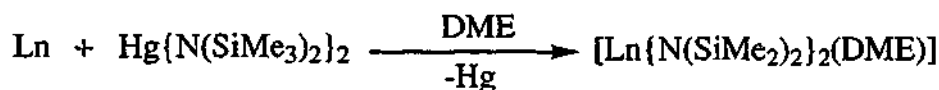
In a similar manner the reaction between ytterbium or samarium diiodide and sodium bis(trimethylsilyl)amide in THF and recrystallisation from toluene and pentane respectively yields the four-coordinate complexes  $[\text{Ln}\{\text{N}(\text{SiMe}_3)_2\}_2(\text{THF})_2]$  ( $\text{Ln} = \text{Sm}, \text{Yb}$ ).[25, 26] The complex  $[\text{Sm}\{\text{N}(\text{SiMe}_3)_2\}_2(\text{THF})_2]$ [25] is isostructural with the Eu analogue,[23, 24] with tetrahedral  $\text{N}_2\text{O}_2$  geometry surrounding the metal centre and further agosite interactions from one of the methyl substituents on each  $\text{SiMe}_3$  unit (*Figure 5.1 (a)*). Alternatively Deacon *et al.* have prepared  $[\text{Ln}\{\text{N}(\text{SiMe}_3)_2\}_2(\text{THF})_2]$  ( $\text{Ln} = \text{Sm}, \text{Yb}$ ) by a halide-free synthesis from the lanthanoid metal,  $\text{HgPh}_2$  and  $\text{HN}(\text{SiMe}_3)_2$ . [27] The reaction of  $[\text{Sm}\{\text{N}(\text{SiMe}_3)_2\}_2(\text{THF})_2]$  with one equivalent of  $\text{NaN}(\text{SiMe}_3)_2$  in DME/THF yielded the mixed amide iodide complex  $[\text{Sm}\{\text{N}(\text{SiMe}_3)_2\}(\mu\text{-I})(\text{DME})(\text{THF})_2]$ . [25] However, the reaction is reversible by cooling a THF solution of the product (*Equation 5.6*).



Equation 5.6

The synthesis of the DME derivative of the smaller ytterbium has also been examined. The reaction of  $\text{YbI}_2$  with two equivalents of bis(trimethylsilyl)amide in DME

and subsequent work up in toluene yielded the bis ligated complex  $[\text{Yb}\{\text{N}(\text{SiMe}_3)_2\}_2(\text{DME})_2]$  (*Figure 5.1 (b)*).<sup>[22]</sup> This complex, which has an octahedral arrangement of the ligated atoms, has a greater steric crowding than the  $[\text{Eu}\{\text{N}(\text{SiMe}_3)_2\}_2(\text{DME})_2]$  analogue<sup>[21]</sup> with the DME ligands unsymmetrically bound to the metal centre. Dissolution of the complex  $[\text{Yb}\{\text{N}(\text{SiMe}_3)_2\}_2(\text{DME})_2]$  in pentane readily displaces one DME to form the mono-DME complex.<sup>[22]</sup> Since this was not observed for the europium complex, it indicates greater steric repulsion with Yb(II) (0.15 Å smaller than Eu(II)). The mono-DME complexes,  $[\text{Ln}\{\text{N}(\text{SiMe}_3)_2\}_2(\text{DME})]$  ( $\text{Ln} = \text{Sm}, \text{Eu}, \text{Yb}$ ) can be prepared in good yield from a halide and alkali-free metal based synthesis, viz. treating elemental lanthanoids with  $\text{Hg}\{\text{N}(\text{SiMe}_3)_2\}_2$  in DME (*Equation 5.7*).<sup>[28]</sup>



Equation 5.7

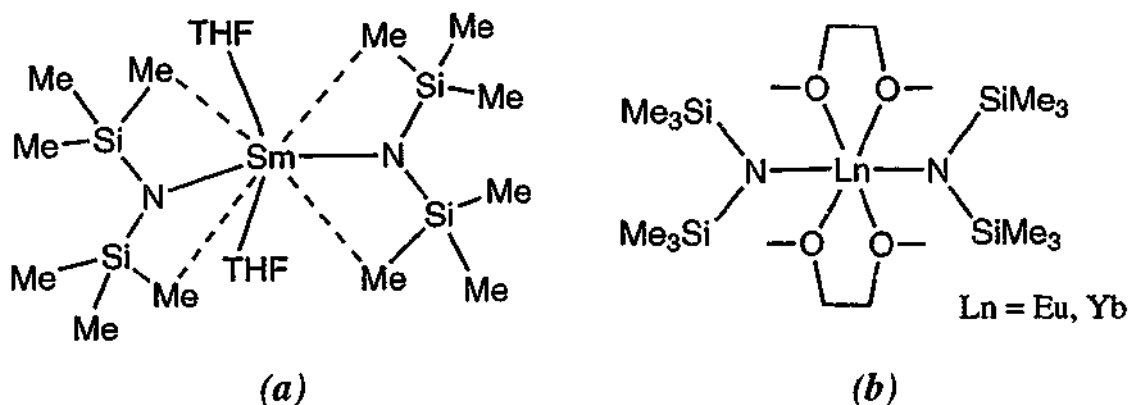
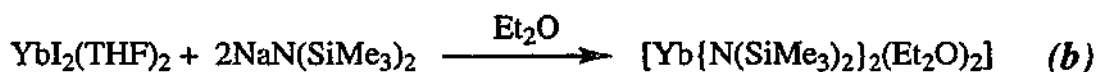
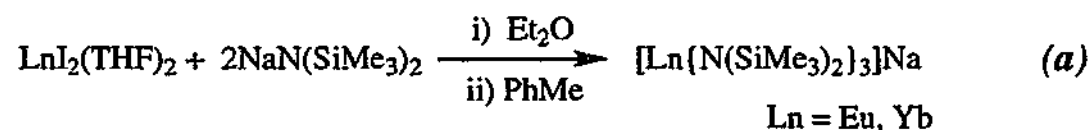


Figure 5.1

In contrast to the preparations above, reaction of  $\text{EuI}_2$  or  $\text{YbI}_2$  with two equivalents of  $\text{NaN}(\text{SiMe}_3)_2$  in  $\text{Et}_2\text{O}$  (1:2 molar ratio) and crystallisation from toluene yielded the bimetallic derivatives  $[\text{Ln}\{\text{N}(\text{SiMe}_3)_2\}_3]\text{Na}$  ( $\text{Ln} = \text{Eu}, \text{Yb}$ ) (*Equation 5.8 (a)*).<sup>[22]</sup> In the case of ytterbium crystallisation from  $\text{Et}_2\text{O}$  gave the solvent adduct  $[\text{Yb}\{\text{N}(\text{SiMe}_3)_2\}_2(\text{OEt}_2)_2]$  (*Equation 5.8 (b)*).<sup>[29]</sup>



Equation 5.8

The ionic complexes  $[\text{Ln}\{\text{N}(\text{SiMe}_3)_2\}_3]\text{Na}$  (Ln = Eu, Yb)<sup>[22]</sup> have similar three-coordinate lanthanoid centres with a planar  $\text{LnN}_3$  arrangement of the amide ligands with one terminal and two bridging nitrogen atoms (*Figure 5.2* (Ln = Eu, Yb)). The sodium forms close inter- and intramolecular  $\text{Na}\dots\text{C}(\text{SiMe}_3)$  contacts thereby linking the  $[\text{Ln}\{\text{N}(\text{SiMe}_3)_2\}_3]\text{Na}$  moieties together. The lanthanoid centre is further saturated by four  $\text{Ln}\dots\text{C}(\text{SiMe}_3)$  agostic interactions (*Figure 5.2*).

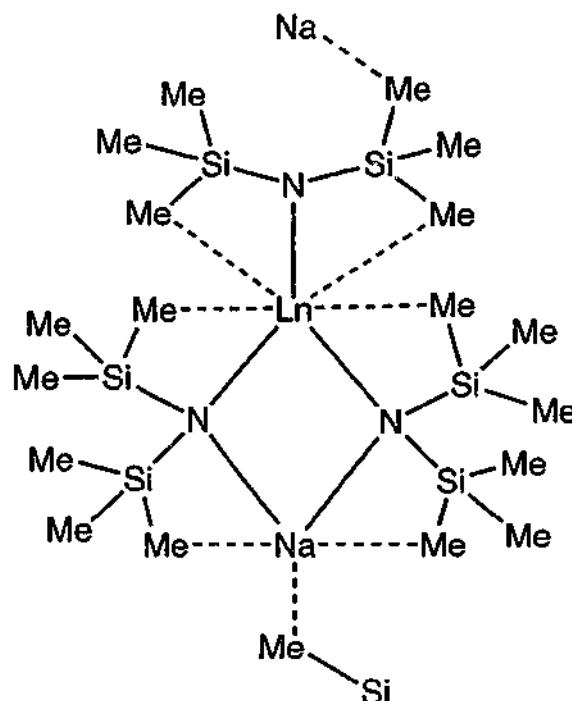


Figure 5.2

The isolation of the solvent-free complex  $[\text{Yb}\{\text{N}(\text{SiMe}_3)_2\}_2]_2$  was successful by heating  $[\text{Yb}\{\text{N}(\text{SiMe}_3)_2\}_2(\text{OEt}_2)]$  to  $80^\circ\text{C}$  in toluene.<sup>[24, 30, 31]</sup> X-ray analysis proved a dimeric species to exist with each ytterbium centre surrounded by two bridging and one terminal amide ligands in addition to two weak  $\text{Yb}\dots\text{C}(\text{SiMe}_3)$  interactions (*Figure 5.3*).

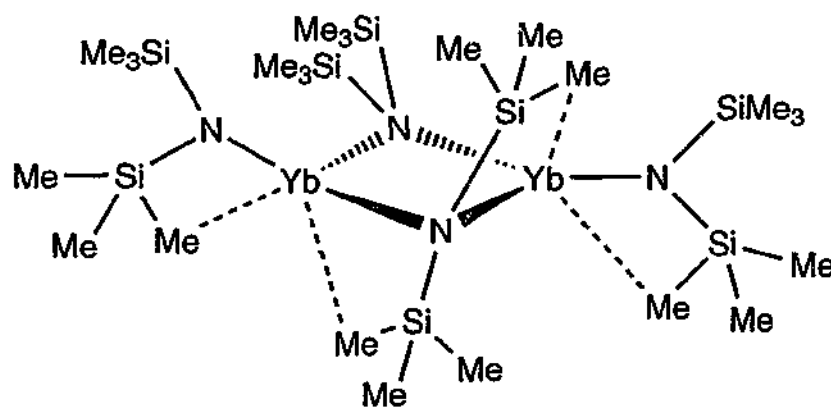
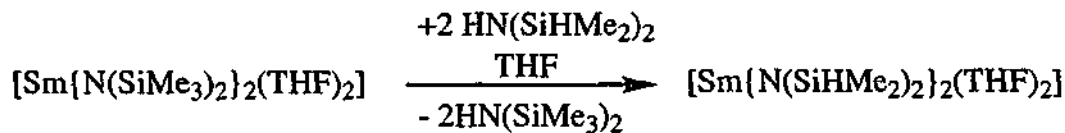


Figure 5.3

The  $\text{N}(\text{SiHMe}_2)_2$  ligand which is less crowded than  $\text{N}(\text{SiMe}_3)_2$  has only recently been examined in lanthanoid(II) chemistry resulting in the stabilisation of the first trinuclear complex  $\text{Sm}[\{\mu\text{-N}(\text{SiHMe}_2)_2\}_2\text{Sm}\{\text{N}(\text{SiHMe}_2)_2\}(\text{THF})_2]$ .<sup>[32]</sup> This species was isolated in low yield from an exchange reaction between  $[\text{Sm}\{\text{N}(\text{SiMe}_3)_2\}_2(\text{THF})_2]$  and two equivalents of  $\text{HN}(\text{SiMe}_2\text{H})_2$  in THF (Equation 5.9). The anticipated complex  $[\text{Sm}\{\text{N}(\text{SiHMe}_2)_2\}_2(\text{THF})_2]$  was isolated and it was found to be structurally similar to  $[\text{Sm}\{\text{N}(\text{SiMe}_3)_2\}_2(\text{THF})_2]$ . A X-ray crystallographic study on the trinuclear species  $\text{Sm}[\{\mu\text{-N}(\text{SiHMe}_2)_2\}_2\text{Sm}\{\text{N}(\text{SiHMe}_2)_2\}(\text{THF})_2]$  revealed that the outer metal centres have a coordinated THF molecule, as well as a bridging and terminal amide ligand. The central samarium atom is solely surrounded by four bridging organoamide ligands. Furthermore, multiple  $\text{Sm}\cdots\text{SiH}$   $\beta$ -interactions were detected which help to sterically and electronically saturate the samarium(II) centres (Figure 5.4).



Equation 5.9

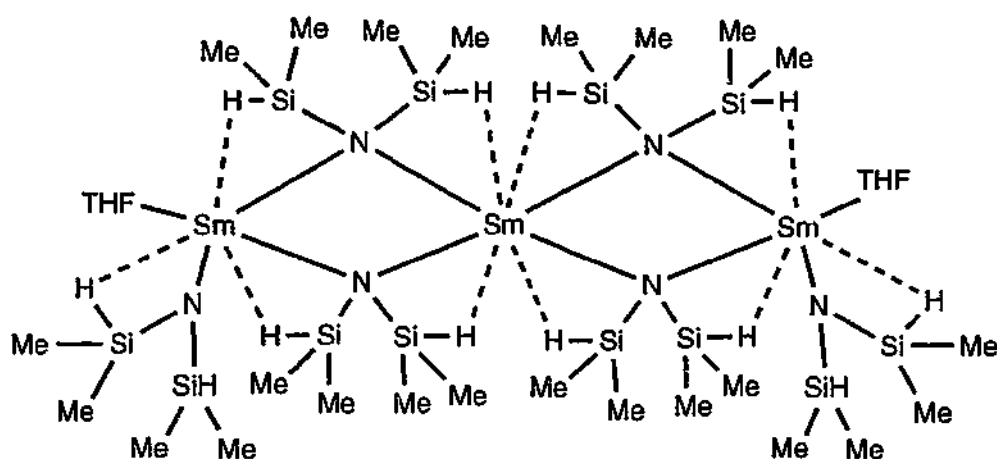
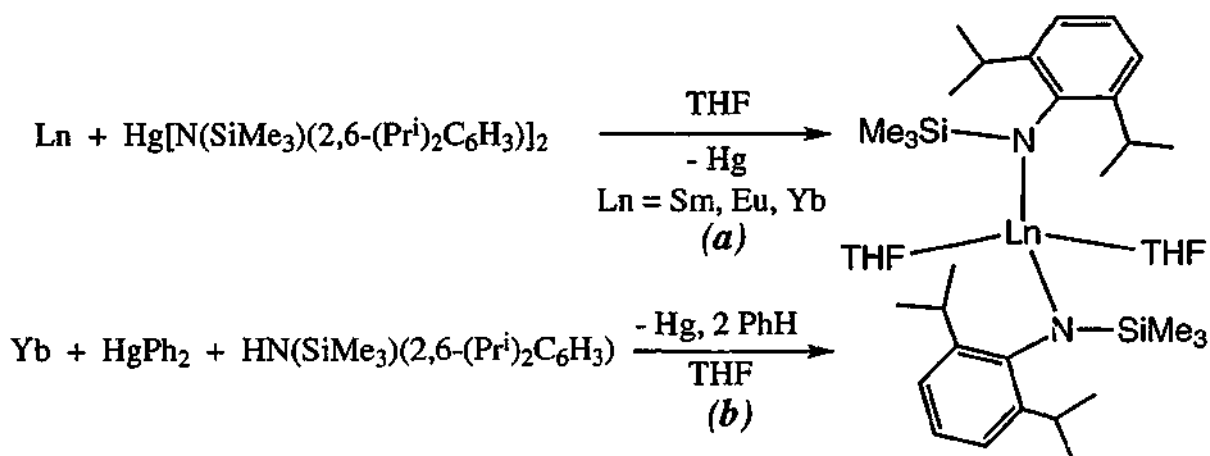


Figure 5.4

Utilising the bulkier organoamide ligand  $N(\text{SiMe}_3)(2,6\text{-}(\text{Pr}^i)_2\text{C}_6\text{H}_3)$  the lanthanoid(II) products ( $[\text{Ln}\{N(\text{SiMe}_3)(2,6\text{-}(\text{Pr}^i)_2\text{C}_6\text{H}_3)\}_2(\text{THF})_2]$   $\text{Ln} = \text{Sm}, \text{Eu}, \text{Yb}$ ) were obtained.[27] Redox transmetallation reactions were carried out using the mercury(II) amide complex  $\text{Hg}\{N(\text{SiMe}_3)(2,6\text{-}(\text{Pr}^i)_2\text{C}_6\text{H}_3)\}_2$  and elemental samarium, europium or ytterbium in THF solvent (Equation 5.10 (a)). Alternatively the ytterbium and samarium derivatives (with the latter isolated in low yield) were also prepared by a redox transmetallation / ligand exchange reaction from elemental ytterbium or samarium,  $\text{HgPh}_2$  and  $\text{HN}(\text{SiMe}_3)(2,6\text{-}(\text{Pr}^i)_2\text{C}_6\text{H}_3)$  (Equation 5.10 (b)).[27] X-ray structure determinations of  $[\text{Ln}\{N(\text{SiMe}_3)(2,6\text{-}(\text{Pr}^i)_2\text{C}_6\text{H}_3)\}_2(\text{THF})_2]$  ( $\text{Ln} = \text{Yb}, \text{Sm}$ ) showed a four-coordinate, distorted tetrahedral metal environment augmented by weak *ortho* phenyl carbon interactions from the organoamide ligand which help saturate the metal centre. These are similar those found in  $[\text{Ln}\{N(\text{SiMe}_3)_2\}_2(\text{S})]$  complexes which have one  $\text{Ln}\cdots\text{C}(\text{SiMe}_3)$  interaction per ligand present.



Equation 5.10

### 5.1.2 Lanthanoid(II) Bidentate Amide Complexes

Reactions using bidentate organoamide ligands in lanthanoid(II) chemistry have had little attention despite the view that the chelate effect should help stabilise Ln(II) centres. The benzamidinate ligand has been utilised in divalent lanthanoid chemistry with the reaction of  $\text{YbI}_2(\text{THF})_2$  with two equivalents of sodium *N, N'*-bis(trimethylsilyl)-benzamidinate in THF yielding the complexes  $[\text{Yb}\{4\text{-RC}_6\text{H}_4\text{C}(\text{NSiMe}_3)_2\}_2(\text{THF})_2]$  ( $\text{R} = \text{H}, \text{OMe}$ ).<sup>[33]</sup> These complexes are very sensitive to oxidation to give the corresponding trivalent homoleptic product  $[\text{Yb}\{4\text{-RC}_6\text{H}_4\text{C}(\text{NSiMe}_3)_2\}_3]$ . An X-ray structure determination on the complex  $[\text{Yb}\{\text{C}_6\text{H}_5\text{C}(\text{NSiMe}_3)_2\}_2(\text{THF})_2]$  revealed the metal centre is surrounded by two *trans* THF molecules and two organoamide ligands in a distorted octahedral environment (*Figure 5.5*).

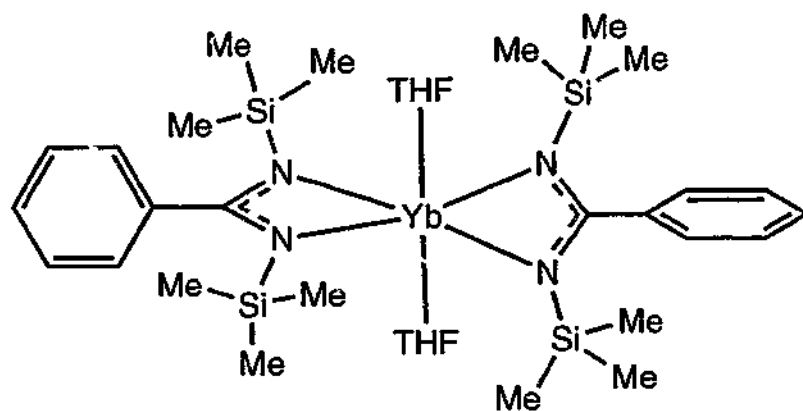
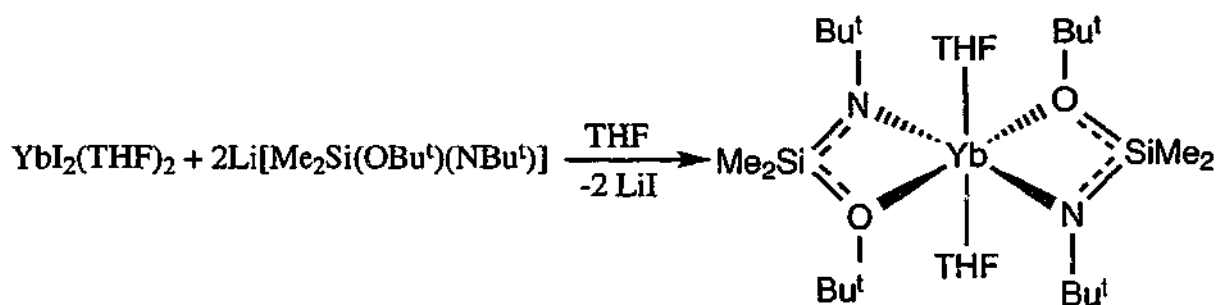


*Figure 5.5*

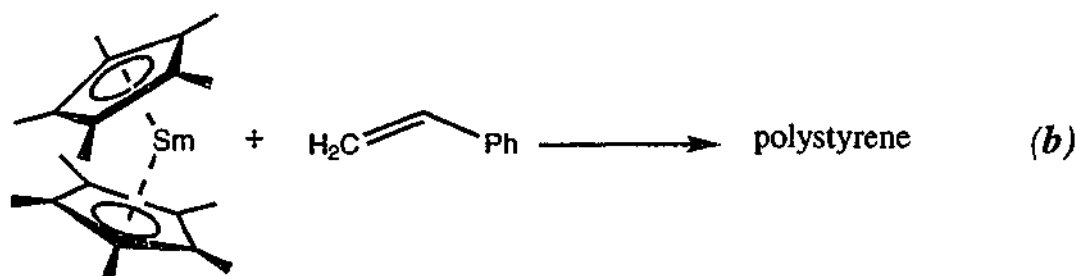
In a similar manner,  $\text{Li}[\text{Me}_2\text{Si}(\text{OBU}^t)(\text{NBu}^t)]$  reacts with  $\text{YbI}_2$  to give the ytterbium(II) alkoxy-silylamide  $[\text{Yb}(\text{Me}_2\text{Si}(\text{OBU}^t)(\text{NBu}^t))_2(\text{THF})_2]$  (*Equation 5.11*) in high yield.<sup>[34]</sup> No X-ray characterisation was performed on this complex but a similar structure to that of  $[\text{Yb}\{\text{C}_6\text{H}_5\text{C}(\text{NSiMe}_3)_2\}_2(\text{THF})_2]$  was presumed. The analogous reaction using  $\text{SmI}_2(\text{THF})_2$  with  $\text{Li}[\text{Me}_2\text{Si}(\text{OBU}^t)(\text{NBu}^t)]$  did not give the Sm(II) product but instead yielded the Sm(III) derivative  $[\text{Sm}\{\text{Me}_2\text{Si}(\text{OBU}^t)(\text{NBu}^t)\}_2(\mu\text{-I})_2\text{Li}(\text{THF})_2]$ .<sup>[34]</sup>



Equation 5.11

### 5.1.3 Oxidation of Lanthanoid(II) Organoamide Complexes

Oxidative pathways utilising the reducing nature of divalent organolanthanoids have yielded many heteroleptic complexes.[35-39] In some cases these have been otherwise unobtainable from the standard metathesis approaches, for example reductive defluorination of fluorocarbons by cyclopentadienyllanthanoid(II) compounds yields complexes of the type  $\text{Ln}(\text{Cp})_2\text{F}$  which cannot be prepared from the very insoluble  $\text{LnF}_3$ . [37, 40-42] The reducing behaviour of  $\text{LnCp}_2$  with other oxidising agents such as metal salts, e.g.  $\text{Hg}(\text{C}_6\text{F}_5)_2$ , has also been explored (e.g. *Equation 5.12 (a)*) giving  $\text{Ln}(\text{Cp})_2\text{R}$  complexes.[2, 37, 43] Furthermore, a diverse range of reactivities has been found for  $\text{Sm}(\text{C}_5\text{Me}_5)_2$  (e.g. olefin polymerisation (*Equation 5.12 (b)*))[35, 44] which indicates that the divalent lanthanoid species is a viable precursor for active lanthanoid(III) catalysts.



Equation 5.12

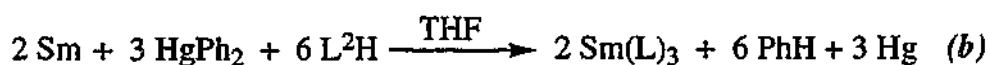
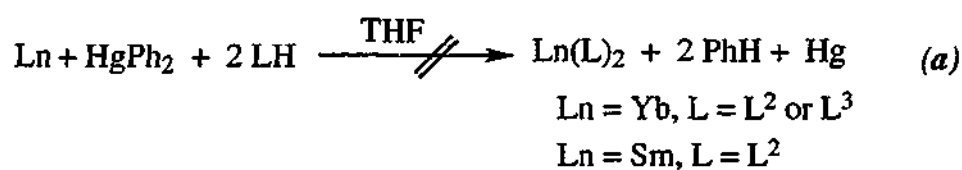
By comparison with oxidation reactions of the cyclopentadienyl ligated lanthanoid(II) complexes,<sup>[2]</sup> reactions of the organoamidolanthanoid(II) derivatives are relatively undeveloped. Preliminary studies of oxidation reactions of  $[\text{Sm}\{\text{N}(\text{SiMe}_3)_2\}_2(\text{THF})_2]$  with carbon monoxide suggest comparable oxidation chemistry to that of the analogous  $\text{C}_5\text{Me}_5$  compound.<sup>[25]</sup> Oxidation reactions of the benzamidinate complexes  $[\text{Yb}\{4\text{-RC}_6\text{H}_4\text{C}(\text{NSiMe}_3)_2\}_2(\text{THF})_2]$  ( $\text{R} = \text{H}, \text{OMe}$ ) were examined with diaryl diselenides and ditellurides to give ytterbium(III) complexes of the type  $[\text{Yb}\{4\text{-RC}_6\text{H}_4\text{C}(\text{NSiMe}_3)_2\}_2(\text{SeR}')(\text{THF})]$  ( $\text{R} = \text{H}, \text{R}' = \text{Ph}; \text{R} = \text{H}, \text{R}' = \text{Mesityl}$ ) and  $[\text{Yb}\{4\text{-RC}_6\text{H}_4\text{C}(\text{NSiMe}_3)_2\}_2(\text{TeR}')(\text{THF})]$  ( $\text{R} = \text{OMe}, \text{R}' = \text{Mesityl}$ ).<sup>[45]</sup> Cleavage of the S—S bond in  $[\text{Me}_2\text{NC}(\text{S})\text{S}]_2$  with  $[\text{Yb}\{\text{C}_6\text{H}_5\text{C}(\text{NSiMe}_3)_2\}_2(\text{THF})_2]$  has also been investigated and yielded the ytterbium(III) dithiocarbamate,  $\text{Yb}\{\text{C}_6\text{H}_5\text{C}(\text{NSiMe}_3)_2\}_2(\text{S}_2\text{CNMe}_2)$ .<sup>[45]</sup> However, oxidation reactions of other bis(organamido)lanthanoid(II) derivatives have not been reported. The current interest in linked cyclopentadienyl-amide lanthanoid complexes for catalysis has recently inspired the application of these ligands in Ln(II) chemistry and the subsequent oxidation reactions. For example,  $[\text{Ln}(\text{C}_5\text{Me}_4\text{SiMe}_2\text{NPh})(\text{THF})_x]$  ( $\text{Ln} = \text{Yb}, x = 3; \text{Ln} = \text{Sm}, x = 0-1$ )<sup>[46]</sup> undergoes oxidation by organic substrates such as azobenzene and fluorenone and has the ability to polymerise ethylene (presumably involving a Ln(III) intermediate) which parallels the behaviour of classical  $\text{Sm}(\text{C}_5\text{Me}_5)_2$  complexes.



## 5.2 Results and Discussion

### 5.2.1 Transmetallation / Ligand Exchange Reactions using $L^2$ and $L^3$

The preparation of ytterbium(II) complexes of the mixed N, O ligands  $L^2$  and  $L^3$  was initially attempted by a redox transmetallation / ligand exchange reaction in THF (Equation 5.13). In an analogous fashion the samarium(II) complex with  $L^2$  was also investigated using this synthetic route.



Equation 5.13

Red-orange crystals were isolated from the ytterbium reaction mixtures in moderate to low yields after work up. In a similar manner the samarium reaction afforded yellow crystals in moderate yield. The colour is typical of Sm(III) (and contrasts the often intensely dark colour of Sm(II) complexes) and the spectroscopic and analytical data confirmed the product to be  $[\text{Sm}(\text{L}^2)_3]$  (see Chapter 8), previously obtained by metathesis (Chapter 3). For the ytterbium complexes the presence of Yb(III) was apparent with  $f \leftarrow f$  transitions near 1000 nm in the electronic spectra.<sup>[47]</sup> Infrared spectroscopy clearly established that  $L^2$  or  $L^3$  amide ligands were coordinated to the metal centres, but the elemental analyses did not fit the corresponding homoleptic compositions  $\text{Yb}(\text{L}^2)_3$  and  $\text{Yb}(\text{L}^3)_3$ . X-ray crystallography subsequently revealed that the products were the methoxide and phenoxide complexes  $[\text{Yb}(\text{L}^2)_2(\mu\text{-OMe})]_2$  and  $[\text{Yb}(\text{L}^3)_2(\text{OPh})(\text{THF})]$ . Although the infrared spectrum of  $[\text{Yb}(\text{L}^2)_2(\mu\text{-OMe})]_2$  has the majority of bands similar to those of the homoleptic complex  $[\text{Yb}(\text{L}^2)_3]$  (Chapter 4) distinct differences in the C—O—C antisymmetric stretching region near  $1000 \text{ cm}^{-1}$  were observed. Whilst in  $[\text{Yb}(\text{L}^2)_3]$  two sets of two absorptions were observed at  $1059$  and  $1051 \text{ cm}^{-1}$  and  $1012$  and  $1000 \text{ cm}^{-1}$ ,  $[\text{Yb}(\text{L}^2)_2(\mu\text{-OMe})]_2$  has three single bands at  $1050$ ,  $1033$  and  $1005 \text{ cm}^{-1}$ . Since only two single bands are present in this region for  $[\text{Yb}(\text{L}^2)_2(\mu\text{-Cl})]_2$ , it suggests that the third absorption in  $[\text{Yb}(\text{L}^2)_2(\mu\text{-OMe})]_2$  is attributable to C—O stretching of the bridging methoxide anion. For

[Yb(L<sup>3</sup>)<sub>2</sub>(OPh)(THF)] the majority of the absorptions are similar to those of [Nd(L<sup>3</sup>)<sub>2</sub>(μ-Cl)]<sub>2</sub>(PhMe)<sub>2</sub> but an additional peak is present near 800 cm<sup>-1</sup>, which is also found in [Yb(L<sup>3</sup>)<sub>3</sub>]. Furthermore, extra bands in the C—O—C stretching region at 1045 and 842 cm<sup>-1</sup>, not observed for [Nd(L<sup>3</sup>)<sub>2</sub>(μ-Cl)]<sub>2</sub>(PhMe)<sub>2</sub>, can be attributed to coordinated THF. In the mass spectrum of [Yb(L<sup>2</sup>)<sub>2</sub>(μ-OMe)]<sub>2</sub> an ion of weak intensity at *m/z* 990 can be assigned to the loss of a L<sup>2</sup> ligand from the dimer molecular ion. In [Yb(L<sup>3</sup>)<sub>2</sub>(OPh)(THF)] the highest mass cluster corresponded to the unsolvated ion [Yb(L<sup>3</sup>)<sub>2</sub>(OPh)]<sup>+</sup> at *m/z* 779.

**Figure 5.6** displays the molecular structure of [Yb(L<sup>2</sup>)<sub>2</sub>(μ-OMe)]<sub>2</sub>, while the crystal refinement details and selected bond distances and angles are given in **Tables 5.1** and **5.2** respectively. The crystal structure of [Yb(L<sup>2</sup>)<sub>2</sub>(μ-OMe)]<sub>2</sub> has two crystallographically independent but closely similar dimeric molecules. Two bridging methoxide ligands and two chelating L<sup>2</sup> moieties surround each of the six-coordinate ytterbium centres in a distorted octahedral environment. Each dimer is situated on a crystallographic twofold axis passing through the methoxide ligands, therefore the Yb<sub>2</sub>O<sub>2</sub> cores are planar. The overall geometry is similar to that of [Yb(L<sup>2</sup>)<sub>2</sub>(μ-Cl)]<sub>2</sub> with the only structural deviation incurred by the closer approach of the methoxy ligands to the metal centre compared with the chloride anions. The *trans* O(1)—Yb—O(2) angle is slightly more linear than the corresponding angle in the heteroleptic [Yb(L<sup>2</sup>)<sub>2</sub>(μ-Cl)]<sub>2</sub> (see Chapter 4). The bridging methoxide ligands are essentially symmetrical with larger O(11)—Yb—O(12) than Yb—O(1X)—Yb (X = 1 or 2) angles which are virtually identical to those of [Ce(η<sup>5</sup>-1,3-(SiMe<sub>3</sub>)<sub>2</sub>C<sub>5</sub>H<sub>3</sub>)<sub>2</sub>(μ-OMe)]<sub>2</sub>.<sup>[48]</sup> The near equivalent Yb—O(11,12)(Me) bond lengths are comparable with the longer of the two Yb—O(Me) distances (2.210(6), 2.152(4) Å) observed in [YbI<sub>2</sub>(μ-OMe)(DME)]<sub>2</sub> where the Yb—O(Me) bond lengthening was attributed to the *trans* influence of the iodide ligand.<sup>[49]</sup> The Yb—N distances are longer (0.06 Å) compared with those found in [Yb(L<sup>2</sup>)<sub>2</sub>(μ-Cl)]<sub>2</sub> and suggests that the methoxide ligands, which are *transoid* to each nitrogen, may exert a *trans* influence (see also below for OAr *trans* influence). It is unlikely that this elongation is attributable to greater steric crowding in the present structure, since the Yb—O(ether) distances in [Yb(L<sup>2</sup>)<sub>2</sub>(μ-OMe)]<sub>2</sub> (**Table 5.2**) are similar to those in [Yb(L<sup>2</sup>)<sub>2</sub>(μ-Cl)]<sub>2</sub> (**Table 4.2**).

**Table 5.1. Summary of Crystallographic Data for  $[\text{Yb}(\text{L}^2)_2(\mu\text{-OMe})_2]$  and  $[\text{Yb}(\text{L}^3)_2(\text{OPh})(\text{THF})]$**

Compound	$[\text{Yb}(\text{L}^2)_2(\mu\text{-OMe})_2]$	$[\text{Yb}(\text{L}^3)_2(\text{OPh})(\text{THF})]$
Formula	$\text{C}_{42}\text{H}_{70}\text{N}_4\text{O}_6\text{Si}_4\text{Yb}_2$	$\text{C}_{40}\text{H}_{49}\text{N}_2\text{O}_4\text{O}_4\text{Si}_2\text{Yb}$
<i>M</i>	1185.47	851.03
<i>a</i> (Å)	24.1340(4)	24.3109(3)
<i>b</i> (Å)	19.1294(3)	15.0605(2)
<i>c</i> (Å)	23.6252(4)	24.5560(2)
$\alpha$ (°)	90	90
$\beta$ (°)	112.150(1)	118.833(1)
$\gamma$ (°)	90	90
<i>V</i> (Å <sup>3</sup> )	10102.1(3)	7876(3)
Crystal system	monoclinic	monoclinic
Space Group	<i>C2/c</i>	<i>P2<sub>1</sub>/n</i>
<i>Z</i>	4	8
Diffractometer	Nonius Kappa CCD	Nonius Kappa CCD
$\rho_{\text{calcd}}$ (g cm <sup>-3</sup> )	1.559	1.435
$\mu(\text{MoK}\alpha)$ (mm <sup>-1</sup> )	3.820	2.476
$2\theta_{\text{max}}$ (°)	60.06	55.80
<i>N</i> , <i>N<sub>o</sub></i>	14634, 12012	17123, 12245
<i>R</i> , <i>R<sub>w</sub></i> (observed data)	0.028, 0.067	0.054, 0.122
<i>R</i> , <i>R<sub>w</sub></i> (all data)	0.044, 0.089	0.100, 0.165

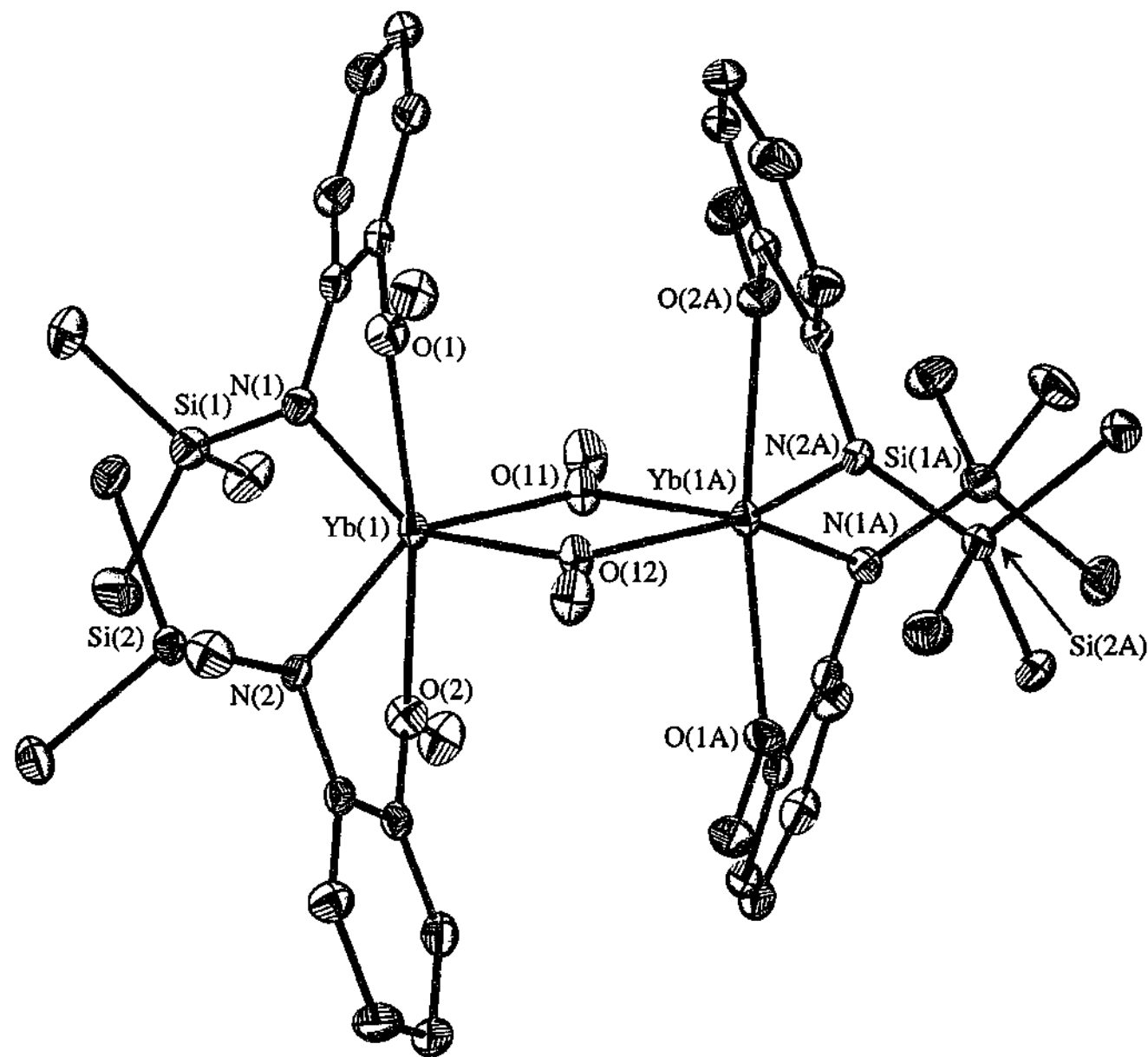


Figure 5.6 Molecular Structure of  $[Yb(L^2)_2(\mu\text{-OMe})_2]$

**Table 5.2** Metal environment in  $[\text{Yb}(\text{L}^2)_2(\mu\text{-OMe})]_2$  (distances in Å, angles °) with estimated standard deviations in parentheses

Yb(1)—N(1)	2.250(3)	N(2)—Yb(1)—O(2)	71.16(9)
Yb(1)—N(2)	2.245(3)	O(11)—Yb(1)—O(12)	72.5(1)
Yb(1)—O(1)	2.346(2)	O(11)—Yb(1)—O(1)	99.85(6)
Yb(1)—O(2)	2.355(2)	O(12)—Yb(1)—O(1)	85.27(6)
Yb(1)—O(11)	2.221(2)	O(11)—Yb(1)—O(2)	85.60(6)
Yb(1)—O(12)	2.217(2)	O(12)—Yb(1)—O(2)	103.17(6)
		O(11)—Yb(1)—N(1)	93.2(1)
N(1)—Yb(1)—N(2)	112.7(1)	O(12)—Yb(1)—N(1)	147.79(8)
N(1)—Yb(1)—O(2)	102.03(9)	O(11)—Yb(1)—N(2)	147.90(7)
N(2)—Yb(1)—O(1)	106.24(9)	O(12)—Yb(1)—N(2)	91.12(9)
O(1)—Yb(1)—O(2)	171.09(8)	Yb(1)—O(11)—Yb(1A) <sup>a</sup>	107.4(1)
N(1)—Yb(1)—O(1)	70.80(9)	Yb(1)—O(12)—Yb(1A) <sup>a</sup>	107.6(1)
<i>Torsion angles</i> (°)		<i>Interplanar angles</i> (°)	
C(13)—C(12)—O(1)—C(10)	10.0(4)	P(1B) <sup>b</sup> —P(1C) <sup>c</sup>	34.2(1)
C(23)—C(22)—O(2)—C(20)	12.1(4)	P(2B) <sup>d</sup> —P(2C) <sup>e</sup>	33.7(1)

<sup>a</sup> symmetry transformation:  $-x, y, -z + 3/2$ ; <sup>b</sup> P(1B) = the plane defined by Yb—N(1)—O(1) atoms; <sup>c</sup> P(1C) = plane defined by the arene backbone (C(11)—C(16)); <sup>d</sup> P(2B) = the plane defined by Yb—N(2)—O(2) atoms; <sup>e</sup> P(2C) = plane defined by the arene backbone (C(21)—C(26)).

The structure of  $[\text{Yb}(\text{L}^3)_2(\text{OPh})(\text{THF})]$  revealed a monomeric complex containing two virtually identical, but independent, monomers in the asymmetric unit one of which is displayed in **Figure 5.7**. Crystal refinement parameters are listed in **Table 5.1** and selected bond distances and angles for one molecule are given in **Table 5.3**. Each ytterbium centre is six-coordinate and contains two chelating  $\text{L}^3$  ligands, a terminal phenoxide and a coordinated THF molecule in an irregular geometry. The  $\text{L}^3$  ligands have a *cisoid* arrangement of the two amide nitrogen atoms (N(1) and N(2)) as well as the ether-OPh atoms (O(1) and O(2)). This is different from the ether environments in  $[\text{Yb}(\text{L}^2)_2(\mu\text{-OMe})]_2$  and  $[\text{Nd}(\text{L}^3)_2(\mu\text{-Cl})]_2(\text{PhMe})_2$ . The phenoxide oxygen (O(3)) is located *transoid* to O(2) while the oxygen atom (O(4)) from the molecule of THF is situated *cis* to N(2), O(1), O(2) and O(4) and is *transoid* to N(1). Whilst the N(1)—Yb(1)—N(2) angle is marginally smaller than in  $[\text{Yb}(\text{L}^2)_2(\mu\text{-OMe})]_2$ , it compares well with those in  $[\text{Nd}(\text{L}^3)_2(\mu\text{-Cl})]_2(\text{PhMe})_2$  (**Table 4.7**, Chapter 4). The C—O bond of the phenyl ether substituent on

each  $L^3$  ligand is in the same plane as the arene backbone (C(13)—C(12)—O(1)—C(111)  $10.7(6)^\circ$ ; C(23)—C(22)—O(2)—C(211)  $28.5(6)^\circ$ ) and rotated near perpendicular to the  $C_6H_4N(O)$  ring (interplanar angles  $75.7(2)^\circ$ ,  $89.1(2)^\circ$ ).

The Yb—N distances in  $[Yb(L^3)_2(OPh)(THF)]$  are nearly equal and are similar to the corresponding lengths in  $[Yb(L^2)_2(\mu-OMe)]_2$ . Subtraction of the six-coordinate ionic radius of  $Yb^{3+}$  gives values ( $\approx 1.38 \text{ \AA}$ ) that are considerably longer than the corresponding values for  $[Nd(L^3)_2(\mu-Cl)]_2 \cdot (PhMe)_2$  (see *Table 5.4*) which presumably reflects the greater steric crowding in the present structure. The steric coordination sum<sup>[50]</sup> of OPh and THF (2.49) is considerably larger than for two chlorides (2.0) and in  $[Nd(L^3)_2(\mu-Cl)]_2 \cdot (PhMe)_2$  the elongation of the Nd—Cl bonds, due to the Nd—Cl—Nd bridging, presumably further reduces steric crowding in this complex. The Yb—O(Ph) bond lengths of  $L^3$  are not symmetrical with Yb—O(2) significantly longer ( $0.08 \text{ \AA}$ ) than Yb—O(1). This lengthening may be attributable to the *trans* influence of the phenoxide ligand. An even greater lengthening of Ln—O(THF) *trans* to 2,6-diphenylphenolates has been reported.<sup>[51]</sup> The O(1) and O(4) oxygen atoms are also in a *trans* position to an anionic nitrogen but the Yb—O(4) distance is comparable to those of the mutually *trans* ether moieties in  $[Yb(L^2)_2(\mu-OMe)]_2$  suggesting that there is no effect of the amide groups upon O(4) and presumably also O(1). Since *trans* influences have been detected in lanthanoid amide systems e.g.  $[Nd(\eta^2-Ph_2pz)_3(OPPh_3)_2] \cdot (DME)$ <sup>[52]</sup> the deviation of the *trans* angles from  $180^\circ$  in the current structure presumably negates bond lengthening for O(1) and O(4). The shorter Yb—O(1) bond length is very similar to those in  $[Nd(L^3)_2(\mu-Cl)]_2 \cdot (PhMe)_2$  (*Table 5.4*) after allowance for ionic radii differences<sup>[17]</sup> and is certainly within the range observed for other lanthanoid complexes containing the  $L^3$  ligand in this thesis ( $1.48$ — $1.62 \text{ \AA}$ ). However the steric coordination sum of OPh and THF (see above) is similar to that of 2,6-di-*tert*-butylphenolate ( $2.41 \text{ \AA}$ ) yet the Yb—O(Ph) distances in  $[Yb(L^3)_2(OAr)]$  ( $OAr = 2,6-(Bu^t)_2C_6H_3O$ ) are much longer than in the current structure. The bonding in the former was influenced by ligand-ligand repulsion (see Chapter 4; Section 4.2.3) and therefore was unusually long.

Subtraction of the ionic radii from the Yb—O(3)(Ph) distance gives a value ( $1.15 \text{ \AA}$ ) slightly shorter than that of the terminal 2,6-( $Bu^t$ )<sub>2</sub> aryloxy ligand (*Table 5.4*) five-coordinate in  $[Yb(L^3)_2(OAr)]$  (Chapter 4) but is much lower than the corresponding

aryloxy distances in  $[\text{Yb}(2,4,6\text{-}(\text{Bu}^t)_3\text{C}_6\text{H}_2\text{O})_3(\text{THF})]$  [53] and  $[\text{Yb}(\text{Odpp})_3(\text{THF})_2]\cdot\text{THF}$  (Table 5.4). [54] However this value is somewhat longer than that derived from the  $\text{Tm}-\text{O}(\text{Ph})$  distance (Table 5.4) in uncrowded  $[\text{TmI}_2(\text{OPh})(\text{DME})_2]$  which is the only other reported lanthanoid complex with a crystallographically established terminal unsubstituted phenoxide ligand. [55] This indicates that in the current structure, greater steric crowding is present. Thus there must be a fine balance between the formation of a six-coordinate THF-free species, e.g.  $[\text{Yb}(\text{L}^3)_2(\mu\text{-OPh})_2]$ , and the current THF complex, since OPh is only marginally bulkier than THF.

Table 5.3 Metal environment in  $[\text{Yb}(\text{L}^3)_2(\text{OPh})(\text{THF})]$  (distances in Å, angles °) with estimated standard deviations in parentheses

Yb(1)—N(1)	2.250(5)	O(3)—Yb(1)—O(4)	86.1(2)
Yb(1)—N(2)	2.247(5)	N(1)—Yb(1)—O(1)	70.7(2)
Yb(1)—O(1)	2.380(4)	N(2)—Yb(1)—O(2)	69.9(2)
Yb(1)—O(2)	2.459(5)	N(1)—Yb(1)—O(2)	82.5(2)
Yb(1)—O(3)	2.023(6)	N(1)—Yb(1)—O(3)	104.3(2)
Yb(1)—O(4)	2.357(4)	N(1)—Yb(1)—O(4)	150.3(2)
N(1)—Yb(1)—N(2)	107.0(2)	N(2)—Yb(1)—O(1)	155.2(2)
O(1)—Yb(1)—O(2)	85.4(2)	N(2)—Yb(1)—O(3)	108.4(2)
O(1)—Yb(1)—O(3)	95.9(2)	N(2)—Yb(1)—O(4)	95.6(2)
O(1)—Yb(1)—O(4)	80.7(2)	<i>Interplanar angles (°)</i>	
O(2)—Yb(1)—O(4)	87.5(2)	P(1A) <sup>a</sup> —P(1B) <sup>b</sup>	15.8(2)
O(2)—Yb(1)—O(3)	173.2(2)	P(1A) <sup>a</sup> —P(1B) <sup>b</sup>	40.0(1)

<sup>a</sup> P(1A) = the plane defined by Yb—N(1)—O(1) atoms; <sup>b</sup> P(1B) = plane defined by the arene backbone (C(11)—C(16)).

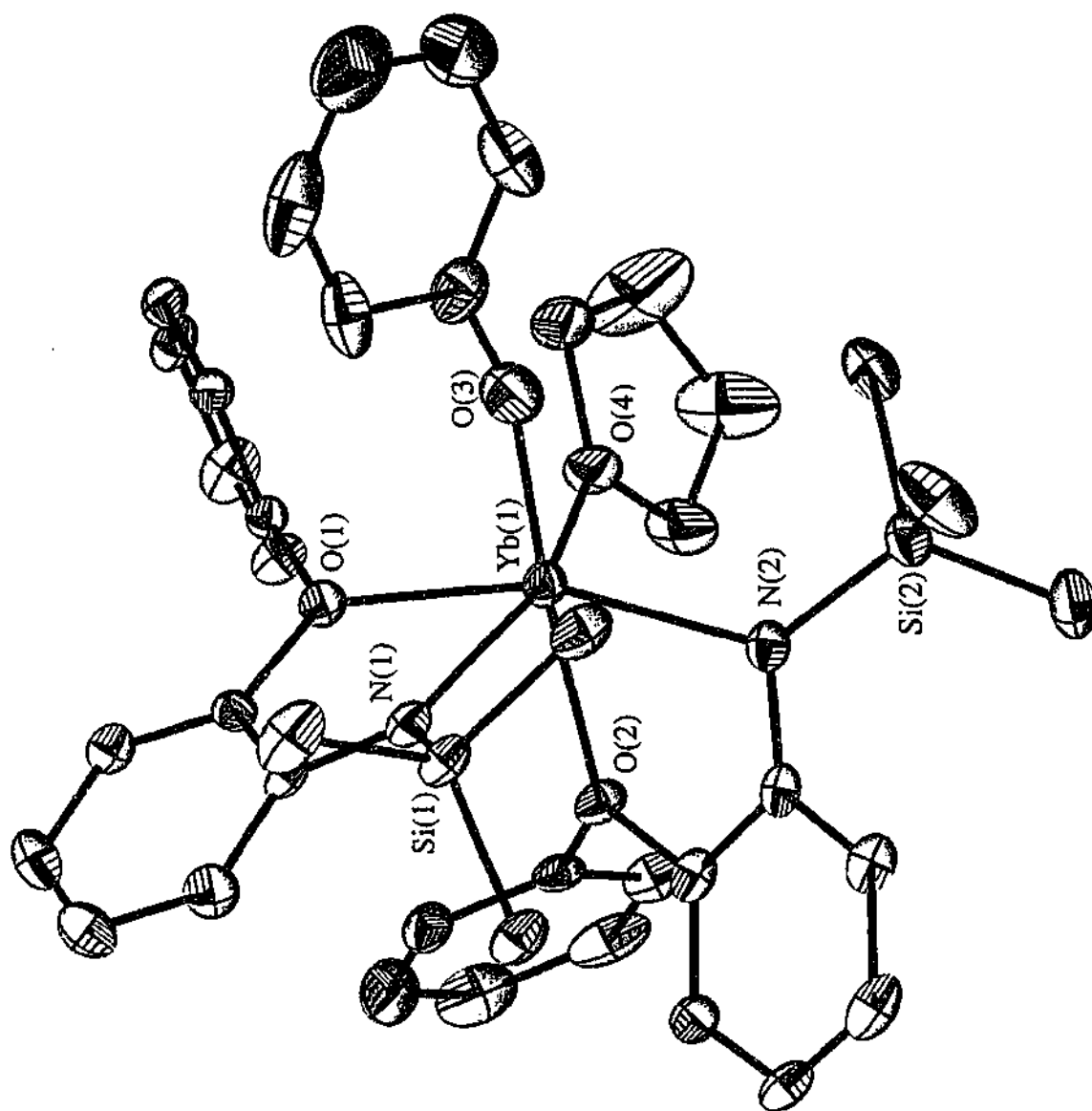


Figure 5.7 Molecular Structure of  $[Yb(L^3)_2(OPh)(THF)]$



Table 5.4 Lanthanoid nitrogen and oxygen distances of a selection of organoamide lanthanoid complexes.

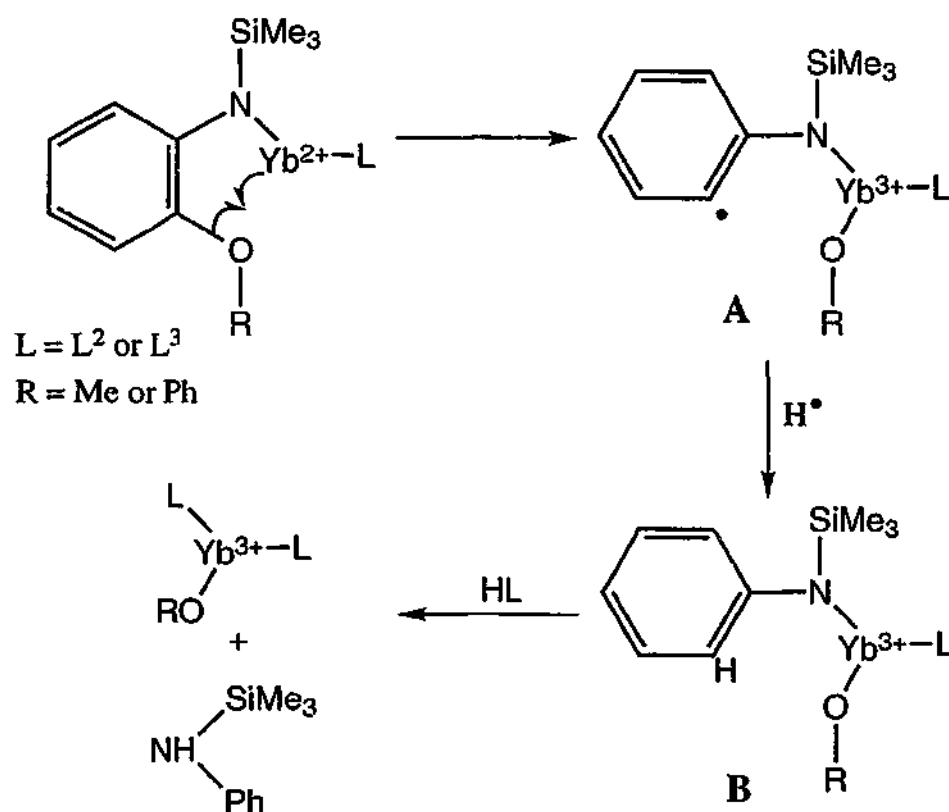
Complex	Ref	Av. Ln—N(amide) distance (d(N)) (Å)	Av. Ln—O(L) distance (d{O(L)}) (Å)	Av. Ln—O(Ar) distance (d{O(Ar)}) (Å)	Ionic radii of Ln <sup>3+</sup> (i.r.) (Å) <sup>a</sup>	d(N)-i.r. (Å)	d{O(L)}-i.r. (Å)	d{O(Ar)}-i.r. (Å)
[Yb(L <sup>3</sup> ) <sub>2</sub> (OPh)(THF)] <sup>a</sup>	this work	2.25	2.38	2.02	0.87	1.38	1.51	1.15
[Yb(L <sup>2</sup> ) <sub>2</sub> (μ-OMe)] <sub>2</sub>	this work	2.25	2.35	—	0.87	1.38	1.48	—
[Nd(L <sup>3</sup> ) <sub>2</sub> (μ-Cl)] <sub>2</sub> ·(PhMe) <sub>2</sub>	Chapter 4	2.31	2.54	—	0.98	1.33	1.56	—
[Yb(L <sup>2</sup> ) <sub>2</sub> (μ-Cl)] <sub>2</sub>	Chapter 4	2.19	2.35	—	0.87	1.32	1.48	—
[Yb(L <sup>3</sup> ) <sub>2</sub> (OAr)] (OAr = 2,6-(Bu <sup>t</sup> ) <sub>2</sub> C <sub>6</sub> H <sub>3</sub> O)	Chapter 4	2.13	2.44	1.98	0.82 <sup>c</sup>	1.31	1.62	1.16
[Yb(L <sup>3</sup> ) <sub>3</sub> ](S) (S = MePh, C <sub>5</sub> H <sub>9</sub> Me)	Chapter 3	2.26	2.37	—	0.87	1.40	1.50	—
[Nd(L <sup>2</sup> ) <sub>3</sub> ]	Chapter 3	2.37	2.54	—	0.98	1.39	1.56	—
[Yb(2,4,6-(Bu <sup>t</sup> ) <sub>3</sub> C <sub>6</sub> H <sub>2</sub> O) <sub>3</sub> (THF)]	[53]	—	—	2.03	0.76	—	—	1.27
[Yb(Odpp) <sub>3</sub> (THF) <sub>2</sub> ].THF	[54]	—	—	2.09	0.82	—	—	1.27
[TmL <sub>2</sub> (OPh)(DME) <sub>2</sub> ]	[55]	—	—	2.03	0.93 <sup>c</sup>	—	—	1.10
[Yb(2,6-(Bu <sup>t</sup> ) <sub>2</sub> -4-MeC <sub>6</sub> H <sub>2</sub> O) <sub>2</sub> (THF) <sub>2</sub> ]	[56]	—	—	2.14	0.92	—	—	1.24
[Nd(Odpp) <sub>3</sub> (THF) <sub>2</sub> ].THF	[51]	—	—	2.19	0.92	—	—	1.27

<sup>a</sup> Values from Shannon's tables<sup>[17]</sup>; <sup>b</sup> Comparison using the short oxygen distance only; <sup>c</sup> Extrapolated from higher coordination numbers from <sup>a</sup>.

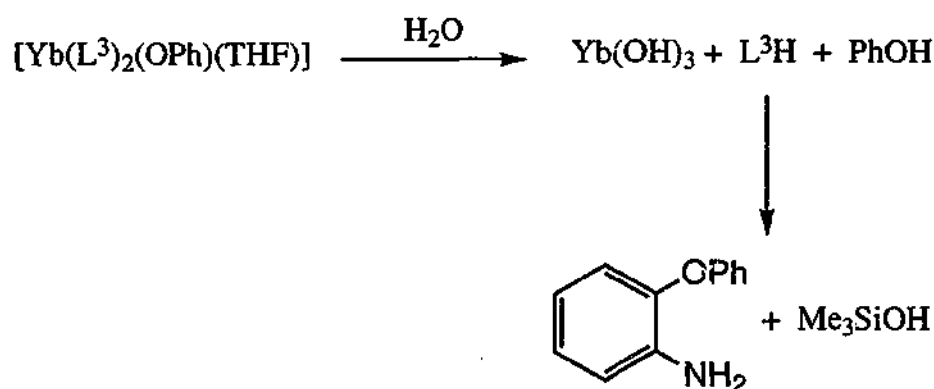
### 5.2.1.1 Proposed Reaction Pathway

Initially the origin of the methoxide group in  $[\text{Yb}(\text{L}^2)_2(\mu\text{-OMe})_2]$  was unclear since recrystallisation of the isolated product involved DME which could be a plausible OMe source.<sup>[48, 49]</sup> On repeating this transmetallation / ligand exchange reaction in the absence of DME, when the product was treated with  $\text{Et}_2\text{O}$  and recrystallised from hexane, the same complex was obtained in similar yield (see Chapter 8). On further investigation it was shown that the initial product was the divalent complex  $[\text{Yb}(\text{L}^2)_2(\text{THF})_2]$  although observation of  $\text{Yb}^{2+}$  and  $\text{Yb}^{3+}$  ions in the electronic spectrum indicated that some oxidation had already occurred prior to work up. The observation of a satisfactory, albeit broad,  $^1\text{H}$  NMR spectrum indicated that the bulk product was the diamagnetic ytterbium(II) complex. Furthermore, the authentic complex  $[\text{Yb}(\text{L}^2)_2(\text{THF})_2]$  (see next section) has been shown to convert into  $[\text{Yb}(\text{L}^2)_2(\mu\text{-OMe})_2]$  in the presence of an excess of  $\text{L}^2\text{H}$  in hexane. It is proposed that the formation of  $[\text{Yb}(\text{L}^2)_2(\mu\text{-OMe})_2]$  and  $[\text{Yb}(\text{L}^3)_2(\text{OPh})(\text{THF})]$  occurs by a one-electron transfer from  $\text{Yb}^{2+}$  to an  $\text{L}^2$  or  $\text{L}^3$  ligand which results in cleavage of the  $\text{Ar-O}$  bond (*Scheme 5.1 (A)*) and formation of an  $\text{Yb}^{3+}\text{-OR}$  ( $\text{R} = \text{Me}, \text{Ph}$ ) bond (*Scheme 5.1*) and  $\text{H}\cdot$  capture by the intermediate radical (*Scheme 5.1 (B)*). Similar mechanisms have been proposed earlier for C—F activation of  $\text{C}_6\text{F}_5\text{CO}_2\text{H}$  by  $\text{YbR}_2$ .<sup>[57, 58]</sup> Subsequent reaction with  $\text{L}^2\text{H}$  or  $\text{L}^3\text{H}$  present as reactants (*Equation 5.13*) gives the observed products and free  $\text{HNPh}(\text{SiMe}_3)$ . Evidence for formation of the latter was obtained by GC-MS analysis of the hydrolysed filtrate after the isolation of  $[\text{Yb}(\text{L}^3)_2(\text{OPh})(\text{THF})]$ . Whilst the analysis showed the presence of phenol and *o*-phenoxyaniline (*Scheme 5.2*), which are the expected products of hydrolysis of  $[\text{Yb}(\text{L}^3)_2(\text{OPh})(\text{THF})]$ , it also detected aniline which is the product of hydrolysis of the proposed  $\text{HNPh}(\text{SiMe}_3)$ . The sensitivity of the *N*-trimethylsilylamine ligands  $\text{L}^2\text{H}$  and  $\text{L}^3\text{H}$  to hydrolysis was established by partial conversion of  $\text{L}^2\text{H}$  into *o*-methoxyaniline on exposure to air. Previous examples of C—O activation by divalent lanthanoid centres are rare and include cleavage of DME by  $\text{YbI}_2$ .<sup>[49]</sup> and  $\text{Ln}(\eta^5\text{-1,3-R}_2\text{C}_5\text{H}_3)_2$  ( $\text{Ln} = \text{Ce}, \text{R} = \text{Bu}^t$  or  $(\text{SiMe}_3)$ ;  $\text{Ln} = \text{Nd}, \text{R} = (\text{SiMe}_3)$ ).<sup>[48]</sup> In the latter, abstraction by the lanthanoid of methoxy radicals was proposed with the other detected product being ethylene. Recently exploration of highly novel Tm(II) chemistry provided an example of reductive cleavage of diethyl ether giving  $[\{\text{Tm}(\text{C}_5\text{Me}_5)_2\}_2(\mu\text{-OEt})_2\{\text{Tm}(\text{C}_5\text{Me}_5)\}(\mu\text{-O})\{\text{Tm}(\text{C}_5\text{Me}_5)_2\}]$ <sup>[59]</sup> showing that not only OR cleavage but also oxygen abstraction may be possible. Other

plausible mechanisms, such as the direct reduction of the aryl ether by ytterbium metal, would seem unlikely under the present conditions, for alkali metal cleavage of ethers is known.[60] Furthermore, methoxy substituted aryloxy ligands have previously been used in the presence of Yb metal without the detection of ether cleavage.[61]



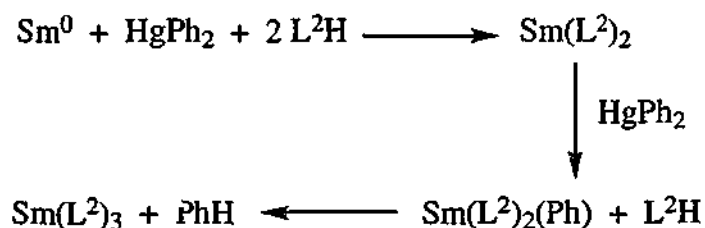
Scheme 5.1



Scheme 5.2

The formation of  $[\text{Sm}(\text{L}^2)_3]$  rather than a  $\text{Sm}(\text{L}^2)_2(\text{OMe})$  species from the redox transmetallation / ligand exchange reaction (Equation 5.13 (b)) may result from oxidation of a transient  $\text{Sm}(\text{L}^2)_2$  complex by  $\text{HgPh}_2$  and subsequent protolysis of the resulting

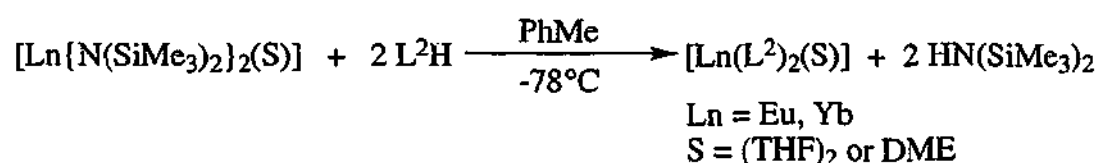
$\text{Sm}(\text{L}^2)_2(\text{Ph})$  by  $\text{L}^2\text{H}$  (Equation 5.14). This oxidation reaction has previously been observed for bis(2-phenylindolyl)samarium(II) but with  $\text{Hg}(\text{C}_6\text{F}_5)_2$  not  $\text{HgPh}_2$ .<sup>[20]</sup> The course of Equation 5.13 (b) is presumably influenced by the stronger reducing potential<sup>[62]</sup> of  $\text{Sm}(\text{II})$  compared with  $\text{Yb}(\text{II})$  allowing rapid reaction of the  $\text{Sm}(\text{II})$  species with  $\text{HgPh}_2$ . It has been shown that  $[\text{Yb}(\text{C}_5\text{H}_5)_2(\text{DME})]$  does not react with  $\text{HgPh}_2$ <sup>[43]</sup> in contrast to the rapid formation of  $[\text{Sm}(\text{C}_5\text{Me}_5)_2(\text{Ph})(\text{THF})]$  from an analogous reaction of  $\text{Sm}(\text{C}_5\text{Me}_5)_2$  with  $\text{HgPh}_2$ .<sup>[63]</sup> Furthermore divalent  $\text{Yb}(\text{II})$  products are favoured from redox transmetallation / ligand exchange reactions utilising  $\text{HgPh}_2$  whereas with more reactive mercurials,  $\text{Yb}(\text{III})$  products are obtained.<sup>[64, 65]</sup>



Equation 5.14

### 5.2.2 Ligand Exchange Reactions using $L^2$ and $L^3$

As a result of difficulties encountered in trying to prepare the divalent lanthanoid derivatives of  $L^2$  or  $L^3$  by a metal-based synthesis, a ligand exchange reaction was used. Thus treatment of  $[Ln\{N(SiMe_3)_2\}_2(S)]$  ( $Ln = Yb$  or  $Eu$ ;  $S = (THF)_2$  or  $DME$ ) with two equivalents of  $L^2H$  in toluene at  $-78^\circ$  afforded the divalent complexes  $[Ln(L^2)_2(S)]$  ( $Ln = Yb$  or  $Eu$ ;  $S = (THF)_2$  or  $DME$ ) (Equation 5.15). However analogous reactions using  $[Yb\{N(SiMe_3)_2\}_2(THF)_2]$  and  $L^3H$  were unsuccessful due to the immediate oxidation to  $[Yb(L^3)_2(OPh)(THF)]$  which was confirmed by electronic and infrared spectroscopy.



Equation 5.15

The THF derivatives  $[Ln(L^2)_2(THF)_2]$  ( $Ln = Eu, Yb$ ) were found to be thermally unstable above  $-20^\circ C$  and as a result satisfactory elemental analyses could not be obtained. Although a similar thermal instability was also encountered for the DME complex  $[Yb(L^2)_2(DME)]$ , a satisfactory ytterbium analysis was obtained (immediately after isolation of the product) establishing the proposed composition. In contrast the product  $[Eu(L^2)_2(DME)]$  showed no signs of decomposition at room temperature and gave satisfactory C, H analyses. Their infrared spectra showed absorptions characteristic of the  $L^2$  ligand and revealed the presence of the ether donors by C—O—C absorptions near 1050 (antisymmetric) and 830 (symmetric)  $cm^{-1}$ . The visible/near-IR spectra in DME of the two divalent ytterbium derivatives immediately on isolation were similar showing a moderately intense band attributable to  $Ln \rightarrow L$  charge transfer and no absorptions attributable to  $Yb^{3+}$  were detected near 1000 nm in the near-infrared region. On standing the DME solution of  $[Yb(L^2)_2(DME)]$  for 48 h, the electronic spectrum showed a significant reduction in the intensity of the  $Ln \rightarrow L$  absorption and the appearance of bands at 905 and 981 nm confirming the presence of  $Yb^{3+}$ .

The  $^1H$  NMR spectra of the diamagnetic ytterbium(II) complexes,  $[Yb(L^2)_2(THF)_2]$  and  $[Yb(L^2)_2(DME)]$  showed the appropriate  $L^2$  to THF (1:2) or DME (1:1) mole ratio. The spectra exhibited similar  $SiMe_3$  and  $OMe$  resonances and aromatic peaks

attributable to coordinated  $L^2$ . The THF resonances of  $[Yb(L^2)_2(THF)_2]$  are at lower frequencies than for free THF suggesting the complex remains relatively intact in solution. In contrast the DME resonances of  $[Yb(L^2)_2(DME)]$  are very broad indicating that the exchange of free and coordinated DME molecules occurs in solution. Heating the NMR solutions resulted in complete loss of the resonances of the divalent complex and presumably those of the product were severely broadened by the presence of paramagnetic  $Yb^{3+}$ .

A single crystal structure determination on each of the divalent complexes  $[Ln(L^2)_2(S)]$  ( $Ln = Yb$  or  $Eu$ ;  $S = (THF)_2$  or  $DME$ ) confirmed the proposed compositions. The tetrahydrofuran complexes are isostructural and an ORTEP diagram of  $[Yb(L^2)_2(THF)_2]$  is shown in *Figure 5.8*. In a similar manner the DME ligated complexes are isostructural with each other having a disordered molecule of 1,2-dimethoxyethane. One particular conformation for  $[Eu(L^2)_2(DME)]$  is displayed in *Figure 5.9*. A summary of the crystal refinement parameters for the  $[Ln(L^2)_2(S)]$  ( $Ln = Yb$  or  $Eu$ ;  $S = (THF)_2$  or  $DME$ ) complexes is listed in *Table 5.5*, while selected bond lengths and angles are compiled in *Table 5.6*. The divalent complexes are monomeric with the six-coordinate lanthanoid atom situated on a two-fold rotation axis surrounded by two chelating  $L^2$  ligands and two *cisoid* THF molecules or one bidentate DME ligand. The arrangement of the  $L^2$  ligand in the two structural types is similar with *cis* silylamide groups and *transoid* OMe substituents. However differences in the coordination polyhedra (best fit polyhedron<sup>[66]</sup>) between the two adducts exist. The  $[Ln(L^2)_2(DME)]$  ( $Ln = Eu, Yb$ ) complexes are distorted octahedral, but the THF complexes do not correspond closely to any polyhedron and are simply irregular. As a result of the fixed bidentate DME angles (compared with two monodentate THF ligands in the former), the DME complexes have a somewhat more ordered polyhedron. The distortion from regular octahedral geometry in the DME derivatives is evident from the large  $N(1)-Ln(1)-N(2)$  angles (see *Table 5.6*). This large distortion is also observed in the THF derivatives and it is not unusual with similar  $N-Ln-N$  angles observed in  $[Yb(cbz)_2(THF)_2(DME)]$  ( $107.3(7)^\circ$ )<sup>[67]</sup> and  $[Sm(NPh_2)_2(THF)_4]$  ( $121.7(2)^\circ$ ).<sup>[18]</sup> An even larger angle ( $134.5(2)^\circ$ ) is evident in the structure of  $[Eu\{N(SiMe_3)_2\}_2(DME)_2]$ .<sup>[21]</sup>

Subtraction of the appropriate ionic radii from the  $Ln-N$  and  $Ln-O$ (ether) bond lengths gives values that can be compared to each other as well as to different

organoamidolanthanoid structures and a list of such is given in *Table 5.7*. Comparison of the lanthanoid—nitrogen distances in the current set of structures show values in a similar region but some differences were observed. A marginally longer Yb—N distance for  $[\text{Yb}(\text{L}^2)_2(\text{THF})_2]$  was found which is consistent with greater steric crowding in the complex resulting from the coordination of two *cisoid* THF ligands compared with one DME molecule and the smaller  $\text{Ln}^{2+}$  (steric coordination numbers; 1.78 and 2.42 (for 2 THF ligands) respectively).<sup>[50]</sup> On the reverse end of the scale, the less sterically crowded complex  $[\text{Eu}(\text{L}^2)_2(\text{DME})]$  also is consistent with this pattern showing a slight contraction of the Eu—N bond length. In general the amide subtraction lengths are shorter than those of the six-coordinate complexes  $[\text{Yb}(\text{cbz})_2(\text{THF})_2(\text{DME})]$ <sup>[67]</sup> and  $[\text{Yb}(\text{L}^2)_2(\mu\text{-OMe})_2]$  but are marginally longer than the corresponding distances in  $[\text{Sm}\{\text{N}(\text{SiMe}_3)_2\}_2(\text{THF})_2]$  (see *Table 5.7*).<sup>[25]</sup> Whilst the Ln—O(ether) distances are significantly shorter in comparison with the other lanthanoid complexes containing the  $\text{L}^2$  ligand, they are longer than the *trans* THF ytterbium bond lengths in  $[\text{Yb}\{\text{PhC}(\text{NSiMe}_3)_2\}_2(\text{THF})_2]$ .<sup>[33]</sup> The Yb—O(THF) and Yb—O(DME) distances of the current divalent products are similar and are longer than the average lanthanoid ether distances found in  $[\text{Yb}\{\text{PhC}(\text{NSiMe}_3)_2\}_2(\text{THF})_2]$ , which has *trans* arrangement of the THF ligands, and in  $[\text{Eu}\{\text{N}(\text{SiMe}_3)_2\}(\text{DME})_2]$ , respectively. Lengthening of Ln—O bonds in the current structures compared to complexes with *trans* THF ligands is due to a greater *trans* influence of N than O(THF). The O(THF)—Ln—O(THF) angle as well as the DME bite angles are similar to those found in  $[\text{Yb}(\text{cbz})_2(\text{THF})_2(\text{DME})]$  (87.6(6) and 65.8(5)° respectively). The orientation of  $\text{L}^2$  in  $[\text{Ln}(\text{L}^2)_2(\text{S})]$  (Ln = Yb or Eu; S = (THF)<sub>2</sub> or DME) has the nitrogen and oxygen substituents in line with the arene backbone plane (average torsional angle C(13)—C(12)—O(1)—C(10) 5.0°). No tilting of the aromatic backbone towards the lanthanoid(II) centre was observed (average interplanar angle 2.0°).

Table 5.5 Summary of crystal refinement data of  $[Ln(L^2)_2(S)]$  ( $Ln = Eu, Yb$ ;  $S = (THF)_2, DME$ ) complexes.

Compound	$[Yb(L^2)_2(THF)_2]$	$[Eu(L^2)_2(THF)_2]^a$	$[Yb(L^2)_2(DME)]$	$[Eu(L^2)_2(DME)]$
Formula	$C_{23}H_{48}N_2O_4Si_2Yb$	$C_{23}H_{48}EuN_2O_4Si_2$	$C_{24}H_{42}N_2O_4Si_2Yb$	$C_{24}H_{42}EuN_2O_4Si_2$
$M$	705.90	684.83	651.82	630.74
$A$ (Å)	15.5139(2)	15.640(9)	15.8486(5)	16.0545(4)
$B$ (Å)	11.3411(2)	11.351(6)	11.0458(3)	11.1445(3)
$c$ (Å)	19.2898(3)	19.198(11)	18.4642(4)	18.7411(3)
$\alpha$ (°)	90	90	90	90
$\beta$ (°)	112.368(1)	111.507(9)	113.190(2)	115.055(1)
$\gamma$ (°)	90	90	90	90
$V$ (Å <sup>3</sup> )	3138.6(11)	3171(5)	2971.2(10)	3037.6(10)
Crystal system	monoclinic	monoclinic	monoclinic	monoclinic
Space Group	$C2/c$	$C2/c$	$C2/c$	$C2/c$
$Z$	4	4	4	4
Diffractometer	Nonius Kappa CCD	Bruker SMART	Nonius Kappa CCD	Nonius Kappa CCD
$\rho_{calcd}$ (g cm <sup>-3</sup> )	1.494	1.434	1.457	1.379
$\mu$ (MoK $\alpha$ ) (mm <sup>-1</sup> )	3.089	2.087	3.257	2.172
$2\theta_{max}$ (°)	60.04	58.0	60.02	55.78
$N, N_o$	4212, 3947	4027, 3870	4209, 3631	3442, 3208
$R, R_w$ (observed data)	0.0291, 0.0825	0.051, 0.014	0.0453, 0.1084	0.0177, 0.0416
$R, R_w$ (all data)	0.0333, 0.0840	0.034, 0.0480	0.0563, 0.1136	0.0210, 0.0429

<sup>a</sup> Crystal data for  $[Eu(L^2)_2(THF)_2]$  were collected by Prof. A.H. White and Dr. B. Skelton, University of Western Australia, Nedlands W.A.



Table 5.6 Metal environment in  $[\text{Ln}(\text{L}^2)_2(\text{S})]$  ( $\text{S} = (\text{THF})_2$  or  $\text{DME}$ ) complexes with estimated standard deviations in parentheses

Compound	$[\text{Yb}(\text{L}^2)_2(\text{THF})_2]$	$[\text{Eu}(\text{L}^2)_2(\text{THF})_2]$	$[\text{Yb}(\text{L}^2)_2(\text{DME})]$	$[\text{Eu}(\text{L}^2)_2(\text{DME})]$
<i>Distances (Å)</i>				
$\text{Ln}(1)-\text{N}(1)$	2.386(2)	2.498(2)	2.353(4)	2.479(1)
$\text{Ln}(1)-\text{O}(1)$	2.458(2)	2.584(3)	2.448(3)	2.585(1)
$\text{Ln}(1)-\text{O}(2)$	2.494(2)	2.604(3)	2.404(10)	2.562(4)
$\text{Ln}(1)-\text{O}(2')^a$	—	—	2.552(12)	2.698(4)
<i>Angles (°)</i>				
$\text{N}(1\text{A})^b-\text{Ln}(1)-\text{N}(1)$	108.81(12)	111.47(9)	111.1(2)	114.95(7)
$\text{O}(1\text{A})^b-\text{Ln}(1)-\text{O}(1)$	165.43(11)	165.77(8)	162.1(2)	160.98(6)
$\text{N}(1\text{A})^b-\text{Ln}(1)-\text{O}(1)$	121.79(8)	125.01(9)	123.3(1)	127.72(5)
$\text{N}(1)-\text{Ln}(1)-\text{O}(1)$	67.71(8)	64.26(9)	68.1(1)	64.27(5)
$\text{N}(1\text{A})^b-\text{Ln}(1)-\text{O}(2)$	154.33(9)	152.31(9)	143.9(3)	140.83(10)
$\text{N}(1\text{A})^b-\text{Ln}(1)-\text{O}(2')^a$	—	—	153.6(3)	150.41(9)
$\text{N}(1)-\text{Ln}(1)-\text{O}(2)$	87.45(9)	89.34(9)	102.8(3)	102.34(11)
$\text{N}(1)-\text{Ln}(1)-\text{O}(2')$	—	—	87.0(3)	87.1(1)
$\text{O}(1)-\text{Ln}(1)-\text{O}(2)$	81.36(9)	79.88(9)	80.5(3)	78.52(9)
$\text{O}(1)-\text{Ln}(1)-\text{O}(2')$	—	—	80.6(3)	78.69(9)
$\text{O}(1)-\text{Ln}(1)-\text{O}(2\text{A})^b$	87.48(8)	89.05(9)	83.3(3)	83.98(9)
$\text{O}(1)-\text{Ln}(1)-\text{O}(2'\text{A})^b$	—	—	86.1(3)	86.82(9)
$\text{O}(2)-\text{Ln}(1)-\text{O}(2\text{A})^b$	80.1(1)	78.2(1)	49.0(7)	46.2(2)
$\text{O}(2)-\text{Ln}(1)-\text{O}(2'\text{A})^b$	—	—	66.2(5)	63.5(2)

<sup>a</sup> the other half of the disorder in  $[\text{Ln}(\text{L}^2)_2(\text{DME})]$  complexes ( $\text{Ln} = \text{Eu}, \text{Yb}$ ); <sup>b</sup> Symmetry transformation:  $-x + 1, y, -z + 3/2$

Table 5.7 Terminal nitrogen- and ether oxygen- lanthanoid distances of a variety of organoamide lanthanoid complexes.

Complex	Ref	Coordination number	Av. Ln—N distance (d(N)) (Å)	Av. Ln—O distance (d(O)) (Å)	Av. Ln—O(S) <sup>a</sup> distance (d(S)) (Å)	Ionic radii of Ln (i.r.) (Å) <sup>b</sup>	d(N)-i.r. (Å)	d(O)-i.r. (Å)	d(S)-i.r. (Å)
[Yb(L <sup>3</sup> ) <sub>2</sub> (THF) <sub>2</sub> ]	this work	6	2.37	2.46	2.49	1.02	1.35	1.44	1.47
[Eu(L <sup>3</sup> ) <sub>2</sub> (THF) <sub>2</sub> ]	this work	6	2.50	2.58	2.60	1.17	1.33	1.41	1.43
[Yb(L <sup>3</sup> ) <sub>2</sub> (DME)]	this work	6	2.35	2.45	2.48	1.02	1.33	1.43	1.46
[Eu(L <sup>3</sup> ) <sub>2</sub> (DME)]	this work	6	2.48	2.59	2.63	1.17	1.31	1.42	1.46
[Yb(L <sup>3</sup> ) <sub>2</sub> (OPh)(THF)] <sup>c</sup>	last section	6	2.25	2.38	2.36	0.87	1.38	1.51	1.49
[Yb(L <sup>3</sup> ) <sub>2</sub> (μ-OMe)] <sub>2</sub>	last section	6	2.25	2.35	—	0.87	1.38	1.48	—
[Yb{N(SiMe <sub>3</sub> )(2,6-(Pr <sup>i</sup> ) <sub>2</sub> C <sub>6</sub> H <sub>3</sub> )} <sub>2</sub> (THF) <sub>2</sub> ]	[27]	4	2.35	—	2.39	0.90 <sup>d</sup>	1.45	—	1.49
[Yb{PhC(NSiMe <sub>3</sub> ) <sub>2</sub> }] <sub>2</sub> (THF) <sub>2</sub>	[33]	6	2.47	—	2.41	1.02	1.45	—	1.39
[Eu{N(SiMe <sub>3</sub> ) <sub>2</sub> }] <sub>2</sub> (DME) <sub>2</sub>	[21]	6	2.53	—	2.70	1.17	1.36	—	1.53
[Sm{N(SiMe <sub>3</sub> ) <sub>2</sub> }] <sub>2</sub> (THF) <sub>2</sub>	[25]	4	2.43	—	2.59	1.12	1.31	—	1.47
[Yb(cbz) <sub>2</sub> (THF) <sub>2</sub> (DME)]	[67]	6	2.44	—	2.44	1.02	1.42	—	1.42
[Yb{N(SiMe <sub>3</sub> ) <sub>2</sub> }] <sub>3</sub> Na	[22]	3	2.38	—	—	0.84 <sup>d</sup>	1.54	—	—
[Eu{N(SiMe <sub>3</sub> ) <sub>2</sub> }] <sub>3</sub> Na	[22]	3	2.45	—	—	1.07 <sup>d</sup>	1.45	—	—

<sup>a</sup>O(S) = THF or DME oxygen distances <sup>b</sup> Values from Shannons Tables<sup>[17]</sup>; <sup>c</sup> Comparison using the short oxygen distance only; <sup>d</sup> Extrapolated from higher coordination numbers from <sup>a</sup>

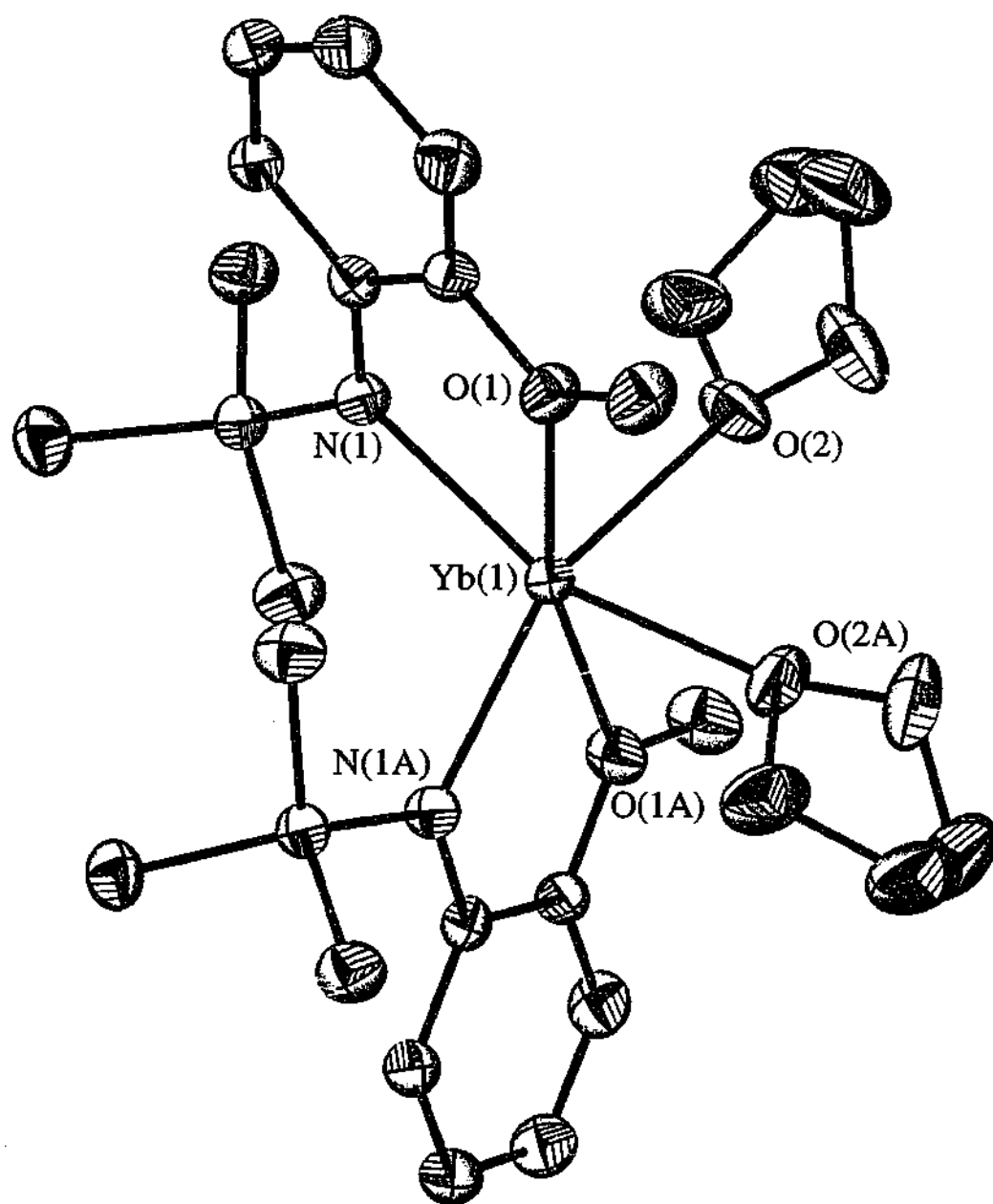
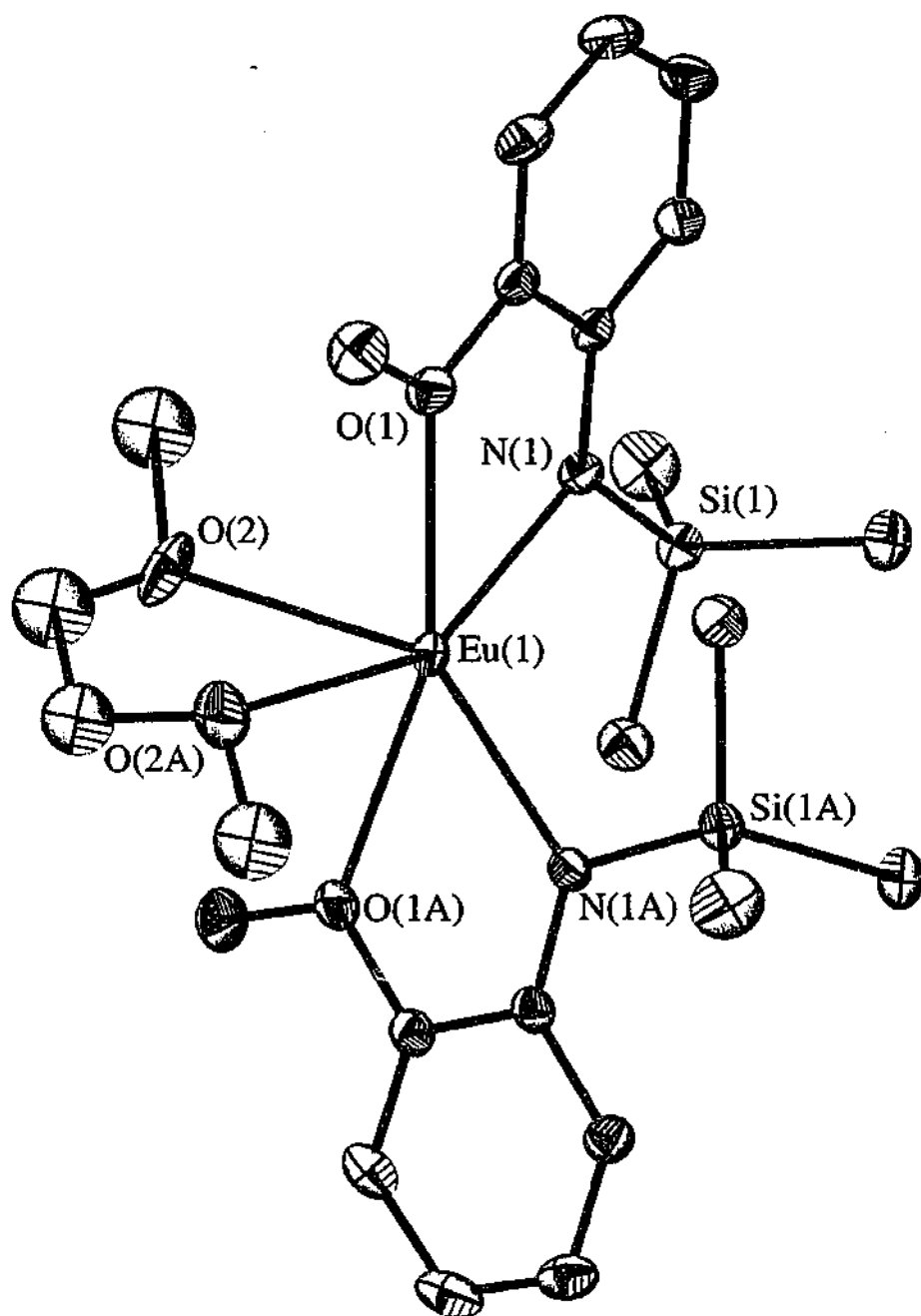


Figure 5.8 ORTEP drawing of  $[Yb(L^2)_2(THF)_2]$   
(Eu analogue is isostructural)

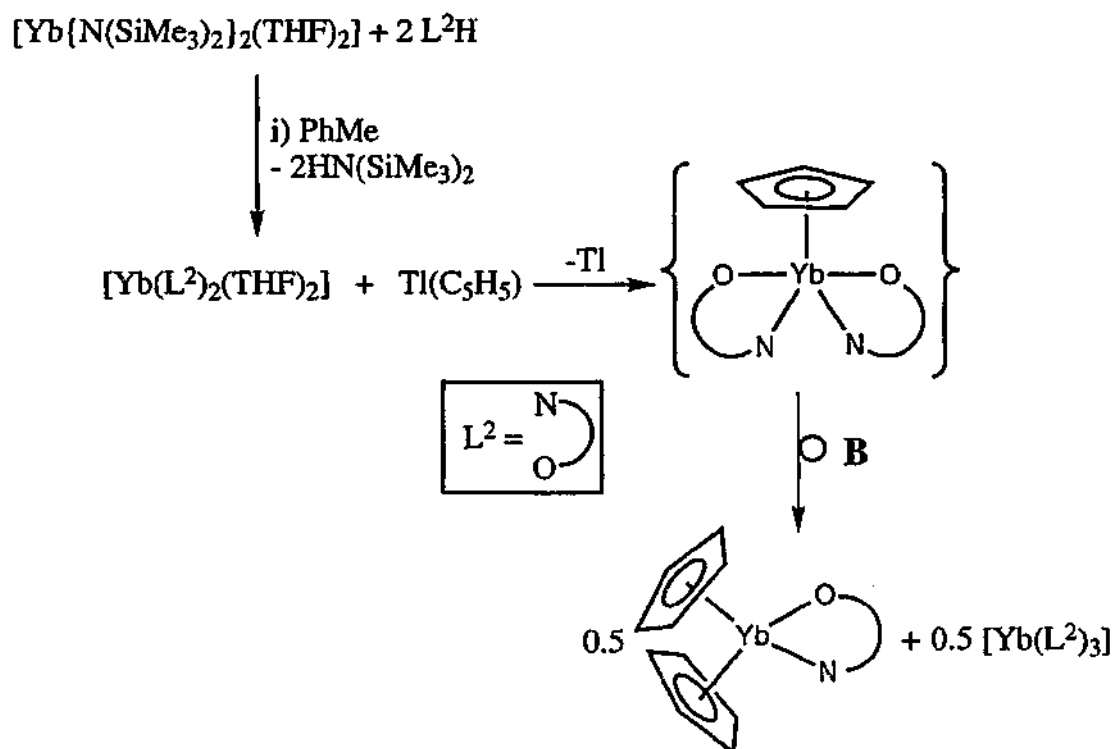


*Figure 5.9* ORTEP drawing of  $[Eu(L^2)_2(THF)_2]$  displaying one DME conformation (Yb analogue is isostructural).

### 5.2.3 Oxidation Chemistry of $[\text{Yb}(\text{L}^2)_2(\text{THF})_2]$

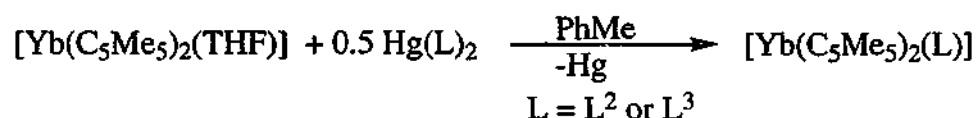
#### 5.2.3.1 Syntheses

Several oxidation reactions of the divalent species  $[\text{Yb}(\text{L}^2)_2(\text{THF})_2]$  were investigated with a variety of reagents (e.g.  $\text{Hg}(\text{SCN})_2$ ,  $\text{TiCl}$ ,  $\text{C}_2\text{Cl}_6$  and  $\text{Ti}(\text{C}_5\text{H}_5)$ ) in an effort to obtain a diverse series of complexes of the type  $[\text{Yb}(\text{L}^2)_2(\text{X})]$  ( $\text{X}$  = anion). One equivalent of oxidant was added to  $[\text{Yb}(\text{L}^2)_2(\text{THF})_2]$  which was prepared *in situ* from an exchange reaction between  $[\text{Yb}\{\text{N}(\text{SiMe}_3)_2\}_2(\text{THF})_2]$  and  $\text{L}^2\text{H}$  at  $-78^\circ\text{C}$  due to the low thermal stability of the complex. For oxidations with  $\text{Hg}(\text{SCN})_2$ ,  $\text{TiCl}$  and  $\text{Ti}(\text{C}_5\text{H}_5)$ , formation of  $\text{Hg}^0$  or  $\text{Ti}^0$  confirmed reduction of the reagents. However apart from the  $\text{Ti}(\text{C}_5\text{H}_5)$  reaction, workup of the reaction mixtures generally gave intractable product mixtures. The isolated materials were oils. Possibly decomposition of the Yb(II) complex was competitive with the oxidation reactions and this may be exacerbated by heat generated if the oxidation reactions are exothermic. This contrasts the successful isolation of  $[\text{Yb}(\text{L}^2)_2(\mu\text{-Cl})]_2$  from metathesis reactions (see Chapter 4). A crystalline compound was obtained from the reaction with  $\text{Ti}(\text{C}_5\text{H}_5)$  but the product was not the expected  $\text{Yb}(\text{L}^2)_2(\text{C}_5\text{H}_5)$  but rather the rearrangement product  $[\text{Yb}(\text{C}_5\text{H}_5)_2(\text{L}^2)]$  (Scheme 5.3). Presumably this is a result of ligand redistribution of an initially formed, but not detected,  $\text{Yb}(\text{L}^2)_2(\text{C}_5\text{H}_5)$  species (Scheme 5.3 (B)).



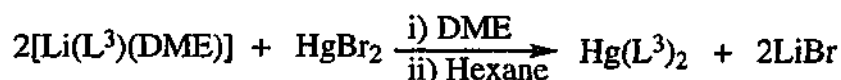
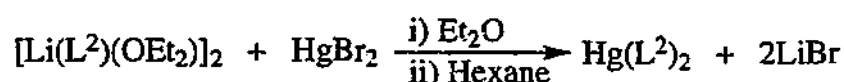
Scheme 5.3

A deliberate preparation of the general compound class  $[\text{Yb}(\text{C}_5\text{R}_5)_2(\text{L})]$  (where  $\text{L} = \text{L}^2, \text{L}^3$ ) involving oxidation of an  $\text{Yb}(\text{C}_5\text{R}_5)_2$  precursor with  $\text{Hg}(\text{L}^2)_2$  or  $\text{Hg}(\text{L}^3)_2$  was explored. Thus  $[\text{Yb}(\text{C}_5\text{Me}_5)_2(\text{THF})]$  was reacted with the mercury amides in toluene affording  $\text{Hg}^0$  and the bis(pentamethylcyclopentadienyl)ytterbium(III) complexes  $[\text{Yb}(\text{C}_5\text{Me}_5)_2(\text{L})]$  ( $\text{L} = \text{L}^2, \text{L}^3$ ) in high yield (Equation 5.16). The two cyclopentadienyl compounds  $[\text{Yb}(\text{C}_5\text{Me}_5)_2(\text{L}^2)]$  and  $[\text{Yb}(\text{C}_5\text{Me}_5)_2(\text{L}^3)]$  and the previously obtained  $[\text{Yb}(\text{C}_5\text{H}_5)_2(\text{L}^2)]$  are an interesting series with variations in the sizes of both the Cp and  $\text{L}^2$  or  $\text{L}^3$  ligands.



Equation 5.16

The required mercury amides were synthesised by standard metathesis reactions from  $[\text{Li}(\text{L}^2)(\text{OEt}_2)]_2$  or  $[\text{Li}(\text{L}^3)(\text{DME})]$  and  $\text{HgBr}_2$  in  $\text{Et}_2\text{O}$  or  $\text{DME}$  respectively (see Equation 5.17).



Equation 5.17

The new mercurial complexes  $\text{Hg}(\text{L}^2)_2$  and  $\text{Hg}(\text{L}^3)_2$  were found to be mildly air- and light-sensitive and elemental analyses (C, H, N) confirmed the proposed compositions. Their infrared spectra showed characteristic absorptions attributable to coordinated  $\text{L}^2$  and  $\text{L}^3$  ligands with the antisymmetric C—O—C stretching region comprising two separate bands at 1052 and 1028  $\text{cm}^{-1}$  for  $\text{L}^2$  and 1056 and 1020  $\text{cm}^{-1}$  for  $\text{L}^3$  which is suggestive of a similar ligand to metal arrangement in the two complexes. The  $^1\text{H}$  NMR spectra of  $\text{Hg}(\text{L}^2)_2$  and  $\text{Hg}(\text{L}^3)_2$  show only one ligand environment in solution. Single resonances attributable to  $\text{SiMe}_3$  were observed, as well as well-defined aromatic protons. The resonance attributable to the OMe substituent on  $\text{L}^2$  in  $\text{Hg}(\text{L}^2)_2$  is only marginally shifted (-0.10 ppm) from the corresponding resonances in  $\text{L}^2\text{H}$  suggesting that it is not coordinated or is only weakly bound to the metal. The  $^{199}\text{Hg}$  NMR spectra of  $\text{Hg}(\text{L}^2)_2$  and  $\text{Hg}(\text{L}^3)_2$  revealed only a singlet at  $\delta = -1270$  ppm ( $\Delta\nu_{1/2}$  195 Hz) and -1316 ppm ( $\Delta\nu_{1/2}$  190 Hz) respectively, consistent with a single mercury environment. Comparable data for  $[\text{Hg}\{\text{N}(\text{SiMe}_3)(2,6\text{-}(\text{Pr}^i)_2\text{C}_6\text{H}_3)\}_2]$ [27] showed one resonance at  $\delta = -1283$  ppm ( $\Delta\nu_{1/2}$  126 Hz) (relative to  $\text{HgMe}_2$ ) at room temperature. The mass spectra of  $\text{Hg}(\text{L}^2)_2$  and  $\text{Hg}(\text{L}^3)_2$  showed the molecular ion  $[\text{Hg}(\text{L})_2]^+$  ( $\text{L} = \text{L}^2$  or  $\text{L}^3$ ) as the highest mass fragment.

The above spectroscopic and analytical data for  $\text{Hg}(\text{L}^2)_2$  and  $\text{Hg}(\text{L}^3)_2$  suggest that they have similar structures. The most likely structure would be a two-coordinate monomer (*Figure 5.10*) with two  $\text{L}^2$  or  $\text{L}^3$  ligands bound in a monodentate fashion. A monomeric arrangement has precedents for Hg complexes of bidentate or bulky monodentate organoamides, e.g.  $[\text{Hg}(\text{PhC}(\text{NSiMe}_3)_2)_2]$ [68] and  $[\text{Hg}\{\text{N}(\text{SiMe}_3)(2,6\text{-}(\text{Pr}^i)_2\text{C}_6\text{H}_3)\}_2]$ [69]. Further saturation of the mercury centre may be provided by weak intramolecular O(R)—Hg interactions from the ether substituent of the  $\text{L}^2$  or  $\text{L}^3$  ligand. Interactions of mercury with pendant donors on the anionic ligand have previously been observed for bis[2-(pyridin-2'-yl)phenyl]mercury where the heterocyclic nitrogen atom is weakly coordinated to the mercury centre.[70] These interactions were supported by a

higher frequency  $\delta(\text{Hg})$  relative to an unsubstituted phenylmercurial reference compound. Whilst the current data seem to suggest coordination of the  $\text{O}(\text{Ph})$  of  $\text{Hg}(\text{L}^3)_2$  to mercury (*Figure 5.10 (a)*) but not of the  $\text{O}(\text{Me})$  of  $\text{Hg}(\text{L}^2)_2$  (*Figure 5.10 (b)*), these conclusions need to be verified by X-ray analysis.

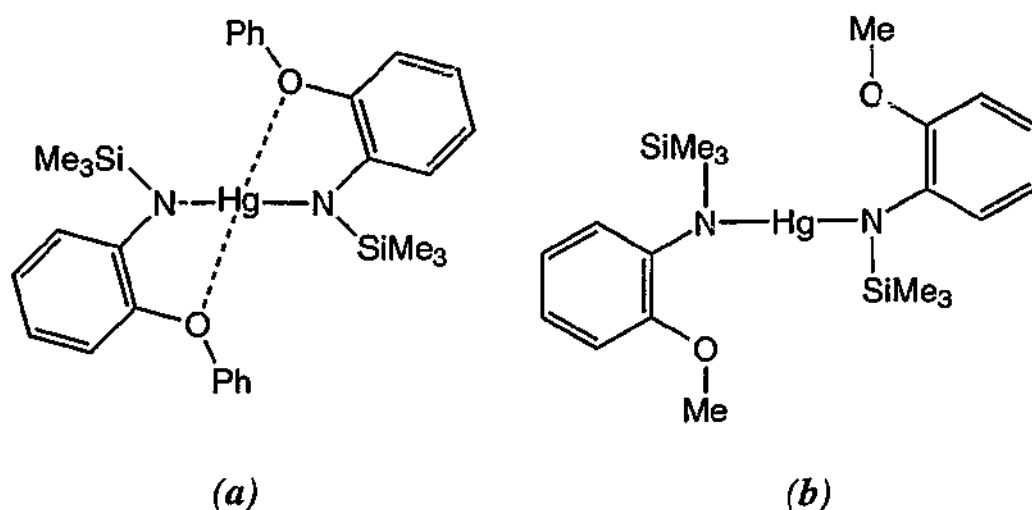


*Figure 5.10*

### 5.2.3.2 Characterisation of $[\text{Yb}(\text{C}_5\text{R}_5)_2(\text{L})]$ ( $\text{R} = \text{H}, \text{Me}, \text{L} = \text{L}^2; \text{R} = \text{Me}, \text{L} = \text{L}^3$ )

The compositions of the oxidation products  $[\text{Yb}(\text{C}_5\text{H}_5)_2(\text{L}^2)]$ ,  $[\text{Yb}(\text{C}_5\text{Me}_5)_2(\text{L}^2)]$  and  $[\text{Yb}(\text{C}_5\text{Me}_5)_2(\text{L}^3)]$  were established by elemental analyses (C, H, N). The presence of trivalent ytterbium was indicated by four weak near-infrared absorptions near 1000 nm attributable to  $\text{Yb}^{3+} f \leftarrow f$  transitions.<sup>[47]</sup> A charge-transfer absorption in the visible region characteristic of the lanthanoid cyclopentadienyl complexes<sup>[71]</sup> was observed at 424, 502 and 518 nm respectively which accounts for their intense but marginally different colours (see Chapter 8). The infrared spectra showed no sign of coordinated THF with absorptions attributable to  $\text{L}^2$  or  $\text{L}^3$  as well as appropriate absorptions for the cyclopentadienyl ligands<sup>[71]</sup> near 1115 and 780  $\text{cm}^{-1}$  being seen. For each complex a single antisymmetric C—O—C stretching absorption at approximately 1050  $\text{cm}^{-1}$  was observed. Their mass spectra gave the appropriate molecular ion as the highest mass ion as well as the breakdown fragments corresponding to the ions  $[\text{Yb}(\text{C}_5\text{R}_5)]^+$ ,  $[(\text{C}_5\text{R}_5)]^+$ , and  $[\text{L}]^+$  ( $\text{L} = \text{L}^2, \text{L}^3; \text{R} = \text{H}$  or  $\text{Me}$ ).

Single crystal X-ray analyses of  $[\text{Yb}(\text{C}_5\text{H}_5)_2(\text{L}^2)]$ ,  $[\text{Yb}(\text{C}_5\text{Me}_5)_2(\text{L}^2)]$  and  $[\text{Yb}(\text{C}_5\text{Me}_5)_2(\text{L}^3)]$  proved unequivocally their monomeric assemblies and they are depicted



in *Figure 5.11*, *5.12* and *5.13* respectively. Their crystal refinement details are listed in *Table 5.8* and selected bond lengths and angles are given in *Table 5.9*. Whilst for the pentamethylcyclopentadienylytterbium(III) complexes one monomer comprises the asymmetric unit, a higher symmetry was observed for  $[\text{Yb}(\text{C}_5\text{H}_5)_2(\text{L}^2)]$  resulting in two virtually identical, but independent, monomers in the asymmetric unit. The complexes  $[\text{Yb}(\text{C}_5\text{H}_5)_2(\text{L}^2)]$ ,  $[\text{Yb}(\text{C}_5\text{Me}_5)_2(\text{L}^2)]$  and  $[\text{Yb}(\text{C}_5\text{Me}_5)_2(\text{L}^3)]$  have very similar structures with an eight-coordinate ytterbium atom surrounded by two  $\eta^5$ -cyclopentadienyl groups and a chelating  $\text{L}^2$  or  $\text{L}^3$  ligand in a distorted pseudo tetrahedral geometry. The distortion away from regular tetrahedral results from the wide  $\text{Cent}(1)\text{---Yb}(1)\text{---Cent}(2)$  angle complemented by the narrow  $\text{N}(1)\text{---Yb}(1)\text{---O}(1)$  angle resulting from the chelating of the amide ligand. The  $\text{Cent}(1)\text{---Yb}(1)\text{---Cent}(2)$  bond angles are similar and are in good agreement with the corresponding values  $132.2$  and  $132.4^\circ$  in  $[\text{Y}(\text{C}_5\text{Me}_5)_2\{\text{N}(\text{SiMe}_3)_2\}]$ <sup>[72]</sup> and  $132.8^\circ$  in  $[\text{Sm}(\text{C}_5\text{Me}_5)_2\{\text{N}(\text{SiMe}_3)_2\}]$ .<sup>[73]</sup> A slightly smaller  $\text{Cent}(1)\text{---Yb}(1)\text{---Cent}(2)$  angle ( $129.8(1)^\circ$ ) for the unsubstituted cyclopentadienyl complex reflects the smaller size of  $\text{C}_5\text{H}_5$  compared with the  $\text{C}_5\text{Me}_5$  ligand.<sup>[50]</sup> This is also consistent with the shorter ( $0.05 \text{ \AA}$ )  $\text{Yb}\text{---C}(\text{ring})$  bond lengths detected in  $[\text{Yb}(\text{C}_5\text{H}_5)_2(\text{L}^2)]$  which range from  $2.602(5)\text{---}2.625(5) \text{ \AA}$ . These values are marginally longer than those of  $[\text{Yb}(\text{C}_5\text{H}_5)_2(\mu\text{-Cl})_2]$  ( $2.57(1)\text{---}2.61(2) \text{ \AA}$ )<sup>[74]</sup> which reflects the larger size of  $\text{L}^2$  in  $[\text{Yb}(\text{C}_5\text{H}_5)_2(\text{L}^2)]$ . Similar average  $\text{Yb}\text{---C}(\text{ring})$  distances ( $2.67 \text{ \AA}$ ) were observed in  $[\text{Yb}(\text{C}_5\text{Me}_5)_2(\text{L}^2)]$  and  $[\text{Yb}(\text{C}_5\text{Me}_5)_2(\text{L}^3)]$  which, after subtraction of the appropriate ionic radii, are shorter than the corresponding average value for  $[\text{Sm}(\text{C}_5\text{Me}_5)_2\{\text{N}(\text{SiMe}_3)_2\}]$ <sup>[73]</sup> and are comparable with  $[\text{Yb}(\text{C}_5\text{Me}_5)_2(\text{NPh}_2)]$  (see *Table 5.10*).<sup>[75]</sup> A list of subtraction values of relevant organolanthanoid complexes is given in *Table 5.10*. For a range of cyclopentadienyl lanthanoid complexes such values were found to lie close to  $1.64 (\pm 0.04) \text{ \AA}$ <sup>[76]</sup> although a later study (which included many  $\text{C}_5\text{Me}_5$  complexes) derived a marginally larger value of  $1.65 (\pm 0.06) \text{ \AA}$ .<sup>[77]</sup> Whilst  $[\text{Yb}(\text{C}_5\text{H}_5)_2(\text{L}^2)]$  was consistent with these values, the larger pentamethylcyclopentadienyl derivatives were at the longer extreme but were shorter than those for  $[\text{Ln}(\text{C}_5\text{Me}_5)_2\{\text{N}(\text{SiMe}_3)_2\}]$  ( $\text{Ln} = \text{Y}$ ,<sup>[72]</sup>  $\text{Sm}$ <sup>[73]</sup>) (*Table 5.10*). The latter pair appear to have unusually long  $\text{Ln}\text{---C}$  distances.  $\text{Ln}\text{---C}_5\text{R}_5$  binding does not correlate well with steric crowding in these systems. Thus, for the series  $[\text{Ln}(\text{C}_5\text{Me}_5)_2\{\text{N}(\text{SiMe}_3)_2\}]$  ( $\text{Ln} = \text{Y}$ ,  $\text{Sm}$ ),  $[\text{Yb}(\text{C}_5\text{Me}_5)_2(\text{NPh}_2)]$ <sup>[75]</sup> and  $[\text{Yb}(\text{MeCp})_2(\text{NPh}_2)(\text{THF})]$ ,<sup>[75]</sup> the sum of the steric coordination numbers are  $7.15$ ,  $6.77$  and  $7.28$  respectively, but  $[\text{Yb}(\text{MeCp})_2(\text{NPh}_2)(\text{THF})]$

has the shortest Ln—C value (*Table 5.10*). Clearly other factors can dominate the bonding of the cyclopentadienyl ligands and it is likely that the observed Ln—C distances are the result of more than one influence.

The steric demands of each of the respective ligands are clearly reflected in the Yb—N and Yb—O bond length variations within the current three complexes (see *Table 5.10*). Thus the Yb—N bond distances are longer (*ca.* 0.05 Å) in the two C<sub>5</sub>Me<sub>5</sub> structures than that in the complex having the smaller C<sub>5</sub>H<sub>5</sub>. Similarly, the Yb—O distances are lengthened for the larger C<sub>5</sub>Me<sub>5</sub> complexes but, for these, the bulkier OPh of L<sup>3</sup> also has a larger (0.1 Å) Yb—O length than for the OMe of L<sup>2</sup>. In the context of L<sup>2</sup> or L<sup>3</sup> coordination, subtraction of the ionic radius of eight-coordinate Yb<sup>3+</sup> (0.99 Å)<sup>[17]</sup> from the Yb—N and Yb—O distances (*Table 5.10*) shows, not surprisingly, both the C<sub>5</sub>Me<sub>5</sub> structures to exhibit weaker binding of the amide ligands than in [Yb(C<sub>5</sub>H<sub>5</sub>)<sub>2</sub>(L<sup>2</sup>)]. However the Yb—N distances are very close to those of typical Ln(C<sub>5</sub>Me<sub>5</sub>)<sub>2</sub>(NR<sub>2</sub>) systems with closely related N(SiMe<sub>3</sub>)<sub>2</sub> or NPh<sub>2</sub> ligands e.g. [Ln(C<sub>5</sub>Me<sub>5</sub>)<sub>2</sub>{N(SiMe<sub>3</sub>)<sub>2</sub>}] (Ln = Sm,<sup>[73]</sup> Y)<sup>[72]</sup> and [Yb(C<sub>5</sub>Me<sub>5</sub>)<sub>2</sub>(NPh<sub>2</sub>)(THF)].<sup>[75]</sup> The [Yb(C<sub>5</sub>H<sub>5</sub>)<sub>2</sub>(L<sup>2</sup>)] complex displays the closest binding of the L<sup>2</sup> ligand of all the lanthanoid complexes in this study. Furthermore, the Yb—N distance is also shorter than for a comparable non-chelated structure [Yb(MeCp)<sub>2</sub>(NPh<sub>2</sub>)(THF)].<sup>[75]</sup> This shows that the near planar L<sup>2</sup> ligand fits neatly into the vacant coordination wedge left by the Cp<sub>2</sub> ligation to the metal centre and this parallels recent examples<sup>[78, 79]</sup> of novel η<sup>2</sup>-pyrazolate-lanthanoid coordination e.g. [Yb(C<sub>5</sub>Me<sub>5</sub>)<sub>2</sub>(Ph<sub>2</sub>pz)].<sup>[80]</sup> Thus both L<sup>2</sup> and R<sub>2</sub>pz are bidentate amide (or pseudoamide) ligands having a near planar centre with bulky substituents on the periphery. The orientation of the L<sup>2</sup> and L<sup>3</sup> ligands to ytterbium in the current set of structures has the ether substituents in the same plane as the arene backbone (for torsion angles see *Table 5.9*) however the phenyl group of L<sup>3</sup> is rotated 69.5(1)° to this plane.

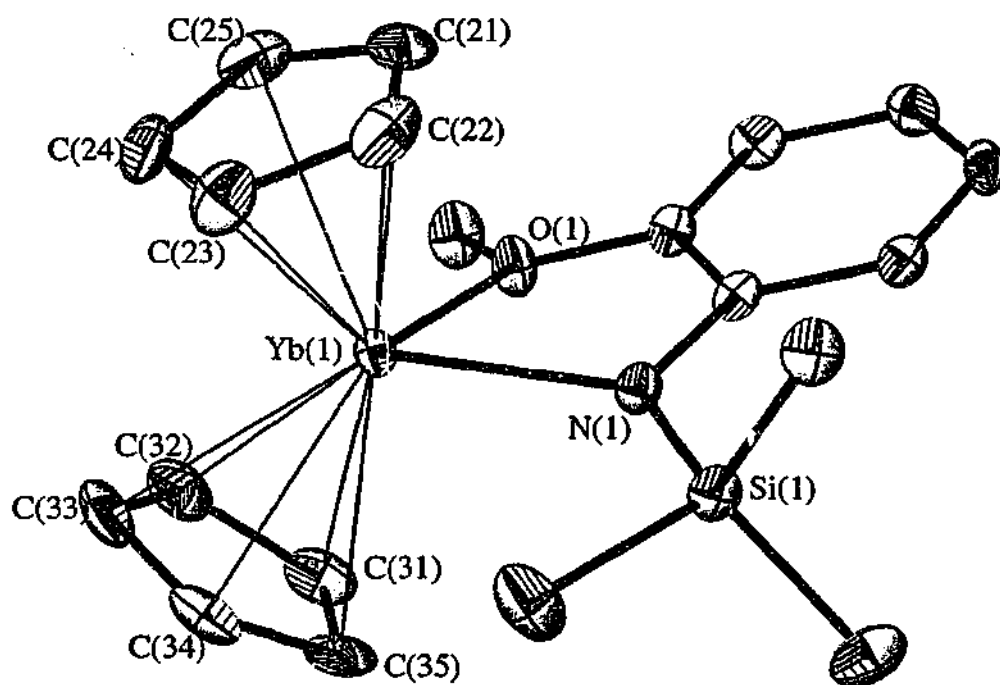


Figure 5.11 Molecular Structure of  $[\text{Yb}(\text{C}_5\text{H}_5)_2(\text{L}^2)]$

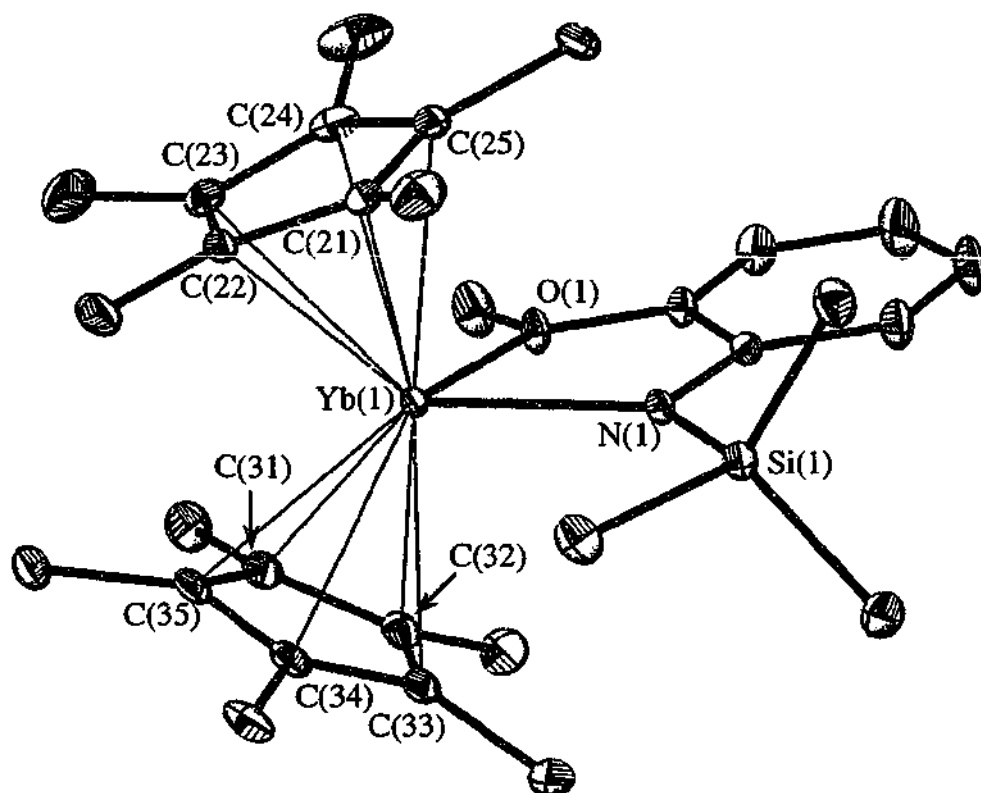


Figure 5.12 Molecular Structure of  $[\text{Yb}(\text{C}_5\text{Me}_5)_2(\text{L}^2)]$

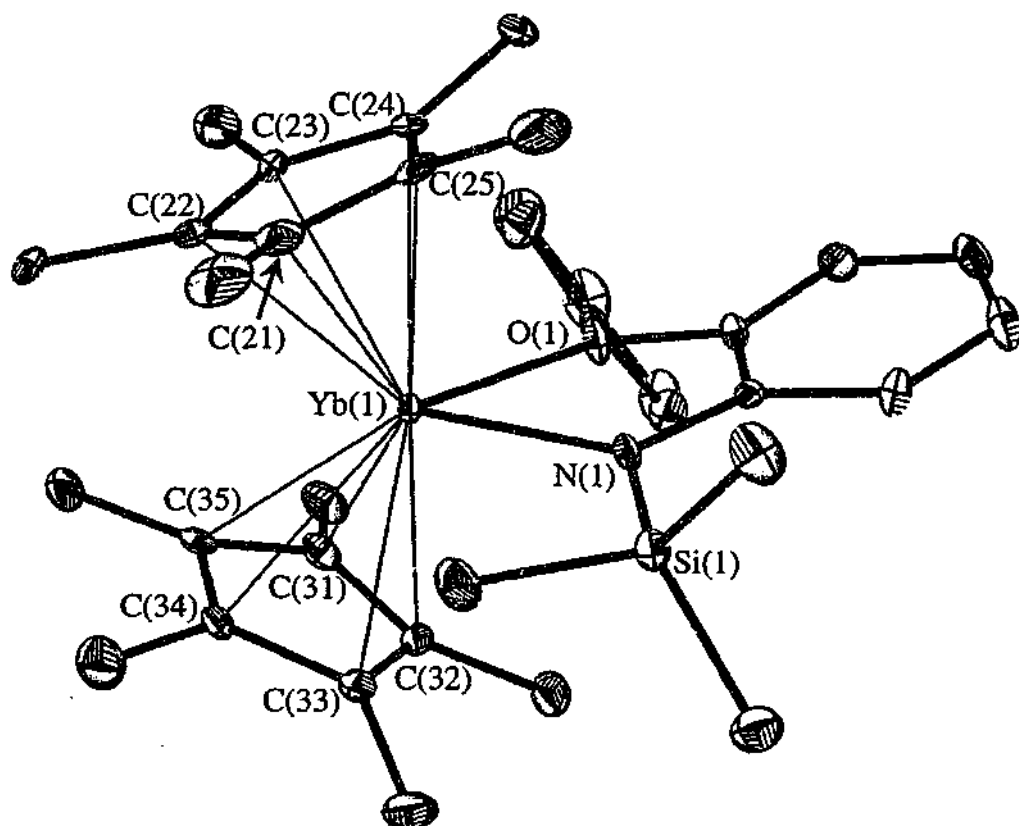


Figure 5.13 Molecular Structure of  $[Yb(C_5Me_5)_2(L^3)]$

Table 5.8 Summary of Crystallographic Data for  $[\text{Yb}(\text{C}_5\text{H}_5)_2(\text{L}^2)]$ ,  $[\text{Yb}(\text{C}_5\text{Me}_5)_2(\text{L}^2)]$  and  $[\text{Yb}(\text{C}_5\text{Me}_5)_2(\text{L}^3)]$

Compound	$[\text{Yb}(\text{C}_5\text{H}_5)_2(\text{L}^2)]$	$[\text{Yb}(\text{C}_5\text{Me}_5)_2(\text{L}^2)]$	$[\text{Yb}(\text{C}_5\text{Me}_5)_2(\text{L}^3)]$
Formula	$\text{C}_{20}\text{H}_{26}\text{NOSiYb}$	$\text{C}_{30}\text{H}_{46}\text{NOSiYb}$	$\text{C}_{35}\text{H}_{48}\text{NOSiYb}$
$M$	497.55	637.81	699.87
$a$ (Å)	11.7682(2)	10.8166(1)	25.0869(3)
$b$ (Å)	13.0233(3)	21.8882(3)	12.1479(1)
$c$ (Å)	25.8591(5)	12.3423(2)	10.3939(1)
$\alpha$ (°)	90	90	90
$\beta$ (°)	91.298(3)	103.611(1)	90
$\gamma$ (°)	90	90	90
$V$ (Å <sup>3</sup> )	3962.2(14)	2838.7(10)	3167.6(11)
Crystal system	monoclinic	monoclinic	orthorhombic
Space Group	$P2_1/c$	$P2_1/n$	$Pna21$
$Z$	8	4	4
Diffractometer	Nonius Kappa CCD	Nonius Kappa CCD	Nonius Kappa CCD
$\rho_{\text{calcd}}$ (g cm <sup>-3</sup> )	1.668	1.492	1.468
$\mu(\text{MoK}\alpha)$ (mm <sup>-1</sup> )	4.787	3.359	3.017
$2\theta_{\text{max}}$ (°)	55.78	56.56	56.56
$N, N_o$	8763, 8041	7022, 6148	7799, 6814
$R, R_w(\text{observed data})$	0.0443, 0.1200	0.0227, 0.0539	0.0274, 0.0613
$R, R_w(\text{all data})$	0.0479, 0.1230	0.0289, 0.0559	0.0361, 0.0642

**Table 5.9** Ytterbium environment in  $[Yb(C_5H_5)_2(L^2)]$ ,  $[Yb(C_5Me_5)_2(L^2)]$  and  $[Yb(C_5Me_5)_2(L^3)]$ .

Compound	$[Yb(C_5H_5)_2(L^2)]^a$	$[Yb(C_5Me_5)_2(L^2)]$	$[Yb(C_5Me_5)_2(L^3)]$
<i>Distances (Å)</i>			
Yb(1)—N(1)	2.224(4)	2.275(2)	2.270(3)
Yb(1)—O(1)	2.309(3)	2.340(2)	2.440(3)
Yb(1)—C(21)	2.625(5)	2.670(3)	2.676(4)
Yb(1)—C(22)	2.622(5)	2.653(3)	2.661(4)
Yb(1)—C(23)	2.602(5)	2.671(3)	2.644(5)
Yb(1)—C(24)	2.616(5)	2.684(3)	2.663(4)
Yb(1)—C(25)	2.624(6)	2.683(3)	2.671(4)
Yb(1)—Cent(2) <sup>b</sup>	2.33(1)	2.38(1)	2.37(1)
Yb(1)—C(31)	2.624(5)	2.675(3)	2.692(4)
Yb(1)—C(32)	2.663(5)	2.652(3)	2.646(4)
Yb(1)—C(33)	2.649(5)	2.639(3)	2.667(5)
Yb(1)—C(34)	2.602(5)	2.659(3)	2.693(4)
Yb(1)—C(35)	2.597(5)	2.685(3)	2.711(4)
Yb(1)—Cent(3) <sup>c</sup>	2.34(1)	2.37(1)	2.39(1)
<i>Angles (°)</i>			
N(1)—Yb(1)—O(1)	72.2(1)	70.6(1)	70.5(1)
N(1)—Yb(1)—Cent(2) <sup>b</sup>	109.1(1)	107.4(1)	109.2(1)
O(1)—Yb(1)—Cent(2) <sup>b</sup>	106.1(1)	105.6(1)	104.5(1)
N(1)—Yb(1)—Cent(3) <sup>c</sup>	117.8(1)	114.4(1)	115.1(1)
O(1)—Yb(1)—Cent(3) <sup>c</sup>	104.3(1)	103.1(1)	105.1(1)
Cent(2) <sup>b</sup> —Yb(1)—Cent(3) <sup>c</sup>	129.8(1)	133.8(1)	132.7(1)
<i>Torsion Angles (°)</i>			
C(13)—C(12)—O(1)—C(10)	12.3(7)	3.4(4)	—
C(13)—C(12)—O(1)—C(111)	—	—	23.6(5)
<i>Interplanar angles (°)</i>			
P(1A) <sup>d</sup> —P(1B) <sup>e</sup>	21.0(7)	9.6(2)	15.4(2)
P(1B) <sup>e</sup> —P(1C) <sup>f</sup>	—	—	69.5(1)

<sup>a</sup> only one independent molecule is listed; <sup>b</sup> Cent(2) = centroid of the C(21)—C(25) ring; <sup>c</sup> Cent(3) = centroid of the C(31)—C(35) ring; <sup>d</sup> P(1A) = the plane defined by Yb—N(1)—O(1) atoms; <sup>e</sup> P(1B) = plane defined by the arene backbone (C(11)—C(16)); <sup>f</sup> P(1C) = plane defined by the arene backbone (C(111)—C(116))

Table 5.10 Comparison of relevant carbon, nitrogen and ether oxygen distances of a range of organolanthanoid complexes.

Complex	Ref	Coordination number	Average Ln—C distance (d(C)) (Å)	Average Ln—N distance (d(N)) (Å)	Average Ln—O(L) distance (d(O)) (Å)	Ionic Radii of Ln (i.r.) (Å) <sup>a</sup>	d(C)—i.r. (Å)	d(N)—i.r. (Å)	d(O)—i.r. (Å)
[Yb(C <sub>3</sub> H <sub>5</sub> ) <sub>2</sub> (L <sup>3</sup> )]	this work	8	2.63	2.22	2.31	0.99	1.63	1.23	1.32
[Yb(C <sub>3</sub> Me <sub>5</sub> ) <sub>2</sub> (L <sup>3</sup> )]	this work	8	2.67	2.28	2.34	0.99	1.68	1.29	1.35
[Yb(C <sub>3</sub> Me <sub>5</sub> ) <sub>2</sub> (L <sup>3</sup> )]	this work	8	2.67	2.27	2.44	0.99	1.68	1.28	1.45
[Yb(C <sub>3</sub> H <sub>5</sub> )(μ-Cl)] <sub>2</sub>	[74]	8	2.58	—	—	0.99	1.59	—	—
[Sm(C <sub>3</sub> Me <sub>5</sub> ) <sub>2</sub> {N(SiMe <sub>3</sub> ) <sub>2</sub> }]	[73]	7	2.75	2.30	—	1.02	1.73	1.28	—
[Y(C <sub>3</sub> Me <sub>5</sub> ) <sub>2</sub> {N(SiMe <sub>3</sub> ) <sub>2</sub> }]	[72]	7	2.68	2.26	—	0.96	1.72	1.30	—
[Yb(C <sub>3</sub> Me <sub>5</sub> ) <sub>2</sub> (NPh <sub>2</sub> )]	[75]	7	2.61	2.22	—	0.93	1.68	1.29	—
[Yb(CpMe) <sub>2</sub> (NPh <sub>2</sub> )(THF)]	[75]	8	2.63	2.29	2.33	0.99	1.64	1.30	1.34
[Sm(C <sub>3</sub> Me <sub>5</sub> ) <sub>3</sub> ]	[81]	9	2.82	—	—	1.13	1.69	—	—
[Yb(MeCp)(L <sup>3</sup> )(μ-Cl)] <sub>2</sub>	Chapter 4	7	2.60	2.21	2.33	0.93	1.67	1.28	1.40
[Yb(MeCp)(L <sup>3</sup> )(μ-Cl)] <sub>2</sub>	Chapter 4	7	2.60	2.21	2.36	0.93	1.67	1.28	1.43
[Yb(L <sup>3</sup> ) <sub>2</sub> (OPh)(THF)] <sup>b</sup>	this Chapter	6	—	2.25	2.38	0.87	—	1.38	1.51
[Yb(L <sup>3</sup> ) <sub>2</sub> (μ-OMe)] <sub>2</sub>	this Chapter	6	—	2.25	2.35	0.87	—	1.38	1.48

<sup>a</sup> Values from R.D. Shannon in [17], <sup>b</sup> Comparison using the shorter Yb—O(L<sup>3</sup>) distance only.

### 5.3 Conclusion

Transmetallation / ligand exchange reactions involving the organoamide ligands  $L^2$  and  $L^3$  found that the Ar—O(R) (R = Me, Ph) bonds were susceptible to C—O cleavage, particularly in the case of  $L^3$ , by a one-electron transfer from the highly reactive divalent lanthanoid(II) centre. As a result the heteroleptic ytterbium(III) complexes  $[Yb(L^2)_2(\mu\text{-OMe})]_2$  and  $[Yb(L^3)_2(\text{OPh})(\text{THF})]$  were obtained. The dimeric and monomeric assemblies of  $[Yb(L^2)_2(\mu\text{-OMe})]_2$  and  $[Yb(L^3)_2(\text{OPh})(\text{THF})]$  respectively, were established by X-ray crystallography and further show the ability of  $L^2$  and  $L^3$  to stabilise heteroleptic lanthanoid(III) complexes with sterically undemanding anions. In an analogous reaction using samarium and  $L^2\text{H}$ , oxidation was again prevalent and the homoleptic product  $[\text{Sm}(L^2)_3]$  was obtained.

Alternatively a ligand exchange reaction was investigated for the synthesis of divalent Ln(II) complexes containing  $L^2$  and  $L^3$  ligands. For  $L^3$ , immediate oxidation to the complex  $[Yb(L^3)_2(\text{OPh})(\text{THF})]$  was observed but for the smaller  $L^2$  ligand a number of thermally unstable divalent lanthanoid(II) complexes  $[\text{Ln}(L^2)_2(\text{S})]$  (Ln = Eu, Yb; S =  $(\text{THF})_2$ , DME) were obtained in good yield. A single crystal X-ray determination for each complex confirmed the monomeric divalent metal centre and these are the first structurally characterised lanthanoid(II) complexes with a mixed N, O-donor ligand.

A brief exploration into the reducing ability of the complex  $[Yb(L^2)_2(\text{THF})_2]$  was attempted using a variety of reducing agents. The findings suggested that oxidation to ytterbium(III) occurred but the products were isolated as oily unmanageable residues and for this reason characterisation was not attempted. However crystals were obtained from the reaction of  $\text{Ti}(\text{C}_5\text{H}_5)_2$  and  $[Yb(L^2)_2(\text{THF})_2]$  and X-ray crystallography revealed the product to be  $[Yb(\text{C}_5\text{H}_5)_2(L^2)]$  which presumably results from rearrangement of the initially formed, but not detected,  $Yb(L^2)_2(\text{C}_5\text{H}_5)$ . The  $[Yb(\text{C}_5\text{Me}_5)_2(L)]$  (L =  $L^2$  and  $L^3$ ) complexes are readily prepared from reaction of  $[Yb(\text{C}_5\text{Me}_5)_2(\text{THF})_2]$  with  $\text{Hg}(L^2)_2$  and  $\text{Hg}(L^3)_2$ , which were prepared from metathesis reactions of  $\text{HgBr}_2$  with  $[\text{Li}(L^2)(\text{OEt}_2)]_2$  or  $[\text{Li}(L^3)(\text{DME})]$ . The pentamethylcyclopentadienyl complexes are highly crystalline and their monomeric structures were established by X-ray analysis.



### 5.4 The Bigger Picture-'edge-on' versus 'face-on'

Chapters 3, 4 and 5 describe coordination of  $L^2$  and  $L^3$  to lanthanoid centres in a variety of structural frameworks. For example, the general compound classes include homoleptic complexes of the type  $LnL_3$ , heteroleptic  $LnL_2X$ , mixed ligand  $LnCpLX$ , classical  $LnCp_2L$  complexes and divalent  $LnL_2(S)_n$  ( $S$  = neutral donor) systems. These results enabled a substantial structural picture for these ligands to be established and this has allowed direct comparisons with 'classical' cyclopentadienyl lanthanoid chemistry. The current ligands can be classified as 'edge-on' coordinators (*Figure 5.14 (a)*) in contrast to the 'face-on' approach of an  $\eta^5$ -cyclopentadienyl ligand (*Figure 5.14 (b)*). The N, O-,  $C_6H_4$  fragment of the  $L^2$  and  $L^3$  ligands is planar and this allows a close approach of the donor atoms despite the presence of the bulky substituents on the periphery of the central plane. As a consequence neighbouring ligands are pushed further away from the metal centre generating the appearance, from bond distances, of a steric similarity of  $L^2$  and  $L^3$  to  $C_3Me_5$  in closely analogous complexes.<sup>[36]</sup> However, the 'edge-on' coordination mode is more flexible and allows ligand arrangements in heteroleptic complexes that match  $C_3H_5$ -lanthanoid chemistry rather than  $C_3Me_5$ .<sup>[36]</sup>

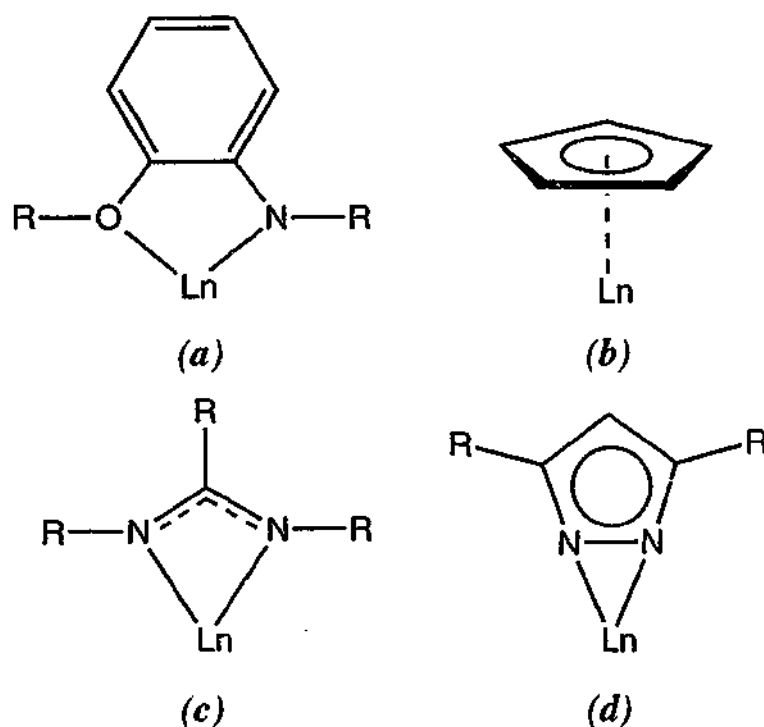
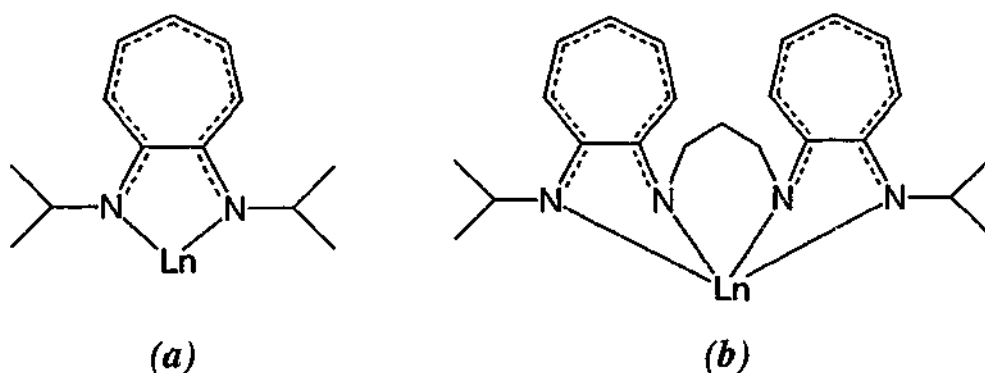


Figure 5.14

The benzamidinate ligand system (*Figure 5.14 (c)*) has also been exploited as a Cp alternative and is generally considered to be the steric equivalent of  $C_5H_5$ .<sup>[82]</sup> In contrast to  $L^2$  and  $L^3$ , it has a smaller bite angle ( $\sim 60^\circ$ ) due to the formation of the four-membered ring when complexed to a metal. With two bulky R groups attached to each nitrogen supplemented by a substituted aryl on the backbone carbon, the benzamidinate ligands are presumably more sterically encumbered than  $L^2$  and  $L^3$  even though there are many similarities in the types of compounds obtained.<sup>[82]</sup> Other planar amide ligands include aminotropiminates (*Figure 5.15 (a)*) that are more closely aligned with the features of  $L^2$  and  $L^3$  than the benzamidinates. However subtle differences exist as shown by the failure of the aminotropiminates<sup>[83]</sup> to stabilise heteroleptic complexes of the type  $Ln(L)_2Cl$  except where two aminotropimate ligands are linked together (*Figure 5.15 (b)*).<sup>[84]</sup> In contrast, although not universally applicable,  $L^2$  and  $L^3$  are capable of forming such complexes.



*Figure 5.15*

A recent observation in lanthanoid chemistry has been the detection of previously unanticipated  $\pi$ -type bonding of neutral arenes to the metal centres. Since both  $L^2$  and  $L^3$  have aryl groups present and indeed the lithium chemistry of  $L^*$ , derived from  $L^3$ , shows outstanding examples of this type of structural feature (see Chapter 7), the possibility for either supplementary coordination by the phenyl substituent of  $L^3$  or tilting of the coordination of  $L^2$  or  $L^3$  allowing the arene backbone to contribute to the overall bonding, may be possible. In the structure of  $[Nd(L^3)_2(\mu-Cl)]_2$  one of the  $L^3$  ligands was inclined toward the metal centre, thus approaching a 'face-on' ligand mode. Similar effects are prevalent in the lanthanoid chemistry of bulky 3,5-disubstituted pyrazolates (*Figure 5.14 (d)*).<sup>[78, 79, 85]</sup> These typically bind in an 'edge-on'  $\eta^2$ -fashion but in coordinatively unsaturated environments progress to 'edge-on'/'face-on' bridging.

## 5.5 References

- 1 G. A. Molander, *Chem. Rev.*, 1992, **92**, 29.
- 2 W. J. Evans, *Coord. Chem. Rev.*, 2000, **206/207**, 263.
- 3 J. L. Namy, P. Girard, and H. B. Kagan, *Nou. J. Chim.*, 1977, **1**, 5.
- 4 P. Girard, J. L. Namy, and H. B. Kagan, *J. Am. Chem. Soc.*, 1980, **102**, 2693.
- 5 H. B. Kagan, *New. J. Chem.*, 1990, **14**, 453.
- 6 L. A. Paquette, in 'Encyclopedia of Reagents for Organic Synthesis, Wiley, New York, 1995, p. 4428.
- 7 J. Collin, N. Giuseppone, and P. Van de Weghe, *Coord. Chem. Rev.*, 1998, **178/180**, 117.
- 8 W. J. Evans, J. W. Grate, H. W. Choi, I. Bloom, W. E. Hunter, and J. L. Atwood, *J. Am. Chem. Soc.*, 1985, **107**, 941.
- 9 W. J. Evans, L. A. Hughes, and T. P. Hanusa, *J. Am. Chem. Soc.*, 1984, **106**, 4270.
- 10 W. J. Evans, L. A. Hughes, and T. P. Hanusa, *Organometallics*, 1986, **5**, 1285.
- 11 R. Anwander, *Top. Organomet. Chem.*, 1999, **2**, 1.
- 12 W. J. Evans, *High Energy Processes in Organometallic Chemistry*, in ACS Symposium Series 333, ed. K.S. Suslick, Washington, D.C., 1987, p. 278.
- 13 W. J. Evans, L. A. Hughes, D. K. Drummond, H. Zhang, and J. L. Atwood, *J. Am. Chem. Soc.*, 1986, **108**, 1722.
- 14 W. J. Evans and D. Drummond, K, *J. Am. Chem. Soc.*, 1986, **108**, 7440.
- 15 M. C. Cassani, D. J. Duncalf, and M. F. Lappert, *J. Am. Chem. Soc.*, 1998, **120**, 12958.
- 16 M. N. Bochkarev, I. L. Fedushkin, A. A. Fagin, T. V. Petrovskaya, J. W. Ziller, R. N. R. Broomhall-Dillard, and W. J. Evans, *Angew. Chem. Int. Ed. Engl.*, 1997, **36**, 133.
- 17 R. D. Shannon, *Acta. Crystallogr., Sect. A*, 1976, **32**, 751.
- 18 R. K. Minhas, Y. Ma, J.-I. Song, and S. Gambarotta, *Inorg. Chem.*, 1996, **35**, 1866.
- 19 W. J. Evans, G. W. Rabe, and J. W. Ziller, *Organometallics*, 1994, **13**, 1641.
- 20 G. B. Deacon, C. M. Forsyth, B. M. Gatehouse, and P. A. White, *Aust. J. Chem.*, 1990, **43**, 795.

- 21 T. D. Tilley, A. Zalkin, R. A. Anderson, and D. H. Templeton, *Inorg. Chem.*, 1981, **20**, 551.
- 22 T. D. Tilley, R. A. Anderson, and A. Zalkin, *Inorg. Chem.*, 1984, **23**, 2271.
- 23 W. J. Evans, R. Anwander, U. H. Berlekamp, and J. W. Ziller, *unpublished results*.
- 24 R. Anwander, *Top. Curr. Chem.*, 1996, **179**, 33.
- 25 W. J. Evans, D. K. Drummond, H. Zhang, and J. L. Atwood, *Inorg. Chem.*, 1988, **27**, 575.
- 26 W. J. Evans, *Polyhedron*, 1987, **6**, 803.
- 27 G. B. Deacon, G. D. Fallon, C. M. Forsyth, H. Schumann, and R. Weimann, *Chem. Ber.*, 1997, **130**, 409.
- 28 Y. F. Rad'kov, E. A. Fedorova, S. Y. Khorshev, G. S. Kalinina, M. N. Bochkarev, and G. A. Razuvaev, *J. Gen. Chem. U.S.S.R.*, 1985, **55**, 1911.
- 29 T. D. Tilley, R. A. Anderson, and A. Zalkin, *J. Am. Chem. Soc.*, 1982, **104**, 3725.
- 30 R. A. Anderson and J. M. Boncella, *Organometallics*, 1985, **4**, 205.
- 31 J. M. Boncella, PhD Thesis, University of California, Berkeley, 1982.
- 32 I. Nagl, W. Scherer, M. Tafipolsky, and R. Anwander, *Eur. J. Inorg. Chem.*, 1999, **1405**.
- 33 M. Wedler, M. Noltemeyer, U. Pieper, H.-G. Schmidt, D. Stalke, and F. T. Edlmann, *Angew. Chem. Int. Ed. Engl.*, 1990, **29**, 894.
- 34 A. Recknagel, A. Steiner, S. Brooker, D. Stalke, and E. T. Edlmann, *J. Organomet. Chem.*, 1991, **415**, 315.
- 35 F. T. Edlmann, in *Comprehensive Organometallic Chemistry*, 2nd edn., eds. G. Wilkinson, F. G. A. Stone, and E. W. Abel, Pergamon, 1995, vol. 4, ch. 2, p. 11.
- 36 H. Schumann, J.-A. Meese-Markscheffel, and L. Esser, *Chem. Rev.*, 1995, **95**, 865.
- 37 C. J. Burns and R. A. Anderson, *J. Chem. Soc., Chem. Commun.*, 1992, 136.
- 38 G. B. Deacon, S. C. Harris, G. Meyer, D. Stellfeldt, and G. Zelesney, *J. Organomet. Chem.*, 1996, **525**, 247.
- 39 Z. Xie, K. Chui, Q. Yang, T. C. W. Mak, and J. Sun, *Organometallics*, 1998, **17**, 3937.
- 40 P. L. Watson, T. H. Tulip, and I. Williams, *Organometallics*, 1990, **9**, 1999.
- 41 G. B. Deacon, G. Meyer, and D. Stellfeldt, *Eur. J. Inorg. Chem.*, 2000, 1061.

- 42 G. B. Deacon, G. Meyer, and D. Stellfeldt, *Z. Anorg. Allg. Chem.*, 1999, **625**, 1252.
- 43 G. B. Deacon and D. L. Wilkinson, *Inorg. Chim. Acta.*, 1988, **144**, 155.
- 44 W. J. Evans, T. A. Ulibarri, and J. W. Ziller, *J. Am. Chem. Soc.*, 1990, **112**, 219.
- 45 M. Wedler, A. Recknagel, J. W. Gilje, M. Noltemeyer, and F. T. Edelmann, *J. Organomet. Chem.*, 1992, **426**, 295.
- 46 Z. Hou, T. Koizumi, M. Nishiura, and Y. Wakatsuki, *Organometallics*, 2001, **20**, 3323.
- 47 F. Calderazzo, R. Pappalardo, and S. Losi, *Inorg. Nucl. Chem.*, 1966, **28**, 987.
- 48 Y. K. Gun'ko, P. B. Hitchcock, and M. F. Lappert, *J. Organomet. Chem.*, 1995, **499**, 213.
- 49 D. J. Duncalf, P. B. Hitchcock, and G. A. Lawless, *Chem. Commun.*, 1996, 269.
- 50 J. Marcalo and A. P. De Matos, *Polyhedron*, 1989, **8**, 2431.
- 51 G. B. Deacon, T. Feng, B. W. Skelton, and A. H. White, *Aust. J. Chem.*, 1995, **48**, 741.
- 52 J. E. Cosgriff, G. B. Deacon, and B. M. Gatehouse, *Aust. J. Chem.*, 1993, **46**, 1881.
- 53 G. B. Deacon, T. Feng, S. Nickel, M. I. Ogden, and A. H. White, *Aust. J. Chem.*, 1992, **45**, 671.
- 54 G. B. Deacon, S. Nickel, P. MacKinnon, and E. R. T. Tiekink, *Aust. J. Chem.*, 1990, **43**, 1245.
- 55 M. N. Bochkarev, A. A. Fagin, I. L. Fedushkin, T. V. Petrovskaya, W. J. Evans, M. A. Greci, and J. W. Ziller, *Russ. Chem. Bull.*, 1999, **48**, 1782.
- 56 G. B. Deacon, T. Feng, P. MacKinnon, R. H. Newnham, N. Siegbert, B. W. Skelton, and A. H. White, *Aust. J. Chem.*, 1993, **46**, 387.
- 57 G. B. Deacon, P. I. MacKinnon, and T. D. Tuong, *Aust. J. Chem.*, 1983, **36**, 43.
- 58 G. B. Deacon, C. M. Forsyth, and J. Sun, *Tetrahedron Lett.*, 1994, **35**, 1095.
- 59 W. J. Evans, N. T. Allen, and J. W. Ziller, *J. Am. Chem. Soc.*, 2001, **123**, 7927.
- 60 A. Maercker, *Angew. Chem. Int. Ed. Engl.*, 1987, **26**, 972.
- 61 S. C. Harris, PhD Thesis, Monash University, Victoria, 1999.
- 62 W. A. Cotton and G. Wilkinson, in *Advanced Inorganic Chemistry*, 5th edn., Wiley-Interscience, New York, 1988, ch. 23, p. 955.

- 63 W. J. Evans, I. Bloom, W. E. Hunter, and J. L. Atwood, *Organometallics*, 1985, **4**, 112.
- 64 G. B. Deacon, E. E. Delbridge, B. W. Skelton, and A. H. White, *Eur. J. Inorg. Chem.*, 1999, 751.
- 65 J. E. Cosgriff, G. B. Deacon, B. N. Gatehouse, H. Hemling, and H. Schumann, *Aust. J. Chem.*, 1994, **47**, 1223.
- 66 M. Johnson, J. C. Taylor, and G. W. Cox, *J. Appl. Crystallogr.*, 1980, **13**, 188.
- 67 C. T. Abrahams, G. B. Deacon, B. M. Gatehouse, and G. N. Ward, *Acta. Cryst.*, 1994, **C50**, 504.
- 68 A. Zinn, K. Dehnicke, D. Fenske, and G. Baum, *Z. Anorg. Allg. Chem.*, 1991, **596**, 47.
- 69 H. Schumann, J. Gottfriedsen, S. Dechert, and F. Girgsdies, *Z. Anorg. Allg. Chem.*, 2000, **626**, 747.
- 70 D. S. C. Black, G. B. Deacon, G. L. Edwards, and B. M. Gatehouse, *Aust. J. Chem.*, 1993, **46**, 1323.
- 71 G. B. Deacon, A. J. Koplick, and T. D. Tuong, *Aust. J. Chem.*, 1984, **37**, 517 and references therein.
- 72 K. H. den Haan, J. L. de Boer, J. H. Teuben, A. L. Spek, B. Kojic-Prodic, G. R. Hays, and R. Huis, *Organometallics*, 1986, **5**, 1726.
- 73 W. J. Evans, R. A. Keyer, and J. W. Ziller, *Organometallics*, 1993, **12**, 2618.
- 74 H. Lueken, J. Schmitz, W. Lamberts, P. Hannibal, and K. Handrick, *Inorg. Chim. Acta.*, 1989, **156**, 119.
- 75 Y. Wang, Q. Shen, F. Xue, and K. Yu, *J. Organomet. Chem.*, 2000, **598**, 359.
- 76 K. N. Raymond and W. Eigenbrot, *Acc. Chem. Res.*, 1980, **13**, 276.
- 77 S. C. Sockwell and T. P. Hanusa, *Inorg. Chem.*, 1990, **29**, 76.
- 78 F. Nief, *Eur. J. Inorg. Chem.*, 2001, 891.
- 79 G. B. Deacon, E. E. Delbridge, and C. M. Forsyth, *Angew. Chem. Int. Ed.*, 1999, **38**, 1766.
- 80 G. B. Deacon, E. E. Delbridge, G. D. Fallon, C. Jones, D. E. Hibbs, and M. B. Hursthouse, *Organometallics*, 2000, **19**, 1713.
- 81 W. J. Evans, S. L. Gonzales, and J. W. Ziller, *J. Am. Chem. Soc.*, 1991, **113**, 7423.

- 
- 82 F. T. Edelmann, *J. Alloys and Compounds*, 1994, **207/208**, 182.
- 83 P. W. Roesky, *Chem. Ber.*, 1997, **130**, 859.
- 84 P. W. Roesky and M. R. Bürgstein, *Inorg. Chem.*, 1999, **38**, 5629.
- 85 G.B. Deacon, A. Gitlits, P. W. Roesky, M. R. Bürgstein, K. C. Lim, B. W. Skelton, and A. H. White, *Chem. Eur. J.*, 2001, **7**, 127.

## Chapter 6

# Structural Characterisation of Some Lanthanoid Trihalide Complexes

### 6.1 Introduction

Anhydrous lanthanoid trihalides, particularly the trichlorides, are important reactants for the synthesis of a variety of lanthanoid complexes, including air-sensitive organometallics,<sup>[1, 2]</sup> aryl or alkoxides,<sup>[3]</sup> and organoamides,<sup>[4, 5]</sup> and have been widely applied as reagents or catalysts in organic synthesis.<sup>[6, 7]</sup> Compared to other elements of the Periodic Table the chemistry of the lanthanoid metals is relatively undeveloped and as a consequence even simple lanthanoid compounds, such as lanthanoid trihalides and their complexes have been neglected. Recently there has been more interest in the structures of complexes of lanthanoid trihalides with simple donors, e.g. THF, as the structures have an effect on their reactivity. The anhydrous chloride, bromide and iodide salts of lanthanoid elements are moisture sensitive and readily form hydrates. The  $\text{LnX}_3$  salts are polymeric with four different structural types known at room temperature owing to the regular decrease in cation coordination number observed with increasing atomic number (*Table 6.1*).<sup>[8]</sup>

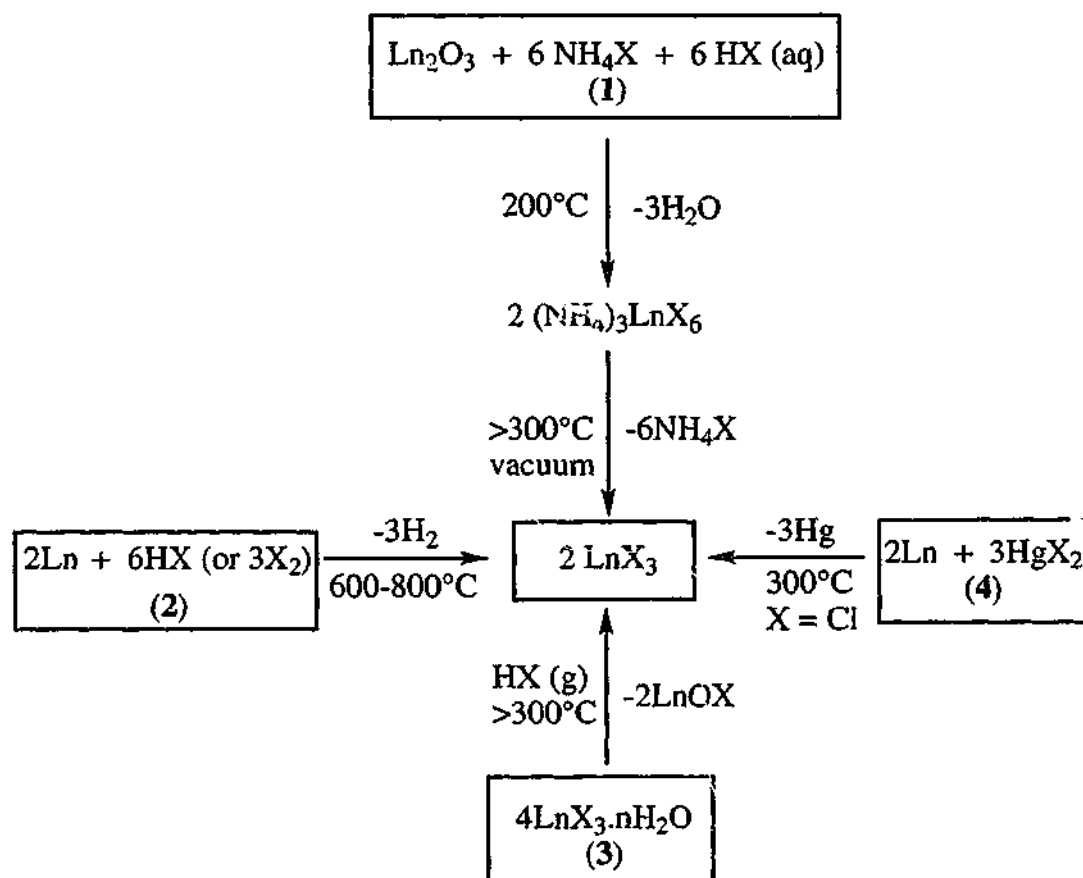
*Table 6.1 Structural Types for the lanthanoid trihalides,  $\text{LnX}_3$*

Structure Type	$\text{UCl}_3$	$\text{PuBr}_3$	$\text{YCl}_3$	$\text{BiI}_3$
Cation Coord. No.	9	8	6	6
(Space Group)	$\text{P6}_3/\text{m}$	$\text{Cmcm}$	$\text{C2}/\text{m}$	$\text{R}\bar{3}$
X = Cl	La-Gd	Tb	Dy-Lu, Y	—
X = Br	La-Pr	Nd-Eu	—	Gd-Lu, Y
X = I	—	La-Nd	—	Sm-Lu <sup>a</sup> , Y

<sup>a</sup>  $\text{EuI}_3$  is unknown.



The anhydrous  $\text{LnX}_3$  ( $X = \text{Cl}, \text{Br}, \text{I}$ ) salts are commercially available at a significant cost, but several synthetic methods exist for preparations on a small scale. The main starting materials used are the hydrated trihalides,[8] the oxides[9-11] or the metals[12] and a variety of preparative methods are listed in *Scheme 6.1*. The conversion of the starting materials to the anhydrous  $\text{LnX}_3$  compounds require strict anaerobic conditions, particularly for preparations involving elevated temperatures (*Scheme 6.1 (1-3)*) to avoid the formation of unwanted  $[\text{LnOX}]$ .



Scheme 6.1

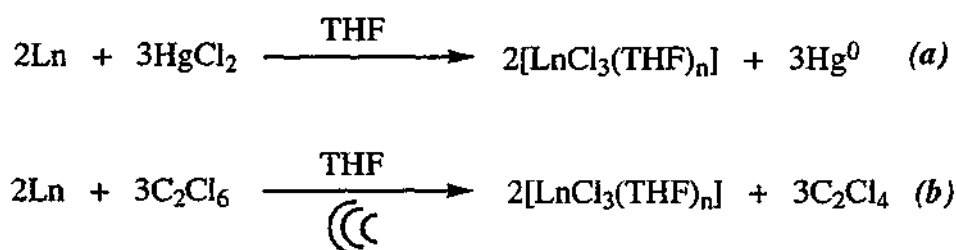
In typical syntheses of lanthanoid organoamide, organometallic, and aryl- or alkoxide complexes utilising the anhydrous trihalides, a strong donor solvent, such as THF, is required. This presumably solubilises the trihalide by coordination to the metal centre and breaks up the polymeric array of  $\text{LnX}_3$ . Thus the more soluble ether adducts  $[\text{LnX}_3(\text{THF})_n]$ [13] can be used as reactants and are well-defined starting materials. As solvated lanthanoid trihalides are the reactive species in solution, the information obtained

from the solid state structure of these complexes is invaluable towards understanding their behaviour in future reactions.

### 6.1.1 Formation of Ether Solvated Lanthanoid Trihalide Complexes

#### 6.1.1.1 $[\text{LnCl}_3(\text{S})_n]$ Compounds

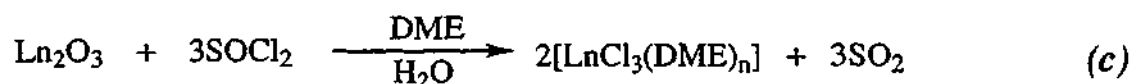
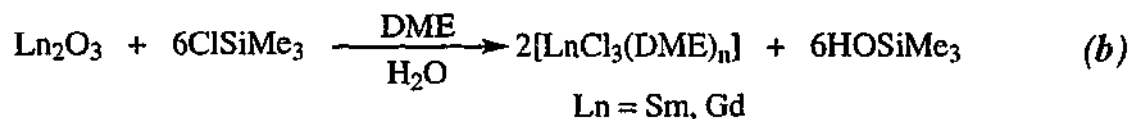
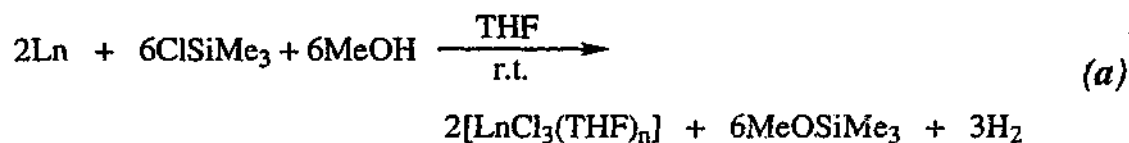
A vast number of methods are available for the preparation of solvated lanthanoid trichlorides  $[\text{LnCl}_3(\text{S})_n]$  especially those where  $\text{S} = \text{THF}$ , than are available for the bromides and iodides. Direct treatment of lanthanoid metals with mercury(II) chloride in THF has been utilised (see *Equation 6.1 (a)*).<sup>[14-16]</sup> The complete removal of mercury is complicated by the low solubility of  $\text{LnCl}_3(\text{THF})_n$  complexes in THF. A simpler metal-based route developed by Deacon *et al.* involved sonication of a mixture of hexachloroethane and lanthanoid metal in THF (see *Equation 6.1 (b)*).<sup>[17, 18]</sup> Despite this reaction demanding an excess of  $\text{C}_2\text{Cl}_6$ , purification is facile due to the solubility differences between the products.



*Equation 6.1*

Treating lanthanoid metal with trimethylsilyl chloride and anhydrous methanol in THF (see *Equation 6.2 (a)*).<sup>[19]</sup> or the addition of a little water to the reaction between lanthanoid oxide ( $\text{Ln} = \text{Sm}, \text{Gd}$ ) and  $\text{ClSiMe}_3$  in DME (see *Equation 6.2 (b)*).<sup>[20]</sup> yields the corresponding solvated lanthanoid trichlorides. Similarly, reaction of  $\text{Ln}_2\text{O}_3$  (or  $\text{Ln}_2(\text{CO}_3)_3$ ) with  $\text{SOCl}_2$  in DME with limited water has also yielded a number of 1,2-dimethoxyethane species,  $[\text{LnCl}_3(\text{DME})_n]$  ( $\text{Ln} = \text{Eu}, \text{Gd}, n = 2$ ;  $\text{Ln} = \text{Nd}, n = 1$ ) (see *Equation 6.2 (c)*).<sup>[21]</sup> The sensitivity of  $[\text{LnCl}_3(\text{DME})_2]$  complexes to hydration disfavours the deliberate addition of water to these reactions as it can lead to contamination by  $[\text{LnCl}_3(\text{DME})(\text{H}_2\text{O})]$  species. Furthermore, there are also problems with

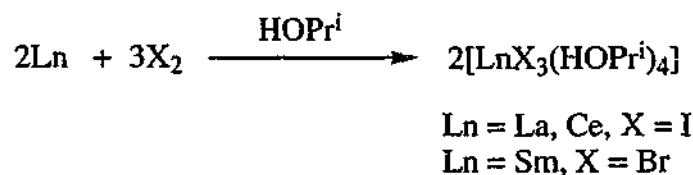
contamination of Schlenk equipment by the corrosive nature of  $\text{SOCl}_2$  and  $\text{ClSiMe}_3$  in work up.



*Equation 6.2*

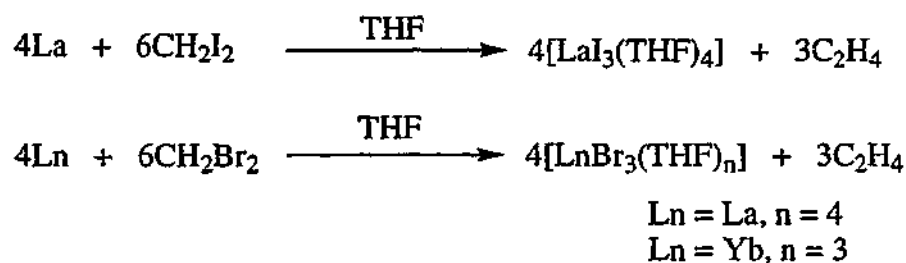
#### 6.1.1.2 $[\text{LnX}_3(\text{S})_n]$ ( $\text{X} = \text{Br, I}$ )

Solvated lanthanoid(III) tribromide and triiodide complexes have been isolated as isopropanol adducts by treating lanthanoid metal with elemental  $\text{Br}_2$  and  $\text{I}_2$  in 2-propanol (*Equation 6.3*).<sup>[22, 23]</sup>



*Equation 6.3*

More recently, Deacon *et al.*<sup>[24]</sup> have reported the direct treatment of lanthanoid metal with  $\text{CH}_2\text{Br}_2$  or  $\text{CH}_2\text{I}_2$  in THF at room temperature. This gave complexes of the type  $[\text{LnX}_3(\text{THF})_n]$  ( $\text{Ln} = \text{La, Ce, X} = \text{I, Br}$  (not Ce),  $n=4$ ;  $\text{Ln} = \text{Yb, X} = \text{Br}$ ,  $n=3$ ) (*Equation 6.4*). Namy and Kagan used this method twenty years ago for the convenient preparation of divalent lanthanoid halide complexes.<sup>[25]</sup>



Equation 6.4

## 6.1.2 Structural Properties of Lanthanoid Trihalide Ether Adducts

### 6.1.2.1 The Trichlorides

A wide range of structural and stoichiometric variations has been found for the  $[\text{LnCl}_3(\text{THF})_n]$  series. A common feature of these complexes, which is also observed for the hydrated trichlorides,<sup>[26]</sup> is an increase in coordination number with increase in metal size. The trichloride tetrahydrofuran adduct of the large lanthanum ion has the highest coordination number of eight. It is polymeric with six bridging halides per metal in a square antiprismatic coordination geometry (*Figure 6.1 (a)*).<sup>[17]</sup> For smaller lanthanoid ions a seven-coordinate polymeric array,  $[\text{LnCl}(\mu\text{-Cl})_2(\text{THF})_2]_n$  ( $\text{Ln} = \text{Ce}$ ,<sup>[17, 27]</sup>  $\text{Pr}$ ,<sup>[17, 28]</sup>  $\text{Nd}$ ,<sup>[27]</sup>  $\text{Y}$ <sup>[29]</sup>) has been characterised. Each metal centre has a terminal chloride atom, four bridging halides and two *cisoid* THF ligands arranged in a pentagonal bipyramidal environment (see *Figure 6.1 (b)*).

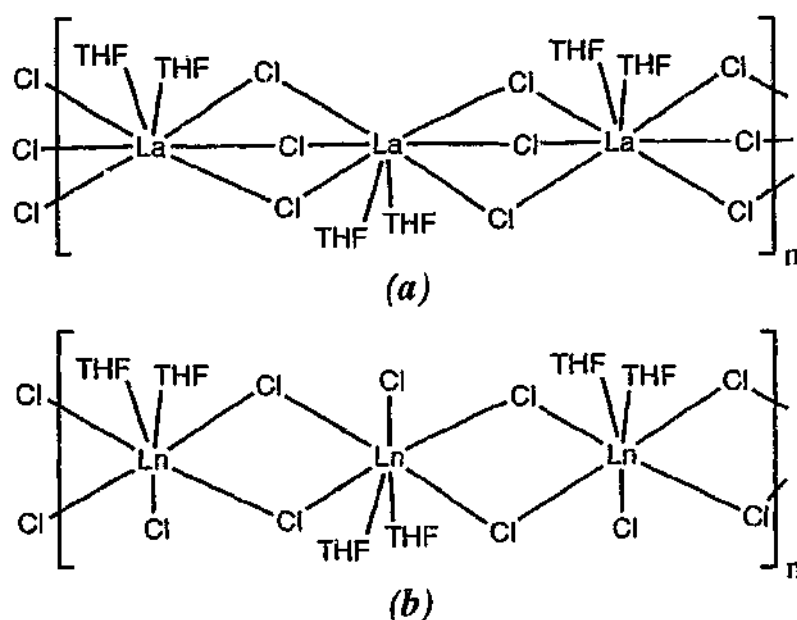


Figure 6.1

Other seven coordinate structural types have been isolated and include monomeric  $[\text{LnCl}_3(\text{THF})_4]$  ( $\text{Ln} = \text{Nd}$ ,<sup>[30]</sup>  $\text{Eu}$ ,<sup>[31]</sup>  $\text{Sm}$ <sup>[32]</sup>  $\text{Gd}$ <sup>[28]</sup>) as well as a mixed seven/six coordinate ionic complex of the type,  $[\text{LnCl}_2(\text{THF})_5][\text{LnCl}_4(\text{THF})_2]$  ( $\text{Ln} = \text{Gd}$ ,<sup>[33]</sup>  $\text{Dy}$ ,<sup>[34, 35]</sup>  $\text{Tb}$ ,<sup>[27]</sup>  $\text{Er}$ ,<sup>[33]</sup>  $\text{Y}$ <sup>[29, 36]</sup>). Six-coordinate species are also known with the later lanthanoid elements, for which there are two structural types; dimeric ( $[\text{YbCl}_2(\mu\text{-Cl})(\text{THF})_2]$ <sup>[17, 18]</sup>) and monomeric ( $[\text{LnCl}_3(\text{THF})_3]$  ( $\text{Ln} = \text{Sc}$ ,<sup>[37]</sup>  $\text{Yb}$ <sup>[17]</sup> and  $\text{Lu}$ <sup>[38]</sup>)).

The replacement of the unidentate THF molecules with a bidentate ligand such as DME results in complexes of the type  $[\text{LnCl}_3(\text{DME})_2]$  ( $\text{Ln} = \text{Y}$ ,<sup>[39]</sup>  $\text{Eu}$ ,<sup>[21]</sup>  $\text{Gd}$ ,<sup>[40]</sup>  $\text{Dy}$ ,<sup>[35]</sup>  $\text{Er}$ <sup>[41]</sup> and  $\text{Yb}$ <sup>[24]</sup>). Alternatively, using a nitrogen-based ligand, such as *N,N,N',N'*-tetramethylethane-1,2-diamine (TMEDA) resulted in incomplete exchange of the THF ligands giving a mixed ligand system,  $[\text{LnCl}_3(\text{THF})_2(\text{TMEDA})]$ .<sup>[20]</sup> Replacement of two *cisoid* THF ligands by a DME has been observed previously (e.g.  $[\text{Ln}\{\text{N}(\text{SiMe}_3)_2\}_2(\text{S})]$   $\text{S} = (\text{THF})_2$ <sup>[33]</sup> or  $\text{DME}$ <sup>[42]</sup>) despite significant differences in steric size as indicated by their steric coordination numbers 1.78 and 2.42 (for 2 THF ligands), respectively.<sup>[43]</sup> However, in situations where steric crowding / unsaturation is critical, as seen in  $[\text{ErCl}_3(\text{THF})_{3.5}]$ ,<sup>[17]</sup> a coordination number change results. Unlike the structural variety observed for the THF analogues (see above) the structurally characterised DME complexes show uniformity across the series. Each of the known  $[\text{LnCl}_3(\text{DME})_2]$

complexes ( $\text{Ln} = \text{Y}, \text{Eu}, \text{Gd}, \text{Dy}, \text{Er}$ ) exists as a monomeric, seven-coordinate structure with a pentagonal bipyramidal geometry. However, this structural series has only been characterised for elements smaller than Sm and it is possible that the larger members have different structures.

### 6.1.2.2 The Tribromides and Triiodides

In terms of reported structures, those of the lanthanoid *trichloride* solvates,  $\text{LnCl}_3(\text{S})_n$  ( $\text{S} = \text{THF}, \text{DME}$ ) have had more attention in comparison to other ligated trihalide complexes. To date, only three ether solvated lanthanoid triiodide compounds have been structurally characterised and fewer for the tribromides. As a consequence little is known about the structural varieties within these lanthanoid series. Whilst *isopropanol* is not an ether solvent, it does behave in a similar manner. Structural studies on the *isopropanol* adducts of lanthanoid tribromides and iodides,  $[\text{LnX}_3(\text{HOPr}^i)_4]$  ( $\text{Ln} = \text{Sm}, \text{X} = \text{Br}; [22]$   $\text{Ln} = \text{La}, \text{Ce}, \text{X} = \text{I} [23]$ ), revealed monomeric seven-coordinate species comprising of three halide atoms and four  $\text{HOPr}^i$  ligands around the metal. The molecular geometry for the  $[\text{LnI}_3(\text{HOPr}^i)_4]$  ( $\text{Ln} = \text{La}, \text{Ce}$ ) complexes is best described as a distorted capped trigonal prism in which an iodide caps the rectangular face defined by the four *isopropanol* oxygen atoms (*Figure 6.2 (a)*). In  $[\text{SmBr}_3(\text{HOPr}^i)_4]$  a pentagonal bipyramidal arrangement about the metal centre was found with two bromide ligands occupying the axial sites (*Figure 6.2 (b)*).

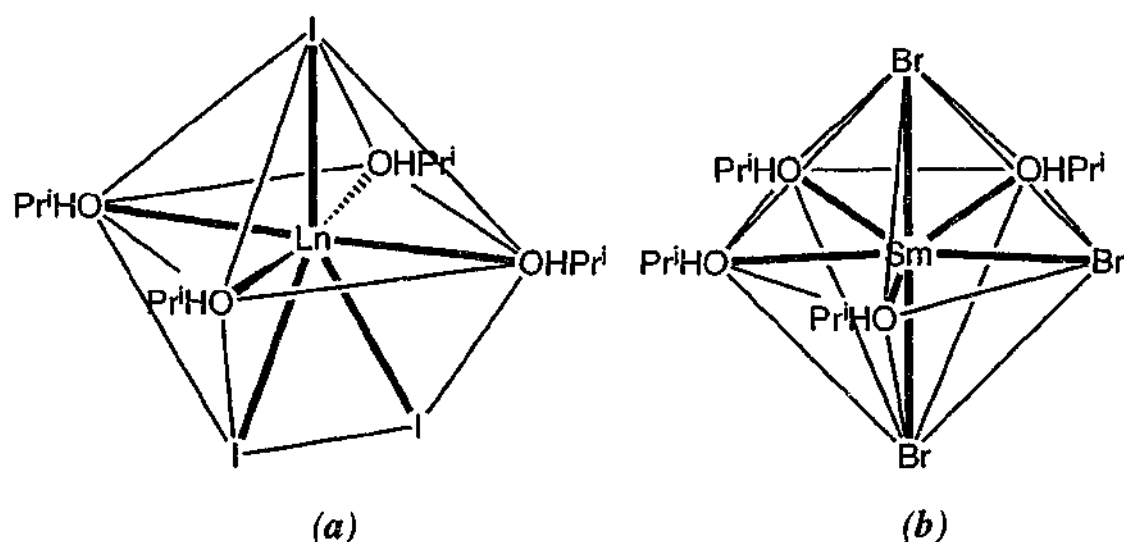


Figure 6.2

In a similar manner, pentagonal bipyramidal coordination geometry was observed for mononuclear lanthanum triiodide and tribromide tetrahydrofuran adducts,  $[\text{LaX}_3(\text{THF})_4]$ .<sup>[24, 44]</sup> A six-coordinate monomer  $[\text{YbBr}_3(\text{THF})_3]$  has also been isolated which presumably results from the decrease in lanthanoid size.<sup>[45]</sup> In contrast, the only other structural arrays known for the triiodides to date are the ionic complexes  $[\text{LaI}_2(\text{THF})_5]\text{I}_3$ <sup>[41]</sup> and  $[\text{SmI}_2(\text{THF})_5][\text{SmI}_4(\text{THF})_2]$ .<sup>[46]</sup> The incorporation of the larger iodide anion results in a lower coordination number for the samarium in the anion compared with the analogous chloride,  $[\text{SmCl}_3(\text{THF})_4]$ . Recrystallisation of the  $[\text{LaBr}_3(\text{THF})_4]$  complex from DME or diglyme afforded an eight-coordinate dimer  $[\text{LaBr}_2(\mu\text{-Br})(\text{DME})_2]_2$  and ionic eight/seven-coordinate  $[\text{LaBr}_2(\text{diglyme})_2][\text{LaBr}_4(\text{diglyme})]$  respectively<sup>[24]</sup> which were published together with the results of this chapter. These have no structural precedents within the chloride series.

### 6.1.3 Current Study

Whilst tetrahydrofuran ligated lanthanoid trichlorides have been extensively investigated, other ether adducts have been neglected. One part of this study seeks to extend the scope of 1,2-dimethoxyethane lanthanoid trichloride compounds. To date, three structurally similar DME ligated lanthanoid trichloride complexes are known. As these complexes contain lanthanoids of similar size, a different structural array may be anticipated with other lanthanoid elements. By preparing new dimethoxyethane ligated lanthanoid trichlorides, using smaller and larger lanthanoid elements, the point of possible structural change (or the 'transition point') in this series will be investigated.

To date little structural information is known for lanthanoid tribromide ether adducts. Since a significant structural variety exists for lanthanoid trichloride tetrahydrofuran adducts one might expect the tetrahydrofuran ligated tribromides to behave similarly. In exploration of this, the synthesis and characterisation of some lanthanoid(III) tribromide ether complexes using THF and DME have been investigated.

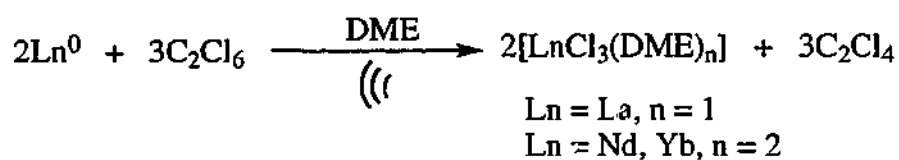
Complexes of the lanthanoids with weak donor ligands are of considerable interest as they can lead to compounds of interesting and useful reactivity.[47, 48] As reports of organoamine ligation of lanthanoid trichlorides are scarce, this study looked at the preparation and potential thermal rearrangement of such compounds. Hence, the synthesis, characterisation and subsequent thermal decomposition of some lanthanoid trichloride organodiamine compounds of the type,  $[\text{LnCl}_3(\text{L})_x]$  ( $\text{L}$  = bidentate amine), using unsubstituted or substituted ethylene diamine ligands have been examined.



## 6.2 Results and Discussion

### 6.2.1 $[\text{LnCl}_3(\text{DME})_x]$ Complexes

In a similar manner to the recent preparations of  $[\text{LnCl}_3(\text{THF})_n]$  complexes, [17, 18] DME analogues were obtained by sonication of lanthanoid metals (pieces or powder) with  $\text{C}_2\text{Cl}_6$  in DME (Equation 6.5).



Equation 6.5

The product formed as a white precipitate and complete reaction was indicated by disappearance of the metal. The relatively insoluble solvated lanthanoid trichloride was purified by washing the reaction mixture with hexane as the organic by-product and excess of  $\text{C}_2\text{Cl}_6$  are highly soluble in this solvent.

The above dimethoxyethane ligated lanthanoid trichlorides were characterised by chloride and / or lanthanoid analyses. IR spectra showed strong bands at 1020-1040  $\text{cm}^{-1}$  which are attributable to antisymmetric C—O—C stretching absorptions of the DME ligand. A far infrared spectrum of  $[\text{LaCl}_3(\text{DME})]$  shows bands at 215 and 182  $\text{cm}^{-1}$  assigned to  $\nu(\text{La}-\text{Cl}_{(\text{br})})$  vibrations. These values are close to those reported for  $([\text{LaCl}_3(\text{THF})_2]_{\infty})$ , [17] (215 and 197  $\text{cm}^{-1}$ ) which contained only bridging chlorides. In addition no bands above 240  $\text{cm}^{-1}$  corresponding to  $\nu(\text{La}-\text{Cl}_{(\text{ter})})$  were observed and this implies that lanthanum is associated with all bridging chloride ligands. Hence, the structure is presumed to be similar to that of  $[\text{LaCl}_3(\text{THF})_2]_{\infty}$  (Figure 6.1 (a)) with replacement of two *cis*-THF ligands with a chelating DME (Figure 6.3). This type of ligand replacement has been observed previously (see Section 6.1.2.1).

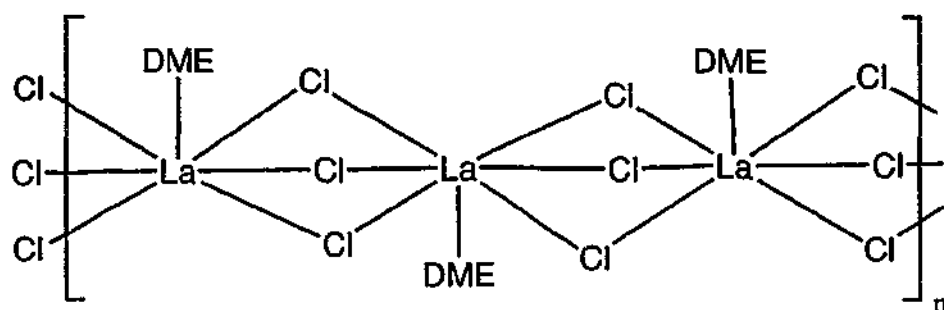


Figure 6.3

Satisfactory far infrared data could not be obtained for the compounds  $[\text{NdCl}_3(\text{DME})_2]$  or  $[\text{YbCl}_3(\text{DME})_2]$ , although significant absorption above  $200\text{ cm}^{-1}$  was observed suggesting that terminally bound chlorides were present. In view of the reported structures of  $[\text{LnCl}_3(\text{DME})_2]$  ( $\text{Ln} = \text{Y}$ ,<sup>[39]</sup>  $\text{Eu}$ ,<sup>[21]</sup>  $\text{Gd}$ ,<sup>[40]</sup>  $\text{Dy}$ ,<sup>[35]</sup> and  $\text{Er}$ <sup>[41]</sup>) which are seven-coordinate monomers, these compounds are likely to be similar and this was confirmed for  $\text{Yb}$  by a single crystal X-ray structure determination.<sup>[24]</sup>

Crystals of  $[\text{YbCl}_3(\text{DME})_2]$  were grown from the surface of a metal piece in a solution of  $\text{C}_2\text{Cl}_6$  in DME and the molecular structure is shown in *Figure 6.4*. Crystallographic data collection and the structure solution were performed by Dr. P. C. Junk at James Cook University, Townsville. Crystal and refinement data, and some selected bond lengths and angles are listed in *Table 6.2* and *Table 6.3*, respectively. The seven-coordinate metal environment comprises three terminal chloride anions and two chelating DME ligands in a pentagonal bipyramidal array. The chloride atoms  $\text{Cl}(1)$  and  $\text{Cl}(3)$  are in axial positions with  $\text{Cl}(1)\text{—Yb—Cl}(3)$  ( $170.10(4)^\circ$ ) being near linear and the equatorial sites are occupied by  $\text{Cl}(2)$  and  $\text{O}(102, 105, 202, 205)$  atoms. The sum of the interligand angles of the equatorial pentagonal plane (made up of  $\text{Cl}(2)$ ,  $\text{O}(102, 105, 202, 205)$ ) is close to  $360^\circ$  ( $366^\circ$ ), as expected for this geometry. The  $[\text{YbCl}_3(\text{DME})_2]$  complex is isostructural with previous  $[\text{LnCl}_3(\text{DME})_2]$  compounds ( $\text{Ln} = \text{Y}$ ,<sup>[39]</sup>  $\text{Eu}$ ,<sup>[21]</sup>  $\text{Gd}$ ,<sup>[40]</sup>  $\text{Dy}$ ,<sup>[35]</sup>  $\text{Er}$ <sup>[41]</sup>). The average  $\text{Ln—Cl}$  and  $\text{Ln—O}(\text{DME})$  distances are comparable as shown by subtraction of the respective metal ionic radii which gives values of  $1.629 \pm 0.003\text{ \AA}$  and  $1.46 \pm 0.01\text{ \AA}$ , respectively. This suggests that the decrease in metal size does not induce significant steric crowding across the series. Whilst one DME ligand has similar  $\text{Yb—O}(102, 105)$  distances, the other DME group has one longer ( $\text{O}(202)$ ) and one shorter ( $\text{O}(205)$ ). As the distance  $\text{Yb}(1)\text{—O}(102)$  is not lengthened with respect to  $\text{Yb}(1)\text{—O}(202)$  it indicates that the long  $\text{Yb}(1)\text{—O}(202)$  is unlikely to be due to a *trans*

influence of Cl(2). More likely the difference in Yb(1)—O(DME) bond lengths arises to relieve ligand-ligand repulsions resulting from the close proximity of the two methyl groups (C(101) and C(201)). These methyl groups are notably placed on opposite sides of the equatorial plane. Comparison of the Yb—O(DME) distances with the corresponding Yb—O(THF) lengths in [YbCl<sub>3</sub>(THF)<sub>3</sub>] shows an approximately 0.1 Å increase for the DME complex. This is greater than anticipated from differences in the ionic radii due to coordination number (coordination number = 7, i.r. Yb<sup>3+</sup> 0.93 Å; 6, Yb<sup>3+</sup> 0.87 Å) and suggests that [YbCl<sub>3</sub>(DME)<sub>2</sub>] is marginally more sterically crowded than the THF analogue. This is despite the two neutral ligand sets (3 x THF or 2 x DME) having similar Σsteric coordination numbers (3.56 and 3.63 respectively).

**Table 6.2** Crystal and refinement data for [YbCl<sub>3</sub>(DME)<sub>2</sub>]

Compound	[YbCl <sub>3</sub> (DME) <sub>2</sub> ]
Formula	C <sub>8</sub> H <sub>20</sub> Cl <sub>3</sub> LnO <sub>4</sub>
<i>M</i>	459.6
<i>a</i> (Å)	11.380(1)
<i>b</i> (Å)	8.993(1)
<i>c</i> (Å)	15.644(9)
$\alpha$ (°)	90
$\beta$ (°)	104.99(4)
$\gamma$ (°)	90
<i>V</i> (Å <sup>3</sup> )	1525
Crystal system	monoclinic
Space Group	<i>P</i> 2 <sub>1</sub> / <i>c</i>
<i>Z</i>	4
Diffractometer	Bruker SMART CCD
$\rho_{\text{calcd}}$ (g cm <sup>-3</sup> )	2.00
$\mu$ (MoK $\alpha$ ) (mm <sup>-1</sup> )	6.6
2 $\theta_{\text{max}}$ (°)	46.6
<i>N</i> , <i>N</i> <sub>o</sub>	6649, 2184
<i>R</i> , <i>R</i> <sub>w</sub> (observed data)	0.0240, 0.0578
<i>R</i> , <i>R</i> <sub>w</sub> (all data)	0.0260, 0.0598

**Table 6.3** Selected bond lengths (Å) and angles (°) with estimated standard deviations in parentheses for  $[\text{YbCl}_3(\text{DME})_2]$ .

Yb(1)—Cl(1)	2.556(1)	Cl(2)-Yb(1)-O(102)	140.83(9)
Yb(1)—Cl(2)	2.559(1)	Cl(2)-Yb(1)-O(105)	80.25(8)
Yb(1)—Cl(3)	2.556(1)	Cl(2)-Yb(1)-O(202)	146.98(8)
Yb(1)—O(102)	2.403(3)	Cl(2)-Yb(1)-O(205)	79.79(9)
Yb(1)—O(105)	2.403(3)	Cl(3)-Yb(1)-O(102)	98.45(9)
Yb(1)—O(202)	2.446(3)	Cl(3)-Yb(1)-O(105)	81.35(7)
Yb(1)—O(205)	2.347(3)	Cl(3)-Yb(1)-O(202)	78.98(8)
		Cl(3)-Yb(1)-O(205)	89.72(8)
Cl(1)-Yb(1)-Cl(2)	90.50(4)		
Cl(1)-Yb(1)-Cl(3)	170.10(4)	O(102)-Yb(1)-O(105)	67.0(1)
Cl(1)-Yb(1)-O(102)	79.35(9)	O(102)-Yb(1)-O(202)	71.6(1)
Cl(1)-Yb(1)-O(105)	106.31(8)	O(102)-Yb(1)-O(205)	135.8(1)
Cl(1)-Yb(1)-O(202)	91.20(8)	O(105)-Yb(1)-O(202)	130.4(1)
Cl(1)-Yb(1)-O(205)	85.4(1)	O(105)-Yb(1)-O(205)	156.9(1)
Cl(2)-Yb(1)-Cl(3)	97.08(4)	O(202)-Yb(1)-O(205)	67.5(1)

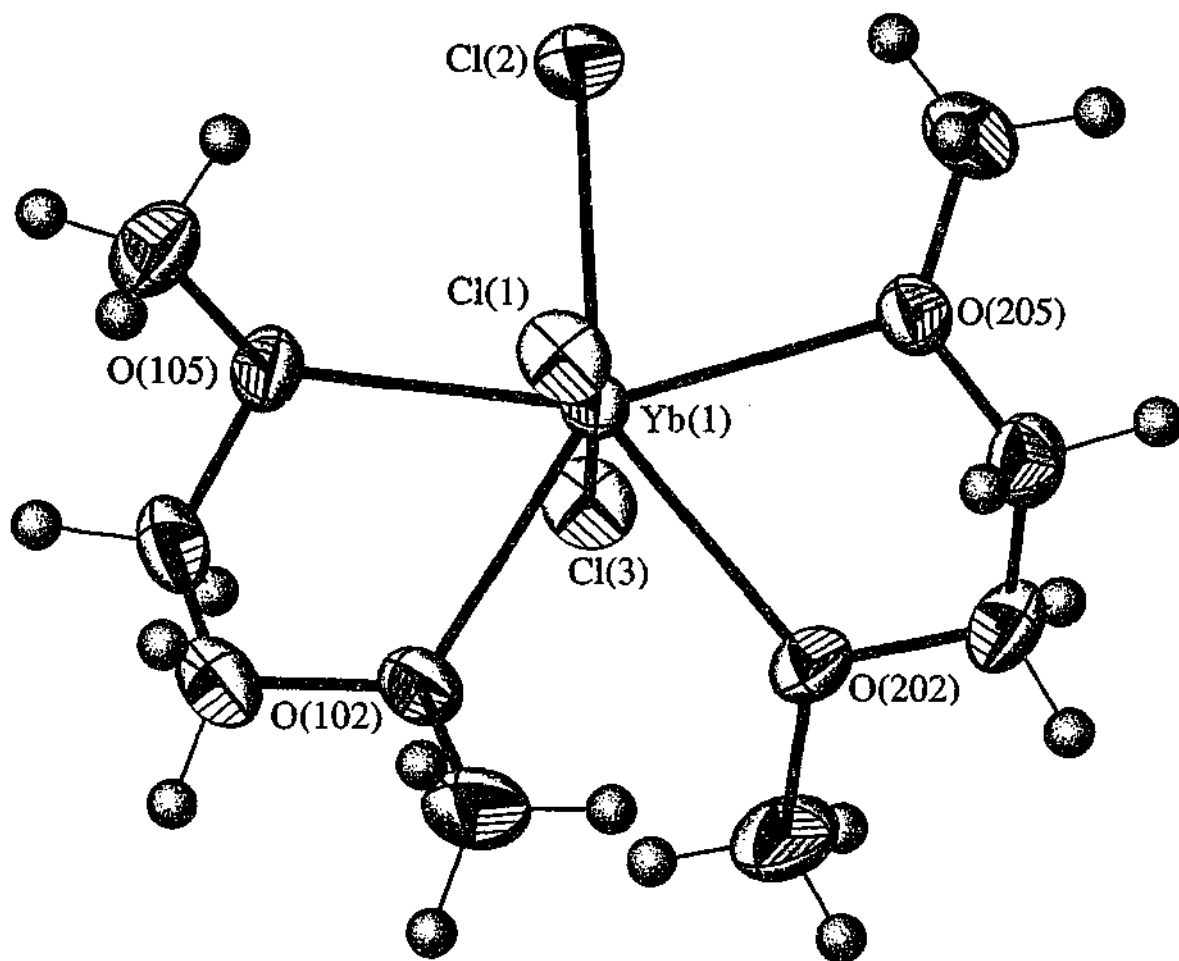
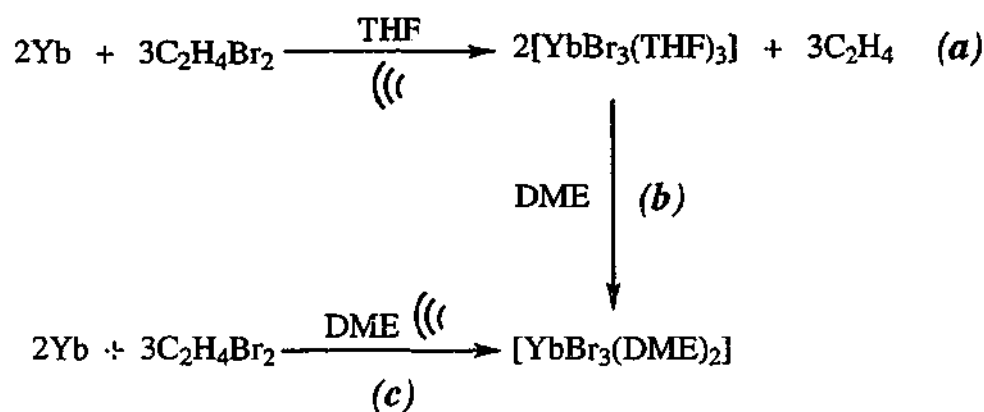


Figure 6.4 Molecular structure of  $[YbCl_3(DME)_2]$

### 6.2.2 $[YbBr_3(S)_x]$ Complexes ( $S = THF, DME$ )

Tetrahydrofuran ligated ytterbium tribromide was prepared in high yield by treatment of the metal powder with an excess of 1,2-dibromoethane in THF (*Scheme 6.2 (a)*). The complete dissolution of metal was aided by sonication of the reaction mixture. The partially THF-soluble  $[YbBr_3(THF)_3]$  complex was precipitated by addition of hexane. Recrystallisation of  $[YbBr_3(THF)_3]$  from dimethoxyethane afforded the DME complex,  $[YbBr_3(DME)_2]$  (*Scheme 6.2 (b)*). This adduct was also prepared from the direct reaction of ytterbium metal and 1,2-dibromoethane in DME (*Scheme 6.2 (c)*).



Scheme 6.2

The compositions of the products were confirmed by halide and/or ytterbium analyses. Infrared spectroscopy revealed the presence of the ether donors by C—O—C absorption bands at the expected values; 1040 (antisymmetric) and 842  $\text{cm}^{-1}$  (symmetric) for  $[\text{YbBr}_3(\text{THF})_3]$  and 1027  $\text{cm}^{-1}$  (antisymmetric) for  $[\text{YbBr}_3(\text{DME})_2]$ . Far infrared data on  $[\text{YbBr}_3(\text{DME})_2]$  showed  $\nu(\text{Yb}-\text{Br}_{(\text{ter})})$  values (172, 150  $\text{cm}^{-1}$ ) consistent with only terminal bromide coordination modes. Hence, for the  $[\text{YbBr}_3(\text{DME})_2]$  a monomeric, seven-coordinate structure, similar to that of  $[\text{LnCl}_3(\text{DME})_2]$  complexes ( $\text{Ln} = \text{Y}$ , [39]  $\text{Eu}$ , [21]  $\text{Gd}$ , [40]  $\text{Dy}$ , [35]  $\text{Er}$  [41] and  $\text{Yb}$  (this work) [24]), is indicated. In the case of the tetrahydrofuran ligated ytterbium tribromide adduct, which is likely to be a six-coordinate monomer in view of the structures of  $[\text{LnCl}_3(\text{THF})_3]$  ( $\text{Ln} = \text{Sc}$ , [37]  $\text{Yb}$ , [17]  $\text{Lu}$  [38]), satisfactory far infrared data could not be obtained.

The structures of the  $[\text{YbBr}_3(\text{THF})_3]$  and  $[\text{YbBr}_3(\text{DME})_2]$  complexes were confirmed by X-ray crystal structure determinations (Figure 6.5, and Figure 6.6, respectively) by Dr. P. C. Junk at James Cook University, Townsville. Single crystals for both solvates were grown on the metal surface in a solution of the ether solvent and 1,2-dibromoethane. A summary of data collection and refinement parameters for both complexes is given in Table 6.4 and selected bond lengths and angles are listed in Table 6.5 and Table 6.6, respectively. For  $[\text{YbBr}_3(\text{THF})_3]$  the structure is monomeric, with *mer*-octahedral stereochemistry around the central metal atom and this closely resembles the structure of  $[\text{YbCl}_3(\text{THF})_3]$ . [17] The Yb atom, Br(1) and O(2) lie on a two fold axis. The two mutually *trans* bromide atoms are near linear (Br(2)—Yb—Br(2') 173.22(4)°) with a similar Yb—Br distance to those (2.719(2) and 2.747(2) Å) found in the six-coordinate anion, *trans*- $[\text{YbBr}_4(\text{THF})_2]$ , [41] however the bond distance of Yb—Br *trans* to the

coordinated THF is significantly shorter (0.043 Å). The mutually *trans* THF ligands have a O(1)—Yb—(O1') angle near 180° and the *trans* Yb—O(THF) bond lengths (2.280 Å) are similar to those of [YbBr<sub>4</sub>(THF)<sub>2</sub>]<sup>-</sup>.<sup>[41]</sup> Interestingly, the Yb—O bond *trans* to Br(2) is marginally longer (0.07 Å), presumably due to a *trans* influence of the negatively charged bromide. A similar effect was observed for the chloride in [YbCl<sub>3</sub>(THF)<sub>3</sub>].<sup>[17]</sup>

Table 6.4. Summary of Crystallographic Data for [YbBr<sub>3</sub>(THF)<sub>3</sub>] and [YbBr<sub>3</sub>(DME)<sub>2</sub>].

Compound	[YbBr <sub>3</sub> (THF) <sub>3</sub> ]	[YbBr <sub>3</sub> (DME) <sub>2</sub> ]
Formula	C <sub>12</sub> H <sub>24</sub> Br <sub>3</sub> O <sub>3</sub> Yb	C <sub>8</sub> H <sub>20</sub> Br <sub>3</sub> YbO <sub>4</sub>
<i>M</i>	629.1	593.0
<i>a</i> (Å)	9.125(1)	11.698(2)
<i>b</i> (Å)	14.249(1)	8.947(2)
<i>c</i> (Å)	14.270(1)	15.905(3)
$\alpha$ (°)	90	90
$\beta$ (°)	90	105.06(3)
$\gamma$ (°)	90	90
<i>V</i> (Å <sup>3</sup> )	1855	1607
Crystal system	orthorhombic	monoclinic
Space Group	<i>Pbcn</i>	<i>P2<sub>1</sub>/c</i>
<i>Z</i>	4	4
Diffractometer	Bruker SMART CCD	Bruker SMART CCD
$\rho_{\text{calcd}}$ (g cm <sup>-3</sup> )	2.25	2.45
$\mu$ (MoK $\alpha$ ) (mm <sup>-1</sup> )	11.5	13.3
$2\theta_{\text{max}}$ (°)	50	50
<i>N</i> , <i>N<sub>o</sub></i>	3149, 1634	7128, 2313
<i>R</i> , <i>R<sub>w</sub></i> (observed data)	0.0324, 0.0811	0.0630, 0.1493
<i>R</i> , <i>R<sub>w</sub></i> (all data)	0.1062, 0.1002	0.0676, 0.1552

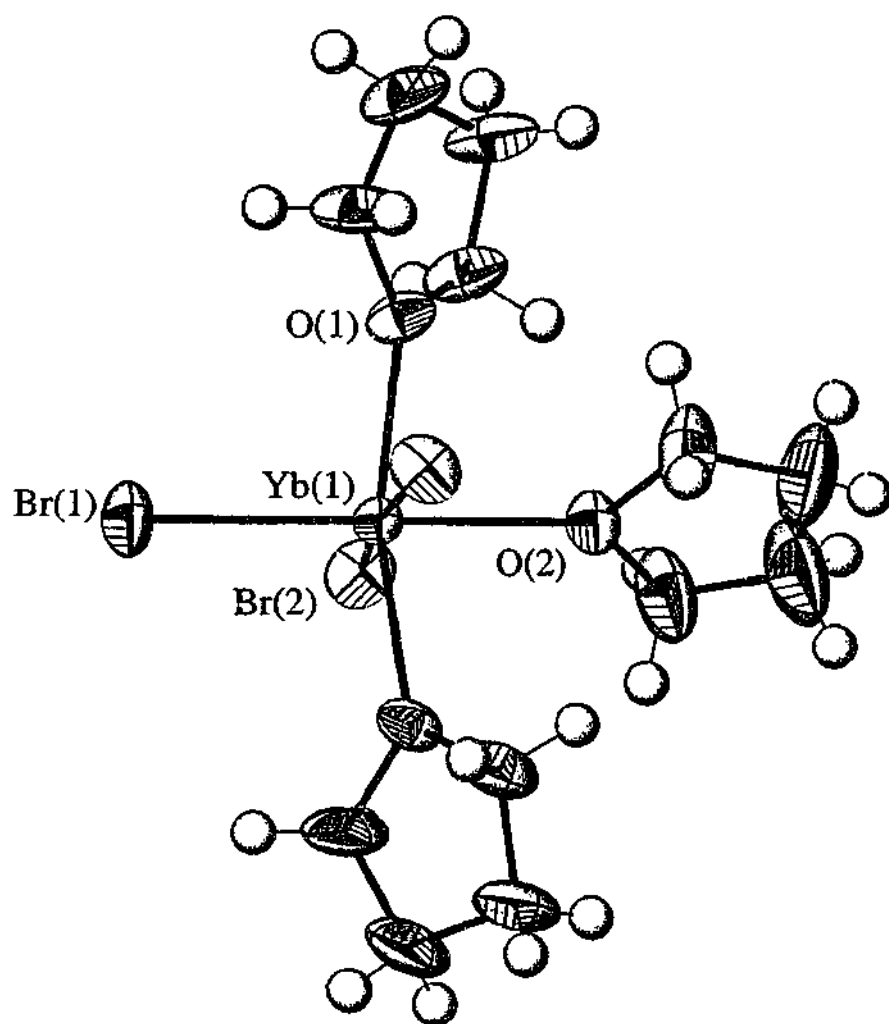


Figure 6.5 Molecular structure of  $[YbBr_3(THF)_3]$ .

Table 6.5 Selected distances ( $\text{\AA}$ ) and angles ( $^\circ$ ) with estimated standard deviations in parentheses for  $[YbBr_3(THF)_3]$  (atoms obtained through symmetry operations are denoted by primes)

Yb(1)—Br(1)	2.665(1)	Br(1)—Yb(1)—Br(2A) <sup>a</sup>	93.39(3)
Yb(1)—Br(2)	2.708(1)	Br(1)—Yb(1)—O(1A) <sup>a</sup>	97.3(2)
Yb(1)—O(1)	2.255(6)	Br(2)—Yb(1)—O(1)	89.4(2)
Yb(1)—C(2)	2.329(9)	Br(2)—Yb(1)—O(2)	86.61(3)
		Br(2)—Yb(1)—Br(2A) <sup>a</sup>	173.22(4)
Br(1)—Yb(1)—Br(2)	93.39(3)	Br(2)—Yb(1)—O(1A) <sup>a</sup>	89.7(2)
Br(1)—Yb(1)—O(1)	97.3(2)	O(1)—Yb(1)—O(1A) <sup>a</sup>	165.4(3)
Br(1)—Yb(1)—O(2)	180(-)	O(1)—Yb(1)—O(2)	82.7(2)

Symmetry transformations used to generate equivalent atoms: <sup>a</sup>  $x, y, \frac{1}{2}-z$ .



The structure of  $[\text{YbBr}_3(\text{DME})_2]$  is shown in *Figure 6.6* and is essentially the same as that of  $[\text{YbCl}_3(\text{DME})_2]$  (see above). The present  $\text{Yb}-\text{Br}_{(\text{axial})}$  and  $\text{Yb}-\text{Br}_{(\text{equat})}$  bond lengths (*Table 6.6*) are similar to those found in  $[\text{YbCl}_3(\text{DME})_2]$  (*Table 6.3*) (bromide consistently just slightly longer) with  $\text{Ln}-\text{X}$  differing by 0.15 and 0.17 Å, respectively (ionic radii of  $\text{Br}^-$  (1.96Å) >  $\text{Cl}^-$  (1.81Å)).<sup>[45]</sup> The  $\text{Yb}-\text{O}(\text{DME})$  distances in  $[\text{YbBr}_3(\text{DME})_2]$  are approximately 0.1 Å longer than the corresponding  $\text{Yb}-\text{O}(\text{THF})$  bond length in six-coordinate  $[\text{YbBr}_3(\text{THF})_3]$  (see above). This is larger than the differences in ionic radii due to coordination number (coordination number = 7, i.r.  $\text{Yb}^{3+}$  0.93 Å; 6,  $\text{Yb}^{3+}$  0.87 Å)<sup>[45]</sup> and suggests that  $[\text{YbBr}_3(\text{DME})_2]$  is marginally more sterically crowded than  $[\text{YbBr}_3(\text{THF})_3]$ .

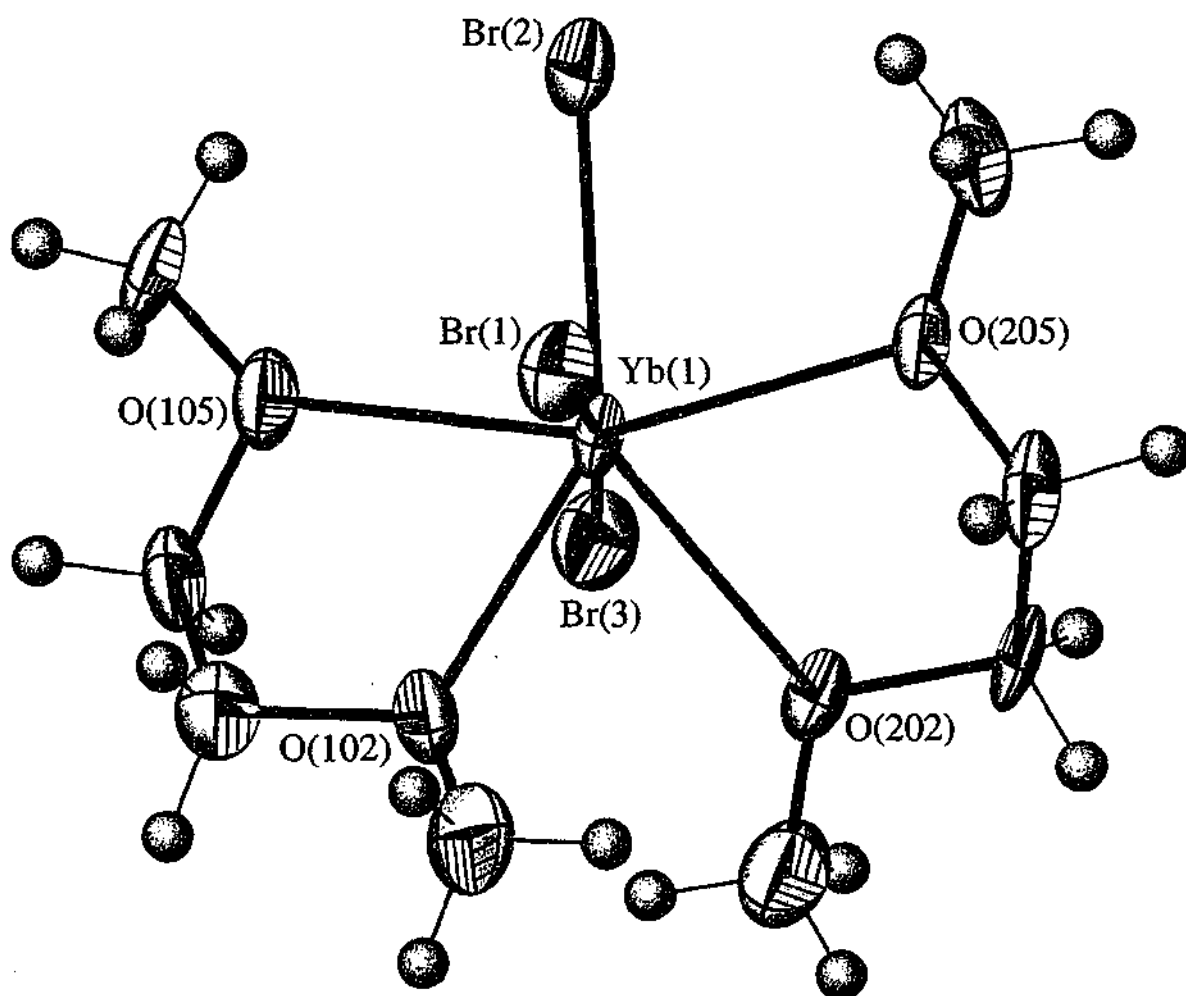


*Figure 6.6* Molecular structure of  $[\text{YbBr}_3(\text{DME})_2]$ .

**Table 6.6** Selected bond lengths (Å) and angles (°) with estimated standard deviations in parentheses for  $[\text{YbBr}_3(\text{DME})_2]$ .

Yb(1)—Br(1)	2.707(1)	Br(2)-Yb(1)-O(102)	140.7(2)
Yb(1)—Br(2)	2.729(1)	Br(2)-Yb(1)-O(105)	80.5(2)
Yb(1)—Br(3)	2.708(1)	Br(2)-Yb(1)-O(202)	147.1(2)
Yb(1)—O(102)	2.374(9)	Br(2)-Yb(1)-O(205)	79.6(2)
Yb(1)—O(105)	2.403(8)	Br(3)-Yb(1)-O(102)	100.0(2)
Yb(1)—O(202)	2.422(7)	Br(3)-Yb(1)-O(105)	81.3(2)
Yb(1)—O(205)	2.354(9)	Br(3)-Yb(1)-O(202)	79.0(2)
		Br(3)-Yb(1)-O(205)	88.7(2)
Br(1)-Yb(1)-Br(2)	88.95(5)		
Br(1)-Yb(1)-Br(3)	171.32(4)	O(102)-Yb(1)-O(105)	67.3(3)
Br(1)-Yb(1)-O(102)	79.4(2)	O(102)-Yb(1)-O(202)	71.6(3)
Br(1)-Yb(1)-O(105)	106.2(2)	O(102)-Yb(1)-O(205)	135.8(3)
Br(1)-Yb(1)-O(202)	92.7(2)	O(105)-Yb(1)-O(202)	129.9(3)
Br(1)-Yb(1)-O(205)	85.9(2)	O(105)-Yb(1)-O(205)	156.5(3)
Br(2)-Yb(1)-Br(3)	96.71(4)	O(202)-Yb(1)-O(205)	67.7(3)

### 6.2.3 Alternative $[\text{LnCl}_3(\text{L})_x(\text{L}')_y]$ Complexes ( $\text{L} = \text{MeCN}$ , $\text{L}' = \text{chelating diamine}$ )

#### 6.2.3.1 Syntheses

The preparation of  $\text{LnCl}_3(\text{L}')$  ( $\text{L}' = \text{bidentate organoamine ligand}$ ) complexes was more complicated than initially expected. The relatively weak donors used in this study had a characteristic ethylene diamine backbone that was substituted to produce a number of ligands with different steric and electronic demands (*Figure 6.7*).

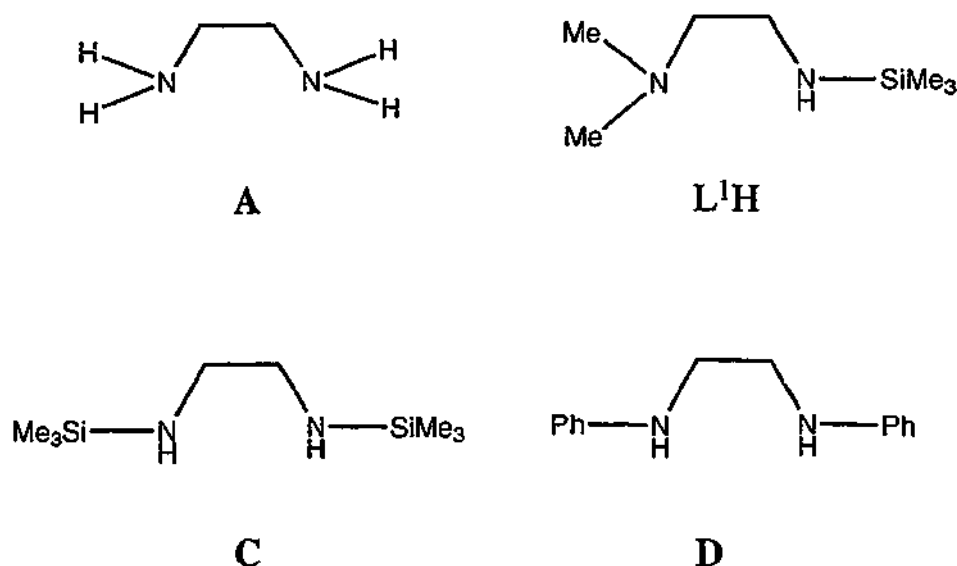
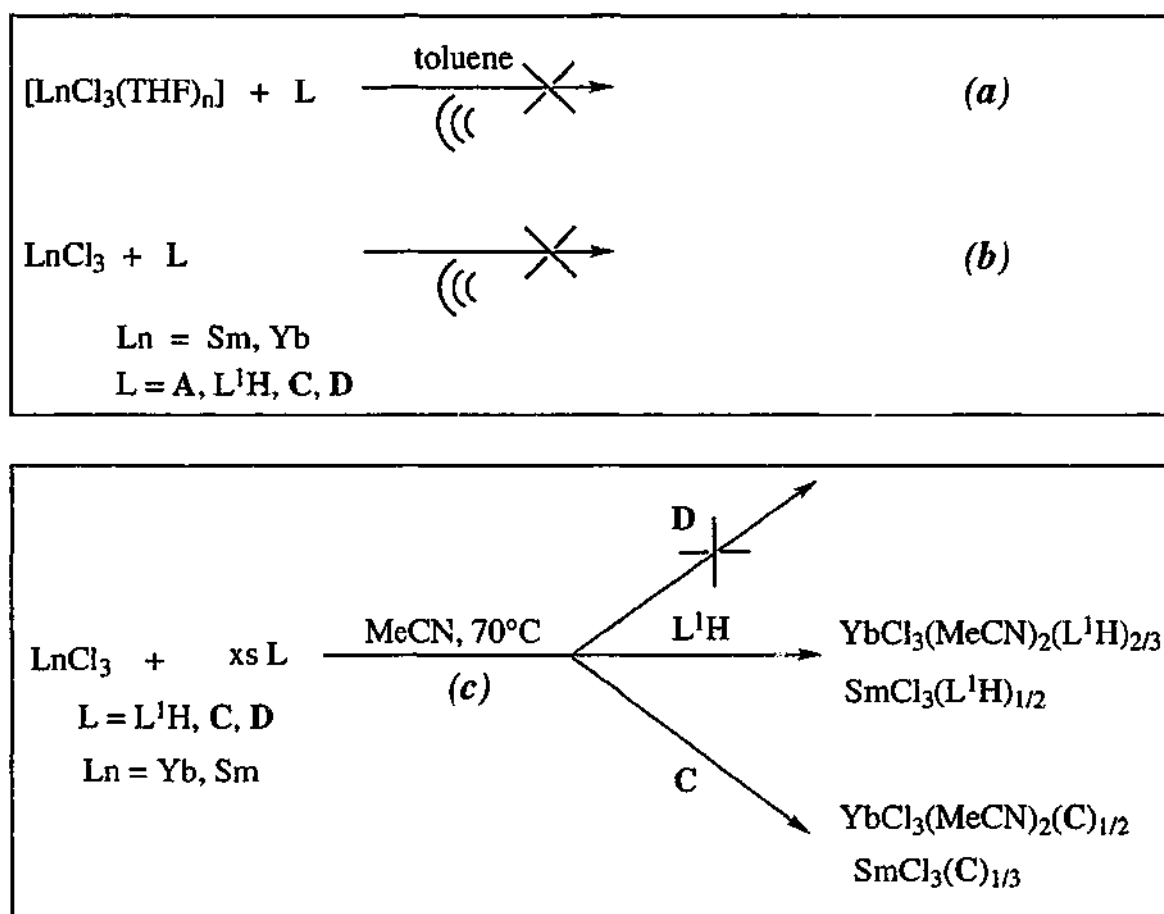


*Figure 6.7*

Since some of these bidentate amines are relatively weak donors ( $\text{L}^1\text{H}$ , **C**, **D**), direct reactions of the ligands with anhydrous lanthanoid trichlorides were carried out in non-polar solvents. Due to the low solubility of  $\text{LnCl}_3$  in hydrocarbons, the more soluble tetrahydrofuran adducts,  $[\text{LnCl}_3(\text{THF})_n]$  were used. The reaction of  $[\text{LnCl}_3(\text{THF})_n]$  with **A**,  $\text{L}^1\text{H}$ , **C** or **D** in a 1:1 ratio in toluene was unsuccessful, despite overnight sonication of the reaction mixture (*Scheme 6.3 (a)*). Solvent-free reactions (see *Scheme 6.3 (b)*), where the anhydrous trichloride is heated (or sonicated) with the amine ligand also failed. Refluxing anhydrous lanthanoid trichloride with excess amine ligand in acetonitrile (*Scheme 6.3 (c)*) was successful for the preparation of samarium and ytterbium complexes using  $\text{L}^1\text{H}$  or **C**. Lanthanum trichloride was also investigated but was unsuccessful in coordinating neutral organoamine ligands. The reaction mixtures of  $\text{L}^1\text{H}$  and **C** were filtered and the residual white powder dried under vacuum. Irrespective of the stoichiometry of mixing, the

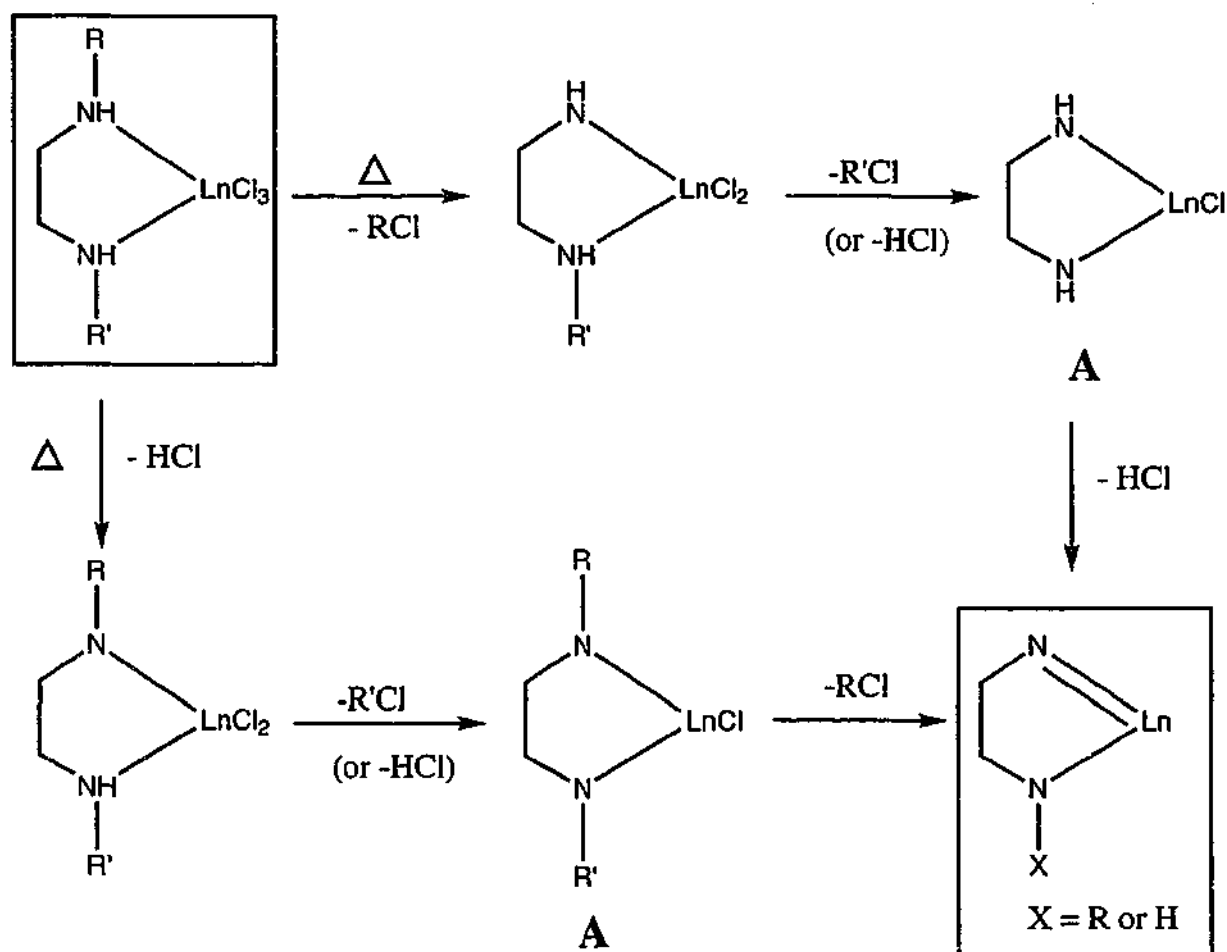
reactions between the lanthanoid halide and excess diamine gave only fractional amounts of ligand to lanthanoid chloride in the end product.



*Scheme 6.3*

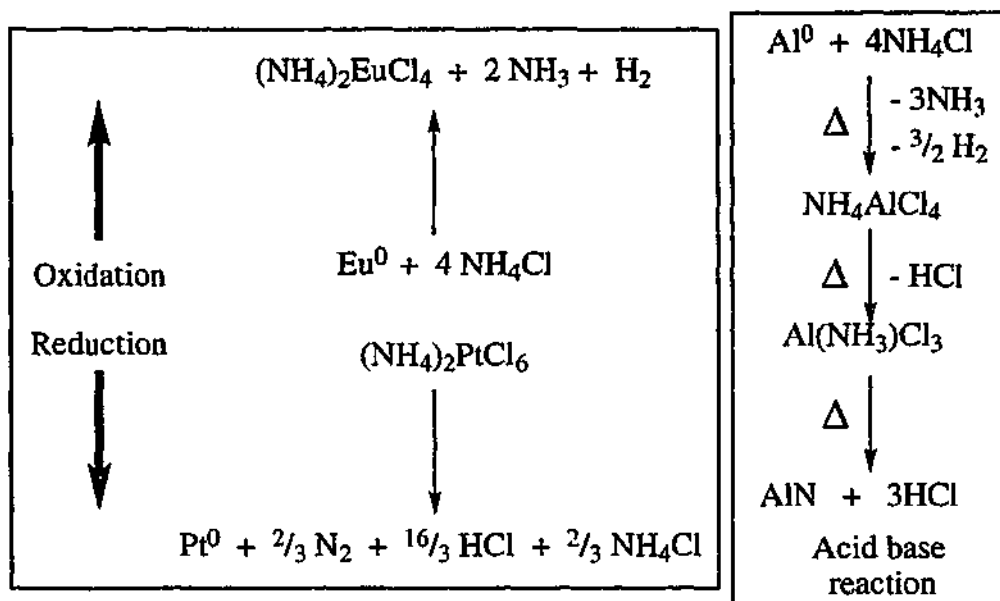
Previous work by Forsberg *et al.*[49] in preparing compounds of the composition  $[\text{LnX}_3(\text{HN}_2\text{CH}_2\text{CH}_2\text{NH}_2)_4]$  ( $\text{Ln} = \text{La-Lu}$ ,  $\text{X} = \text{Cl}$ ; or for  $\text{Ln} = \text{La, Nd, Gd}$ ,  $\text{X} = \text{Br}$ ) used a similar method to *Scheme 6.3 (c)*. They state that the reaction conditions required careful control with strict exclusion of air. Although the ethylenediamine ligated lanthanoid trihalides have been prepared, it is not surprising that similar complexes incorporating the less basic ligands  $\text{L}^1\text{H}$ ,  $\text{C}$  and  $\text{D}$  are more difficult to synthesize. This is evident by the preferred coordination of  $\text{MeCN}$  to the metal centre. As the  $\text{L}^1\text{H}$  and  $\text{C}$  diamines can be (partly) coordinated to  $\text{LnCl}_3$  salts, the diphenyl substituted ethylene diamine ( $\text{D}$ ) ligand must not have sufficient donor ability to coordinate to the lanthanoid trichloride under the reaction conditions investigated. This insufficient ability of  $\text{D}$  to coordinate suggests that the lone pair of the nitrogen atom is partially delocalised into the electron withdrawing phenyl substituent.

The motivation to prepare these lanthanoid amine adducts was to explore their thermal decomposition pathways which may result in the isolation of a highly reactive lanthanoid species. It was anticipated that upon heating, loss of trimethylsilylchloride and hydrogen chloride would occur resulting in the stepwise formation of a metal amide to nitride species (see *Scheme 6.4*).



*Scheme 6.4*

The ammonium ion has been found to act as an oxidising or reducing agent when coordinated as a counter ion to a metal during thermal treatment. For example, oxidation of europium metal with NH<sub>4</sub>Cl gives [(NH<sub>4</sub>)<sub>2</sub>EuCl<sub>4</sub>] whereas [(NH<sub>4</sub>)<sub>2</sub>PtCl<sub>6</sub>] undergoes an internal reduction to give in Pt<sup>0</sup> (see *Scheme 6.5*).<sup>[10]</sup> The ammonium ion can also behave as a base by reacting with an acid such as M<sup>n+</sup> and it has been used to prepare a number of pure nitride metal complexes through intramolecular rearrangement (one example is shown in *Scheme 6.5*). Furthermore, the use of the ammonium ion in lanthanoid chemistry to synthesize anhydrous LnCl<sub>3</sub> compounds is widely applied in the thermal decomposition of [(NH<sub>4</sub>)<sub>3</sub>LnCl<sub>6</sub>] which releases NH<sub>4</sub>Cl.<sup>[10]</sup>



Scheme 6.5

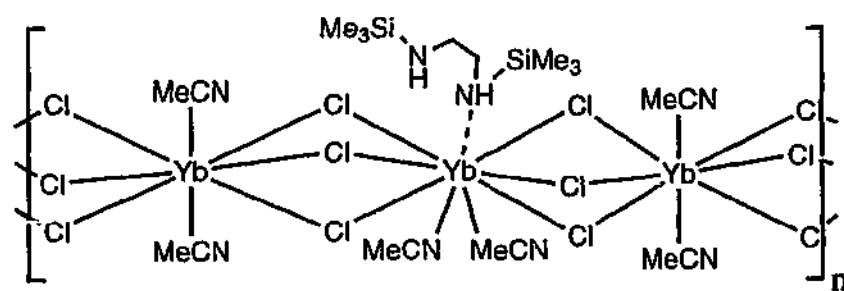
Analogous lanthanoid trihalide complexes undergoing thermal intramolecular rearrangement have not been reported. Throughout this thesis, the research is directed toward complexes with bidentate diorganoamide ligands. Consequently, a synthetic method involving reactions of ligands with a simple halide precursor may provide a straightforward route to the target molecules (*Scheme 6.4 giving (A)*). Hence the range of solvated lanthanoid trichloride complexes with bidentate diamines prepared above was investigated for possible thermal rearrangement giving  $\text{ClSiMe}_3$  and  $\text{HCl}$ . Decomposition was followed by the simultaneous TG/MS technique.

### 6.2.3.2 Characterisation

The compositions of the complexes  $\text{LnCl}_3(\text{MeCN})_x(\text{L}^1\text{H})_y$  (where  $\text{Ln} = \text{Yb}$ ,  $x = 2$ ,  $y = \frac{2}{3}$ ;  $\text{Ln} = \text{Sm}$ ,  $x = 0$ ,  $y = \frac{1}{2}$ ) and  $\text{LnCl}_3(\text{MeCN})_x(\text{C})_y$  (where  $\text{Ln} = \text{Yb}$ ,  $x = 2$ ,  $y = \frac{1}{2}$ ;  $\text{Ln} = \text{Sm}$ ,  $x = 0$ ,  $y = \frac{1}{3}$ ) were established by both lanthanoid and chloride analyses. The infrared spectra of these complexes show peaks attributable to the corresponding ligands. The key features of the spectra were broad  $\nu(\text{N-H})$  bands near  $3000 \text{ cm}^{-1}$ , as well as weaker  $\delta(\text{CH}_3)$  frequencies between  $1466\text{-}1401 \text{ cm}^{-1}$  (asymmetric deformation) and  $1255\text{-}1239 \text{ cm}^{-1}$  (symmetric deformation) owing to the  $\text{SiMe}_3$  groups. In the case of acetonitrile ligated ytterbium trichloride, vibrations associated with the  $\nu(\text{C-N})$  mode<sup>[50]</sup> were observed around  $2250 \text{ cm}^{-1}$ . Absorptions attributable to C-C-N bending<sup>[50]</sup> at approximately  $380 \text{ cm}^{-1}$  were not apparent in the far infrared spectra of these compounds. The far infrared

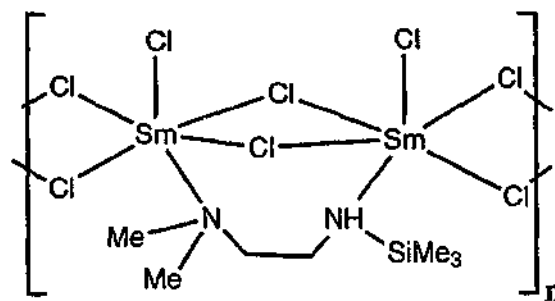
spectra of the lanthanoid trichloride amine complexes all have strong absorptions above  $230\text{ cm}^{-1}$  attributable to  $\nu(\text{Ln-Cl}_{(\text{br})})$  as reported for  $[\text{LnCl}_3(\text{THF})_2]_n$  complexes.[17] For  $\text{SmCl}_3(\text{L}^1\text{H})_{1/2}$  and  $\text{SmCl}_3(\text{C})_{1/3}$  complexes, absorptions between  $205 - 122\text{ cm}^{-1}$  can be assigned to  $\nu(\text{Sm-Cl}_{(\text{ter})})$ .

As single crystals of these diamine ligated complexes have proven elusive, definitive structural conclusions are not possible. It is impossible to speculate if the diamine ligands are coordinated directly to, or are a ligand of crystallisation about the lanthanoid centre. Comparing the infrared spectra of the free diamine ligands with their lanthanoid complexes did not provide conclusive evidence. Interestingly, for samarium the organoamine ligands were stronger donors than acetonitrile, by contrast with ytterbium. As far infrared data for the ytterbium complexes suggest that only bridging chlorides are present it may be similar to the polymeric array found for  $[\text{LaCl}_3(\text{THF})_2]_\infty$ [17] with the *cisoid* THF ligands replaced by acetonitrile molecules with the amine ligand weakly coordinated to the lanthanoid centre (*Figure 6.7 (a)*). However for  $\text{YbCl}_3(\text{MeCN})_2(\text{L})$  ( $\text{L} = (\text{L}^1\text{H})_{2/3}, \text{C}_{1/2}$ ) a higher coordination number of nine would result due to the chelation of the bidentate donor but this is consistent with MeCN (steric coordination number = 0.90) having lower steric demands than THF (steric coordination number = 1.21). For  $\text{SmCl}_3(\text{L})$  complexes ( $\text{L} = (\text{L}^1\text{H})_{1/2}$  and  $\text{C}_{1/3}$ ) both bridging and terminal chlorides are present, hence a variety of polymeric structures can be postulated (*Figure 6.7 (b)-(c)*) comprising two bridging chlorides and a terminal chloride per metal. Since the incorporation of acetonitrile was not detected, the diamine ligands are sufficient to break up the polymeric array of the anhydrous starting material in this case. The neutral diamine ligands can either bond directly (*Figure 6.7 (b)*), or coordinate weakly (*Figure 6.7 (c)*) to the metal centre shielding the complex from possible acetonitrile interaction.



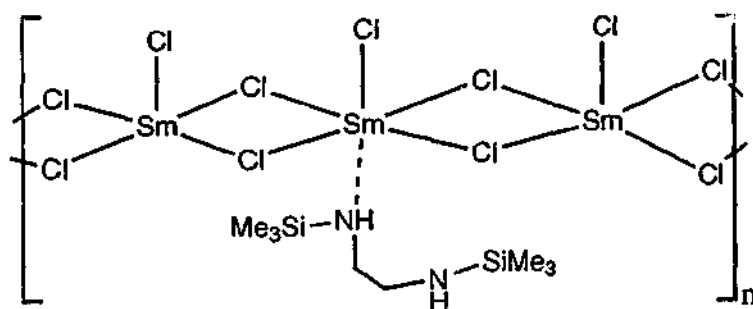
*Proposed structure of  $\text{YbCl}_3(\text{MeCN})_2(\text{C})_{1/3}$*

(a)



*Proposed structure of  $\text{SmCl}_3(\text{L}^1\text{H})_{1/2}$*

(b)



*Proposed structure of  $\text{SmCl}_3(\text{C})_{1/3}$*

(c)

**Figure 6.7**



### 6.2.3.3 Thermal Evaluation of $\text{LnCl}_3(\text{L})_x\text{L}'_y$ Complexes ( $\text{L} = \text{MeCN}$ , $\text{L}' = \text{chelating diamine}$ )

The ligated diamine lanthanoid trichlorides prepared above were heated to elevated temperatures under an inert atmosphere with mass loss and evolved gases monitored simultaneously by TGA/MS (Thermal Gravimetric Analysis/Mass Spectroscopy). The TGA results for the four complexes were extremely complex and difficult to interpret. In general, the thermal decomposition of the lanthanoid trichloride amine adducts did not occur in discrete steps but was nearly continuous until pure  $\text{LnCl}_3$  was formed around  $500^\circ\text{C}$ . Furthermore, the accompanying DSC data (which indicates exothermic or endothermic behaviour) showed that no clear decomposition steps occurred for these compounds (for example see *Figure 6.8*).

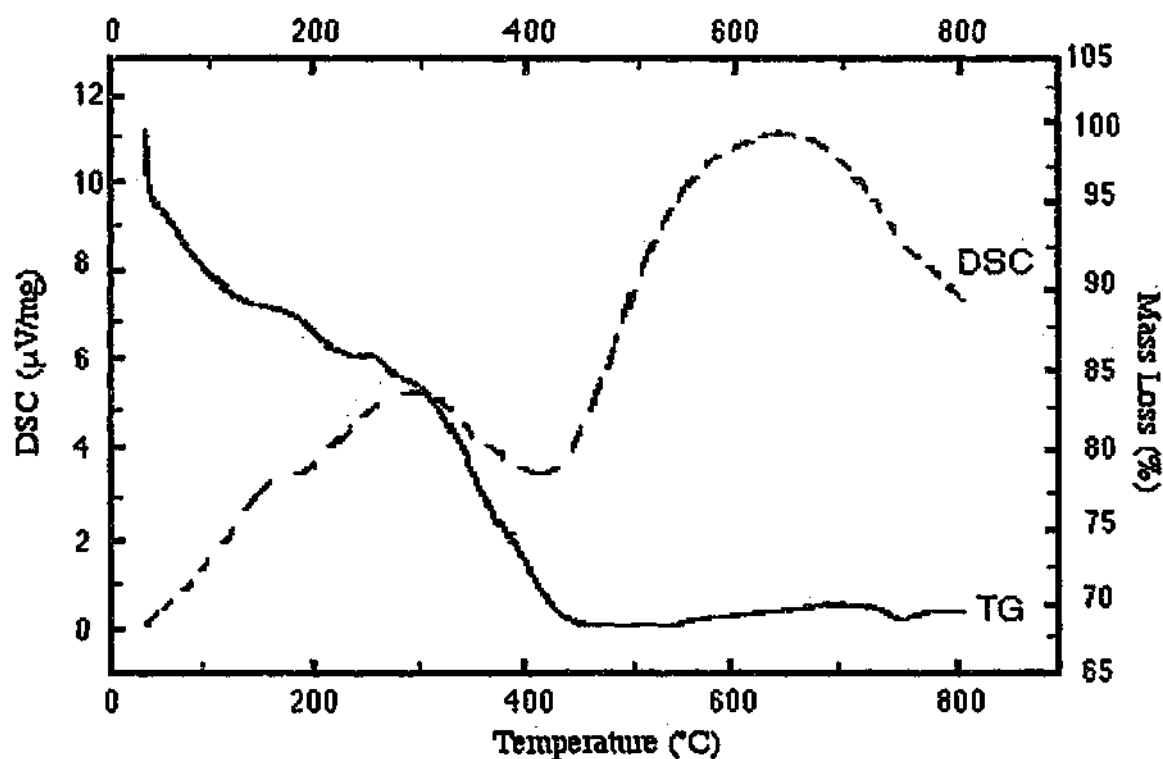


*Figure 6.8* TGA and DCS curves from the thermal decomposition of  $\text{YbCl}_3(\text{C})_{12}(\text{MeCN})_2$

Whilst the decomposition of all four compounds did not occur in discrete steps, the mass spectra indicate that the diamine ligands are dissociating from the metal but subsequently decompose before intramolecular rearrangement can take place (for decomposition fragments see *Table 6.7*). However in the case of  $\text{YbCl}_3(\text{MeCN})_2(\text{L}'\text{H})_{2/3}$  there was evidence of the elimination of  $\text{ClSiMe}_3$  in the mass spectrum confirming at least in principle that the target species may be formed under these conditions. In all cases, the

molecular fragment from the free diamine was detected, but no mass loss attributable to the clean formation of an amide (*Scheme 6.4 (A)*) was observed upon heating.

*Table 6.7 Results from simultaneous TG/MS of the gases released during the 'thermal decomposition' of the ligated amine lanthanoid trichloride complexes.*

Compound	$m/z$	Temp °C	Fragment
$[\text{LnCl}_3(\text{MeCN})_x(\text{L}^1\text{H})_y]$	58	120	$[\text{CH}_2\text{N}(\text{Me})_2]^+$
(Ln = Yb, $x = 2$ , $y = 2/3$ ;	73	205	$[\text{SiMe}_3]^+$
Ln = Sm, $x = 0$ , $y = 1/2$ )	102 (Yb only)	195	$[\text{SiMe}_3\text{NHCH}_2]^+$
	108 (Yb only)	250	$[\text{SiMe}_3\text{Cl}]^+$
<hr/>			
$[\text{LnCl}_3(\text{MeCN})_x(\text{C})_y]$	102	195	$[\text{Me}_3\text{SiNHCH}_2]^+$
(Ln = Yb, $x = 2$ , $y = 1/2$ ;	73	205	$[\text{SiMe}_3]^+$
Ln = Sm, $x = 0$ , $y = 1/2$ )			

Since fractional quantities of diamines are present in these complexes, it is impossible to speculate whether a higher ligand to  $\text{LnCl}_3$  ratio will give the same result. This study was hindered by the unsuccessful preparation of stoichiometric diamine ligated  $\text{LnCl}_3$  complexes, however it provided a qualitative examination of decomposition pathways of lanthanoid trichloride diamine adducts.

### 6.3 Conclusions

A new approach was successfully used to prepare a number of  $[\text{LnCl}_3(\text{DME})_n]$  ( $\text{Ln} = \text{La}$ ,  $n = 1$ ;  $\text{Ln} = \text{Nd}$ ,  $\text{Yb}$ ,  $n = 2$ ) complexes by treating lanthanoid metals with hexachloroethane in DME. These lanthanoid complexes were fully characterised to explore whether a transition point of structural change exists within the series. Surprisingly, unlike the several transition points that occur in analogous tetrahydrofuran complexes, the dimethoxyethane complexes have the general formula  $[\text{LnCl}_3(\text{DME})_2]$  except for  $[\text{LaCl}_3(\text{DME})]_\infty$ . X-ray crystallographically suitable single crystals were isolated for  $[\text{YbCl}_3(\text{DME})_2]$  which was found to be isostructural with the other members of the series. Evidence that  $[\text{LaCl}_3(\text{DME})]_\infty$  is an 8-coordinate polymer was obtained from far infrared spectroscopy.

The formation of lanthanoid tribromide ether adducts can be achieved using 1,2-dibromoethane as the reagent with ytterbium metal in ether solvents in good yields. The complexes,  $[\text{YbBr}_3(\text{THF})_3]$  and  $[\text{YbBr}_3(\text{DME})_2]$  are the first reported ether-ligated tribromide compounds and were prepared along with  $[\text{LaBr}_2(\mu\text{-Br})(\text{DME})]_2$  and  $[\text{LaBr}_2(\text{diglyme})_2][\text{LaBr}_4(\text{diglyme})]$  obtained by another co-worker.<sup>[24]</sup> Structure determination of  $[\text{YbBr}_3(\text{THF})_3]$  and  $[\text{YbBr}_3(\text{DME})_2]$  revealed that they were similar to the corresponding ytterbium trichloride adducts.

Lanthanoid trichloride amine adducts,  $\text{LnCl}_3(\text{MeCN})_x(\text{L}^1\text{H})_y$  (where  $\text{Ln} = \text{Yb}$ ,  $x = 2$ ,  $y = 2/3$ ;  $\text{Ln} = \text{Sm}$ ,  $x = 0$ ,  $y = 1/2$ ) and  $\text{LnCl}_3(\text{MeCN})_x(\text{C})_y$  (where  $\text{Ln} = \text{Yb}$ ,  $x = 2$ ,  $y = 1/2$ ;  $\text{Ln} = \text{Sm}$ ,  $x = 0$ ,  $y = 1/3$ ), were prepared by refluxing anhydrous  $\text{LnCl}_3$  in acetonitrile with excess diamine. Surprisingly, no coordinated acetonitrile was present for the samarium adducts unlike the ytterbium complexes. The thermal decomposition of these complexes did not occur in discrete steps, but in the case of  $\text{YbCl}_3(\text{MeCN})_2(\text{L}^1\text{H})_{2/3}$  there was evidence of the elimination of  $\text{ClSiMe}_3$  in the mass spectrum confirming in principle that intramolecular rearrangement is possible within this system. Further work is necessary to synthesize amine compounds with a higher mole ratio of ligand to  $\text{LnCl}_3$  so that thermal decomposition can be explored more satisfactorily.

## 6.4 References

- 1 H. Schumann and W. Genthe, *Organometallic Compounds of the Rare Earths*, in *Handbook on the Physics and Chemistry of Rare Earths*, eds. K. A. Gshneidner and L. Eyring, Elsevier, Amsterdam, 1984, vol. 7, ch. 53.
- 2 F. A. Hart, in *Comprehensive Organometallic Chemistry*, eds. G. A. Wilkinson, R. D. Gillard, and J. A. McLeverly, Pergamon, Oxford, 1987, vol. 3, ch. 39.
- 3 R. C. Mehrotra, A. Singh, and U. M. Tripathi, *Chem. Rev.*, 1991, **91**, 1287.
- 4 R. Anwander, *Top. Curr. Chem.*, 1996, **179**, 33.
- 5 D. C. Bradley, R. C. Mehrotra, I. P. Rothwell, and A. Singh, *Alkoxo and Aryloxo Derivatives of Metals*, Academic Press, London, 2001.
- 6 G. A. Molander, *Chem. Rev.*, 1992, **92**, 29.
- 7 G. A. Molander and C. R. Harris, *Chem. Rev.*, 1996, **96**, 307.
- 8 J. M. Haschke, *Halides*, in *Handbook on the Physics and chemistry of Rare Earths*, eds. K. A. Gshneidner and L. Eyring, Elsevier, North-Holland, Amsterdam, 1979, vol 4, ch. 32.
- 9 H. A. Eick, *Lanthanide and Actinide Halides*, in *Handbook on the Physics and Chemistry of Rare Earths*, eds. K. A. Gshneidner, L. Eyring, G. R. Choppin, and G. H. Lander, Elsevier, North-Holland, Amsterdam 1994, vol. 18, ch. 124, p. 365.
- 10 G. Meyer, *The Ammonium Ion for Inorganic Synthesis*, in *Advances in the Synthesis and Reactivity of Solids*, 1994, vol. 2, p. 1.
- 11 M. D. Taylor and C. P. Carter, *J. Inorg. Nucl. Chem.*, 1962, **24**, 387.
- 12 J. D. Corbett, *Inorg. Synth.*, 1983, **22**, 39.
- 13 K. Rossmannith and C. Auer-Welsbach, *Mh. Chem.*, 1965, **96**, 602.
- 14 G. B. Deacon and A. J. Koplick, *Inorg. Nucl. Chem. Lett.*, 1979, **15**, 263.
- 15 G. B. Deacon, T. D. Tuong, and D. L. Wilkinson, *Inorg. Synth.*, 1990, **27**, 136.
- 16 G. B. Deacon, T. D. Tuong, and D. L. Wilkinson, *Inorg. Synth.*, 1990, **8**, 86.
- 17 G. B. Deacon, T. Feng, P. C. Junk, B. W. Skelton, A. N. Sobolev, and A. H. White, *Aust. J. Chem.*, 1998, **51**, 75.
- 18 G. B. Deacon, T. Feng, S. Nickel, B. W. Skelton, and A. H. White, *J. Chem. Soc., Chem. Comm.*, 1993, 1328.

- 19 S.-H. Wu, Z.-B. Ding, and X.-J. Li, *Polyhedron*, 1994, **13**, 2679.
- 20 S. Petricek, A. Demsar, and L. Golic, *Polyhedron*, 1999, **18**, 529.
- 21 D. Belli Dell'Amico, F. Calderazzo, C. della Porta, A. Merigo, P. Biagini, G. Lugli, and T. Wagner, *Inorg. Chim. Acta*, 1995, **240**, 1.
- 22 L. E. Depero, M. T. Arienti, M. Zocchi, and M. C. Gallazzi, *Inorg. Chem.*, 1991, **2**, 595.
- 23 D. M. Barnhart, T. M. Frankcom, P. L. Gordon, N. N. Sauer, J. A. Thompson, and J. G. Watkins, *Inorg. Chem.*, 1995, **34**, 4862.
- 24 G. B. Deacon, T. Feng, P. C. Junk, G. Meyer, N. M. Scott, B. W. Skelton, and A. H. White, *Aust. J. Chem.*, 2000, **53**, 853.
- 25 J. L. Namy, P. Girard, and H. B. Kagan, *Nouveau J. De Chimie*, 1981, **5**, 479.
- 26 C. J. Kepert, B. W. Skelton, and A. H. White, *Aust. J. Chem.*, 1994, **47**, 385.
- 27 W. J. Evans, J. L. Shreeve, J. W. Ziller, and R. J. Doedens, *Inorg. Chem.*, 1995, **34**, 576.
- 28 G. R. Willey, T. J. Woodman, and M. G. B. Drew, *Polyhedron*, 1997, **16**, 3385.
- 29 P. Sobota, J. Utko, and S. Szafert, *Inorg. Chem.*, 1994, **33**, 5203.
- 30 C. Wenqi, X. Y. Zhongsheng, F. Yuguo, and Y. Guangdi, *Inorg. Chim. Acta*, 1987, **130**, 125.
- 31 S.-H. Lin, Z.-C. Dong, J.-S. Huang, Q.-F. Zhang, and J.-X. Lu, *Acta Cryst.*, 1991, **C47**, 426.
- 32 G.-Y. Lin, G.-C. Wei, Z.-S. Jin, and W.-Q. Chen, *Jiegou Huaxua (J. Struct. Chem.)*, 1992, **11**, 200.
- 33 G. B. Deacon, G. D. Fallon, C. M. Forsyth, H. Schumann, and R. Weimann, *Chem. Ber.*, 1997, **130**, 409.
- 34 G. R. Willey, P. R. Meehan, T. J. Woodman, and M. G. B. Drew, *Polyhedron*, 1997, **16**, 623.
- 35 S. Anfang, K. Dehnicke, and J. Magull, *Z. Naturforsch.*, 1996, **51b**, 531.
- 36 Z.-W. Xie, C.-T. Qian, Z.-S. Jin, and W.-Q. Chen, *Jiegou Huaxua (J. Struct. Chem.)*, 1993, **12**, 107.
- 37 J. L. Atwood and K. D. Smith, *J. Chem. Soc., Dalton Trans.*, 1974, 921.

- 38 G. K.-I. Magomedov, A. Z. Voskoboinikov, N. I. Kirillova, A. I. Gusev, I. N. Parshina, and I. P. Beletskaya, *Metallorg. Khim. (Organomet. Chem. USSR)*, 1992, **5**, 679.
- 39 W. J. Evans, T. J. Boyle, and J. W. Ziller, *J. Am. Chem. Soc.*, 1993, **115**, 5084.
- 40 W. Gecheng, G. Hanrong, and J. Zhongsheng, *Jiegou Hauxue (J. Struct. Chem.)*, 1989, **8**, 61.
- 41 S. Anfang, M. Karl, N. Faza, W. Massa, J. Magull, and K. Dehnicke, *Z. Anorg. Allg. Chem.*, 1997, **623**, 1425.
- 42 T. D. Tilley, A. Zalkin, R. A. Anderson, and D. H. Templeton, *Inorg. Chem.*, 1981, **20**, 551.
- 43 J. Marcalo and A. P. De Matos, *Polyhedron*, 1989, **8**, 2431.
- 44 A. A. Trifonov, P. Van der Weghe, J. Collin, A. Domingos, and I. Santos, *J. Organomet. Chem.*, 1997, **527**, 225.
- 45 R. D. Shannon, *Acta. Crystallogr., Sect. A*, 1976, **32**, 751.
- 46 Z. Xie, K.-Y. Chui, B. Wu, and T. C. W. Mak, *Inorg. Chem.*, 1996, **35**, 5957.
- 47 M. Allen, H. C. Aspinall, S. R. Moore, M. B. Hursthouse, and A. I. Karvalov, *Polyhedron*, 1992, **11**, 409.
- 48 H. C. Aspinall, S. R. Moore, and A. K. Smith, *J. Chem. Soc., Dalton Trans.*, 1992, 153.
- 49 J. H. Forsberg and T. Moeller, *Inorg. Chem.*, 1969, **8**, 883.
- 50 R. A. Walton, *Q. Rev., Chem. Soc.*, 1965, **19**, 126.

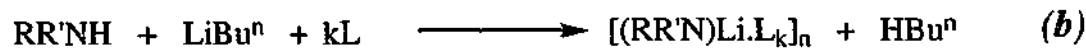
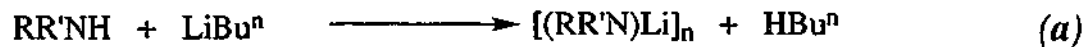
## Chapter 7

# Diorganoamidolithium Complexes - Preparation, Properties and Crystal Structures

### 7.1 Introduction

The present interest in the structural architecture of lithium amide complexes is in response to the need to understand these important ligand transfer reagents for metathesis reactions in lanthanoid chemistry. They are also used in the preparation of organoamidometallic compounds of other elements and have the ability to act as selective bases in organic synthesis. Lithium amide complexes have been shown to exhibit fascinating structures in the solid state that range from monomeric to polymeric species,<sup>[1, 2]</sup> and their reactivity is related to the degree of association and solvation. Knowledge of their structures is vital in understanding their subsequent chemistry.

The preparation of lithium amide complexes often involves strongly basic alkyl lithium reagents such as  $\text{LiBu}^n$ , which remove weakly acidic protons of organoamines. These reactions can be performed in the presence (*Equation 7.1 (a)*) or absence (*Equation 7.1 (b)*) of a Lewis base solvent.



R,R' = alkyl, aryl, H

L = Lewis base

k = number of Lewis donor atoms

*Equation 7.1*

Primarily, the architecture of all organolithium derivatives is determined by the need of the polar  $\text{Li}^+$  cations to attract as many negative centres (anions) or poles (polar ligands) as possible.<sup>[1]</sup> Commonly, lithium has a coordination number of four within a tetrahedral (or pseudo tetrahedral) environment, but lower coordination numbers of 2 or 3 can be achieved with bulkier ligands.<sup>[2]</sup> Rather than the need to satisfy the 'octet rule' by involving the four  $sp^3$  bonding orbitals of lithium, electrostatic forces dictate bonding, thereby ensuring the maximum number of metal-ligand contacts.<sup>[1, 2]</sup> However steric factors such as van der Waals repulsions between ligands compete and as a consequence limit the number of these interactions, especially given the small size of  $\text{Li}^+$ . For this reason, bulky ligands form lithium complexes of lower coordination numbers, whereas less sterically demanding groups can give complexes of higher coordination number. The structural nature of a selection of lithium amide complexes is discussed below in three sections. The first two focus on lithium compounds of monodentate amide ligands either in *non-polar* (section 7.1.1) or *polar* (section 7.1.2) solvents. The third examines some multidentate amide ligands in both solvent environments.

### 7.1.1 Uncomplexed Lithium Amides ( $\text{RR}'\text{NLi}$ )<sub>n</sub>

The chemistry of unsolvated lithium amides is dictated by the formation of the maximum number of nitrogen-lithium contacts. This is often gained laterally with the formation of a ring-ladder structure (*Figure 7.1*).<sup>[1, 3]</sup> Vertical association is prevented due to the  $\text{RR}'$  groups adequately projecting above and below the  $(\text{NLi})_n$  ring plane as a result of the distorted tetrahedral geometry at the  $sp^3$  hybridized N centre.<sup>[1]</sup> The most favoured arrangement of unsolvated lithium amides involves polymeric ladder structures of infinite arrays (see *Figure 7.1*). These complexes are amorphous, exhibit high melting points ( $>250^\circ\text{C}$ ) and have low solubility in hydrocarbon solvents.<sup>[4]</sup>



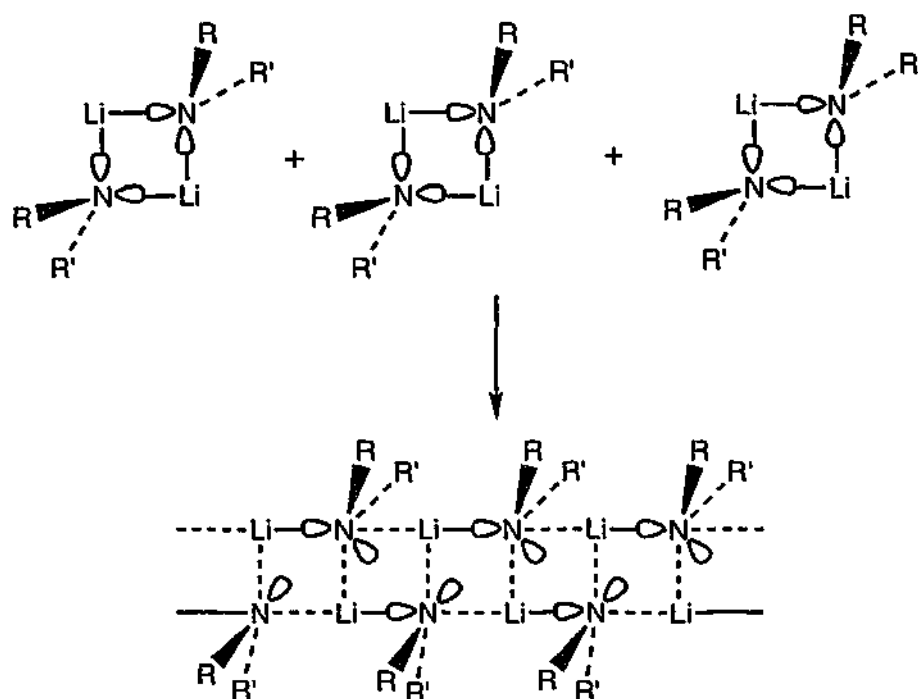


Figure 7.1

Smaller polymeric arrays, or oligomers, have less amorphous behaviour and as a result more crystallographic information is known for them. Most of these arrays contain a planar  $(\text{NLi})_n$  ring arrangement with the exception of  $[\text{LiN}((\text{CH}_2)_5\text{CH}_2)]_6$  [5, 6] which consists of three  $(\text{NLi}_2)$  units joined in a cyclic ladder. This arrangement is sterically prevented in most of the other cases. By increasing the size of the  $\text{RR}'$  groups on the nitrogen atom, the space surrounding the  $(\text{NLi})_n$  rings is decreased. For this reason, the aggregation size is largely dependent on the size of the R groups. For example, in  $[\text{Li}\{\text{NCMe}_2(\text{CH}_2)_3\text{CMe}_2\}]_4$  [7] the ligand-ligand repulsions from the large tetramethylpiperidinato anion gives rise to the formation of one of only two known tetrameric lithium amide complexes. The other tetranuclear species,  $[\text{Li}\{\text{N}(\text{SiMe}_3)(\text{Ph})\}]_4$ , recently reported by Lappert *et al.* [8] consists of four lithium atoms arranged in a stair-like fashion (see *Figure 7.2 (a)*). The more common trimeric arrangement can be achieved using sterically demanding amides such as  $[\text{Li}\{\text{N}(\text{SiMe}_3)_2\}]_3$  [9, 10]  $[\text{Li}\{\text{N}(\text{PhCH}_2)_2\}]_3$  [11] and  $[\text{Li}\{\text{N}(\text{GeMe}_3)_2\}]_3$  [12]. The complex  $[\text{Li}\{\text{N}(\text{SiMe}_3)_2\}]_3$  was the first structurally characterised substituted lithium amide. The molecular structure of  $[\text{Li}\{\text{N}(\text{PhCH}_2)_2\}]_3$  [11] (*Figure 7.2(b)*) has a planar ring arrangement of three lithium and three nitrogen centres. Each lithium atom has a primary coordination number of two that is stabilised through additional interactions from the aryl and methyl groups.

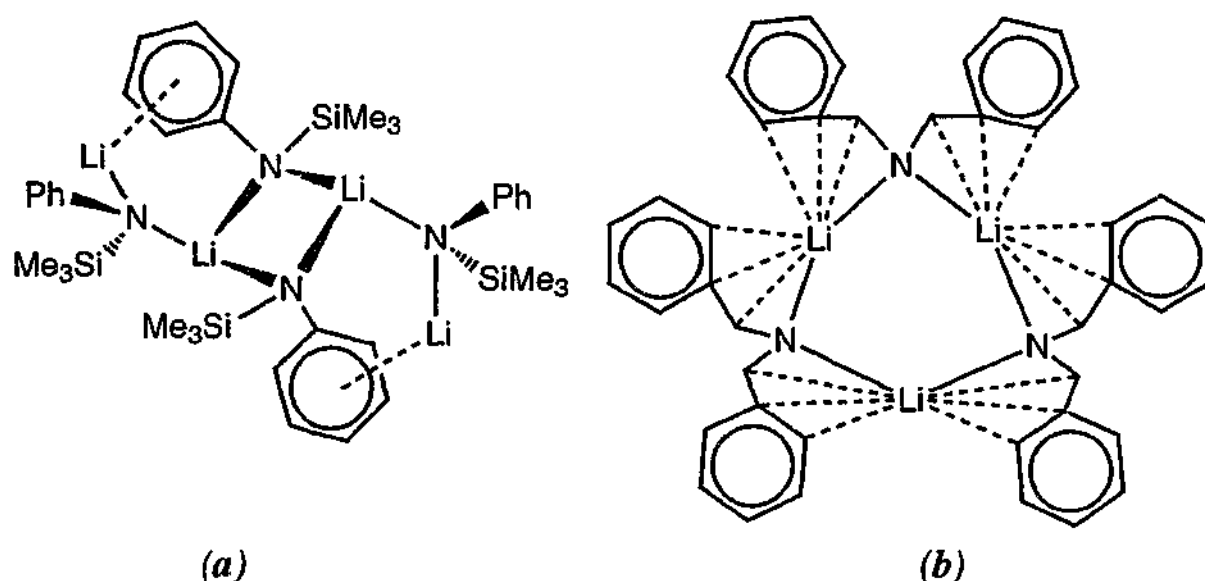


Figure 7.2

Whilst an electron diffraction study of  $[\text{Li}\{\text{N}(\text{SiMe}_3)_2\}]_3$  detected the presence of a dimeric species in the gas phase,<sup>[13]</sup> monomeric and dimeric forms of unsolvated lithium amides complexes were thought to be too unstable to exist in the solid state.<sup>[1, 13]</sup> Since then, there have been two dinuclear complexes reported. The complexes,  $[\text{Li}\{\text{N}(\text{SiMe}_3)(2,6\text{-}(\text{Pr}^i)_2\text{C}_6\text{H}_3)\}]_2$ <sup>[14]</sup> and  $[\text{Li}\{\text{N}(\text{SiMe}_3)(\text{SiMe}_2\text{Ph})\}]_2$  (Figure 7.3),<sup>[8]</sup> have a  $(\text{LiN})_2$  ring with the two-coordinate central Li atom supported by additional interactions with the *ipso*-carbons.

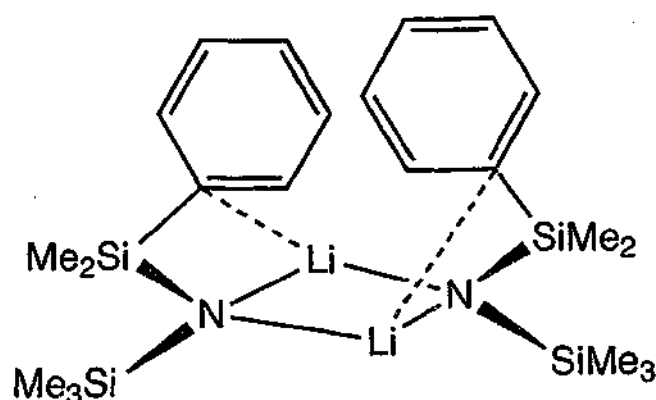


Figure 7.3

As most unsolvated lithium amides have low solubility in non-coordinating solvents, solution studies of such are rare. However, for  $[\text{Li}\{\text{N}(\text{CH}_2\text{Ph})_2\}]_3$ <sup>[11]</sup> which readily dissolves in arene solvents, NMR and cryoscopic measurements were obtained. These data suggest that an equilibrium between the trimeric and monomeric structures

exists in solution.[15] Presumably, the formerly one-coordinate Li centre in the latter is stabilised by additional aryl-interactions either from the solvent or from the amide ligand. De-aggregation in solution has also been reported for the tetranuclear complex,  $[\text{Li}\{\text{N}(\text{SiMe}_3)(\text{Ph})\}]_4$ . [16]

### 7.1.2 Complexed Lithium Amides $[\text{RR}'\text{NLi}(\text{L})_2]_n$

The breakdown of polymeric ladders into smaller subunits can be achieved by using coordinating solvents such as *N,N,N',N'*-tetramethylethylenediamine (TMEDA) and  $\text{Et}_2\text{O}$ . The solvent molecules coordinate to the lithium centre affording compounds of low aggregation states that have a higher solubility and hence greater reactivities. The availability of Lewis donor sites determines the extent of deaggregation of the unsolvated lithium species.[3] Where there are insufficient donors to completely saturate the lithium centres, a limited ladder structure may be formed. For example, the addition of TMEDA to the parent compound  $[\text{LiN}\{(\text{CH}_2)_3\text{CH}_2\}]_n$  yields the crystalline complex,  $[\text{LiN}\{(\text{CH}_2)_3\text{CH}_2\}(\text{TMEDA})]_2$  in which a four (N—Li) rung ladder results (*Figure 7.4*).

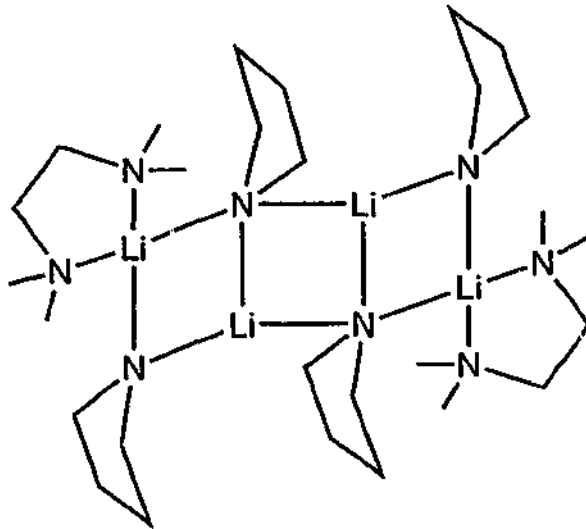


*Figure 7.4*

In the case of a 1:1 ratio of solvent molecules to lithium centres, a dimeric  $(\text{NLi})_2$  ring species commonly results,[1] e.g.  $[\text{Li}\{\text{N}(\text{SiMe}_3)_2\}]_3$ [9, 10] in the presence of monodentate coordinating solvents, such as THF[17] and  $\text{Et}_2\text{O}$ [7, 18] (*Figure 7.5*). In a similar manner, the addition of polar solvents to  $[\text{Li}\{\text{N}(\text{CH}_2\text{Ph})_2\}]_3$  results in a dimeric

species of the type  $[\text{Li}\{\text{N}(\text{CH}_2\text{Ph})_2\}_2\text{L}]_2$  ( $\text{L} = \text{THF}, \text{Et}_2\text{O}$  and hexamethylphosphoramide (HMPA)[11, 15]). Additional  $\pi$ -arene—Li interactions help stabilise the Li centre.

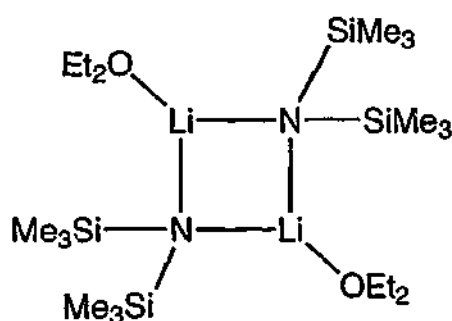


Figure 7.5

The use of the bidentate donor TMEDA can also give dimeric complexes, for example  $[\text{Li}\{\text{N}(\text{Ph})(\text{Me})\}(\text{TMEDA})]_2$ [19] and  $[\text{Li}\{\text{N}(\text{SiMe}_3)_2\}(\text{TMEDA})]_2$ [20] but in these each lithium atom is four-coordinate, although for the latter complex a three-coordinate monomer can also result.[20] The formation of monomeric lithium amide complexes often requires polydentate donors, such as *N,N,N',N',N''*-pentamethylethylenetriamine (PMDETA). As this ligand contains multiple donor sites that are capable of coordinating to lithium they stabilise the monomeric metal centre as seen in four-coordinate  $[\text{Li}\{\text{N}(\text{SiMe}_3)_2\}(\text{PMDETA})]$ [21]. In four-coordinate  $[\text{Li}\{\text{N}(\text{Ph})(\text{naphthyl})\}(\text{PMDETA})]$ [19] the tridentate donor prevents further dimerisation despite the R groups on the amide nitrogen being flat and free to rotate about the C—N bond (Figure 7.6 (a)). However, in the TMEDA analogue  $[\text{Li}\{\text{N}(\text{Ph})(\text{naphthyl})\}(\text{TMEDA})]$ [22] the coordination number of lithium is reduced to three and the structure displays features between that of a monomer and a dimer by forming 'slipped' vertical pairs (see Figure 7.6 (b)).

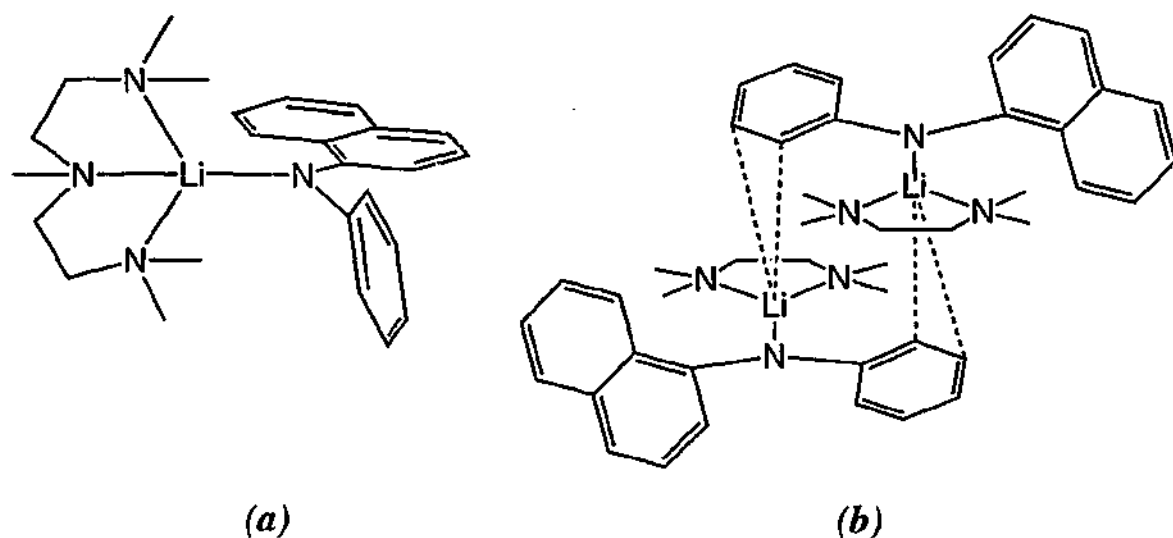


Figure 7.6

The tetradentate donor 12-crown-4 results in an unusual lithium amide complex,  $[\text{Li}(12\text{-crown-4})\{\text{N}(\text{SiMe}_3)_2\}]$  which contains a five-coordinate lithium atom (Figure 7.7).

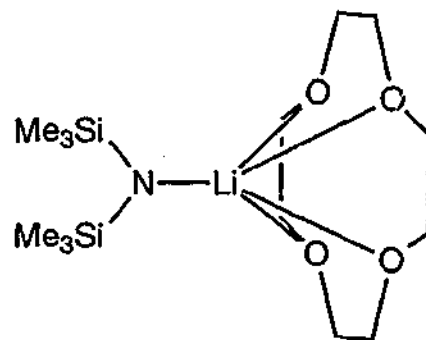
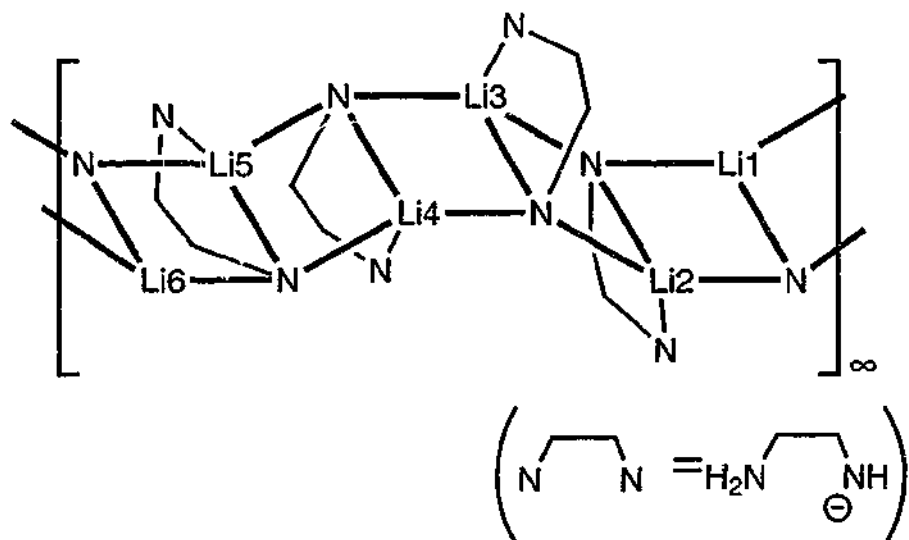


Figure 7.7

Due to the higher solubility of solvated dimeric lithium amide species in non-coordinating solvents, extensive investigations in solution have been undertaken.<sup>[1]</sup> In this state, the lithium amide complexes often display different features from those of the solid state structures. On dissolution of the solid state dimer  $[\text{Li}\{\text{N}(\text{CH}_2\text{Ph})_2\}(\text{OEt}_2)]_2$ <sup>[11]</sup> in arene solvents, two species were observed. The dimer undergoes cleavage of the  $\text{Li}-\text{OEt}_2$  bond and gives trimeric and monomeric units which were previously observed for unsolvated  $[\text{Li}\{\text{N}(\text{CH}_2\text{Ph})_2\}]_3$  (see section 7.1.1). However, the NMR spectra of  $[\text{Li}\{\text{NR}(\text{Ph})\}(\text{OEt}_2)]_2$  ( $\text{R} = \text{SiMe}_3$  or  $\text{CH}_2\text{Bu}^t$ )<sup>[16]</sup> in arene solutions at ambient temperature show only one lithium environment. Presumably the symmetrical dimer is present.

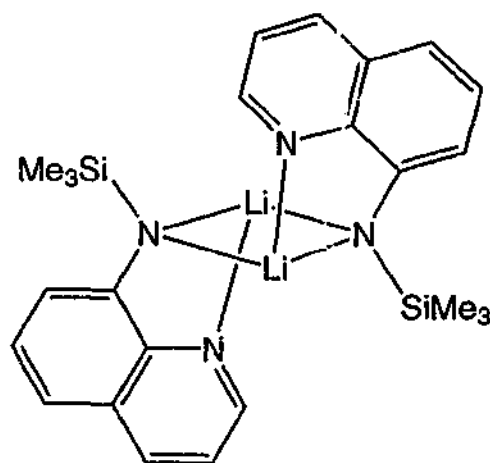
### 7.1.3 Lithium Complexes Containing Multidentate Amide Ligands

The size and shape of the amide group can be further altered by the addition of a pendant donor(s) to form a multidentate ligand. In the absence of a neutral donor a polymeric species can be formed as seen in the complex  $[\text{Li}\{(\text{H})\text{NCH}_2\text{CH}_2\text{NH}_2\}]_\infty$ ,<sup>[4]</sup> which was the first polymeric lithium amide to be identified crystallographically (*Figure 7.8*). It established continual 'S' shaped  $(\text{LiN})_\infty$  ladders in lithium amide chemistry.



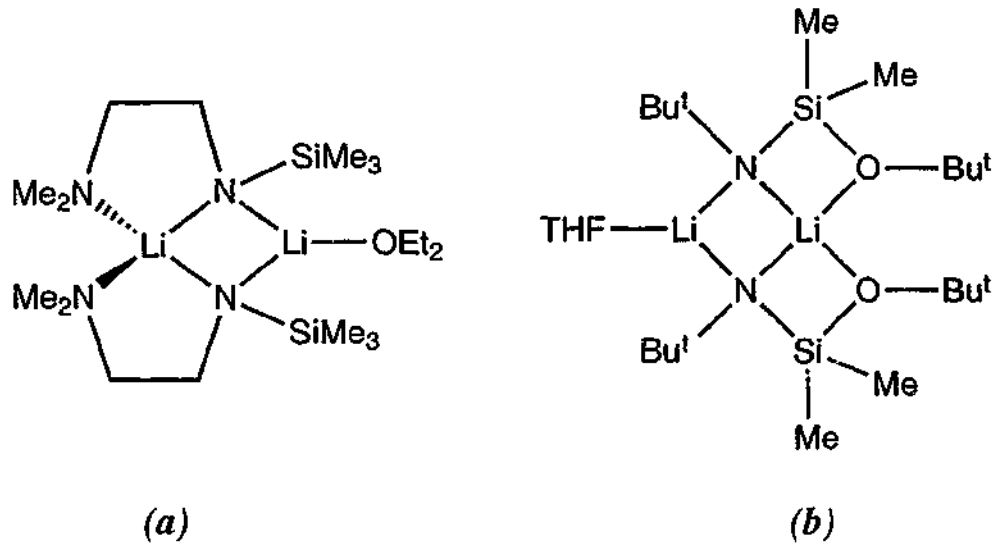
*Figure 7.8*

For the bulkier 8-trimethylsilylaminoquinoline (*qsta*) a dimeric species,  $[\text{Li}(\text{qsta})]_2$  (*Figure 7.9*), in which each lithium atom is three-coordinate,<sup>[23]</sup> is observed.



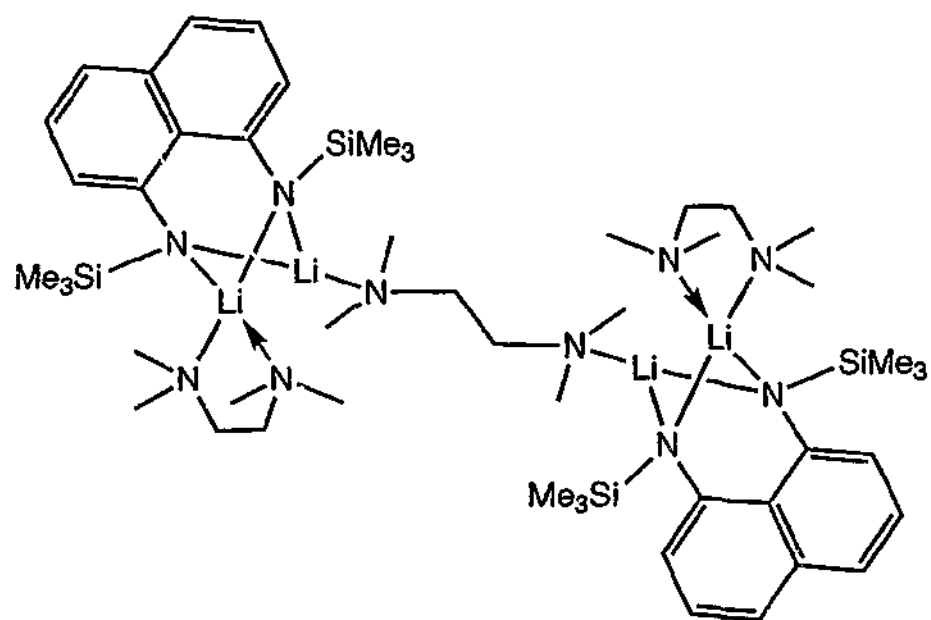
*Figure 7.9*

As seen for complexes of monodentate amides, the presence of coordinating solvents with multidentate lithium amides influences the observed structural type. For example, when  $[\text{Li}(\text{qsta})]_2$  is in the presence of  $\text{Et}_2\text{O}$  a symmetrical dimer results with each lithium atom being four-coordinate.[23] The deprotonation of  $\text{L}^1\text{H}$  ( $\text{L}^1\text{H} = N,N$ -dimethyl- $N'$ -trimethylsilylethane-1,2-diamine) with  $\text{LiBu}^n$  in  $\text{Et}_2\text{O}$  results in a discrete dinuclear complex with two different lithium centres (*Figure 7.10 (a)*).[24] A similar lithium arrangement in the solid state has also been observed for  $[\text{Li}\{\text{Bu}^n\text{NSiOMe}_2\text{O}(\text{Bu}^n)\}_2\text{Li}(\text{THF})]$ ,[25] where a central four-membered  $(\text{LiN})_2$  ring is supported by two Li-N-Si-O rings resulting from the chelating ligand (*Figure 7.10 (b)*). The outlying lithium atom is three-coordinate including a molecule of THF, whereas the central lithium is four-coordinate. The formation of these unsymmetrical lithium complexes presumably arises from the steric demands of the chelating amide ligands.



*Figure 7.10*

The addition of bulkier ligands, such as TMEDA, can result in the formation of monomeric complexes, as seen for  $[\text{Li}(\text{qsta})(\text{TMEDA})]$ . [23] In this case the TMEDA acts as a bidentate ligand resulting in a four-coordinate lithium centre. This neutral ligand can also coordinate in a monodentate mode as exemplified by a recent structure in which the TMEDA bridges two lithium aggregates (*Figure 7.11*). [16]

*Figure 7.11*

NMR data obtained for the dinuclear species  $[\text{Li}(\text{L}^1)_2\text{Li}(\text{OEt}_2)]$ <sup>[24]</sup> in solution shows only one  $^7\text{Li}$  environment, even at low temperature. As the solid state structure of  $[\text{Li}(\text{L}^1)_2\text{Li}(\text{OEt}_2)]$  shows two different lithium environments, the NMR data presumably indicate a rapidly exchanging species.



### 7.1.4 Current Study

Due to the large number of variables ranging from the size of the incoming amide group to competition from the coordinating solvent, lithium chemistry is an expanding field. The above review provides a background into the general principles of amidolithium chemistry with a focus on the structural variety of both solvated and unsolvated lithium amide species.<sup>[1, 2]</sup> In this chapter the synthesis and crystallisation of lithium compounds of  $L^2$  and  $L^3$  is examined. The necessity of identifying these lithium complexes in the solid state arises from the need to obtain greater stoichiometric control, as well as an understanding of the functionalisation in subsequent reactions with lanthanoid metal salts.

During the course of this research an interesting reaction between the  $LiL^3$  and the highly reactive  $LiBu^n$  was found. Under certain reaction conditions, metallation of the phenoxy substituent at the *o*-carbon site gives  $N(SiMe_3)(2-C_6H_4(2'-C_6H_4O)) (L^*)$  (Figure 7.12).

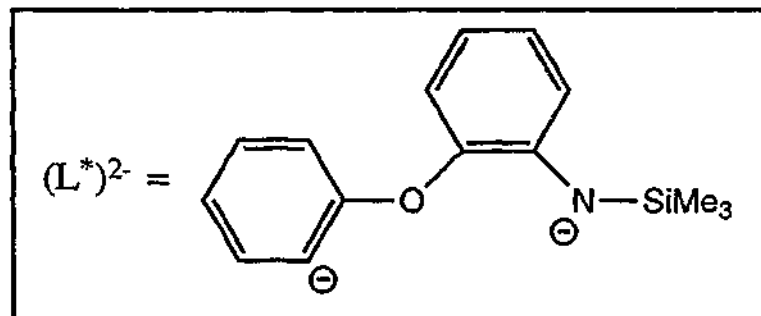
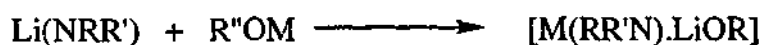


Figure 7.12

Whilst the metallation of 'activated' arenes has previously been observed<sup>[26]</sup> the behaviour of  $L^*$  in sequestering small anions (e.g.  $Bu^n$ ,  $EtO^-$ ) resulting in the self-assembly of lithium aggregates in the solid state was unexpected. The multifunctionalised lithium species are also significant in relation to the 'superbase' phenomenon when mixed anions are present.<sup>[27]</sup> It has been shown that the addition of lithium amides ( $RR'NLi$ ) to metal alkoxides ( $M = Na$  or  $K$ ) (Equation 7.2) results in superbase aggregates having a dramatically enhanced selectivity and deprotonating ability that can be harnessed in organic synthesis.



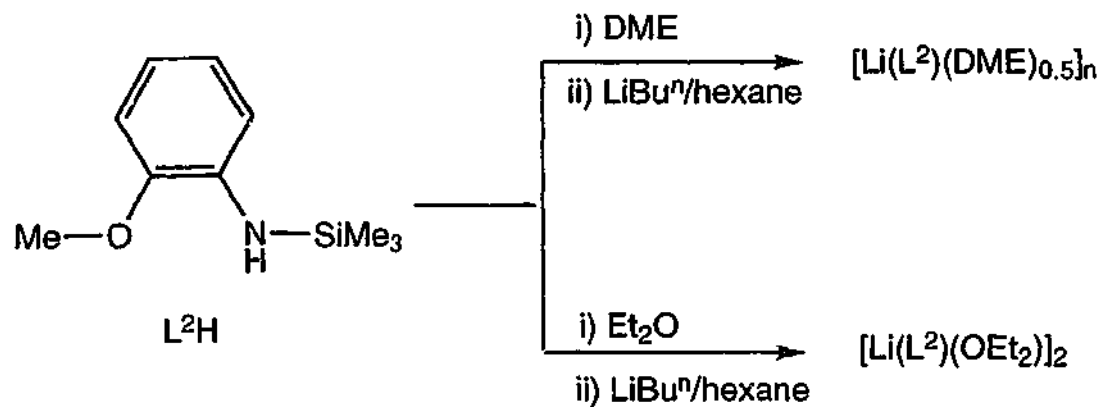
Equation 7.2

One of the aggregates to be described below contains *three* superbase anions and is unique with alkoxy, aryl and organoamide ligation in a single complex.<sup>[27]</sup>

## 7.2 Results and Discussion

### 7.2.1 Reaction of $L^2H$ with $LiBu^n$

The lithiation of  $L^2H$  with one equivalent of *n*-butyllithium at 0°C in DME or  $Et_2O$  affords a white precipitate of  $[Li(L^2)(DME)_{0.5}]_n$  or  $[Li(L^2)_2(OEt_2)]_2$ , respectively (Scheme 7.1).



Scheme 7.1

The composition of  $[Li(L^2)(DME)_{0.5}]_n$  was determined from elemental analysis (C, H, N). Satisfactory elemental analyses, despite numerous attempts, could not be obtained for  $[Li(L^2)_2(OEt_2)]_2$  due to the light-sensitivity of the bulk product however  $^1H$  NMR spectra of  $[Li(L^2)(DME)_{0.5}]_n$  and  $[Li(L^2)_2(OEt_2)]_2$  established the  $L^2:S_x$  ( $S = DME, x = 0.5$ ;  $Et_2O, x = 1$ ) ratios. Their IR spectra contained absorptions typical of either coordinated DME or  $Et_2O$  molecules and of the  $L^2$  ligand. No  $\nu(N-H)$  band attributable to  $L^2H$  ( $3401\text{ cm}^{-1}$ ) was observed. The  $^1H$  NMR spectra of  $[Li(L^2)(DME)_{0.5}]_n$  (in  $C_6D_6$ ) and  $[Li(L^2)_2(OEt_2)]_2$  ( $C_7D_8$ ) have a single methoxy ether peak as well as characteristic arene backbone signals (H3-H6). The room temperature  $^7Li$  NMR spectra of  $[Li(L^2)(DME)_{0.5}]_n$  and  $[Li(L^2)_2(OEt_2)]_2$  show a single lithium environment. Whilst  $[Li(L^2)_2(OEt_2)]_2$  has a narrow ( $\Delta\nu_{1/2}$  14 Hz) resonance at 1.85 ppm,  $[Li(L^2)(DME)_{0.5}]_n$  has a very broad resonance ( $\Delta\nu_{1/2}$  58 Hz) and at a lower frequency (-0.97 ppm). The broadness of the lithium peak in  $[Li(L^2)(DME)_{0.5}]_n$  indicates that there may be rapidly exchanging species in solution.

Crystals of  $[Li(L^2)_2(OEt_2)]_2$  suitable for X-ray crystallography were obtained by recrystallisation of the crude material from diethyl ether. The structure of the complex  $[Li(L^2)_2(OEt_2)]_2$  is dimeric, as illustrated in Figure 7.13. Crystallographic details and

selected geometric data are listed *Table 7.1* and *Table 7.2* respectively. Each four-coordinate lithium atom is surrounded by one diethyl ether, two bridging amido nitrogens (N(1) and N(1A)) and an oxygen atom from the methoxy group on bidentate  $L^2$  in a distorted tetrahedral array. This distortion from regular tetrahedral geometry presumably arises from the restriction of the N—Li—O(Me) bite angle ( $83.6(2)^\circ$ ) as well as the ligation of the bridging amide nitrogens, N(1) and N(1A), to Li(1,1A). The N(1)Li(1)N(1A)Li(1A) ring is essentially planar having the bidentate  $L^2$  ligands parallel to each other, with the arene backbone approximately perpendicular to the central (NLi)<sub>2</sub> plane ( $74.9(1)^\circ$ ). In comparison to  $L^2H$ , binding of  $L^2$  to lithium has had little effect on the methoxy position in relation to the arene backbone plane (torsion angle: C(13)—C(12)—O(1)—C(10)  $11.7(3)^\circ$ ). The structure of  $[Li(L^2)_2(OEt_2)]_2$  can be compared with those of less sterically-crowded  $[Li(\mu-L)(OEt_2)]_2$  complexes ( $L = 8$ -quinolinyl(trimethylsilyl)amide (qsta)<sup>[23]</sup> or *N,N'*-di-*p*-tolylformamidinate (dtf)<sup>[28]</sup>). However, the steric requirements for  $L^2$  must be less than that of  $L^1$  which coordinates to lithium in an unsymmetrical dinuclear configuration e.g.  $[Li(L^1)_2Li(OEt_2)]$ <sup>[24]</sup> with one four-coordinate and one three-coordinate Li. The Li—O(1) and Li—O(2) ether distances (2.000(4) Å, 1.991(4) Å respectively) in  $[Li(L^2)_2(OEt_2)]_2$  are similar to those in the related etherates above (for example, 1.94(3) Å in four-coordinate  $[Li(qsta)(OEt_2)]_2$  and 1.943(6) in three-coordinate  $[Li(N(SiMe_3)_2(OEt_2)]_2$ <sup>[29]</sup>). The lithium bridging is not symmetrical as shown by the significant difference in the Li(1)—N(1) and Li(1)—N(1A) bond lengths of 0.129 Å. This unsymmetrical behaviour has been observed in the related  $[Li(qsta)(OEt_2)]_2$  complex with bridging Li—N (amide) distances of 2.07(2) and 2.21(2) Å. Such distortions, which are presumably due to the steric crowding by the chelating  $L^2$  ligand, may suggest that dissociation is quite likely if crowding is increased further. The sharp  $^7Li$  and  $^1H$  NMR spectra of  $[Li(L^2)_2(OEt_2)]_2$  support the findings in the solid state with only one  $LiL^2$  environment detected.

Table 7.1. Summary of Crystallographic Data for  $[\text{Li}(\text{L}^2)_2(\text{OEt}_2)]_2$ 

Compound	$[\text{Li}(\text{L}^2)_2(\text{OEt}_2)]_2$
Formula	$\text{C}_{28}\text{H}_{32}\text{Li}_2\text{N}_2\text{O}_4\text{Si}_2$
$M$	550.78
$a$ (Å)	9.9320(5)
$b$ (Å)	10.0400(5)
$c$ (Å)	10.4465(4)
$\alpha$ (°)	117.651(3)
$\beta$ (°)	94.472(3)
$\gamma$ (°)	111.482(2)
$V$ (Å <sup>3</sup> )	818.9(3)
Crystal system	triclinic
Space Group	P(-1)
$Z$	1
Diffractometer	Nonius Kappa CCD
$\rho_{\text{calc}}$ (g cm <sup>-3</sup> )	1.117
$\mu(\text{MoK}\alpha)$ (mm <sup>-1</sup> )	0.140
$2\theta_{\text{max}}$ (°)	56.5
$N, N_o$	3887, 2831
$R, R_w$ (observed data)	0.0589, 0.1394
$R, R_w$ (all data)	0.0912, 0.1544

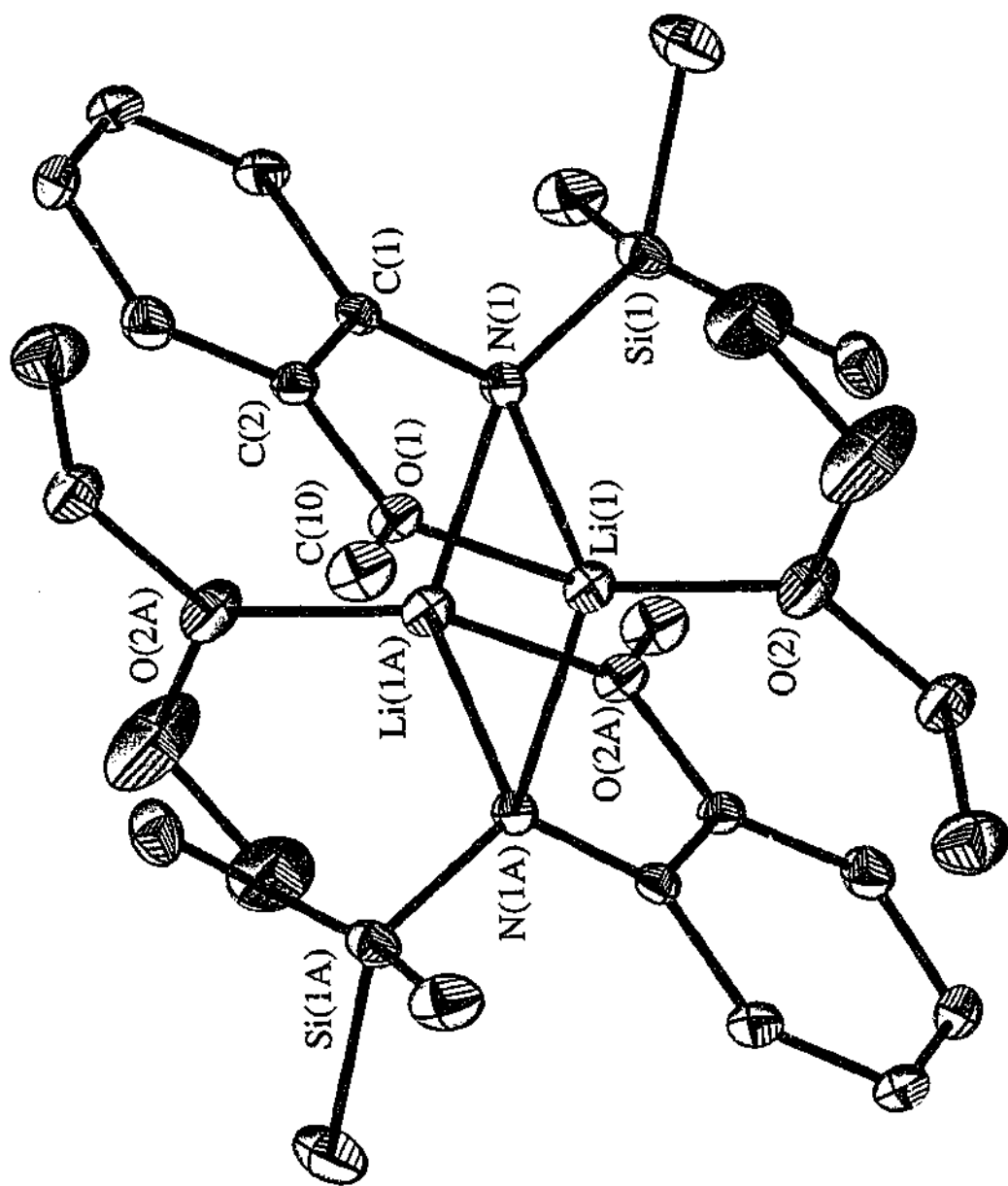
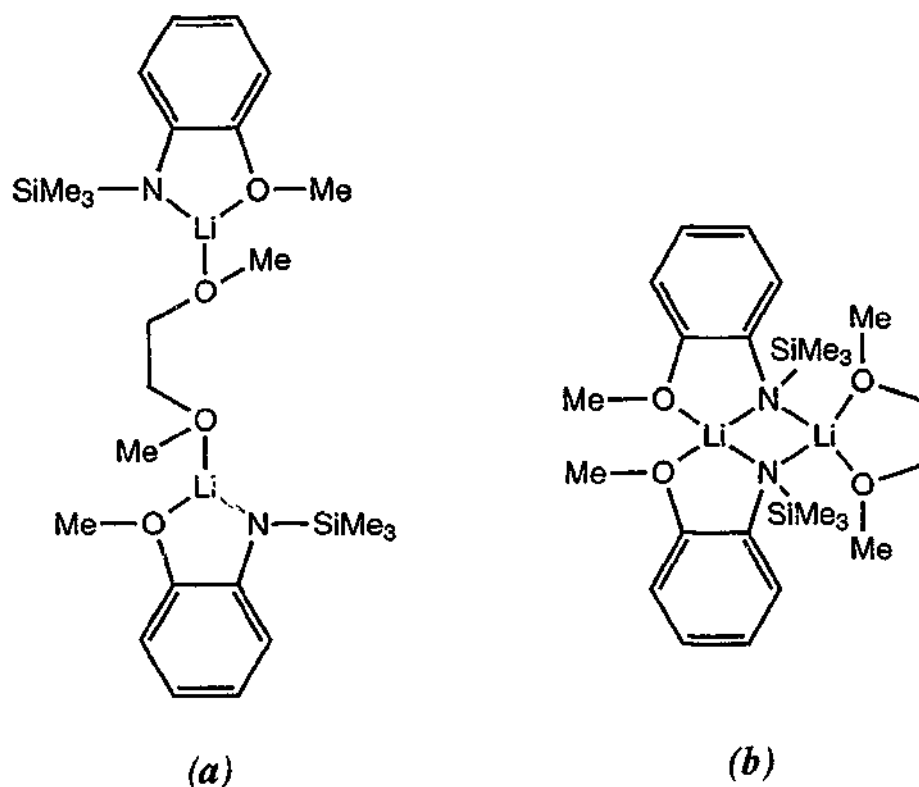


Figure 7.13 Molecular structure of  $[\text{Li}(\text{L}^2)_2(\text{OEt}_2)]_2$

**Table 7.2** Selected bond lengths (Å) and angles (°) with estimated standard deviations in parentheses for  $[\text{Li}(\text{L}^2)_2(\text{OEt}_2)]_2$

Li(1)—N(1)	2.025(4)	O(2)—Li(1)—O(1)	107.2(2)
Li(1)—N(1A)	2.157(4)	O(2)—Li(1)—N(1)	124.3(2)
Li(1)—O(1)	2.000(4)	O(1)—Li(1)—N(1)	83.6(2)
Li(1)—O(2)	1.991(4)	O(2)—Li(1)—N(1A)	120.7(2)
		O(1)—Li(1)—N(1A)	109.4(2)
		N(1)—Li(1)—N(1A)	104.9(2)

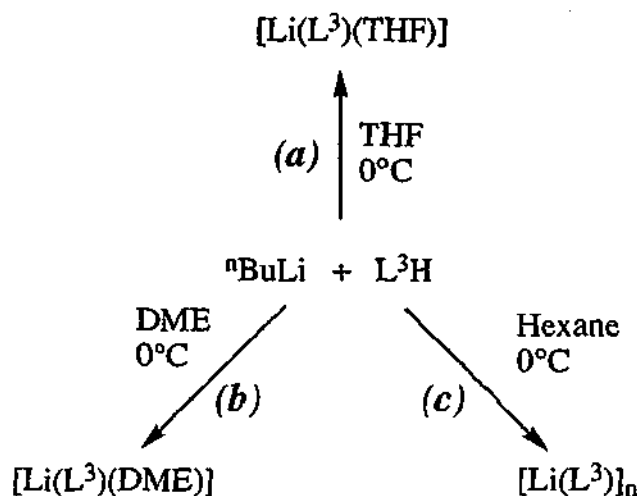
To date, suitable single crystals of  $[\text{Li}(\text{L}^2)(\text{DME})_{0.5}]_n$ , have not been obtained due to its extreme sensitivity to light, however a number of possible structures for  $[\text{Li}(\text{L}^2)(\text{DME})_{0.5}]_n$  can be postulated in view of the solid state structure of  $[\text{Li}(\text{L}^2)_2(\text{OEt}_2)]_2$  (see above). These include a dinuclear species bridged by DME (*Figure 7.14 (a)*) which would have a structural architecture similar to  $[\{\text{Li}(\text{N}(\text{SiMe}_3)_2)(\text{TMEDA})\}]$  which has a bridging bidentate neutral donor. Alternatively an unsymmetrical arrangement (*Figure 7.14 (b)*) which has a chelating DME bound to one lithium may also be possible and this structural type has previously been seen in  $[\text{Li}(\text{N}(\text{SiMe}_3)_2)_2\text{Li}(\text{DME})]$ .



**Figure 7.14**

### 7.2.2 Reaction of $L^3H$ with $LiBu^n$

Treatment of  $L^3H$  with a slight excess of  $n$ -butyllithium in THF or DME at low temperature gave  $[Li(L^3)(THF)]$  and  $[Li(L^3)(DME)]$ , respectively in high yield (>80%) (Scheme 7.2 (a), (b)). A similar reaction using non-coordinating hexane resulted in the donor free lithium salt  $[Li(L^3)]_n$ , which was also synthesized in good yield (see Scheme 7.2 (c)).



Scheme 7.2

The compositions and identities of the colourless, crystalline lithium products were established by elemental analyses (C, H, N) and infrared spectroscopy. Intense infrared absorptions of  $[Li(L^3)(THF)]$  attributable to a molecule of coordinated THF were seen at 1046 and 868  $cm^{-1}$ .<sup>[30]</sup> In  $[Li(L^3)(DME)]$  a strong absorption at 1082  $cm^{-1}$  confirmed the presence of ligated DME.<sup>[31]</sup> Room temperature  $^1H$  NMR spectra of  $[Li(L^3)(THF)]$  and  $[Li(L^3)(DME)]$  in  $C_7D_8$  solutions revealed a 1:1 ratio of coordinated THF or DME to a single  $L^3$  ligand. Each of the backbone aromatic protons (H3–H6) had a distinctive  $^1H$  NMR resonance and characteristic phenyl signals were observed for the phenoxy group (see Chapter 8). A single resonance peak for each of  $[Li(L^3)(THF)]$  and  $[Li(L^3)(DME)]$  attributable to the trimethylsilyl group is consistent with their  $^7Li$  NMR spectra at room temperature. These showed narrow ( $\Delta\nu_{1/2}$  20–30 Hz) single peaks at 1.68 and 1.43 ppm, respectively. Thus, both the  $^1H$  and  $^7Li$  NMR spectra of  $[Li(L^3)(THF)]$  and  $[Li(L^3)(DME)]$  have discrete signals attributable to only one species in solution (for assignments, see Chapter 8).

An X-ray structure determination on single crystals of  $[\text{Li}(\text{L}^3)(\text{DME})]$  confirmed the proposed composition. The molecular structure of  $[\text{Li}(\text{L}^3)(\text{DME})]$  is shown in *Figure 7.15* with crystallographic details and selected bond lengths and angles listed in *Table 7.3* and *Table 7.4* respectively. The structure comprises a mononuclear lithium centre that is coordinated by chelating  $\text{L}^3$  and DME ligands in a very distorted tetrahedral array (*Table 7.4*). The deviation from a regular tetrahedron presumably results from the narrow bite angles of the  $\text{L}^3$  ( $85.2(1)^\circ$ ) and DME ( $83.4(1)^\circ$ ). The  $\text{Li}(1)\text{—N}(1)$  bond length ( $1.930(3)$  Å) is marginally shorter than in other four-coordinate monomeric lithium amide complexes (e.g.  $[\text{Li}\{\text{N}(\text{SiMe}_3)_2\}(\text{PMDETA})]$  ( $\text{Li—N}(\text{amide})$   $1.988(6)$  Å)<sup>[21]</sup> and  $[\text{Li}\{\text{N}(\text{Ph}(\text{Me})\text{CH})(\text{PhCH}_2)\}(\text{PMDETA})]$  ( $\text{Li—N}(\text{amide})$   $1.959(7)$  Å)).<sup>[32]</sup> The ether units of  $[\text{Li}(\text{L}^3)(\text{DME})]$  have one longer ( $\text{Li—O}(\text{Ph})$ ) and two somewhat shorter ( $\text{Li—O}(\text{DME})$ )  $\text{Li—O}$  bond lengths. This is consistent with the more sterically demanding and electron withdrawing Ph and Ar substituents at the ether oxygen atom. The twist angles of the arene rings (torsion angle  $\text{C}(13)\text{—C}(12)\text{—O}(1)\text{—C}(111)$   $55.5(2)^\circ$ ; interplanar angle  $67.6(5)^\circ$ ) are in similar dispositions to those observed in  $\text{L}^3\text{H}$  (see Chapter 3).



Table 7.3. Summary of Crystallographic Data for  $[\text{Li}(\text{L}^3)(\text{DME})]$ 

Compound	$[\text{Li}(\text{L}^3)(\text{DME})]$
Formula	$\text{C}_{19}\text{H}_{28}\text{LiNO}_3\text{Si}$
$M$	353.45
$a$ (Å)	10.1225(2)
$b$ (Å)	12.8885(2)
$c$ (Å)	16.4847(3)
$\alpha$ (°)	90
$\beta$ (°)	107.395(1)
$\gamma$ (°)	90
$V$ (Å <sup>3</sup> )	2052.3(7)
Crystal system	Monoclinic
Space Group	$P2_1/c$
$Z$	4
Diffractometer	Nonius Kappa CCD
$\rho_{\text{calcd}}$ (g cm <sup>-3</sup> )	1.144
$\mu(\text{MoK}\alpha)$ (mm <sup>-1</sup> )	0.130
$2\theta_{\text{max}}$ (°)	56.5
$N, N_o$	5063, 3500
$R, R_w$ (observed data)	0.046, 0.099
$R, R_w$ (all data)	0.082, 0.113

Table 7.4 Selected bond lengths (Å) and angles (°) with estimated standard deviations in parentheses for  $[\text{Li}(\text{L}^3)(\text{DME})]$ 

Li(1)—N(1)	1.930(3)	N(1)—Li(1)—O(2)	117.2(1)
Li(1)—O(2)	1.963(3)	N(1)—Li(1)—O(3)	144.2(2)
Li(1)—O(3)	1.986(3)	O(2)—Li(1)—O(3)	83.4(1)
Li(1)—O(1)	2.062(3)	N(1)—Li(1)—O(1)	85.2(1)
		O(2)—Li(1)—O(1)	119.6(1)
		O(3)—Li(1)—O(1)	111.0(1)

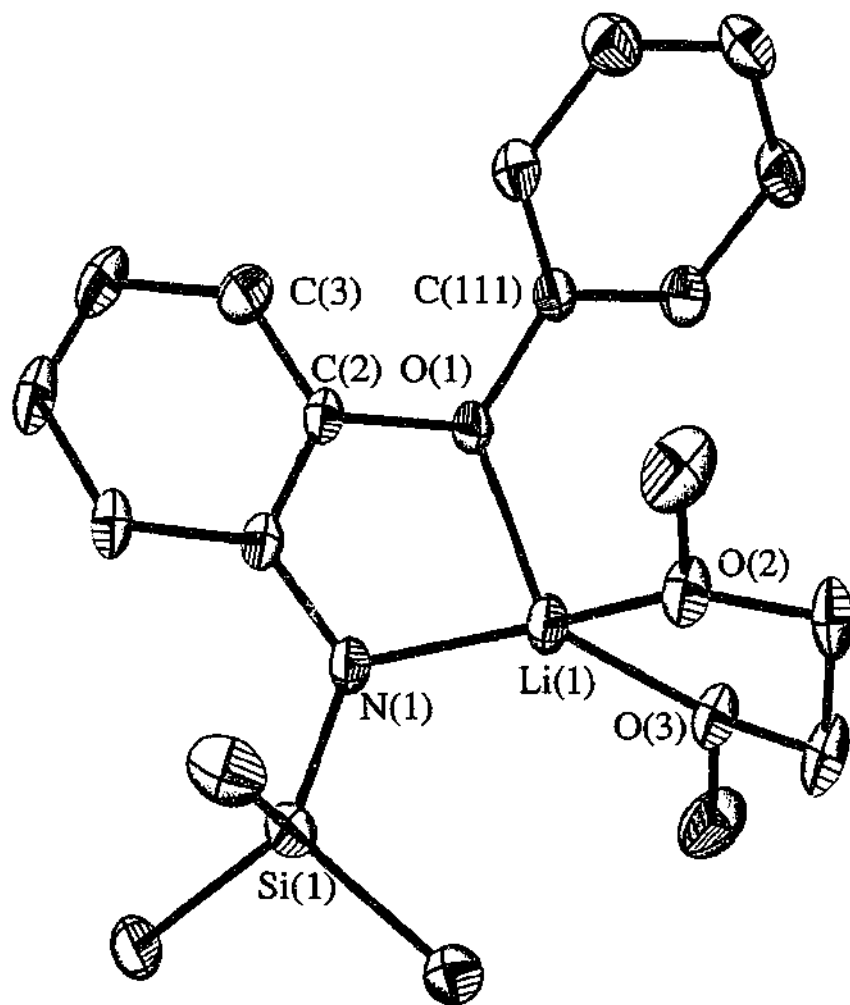


Figure 7.15 Molecular Structure of  $[\text{Li}(\text{L}^3)(\text{DME})]$

By contrast with the spectra of  $[\text{Li}(\text{L}^3)(\text{THF})]$  and  $[\text{Li}(\text{L}^3)(\text{DME})]$ , those of the donor-free  $[\text{Li}(\text{L}^3)]_n$  are more complex and need more consideration. The  $^1\text{H}$  NMR spectrum of  $[\text{Li}(\text{L}^3)]_n$  was found to have temperature-dependence with that obtained at  $30^\circ\text{C}$  being poorly resolved in the aromatic region. At  $-90^\circ\text{C}$ , the  $\text{C}_7\text{D}_8$  solution of  $[\text{Li}(\text{L}^3)]_n$  showed two sets of resonances for the trimethylsilyl group and three of the aromatic protons of  $\text{L}^3$  in a 1:3 ratio. This suggests that two unique  $\text{L}^3$  ligand environments are present in  $[\text{Li}(\text{L}^3)]_n$ . At room temperature  $^7\text{Li}$  NMR data on  $[\text{Li}(\text{L}^3)]_n$  show a single resonance which is in the same spectral window (1.65 ppm) as the signals of  $[\text{Li}(\text{L}^3)(\text{THF})]$  and  $[\text{Li}(\text{L}^3)(\text{DME})]$ , but is somewhat ( $\Delta\nu_{1/2}$  50 Hz) broader. On cooling to  $0^\circ\text{C}$ , the broad  $^7\text{Li}$  resonance splits into two broad peaks at 2.6 and 1.1 ppm and this is maintained at temperatures between  $-30$  and  $-60^\circ\text{C}$ . Further resolution into three sharp signals (-1.77, 2.60, 2.96 ppm) was achieved by  $-90^\circ\text{C}$  (*Figure 7.16*). The assignment of the three  $^7\text{Li}$  NMR signals of  $[\text{Li}(\text{L}^3)]_n$  is difficult, but the overall NMR behaviour of  $[\text{Li}(\text{L}^3)]_n$  is typical of the presence of rapidly exchanging species. The higher resolution at low temperatures suggests that  $[\text{Li}(\text{L}^3)]_n$  may form one or more aggregates with different Li environments (see below). In the recently prepared  $[\text{LiN}\{(\text{SiMe}_3)(\text{Ph})\}]_4$ , comparable data showed two  $^7\text{Li}$  resonances (0.9 and -4.6 ppm) at  $-110^\circ\text{C}$  with the low frequency peak being assigned to a terminal Li nucleus with an intramolecular  $\eta^6$ - $\pi$ -phenyl interaction.[8]

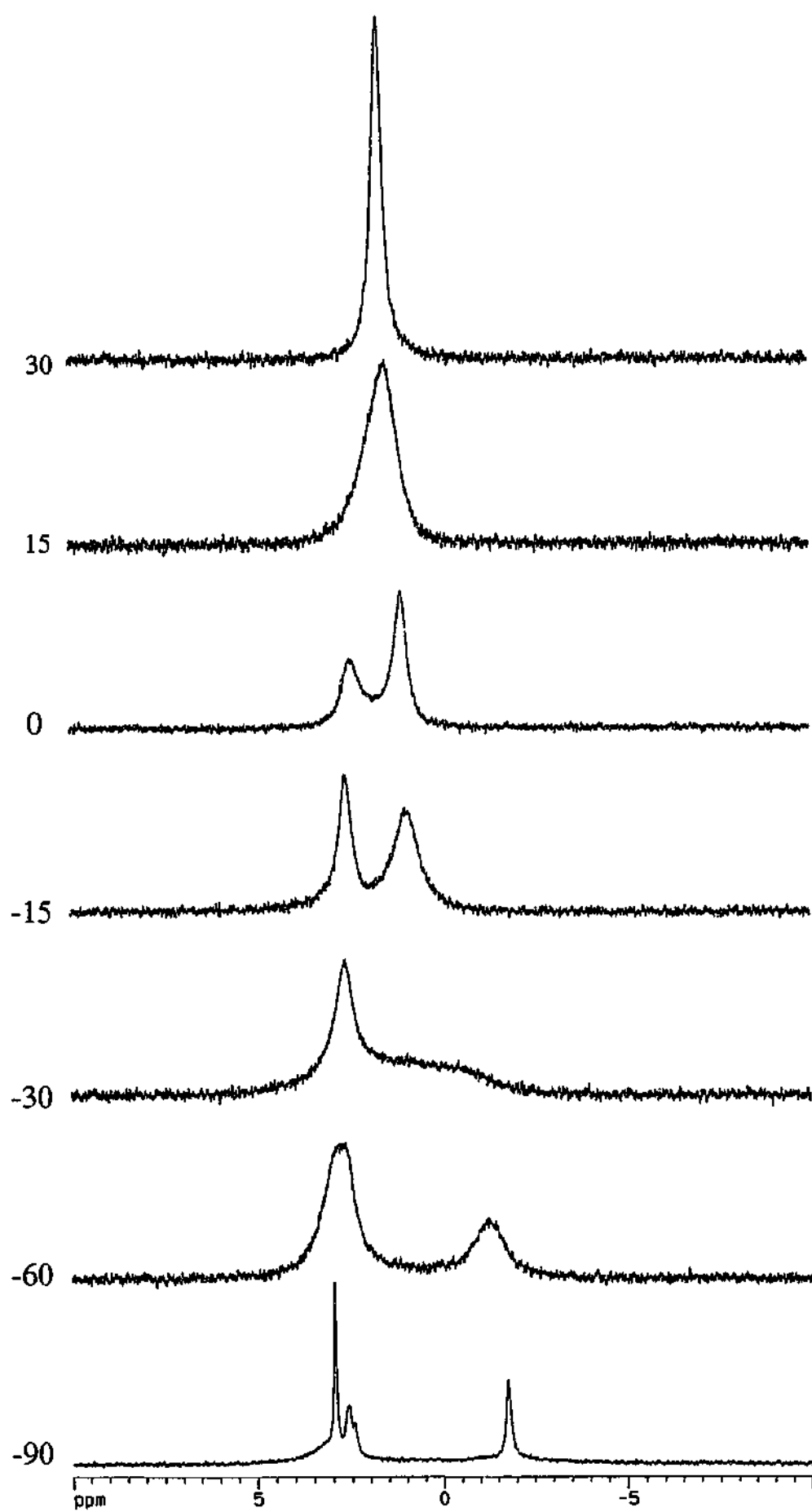
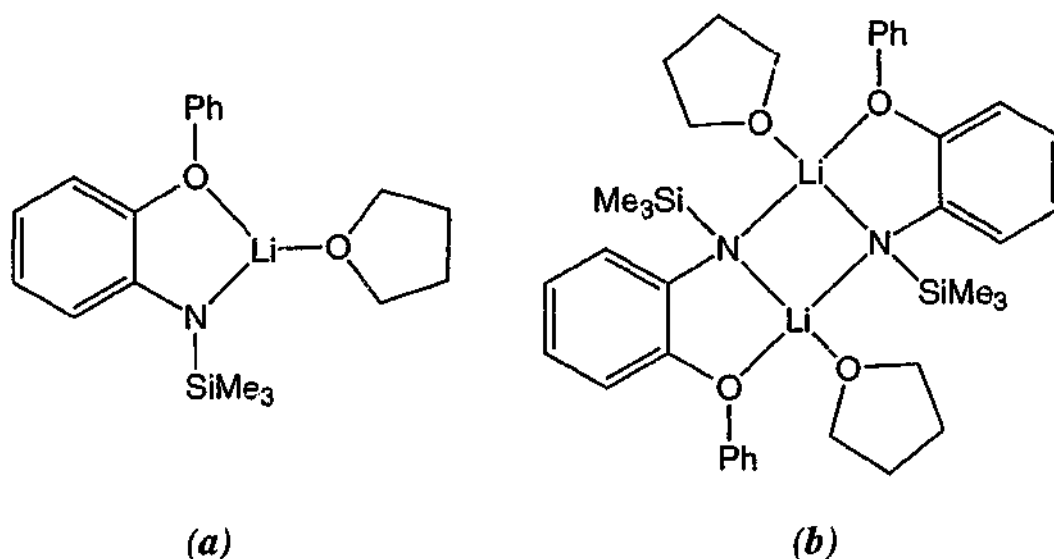


Figure 7.16  $^7\text{Li}$  NMR spectra for  $[\text{Li}(\text{L}^3)]_n$  in  $\text{C}_7\text{H}_8$  at variable temperatures

In view of the structure of  $[\text{Li}(\text{L}^3)(\text{DME})]$  two structural proposals can be made for  $[\text{Li}(\text{L}^3)(\text{THF})]$ , one being a three-coordinate monomer (*Figure 7.17 (a)*) similar to  $[\text{Li}(\text{L}^3)(\text{DME})]$  but with a monodentate THF, the other a four-coordinate dimer (*Figure 7.17 (b)*) which is related to the lithium compound obtained using the less sterically hindered  $\text{L}^2$  ligand in  $[\text{Li}(\text{L}^2)(\text{Et}_2\text{O})]_2$  (see section 7.2.1). Utilizing a more sterically crowded amide ligand, such as  $\text{L}^1$ , results in an unsymmetrical dinuclear species,  $[\text{Li}(\text{L}^1)_2\text{Li}(\text{OEt}_2)]$ .<sup>[24]</sup> However the  $^7\text{Li}$  and  $^1\text{H}$  NMR spectra for  $[\text{Li}(\text{L}^3)(\text{THF})]$  shows only one lithium and one  $\text{L}^3$  environment suggesting that an unsymmetrical structural type is less probable. In contrast to the  $\text{L}^2$  ligand, the steric demands of the diaryl ether moiety of  $\text{L}^3$  would be more likely to stabilise a monomeric arrangement rather than a symmetrical dimer.



*Figure 7.17*

A possible structure for unsolvated  $[\text{Li}(\text{L}^3)]_n$  is more contentious. Low temperature  $^7\text{Li}$  NMR studies on  $[\text{Li}(\text{L}^3)]_n$  revealed that three unique lithium environments are present. This excludes a two-coordinate monomer and suggests that one or more higher oligomeric species are present. In the related solvent-free bidentate organoamidolithium complex  $[\text{Li}(\text{qsta})]_2$  structural characterisation revealed a symmetrical dimer with each three-coordinate Li having two bridging amide nitrogen atoms.<sup>[23]</sup> Accordingly, this complex has only a single  $^7\text{Li}$  resonance. However  $[\text{Li}(\text{L}^3)]_n$  could be a mixture of two dimers, with one lithium environment coming from a symmetrical dimer (*Figure 7.18 (a)*) with the other two resonances from the unsymmetrical dimer (*Figure 7.18 (b)*). Alternatively, a symmetrical and unsymmetrical dimers can be combined giving

a tetranuclear species (*Figure 7.18 (c)*) with at least three different Li environments and two  $L^3$  types in a 1:3 ratio as observed. A recent example of a higher aggregate is the tetranuclear species  $[\text{LiN}((\text{SiMe}_3)(\text{Ph}))]_4$  (*Figure 7.2 (a)*), which has central bridging amide ligands with the outer lithium atoms capped by  $\eta^6\text{-Li-Ph}$  interactions.[8]

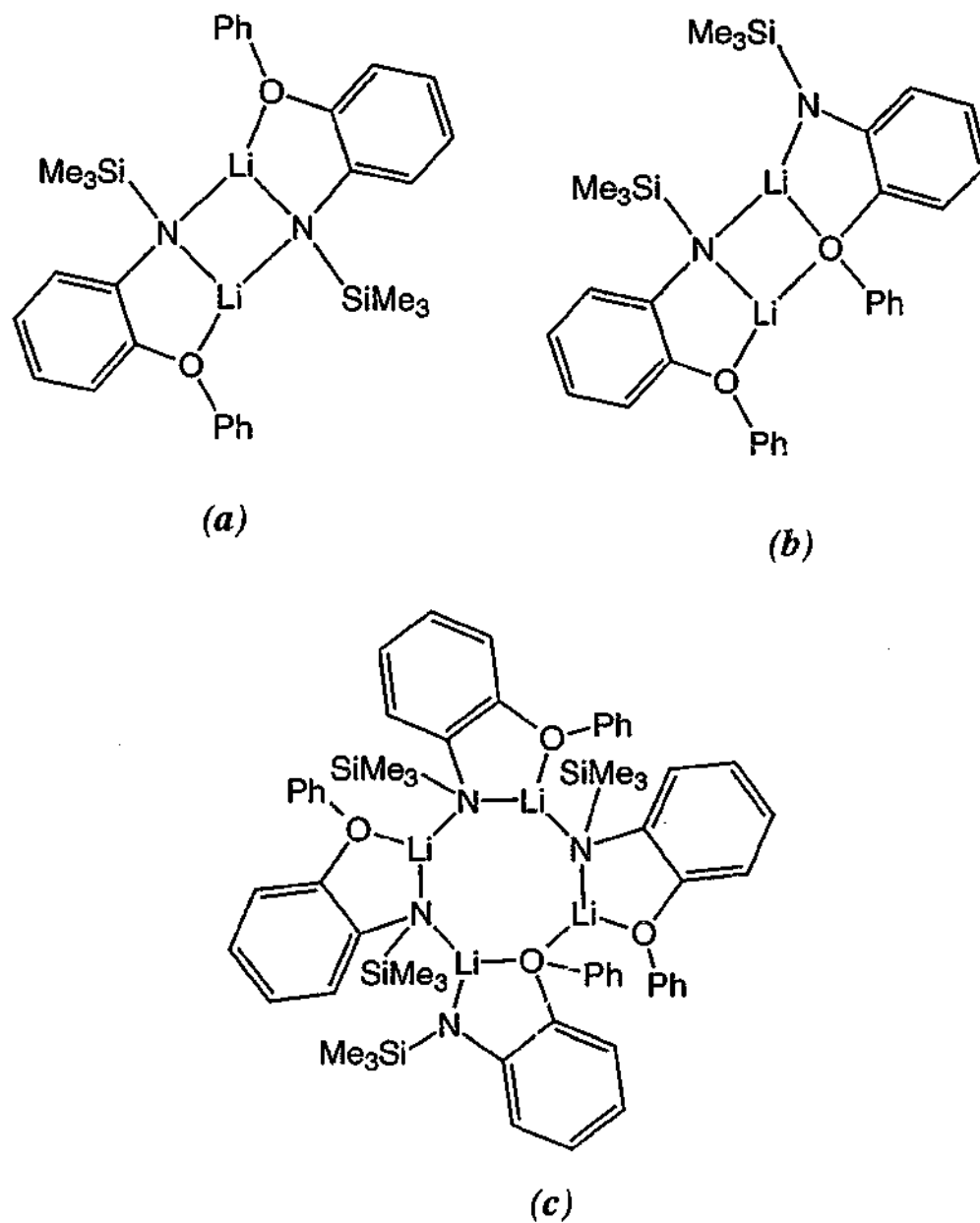
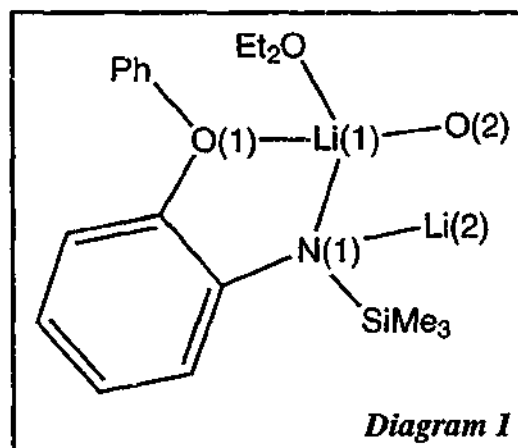


*Figure 7.18*

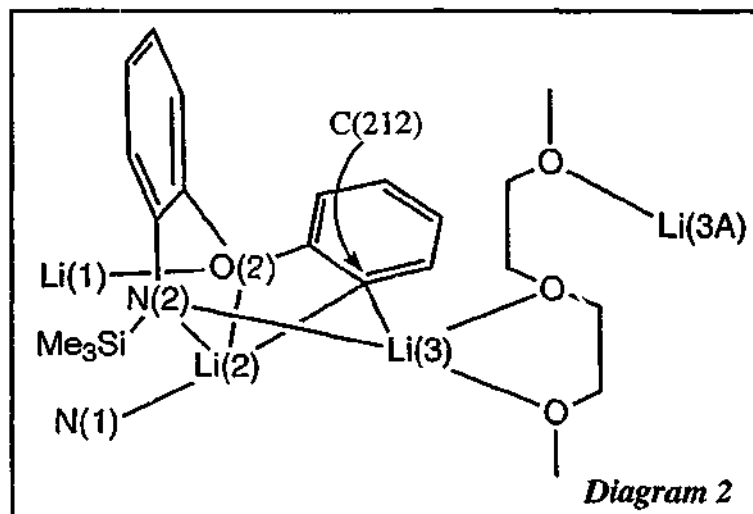
### 7.2.3 Reaction of $L^3H$ with Excess $LiBu^n$

The deprotonation of  $L^3H$  with an excess of  $LiBu^n$  in diethyl ether and work up in hexane gave a very low yield of colourless crystals. The crystals were later identified by X-ray crystallography and showed not only the expected  $Li(L^3)(OEt_2)$  group in the asymmetric unit, but also a doubly deprotonated ligand,  $L^*$  ( $L^* = N(SiMe_3)(2-(2'-C_6H_4O)C_6H_4)$ ) (Figure 7.12) from which a hydrogen in the *ortho* position on the phenoxy substituent has been removed, resulting in a novel hexanuclear lithium complex  $[[Li(L^3)(OEt_2)Li_2(L^*)]_2(\text{diglyme})]$ . The hexane was subsequently shown to contain trace amounts of adventitious bis(2-methoxyethyl) ether (diglyme). The molecular structure is shown in Figure 7.19, crystallographic details are listed in Table 7.5, and selected bond distances and angles are presented in Table 7.6. The  $Li(L^3)(OEt_2)$  moiety contains a four coordinate lithium (Li(1)) not dissimilar to the lithium environment in  $[Li(L^2)(OEt_2)]_2$  (Figure 7.13). However instead of bridging to a nitrogen atom on another  $L^3$  ligand, Li(1) is further coordinated by an oxygen atom (O(2)) from the aryl ether substituent of the neighbouring  $L^*$  (see Diagram 1). Whilst N(1) and O(1) are chelated to Li(1), N(1) is also bridging to Li(2) which is bound to  $L^*$ . The  $L^3$  bite angle (O(1)—Li(1)—N(1)  $83.5(2)^\circ$ ) in the



current structure is similar to the corresponding angle in  $[Li(L^2)(OEt_2)]_2$  and  $[Li(L^3)(DME)]$  ( $83.6(2)^\circ$  and  $85.2(1)^\circ$  respectively). Whilst the Li(1)—N(1) distance is significantly longer ( $0.08 \text{ \AA}$ ) than the equivalent Li—N distance in  $[Li(L^3)(DME)]$  as expected for bridging atoms, it is slightly shorter ( $0.02 \text{ \AA}$ ) than the shortest Li— $N_{br}$  bond length in  $[Li(L^2)(OEt_2)]_2$  (Table 7.2). The terminal Li(1)—O(3)( $OEt_2$ ) distance in  $[[Li(L^3)(OEt_2)Li_2(L^*)]_2(\text{diglyme})]$  is comparable to the equivalent bond lengths in  $[Li(L^2)(OEt_2)]_2$  (Table 7.2). The relative disposition of the arene substituents on the  $L^3$  ligand has the phenoxy group linear with the arene backbone (torsion angle C(13)—C(12)—O(1)—C(111)  $-2.8(3)^\circ$ ) but the ring plane is tilted almost perpendicular (interplanar angle  $84.18(9)^\circ$ ).

As mentioned above, the  $\text{Li}_2\text{L}^*$  unit is situated between  $\text{LiL}^3$  and diglyme with bonding of O(2) and Li(2) to Li(1) and N(1) of  $\text{LiL}^3$ , respectively (see *Diagram 2*). The phenoxy oxygen (O(2)) of  $\text{L}^*$  is also bridged to Li(2) and is only the second example in lithium organoamides<sup>[26]</sup> to contain a diaryl ether bridging two lithium centers. The other is  $[\text{O}(2\text{-C}_6\text{H}_4\text{N}(\text{Li})\text{CH}_2\text{CH}_2\text{OMe})_2]_2$ .<sup>[26]</sup> As in the present case, it is further supported by donor groups on the aryl ether unit. The lithium atom Li(2), is further bound by another



amide nitrogen (N(2)) and the *ortho* carbon C(212) of the phenoxy substituent of the  $\text{L}^*$  ligand, which is tridentate to Li(2), to have a coordination number of four. Furthermore, the N(2) and C(212) atoms each bridge to Li(3). The molecule of diglyme is positioned

between the two trilithium units with the three donor oxygen atoms linking Li(3) to the symmetry generated Li(3A). As the diglyme is disordered over a symmetry site, one component has two oxygen atoms chelating to one lithium (Li(3)), while the other oxygen atom is coordinated to the corresponding atom (Li(3A)) in the symmetry generated trilithium unit. In the other component of the disorder, the bonding of the diglyme oxygen atoms to Li(3A) and Li(3) is reversed. This highly strained behaviour of sharing of a single diglyme between two separate trilithium aggregates is reflected by the unsymmetrical bonding of the diglyme to Li(3)/Li(3A) (*Table 7.6*). The Li(2)—N(1) or N(2) bond length is similar to the corresponding distance in the  $\text{LiL}^3$  fragment (see above) and comparable with the Li—N<sub>br</sub> bond length in  $[\text{Li}(\text{N}(\text{SiMe}_3)_2(\text{OEt}))_2]_2$  (2.055(5) Å). As expected, the terminal Li(1)—O(1) distance in the  $\text{LiL}^3$  moiety is shorter than the bridging Li(x)—O(2) (x = 1 and 2) bond distances. However, these bridging distances are unsymmetrical with the distance Li(2)—O(2) being considerably longer (0.077 Å) than Li(1)—O(2) reflecting the more crowded lithium environment in the  $\text{Li}_2\text{L}^*$  unit. The remarkable deprotonation of the phenoxy substituent of  $\text{L}^*$  results in a  $\text{Li}_2(\mu\text{-}\eta^1\text{:}\eta^1\text{-Ar})$  unit. The Li—C(212) bond lengths are uneven, with the longer distance (Li(2)—C(212)) being comparable to the Li—C distances previously reported for dimeric  $[\text{Li}(\mu\text{-}\eta^1\text{:}\eta^1\text{-Ar})_2]$  (Ar = 2,6-(CH(Me)NMe<sub>2</sub>)<sub>2</sub>C<sub>6</sub>H<sub>3</sub> 2.21(1)-2.26(2) Å)<sup>[33]</sup> whilst the shorter Li(3)—C(212) bond length is within the range for  $[\text{Li}(\mu\text{-}\eta^1\text{:}\eta^1\text{-Ar})_4]$  (Ar = 2,6-(OBu<sup>t</sup>)<sub>2</sub>C<sub>6</sub>H<sub>3</sub> 2.139(5)-



2.160(6) Å).<sup>[34]</sup> Furthermore, C(211) shows a close approach (2.509(5) Å) to Li(2) resulting from the O(2) and C(212) from the same phenoxy ring chelating also to this lithium. However, this approach may not represent significant bonding. As seen in the related complexes  $[\text{Li}(\text{L}^3)(\text{OEt}_2)]_2$  and  $[\text{Li}(\text{L}^3)(\text{DME})]$ , the geometry of the lithium centre is severely distorted from tetrahedral owing to the restriction of the chelating  $\text{N}-\text{Li}-\text{O}$  angle. In  $[\{\text{Li}(\text{L}^3)(\text{Et}_2\text{O})\text{Li}_2(\text{L}^*)\}_2(\text{diglyme})]$ , Li(2) experiences a greater distortion compared with Li(1) and the appropriate component in Li(3) as evidenced by the narrow  $\text{O}(2)-\text{Li}(2)-\text{C}(212)$  angle, resulting from the coordination of N(2), O(2) and C(212) from the  $\text{L}^*$  to the same lithium atom (Li(2)). The placement of the arene substituents on  $\text{L}^*$  in  $[\{\text{Li}(\text{L}^3)(\text{Et}_2\text{O})\text{Li}_2(\text{L}^*)\}_2(\text{diglyme})]$  is different to the  $\text{LiL}^3$  moiety (see above) and is similar to  $\text{L}^3\text{H}$  and  $[\text{Li}(\text{L}^3)(\text{DME})]$  despite the restriction caused by the deprotonated phenyl group. However, the phenoxy ring on  $\text{L}^*$  is pulled further out of the plane of the arene backbone (torsion angle  $\text{C}(23)-\text{C}(22)-\text{O}(2)-(\text{C}211)$   $89.7(3)^\circ$ ) but the ring plane is not as rotated (interplanar angle  $53.04(9)^\circ$ ).

Table 7.5. Summary of Crystallographic Data for  $[\{\text{Li}(\text{L}^3)(\text{OEt}_2)\text{Li}_2(\text{L}^*)\}_2(\text{diglyme})]$

Compound	$[\{\text{Li}(\text{L}^3)(\text{OEt}_2)\text{Li}_2(\text{L}^*)\}_2(\text{diglyme})]$
Formula	$\text{C}_{74}\text{H}_{104}\text{Li}_6\text{N}_4\text{O}_9\text{Si}_4$
<i>M</i>	1347.62
<i>a</i> (Å)	40.3030(1)
<i>b</i> (Å)	10.5611(3)
<i>c</i> (Å)	18.7239(3)
$\alpha$ (°)	90
$\beta$ (°)	99.263(1)
$\gamma$ (°)	90
<i>V</i> (Å <sup>3</sup> )	7866(3)
Crystal system	monoclinic
Space Group	<i>C2/c</i>
<i>Z</i>	4
Diffractometer	Nonius Kappa CCD
$\rho_{\text{calcd}}$ (g cm <sup>-3</sup> )	1.138
$\mu(\text{MoK}\alpha)$ (mm <sup>-1</sup> )	0.129
$2\theta_{\text{max}}$ (°)	56.5
<i>N</i> , <i>N</i> <sub>o</sub>	9449, 5969
<i>R</i> , <i>R</i> <sub>w</sub> (observed data)	0.070, 0.139
<i>R</i> , <i>R</i> <sub>w</sub> (all data)	0.122, 0.162

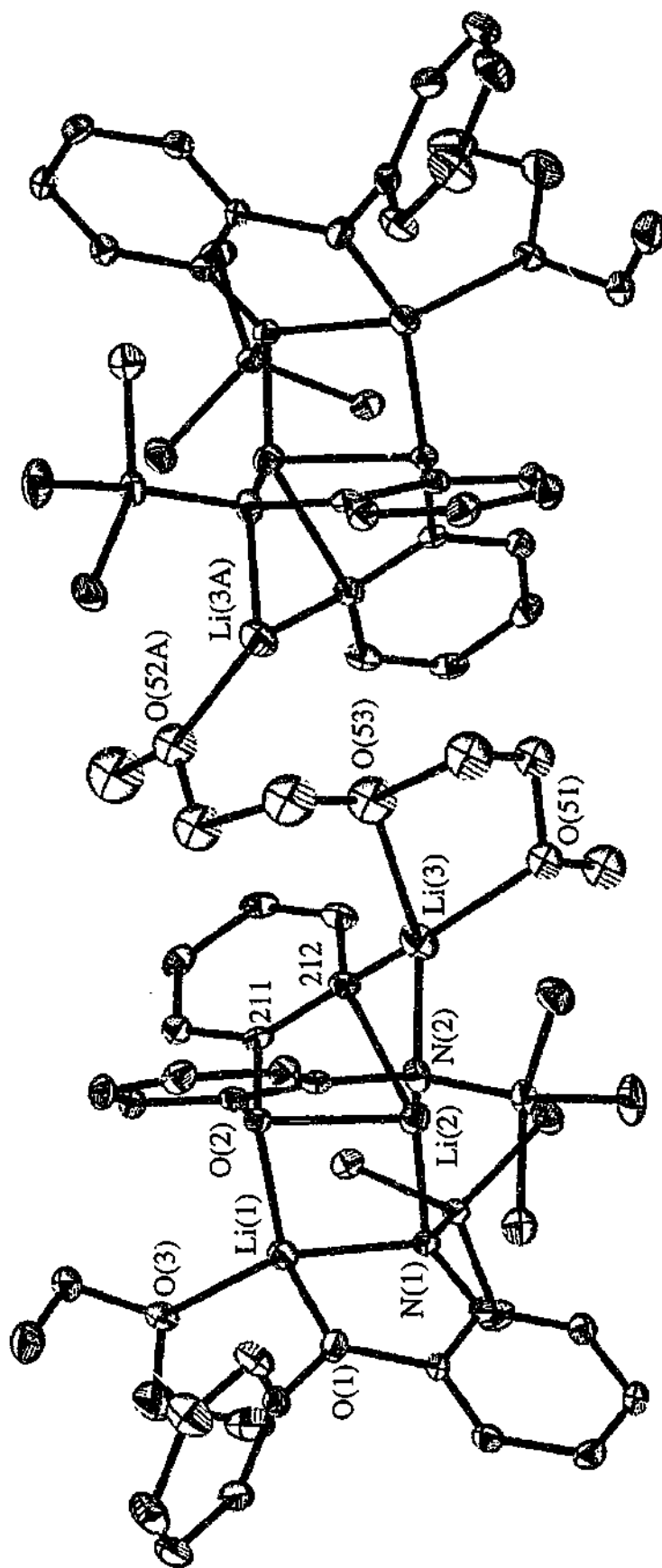


Figure 7.19 Molecular Structure of  $[Li(L)(OEt)_2Li_2(L^*)]_2$  (diglyme)

**Table 7.6** Selected bond lengths (Å) and angles (°) with estimated standard deviations in parentheses for  $[\{\text{Li}(\text{L}^3)(\text{OEt}_2)\text{Li}_2(\text{L}^*)\}_2(\text{diglyme})]$

Li(1)—O(1)	1.980(5)	O(1)—Li(1)—O(3)	106.1(2)
Li(1)—O(3)	1.979(5)	O(1)—Li(1)—N(1)	83.5(2)
Li(1)—N(1)	2.009(5)	O(3)—Li(1)—N(1)	139.4(3)
Li(1)—O(2)	2.033(5)	O(1)—Li(1)—O(2)	108.0(2)
		O(3)—Li(1)—O(2)	112.7(2)
		N(1)—Li(1)—O(2)	100.8(2)
Li(2)—N(1)	2.073(5)	N(1)—Li(2)—N(2)	139.7(2)
Li(2)—N(2)	2.020(5)	N(1)—Li(2)—O(2)	96.2(2)
Li(2)—O(2)	2.110(5)	N(1)—Li(2)—C(212)	120.3(2)
Li(2)—C(212)	2.254(5)	N(2)—Li(2)—O(2)	86.4(2)
Li(2)—C(211)	2.509(5)	N(2)—Li(2)—C(212)	97.9(2)
		O(2)—Li(2)—C(212)	67.4(2)
Li(3)—N(2)	2.060(6)	N(2)—Li(3)—C(212)	100.6(2)
Li(3)—C(212)	2.133(6)	N(2)—Li(3)—O(51)	121.7(3)
Li(3)—O(51)	2.032(7)	N(2)—Li(3)—O(53)	121.6(3)
Li(3)—O(52)	1.835(7)	C(212)—Li(3)—O(51)	117.9(3)
Li(3)—O(53)	2.181(7)	C(212)—Li(3)—O(53)	116.7(3)
		O(51)—Li(3)—O(53)	79.2(2)
		N(2)—Li(3)—O(52)	123.9(3)
		C(212)—Li(3)—O(52)	133.3(3)

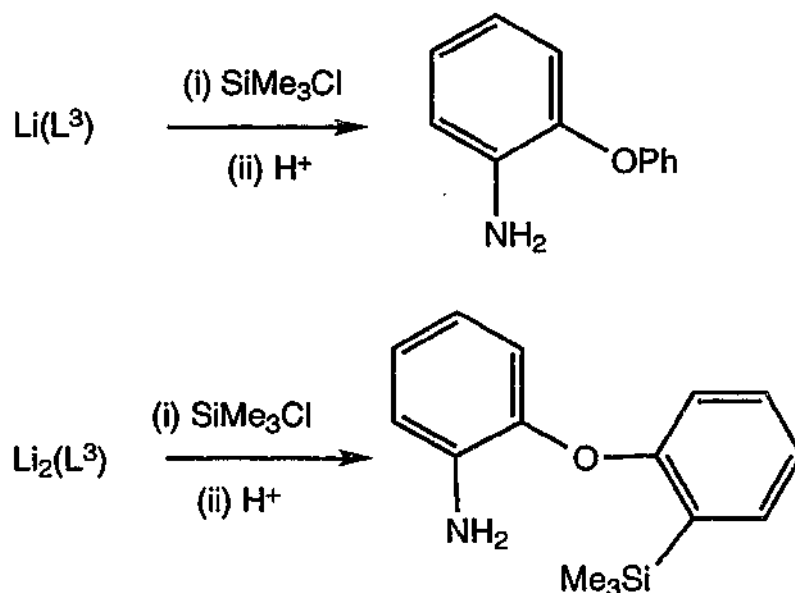
Symmetry transformations used to generate equivalent atoms:

<sup>a</sup> -x, y, -z+1/2

<sup>1</sup>H and <sup>7</sup>Li NMR studies of  $[\{\text{Li}(\text{L}^3)(\text{OEt}_2)\text{Li}_2(\text{L}^*)\}_2(\text{diglyme})]$  in  $\text{C}_7\text{D}_8$  revealed temperature dependent spectra. The room temperature <sup>1</sup>H NMR spectrum exhibited many broad features. Two distinct SiMe<sub>3</sub> peaks in a 1:1 ratio were observed, one from each of the two types of silylated amide ligands, L<sup>3</sup> and L<sup>\*</sup>. However one peak is sharp (0.17 ppm) and the other is broad (0.24 ppm) suggesting that one SiMe<sub>3</sub> environment is rotating freely while the other is somewhat restricted. The signals attributable to diglyme are broad and are positioned further to low frequency than those of free diglyme. This suggests that in  $[\{\text{Li}(\text{L}^3)(\text{OEt}_2)\text{Li}_2(\text{L}^*)\}_2(\text{diglyme})]$  both free and coordinated diglyme are present resulting in an average peak position. By contrast, the Et<sub>2</sub>O resonance pattern is sharp and is close to that of free diethyl ether. A mixture of broad and sharp peaks in the aromatic region suggests there is some mobility of the arene groups in solution. At 0°C the two SiMe<sub>3</sub>

resonances merge into a broad peak at 0.24 ppm, while the Et<sub>2</sub>O signals broaden out suggesting that the motion observed in the room temperature spectrum is starting to slow down, however the diglyme and aromatic peaks remain broad. On cooling to -90 °C solubility problems were encountered with the sample starting to precipitate out. Despite this, the diglyme appears to broaden further suggesting that exchange has not been halted entirely. This broadening may also be a result of an overlap caused by the unsymmetrical binding of diglyme present in the solid structure of  $[\{\text{Li}(\text{L}^3)(\text{OEt}_2)\text{Li}_2(\text{L}^*)\}_2(\text{diglyme})]$ , further compounded by the precipitation of the product during data collection. With decreasing temperature the Et<sub>2</sub>O signals progressively broaden and at -90 °C start to split into two, as expected for a non-exchanging structure. In the room temperature <sup>7</sup>Li NMR of  $[\{\text{Li}(\text{L}^3)(\text{Et}_2\text{O})\text{Li}_2(\text{L}^*)\}_2(\text{diglyme})]$  a broad single resonance ( $\Delta\nu_{1/2} = 40$  Hz, 1.67 ppm) is observed. On cooling to -90 °C this resonance is resolved into four separate peaks (0.83, 1.50, 2.08, 3.50 ppm). This is consistent with the four lithium atom environments observed in the solid state structure of  $[\{\text{Li}(\text{L}^3)(\text{Et}_2\text{O})\text{Li}_2(\text{L}^*)\}_2(\text{diglyme})]$ .

Deliberate syntheses of Li<sub>2</sub>(L<sup>\*</sup>) were investigated by reactions of two equivalents of LiBu<sup>n</sup> with L<sup>3</sup>H. These reactions were found to be highly solvent dependent. Consequently, reactions in strong *polar* solvents e.g THF, DME do not yield L<sup>\*</sup> but simply the mono-deprotonated LiL<sup>3</sup> complexes (60-70% yield). In contrast to the preparations of Li<sub>2</sub>(L<sup>3</sup>) with diethyl ether (see below), reactions in the *less polar* hexane give only a compound containing the mono-deprotonated ligand, L<sup>3</sup>. Whilst a structure of [Li(L<sup>3</sup>)]<sub>n</sub> could not be obtained, the presence of solely the L<sup>3</sup> ligand from the reaction of L<sup>3</sup>H / LiBu<sup>n</sup> (mole ratio 1:2) in hexane was proven by treatment of the product with SiMe<sub>3</sub>Cl followed by hydrolysis (*Scheme 7.3*). This gave only the compound H<sub>2</sub>N(2-PhOC<sub>6</sub>H<sub>4</sub>) which was derived from L<sup>3</sup>. No H<sub>2</sub>N(2-(2'-C<sub>6</sub>H<sub>4</sub>SiMe<sub>3</sub>)C<sub>6</sub>H<sub>4</sub>) was detected which was the expected product from L<sup>\*</sup>.

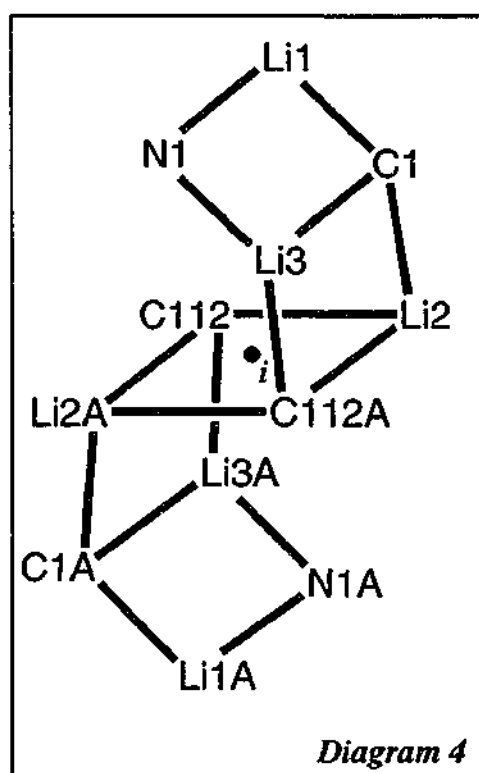
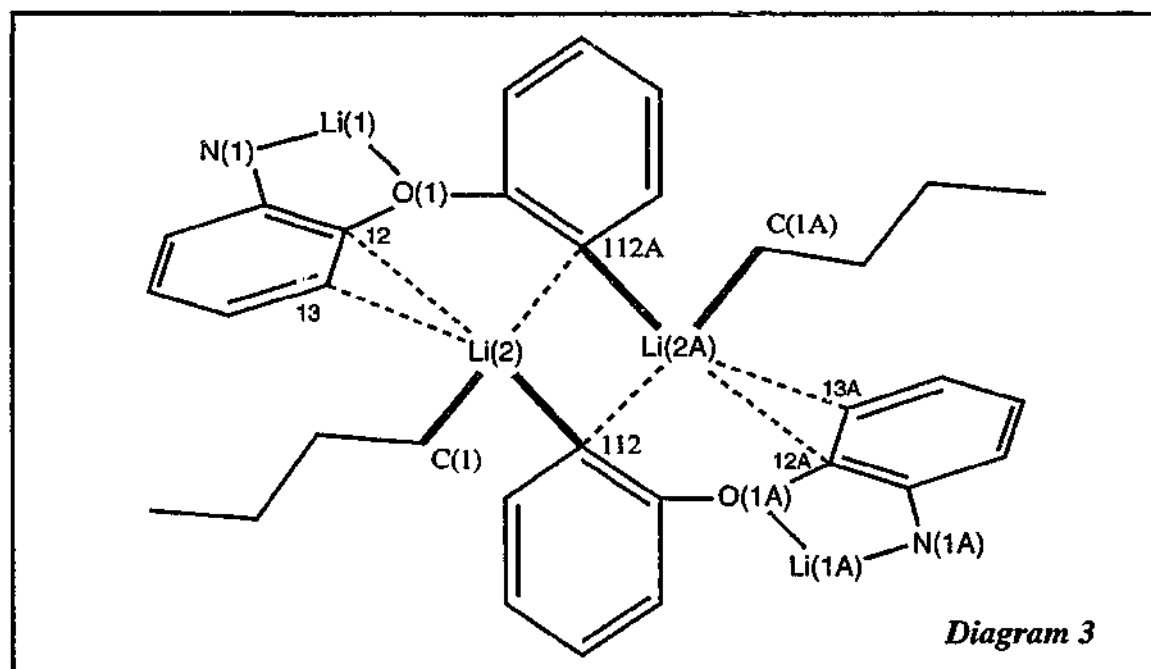


Scheme 7.3

The *intermediate polarity* diethyl ether was found to be the only solvent environment to yield the doubly deprotonated unit,  $\text{Li}_2(\text{L}^*)$ . The lithiation of  $\text{L}^3\text{H}$  using two equivalents of  $\text{LiBu}^n$  in diethyl ether, afforded after work up in hexane (freed from donor impurities) colourless crystals in low yield. These crystals were found not only to contain the desired  $\text{Li}_2(\text{L}^*)$  unit but also, unexpectedly, a molecule of  $\text{LiBu}^n$  resulting in an overall composition of  $[\text{Li}_2(\text{L}^*)(\text{OEt}_2)\text{Li}(\text{Bu}^n)]_2$ . Repeating this synthesis followed by work up in a mixture of hexane and DME (30:1) removed the residual  $\text{LiBu}^n$  to yield pure  $[\text{Li}_2(\text{L}^*)(\text{DME})]_2$  in moderate yield. The crystal structures of  $[\text{Li}_2(\text{L}^*)(\text{OEt}_2)\text{Li}(\text{Bu}^n)]_2$  and  $[\text{Li}_2(\text{L}^*)(\text{DME})]_2$  have been determined (see below) with elemental analyses (C, H, N) supporting each composition for the bulk sample. The entrapment of molecules of organolithium reagents in the structures of derived lithiated products is rare and unusual but this phenomenon has been observed before. For example, in the complex,  $[(\text{Ph}_2\text{NLi})\{((2\text{-LiC}_6\text{H}_4)\text{Ph})(\text{NLi})\}_2(\text{LiBu}^n)_2(\text{Et}_2\text{O})_4]$ ,<sup>[35]</sup> two doubly deprotonated amide ligands ( $\text{LiN}(2\text{-LiC}_6\text{H}_4)\text{Ph}$ ) and two  $\text{Li}_3\text{---}\mu_3\text{-Bu}^n$  units form an array not that dissimilar to that of  $[\text{Li}_2(\text{L}^*)(\text{OEt}_2)\text{Li}(\text{Bu}^n)]_2$  (see below).

The solid state structure of  $[\text{Li}_2(\text{L}^*)(\text{OEt}_2)\text{Li}(\text{Bu}^n)]_2$ , shown in *Figure 7.20*, consists of a hexalithium aggregate built up by two  $\text{Li}_2(\text{L}^*)(\text{OEt}_2)$  units and two  $\text{LiBu}^n$  molecules. The crystallographic details are given in *Table 7.7*, and selected bond distances and angles are tabulated in *Table 7.8*. The two  $\text{Li}_2(\text{L}^*)(\text{OEt}_2)$  units are linked by a central  $\text{Li}_2\text{C}_2$  core that is situated on a crystallographic inversion centre. This core comprises the phenyl

carbons C(112) on  $L^*$  and its symmetry equivalent (C(112A)) which bridge between Li(2) and Li(2A) (see *Diagram 3*). The  $L^*$  binds to Li(1) and Li(3) via  $\mu$ -NSiMe<sub>3</sub> and chelates to Li(1) by coordination of the OPh arm. The remaining lithium Li(2), and its symmetry generated Li(2A) are bound to  $L^*$  solely by the  $\mu$ - $\eta^1:\eta^1$ -C<sub>6</sub>H<sub>4</sub> unit, each further supported by a  $\pi$ - $\eta^2$ -arene—lithium interaction with the  $L^*$  backbone. This contrasts the situation in  $[\text{Li}(L^*)(\text{OEt}_2)\text{Li}_2(L^*)]_2(\text{diglyme})$  which shows N,O,C chelation to a single lithium, in addition to  $\mu$ -NSiMe<sub>3</sub>,  $\mu$ -OPh and  $\mu$ -C<sub>6</sub>H<sub>4</sub> fragments.

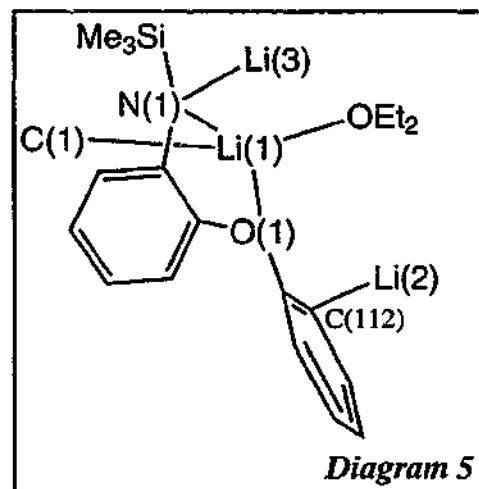


The lithium atom (Li(1)) attached to the  $\text{Li}_2(L^*)(\text{OEt}_2)$  unit, is binding to N(1) and O(1) atoms and is in the plane with the arene backbone (C(11)-C(16)). The C—O(phenoxy) bond (C(111)—O(1)) is also in this plane (torsion angle C(13)—C(12)—O(1)—C(111)  $-18.7(3)^\circ$ ) but the arene ring planes are twisted by  $88.55(6)^\circ$ . A molecule of LiBu<sup>n</sup> (Li(3)) is positioned above and another below (Li(3A)) the central  $\text{Li}_2\text{C}_2$  core resulting in a central organolithium array (comprising Li(3), C(1), Li(2), C(112), C(112A), Li(2A), C(1A) and Li(3A)). Each butyl group is attached to Li(1-3) through the  $\alpha$ -carbon atom (C(1),

C(1A)). The array is sandwiched between two organoamidolithium units with the overall central corridor consisting of Li, N and C atoms in an 'S' shaped ladder (*Diagram 4*).

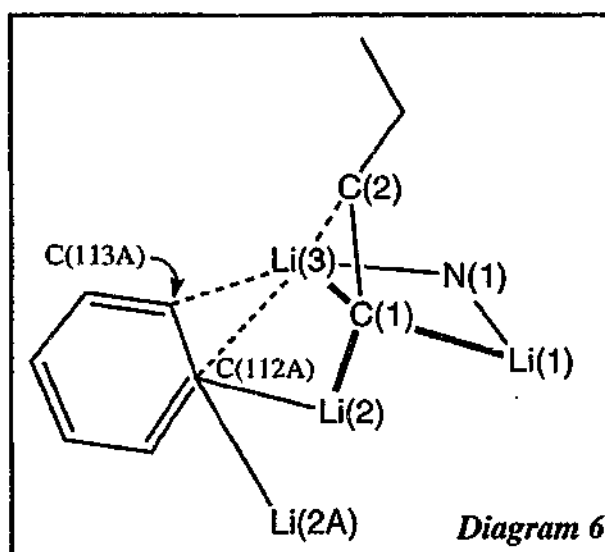
Each lithium atom in the asymmetric unit in  $[\text{Li}_2(\text{L}^*)(\text{OEt}_2)\text{Li}(\text{Bu}^n)]_2$  is unique. The four-coordinate Li(1) environment comprises an amide nitrogen atom (N(1)), the phenoxy oxygen and diethyl ether oxygen atoms (O(1) and O(2)) and the  $\alpha$ -carbon atom (C(1)) of the  $\text{Bu}^n$  group in an approximately tetrahedral geometry (*Diagram 5*). The amide nitrogen (N(1)) and the  $\alpha$ -C (C(1)) are bridging to Li(3).

Similarly  $[\{\text{Li}(\text{L}^3)(\text{Et}_2\text{O})\text{Li}_2(\text{L}^*)\}_2(\text{diglyme})]$  has the amide nitrogen atoms on  $\text{L}^3$  and  $\text{L}^*$  bridging two lithium atoms (*Figure 7.19*). The Li—N(1) and Li(1)—O(OAr<sub>2</sub> and OEt<sub>2</sub>) bond distances in  $[\text{Li}_2(\text{L}^*)(\text{OEt}_2)\text{Li}(\text{Bu}^n)]_2$  (*Table 7.8*) are similar to the corresponding bond lengths in the related complex  $[\{\text{Li}(\text{L}^3)(\text{OEt}_2)\text{Li}_2(\text{L}^*)\}_2(\text{diglyme})]$ . A different combination of atoms surrounds the second lithium,



Li(2), which is coordinated solely by the carbon atoms C(1), C(112), C(12) and C(13) (*Diagram 5*). The closest interactions are to the  $\alpha$ -carbon (C(1)) on the  $\text{Bu}^n$  group and the *ortho* carbon atom (C(112)) on  $\text{L}^*$ . Carbon atoms C(112) and C(112A) are bridging between Li(2) and Li(2A) and are highly unsymmetrical (difference *ca.* 0.40 Å), contrasting the  $\mu$ - $\eta^1:\eta^1$ -Ar bridging (difference *ca.* 0.10 Å) in  $[\{\text{Li}(\text{L}^3)(\text{OEt}_2)\text{Li}_2(\text{L}^*)\}_2(\text{diglyme})]$ . The Li(2)—C(112) bond length is comparable to the analogous bonding in  $[\{\text{Li}(\text{L}^3)(\text{OEt}_2)\text{Li}_2(\text{L}^*)\}_2(\text{diglyme})]$  but Li(2)—C(112A) is remarkably long for a  $\sigma$ -Li—C bond and even approaches the limit for a neutral  $\pi$ -arene—Li interaction (see below). Furthermore, Li(2) is supported by secondary interactions from C(12A) and C(13A) of the arene backbone of the symmetry generated ligand  $\text{L}^*$ . The Li(2)—C(12A) and Li(2)—C(13A) bond lengths are near equal ( $\pm 0.013$  Å) and are significantly longer than Li(2)—C(112) and Li(2)—C(1) but are shorter than Li(2)—C(112A). The bonding is best described as a neutral  $\pi$ - $\eta^2$ -arene—Li interaction since Li(2) is almost perpendicular to the C(11A)—C(16A) ring plane (the angle defined by Li(2)—centre of the C(12A) and C(13A) bond—centre of arene ring (C11A)-C(16A)) is 98.7°). Many examples are known with this bonding type and typical Li—C values are between 2.28—2.77 Å. [36-38]

The remaining Li(3) atom is ligated by a bridging amide nitrogen (N(1)) and the  $\alpha$ -carbon atom C(1) of the Bu<sup>n</sup> group. The latter atom C(1) is bonded to all three lithium atoms (see *Diagram 6*). The bridging amide nitrogen distance Li(3)—N(1) is similar to Li(1)—N(1) in [Li<sub>2</sub>(L\*)(OEt<sub>2</sub>)Li(Bu<sup>n</sup>)]<sub>2</sub> (see above) but Li(3)—C(1) is 0.207 Å shorter than Li(1)—C(1) (*Table 7.8*). In a manner similar to Li(2) (see above), Li(3) interacts with two arene carbon atoms (C112A and



C(113A)), in this case from the phenyl substituent of L\*A. The *ortho* phenyl carbon atoms, C(112) and C(112A), each bridge three lithium atoms, but only two are unique (Li(2), Li(3)) with the other (Li(2A)) generated by symmetry. The similar Li(3)—C(112A)/C(113A) bond distances (*Table 7.8*) are near the lower limit of the range for a  $\pi$ - $\eta^2$ -arene—Li interaction (see above), they are significantly shorter than Li(2)—C(112A)/C(113A) and are close to the  $\sigma$ -bonded Li(2)—C(1) and Li(1)—C(1) distances. Accordingly they have considerable  $\sigma$ -bond character as is also indicated by the Li(3)—centre of the C(112A) and C(113A) bond—centre of the phenyl ring (C(111A)—C(116A)) angle (131.9°) which is much larger than expected (90°) for a  $\pi$ -phenyl-Li interaction.

The coordination of the butyl group is primarily from C(1) which bridges three unique Li atoms (Li(1), Li(2) and Li(3)). This parallels the bonding in [Li(Bu<sup>n</sup>)]<sub>6</sub> and is further supplemented by a weak agostic interaction between the lithium atom Li(3) and the  $\beta$ -C (C(2)) of the Bu<sup>n</sup> chain (*Table 7.8*). This Li(3)—C(2) distance is longer than in the parent [Li(Bu<sup>n</sup>)]<sub>6</sub> (Li— $\beta$ -C 2.287 Å)<sup>[39]</sup> but is presumably shorter than in the related complex [(Ph<sub>2</sub>NLi){2-LiC<sub>6</sub>H<sub>4</sub>}NLi]<sub>2</sub>(LiBu<sup>n</sup>)<sub>2</sub>(Et<sub>2</sub>O)<sub>4</sub> for which no Li— $\beta$ -C distance was given.<sup>[35]</sup> Whilst in [Li<sub>2</sub>(L\*)(OEt<sub>2</sub>)Li(Bu<sup>n</sup>)]<sub>2</sub> the  $\mu_3$ - $\alpha$ -C distances vary considerably (2.143(4)-2.359(4) Å), the corresponding  $\mu_3$ - $\alpha$ -C distances of [Li(Bu<sup>n</sup>)]<sub>6</sub> have two shorter (in the range 2.137(3)-2.175(3) Å) and one longer bond (in the range 2.227(3)-2.262(3) Å).



Table 7.7 Summary of Crystallographic Data for  $[\text{Li}_2(\text{L}^*)(\text{OEt}_2)\text{Li}(\text{Bu}^n)]_2$  and  $[\text{Li}_2(\text{L}^*)(\text{DME})]_2$

Compound	$[\text{Li}_2(\text{L}^*)(\text{OEt}_2)\text{Li}(\text{Bu}^n)]_2$	$[\text{Li}_2(\text{L}^*)(\text{DME})]_2$
Formula	$\text{C}_{36}\text{H}_{68}\text{Li}_6\text{N}_2\text{O}_4\text{Si}_2$	$\text{C}_{38}\text{H}_{54}\text{Li}_4\text{N}_2\text{O}_6\text{Si}_2$
<i>M</i>	810.84	718.78
<i>a</i> (Å)	12.9117(2)	22.1749(10)
<i>b</i> (Å)	11.5166(3)	14.3421(6)
<i>c</i> (Å)	16.9667(5)	34.5285(11)
$\alpha$ (°)	90	90
$\beta$ (°)	100.243(2)	105.890(3)
$\gamma$ (°)	90	90
<i>V</i> (Å <sup>3</sup> )	2482.7(9)	10562(4)
Crystal system	<i>P2<sub>1</sub>/n</i>	<i>P2<sub>1</sub>/n</i>
Space Group	monoclinic	monoclinic
<i>Z</i>	2(dimers)	10(dimers)
Diffractometer	Nonius Kappa CCD	Nonius Kappa CCD
$\rho_{\text{calc}}$ (g cm <sup>-3</sup> )	1.085	1.130
$\mu(\text{MoK}\alpha)$ (mm <sup>-1</sup> )	0.111	0.126
$2\theta_{\text{max}}$ (°)	56.5	56.6
<i>N</i> , <i>N<sub>o</sub></i>	5851, 3955	14985, 6567
<i>R</i> , <i>R<sub>w</sub></i> (observed data)	0.056, 0.126	0.110, 0.274
<i>R</i> , <i>R<sub>w</sub></i> (all data)	0.100, 0.143	0.228, 0.343

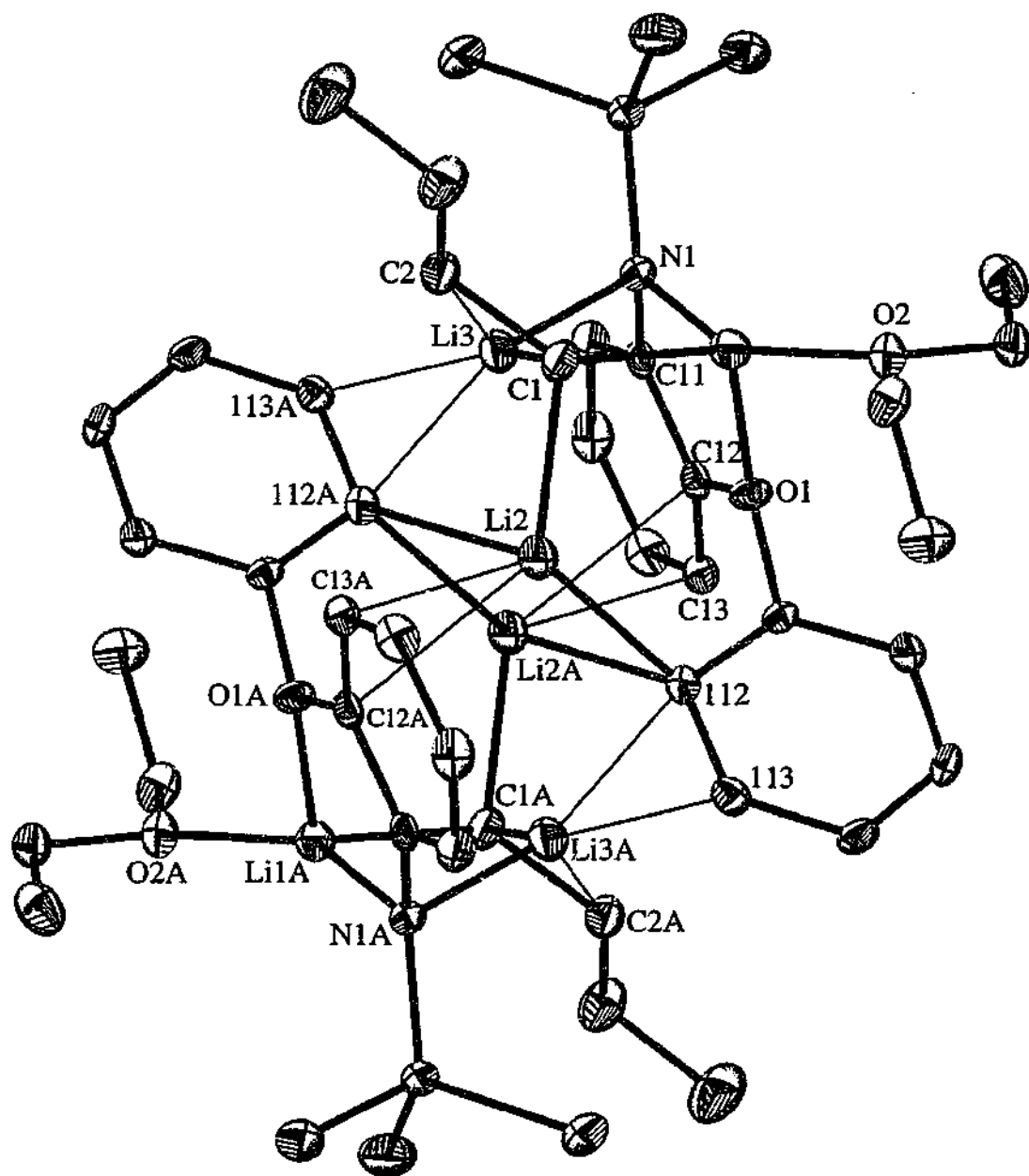


Figure 7.20 Molecular Structure of  $[\text{Li}_2(\text{L}^*)(\text{OEt}_2)\text{Li}(\text{Bu}^n)]_2$

Table 7.8 The lithium environments in  $[\text{Li}_2(\text{L}^*)(\text{OEt}_2)\text{Li}(\text{Bu}^n)]_2$ 

Li(1)—O(1)	1.948(4)	O(1)—Li(1)—O(2)	102.7(2)
Li(1)—O(2)	1.973(4)	O(1)—Li(1)—N(1)	82.8(1)
Li(1)—N(1)	2.057(4)	O(2)—Li(1)—N(1)	147.5(2)
Li(1)—C(1)	2.350(4)	O(1)—Li(1)—C(1)	116.1(2)
		O(2)—Li(1)—C(1)	105.3(2)
		N(1)—Li(1)—C(1)	100.5(2)
Li(2)—C(112)	2.189(4)	C(112)—Li(2)—C(112A) <sup>a</sup>	109.8(2)
Li(2)—C(112A) <sup>a</sup>	2.660(4)	C(1)—Li(2)—C(112)	128.9(2)
Li(2)—C(1)	2.226(4)	C(1)—Li(2)—C(112A) <sup>a</sup>	97.1(2)
Li(2)—C(12A) <sup>a</sup>	2.596(4)	C(112)—Li(2)—C(1C) <sup>b</sup>	115.7(5)
Li(2)—C(13A) <sup>a</sup>	2.583(4)	C(112A)—Li(2)—C(1C) <sup>a,b</sup>	79.9(5)
		C(1)—Li(2)—C(1C) <sup>b</sup>	111.1(5)
Li(3)—N(1)	2.016(4)	N(1)—Li(3)—C(1)	109.3(2)
Li(3)—C(1)	2.143(4)	N(1)—Li(3)—C(11C) <sup>c</sup>	121.8(5)
Li(3)—C(2)	2.419(4)	C(1)—Li(3)—C(11C) <sup>c</sup>	127.1(5)
Li(3)—C(112A) <sup>a</sup>	2.241(4)		
Li(3)—C(113A) <sup>a</sup>	2.304(4)		

Symmetry transformations used to generate equivalent atoms:

<sup>a</sup>  $-x, -y+1, -z$ , <sup>b</sup> C(1C) = centroid of C(12A) and C(13A), <sup>c</sup> C(11C) = centroid of C(112A) and C(113A)

$^1\text{H}$  NMR studies on a  $\text{C}_7\text{D}_8$  solution of  $[\text{Li}_2(\text{L}^*)(\text{OEt}_2)\text{Li}(\text{Bu}^n)]_2$  revealed a temperature dependent species to be present. At room temperature the  $^1\text{H}$  spectrum shows broad  $\alpha$ ,  $\beta$  and  $\gamma$ - $\text{CH}_2$  resonances from the  $\text{LiBu}^n$  unit in addition to a single peak for the  $\text{SiMe}_3$  group and poorly resolved aromatic signals from  $\text{L}^*$ . In contrast, the signal from  $\text{Et}_2\text{O}$  is well defined and in a similar position to that of free diethyl ether. On cooling to  $-90^\circ\text{C}$  the spectrum is well resolved and reveals a single set of  $\text{L}^*$  peaks as expected from the solid state structure. The  $\alpha$ - $\text{CH}_2$  methylene signal of butyllithium splits into two broad multiplets centred at  $-1.16$  and  $-1.02$  ppm, close to the values observed for  $\text{LiBu}^n$ . Similarly, the  $\text{Et}_2\text{O}$  signal divides into two resonances and suggests that the ether ligands are also mobile in solution. These data could suggest that  $[\text{Li}_2(\text{L}^*)(\text{OEt}_2)\text{Li}(\text{Bu}^n)]_2$  dissociates into  $\text{Li}_2(\text{L}^*)$  and  $\text{LiBu}^n$  species in solution. However, the variable temperature  $^7\text{Li}$  NMR spectra (*Figure 7.21*) resolves into three peaks at  $-90^\circ\text{C}$  in agreement with the solid state structure of  $[\text{Li}_2(\text{L}^*)(\text{OEt}_2)\text{Li}(\text{Bu}^n)]_2$  which has three different lithium environments. When the sample is heated the lithium resonances broaden to become two at  $-60^\circ\text{C}$  then a singlet at  $0^\circ\text{C}$ , observations which are consistent with the ill-resolved  $^1\text{H}$  NMR spectra at such temperatures.

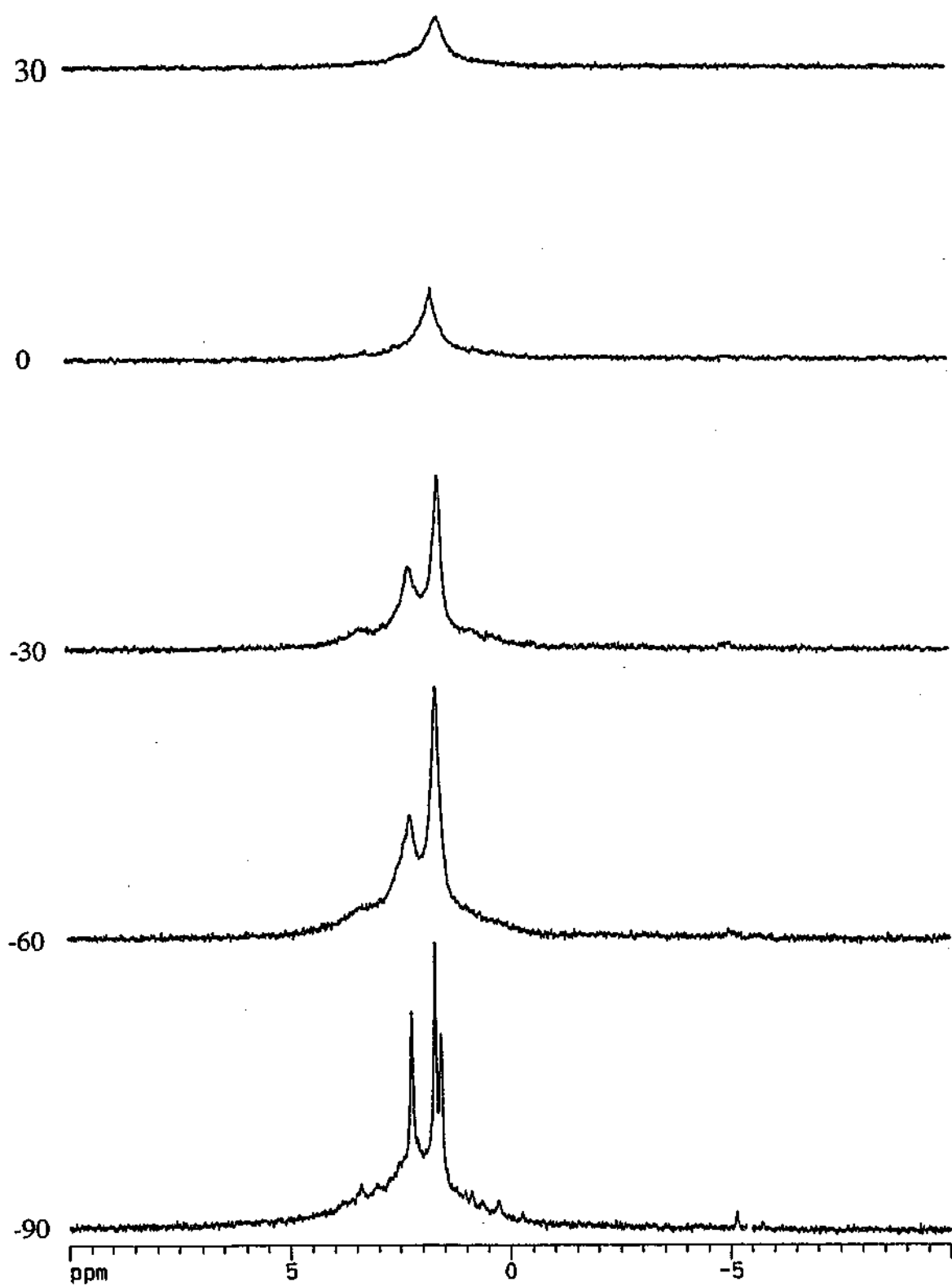


Figure 7.21  ${}^7\text{Li}$  NMR Spectra for  $[\text{Li}_2(\text{L}^*)(\text{OEt}_2)\text{Li}(\text{Bu}^n)]_2$  in  $\text{C}_7\text{H}_8$  at variable temperatures

The removal of  $\text{LiBu}^n$  from  $[\text{Li}_2(\text{L}^*)(\text{OEt}_2)\text{Li}(\text{Bu}^n)]_2$  was achieved using the chelating donor DME giving  $[\text{Li}_2(\text{L}^*)(\text{DME})]_2$  (Figure 7.22). Suitable crystals for X-ray analysis were grown on work up from a mixture of DME:hexane (1:30). The molecular structure was a dimer with the crystal lattice composed of 5 dimers per unit cell. Due to rapid decomposition of the crystal within the X-ray beam only limited data were collected, but these were sufficient to unambiguously establish atom connectivity of  $[\text{Li}_2(\text{L}^*)(\text{DME})]_2$ . Selected bond distances and angles for one dimer are listed in Table 7.9.

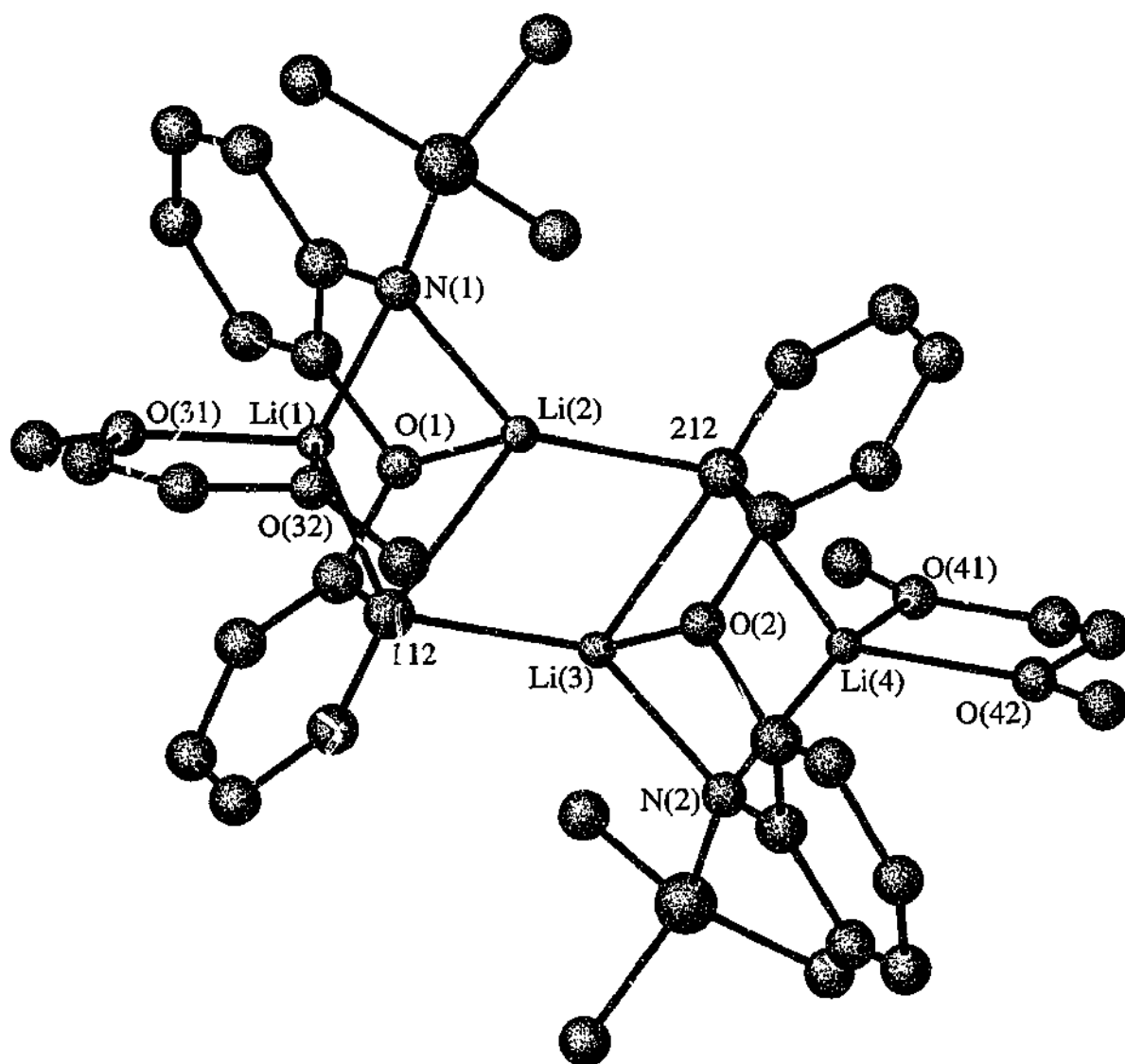
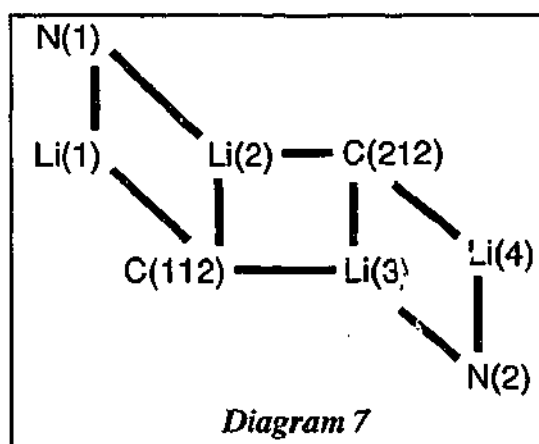


Figure 7.22 Molecular Structure of  $[\text{Li}_2(\text{L}^*)(\text{DME})]_2$

In a similar manner to  $[\text{Li}_2(\text{L}^*)(\text{OEt}_2)\text{Li}(\text{Bu}^n)]_2$  the *ortho* phenyl carbon atoms (C(112) and C(212)) from two  $\text{L}^*$  ligands in  $[\text{Li}_2(\text{L}^*)(\text{DME})]_2$  each bridge to the same two lithium atoms (Li(2) and Li(3)) and result in a central Li(2)C(112)Li(3)C(212) core. However, Li(2) and Li(3) are also bonded to the N and O donor atoms on their respective  $\text{L}^*$  group which is similar to the  $\text{L}^*$  environment in  $[\{\text{Li}(\text{L}^3)(\text{Et}_2\text{O})\text{Li}_2(\text{L}^*)\}_2(\text{diglyme})]$ , rather than to the carbon atoms in  $[\text{Li}_2(\text{L}^*)(\text{OEt}_2)\text{Li}(\text{Bu}^n)]_2$ . The carbon atoms C(112) and C(212) of the deprotonated phenyl substituent also bridge to Li(1) and Li(4) respectively, and thus are both coordinated to three lithium atoms (C(112) to Li(1), Li(2) and Li(3); C(212) to Li(2), Li(3) and Li(4)). The Li(1) and Li(4) environments are completed by a bridging amide nitrogen atom (N(1) or N(2)) on the respective  $\text{L}^*$  ligands and two oxygen atoms from a chelating DME. Overall a four-rung ladder comprising only Li, N and C atoms is formed (*Diagram 7*), with a molecule of DME coordinatively saturating the Li(1) and Li(4) atoms and preventing further association.



The arene ring disposition in  $[\text{Li}_2(\text{L}^*)(\text{DME})]_2$  is similar to those of  $\text{L}^*$  in  $[\{\text{Li}(\text{L}^3)(\text{OEt}_2)\text{Li}_2(\text{L}^*)\}_2(\text{diglyme})]$  rather than in  $[\text{Li}_2(\text{L}^*)(\text{OEt}_2)\text{Li}(\text{Bu}^n)]_2$ , with the phenoxy substituent pulled out of the plane of the arene backbone (C(X3)—C(X2)—O(X)—C(X11) (X= 1,2,5,6,9 derived from the 2.5 dimers per asymmetric unit) 93.7(3)-98.4(3)°) and the phenyl ring rotated by 58.2(2)-65.3(2)°. This presumably results from the interaction of the *ortho* phenyl carbon atom and the oxygen with the same lithium atom.

Table 7.9 The lithium environments in  $[\text{Li}_2(\text{L}^*)(\text{DME})]_2^a$ .

Li(1)—N(1)	2.04(1)	N(1)—Li(1)—C(112)	103.0(7)
Li(1)—C(112)	2.25(1)	N(1)—Li(1)—O(31)	115.0(5)
Li(1)—O(31)	1.96(1)	N(1)—Li(1)—O(32)	131.0(6)
Li(1)—O(32)	1.98(2)	C(112)—Li(1)—O(31)	114.7(5)
Li(2)—N(1)	2.01(1)	C(112)—Li(1)—O(32)	109.3(5)
Li(2)—O(1)	2.015(9)	O(31)—Li(1)—O(32)	83.7(6)
Li(2)—C(112)	2.30(1)	N(1)—Li(2)—O(1)	86.9(4)
Li(2)—C(212)	2.18(1)	N(1)—Li(2)—C(112)	102.3(5)
		N(1)—Li(2)—C(212)	130.0(5)
		O(1)—Li(2)—C(112)	67.7(3)
		O(1)—Li(2)—C(212)	139.5(7)
		C(112)—Li(2)—C(212)	111.3(4)

<sup>a</sup> for one of the independent molecules only.

At room temperature the  $^1\text{H}$  NMR spectrum of  $[\text{Li}_2(\text{L}^*)(\text{DME})]_2$  is well resolved and shows the expected single  $\text{L}^*$  pattern as well as DME resonances in a 1:1 ratio. These DME resonances are in the region found for free DME and this suggests that they are mobile in solution. However, only one  $^7\text{Li}$  NMR resonance was observed both at room temperature and on cooling to  $-90^\circ\text{C}$ . This is not consistent with the two lithium environments observed in the solid state and may be the result of a rapidly exchanging species in solution, or simply a coincidence of two overlapping lithium resonances.

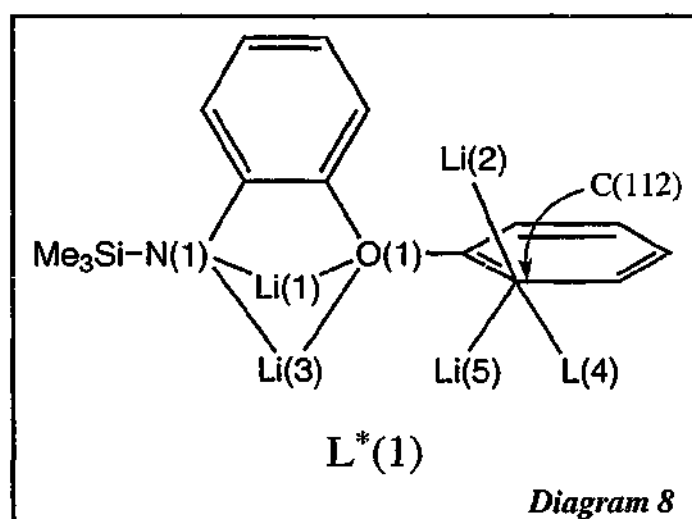


### 7.2.4 Attempted Reactions of $\text{Li}_2(\text{L}^*)$ with Lanthanoid Chlorides

The chemistry of the doubly deprotonated  $\text{L}^*$  ligand with the lanthanoid elements was briefly explored with a surprising and exciting outcome. An *in situ* metathesis reaction was examined where  $\text{L}^*\text{H}$  was treated with two equivalents of  $\text{LiBu}^n$  in diethyl ether and, after the reaction was complete, one equivalent of anhydrous  $\text{LnCl}_3$  (La, Nd, Yb) was added. No reaction was observed for neodymium and ytterbium, but work up of the lanthanum reaction mixture with hexane yielded colourless crystals. The crystals were identified as a decalithium aggregate,  $[\{\text{Li}_2(\text{L}^*)\}_2(\text{LiOEt})(\text{OEt}_2)]_2 \cdot (\text{hexane})$ , rather than a lanthanum complex.

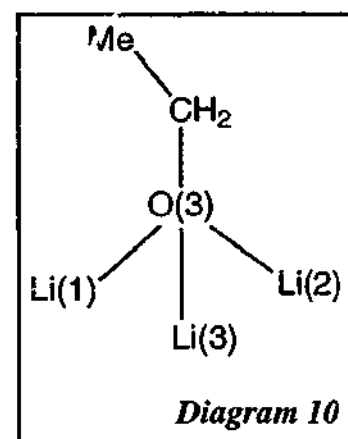
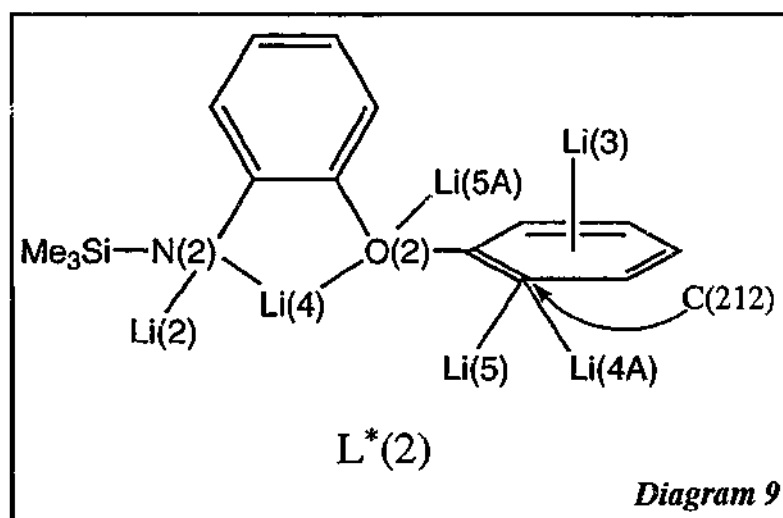
The X-ray structure of  $[\{\text{Li}_2(\text{L}^*)\}_2(\text{LiOEt})(\text{OEt}_2)]_2 \cdot (\text{hexane})$  shows a centrosymmetric decalithium aggregate (*Figure 7.23*) located at each of the eight unit cell vertices, with a molecule of hexane positioned in a channel parallel to the *a* axis in the centre of the unit cell (*Figure 7.24*). The complex  $[\{\text{Li}_2(\text{L}^*)\}_2(\text{LiOEt})(\text{OEt}_2)]_2$  has four  $\text{Li}_2(\text{L}^*)$  units and two  $\text{Li}(\text{OEt})$  groups with the latter presumably derived from ether cleavage. The asymmetric unit consists of five different lithium coordination spheres with two  $\text{L}^*$  ligands ( $\text{L}^*(1)$  and  $\text{L}^*(2)$ ) and an ethoxide group. Crystallographic details and refinement parameters are presented in *Table 7.10*. Important bond lengths and angles are listed in *Table 7.11*. The outer  $\text{L}^*(1)$

ligand (*Diagram 8*) is coordinated to five lithium atoms, with two Li atoms ( $\text{Li}(1)$  and  $\text{Li}(3)$ ) chelated by  $\text{N}(1)$  and  $\text{O}(1)$  and the remaining  $\text{Li}(2)$ ,  $\text{Li}(4)$  and  $\text{Li}(5)$  atoms ligated by the *ortho* phenyl carbon ( $\text{C}(112)$ ) in a  $\mu_3$ -arrangement. The  $\text{N}(1)$  and  $\text{O}(1)$  atoms are in the plane of the arene backbone ( $\text{C}(11)$ – $\text{C}(16)$ ) with



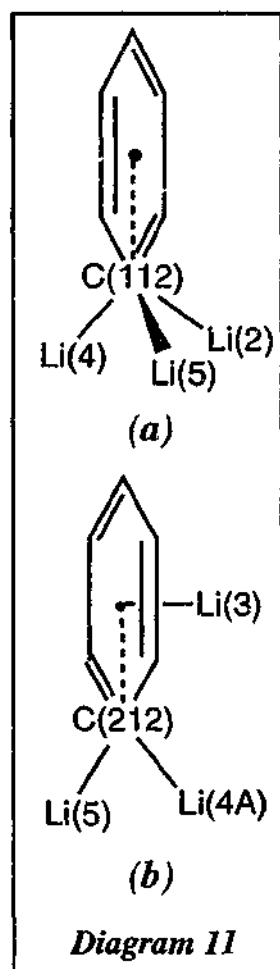
the  $\text{C}-\text{O}(\text{phenoxy})$  bond ( $\text{C}(111)-\text{O}(1)$ ) in this plane (torsion angle  $\text{C}(13)-\text{C}(12)-\text{O}(1)-\text{C}(111) -21.9(4)^\circ$ ) but the arene ring planes are rotated (interplanar angle  $70.6(1)^\circ$ ) similar to the relative disposition of the arene rings in  $[\text{Li}_2(\text{L}^*)(\text{OEt}_2)\text{Li}(\text{Bu}^n)]_2$  (torsion angle  $\text{C}(13)-\text{C}(12)-\text{O}(1)-\text{C}(111) -18.7(3)^\circ$ ; interplanar angle  $85.51(6)^\circ$ ).

The hexalithium arrangement surrounding  $L^*(2)$  (*Diagram 9*) has N(2) and O(2) chelating to one lithium atom (Li(4)) and each bridging separately to two other lithium centres (Li(2) and Li(5A) respectively). The *ortho* phenyl carbon (C(212)) bridges three lithium centres with two lithium atoms (Li(4A) and Li(5)) binding to C(212) in a  $\mu\text{-}\eta^1\text{:}\eta^1$  fashion and Li(3) to the phenyl substituent (C(211)-C(216)) in an  $\eta^6$ -arrangement. The ring planes (C(21)-C(26), C(211)-C(216)) in  $L^*(2)$  (interplanar angle  $63.3(1)^\circ$ ) have a similar rotation to  $L^*(1)$  (see above) but the phenyl ring is pulled further out from the arene backbone plane (C(23)—C(22)—O(2)—C(211)  $-52.0(3)^\circ$ ). The rotation between the arene planes in  $L^*(1)$  and  $L^*(2)$  differs from other  $L^*$  ligands (see above) and resembles  $L^3$  in  $[\text{Li}(L^3)(\text{DME})]$ . The third anion in the asymmetric unit is the ethoxide group (*Diagram 10*) which is bound to three lithium atoms, Li1, Li2 and Li3. The bridging nitrogen atoms in  $L^*(1)$  and  $L^*(2)$  have Li—N(amide) distances (*Table 7.II*) well within the range seen for  $L^*$  in  $[\{\text{Li}(L^3)(\text{OEt}_2)\text{Li}_2(L^*)\}_2(\text{diglyme})]$ ,  $[\text{Li}_2(L^*)(\text{OEt}_2)\text{Li}(\text{Bu}^n)]_2$  and  $[\{\text{Li}_2(L^*)\}_2(\text{LiOEt})(\text{OEt}_2)]_2$ .



The outer lithium (Li(1)) is four-coordinate with chelating N(1) and O(1) atoms from  $L^*(1)$ , an ethoxide oxygen (O(3)) and a molecule of  $\text{Et}_2\text{O}$  which presumably inhibits further association, in a distorted tetrahedral geometry. The N(1), O(1) and O(3) atoms are also bound to Li(3) which is also coordinated in an  $\eta^6$ -arrangement by the phenyl group on  $L^*(2)$ . In addition, the ethoxide oxygen (O(3)) further binds to Li(2) and also Li(1). The three-coordinate Li(2) is bound by O(3), N(2) and C(112) atoms in a trigonal planar geometry ( $\Sigma 359.9^\circ$ ). Thus the three superbases - alkoxide, amide and carbanion surround this single lithium atom. The nearest related system is the

bimetallic complex  $[\text{Li}_4\text{Na}_4(\text{Bu}'\text{O})_4\{\text{PhN}(\text{H})\}_4(\text{NaOH})(4\text{-Me-py})_4]$ , which displays a lithium atom coordinated by hydroxide, alkoxide and amide groups.<sup>[40]</sup> The phenyl carbon C(112) of L\*(1) also coordinates to Li(4) and Li(5) whilst the nitrogen N(2) chelates with O(2) to Li(4). The Li(2)—C(112) bond length (2.367(5) Å) is considerably longer than Li(4)—C(112) (2.251(5) Å) or Li(5)—C(112) (2.171(5) Å) or lithium—carbon distances in other aryl lithium aggregates which contain a similar  $\mu_3$ -aryl—Li<sub>3</sub> unit (e.g.



$[\text{Li}(3,5\text{-}(\text{Bu}')_2\text{C}_6\text{H}_3)]_6$ : Li—C 2.119(7) – 2.247(7) Å<sup>[41]</sup>). Whilst the *ortho* phenyl carbon in L\*(2) interacts in a  $\mu\text{-}\eta^1\text{:}\eta^1$  fashion to Li(5) and the symmetry related Li(4A), it also coordinates more weakly to Li(3) through a  $\eta^6\text{-}\pi\text{-Ph}$  interaction. The Li— $\mu\text{-C}$ (212) distances are shorter than Li— $\mu\text{-C}$ (112) of L\*(1) (see above). The orientation of the lithium atoms Li(2), Li(4) and Li(5) (*Diagram 11 (a)*) and Li(4A) and Li(5) (*Diagram 11 (b)*) with respect to the associated phenyl ring plane (Li—C to C<sub>6</sub> ring plane angles 0.4 – 59.2°) suggest predominately  $\sigma\text{-Li—C}$  bonding. Likewise the Li(3)—centre of C(211)—C(216)—C(21X) (X = 1-6) angles are close to 90° as expected for a neutral  $\pi\text{-}\eta^6\text{-arene—Li}$  interaction. The Li(3)—C(21X) (X = 1-6) distances (av. 2.62 Å) are towards the longer extreme of the range (2.28 – 2.77 Å)<sup>[36-38]</sup> previously reported for neutral arene lithium interactions, though the Li—C( $\pi\text{-phenyl}$ ) distances are much less than the sum (3.30 Å) of the metallic radius for Li<sup>[42]</sup> and the van der Waals radius of an arene ring.<sup>[43]</sup> A closer approach of Li(3) to the phenyl ring (C(211) – C(216)) is most likely prevented by the bonding of the *ortho*

phenyl carbon (C(212)) and of O(2) to Li(4A) and Li(5) to give a constraining four-membered ring. The geometry about the three-coordinate Li(3) environment is pyramidal but with the  $\eta^6\text{-}\pi\text{-Ph}$  interaction it becomes pseudo tetrahedral and six-coordinate. The Li(4) centre is four-coordinate in a triangular pyramidal arrangement and Li(5), like Li(2), is trigonal planar ( $\Sigma(\circ)$  351.0), though with more deviation from triangular.

The Li—O(3) bond lengths are unsymmetrical with one shorter Li(2)—O(3) (1.839(5) Å) and two longer (Li(1)—O(3) 1.918(5) Å, Li(3)—O(3) 1.890(5) Å) distances, though all are in the reported range for RO—Li. The  $\mu_3$ -alkoxide—Li<sub>3</sub> configuration is

typical of lithium aggregates containing bulky alkoxides,  $[\text{Li}(\text{OR})]_n$  ( $n = 4, 6$ )<sup>[44-46]</sup> and the rarely incorporated small OEt anion of  $[\{\text{Li}_2(\text{L}^*)\}_2(\text{LiOEt})(\text{OEt}_2)]_2$  is presumably stabilised against dissociation by the two bulky  $\text{SiMe}_3$  groups on  $\text{L}^*(1)$  and  $\text{L}^*(2)$  and the  $\text{OEt}_2$  ligand.

A  $^7\text{Li}$  and  $^1\text{H}$  NMR study on  $[\{\text{Li}_2(\text{L}^*)\}_2(\text{LiOEt})(\text{OEt}_2)]_2$ .hexane in  $\text{C}_7\text{D}_8$  reveals a temperature dependent species which at room temperature shows some broad peaks which are better resolved at low temperatures. The  $^7\text{Li}$  spectrum at room temperature showed four peaks at -2.57, 0.68, 1.16, 2.27 ppm with the last being relatively sharp despite having a broad baseline. On lowering the temperature to  $0^\circ\text{C}$  the peak which appeared at 1.16 ppm at room temperature splits into two (1.67 and 1.12 ppm) while the peak at -2.57 ppm broadens. Further cooling to  $-60^\circ\text{C}$  results in a very broad spectrum but at  $-90^\circ\text{C}$  higher resolution is achieved. At this temperature, five distinct lithium environments are observed which suggests that the solid state structure of  $[\{\text{Li}_2(\text{L}^*)\}_2(\text{LiOEt})(\text{OEt}_2)]_2$ .hexane is attained in solution. The  $^1\text{H}$  NMR spectrum at room temperature has features revealing two  $\text{SiMe}_3$  groups and two sets of  $\text{L}^*$  resonances consistent with the two different ligands  $\text{L}^*(1, 2)$ . Whilst the methyl protons on the  $\text{Et}_2\text{O}$  and  $\text{OEt}$  ligands are well resolved suggesting they are freely rotating in solution, the methylene protons cannot be seen due to overlap with the hexane signal. Decreasing the temperature to  $-60^\circ\text{C}$  resulted in better resolution, in particular for the aromatic region which showed two well defined  $\text{L}^*$  ligand environments. In a similar manner to the NMR data obtained for  $[\text{Li}_2(\text{L}^*)(\text{OEt}_2)\text{Li}(\text{Bu}^n)]_2$  (see above), the methylene groups of  $[\{\text{Li}_2(\text{L}^*)\}_2(\text{LiOEt})(\text{OEt}_2)]_2$ .hexane divide into two resonances which suggests that they are still mobile at this temperature. The NMR results suggest that the solid state structure of  $[\{\text{Li}_2(\text{L}^*)\}_2(\text{LiOEt})(\text{OEt}_2)]_2$  remains intact at  $-90^\circ$  (although the signals are broad due to precipitation of the complex at this temperature) as was also observed for  $[\{\text{Li}(\text{L}^3)(\text{OEt}_2)\text{Li}_2(\text{L}^*)\}_2(\text{diglyme})]$  and  $[\text{Li}_2(\text{L}^*)(\text{OEt}_2)\text{Li}(\text{Bu}^n)]_2$ .

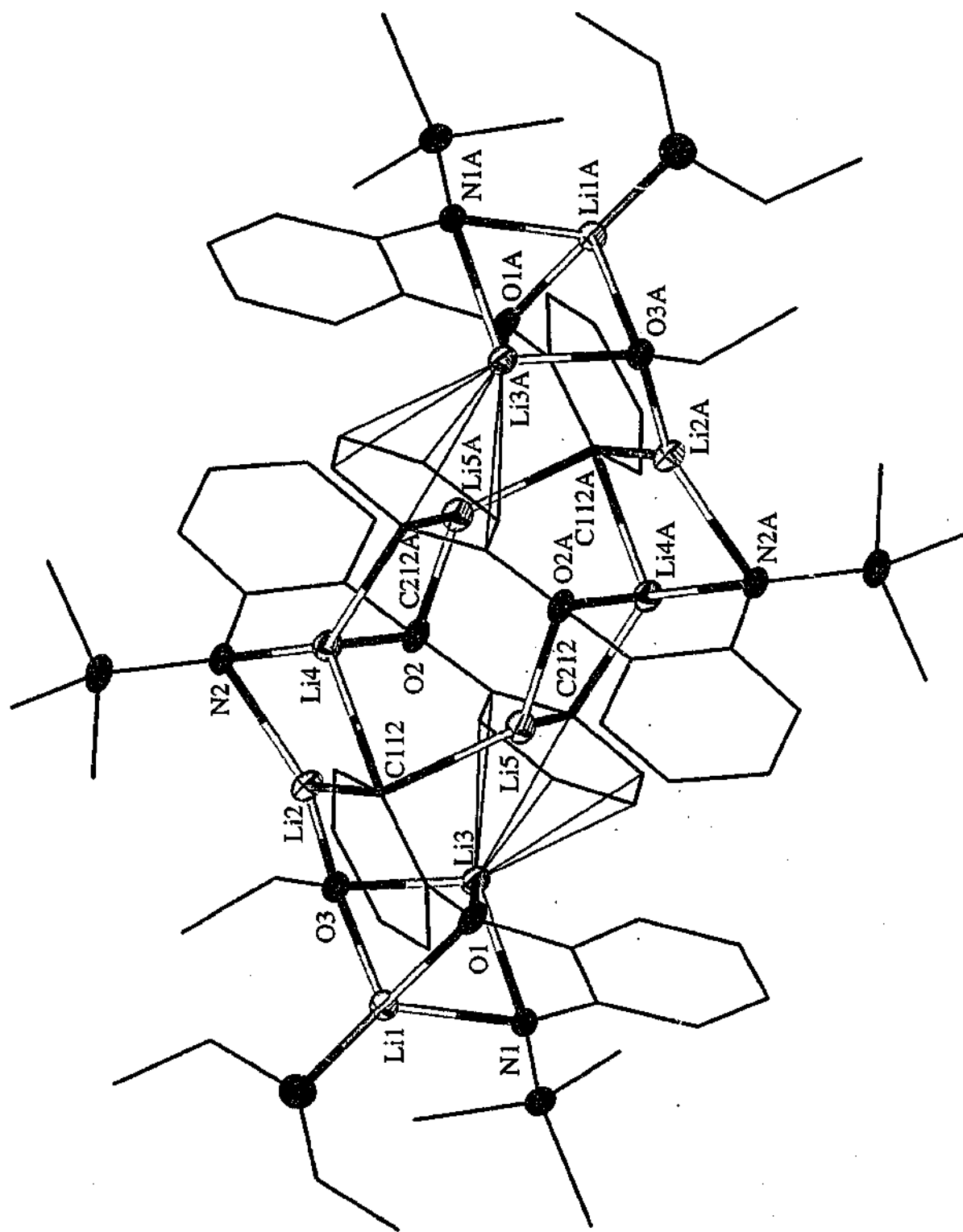


Figure 7.23 Molecular structure of  $[\text{Li}_2(\text{L}^*)]_2(\text{LiOEt})(\text{OEt})_2$  (hexane is omitted for clarity)

Table 7.10 Summary of Crystallographic Data for  $[(Li_2(L^*))_2(LiOEt)(OEt_2)]_2 \cdot (hexane)$ 

Compound	$[(Li_2(L^*))_2(LiOEt)(OEt_2)]_2 \cdot hexane$
Formula	$C_{78}H_{112}Li_{10}N_4O_8Si_4$
$M$	1415.5
$a$ (Å)	10.7828(3)
$b$ (Å)	13.1998(5)
$c$ (Å)	16.1826(7)
$\alpha$ (°)	105.724(2)
$\beta$ (°)	103.774(2)
$\gamma$ (°)	92.199(3)
$V$ (Å <sup>3</sup> )	2140.2(7)
Crystal system	triclinic
Space Group	$P(-1)$
$Z$	1
Diffractometer	Enraf Nonius CCD
$\rho_{calc}$ (g cm <sup>-3</sup> )	1.098
$\mu(MoK\alpha)$ (mm <sup>-1</sup> )	0.120
$2\theta_{max}$ (°)	56.5
$N, N_o$	10232, 6194
$R, R_w$ (observed data)	0.073, 0.169
$R, R_w$ (all data)	0.134, 0.198

**Table 7.11** Bond distances (Å) and angles (°) for the lithium environments in  $[\text{Li}_2(\text{L}^*)]_2(\text{LiOEt})(\text{OEt}_2)_2(\text{hexane})$

Li(1)—N(1)	2.052(5)	N(1)—Li(1)—O(1)	77.95(2)
Li(1)—O(1)	2.125(5)	N(1)—Li(1)—O(3)	104.1(2)
Li(1)—O(3)	1.918(5)	N(1)—Li(1)—O(4)	133.3(2)
Li(1)—O(4)	1.942(4)	O(1)—Li(1)—O(3)	88.72(2)
		O(1)—Li(1)—O(4)	110.0(2)
Li(2)—N(2)	2.072(5)	O(3)—Li(1)—O(4)	121.6(2)
Li(2)—O(3)	1.839(5)		
Li(2)—C(112)	2.367(5)	N(2)—Li(2)—O(3)	137.1(3)
		N(2)—Li(2)—C(112)	106.2(2)
Li(3)—N(1)	2.064(5)	O(3)—Li(2)—C(112)	116.6(2)
Li(3)—O(1)	2.439(5)		
Li(3)—O(3)	1.890(5)	N(1)—Li(3)—O(1)	70.85(2)
Li(3)—C(211)	2.591(5)	N(1)—Li(3)—O(3)	104.7(2)
Li(3)—C(212)	2.757(6)	O(1)—Li(3)—O(3)	80.59(2)
Li(3)—C(213)	2.711(5)		
Li(3)—C(214)	2.636(5)	N(2)—Li(4)—O(2)	75.29(2)
Li(3)—C(215)	2.532(5)	N(2)—Li(4)—C(112)	112.6(2)
Li(3)—C(216)	2.521(5)	N(2)—Li(4)—C(212A)	137.1(3)
		C(112)—Li(4)—O(2)	100.9(2)
Li(4)—N(2)	2.018(5)	C(212A)—Li(4)—C(112)	110.3(2)
Li(4)—O(2)	2.407(5)	C(212A)—Li(4)—O(2)	97.2(2)
Li(4)—C(112)	2.251(5)		
Li(4A)—C(212)	2.167(6)	O(2A)—Li(5)—C(212)	110.6(2)
		O(2A)—Li(5)—C(112A)	113.1(2)
Li(5)—O(2A)	2.050(6)	C(212)—Li(5)—C(112A)	127.3(3)
Li(5)—C(112A)	2.171(5)		
Li(5)—C(212)	2.128(5)	Li(1)—N(1)—Li(3)	69.72(2)
		Li(1)—O(3)—Li(2)	115.8(2)
Li(3)—C(1A)—C(211)	90.7	Li(1)—O(3)—Li(3)	76.31(2)
Li(3)—C(1A)—C(212)	89.6	Li(2)—N(2)—Li(4)	70.7(2)
Li(3)—C(1A)—C(213)	94.6		
Li(3)—C(1A)—C(214)	94.9	C(1A)—Li(3)—N(1)	128.9
Li(3)—C(1A)—C(215)	85.4	C(1A)—Li(3)—O(1)	113.4
Li(3)—C(1A)—C(216)	84.7	C(1A)—Li(3)—O(3)	126.4

Symmetry transformations used to generate equivalent atoms:

<sup>a</sup>  $-x, -y+2, -z$ , <sup>b</sup>  $-x+1, -y+1, -z+1$ , <sup>c</sup> C(1A) = centroid of C(211-216)

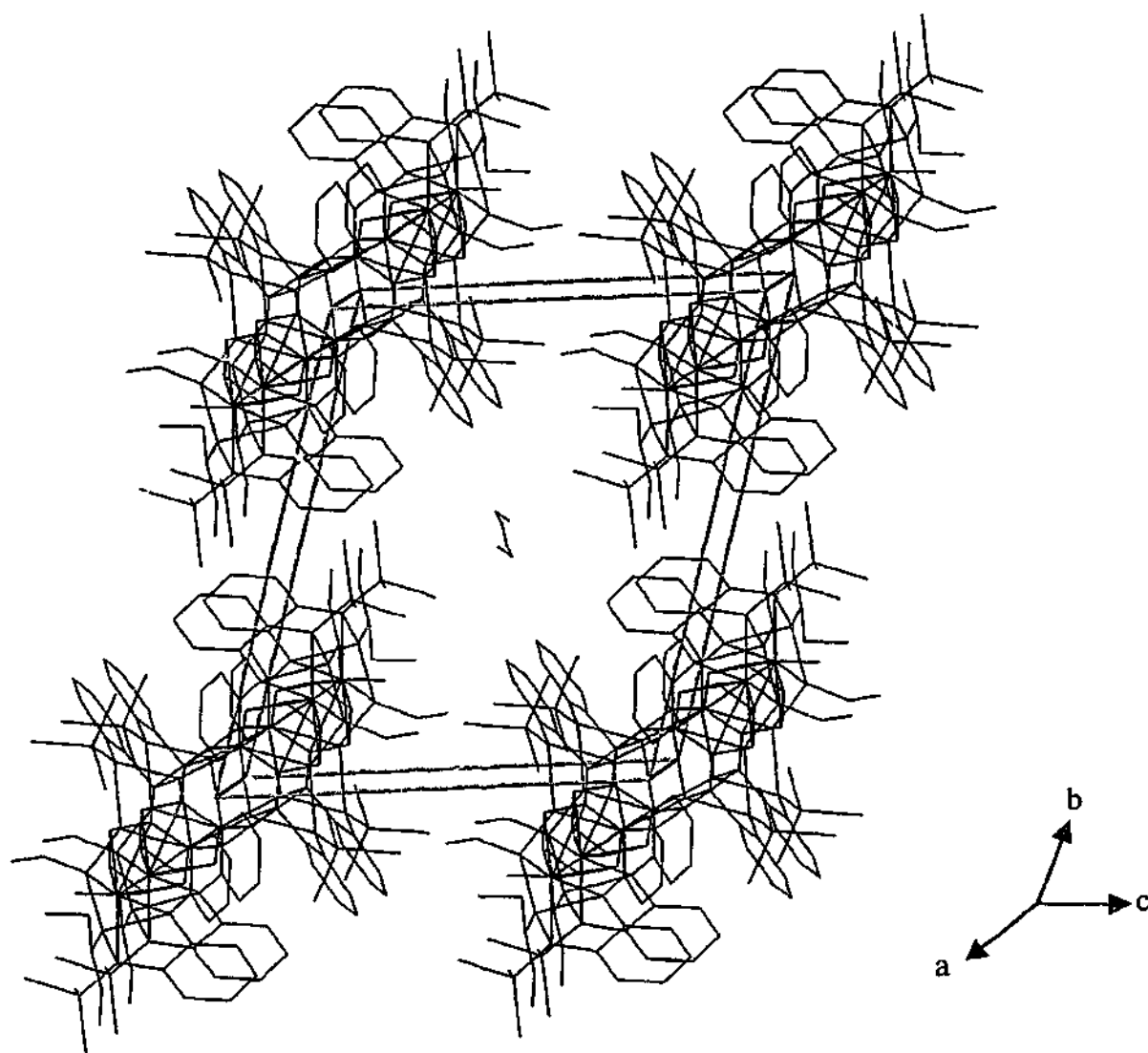
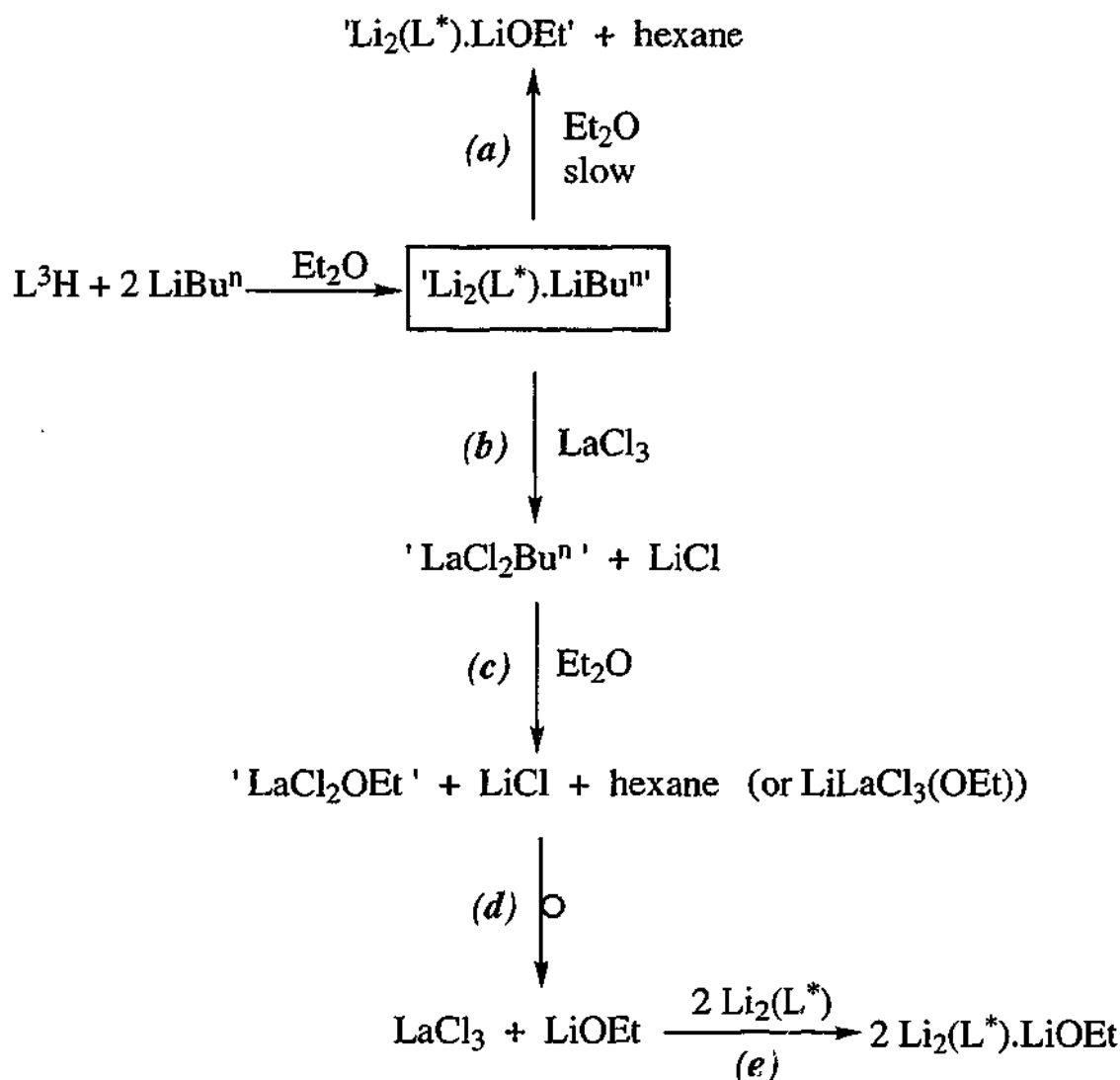


Figure 7.24 Unit cell of  $[(\text{Li}_2(\text{L}^*))_2(\text{LiOEt})(\text{OEt}_2)]_2 \cdot (\text{hexane})$  along the *a* axis

The source of ethoxide in  $[(\text{Li}_2(\text{L}^*))_2(\text{LiOEt})(\text{OEt}_2)]_2 \cdot \text{hexane}$  is presumably from ether cleavage and as the product was only isolated in low yield (18%), it may be a minor component. Whilst the isolation conditions for  $[(\text{Li}_2(\text{L}^*))_2(\text{LiOEt})(\text{OEt}_2)]_2 \cdot \text{hexane}$  were mild in comparison with those for the complex  $[\text{Li}_2(\text{L}^*)(\text{OEt}_2)\text{Li}(\text{Bu}^n)]_2$  (see Chapter 8), the longer reaction time in the former, after the addition of  $\text{LaCl}_3$ , may have caused the cleavage of ether by  $\text{LiBu}^n$ .<sup>[47]</sup> However as the incorporation of OEt has only been observed from a reaction of  $[\text{Li}_2(\text{L}^*)(\text{OEt}_2)\text{Li}(\text{Bu}^n)]_2$  with  $\text{LaCl}_3$ , it suggests that the formation of ethoxide is more likely to be mediated by the lanthanoid (see *Scheme 7.4 (a)*). A possible reaction scenario (*Scheme 7.4 (b)-(e)*) may be the formation of a



'LaCl<sub>2</sub>(Bu<sup>n</sup>)' species from the LiBu<sup>n</sup> trapped in the initially formed [Li<sub>2</sub>(L\*)(OEt<sub>2</sub>)Li(Bu<sup>n</sup>)]<sub>2</sub> and LaCl<sub>3</sub> ((*Scheme 7.4 (b)*). In a closely related example, the reaction between GdCl<sub>3</sub> and PhLi resulted in the heteroleptic [GdCl<sub>2</sub>Ph].[48] The 'LaCl<sub>2</sub>(Bu<sup>n</sup>)' could undergo reaction with diethyl ether giving a 'LaCl<sub>2</sub>OEt' species ((*Scheme 7.4 (c)*). Facile diethyl ether cleavage has previously been shown by Schumann in his pioneering work with [Ln(C<sub>5</sub>Me<sub>5</sub>)<sub>2</sub>Me].[49] The resulting 'LaX<sub>2</sub>OEt' species rearranges ((*Scheme 7.4 (d)*) yielding LaCl<sub>3</sub> and releasing the OEt which is subsequently trapped by the Li<sub>2</sub>(L\*) fragment. Ether scission of the L<sup>2</sup> and L<sup>3</sup> ligands accompanying oxidation of Ln(L)<sub>2</sub> (L = L<sup>2</sup> or L<sup>3</sup>) has been observed resulting in the complexes [Yb(L<sup>2</sup>)<sub>2</sub>(μ-OMe)]<sub>2</sub> and [Yb(L<sup>3</sup>)<sub>2</sub>(OPh)(THF)] as discussed in Chapter 5.



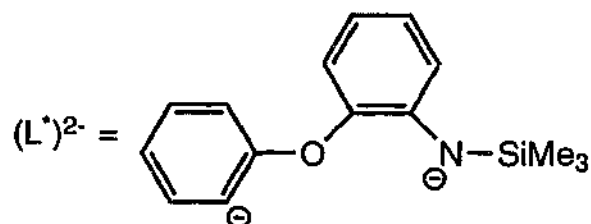
Scheme 7.4

Other attempts to prepare a Ln containing  $L^*$  species by adding  $[Yb(C_5Me_5)_2Cl(THF)]$  to a  $L^3H / 2LiBu^n$  diethyl ether mixture resulted in a highly reactive species (A) which could not be isolated. However no reaction was observed between the isolated lithium complex  $[Li_2(L^*)(dme)]_2$  and one equivalent of  $[Yb(C_5Me_5)_2Cl(THF)]$  in hexane despite gentle reflux and in addition to changing to a coordinating solvent (THF or DME). This suggests the lithium aggregate is remarkably stable and the highly reactive species (A) from the *in situ* reaction is formed from the trapped  $LiBu^n$  and the Yb complex. Thus, a resulting  $Yb(C_5Me_5)_2Bu^n$  species could undergo  $\beta$ -hydride elimination and decomposition. These observations support the proposal of involvement of an intermediate unstable La complex (*Scheme 7.4 (b)-(e)*) in the formation of  $[Li_2(L^*)]_2(LiOEt)(OEt)_2$  (hexane).

### 7.3 Conclusions

Lithiation of  $L^2H$  and  $L^3H$  in a variety of solvents generally gave the expected monodeprotonated lithium amides (e.g.  $[Li(L^2)(OEt_2)]_2$ ,  $[Li(L^3)(DME)_{0.5}]$ ,  $[Li(L^3)(THF)]$ ,  $[Li(L^3)(DME)]$  and  $[Li(L^3)]_n$ ) in good yields. These materials were readily purified by recrystallisation and in several cases were structurally characterized. They are versatile sources of  $L^2$  and  $L^3$  for use in the preparation of lanthanoid complexes (Chapter 3-5) and presumably also for other metals.

A remarkable and unexpected result was achieved in the reaction of  $L^3H$  with  $LiBu^n$  in diethyl ether where further deprotonation of  $L^3$  was observed resulting in the new N, C-dianion  $L^*$ .



Lithium salts of the  $L^*$  ligand exhibited a fascinating structural chemistry with the observation of elegant multilithium aggregates each with their own unique features. For example, mixed  $L^*/L^3$  species  $\{[Li(L^3)(OEt_2)Li_2(L^*)]_2(\text{diglyme})\}$  and incorporation of  $LiBu^n$   $\{[Li_2(L^*)(OEt_2)Li(Bu^n)]_2\}$ . Furthermore a convenient low aggregate form of  $L^*$   $[Li(L^*)_2(DME)]_2$  can be isolated in good yield from DME and this should provide a valuable precursor for further synthetic reactions. Initial attempts to transfer the  $L^*$  ligand to lanthanoids, whilst unsuccessful, gave an even more fascinating lithium array with the inclusion of  $LiOEt$  in a decalithium aggregate  $\{[Li_2(L^*)]_2(LiOEt)(OEt_2)\}_2(\text{hexane})$ . This structure has implications for 'superbase' chemistry where it is the first example containing more than two different superbases anions, alkoxide, amide and carbanion, and indeed all three were found surrounding a single lithium atom (see *Figure 7.25*).

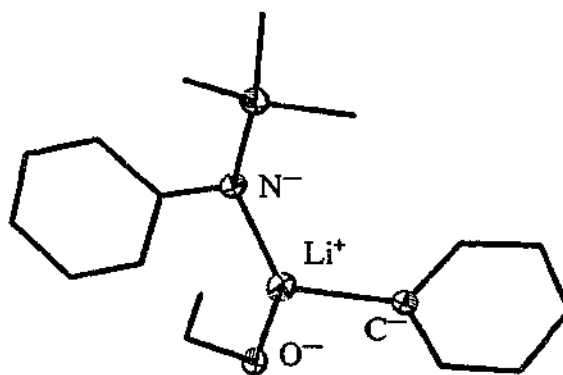


*Figure 7.25*

## 7.4 References

- 1 R. E. Mulvey, *Chem. Soc. Rev.*, 1991, **20**, 176.
- 2 A. M. Sapsa and P. v. R. Schleyer, in *Lithium Chemistry: A theoretical and Experimental Overview*, Wiley-Interscience, New York, 1995.
- 3 K. Gregory, P. v. R. Schleyer, and R. Snaith, *Adv. Inorg. Chem.*, 1991, **37**, 47.
- 4 G. Kowach, C. Warren, R. Haushalter, and F. Di Salvo, *Inorg. Chem.*, 1998, **39**, 156.
- 5 R. Snaith, D. Barr, D. S. Wright, W. Clegg, S. M. Hodgson, G. R. Lamming, A. J. Scott, and R. E. Mulvey, *Angew. Chem., Int. Ed. Engl.*, 1989, **28**, 1741.
- 6 R. Snaith, D. Barr, D. S. Wright, W. Clegg, S. M. Hodgson, G. R. Lamming, A. J. Scott, and R. E. Mulvey, *Angew. Chem.*, 1989, **101**, 1279.
- 7 M. F. Lappert, M. J. Slade, A. Singh, J. L. Atwood, R. D. Rodgers, and R. Shakir, *J. Am. Chem. Soc.*, 1983, **105**, 302.
- 8 F. Antolini, P. B. Hitchcock, M. F. Lappert, and P. Merle, *Chem. Commun.*, 2000, 1301.
- 9 D. Mootz, A. Zinnius, and B. Böttcher, *Angew. Chem., Int. Ed. Engl.*, 1969, **8**, 378.
- 10 R. D. Rodgers, J. L. Atwood, and R. Grüning, *J. Organomet. Chem.*, 1978, **157**, 229.
- 11 D. Barr, W. Clegg, R. E. Mulvey, and R. Snaith, *J. Chem. Soc., Chem. Commun.*, 1984, 285, 287.
- 12 M. Rannenber, H.-D. Hausen, and J. Weidlein, *J. Organomet. Chem.*, 1989, **376**, C27.
- 13 T. Fjeldberg, P. B. Hitchcock, M. F. Lappert, and A. J. Thorne, *J. Chem. Soc., Chem. Commun.*, 1984, 822.
- 14 D. K. Kennepohl, S. Brooker, G. M. Sheldrick, and H. W. Roesky, *Chem. Ber.*, 1991, **124**, 2223.
- 15 D. R. Armstrong, R. E. Mulvey, G. T. Walker, D. Barr, and R. Snaith, *J. Chem. Soc., Dalton Trans.*, 1988, 617.
- 16 J. P. Bezombes, P. B. Hitchcock, M. F. Lappert, and P. G. Merle, *J. Chem. Soc., Dalton Trans.*, 2001, 816.

- 17 L. M. Engelhardt, B. S. Jolly, P. C. Junk, C. L. Raston, B. W. Skelton, and A. H. White, *Aust. J. Chem.*, 1986, **39**, 1337.
- 18 L. M. Engelhardt, A. S. May, C. L. Raston, and A. H. White, *J. Chem. Soc., Dalton Trans.*, 1983, 1671.
- 19 D. Barr, W. Clegg, R. E. Mulvey, R. Snaith, and D. S. Wright, *J. Chem. Soc., Chem. Commun.*, 1987, 716.
- 20 J. L. Atwood, M. F. Lappert, W.-P. Leung, and H. Zhang, *Unpublished Results cited in R. E. Mulvey, Chem. Soc. Rev.*, 1991, **20**, 176..
- 21 K. W. Henderson, A. E. Dorigo, Q. Liu, -Y, and P. G. Williard, *J. Am. Chem. Soc.*, 1997, **119**, 11855.
- 22 D. Barr, W. Clegg, R. E. Mulvey, and R. Snaith, *J. Chem. Soc., Chem. Commun.*, 1984, 700.
- 23 L. M. Engelhardt, G. E. Jacobsen, P. C. Junk, C. L. Raston, B. W. Skelton, and A. H. White, *J. Chem. Soc., Dalton Trans.*, 1988, 1011.
- 24 G. B. Deacon, C. M. Forsyth, P. C. Junk, B. W. Skelton, and A. H. White, *J. Chem. Soc., Dalton Trans.*, 1998, 1381.
- 25 M. Veith, J. Bönlein, and V. Huch, *Chem. Ber.*, 1989, **122**, 841.
- 26 I. Cragg-Hine, M. G. Davidson, O. Kocian, F. S. Mair, E. Pohl, P. R. Raithby, R. Snaith, N. Spencer, and J. F. Stoodart, *Angew. Chem. Int. Ed. Engl.*, 1993, **32**, 1182.
- 27 L. Lochmann, *Eur. J. Inorg. Chem.*, 2000, 1115.
- 28 F. A. Cotton, S. C. Haefner, J. H. Matonic, X. Wang, and C. A. Murillo, *Polyhedron*, 1997, **16**, 541.
- 29 M. F. Lappert, M. J. Slade, A. Singh, J. L. Atwood, R. D. Rodgers, and R. Shakir, *J. Am. Chem. Soc.*, 1983, **105**, 302.
- 30 J. Lewis, J. R. Miller, R. L. Richards, and A. Thompson, *J. Chem. Soc.*, 1965, 5850.
- 31 R. J. H. Clark, J. Lewis, D. J. Machin, and R. S. Nyholm, *J. Chem. Soc.*, 1963, 379.
- 32 P. C. Andrews, P. J. Duggan, G. D. Fallon, T. D. McCarthy, and A. C. Peatt, *J. Chem. Soc., Dalton Trans.*, 2000, 1937.
- 33 S. Harder, J. Boesma, L. Brandsma, J. A. Kanters, A. J. M. Duisenberg, and J. H. van Lenthe, *Organometallics*, 1991, **10**, 1623.

- 34 J. G. Dondervoort, J. L. Vicario, E. Rijnberg, J. T. B. H. Jastrzebski, H. Kooijman, A. L. Spek, and G. van Koten, *J. Organomet. Chem.*, 1998, **463**, 463.
- 35 P. Davies, P. R. Raithby, and R. Snaith, *Angew. Chem. Int. Ed. Engl.*, 1997, **36**, 1215.
- 36 K. Ruhlandt-Senge, J. J. Ellison, R. J. Wehmschulte, F. Pauer, and P. P. Power, *J. Am. Chem. Soc.*, 1993, **115**, 11353.
- 37 B. Schiemenz and P. P. Power, *Angew. Chem. Int. Ed. Engl.*, 1996, **35**, 2150.
- 38 M. Niemeyer and P. P. Power, *Inorg. Chem.*, 1996, **35**, 7264.
- 39 T. Kottke and D. Stalke, *Angew. Chem. Int. Ed. Engl.*, 1993, **32**, 580.
- 40 A. R. Kennedy, J. G. MacLellan, R. E. Mulvey, and A. Robertson, *J. Chem. Soc., Dalton Trans.*, 2000, 4112.
- 41 R. J. Wehmschulte and P. P. Power, *J. Am. Chem. Soc.*, 1997, **119**, 2847.
- 42 A. F. Wells, in *Structural Inorganic Chemistry*, 5th edn., Clarendon, Oxford, 1984, p. 1288.
- 43 L. C. Pauling, *The Nature of the Chemical Bond*, Cornell University Press, New York, 1960.
- 44 M. Marsch, K. Harms, L. Lochmann, and G. Boche, *Angew. Chem.*, 1990, **102**, 334.
- 45 M. Marsch, K. Harms, L. Lochmann, and G. Boche, *Angew. Chem. Int. Ed. Engl.*, 1990, **29**, 308.
- 46 F. Pauer and P. Power, in *Lithium Chemistry; A Theoretical and Experimental Overview*, eds. A.-M. Sapse and P. v. R. Schleyer, John Wiley and Sons, 1995, ch. 9.
- 47 G. E. Coates and K. Wade, *The Main Group Elements*, in *Organometallic Compounds*, 3rd edn., eds. G. E. Coates, M. L. H. Green, and K. Wade, Methuen, London, 1967, vol. 1, p. 9.
- 48 G. Lin, Z. Jiu, Y. Zhang, and W. Chen, *J. Organomet. Chem.*, 1990, **396**, 307.
- 49 H. Schumann, W. Genthe, and N. Bruncks, *Angew. Chem.*, 1981, **93**, 126.

## Chapter 8

# Experimental Section

### 8.1 General Experimental

All experiments involving lanthanoid and lithium organoamide complexes were handled and stored under a purified nitrogen atmosphere. Synthetic manipulations were carried out using a vacuum-line and Schlenk glassware as well as a recirculating atmosphere dry box (Vacuum atmospheres HE43-2 Drilab or Miller Howe Type 100 Glove Box). Nitrogen was purified by being passed through activated BASF R3/11 copper oxide 'catalyst' and 4Å molecular sieves. All glassware was dried (130°C) for at least 30 min, or flame dried under vacuum, to remove residual water before use.

### 8.2 Analysis

#### 8.2.1 Elemental Analyses

Elemental analyses (C, H and N) were performed by the Campbell Microanalytical Service of the University of Otago, New Zealand. Microanalytical samples of air- and moisture-sensitive compounds were submitted sealed under nitrogen in a glass ampoule.

Lanthanoid analyses were carried out on accurately weighed samples (*ca.* 0.1 g) by complexometric titration.[1, 2] These samples were digested in concentrated  $\text{HNO}_3/\text{H}_2\text{SO}_4$  and the  $\text{HNO}_3$  was then distilled off. The resulting colourless solutions were diluted with distilled water to a standard volume. Aliquots were buffered to pH 6.3 with hexamethylenetetramine and titrated against a standard solution of  $\text{Na}_2\text{H}_2\text{EDTA}$  (*ca.* 0.01M), with xylol orange. This procedure was modified for complexes not containing organic ligands where digestion of the sample was carried out by the addition of 1-2  $\text{cm}^3$  2 M HCl.

### 8.2.2 IR-, FIR-, UV-, VIS-, NIR- Spectroscopy

Infrared spectra ( $4000 - 650 \text{ cm}^{-1}$ ) were obtained from Nujol mulls (using degassed sodium-dried Nujol) of the sample between NaCl plates with a Perkin Elmer 1600 Fourier transform infrared spectrometer or as KBr disks (Chapter 6) with a Bruker 66V/S instrument. In each case, the air- and moisture-sensitive compound was prepared for spectroscopy in a dry box and the spectrum run immediately after removal from the dry box with no decomposition observed. Far infrared spectra ( $600 - 50 \text{ cm}^{-1}$ ) were recorded on either a Bruker IFS 120 HR spectrometer as vaseline mulls or a Bruker IFS 66V/S instrument as polyethylene disks.

UV/VIS/near-infrared spectra (350 - 1500 nm) were recorded on a Cary 17 spectrophotometer. Accurately weighed samples were dissolved in a known amount of solvent (DME) in a dry box and transferred to a quartz 1mm cell fitted with a teflon tap.

### 8.2.3 Mass Spectroscopy, TGA/DSC/DTA/MS and GC/MS

Mass spectra were recorded with a VG Trio-1 GC mass spectrometer. Samples were loaded in a drybox into a specially designed air-tight probe and immediately run. Each listed  $m/z$  value for a Ln-containing ion is the most intense peak of a cluster pattern in good agreement with the calculated pattern.

TGA/DSC and DTA/TG/MS measurements were obtained using a NETZSCH STA 409 instrument interfaced to a BALZERS QMS 421 quadrupole mass spectrometer. The system was calibrated using melting points of pure metals. All measurements were done in a continual flow of Ar with an aluminium oxide reference.

GC/MS measurements were recorded on a Hewlett-Packard 5890A instrument interfaced to a VG Trio-1 GC mass spectrometer with helium as a carrier gas. Separation was achieved with an XTI-5 column (30m, 0.32 mm id) (bonded 5% phenyl — 95% dimethylpolysiloxane) with the temperature program starting at  $50^\circ\text{C}$  (2 min) and then increased by  $10^\circ\text{C}/\text{min}$  to  $280^\circ\text{C}$ . Retention times were measured in minutes from injection.



### 8.2.4 $^1\text{H}$ and Heteronuclear NMR spectroscopy

NMR experiments were carried out with either a Bruker AC 200 MHz ( $^1\text{H}$ ), Bruker AC 300 MHz ( $^1\text{H}$ ) or Bruker AC 400 MHz ( $^1\text{H}$ ,  $^7\text{Li}$ ,  $^{199}\text{Hg}$ , VT) spectrometers as indicated. Samples were prepared in the deuterio solvent in 5mm NMR tubes sealed with a teflon stopcock.  $\text{C}_4\text{D}_8\text{O}$ ,  $\text{C}_6\text{D}_6$ ,  $\text{C}_7\text{H}_8$  were distilled from Na/K alloy and degassed.  $^1\text{H}$  NMR spectra were referenced to the residual protonated solvent signal. Chemical shifts at room temperature for  $^7\text{Li}$  spectra are given relative to external 1 M LiBr in  $\text{H}_2\text{O}$ .  $^{199}\text{Hg}$  chemical shifts are reported relative to  $\text{HgMe}_2$  at room temperature with 1 M  $\text{Hg}(\text{OAc})(\text{Ph})$  in DMSO used as a secondary external standard ( $\delta = -1430$  ppm).

### 8.2.5 X-ray Crystallography

Unless otherwise stated crystal structure determinations in this thesis were carried out by Dr. C. M. Forysth, Monash University, Victoria.

## 8.3 Reagents and Solvents

Tetrahydrofuran, 1,2-dimethoxyethane, *n*hexane, diethyl ether and toluene were predried over sodium wire for at least 24 h and distilled from benzophenone / sodium wire under purified nitrogen. Tetraethylene glycol dimethyl ether (tetraglyme) was added to the *n*hexane to solubilise the keytl. When tetraglyme was not available dimethyl ethylene glycol (diglyme) was added. Acetonitrile was dried and distilled from  $\text{CaH}_2$ . 2-Methoxyaniline, hexamethyldisilazane, 1,2-diaminoethane and *N,N*-dimethyl-1,2-diaminoethane were dried over molecular sieves for 24h, then fractionally distilled and stored under nitrogen. Hexachloroethane, diphenylmercury, dibromomercury, 2-phenoxyaniline, trimethylsilyl chloride and *N,N'*-diphenyl-1,2-diaminoethane were used as received from Aldrich. *n*-Butyllithium (1.6 M) (Aldrich) was used unstandardised but transferred to and stored in a Schlenk flask under nitrogen. Solvents and liquid reagents were stored under nitrogen and introduced into reaction vessels by a syringe or cannula that was preflushed with nitrogen.

Lanthanoid metals were obtained from Johnson Matthey Rare Earth Products or Rhone-Poulenc U.S.A. and were stored under nitrogen in a drybox. Anhydrous terbium and samarium trichloride were obtained from Aldrich and stored under nitrogen in a drybox.

### 8.3.1 Preparation of starting materials

The following reagents were prepared according to their literature methods;  $\text{LnCl}_3(\text{THF})_n$ ,<sup>[3]</sup>  $\text{LnCl}_3$ ,<sup>[4]</sup>  $\text{HN}(\text{SiMe}_3)\text{CH}_2\text{CH}_2\text{NMe}_2$  ( $\text{L}^1\text{H}$ ),<sup>[5]</sup>  $[\text{Yb}(2,6\text{-}(\text{Bu}^t)_2\text{C}_6\text{H}_3\text{O})_3]$  was prepared analogously to Sc, Y, La and Sm derivatives,<sup>[6]</sup>  $[\text{Ln}\{\text{N}(\text{SiMe}_3)_2\}_2(\text{THF})_2]$ <sup>[7]</sup> and  $[\text{Ln}\{\text{N}(\text{SiMe}_3)_2\}_2(\text{DME})]$ <sup>[8, 9]</sup> (where Ln = Yb, Eu),  $\text{TlMeCp}$  and  $\text{Tl}(\text{C}_5\text{H}_5)$ ,<sup>[10]</sup>  $[\text{Yb}(\text{C}_5\text{Me}_5)_2(\text{THF})]$ ,<sup>[11]</sup>  $[\text{HN}(\text{SiMe}_3)\text{CH}_2]_2$ ,<sup>[12]</sup>  $[\text{Yb}(\text{C}_5\text{Me}_5)_2\text{Cl}(\text{THF})]$ ,<sup>[13]</sup> and  $\text{Li}(\text{Ph}_2\text{pz})$  was generated *in situ* from  $\text{HPh}_2\text{pz}$  and  $\text{LiBu}^f$  in THF.

#### 8.3.1.1 Synthesis and Characterisation of $[\text{Yb}(\text{MeCp})\text{Cl}_2(\text{THF})]$

The compound  $[\text{Yb}(\text{MeCp})\text{Cl}_2(\text{THF})]$  was prepared in a metathesis reaction similar to the synthesis of  $[\text{Er}(\text{C}_5\text{H}_5)\text{Cl}_2(\text{THF})_3]$ .<sup>[14]</sup> THF was added to the solids  $\text{YbCl}_3(\text{THF})_3$  (1.05 g, 2.11 mmol) and  $\text{Tl}(\text{MeCp})$  (0.60 g, 2.11 mmol). The reaction mixture was stirred at room temperature for 12 h and filtered at  $-78^\circ\text{C}$ . The filtrate volume was evaporated to dryness, and after drying at room temperature under vacuum, a dark red material was afforded (yield 0.52 g, 62 %). (Found: C, 28.95; H, 4.96.  $\text{C}_{10}\text{H}_{15}\text{Cl}_2\text{OYb}$  requires C, 30.39; H, 3.83 %) Infrared (Nujol,  $\text{v}/\text{cm}^{-1}$ ): 1299 w, 1170 w, 1074 w, 1013 s, 921 m, 863 br s, 771 w, 722 s, 668 w.

## 8.4 Experimental Procedures for Chapter 2

### 8.4.1 Synthesis of $[Ln(L^1)_2(\mu-Cl)]_2$ Complexes ( $Ln = Yb, Er, Nd, Sm, La$ )

#### 2a) $[Yb(L^1)_2(\mu-Cl)]_2$

To a stirred solution of  $L^1H$  (0.88 g, 1.0 cm<sup>3</sup>, 5.5 mmol) in THF (50 cm<sup>3</sup>) at 0°C was slowly added  $LiBu^a$  (3.75 cm<sup>3</sup>, 6.0 mmol) and the resulting solution was warmed to room temperature over *ca.* 1 h. To this solution,  $YbCl_3(THF)_3$  (1.36 g, 2.75 mmol) was added, and the reaction mixture was rapidly stirred for 12 h. The solvent was removed *in vacuo*, and hexane added affording a white precipitate. The orange solution was filtered and the filtrate volume reduced to *ca.* 2 cm<sup>3</sup> under vacuum. Orange crystals deposited on standing overnight (yield 0.79 g, 55 %). (Found: C, 31.35; H, 7.28; N, 9.60; Yb, 33.18  $C_{28}H_{76}Cl_2N_3Si_4Yb_2$  requires C, 31.90; H, 7.27; N, 10.66; Yb, 32.83 %) Infrared (Nujol,  $\nu/cm^{-1}$ ): 1351 m, 1270 w, 1238 m, 1157 w, 1078 m, 1031 w, 1010 s, 952 s, 925 s, 858 m, 832 m, 778 w, 740 m, 679 w. Mass Spectrum:  $m/z$  736 (<1%)  $[M(dimer) - (2L^1)]^+$ , 701 (<1)  $[Yb_2(L^1)_2Cl]^+$ , 527 (2)  $[Yb(L^1)_2Cl]^+$ , 333 (50)  $[Yb(L^1)]^+$ , 73 (45)  $[SiMe_3]^+$ , 58 (100)  $[SiMe_2]^+$ .

#### 2b) $[Er(L^1)_2(\mu-Cl)]_2$

A similar preparation method to that used for compound 2a gave pink crystals of 2b (yield 0.76 g, 53 %). Infrared (Nujol,  $\nu/cm^{-1}$ ): 1348 m, 1259 m, 1246 s, 1168 w, 1104 m, 1079 m, 1036 w, 1020 s, 924 s, 827 br s, 734 m, 662 m. Mass Spectrum:  $m/z$  883 (>1%)  $[M(dimer) - (L^1)]^+$ , 724 (1)  $[M(dimer) - (2L^1)]^+$ , 521 (1)  $[Er(L^1)_2Cl]^+$ , 325 (25)  $[Er(L^1)]^+$ , 73 (35)  $[SiMe_3]^+$ , 58 (100)  $[SiMe_2]^+$ .

2c)  $[Sm(L^1)_2(\mu-Cl)]_2$ 

A similar procedure to that used for compound 2a gave yellow crystals of 2c (yield 0.58 g, 42 %). Infrared (Nujol,  $\nu/cm^{-1}$ ): 1347 m, 1258 m, 1246 s, 1169 w, 1103m, 1079 m, 1035 w, 1020 s, 924 s, 828 br s, 735 m, 676 w, 662 m, 619 w. Mass Spectrum:  $m/z$  689 (>1 %)  $[M(\text{dimer}) - (2L^1)]^+$ , 507 (1)  $[Sm(L^1)_2Cl]^+$ , 348 (20)  $[Sm(L^1)Cl]^+$ , 311 (15)  $[Sm(L^1)]^+$ , 281 (25)  $[Sm(L^1) - 2Me]^+$ , 73 (50)  $[SiMe_3]^+$ , 58 (100)  $[SiMe_2]^+$ .

2d)  $[Nd(L^1)_2(\mu-Cl)]_2$ 

A similar procedure to that used for compound 2a gave blue crystals of 2d (yield 0.70 g, 51 %). (Found: Nd, 29.15.  $C_{28}H_{76}Cl_2N_8Nd_2Si_4$  requires Nd, 28.94 %) Infrared (Nujol,  $\nu/cm^{-1}$ ): 1348 m, 1259 m, 1246 s, 1168 w, 1104 m, 1079 m, 1036 w, 1020 s, 924 s, 827 br s, 734 m, 662 m. Mass Spectrum:  $m/z$  835 (<1%)  $[^{144}Nd(L^1)_2(\mu-Cl)]_2 - (L^1)]^+$ , 676 (<1)  $[^{144}Nd(L^1)_2(\mu-Cl)]_2 - (2L^1)]^+$ , 482 (1)  $[^{144}Nd_2(L^1)Cl]^+$ , 338 (50)  $[^{144}Nd(L^1)Cl]^+$ , 73 (45)  $[SiMe_3]^+$ , 58 (100)  $[SiMe_2]^+$ .

2e)  $[La(L^1)_2(\mu-Cl)]_2$ 

A similar preparation to that for compound 2a gave colourless crystals of 2e (yield 0.63 g, 46 %) (Found: La, 28.02.  $C_{28}H_{76}Cl_2La_2N_8Si_4$  requires La, 28.17 %) Infrared (Nujol,  $\nu/cm^{-1}$ ): 1348 w, 1259 m, 1246 s, 1168 w, 1107 m, 1084 s, 1068 m, 1037 w, 1021 s, 938 m, 923 vs, 848 vs, 827 vs, 797 m, 735 m, 664 w. Mass Spectrum  $m/z$  825 (5%)  $[M(\text{dimer}) - (L^1)]^+$ , 457 (30)  $[La(L^1)_2]^+$ , 333 (80)  $[La(L^1)Cl]^+$ , 73 (20)  $[SiMe_3]^+$ , 58 (100)  $[SiMe_2]^+$ .

### 8.4.2 Synthesis of $[Nd(L^1)(Ph_2pz)_3][Li(DME)_3]$

To a stirred solution of  $L^1H$  (0.88 g, 5.5 mmol) in THF (40 cm<sup>3</sup>) at 0°C was slowly added  $LiBu^n$  (3.75 cm<sup>3</sup>, 6.0 mmol) and the resulting solution was warmed to room temperature over *ca.* 1 h. To the mixture,  $NdCl_3(THF)_2$  (1.08 g, 2.75 mmol) and  $LiPh_2pz$  (0.60 g, 2.75 mmol) were added and the resulting suspension rapidly stirred and heated at 70°C for 12 h. The solvent was removed under vacuum and hexane was added giving a white precipitate. The blue solution was then filtered, the filtrate evaporated to dryness and DME (15 cm<sup>3</sup>) was added. On standing overnight, suitable X-ray quality blue crystals of the title complex were deposited (yield 0.32 g, 28 %). (Found: C, 56.61; H, 5.93; N, 9.83.  $C_{64}H_{82}LiN_8NdO_6Si$  requires C, 62.06; H, 6.67; N, 9.05 %). Infrared (Nujol,  $\nu/cm^{-1}$ ): 1603 vs, 1273 w, 1246 s, 1192 s, 1171 w, 1123 vs, 1082 s, 1026 s, 970 vs, 945 vs, 826 s, 755 vs, 695 vs, 683 vs. Mass Spectrum:  $m/z$  522 (4 %) [ $^{144}Nd(L^1)(Ph_2pz)$ ]<sup>+</sup>, 361 (3) [ $^{142}Nd(Ph_2pz)$ ]<sup>+</sup>, 229 (2) [ $^{142}Nd(NSiMe_3)$ ]<sup>+</sup>, 144 (40) [ $L^1 - Me$ ]<sup>+</sup>, 129 (20) [ $L^1 - 2Me$ ]<sup>+</sup>, 114 [ $L^1 - 3Me$ ]<sup>+</sup>, 101 (90) [ $CH_2NSiMe_3$ ]<sup>+</sup>, 73 (100) [ $SiMe_3$ ]<sup>+</sup>, 58 (80) [ $SiMe_2$ ]<sup>+</sup>. *Very weak* higher mass ion fragments were detected and could be assigned to 967 (<1) [ $^{144}Nd(L^1)(Ph_2pz)_3Li$ ]<sup>+</sup>, 748 (<1) [ $^{144}Nd(L^1)(Ph_2pz)_2Li$ ]<sup>+</sup>, 688 (<1) [ $^{144}Nd(L^1)_2(Ph_2pz)Li$ ]<sup>+</sup>, 621 (<1) [ $^{144}Nd(L^1)_3$ ]<sup>+</sup>, 462 (<1) [ $^{144}Nd(L^1)_2$ ]<sup>+</sup>.

## 8.5 Experimental Procedures for Chapter 3

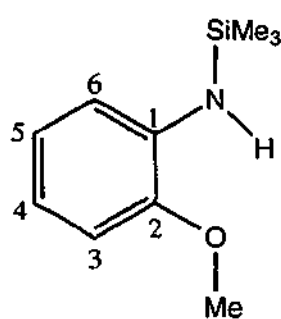
### 8.5.1 Synthesis of $L^2H$

#### 3a) $[o\text{-MeOC}_6\text{H}_4\text{NHLi}]$

To a stirred solution of  $[o\text{-MeOC}_6\text{H}_4\text{NH}_2]$  (18 cm<sup>3</sup>, 0.16 mol) in Et<sub>2</sub>O (100 cm<sup>3</sup>) at 0°C was slowly added LiBu<sup>n</sup> (100 cm<sup>3</sup>, 0.16 mol). After complete addition a white solid was obtained which was stirred to warm to room temperature (*ca.* 1 h). The solid was then filtered and washed with hexane (50 cm<sup>3</sup>) and dried under vacuum. (yield 20 g, 97%) An attempt to obtain consistent analytical and spectroscopic data was thwarted due to the extreme air- and moisture-sensitivity of the complex.

#### 3b) $[o\text{-MeOC}_6\text{H}_4\text{NH}(\text{SiMe}_3)] (L^2H)$

To a stirred suspension of 3a (18.86 g, 0.15 mol) in Et<sub>2</sub>O (100 cm<sup>3</sup>) at 0°C was slowly added ClSiMe<sub>3</sub> (18.5 cm<sup>3</sup>, 0.15 mol), and the mixture was stirred until it had warmed to room temperature (*ca.* 1 h). The solvent volume was then reduced *in vacuo* until a residual oil remained which was vacuum distilled as a colourless, moisture sensitive liquid (yield 26.7g, 85 %). (Found: C, 61.66; H, 8.89; N, 7.29. C<sub>10</sub>H<sub>16</sub>N<sub>3</sub>OSi requires C, 61.46; H, 8.77; N, 7.17 %) Infrared (Nujol, v/cm<sup>-1</sup>): 3401 vs, 3043 s, 2956 vs, 2901 s, 2884 s, 1599 vs, 1504 vs, 1460 s, 1446 s, 1386 vs, 1322 vs, 1289 vs, 1238 vs, 1215 vs, 1174 s, 1113 vs, 1050 s, 1031 vs, 902 vs, 842 vs, 776 s, 735 vs, 689 s, 620 s, 590 m. Mass Spectrum *m/z* 195 (80%)  $[L^2H]^+$ , 180 (50)  $[L^2H - \text{Me}]^+$ , 165 (100)  $[L^2H - 2\text{Me}]^+$ , 150 (60)  $[L^2H - 3\text{Me}]^+$ , 135 (45)  $[\text{C}_6\text{H}_4\text{ONHSi}]^+$ , 108 (19)  $[\text{C}_6\text{H}_5\text{OMe}]^+$ , 73 (75)  $[\text{SiMe}_3]^+$ , 58  $[\text{SiMe}_2]^+$ . <sup>1</sup>H NMR. (300 MHz, C<sub>6</sub>D<sub>6</sub>, 298 K): δ 0.16 (9 H, s, SiMe<sub>3</sub>), 3.31 (3 H, s, OMe), 4.26 (1 H, br s, NH), 6.57 (1 H, dd, <sup>3</sup>J 7.5 Hz, <sup>4</sup>J 1.0 Hz, H6), 6.74 (1H, ddd, H5), 6.88 (2 H, m, H3, H4).

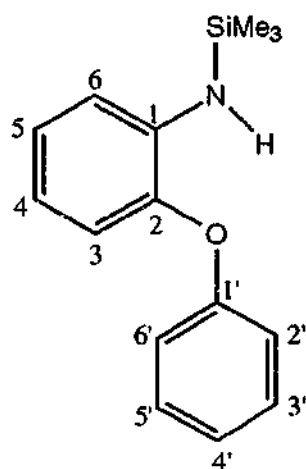


8.5.2 Synthesis of  $L^3H$ 3c)  $o\text{-PhOC}_6\text{H}_4\text{NHLi}$ 

To a stirred solution of  $o\text{-PhOC}_6\text{H}_4\text{NH}_2$  (5.0 g, 27.0 mmol) in  $\text{Et}_2\text{O}$  (50  $\text{cm}^3$ ) which was cooled to  $0^\circ\text{C}$  was added dropwise 16.9  $\text{cm}^3$  of a solution of  $\text{LiBu}^n$ . After complete addition a white solid was obtained which was stirred to warm to room temperature (*ca.* 1 h). The solid was then filtered and washed with 50  $\text{cm}^3$  of  $\text{Et}_2\text{O}$ .

3d)  $[o\text{-PhOC}_6\text{H}_4\text{NH}(\text{SiMe}_3)] (L^3H)$ 

To a stirred solution of 3c (5.15 g, 27.0 mmol) in  $\text{Et}_2\text{O}$  (50  $\text{cm}^3$ ) at  $0^\circ\text{C}$  was slowly added  $\text{ClSiMe}_3$  (3.5  $\text{cm}^3$ , 27.0 mmol). The reaction mixture was warmed to room temperature (*ca.* 1 h) and stirred for another 5 h. The reaction solution was decanted from the  $\text{LiCl}$  formed in the conversion. The solvent volume was then reduced *in vacuo* until a residual oil remained which was vacuum distilled and upon cooling formed a colourless



crystalline solid (yield 5.3 g, 76 %). (Found: C, 69.98; H, 7.57; N, 5.60.  $\text{C}_{15}\text{H}_{19}\text{NOSi}$  requires C, 69.99; H, 7.44; N, 5.44 %) Infrared (Nujol,  $\text{v}/\text{cm}^{-1}$ ) 3401 vs, 1606 vs, 1589 s, 1583 s, 1499 s, 1462 br s, 1377 vs, 1307 vs, 1253 vs, 1240 vs, 1217 s, 1179 w, 1161 s, 1099 s, 1072 w, 1038 s, 1024 w, 912 vs, 841 s, 750 vs, 689 vs. Mass Spectrum  $m/z$  257 (60%)  $[L^3H]^+$ , 242 (61)  $[L^3H - \text{Me}]^+$ , 226 (15)  $[L^3 - \text{Me}_2]^+$ , 211 (5)  $[L^3 - \text{Me}_3]^+$ , 165 (100)  $[\text{OC}_6\text{H}_4\text{NHSiMe}_2]^+$ , 150 (40)  $[\text{C}_6\text{H}_4\text{ONHSiMe}]^+$ , 135 (30)  $[\text{C}_6\text{H}_4\text{OSiNH}]^+$ , 73 (35)  $[\text{SiMe}_3]^+$ , 58 (10)  $[\text{SiMe}_2]^+$ .  $^1\text{H NMR}$  (300 MHz,  $\text{C}_6\text{D}_6$ , 298 K):  $\delta$  0.07 (9 H, s,  $\text{SiMe}_3$ ), 6.57-6.63 (1 H, ddd, H4), 6.76-6.80 (1 H, tt, H5), 6.82-6.88 (1 H, dd, H3), 6.90-7.02 (6 H, m, H6, H2', H3', H4', H5', H6').

### 8.5.3 Synthesis of Homoleptic Lanthanoid Complexes Containing $L^2$

#### 3e) $[Yb(L^2)_3]$

a) To a stirred suspension of  $YbCl_3(THF)_3$  (0.37 g, 0.75 mmol) in THF (40 cm<sup>3</sup>) was added  $[Li(L^2)_2(OEt_2)]_2$  (0.62 g, 1.12 mmol) and the resulting mixture was stirred for 12 h. The solvent was removed under vacuum and hexane added (30 cm<sup>3</sup>) giving a white precipitate. The red solution was filtered and the filtrate concentrated to 15 cm<sup>3</sup>. A red crystalline product was obtained on standing for 2 h (yield 0.41 g, 72 %) (Found: C, 47.88; H, 6.44; N, 5.63.  $C_{30}H_{48}N_3O_3Si_3Yb$  requires C, 47.66; H, 6.40; N, 5.56 %). Infrared (Nujol, v/cm<sup>-1</sup>): 1593 vs, 1561 vs, 1485 s, 1465 m, 1321 vs, 1294 vs, 1283 s, 1245 vs, 1209 s, 1159 w, 1059 w, 1051 s, 1012 s, 1000 vs, 913 br s, 843 br vs, 822 s, 787 m, 770 s, 743 s, 681 s, 629 s, 598 s. Vis-near IR [ $\lambda_{max}$  ( $\epsilon$ )] (DME): 431 (185), 874 (9), 911 (14), 945 (6), 978 (35) nm (dm<sup>3</sup> mol<sup>-1</sup>).

b) (2:1 Li to Ln mole ratio (*in situ*)) To a stirred solution of compound  $L^2H$  (0.71 g, 3.6 mmol) in THF (40 cm<sup>3</sup>) at 0°C was slowly added  $LiBu^p$  (2.31 cm<sup>3</sup>, 3.7 mmol) and the resulting solution was warmed to room temperature over *ca.* 1 h. To the resulting solution  $YbCl_3(THF)_2$  (0.76 g, 1.80 mmol) was added, and the reaction mixture rapidly stirred for 12 h. The solvent was removed *in vacuo*, and hexane (30 cm<sup>3</sup>) was added affording a white precipitate. The red solution was filtered and the filtrate volume reduced to *ca.* 2 cm<sup>3</sup> under vacuum and red crystals of  $[Yb(L^2)_3]$  **3a** were deposited on standing overnight. (infrared identification)



3f)  $[Er(L^2)_3]$ 

To a stirred solution of compound  $L^2H$  (0.72g., 3.7 mmol) in THF (40  $cm^3$ ) at  $0^\circ C$  was added  $LiBu^n$  (2.30  $cm^3$ , 3.7 mmol), and the resulting solution was warmed to room temperature over *ca.* 1 h. The compound  $ErCl_3(THF)_{3.5}$  (0.63 g, 1.20 mmol) was then added and the reaction mixture stirred for 15 h. The solvent was then removed under vacuum and hexane (30  $cm^3$ ) was added giving a white precipitate. The light pink solution was filtered and the filtrate volume reduced to 10  $cm^3$  under vacuum. The light pink crystals deposited on standing for 12 h (yield 0.43 g, 48 %) (Found: C, 48.16; H, 6.70; N, 5.73.  $C_{30}H_{48}ErN_3O_3Si_3$  requires C, 48.03; H, 6.45; N, 5.60 %). Infrared (Nujol,  $\nu/cm^{-1}$ ): 1593 vs, 1561 vs, 1485 s, 1464 m, 1321 vs, 1284 vs, 1240 s, 1209 s, 1156 vs, 1117 vs, 1058 w, 1051 s, 1011 s, 1000 vs, 911 br s, 841 br vs, 784 s, 768 s, 735 s, 681 s, 627 s, 597 s. Mass Spectrum:  $m/z$  646 (<1%)  $[Er(L^2)_2NC_6H_4]^+$ , 556 (<1)  $[Er(L^2)_2]^+$ , 480 (<1)  $[Er(L^2)(C_6H_4NSi)]^+$ , 195 (35)  $[(L^2H)]^+$ , 180 (20)  $[(L^2H) - Me]^+$ , 165 (100)  $[(L^2H) - 2Me]^+$ , 150 (35)  $[(L^2H) - 3Me]^+$ , 135 (20)  $[C_6H_5ONSi]^+$ , 73 (20)  $[SiMe_3]^+$ , 58 (10)  $[SiMe_2]^+$ .

3g)  $[Sm(L^2)_3]$ 

A similar preparation method to that used for compound 3f gave yellow crystals of 3g (yield 0.36 g, 41 %). (Found: C, 48.55; H, 6.67; N, 5.67.  $C_{30}H_{48}N_3O_3Si_3Sm$  requires C, 49.13; H, 6.60; N, 5.73 %) Infrared (Nujol,  $\nu/cm^{-1}$ ): 1585 vs, 1559 vs, 1481 s, 1307 vs, 1279 vs, 1237 s, 1211 s, 1173 vs, 1117 vs, 1076 vs, 1058 w, 1050 vs, 1030 vs, 937 s, 919 s, 842 s, 825 s, 772 vs, 741 vs, 735 s, 662 vs, 616 s, 597 s. Mass Spectrum:  $m/z$  734 (<1%)  $[Sm(L^2)_3]^+$ , 630 (<1)  $[Sm(L^2)_2NC_6H_4]^+$ , 540 (<1)  $[Sm(L^2)_2]^+$ , 464 (<1)  $[Sm(L^2)(C_6H_4NSi)]^+$ , 195 (35)  $[(L^2H)]^+$ , 180 (20)  $[(L^2H) - Me]^+$ , 165 (100)  $[(L^2H) - 2Me]^+$ , 150 (35)  $[(L^2H) - 3Me]^+$ , 135 (20)  $[C_6H_5ONSi]^+$ , 73 (20)  $[SiMe_3]^+$ , 58 (10)  $[SiMe_2]^+$ .

3h)  $[\text{Nd}(\text{L}^2)_3]$ 

a) A similar preparation method to that used for compound 3f gave blue crystals of 3h (yield 0.57 g, 65 %). (Found: C, 49.85; H, 6.81; N, 5.73.  $\text{C}_{30}\text{H}_{48}\text{N}_3\text{NdO}_3\text{Si}_3$  requires C, 49.55; H, 6.65; N, 5.78 %) Infrared (Nujol,  $\text{v}/\text{cm}^{-1}$ ): 1590 vs, 1560 m, 1484 s, 1319 vs, 1285 vs, 1246 m, 1209 s, 1163 s, 1117 vs, 1058 w, 1050 s, 1011 s, 1002 vs, 914 br s, 841 br vs, 767 s, 743 vs, 675 m, 625 s, 597 s. Mass Spectrum:  $m/z$  726 (10 %)  $[\text{Nd}(\text{L}^2)_3]^+$ , 622 (5)  $[\text{Nd}(\text{L}^2)_2\text{C}_6\text{H}_4\text{N}]^+$ , 532 (30)  $[\text{Nd}(\text{L}^2)_2]^+$ , 305 (5)  $[\text{Nd}(\text{L}^2) - \text{OMe}]^+$ , 195 (40)  $[(\text{L}^2\text{H})]^+$ , 180 (15)  $[(\text{L}^2\text{H}) - \text{Me}]^+$ , 165 (70)  $[(\text{L}^2\text{H}) - 2\text{Me}]^+$ , 150 (30)  $[(\text{L}^2\text{H}) - 3\text{Me}]^+$ , 135 (25)  $[\text{C}_6\text{H}_5\text{ONSi}]^+$ , 73 (100)  $[\text{SiMe}_3]^+$ , 58 (35)  $[\text{SiMe}_2]^+$ . NMR (300 MHz,  $\text{C}_6\text{D}_6$ , 298 K):  $^1\text{H}$ ,  $\delta$  -16.98 (9 H, br s, OMe), -4.20 (27 H, br s,  $\text{SiMe}_3$ ), 1.14 (3 H, s, H4 or H5), 7.88 (3H, s, H4 or H5), 14.18 (3H, s, H3 or H6), 23.60 (3H, s, H3 or H6).

b) (using 1:2 Ln to  $\text{L}^3$  mole ratio (*in situ*)) - To a stirred solution of compound  $\text{L}^2\text{H}$  (0.71 g, 3.6 mmol) in THF (40  $\text{cm}^3$ ) at 0°C was slowly added  $\text{LiBu}^n$  (2.31  $\text{cm}^3$ , 3.7 mmol) and the resulting solution was warmed to room temperature over *ca.* 1 h. To the resulting solution  $\text{NdCl}_3(\text{THF})_2$  (0.71 g, 1.80 mmol) was added, and the reaction mixture rapidly stirred for 12 h. The solvent was removed *in vacuo*, and hexane (30  $\text{cm}^3$ ) was added affording a white precipitate. The blue solution was filtered and the filtrate volume reduced to *ca.* 2  $\text{cm}^3$  under vacuum. Blue crystals deposited on standing overnight. The infrared spectrum was similar to that of  $[\text{Nd}(\text{L}^2)_3]$  (3e). Unit Cell data- $\text{C}_{30}\text{H}_{48}\text{N}_3\text{NdO}_3\text{Si}_3$ ,  $M$  724.2, monoclinic,  $a$  10.121(1),  $b$  18.876(1),  $c$  18.814(1) Å;  $\alpha = 90$ ,  $\beta = 104.37(1)$ ,  $\gamma = 90^\circ$ ;  $V$  3500.2 Å<sup>3</sup>,  $T \sim 123$  K were in agreement with those obtained previously (Chapter 3; section 3.2.1).

c) (using 1:2 Ln to Li (*isolated*) ratio)  $\text{NdCl}_3(\text{THF})_2$  (0.30 g, 0.75 mmol) and  $[\text{Li}(\text{L}^2)(\text{OEt}_2)]_2$  (0.42 g, 0.75 mmol) were stirred together in THF (40  $\text{cm}^3$ ). After 12 h, the pale yellow solution was evaporated to dryness under reduced pressure and hexane added. The resulting white solid was filtered and the filtrate evaporated to dryness under vacuum affording a blue crystalline material (yield 0.20 g, 55 %). The infrared and  $^1\text{H}$  NMR spectra were identical to those of  $[\text{Nd}(\text{L}^2)_3]$ .

3i)  $[Pr(L^2)_3]$ 

A similar preparation method to that used for compound 3f gave green crystals of 3i (yield 0.49 g, 57 %). (Found: C, 49.56; H, 6.71; N, 5.97.  $C_{30}H_{48}N_3O_3PrSi_3$  requires C, 49.78; H, 6.68; N, 5.80 %) Infrared (Nujol,  $\nu/cm^{-1}$ ): 1590 vs, 1561 vs, 1484 s, 1449 s, 1320 vs, 1285 vs, 1246 br s, 1210 s, 1164 vs, 1117 vs, 1058 w, 1050 s, 1011 s, 1002 vs, 915 br s, 841 br s, 768 s, 743 s, 674 s, 625 s, 597 s.

8.5.4 Synthesis of Homoleptic Lanthanoid Complexes Containing  $L^3$ 3j)  $[Yb(L^3)_3] \cdot (PhMe)$ 

To a stirred solution of compound  $L^3H$  (0.77g, 3.0 mmol) in THF (40  $cm^3$ ) at  $0^\circ C$  was added  $LiBu^a$  (1.88  $cm^3$ , 3.0 mmol), and the resulting solution was warmed to room temperature over *ca.* 1 h. The compound  $YbCl_2 \cdot (THF)_2$  (0.42 g, 1.0 mmol) was then added and the reaction mixture stirred for 12 h. The solvent was then removed under vacuum and toluene (30  $cm^3$ ) added giving a white precipitate. The red solution was filtered at  $-78^\circ C$  and the filtrate volume reduced to 25  $cm^3$  under vacuum. Red crystals of good X-ray quality were deposited on standing overnight (yield 0.70 g, 68 %). (Found: C, 59.69; H, 6.42; N, 4.35.  $C_{52}H_{62}N_3O_3Si_3Yb$  requires C, 60.38; H, 6.04; N, 4.06 %) Infrared (Nujol,  $\nu/cm^{-1}$ ): 1589 vs, 1557 m, 1480 s, 1287 vs, 1249 vs, 1188 vs, 1153 vs, 1124 w, 1098 s, 1072 w, 1052 s, 1022 m, 1006 w, 919 s, 858 w, 824 m, 803 vs, 770 vs, 694 vs, 675 w, 618 s, 592 s, 562 w. Mass Spectrum  $m/z$  942 (<1%)  $[Yb(L^3)_3]^+$ , 849 (<1)  $[Yb(L^3)_3(C_6H_4NSiMe_3)]^+$ , 776 (16)  $[Yb(L^3)_2(C_6H_4N)]^+$ , 686 (35)  $[Yb(L^3)_2]^+$ , 671 (15)  $[Yb(L^3)_2 - Me]^+$ , 609 (18)  $[Yb(L^3)_2(OC_6H_4NSiMe_3)]^+$ , 593 (3)  $[Yb(L^3)(C_6H_4NSiMe_3)]^+$ , 523 (4)  $[Yb(L^3)OC_6H_5]^+$ , 430 (30)  $[Yb(L^3)]^+$ , 415 (35)  $[Yb(L^3) - Me]^+$ , 400 (7)  $[Yb(L^3) - 2Me]^+$ , 353 (3)  $[Yb(OC_6H_4NSiMe_3)]^+$ , 337 (5)  $[Yb(C_6H_4NSiMe_3)]^+$ , 257 (20)  $[(L^3H)]^+$ , 242 (16)  $[(L^3H) - Me]^+$ , 226 (10)  $[(L^3) - 2Me]^+$ , 165 (50)  $[OC_6H_4NHSiMe_2]^+$ , 150 (15)  $[C_6H_4ONHSiMe]^+$ , 73 (100)  $[SiMe_3]^+$ .

3k)  $[\text{Yb}(\text{L}^3)_3] \cdot (\text{C}_5\text{H}_9\text{Me})$  (using a 1:2 Ln:Li ratio)

a) THF (40 cm<sup>3</sup>) was added to the solids  $[\text{Li}(\text{L}^3)(\text{DME})]$  (0.53g, 1.5 mmol) and  $\text{YbCl}_3(\text{THF})_2$  (0.32 g, 0.75 mmol) and the resulting mixture was stirring for 12 h. The solvent was then removed under vacuum and toluene (25 cm<sup>3</sup>) added giving a white precipitate. The red solution was filtered at -78°C and the filtrate volume reduced to 20 cm<sup>3</sup> under vacuum. Red crystals suitable for X-ray analysis deposited on standing overnight (yield 0.15g, 24% (based on L<sup>3</sup>)). (Found: C, 57.47; H, 6.01; N, 4.22.  $\text{C}_{31}\text{H}_{66}\text{N}_3\text{O}_3\text{Si}_3\text{Yb}$  (solvate) requires C, 59.68; H, 6.48; N, 4.09;  $\text{C}_{45}\text{H}_{54}\text{N}_3\text{O}_3\text{Si}_3\text{Yb}$  ( $[\text{Yb}(\text{L}^3)_3]$ ) requires C, 57.36; H, 5.78; N, 4.46 %) Infrared (Nujol, v/cm<sup>-1</sup>): 1593 vs, 1560 m, 1480 sh w, 1307 w, 1280 s, 1242 s, 1185 s, 1098 s, 1072 m, 1052 s, 1020 m, 1004 w, 908 s, 858 sh w, 840 s, 802 w, 780 w, 726 s, 691 s, 618 s. Mass Spectrum *m/z* 776 (<1%)  $[\text{Yb}(\text{L}^3)_2(\text{C}_6\text{H}_4\text{N})]^+$ , 686 (4)  $[\text{Yb}(\text{L}^3)_2]^+$ , 507 (4)  $[\text{Yb}(\text{L}^3)(\text{OC}_6\text{H}_5)]^+$ , 430 (10)  $[\text{Yb}(\text{L}^3)]^+$ , 415 (10)  $[\text{Yb}(\text{L}^3) - \text{Me}]^+$ , 353 (10)  $[\text{Yb}(\text{OC}_6\text{H}_4\text{NSiMe}_3)]^+$ , 337 (10)  $[\text{Yb}(\text{C}_6\text{H}_4\text{NSiMe}_3)]^+$ , 257 (45)  $[(\text{L}^3)]^+$ , 242 (40)  $[(\text{L}^3) - \text{Me}]^+$ , 226 (5)  $[(\text{L}^3) - 2\text{Me}]^+$ , 165 (100)  $[\text{OC}_6\text{H}_4\text{NSiMe}_2]^+$ , 150 (35)  $[\text{C}_6\text{H}_4\text{ONSiMe}]^+$ , 73 (50)  $[\text{SiMe}_3]^+$ .

b) (2:1 Li to Ln mole ratio (*in situ*)) To a stirred solution of compound L<sup>3</sup>H (0.64 g, 2.5 mmol) in THF (40 cm<sup>3</sup>) at 0°C was slowly added LiBu<sup>n</sup> (1.65 cm<sup>3</sup>, 2.6 mmol) and the resulting solution was warmed to room temperature over *ca.* 1 h. To the resulting solution  $\text{YbCl}_3(\text{THF})_{3.5}$  (0.66 g, 1.25 mmol) was added, and the reaction mixture rapidly stirred for 12 h. The solvent was removed *in vacuo*, and hexane (30 cm<sup>3</sup>) added affording a white precipitate. The pale yellow solution was filtered and the filtrate volume reduced to *ca.* 15 cm<sup>3</sup> under vacuum. Yellow crystals deposited on standing and were dried at room temperature under vacuum. The infrared spectrum was similar to that of  $[\text{Yb}(\text{L}^3)_3] \cdot (\text{C}_5\text{H}_9\text{Me})$  (3j).

3l)  $[Y(L^3)_3] \cdot (C_5H_9Me)$ 

A similar procedure to that used for compound 3j gave colourless crystals of 3l (yield 0.61 g, 71 %). (Found: C, 65.70; H, 7.49; N, 4.46.  $C_{51}H_{66}N_3O_3Si_3Y$ (solvate) requires C, 65.01; H, 7.06; N, 4.46;  $C_{45}H_{54}N_3O_3Si_3Y$  ( $[Y(L^3)_3]$ ) requires C, 62.99; H, 6.34; N, 4.90 %) Infrared (Nujol,  $\nu/cm^{-1}$ ): 1592 vs, 1557 m, 1489 s, 1278 vs, 1239 vs, 1210 s, 1170 s, 1152 vs, 1099 vs, 1071 m, 1049 s, 1020 m, 1004 w, 911 br s, 860 w, 824 s, 776 s, 735 vs, 692 vs, 675 w, 625 w, 592 s, 560 w. Mass Spectrum  $m/z$  857 (<1%)  $[Y(L^3)_3]^+$ , 601 (20)  $[Y(L^3)_2]^+$ , 524 (5)  $[Y(L^3)(OC_6H_4NSiMe_3)]^+$ , 438 (5)  $[Y(L^3)(OC_6H_5)]^+$ , 330 (5)  $[Y(L^3) - Me]^+$ , 257 (40)  $[(L^3H)]^+$ , 242 (20)  $[(L^3H) - Me]^+$ , 164 (60)  $[OC_6H_4NSiMe_2]^+$ , 149 (25)  $[C_6H_4ONSiMe]^+$ , 73 (100)  $[SiMe_3]^+$ . NMR (300 MHz,  $C_6D_6$ , 298 K):  $^1H$ ,  $\delta$  0.43 (27 H, s,  $SiMe_3$ ), 0.89-1.45 (br m, 6 H,  $C_5H_9Me$ ), 5.97-6.15 (3 H, dd,  $^3J$  7.1 Hz,  $^4J$  1.2 Hz, H6), 6.20-6.30 (3 H, ddd,  $^3J$  6.9 Hz,  $^4J$  1.5 Hz, H5), 6.40-6.97 (21 H, br m, H3, H4, H2'-6').

3m)  $[Sm(L^3)_3] \cdot (PhMe)$ 

A similar preparation method to that used for compound 3j gave yellow crystals of 3m (yield 0.56 g, 56 %). (Found: C, 62.83; H, 6.74; N, 4.22.  $C_{52}H_{62}N_3O_3Si_3Sm$  requires C, 61.73; H, 6.18; N, 4.15 %) Infrared (Nujol,  $\nu/cm^{-1}$ ): 1591 vs, 1557 w, 1480 s, 1283 vs, 1248 vs, 1186 vs, 1155 vs, 1102 vs, 1071 w, 1053 s, 1021 w, 1005 w, 915 s, 826 s, 802 vs, 774 s, 727 vs, 694 vs, 676 w, 622 s, 593 s. Mass Spectrum  $m/z$  922 (<1%)  $[Sm(L^3)_3]^+$  827 (<1),  $[Sm(L^3)_2(C_6H_4NSiMe_3)]^+$ , 757 (<1)  $[Sm(L^3)_2(OC_6H_5)]^+$ , 664 (10)  $[Sm(L^3)_2]^+$ , 587 (<1)  $[Sm(L^3)(OC_6H_4NSiMe_3)]^+$ , 408 (3)  $[Sm(L^3)_2]^+$ , 392 (3)  $[Sm(L^3) - Me]^+$ , 331 (4)  $[Sm(OC_6H_4NSiMe_3)]^+$ , 315 (5)  $[Sm(C_6H_4NSiMe_3)]^+$ , 257 (100)  $[(L^3H)]^+$ , 242 (100)  $[(L^3H) - Me]^+$ , 226 (20)  $[(L^3) - 2Me]^+$ , 165 (100)  $[OC_6H_4NHSiMe_2]^+$ , 150 (40)  $[C_6H_4ONHSiMe]^+$ , 73 (70)  $[SiMe_3]^+$ . NMR (300 MHz,  $C_6D_6$ , 298 K):  $^1H$   $\delta$  -1.63 (27 H, s,  $SiMe_3$ ), 2.10 (3H, s, Me (Tol)), 4.26 (6 H, br s, H2', H6'), 5.31-5.45 (6 H, br s, H3', H5'), 5.49-5.60 (3 H, br s, H4'), 6.30-6.50 (3H, dd, H3 or H6), 6.90-7.10 (5 H, *PhMe* (Tol)), 7.40-7.46 (3 H, ddd, H4 or H5), 8.28-8.31 (3H, ddd, H5 or H5), 10.67-10.70 (3H, dd, H3 or H6).

**3n) [Nd(L<sup>3</sup>)<sub>3</sub>].(PhMe)<sub>2</sub>**

a) A similar preparation method to that used for compound **3j** gave blue crystals of **3n** (yield 0.68 g, 62 %). (Found: C, 64.48; H, 6.54; N, 4.13. C<sub>59</sub>H<sub>70</sub>N<sub>3</sub>NdO<sub>3</sub>Si<sub>3</sub> requires C, 64.56; H, 6.43; N, 3.83 %) Infrared (Nujol, v/cm<sup>-1</sup>): 1591 vs, 1557 w, 1481 s, 1337 vs, 1285 vs, 1249 vs, 1187 vs, 1155 vs, 1103 vs, 1070 w, 1071 w, 1052 s, 1020 w, 1005 w, 916 vs, 826 s, 802 s, 773 s, 728 vs, 694 vs, 676 w. NMR (300 MHz, C<sub>6</sub>D<sub>6</sub>, 298 K): <sup>1</sup>H δ - 8.05 (6 H, br s, H2',H6'), -1.22 (27 H, br s, SiMe<sub>3</sub>), 0.48 (6 H, br s, H3',H5'), 0.90 (3 H, s, H4 or H5), 1.20 (3 H, br s, H4'), 2.11 (6H, s, Me (Tol)), 6.97-7.14 (13 H, m, H4 or H5 and PhMe (Tol)), 13.90 (3H, br s, H3 or H6), 23.28 (3H, br s, H3 or H6). Recrystallisation of [Nd(L<sup>3</sup>)<sub>3</sub>].(PhMe)<sub>2</sub> from hexane afforded crystals of solvent free [Nd(L<sup>3</sup>)<sub>3</sub>].

b) (2:1 Li to Ln mole ratio (*in situ*)) To a stirred solution of compound L<sup>3</sup>H (0.64 g, 2.5 mmol) in THF (40 cm<sup>3</sup>) at 0°C was slowly added LiBu<sup>n</sup> (1.65 cm<sup>3</sup>, 2.6 mmol) and the resulting solution was warmed to room temperature over *ca.* 1 h. To the resulting solution NdCl<sub>3</sub>(THF)<sub>2</sub> (0.49 g, 1.25 mmol) was added, and the reaction mixture rapidly stirred for 12 h. The solvent was removed *in vacuo*, and hexane (30 cm<sup>3</sup>) added affording a white precipitate. The blue solution was filtered and the filtrate volume reduced to *ca.* 15 cm<sup>3</sup> under vacuum. Blue crystals of [Nd(L<sup>3</sup>)<sub>3</sub>] deposited on standing. (Infrared identification) Unit Cell data-C<sub>45</sub>H<sub>54</sub>N<sub>3</sub>NdO<sub>3</sub>Si<sub>3</sub>, *M* 910.3, monoclinic, *a* 16.154(1), *b* 15.459(1), *c* 17.992(1) Å; α = 90, β = 103.0(1), γ = 90°; *V* 4378.1 Å<sup>3</sup>, *T* ~ 123 K were in agreement with those obtained previously (Chapter 3; Section 3.2.2).

3o)  $[La(L^3)_3](PhMe)$ 

A similar preparation method to that used for compound **3j** gave yellow crystals of **3o** (yield 0.35 g, 35 %). (Found: C, 62.27; H, 6.35; N, 4.32.  $C_{52}H_{62}LaN_3O_3Si_3$  requires C, 62.44; H, 6.25; N, 4.20 %) Infrared (Nujol,  $\nu/cm^{-1}$ ): 1589 vs, 1557 m, 1480 s, 1287 vs, 1249 vs, 1188 vs, 1155 vs, 1103 vs, 1070 w, 1050 s, 1020 m, 1004 w, 919 s, 858 w, 824 m, 803 vs, 770 vs, 694 vs, 675 w, 618 s, 592 s, 562 w. Mass Spectrum  $m/z$  651 (3)  $[La(L^3)_2]^+$ , 395 (<1)  $[La(L^3)]^+$ , 257 (70)  $[(L^3H)]^+$ , 242 (65)  $[(L^3H) - Me]^+$ , 226 (15)  $[(L^3) - 2Me]^+$ , 165 (100)  $[OC_6H_4NHSiMe_2]^+$ , 150 (40)  $[C_6H_4ONHSiMe]^+$ , 135 (30)  $[C_6H_4OSiNH]^+$ , 73 (50)  $[SiMe_3]^+$ . NMR (300 MHz,  $C_6D_6$ , 298 K):  $^1H$ ,  $\delta$  0.07 (27 H, s,  $SiMe_3$ ), 2.10 (3 H, s, Me (*MePh*)), 6.57-6.63 (3 H, dd, H6), 6.76-6.80 (3 H, ddd, H5), 6.82-6.88 (3H, ddd, H4), 6.90-7.02 (18 H, m, H3, H2'-6'), 7.03-7.12 (5 H, m, Ph (*MePh*)).

3p)  $[La(L^3)_3]$  (using a 1:2 Ln to Li ratio)

a)  $LaCl_3$  (0.18 g, 0.75 mmol) and  $[Li(L^3)(DME)]$  (0.53 g, 1.50 mmol) were stirred together in THF (40  $cm^3$ ). After 12 h, the pale yellow solution was evaporated to dryness under reduced pressure and toluene was added. The resulting white solid was filtered, the filtrate was evaporated to dryness and  $Et_2O$  was added (20  $cm^3$ ). The solution was concentrated to *ca.* 10  $cm^3$  and on standing for 2 days colourless crystals of **3p** (suitable for an X-ray crystallographic study) were deposited (yield 0.35 g, 77 %). Infrared (Nujol,  $\nu/cm^{-1}$ ): 1590 vs, 1557 m, 1480 s, 1444 s, 1288 vs, 1251 vs, 1189 vs, 1155 vs, 1102 vs, 1072 w, 1052 s, 1020 m, 1004 w, 964 w, 917 s, 858 w, 826 m, 801 s, 771 s, 735 s, 722 s, 695 s, 674 w, 632 w, 622 s, 594 s, 559 w. NMR (300 MHz,  $C_6D_6$ , 298 K):  $^1H$ ,  $\delta$  0.35 (27 H, s,  $SiMe_3$ ), 6.10 (3 H, dd,  $^3J$  7.6 Hz,  $^4J$  1.2 Hz, H6), 6.75 (3 H, ddd,  $^3J$  7.3 Hz,  $^4J$  1.6 Hz, H5), 6.79-6.90 (21 H, m, H3, H4, H2'-6').

b) (2:1 Li to Ln ratio (*in situ*)) To a stirred solution of compound  $L^3H$  (0.64 g, 2.5 mmol) in THF (40 cm<sup>3</sup>) at 0°C was slowly added  $LiBu^n$  (1.65 cm<sup>3</sup>, 2.6 mmol) and the resulting solution was warmed to room temperature over *ca.* 1 h. To the resulting solution  $LaCl_3(THF)_2$  (0.49 g, 1.25 mmol) was added, and the reaction mixture rapidly stirred for 12 h. The solvent was removed *in vacuo*, and hexane (30 cm<sup>3</sup>) added affording a white precipitate. The pale yellow solution was filtered and the filtrate volume reduced to *ca.* 15 cm<sup>3</sup> under vacuum. Light yellow crystals deposited on standing. The infrared spectrum was identical to that of  $[La(L^2)_3]$  (**3p (a)**).

## 8.6 Experimental Procedures for Chapter 4

### 8.6.1 Synthesis of $[Ln(L^2)_2(\mu-Cl)]_2$ Complexes (Ln = Yb, Er and Tb)

#### 4a) $[Yb(L^2)_2(\mu-Cl)]_2$

##### Method 1

To a stirred suspension of  $YbCl_3(THF)_3$  (0.68 g, 1.37 mmol) in THF (40 cm<sup>3</sup>) was added  $[Li(L^2)(OEt_2)]_2$  (0.76 g, 1.37 mmol). The solution was stirred for 15 h, the solvent was removed under vacuum and hexane (30 cm<sup>3</sup>) was added. After heating the stirred solution for 2 h, the warm mixture was filtered and on cooling to room temperature the filtrate afforded red crystals (suitable for X-ray analysis) of the title complex (yield 0.51 g, 63 %). (Found: C, 39.15; H, 5.57; N, 4.72.  $C_{40}H_{64}Cl_2N_4O_4Si_4Yb_2$  requires C, 40.23; H, 5.40; N, 4.69 %) Infrared (Nujol, v/cm<sup>-1</sup>): 1594 s, 1563 w, 1318 w, 1290 s, 1277 s, 1242 vs, 1210 m, 1158 s, 1117 vs, 1051 m, 1002 s, 917 s, 844 vs, 826 s, 792 w, 768 m, 730 vs, 679 m, 627 w, 597 w. Vis-near IR [ $\lambda_{max}$  (ε)] (DME): 457 (156), 935 (4), 982 (18), 985 (17) nm (dm<sup>3</sup> mol<sup>-1</sup>).



**Method 2**

Tetrahydrofuran (40 cm<sup>3</sup>) was added to the solids [Li(L<sup>2</sup>)(OEt<sub>2</sub>)<sub>2</sub>] (0.29 g, 0.50 mmol) and [Yb(MeCp)Cl<sub>2</sub>(THF)<sub>3</sub>] (0.28 g, 0.50 mmol). The resulting dark red mixture was stirred for 12 h, the solvent was removed under vacuum and hexane was added (30 cm<sup>3</sup>). The mixture was filtered and the red filtrate concentrated to *ca.* 15 cm<sup>3</sup> to yield large red crystals of **4a** (yield 0.22 g, 74 %). The infrared spectrum was identical to that above. Unit Cell data-C<sub>40</sub>H<sub>64</sub>Cl<sub>2</sub>N<sub>4</sub>O<sub>4</sub>Si<sub>4</sub>Yb<sub>2</sub>, *M* 1194.3, monoclinic, *a* 14.614(1), *b* 18.063(1), *c* 19.012(1) Å; α = 90, β = 92.44, γ = 90°; *V* 5015 Å<sup>3</sup>, *T* ~ 123 K, *N* 1263 were in agreement with those obtained previously (Chapter 4; section 4.2.2.1).

**4b) [Er(L<sup>2</sup>)<sub>2</sub>(μ-Cl)]<sub>2</sub>**

Addition of [Li(L<sup>2</sup>)(OEt<sub>2</sub>)<sub>2</sub>] (0.55 g, 1.0 mmol) to a suspension of ErCl<sub>3</sub>(THF)<sub>2</sub> (0.42 g, 1.0 mmol) in THF (40 cm<sup>3</sup>) resulted in precipitation of a white solid and formation of a pink solution. The solvent was removed under vacuum and hexane added (30 cm<sup>3</sup>). The mixture was warmed and filtered. The filtrate was concentrated to *ca.* 25 cm<sup>3</sup> affording X-ray quality pink crystals of **4b** (yield 0.36 g, 61 %). (Found: C, 39.79; H, 5.54; N, 4.96. C<sub>40</sub>H<sub>64</sub>Er<sub>2</sub>Cl<sub>2</sub>N<sub>4</sub>O<sub>4</sub>Si<sub>4</sub> requires C, 40.62; H, 5.45; N, 4.74 %). Infrared (Nujol, ν/cm<sup>-1</sup>): 1593 s, 1563 w, 1318 w, 1291 s, 1277 m, 1242 s, 1210 w, 1158 s, 1116 vs, 1051 m, 1001 s, 916 vs, 843 vs, 822 s, 788 m, 768 m, 729 vs, 679 m, 626 s, 597 s.

**4c) [Tb(L<sup>2</sup>)<sub>2</sub>(μ-Cl)]<sub>2</sub>**

A similar preparation method to that used for compound **4b** gave large pale yellow crystals of **4c** (yield 0.40 g, 68 %). (Found: C, 41.42; H, 5.39; N, 4.76. C<sub>40</sub>H<sub>64</sub>Cl<sub>2</sub>N<sub>4</sub>O<sub>4</sub>Si<sub>4</sub>Tb<sub>2</sub> requires C, 41.20; H, 5.53; N, 4.80 %). Infrared (Nujol, ν/cm<sup>-1</sup>): 1593 s, 1563 w, 1504 s, 1320 w, 1293 s, 1265 s, 1240 s, 1210 w, 1158 s, 1115 vs, 1051 m, 1001 s, 914 vs, 842 vs, 826 sh w, 783 m, 766 m, 727 vs, 669 m, 625 s, 596s.

### 8.6.2 Synthesis of $[Ln(L^3)_2(\mu-Cl)]_2$

#### 4d) $[Nd(L^3)_2(\mu-Cl)]_2(PhMe)_2$

To a stirring solution of  $NdCl_3(THF)_2$  (0.40 g, 1.0 mmol) in THF (40 cm<sup>3</sup>) was added  $[Li(L^3)(DME)]$  (0.72 g, 2.0 mmol). The resulting blue solution was evaporated to dryness and toluene was added (30 cm<sup>3</sup>). The reaction mixture was filtered and the filtrate volume was reduced under vacuum (ca. 15 cm<sup>3</sup>). Upon standing overnight suitable single blue crystals for X-ray crystallography of the title compound formed (0.35 g, yield 72 %). (Found: C, 54.47; H, 5.53; N, 3.63.  $C_{74}H_{88}Cl_2N_4Nd_2O_4Si_4$  requires C, 54.64; H, 5.65; N, 3.57 %) Infrared (Nujol,  $\nu/cm^{-1}$ ): 1585 s, 1294 s, 1266 m, 1243 s, 1185 s, 1160 s, 1100 s, 1074 w, 1036 m, 1022 w, 936 vs, 859 m, 828 br s, 774 m, 746 s, 727 s, 690 s, 679 w, 623 w. Vis-near IR [ $\lambda_{max}$  ( $\epsilon$ )] (DME): 428 (241), 926 (6), 949 (13), 988 (78), 995 (22) nm (dm<sup>3</sup> mol<sup>-1</sup>). NMR (300 MHz,  $C_6D_6$ , 298 K): <sup>1</sup>H,  $\delta$  -8.73 (8 H, br s, H2',6'), -5.04 (36 H, br s, SiMe<sub>3</sub>), 0.08 (8 H, s, H3',H5'), 1.18 (4H, s, H4'), 1.49 (8H, br s, H4, H5), 2.10 (6H, s, Me (Tol)), 7.02-7.20 (10H, m, Ar (Tol)), 15.4 (4 H, br s, H3 or H6), 30.95 (4 H, br s, H3 or H6).

#### 4e) $Yb(L^3)_2Cl(THF)_n$

To a stirring solution of  $YbCl_3(THF)_2$  (0.42 g, 1.0 mmol) in THF (40 cm<sup>3</sup>) was added  $[Li(L^3)(DME)]$  (0.72 g, 2.0 mmol). The resulting red solution was evaporated to dryness and this residue was extracted with toluene (30 cm<sup>3</sup>). The filtrate volume was evaporated to dryness under vacuum and Et<sub>2</sub>O (ca. 10 cm<sup>3</sup>) added. The solution was concentrated (1 cm<sup>3</sup>) and cooled to ca. -20°C where upon a brown oily residue was obtained. Infrared (Nujol,  $\nu/cm^{-1}$ ): 1589 s, 1558 w, 1289 s, 1243 s, 1192 s, 1162 s, 1122 s, 1102 s, 1082 w, 1025 w, 925 vs, 866 m, 834 br s, 785 w, 749 br m, 691 s.

### 8.6.3 Synthesis of $[Yb(L^3)_2(OAr)]$ ( $OAr = 2,6-(Bu^t)_2C_6H_3O$ )

#### 4f) $[Yb(L^3)_2(OAr)]$

Tris(2,6-di-*tert*-butylphenolato)ytterbium(III) (0.09 g, 0.11 mmol),  $[Li(L^3)]_n$  (0.06 g, 0.22 mmol) and hexane (20 cm<sup>3</sup>) were added to a flask, and the mixture was stirred for 15 h. The red reaction mixture was cooled to -78°C affording a white precipitate. The mixture was filtered and the filtrate allowed warmed to room temperature. After standing for 2 h, orange crystals (suitable for X-ray analysis) of the title complex formed (yield 0.07 g, 73 %). (Found: C, 59.01; H, 6.82; N, 2.94.  $C_{44}H_{57}N_2O_3Si_2Yb$  requires C, 59.30; H, 6.45; N, 3.14 %) Infrared (Nujol,  $v/cm^{-1}$ ): 1594 s, 1558 w, 1478 s, 1411 vs, 1351 w, 1280 vs, 1244 s, 1183 s, 1158 s, 1098 vs, 1074 w, 1048 br m, 1022 w, 1004 w, 916 vs, 861 s, 845 s, 827 s, 801 vs, 755 s, 734 s, 693 vs, 680 w, 659 m, 628 w, 593 w.

### 8.6.4 Synthesis of $[Yb(MeCp)(L)(\mu-Cl)]_2$ Complexes ( $L = L^2, L^3$ )

#### 4g) $[Yb(MeCp)(L^2)(\mu-Cl)]_2$ (using a Ln:Li ratio of 1:1)

To a THF solution (40cm<sup>3</sup>) of  $[Yb(MeCp)Cl_2(THF)]$  (0.20 g, 0.50 mmol) was added  $[Li(L^2)(OEt_2)]_2$  (0.14 g, 0.25 mmol). After stirring for 12 h, the solvent was removed under reduced pressure, and hexane (30 cm<sup>3</sup>) was added giving a white precipitate. The red solution was filtered and the filtrate volume reduced to 15 cm<sup>3</sup> under vacuum. The dark red/green crystals of the title compound were collected on standing for 2 weeks (yield 0.17 g, 72 %). (Found: C, 39.68; H, 4.71; N, 2.96.  $C_{32}H_{46}Cl_2N_2O_2Si_2Yb_2$  requires C, 39.88; H, 4.81; N, 2.91 %) Infrared (Nujol,  $v/cm^{-1}$ ): 1594 s, 1560 w, 1486 s, 1320 w, 1283 vs, 1247 vs, 1238 s, 1214 m, 1164 vs, 1119 vs, 1068 w, 1052 m, 1032 m 1011s, 911 vs, 897 w, 827 vs, 790 w, 768 vs, 746 w, 732 vs, 678 s, 629 s, 599 w. Vis-near IR [ $\lambda_{max}$  ( $\epsilon$ )] (DME): 426 (230), 938 (4), 982 (42), 994 (18) nm (dm<sup>3</sup> mol<sup>-1</sup>).

4h)  $[Yb(MeCp)(L^3)(\mu-Cl)]_2$ 

THF (40 cm<sup>3</sup>) was added to the solids  $[Yb(MeCp)Cl_2(THF)]$  (0.27g, 0.72 mmol) and  $[Li(L^3)(DME)]$  (0.26g, 0.72 mmol). The solvent was evaporated to dryness and hexane (30 cm<sup>3</sup>) was added giving a white precipitate. The orange solution was filtered and the filtrate volume reduced to 15 cm<sup>3</sup> under vacuum. The dark purple crystals (suitable for X-ray analysis) of the title compound deposited on standing for 12 h (yield 0.24 g, 62 %). (Found: C, 46.13; H, 4.65; N, 2.73.  $C_{42}H_{50}Cl_2N_2Yb_2O_2Si_2$  requires C, 46.37; H, 4.63; N, 2.57 %) Infrared (Nujol,  $\nu/cm^{-1}$ ): 1586 s, 1558 w, 1303 w, 1281 vs, 1245 vs, 1183 s, 1157 vs, 1100 vs, 1047 s, 1026 m, 960 w, 908 vs, 850 s, 831 vs, 786 s, 726 m, 695 s, 680 w, 632 w. Mass Spectrum:  $m/z$  509 (20 %)  $[Yb(L^3)(C_5H_4Me)]^+$ , 464 (5)  $[Yb(L^3)(C_5H_4Me) - 3Me]^+$ , 432 (<1)  $[Yb(L^3)(C_5H_4Me) - C_6H_5]^+$ , 416 (<1)  $[Yb(L^3)(C_5H_4Me) - OC_6H_5]^+$ , 337 (5)  $[Yb(C_6H_4NSiMe_3)]^+$ , 257 (10)  $[(L^3H)]^+$ , 226 (10)  $[(L^3) - 2Me]^+$ , 165 (15)  $[OC_6H_4NHSiMe_2]^+$ , 150 (15)  $[C_6H_4ONHSiMe]^+$ , 135 (20)  $[C_6H_5ONHSi]^+$ , 73 (100)  $[SiMe_3]^+$ , 58 (25)  $[SiMe_2]^+$ . Vis-near IR [ $\lambda_{max}$  ( $\epsilon$ )] (DME): 428 (241), 926 (6), 949 (13), 988 (78), 995 (22) nm (dm<sup>3</sup> mol<sup>-1</sup>).

*Reaction of  $[Yb(MeCp)Cl_2(THF)]$  with  $[Li(L^2)(OEt_2)]_2$  (from a Ln:Li mole ratio of 1:2)*

Tetrahydrofuran (40 cm<sup>3</sup>) was added to the solids  $[Li(L^2)(OEt_2)]_2$  (0.29 g, 0.50 mmol) and  $[Yb(MeCp)Cl_2(THF)]$  (0.28 g, 0.50 mmol). The resulting dark red mixture was stirred for 12 h at room temperature, the solvent was removed under vacuum and hexane was added (30 cm<sup>3</sup>). The mixture was filtered and the red filtrate concentrated to ca. 15 cm<sup>3</sup> to yield large red crystals of (Infrared identification)  $[Yb(L^2)_2(\mu-Cl)]_2$  4a (yield 0.22 g (1.8 mmol), 74%). Unit Cell data- $C_{40}H_{64}Cl_2N_4O_4Si_4Yb_2$ ,  $M$  1194.3, monoclinic,  $a$  14.614(1),  $b$  18.063(1),  $c$  19.012(1) Å;  $\alpha = 90^\circ$ ,  $\beta = 92.44^\circ$ ,  $\gamma = 90^\circ$ ;  $V$  5015 Å<sup>3</sup>,  $T \sim 123$  K,  $N$  1263 were in agreement with those obtained previously (Chapter 4; section 4.2.2.1).

*Reaction of  $[Yb(MeCp)(L^2)(\mu-Cl)]_2$  with  $[Li(L^2)(OEt_2)]_2$  (by a 1:1 ratio of Ln:Li)*

Treatment of  $[Yb(MeCp)(L^2)(\mu-Cl)]_2$  (0.10 g, 0.10 mmol) with  $[Li(L^2)(OEt_2)]_2$  (0.06 g, 0.10 mmol) in hexane resulted in a white precipitate and a red solution. The reaction mixture was filtered and the filtrate volume reduced affording red crystals of  $[Yb(L^2)_2(\mu-Cl)]_2$  4a (yield 0.06 g, 51%). The infrared spectrum was similar to that of the authentic compound ((4a) section 8.6.1).

## 8.7 Experimental Procedures for Chapter 5

### 8.7.1 Oxidation / Transmetalation Reactions

#### 5a) $[Yb(L^2)_2(THF)_2]$ (Method 1) (see next section for Method 2 (Ligand Exchange))

A mixture of ytterbium powder (0.69 g, 4.0 mmol),  $HgPh_2$  (0.71 g, 2.0 mmol) and  $L^2H$  (0.82 cm<sup>3</sup>, 4.0 mmol) in THF (60 cm<sup>3</sup>) was stirred and heated at 60°C for 8 h. The resulting mixture was filtered and the dark red filtrate evaporated to dryness leaving a dark red powder (crude yield 1.03g, 73 %). Infrared (Nujol, v/cm<sup>-1</sup>): 1583 vs, 1560 w, 1483 w, 1319 sh s, 1298 br s, 1251 s, 1203 s, 1162 vs, 1116 vs, 1054 s, 1033 w, 1011 s, 933 br s, 830 br s, 765 w, 723 s. Vis-near IR (DME):  $\lambda_{max}$  ( $\epsilon$ ) 487 sh (201), 906 (13), 978 (19) nm (dm<sup>3</sup> mol<sup>-1</sup>). <sup>1</sup>H NMR (300 MHz, C<sub>6</sub>D<sub>6</sub>, 298 K):  $\delta$  = 0.44 [s, 18 H, SiMe<sub>3</sub>], 1.23 [br s, 8 H,  $\beta$ -H (THF)], 3.29 [br s, 8 H,  $\alpha$ -H (THF)], 3.44 [s, 6 H, OMe], 6.56 - 6.59 [m, 4 H, H5, H6], 7.04 [s, 4 H, H3, H4].

#### 5b) $[Yb(L^2)_2(\mu-Ome)]_2$

##### Method 1

A mixture of Yb<sup>0</sup> metal (0.69g, 4.0 mmol),  $HgPh_2$  (0.71g, 2.0 mmol) and  $L^2H$  (0.82g, 4.0 mmol) in THF (60cm<sup>3</sup>) was stirred and heated at 60°C for 24 h. Evaporation of the filtered reaction mixture to dryness gave a red oil. Treatment of the residue with DME (20 cm<sup>3</sup>), evaporation to dryness, and then treatment with hexane (15 cm<sup>3</sup>) afforded X-ray quality red/orange crystals of **5b** on standing (yield 0.45 g, 19%). (Found: C, 42.55; H, 5.68; N, 4.91. C<sub>42</sub>H<sub>70</sub>N<sub>4</sub>O<sub>6</sub>Si<sub>4</sub>Yb<sub>2</sub> requires C, 42.55; H, 5.95; N, 4.73 %) Infrared (Nujol, v/cm<sup>-1</sup>): 1590 vs, 1560 vs, 1314 w, 1287 s, 1242 s, 1204 vs, 1160 vs, 1115 vs, 1050 vs, 1033 vs, 1005 vs, 916 br s, 843 s, 832 s, 782 vs, 768 vs, 723 s, 670 s, 642 vs, 596 vs. Vis-near IR [ $\lambda_{max}$  ( $\epsilon$ )] (DME): 431 (304), 911 (22), 978 (63) nm (dm<sup>3</sup> mol<sup>-1</sup>). Mass Spectrum  $m/z$  990 (<1) [M(dimer) - L<sup>2</sup>]<sup>+</sup>, 368 (<1) [YbL<sup>2</sup>]<sup>+</sup>.

**Method 2**

From a similar reaction (using  $\text{Yb}^0$  (0.30 g 1.7 mmol),  $\text{HgPh}_2$  (0.35 g 1.0 mmol and  $\text{L}^2\text{H}$  (0.41 g, 2.0 mmol)) the red oil was treated with diethyl ether instead of DME. Evaporation and recrystallisation of the residue from hexane (20  $\text{cm}^3$ ) gave **5b** (yield 0.22 g, 23 %). The spectroscopic and X-ray properties were identical with those of the product from *Method 1*.

**Method 3**

To **5a** (0.47 g, 0.66 mmol) in hexane (30  $\text{cm}^3$ ) was added  $\text{L}^2\text{H}$  (0.13 g, 0.66 mmol). The resulting mixture was heated to 60°C for 12 h. The reaction mixture was then allowed to stand for 3 weeks at room temperature and the solvent volume concentrated to 3  $\text{cm}^3$  giving crystals of **5b** which was identified by a unit cell determination, mass and IR spectra.

**5c) [Sm(L<sup>2</sup>)<sub>3</sub>] (Method 2) (For Method 1 (metathesis) see Section 8.5.3)**

A mixture of samarium powder (0.43g, 4.0 mmol),  $\text{HgPh}_2$  (0.71 g, 2.0 mmol) and  $\text{L}^2\text{H}$  (0.82  $\text{cm}^3$ , 4.0 mmol) in THF (60  $\text{cm}^3$ ) was stirred and heated at 60°C for 48 h. The resulting mixture was filtered and the pale yellow filtrate was evaporated to dryness. Recrystallisation of the yellow residue from hexane (20  $\text{cm}^3$ ) gave yellow crystals of **5c** (yield 0.24 g, 49 %). (Found: C, 48.55; H, 6.67; N, 5.67.  $\text{C}_{30}\text{H}_{48}\text{N}_3\text{O}_3\text{Si}_3\text{Sm}$  requires C, 49.13; H, 6.60; N, 5.73 %) Infrared (Nujol,  $\text{v}/\text{cm}^{-1}$ ): 1590 vs, 1560 vs, 1484 s, 1320 w, 1296 s, 1285 s, 1246 s, 1209 vs, 1156 vs, 1118 vs, 1055 w, 1050 s, 1010 m, 1001 s, 914 br s, 842 s, 832 s, 782 vs, 768 vs, 723 s, 670 s, 642 vs, 596 vs. Mass Spectrum:  $m/z$  734 (>1%)  $[\text{M}]^+$ , 630 (<1)  $[\text{Sm}(\text{L}^2)_2\text{C}_6\text{H}_4\text{N}]^+$ , 540 (5)  $[\text{Sm}(\text{L}^2)_2]^+$ , 316 (70)  $[\text{Sm}(\text{L}^2) - \text{OCH}_2]^+$ , 195 (65)  $[\text{L}^2\text{H}]^+$ , 165 (100)  $[\text{L}^2\text{H} - 2\text{Me}]^+$ , 150 (65)  $[\text{L}^2\text{H} - 3\text{Me}]^+$ , 135 (40)  $[\text{C}_6\text{H}_5\text{ONSi}]^+$ , 73 (100)  $[\text{SiMe}_3]^+$ , 58 (30)  $[\text{SiMe}_2]^+$ . NMR (300 MHz,  $\text{C}_6\text{D}_6$ , 298 K):  $^1\text{H}$ ,  $\delta$  - 2.34 (9 H, s, OMe), -1.85 (27 H, br s,  $\text{SiMe}_3$ ), 6.44 (3 H, dd, H3 or H6), 7.56 (3H, ddd, H4 or H5), 8.35 (3 H, m, H4 or H5), 10.67 (3 H, m, H3 or H6).

5d)  $[Yb(L^3)_2(OPh)(THF)]$  (Method 1)

A mixture of ytterbium powder (0.17 g, 1.0 mmol),  $HgPh_2$  (0.35 g, 1.0 mmol) and  $L^3H$  (0.51 g, 2.0 mmol) in THF (40 cm<sup>3</sup>) was stirred and heated at 60°C for 24 h. The resulting mixture was filtered and the dark red filtrate evaporated to dryness. Recrystallisation from toluene (20 cm<sup>3</sup>) gave orange crystals (suitable for X-ray crystallography) upon standing overnight (yield 0.18 g, 21 %). (Found C 56.41, H 5.77, N 3.59.  $C_{40}H_{49}N_2O_4Si_2Yb$  requires C 56.45, H 5.80, N 3.29 %). Infrared (Nujol,  $\nu/cm^{-1}$ ): 1718 w, 1621 s, 1588 vs, 1554 s, 1307 vs, 1288 s, 1241 s, 1190 vs, 1158 vs, 1101 vs, 1070 vs, 1045 vs, 863 m, 842 sh s, 830 br s, 807 m, 786 m, 756 s, 736 s, 706 s, 695 vs, 630 vs, 602 s, 594 s  $cm^{-1}$ . Mass Spectrum:  $m/z$  779 (<1)  $[M - THF]^+$ , 686 (<1)  $[Yb(L^3)_2]^+$ , 613 (<1)  $[Yb(L^3)_2 - SiMe_3]^+$ , 430 (<1)  $[Yb(L^3)]^+$ . Vis-near IR [ $\lambda_{max}$  ( $\epsilon$ )] (DME): 416 (401), 919 (31), 982 (73) nm (dm<sup>3</sup> mol<sup>-1</sup>). The reaction filtrate of **6g** was hydrolysed with H<sub>2</sub>O (15 cm<sup>3</sup>) followed by extraction with CHCl<sub>3</sub> (30 cm<sup>3</sup>) which was evaporated under vacuum to 5 cm<sup>3</sup> and analysed by GC-MS. — GC-MS:  $R_f$ : (rel. int.)  $m/z$  (%): 2.62 (80), 93 ( $C_6H_5NH_2^+$ , 10);  $R_f$ : 7.12 (5). 94 ( $C_6H_5OH^+$ , 100);  $R_f$ : 17.35 (95). 185 ( $C_6H_5O C_6H_4NH_2^+$ , 100).

**Method 2**

$L^3H$  (0.51 g, 2.0 mmol) in a hexane (5 cm<sup>3</sup>) was added to  $[Yb\{N(SiMe_3)_2\}_2(THF)_2]$  (0.65g, 1.0 mmol) in hexane (40 cm<sup>3</sup>) at -78°C. The resulting orange solution was warmed to room temperature whereupon the solvent volume was evaporated under vacuum to ca. 15 cm<sup>3</sup>. On cooling to -20°C the reaction mixture afforded orange crystals of  $[Yb(L^3)_2(OPh)(THF)]$  (yield 0.15 g, 18%). The infrared and UV/Vis/NIR spectra were identical with those of  $[Yb(L^3)_2(OPh)(THF)]$  obtained above.

## 8.7.2 Synthesis of Diorganoamidolanthanoid(II) Complexes By Ligand Exchange Reactions

### 5e) $[Yb(L^2)_2(THF)_2]$ Method 2 (For Method 1 see previous section (8.7.1))

$L^2H$  (0.39 g, 2.0 mmol) in a toluene (5 cm<sup>3</sup>) was added to  $[Yb\{N(SiMe_3)_2\}_2(THF)_2]$  (0.65g, 1.0 mmol) in toluene (40 cm<sup>3</sup>) at -78°C. The resulting orange solution was warmed to -20°C where upon dark red crystals of good X-ray quality formed overnight (yield 0.54 g, 76%). (Found: C, 41.75; H, 5.90; N, 4.63; Yb, 25.59.  $C_{28}H_{48}N_2YbO_4Si_2$  requires C, 47.64; H, 6.85; N, 3.97; Yb, 24.51 %) Infrared (Nujol, v/cm<sup>-1</sup>): 1584 vs, 1552 vs, 1482 s, 1320 sh s, 1296 br s, 1251 s, 1203 vs, 1162 vs, 1116 vs, 1054 vs, 1010 vs, 934 br s, 831 br s, 765 s, 723 s, 668 s, 617 vs, 593 vs. Vis-near IR [ $\lambda_{max}$  ( $\epsilon$ )] (DME): 499 sh (414) nm (dm<sup>3</sup> mol<sup>-1</sup>). NMR (300 MHz, C<sub>6</sub>D<sub>6</sub>, 298 K): <sup>1</sup>H,  $\delta$  0.44 (18 H, s, SiMe<sub>3</sub>), 1.19 (8 H, br s,  $\beta$ -H (THF)), 3.35 (8H, s,  $\alpha$ -H (THF)), 3.47 (6 H, s, OMe), 6.54-6.59 (4H, m (br), H5, H6), 7.03 (4H, s (br), H3, H4). A sample of diamagnetic 5e in C<sub>6</sub>D<sub>6</sub> was shown by <sup>1</sup>H NMR to convert to a paramagnetic species upon heating at 60°C for 24 h.

### 5f) $[Yb(L^2)_2(DME)]$

To a toluene solution (5 cm<sup>3</sup>) of  $L^2H$  (0.39g, 2.0 mmol) was added a toluene solution (40 cm<sup>3</sup>) of  $[Yb\{N(SiMe_3)_2\}_2(DME)]$  (0.56g, 1.0 mmol) at -78°C. The resulting purple solution was warmed to -20°C where upon dark red crystals (suitable for X-ray crystallography) formed overnight (yield 0.42 g, 64 %). (Found: C, 40.65; H, 6.40; N, 4.65; Yb 26.69.  $C_{24}H_{42}N_2O_4Si_2Yb$  requires C, 44.22; H, 6.49; N, 4.30; Yb, 26.55 %) Infrared (Nujol, v/cm<sup>-1</sup>): 1591vs, 1560vs, 1480br s, 1320sh w, 1283br s, 1244s, 1205vs, 1160vs, 1116vs, 1050vs, 1033vs, 1006vs, 918br s, 843br s, 785w, 768vs, 732br s, 674s, 625w, 567vs. Vis-near IR [ $\lambda_{max}$  ( $\epsilon$ )] (DME): 499 (381) nm (dm<sup>3</sup> mol<sup>-1</sup>); repeated after 48 h 405 (250), 905 (11), 981 (30), 985 (21) nm (dm<sup>3</sup> mol<sup>-1</sup>); NMR (300 MHz, C<sub>6</sub>D<sub>6</sub>, 298 K): <sup>1</sup>H,  $\delta$  0.49 (18 H, s, SiMe<sub>3</sub>), 2.54 (4 H, vbr s, CH<sub>2</sub> (DME)), 2.60 (6 H, vbr s, Me (DME)), 3.48 (6 H, s, OMe), 6.55-6.64 (4H, m, H5, H6), 7.05 (4H, m, H3, H4).



5g)  $[Eu(L^2)_2(THF)_2]$ 

A similar preparation method to that used for compound 5e gave orange crystals of 5g (yield 0.35 g, 51 %). (Found: C, 47.10; H, 7.21; N, 4.43;  $C_{28}H_{48}N_2EuO_4Si_2$  requires C, 49.11; H, 7.06; N, 4.09 %) Infrared (Nujol,  $\nu/cm^{-1}$ ): 1582 vs, 1551 vs, 1483 vs, 1320 vs, 1301 s, 1251 s, 1203 vs, 1164 vs, 1116 vs, 1054 vs, 1037 s, 1013 vs, 941 vs, 888 vs, 828 s, 760 s, 723 vs, 668 s, 615 s, 592 s.

5h)  $[Eu(L^2)_2(DME)]$ 

In a similar preparation method that used for compound 5f gave yellow crystals of 5h upon warming to  $-20^\circ C$  overnight (yield 0.27g, 43 %). (Found: C, 46.07; H, 6.35; N, 5.12;  $C_{24}H_{42}EuN_2O_4Si_2$  requires C, 45.70; H, 6.71; N, 4.44 %). Infrared (Nujol,  $\nu/cm^{-1}$ ): 1600vs, 1564vs, 1505vs, 1322vs, 1302s, 1252s, 1238vs, 1205s 1164s, 1114vs, 1052s, 1035w, 1012s, 941w, 909s, 842br s, 748 sh m, 733vs, 668w, 616 w, 567 w.

## 8.7.3 Oxidations of Ln(II) Species

i) Attempted Reaction of  $Hg(SCN)_2$  with  $[Yb(L^2)_2(THF)_2]$ .

To a THF solution ( $30\text{ cm}^3$ ) of  $[Yb\{N(SiMe_3)_2\}_2(THF)_2]$  (0.65 g, 1.0 mmol) at  $25^\circ C$  was added  $L^2H$  (0.30 g, 2.0 mmol) to give a red solution of  $[Yb(L^2)_2(THF)_2]$ . To this solution  $Hg(SCN)_2$  (0.16g, 0.5 mmol) was added resulting in rapid deposition of Hg metal. The mixture was filtered and the filtrate evaporated to dryness and toluene ( $20\text{ cm}^3$ ) added. The toluene was removed under vacuum resulting in a red/brown intractable product. Infrared (Nujol,  $\nu/cm^{-1}$ ): 2045vs, 1593m, 1560w, 1299m, 1282m, 1248s, 1206w, 1156 m, 1117 s, 1056 w, 1002 m, 910 br m, 842vs, 553 w, 733 s.

ii) *Attempted Reaction of TiCl with  $[Yb(L^2)_2(THF)_2]$ .*

To a toluene solution (30 cm<sup>3</sup>) of  $[Yb\{N(SiMe_3)_2\}_2(THF)_2]$  (0.65 g, 1.0 mmol) at 25°C was added L<sup>2</sup>H (0.30 g, 2.0 mmol) to give a red solution of  $[Yb(L^2)_2(THF)_2]$ . To this solution TiCl (0.24 g, 1.0 mmol) was added resulting in rapid deposition of Ti metal. The reaction mixture was filtered and evaporated to dryness affording a red/brown intractable product.

iii) *Attempted Reaction of C<sub>2</sub>Cl<sub>6</sub> with  $[Yb(L^2)_2(THF)_2]$ .*

To a THF solution (30 cm<sup>3</sup>) of  $[Yb\{N(SiMe_3)_2\}_2(THF)_2]$  (0.65 g, 1.0 mmol) at 25°C was added L<sup>2</sup>H (0.30 g, 2.0 mmol) to give a red solution of  $[Yb(L^2)_2(THF)_2]$ . To this solution C<sub>2</sub>Cl<sub>6</sub> (0.12g, 0.5 mmol) was added and the resulting mixture stirred for 12 h. The reaction mixture was evaporated to dryness and toluene added (15 cm<sup>3</sup>). The solution was evaporated to dryness under vacuum to afford a red/brown intractable product.

5i)  $[Yb(L^2)(C_5H_5)_2]$

To a toluene solution (40 cm<sup>3</sup>) of  $[Yb\{N(SiMe_3)_2\}_2(THF)_2]$  (0.65 g, 1.0 mmol) at 25°C was added L<sup>2</sup>H (0.30 g, 2.0 mmol) to give a red solution of  $[Yb(L^2)_2(THF)_2]$ . To this solution Ti(C<sub>5</sub>H<sub>5</sub>) (0.12 g, 1.0 mmol) was added where upon thallium metal immediately formed. The reaction mixture was filtered at -78°C and the filtrate was evaporated under vacuum (15 cm<sup>3</sup>). Upon standing overnight dark red/brown crystals of **5i** (suitable for X-ray crystallography) were formed (0.15 g, 69 % (based on 0.5 mmol of product maximum)). (Found: C, 47.99 H, 5.79; N, 2.93. C<sub>20</sub>H<sub>26</sub>NOSiYb requires C, 48.28; H, 5.27; N, 2.82 %). Infrared (Nujol, v/cm<sup>-1</sup>): 1651w, 1590vs, 1558s, 1484br s, 1319w, 1290vs, 1255s, 1245s, 1207s, 1155s, 1118vs, 1052s, 1011s, 918br s, 840s, 778br s, 741m, 676s, 630s, 599s. Mass Spectrum: *m/z* 498 (90%) [M]<sup>+</sup>, 433 (55) [M - C<sub>5</sub>H<sub>5</sub>]<sup>+</sup>, 418 (25) [Yb(C<sub>5</sub>H<sub>5</sub>)(L<sup>2</sup>) - Me]<sup>+</sup>, 338 (45) [Yb(L<sup>2</sup>) - 2Me]<sup>+</sup>, 304 (10) [Yb(C<sub>5</sub>H<sub>5</sub>)<sub>2</sub>]<sup>+</sup>, 239 (90) [Yb(C<sub>5</sub>H<sub>5</sub>)]<sup>+</sup>, 195 (15) [L<sup>2</sup>H]<sup>+</sup>, 165 (80) [L<sup>2</sup>H - 2Me]<sup>+</sup>, 150 (30) [L<sup>2</sup>H - 3Me]<sup>+</sup>, 135 (20) [C<sub>6</sub>H<sub>5</sub>ONSi]<sup>+</sup>, 73 (30) [SiMe<sub>3</sub>]<sup>+</sup>, 65 (35) [C<sub>5</sub>H<sub>5</sub>]<sup>+</sup>. Vis-near IR[ λ<sub>max</sub> (ε)] (DME): 424 (405), 547 (272), 886 (36), 909 (45), 960 (19), 994 (29) nm (dm<sup>3</sup> mol<sup>-1</sup>).

5j)  $[\text{Hg}(\text{L}^2)_2]$ 

$\text{HgBr}_2$  (3.49g, 9.70 mmol) was added to a stirring suspension of  $[\text{Li}(\text{L}^2)(\text{OEt}_2)]_2$  (5.30 g, 9.70 mmol) in  $\text{Et}_2\text{O}$  ( $60 \text{ cm}^3$ ). The resulting mixture was stirred for 3h, evaporated to dryness and hexane added ( $30 \text{ cm}^3$ ). The green filtrate was filtered and reduced in volume ( $5 \text{ cm}^3$ ) and on standing gave a moisture- and light-sensitive white solid. The solid was dried under vacuum at room temperature. (yield 4.10 g, 71 %). (Found: C, 40.00; H, 5.30; N, 4.81.  $\text{C}_{20}\text{H}_{32}\text{HgN}_2\text{O}_2\text{Si}_2$  requires C, 40.77; H, 5.47; N, 4.75 %). Infrared (Nujol,  $\text{v}/\text{cm}^{-1}$ ): 1590vs, 1560 w, 1490vs, 1285vs, 1251s, 1219s, 1177s, 1125vs, 1052s, 1028s, 920vs, 840vs, 774s, 733vs, 681s. Mass Spectrum:  $m/z$  590 (5%)  $[\text{M}]^+$ , 559 (<1)  $[\text{Hg}(\text{L}^2)_2 - \text{OMe}]^+$ , 396 (1)  $[\text{Hg}(\text{L}^2)]^+$ , 381 (1)  $[\text{Hg}(\text{L}^2) - \text{Me}]^+$ , 195 (100)  $[\text{L}^2\text{H}]^+$ , 165 (50)  $[\text{L}^2\text{H} - 2\text{Me}]^+$ , 150 (25)  $[\text{L}^2\text{H} - 3\text{Me}]^+$ , 135 (10)  $[\text{C}_6\text{H}_5\text{ONSi}]^+$ , 73 (30)  $[\text{SiMe}_3]^+$ . NMR (300 MHz,  $\text{C}_7\text{D}_8$ , 298 K):  $^1\text{H}$ ,  $\delta$  0.34 (18 H, s,  $\text{SiMe}_3$ ), 3.23 (6 H, s, OMe), 6.49 (2 H, dd,  $^3\text{J}$  8.0 Hz,  $^4\text{J}$  1.4 Hz, H6), 6.66 (2H, ddd,  $^3\text{J}$  7.5 Hz,  $^4\text{J}$  1.4 Hz, H5), 6.85 (4 H, m, H3, H4);  $^{199}\text{Hg}$  (71.67 MHz, 298K),  $\delta$  -1270.

5k)  $[\text{Hg}(\text{L}^3)_2]$ 

Dimethoxyethane ( $40 \text{ cm}^3$ ) was added to solid  $[\text{Li}(\text{L}^3)(\text{DME})]$  (1.24 g, 3.5 mmol) and  $\text{HgBr}_2$  (0.63 g, 1.75 mmol) and the mixture was stirred at room temperature in the dark for 5 h. The solvent was evaporated to dryness and hexane ( $25 \text{ cm}^3$ ) added. The resulting solution was filtered at  $-78^\circ\text{C}$  and, after reduction of the solvent volume to dryness, the title complex was obtained as a white moisture- and light-sensitive solid (yield 0.83g, 67 %). (Found: C, 50.81; H, 5.34; N, 4.15.  $\text{C}_{30}\text{H}_{36}\text{HgN}_2\text{O}_2\text{Si}_2$  requires C, 50.51; H, 5.09; N, 3.93 %) Infrared (Nujol,  $\text{v}/\text{cm}^{-1}$ ): 1589vs, 1488vs, 1283s, 1249s, 1206s, 1162w, 1112vs, 1056w, 1020w, 923br s, 856s, 835s, 798m, 732s, 690s. Mass Spectrum:  $m/z$  714 (12%)  $[\text{M}]^+$ , 458 (<1)  $[\text{Hg}(\text{L}^3)]^+$ , 428 (<1)  $[\text{Hg}(\text{L}^3) - 2\text{Me}]^+$ , 413 (<1)  $[\text{Hg}(\text{L}^3) - 3\text{Me}]^+$ , 257 (50)  $[\text{L}^3\text{H}]^+$ , 242 (45)  $[\text{L}^3\text{H} - \text{Me}]^+$ , 226 (20)  $[\text{L}^3 - 2\text{Me}]^+$ , 165 (60)  $[\text{C}_6\text{H}_4\text{ONHSiMe}_2]^+$ , 150 (35)  $[\text{C}_6\text{H}_4\text{ONHSiMe}]^+$ , 73 (100)  $[\text{SiMe}_3]^+$ . NMR (300 MHz,  $\text{C}_7\text{D}_8$ , 298 K):  $^1\text{H}$ ,  $\delta$  0.21 (18 H, s,  $\text{SiMe}_3$ ), 6.57 (2 H, ddd,  $^3\text{J}$  7.3 Hz,  $^4\text{J}$  1.5 Hz, H5), 6.70-6.80 (8 H, m, H6, H3', H4', H5'), 6.85-7.00 (6 H, m, H4, H2', H6'), 7.12 (2 H, dd,  $^3\text{J}$  7.2 Hz);  $^{199}\text{Hg}$  (71.58 MHz, 298K),  $\delta$  -1316.

5l)  $[Yb(C_5Me_5)_2(L^2)]$ 

To a stirring solution of  $[Yb(C_5Me_5)_2(THF)]$  (0.52 g, 1.0 mmol) in toluene (30 cm<sup>3</sup>) was added  $Hg(L^2)_2$  (0.30 g, 0.50 mmol) whereupon mercury metal immediately formed. The reaction mixture was filtered and the filtrate evaporated to *ca.* 10 cm<sup>3</sup>. On standing purple crystals of **5l** suitable for X-ray analysis deposited (yield 0.38 g, 60 %). (Found C, 56.79; H, 7.32; N, 2.39, Yb, 26.84.  $C_{30}H_{46}NOSiYb$  requires C, 56.49; H, 7.27; N, 2.20; Yb, 27.12 %). Infrared (Nujol,  $\nu/cm^{-1}$ ): 1593 s, 1488 s, 1320 w, 1289 s, 1258 s, 1247 s, 1212 m, 1158 m, 1016 vs, 916 vs, 833 s, 786 w, 772 w, 722 s, 668 w. Mass Spectrum:  $m/z$  638 (5%)  $[M]^+$ , 503 (35)  $[M - C_5Me_5]^+$ , 488 (25)  $[Yb(C_5Me_5)(L^2) - Me]^+$ , 353 (20)  $[Yb(L^2) - Me]^+$ , 338 (30)  $[Yb(L^2) - 2Me]^+$ , 309 (5)  $[Yb(C_5Me_5)]^+$ , 264 (3)  $[Yb(C_5Me_2)]^+$ , 195 (10)  $[L^2H]^+$ , 165 (25)  $[L^2H - 2Me]^+$ , 150 (5)  $[L^2H - 3Me]^+$ , 135 (80)  $[C_6H_5ONSi]^+$ , 120 (100)  $[C_5Me_4]^+$ , 105 (90)  $[C_5Me_3]^+$ , 90 (70)  $[C_5Me_2]^+$ , 73 (30)  $[SiMe_3]^+$ . Vis-near IR  $[\lambda_{max} (\epsilon)]$  (DME): 502 (217), 889 (16), 917 (14), 923 (11), 1010 (59) nm (dm<sup>3</sup> mol<sup>-1</sup>).

5m)  $[Yb(C_5Me_5)_2(L^3)]$ 

To a stirring solution of  $[Yb(C_5Me_5)_2(THF)]$  (0.52g, 1.0 mmol) in toluene (30 cm<sup>3</sup>) was added  $Hg(L^3)_2$  (0.36g, 0.50 mmol) where upon mercury metal immediately formed. The reaction mixture was filtered and the filtrate was reduced in volume to *ca.* 10 cm<sup>3</sup>. Purple crystals of **5m** suitable for an X-ray crystallographic study were isolated (yield 0.33g, 59 %). (Found: C, 59.71; H, 7.01; N, 2.10.  $C_{35}H_{48}NOSiYb$  requires C, 60.06; H, 6.91; N, 2.00 %). Infrared (Nujol,  $\nu/cm^{-1}$ ): 1588 s, 1556 w, 1487 s, 1286 s, 1254 s, 1184 s, 1153 s, 1102 s, 1054 m, 1023 w, 914 vs, 838 br s, 800 s, 786 w, 734 s, 696 w. Vis-near IR  $[\lambda_{max} (\epsilon)]$  (DME): 518 (434), 892 (39), 920 (37), 925 (36), 1013 (90) nm (dm<sup>3</sup> mol<sup>-1</sup>). Mass Spectrum:  $m/z$  700 (<1%)  $[M]^+$ , 562 (<1)  $[Yb(C_5Me_5)_2(C_6H_4NSi)]^+$ , 534 (<1)  $[Yb(C_5Me_5)_2(C_6H_4N)]^+$ , 444 (<1)  $[Yb(C_5Me_5)_2]^+$ , 309 (5)  $[Yb(C_5Me_5)]^+$ , 264 (5)  $[Yb(C_5Me_2)]^+$ , 257 (10)  $[L^3H]^+$ , 241 (12)  $[L^3 - Me]^+$ , 226 (2)  $[L^3 - 2Me]^+$ , 165 (40)  $[OC_6H_4NHSiMe_2]^+$ , 150 (20)  $[C_6H_4ONHSiMe]^+$ , 135 (100)  $[C_5Me_3]^+$ , 120 (45)  $[C_5Me_4]^+$ , 105 (70)  $[C_5Me_3]^+$ , 90 (45)  $[C_5Me_2]^+$ , 73 (50)  $[SiMe_3]^+$ , 70 (30)  $[C_5Me]^+$ , 58 (25)  $[SiMe_2]^+$ .

## 8.8 Experimental Procedures for Chapter 6

### 8.8.1 Synthesis of $[LnCl_3(DME)_x]$ Complexes ( $Ln = La, Nd, Yb$ )

In typical syntheses, lanthanoid metal powder or lump (0.5 g, 2.87-3.60 mmol) and hexachloroethane (1.50 g, 6.34 mmol) in 1,2-dimethoxyethane (40 cm<sup>3</sup>) were sonicated under N<sub>2</sub> or Ar until all traces of metal disappeared and a milk-like suspension remained. Hexane (20 cm<sup>3</sup>) was added to the reaction mixture separating insoluble  $[LnCl_3(DME)_n]$ , the supernatant liquid was decanted, and the residue was washed with hexane, and dried at room temperature under vacuum.

#### 6a) $[LaCl_3(DME)]_n$ ( $n = 1-\infty$ )

Sonication time: 20 h (yield 1.23 g, 81 %). (Found: La, 41.82. C<sub>4</sub>H<sub>10</sub>Cl<sub>3</sub>LaO<sub>2</sub> requires La, 41.43 %). Infrared (Nujol, v/cm<sup>-1</sup>): 1343 m, 1297 w, 1244 w, 1178 w, 1020 s, 956 w, 925 m, 865 s, 835 s, 722 w, 667 w. Far infrared (Polyethylene, v/cm<sup>-1</sup>): 542 m, 419 w, 385 m, 353 w, 323 w, 215 s, 195 s, 121 s, 87 w, 81 w, 73 s.

#### 6b) $[NdCl_3(DME)_2]$

Sonication time: 38 h (yield 1.11 g, 74 %). (Found: Cl, 24.81; Nd, 33.20. C<sub>8</sub>H<sub>20</sub>Cl<sub>3</sub>NdO<sub>4</sub> requires Cl, 24.69; Nd, 33.48 %). Infrared (Nujol, v/cm<sup>-1</sup>): 1289 w, 1251 w, 1191 w, 1119 m, 1094 m, 1040 s, 986 m, 858 s, 722 w, 550 w.

#### 6c) $[YbCl_3(DME)_2]$

Sonication time: 54 h (yield 1.12 g, 84 %). (Found: Cl, 23.10; Yb, 37.75. C<sub>8</sub>H<sub>20</sub>Cl<sub>3</sub>YbO<sub>4</sub> requires Cl, 23.14; Yb, 37.65 %). Infrared (Nujol, v/cm<sup>-1</sup>): 1352 m, 1284 w, 1240 m, 1167 w, 1154 w, 1116 m, 1032 br s, 978 m, 860 s, 834 s, 722 w, 566 w. Crystals of 6c were grown from the surface of a Yb metal piece within a solution of DME and C<sub>2</sub>Cl<sub>6</sub>.

### 8.8.2 Synthesis of $[YbBr_3(L)]$ Complexes ( $L = THF_3$ or $DME_2$ )

#### 6d) $[YbBr_3(THF)_3]$

Ytterbium metal powder (0.50 g, 2.9 mmol) and 1,2-dibromomethane (2.0 cm<sup>3</sup>, 29 mmol) in THF (40 cm<sup>3</sup>) were sonicated under N<sub>2</sub> (36 h) until all traces of metal disappeared and a milk-like suspension remained. Hexane (20 cm<sup>3</sup>) was added to the reaction mixture and the resulting filtrate was decanted. The remaining residue was washed with hexane and dried under vacuum (yield 1.40 g, 77 %). (Found: Yb, 28.12. C<sub>16</sub>H<sub>32</sub>Br<sub>3</sub>YbO<sub>4</sub> requires Yb, 27.51 %) Infrared (Nujol, v/cm<sup>-1</sup>): 1305 w, 1260 w, 1181 w, 1040 s, 1003 s, 912 w, 842 s, 722 s. Single crystals were grown on the surface of the metal within a mixture of C<sub>2</sub>H<sub>4</sub>Br<sub>2</sub> and THF.

#### 6e) $[YbBr_3(DME)_2]$

Recrystallisation of  $[YbBr_3(THF)_3]$  (0.62g, 1.0 mmol) from DME (35 cm<sup>3</sup>) yielded a white precipitate of the title complex (yield 0.45 g, 76 %). (Found: Br, 38.79; Yb, 30.01%. C<sub>8</sub>H<sub>20</sub>Br<sub>3</sub>YbO<sub>4</sub> requires Br, 40.42; Yb, 29.18 %). Infrared (Nujol, v/cm<sup>-1</sup>): 1458 m, 1367 m, 1184 w, 1116 w, 1077 s, 1027 s, 975 w, 859 s. Far infrared (Polyethylene, v/cm<sup>-1</sup>): 581 w, 562 w, 542 w, 463 w, 399 m, 324 w, 274 w, 172 s, 150 m, 106 m, 73 w, 54 w. Single crystals were grown on the surface of the metal within a mixture of C<sub>2</sub>H<sub>4</sub>Br<sub>2</sub> and DME.

### 8.8.3 Synthesis of Diorganoaminolanthanoid Halide Complexes

#### 8.8.3.1 Attempted preparations of $\text{LnCl}_3(\text{HL})$ ( $\text{Ln} = \text{Sm}, \text{Yb}$ ; $\text{HL} = \text{A}, \text{L}^1\text{H}, \text{C}, \text{D}$ )

*i)* HL (1.0 mmol) was added to anhydrous  $\text{LnCl}_3$  (1.0 mmol,  $\text{Ln} = \text{Yb}$ , 0.28 g or  $\text{Ln} = \text{Sm}$ , 0.26 g) and the reaction mixture heated at  $70^\circ\text{C}$  for 8 h. The white suspension was evaporated to dryness to afford a white solid. Lanthanoid analyses on the products obtained from the reaction of **A**, **L<sup>1</sup>H** and **C**, confirmed the isolated white solid to be  $\text{LnCl}_3$ . In the case of **D** with either **Yb** or **Sm** no reaction between the two solid starting materials was observed on heating at  $90^\circ\text{C}$  for a further 6 h.

*ii)* In typical syntheses, HL (**L** = **A**, **L<sup>1</sup>H**, **C** or **D**) (1.0 mmol) was added to a stirring suspension of  $\text{LnCl}_3(\text{THF})_2$  (1.0 mmol,  $\text{Ln} = \text{Yb}$ , 0.42 g or  $\text{Ln} = \text{Sm}$ , 0.41 g) in toluene (20  $\text{cm}^3$ ). The white suspension was heated to  $60^\circ\text{C}$  for 6 h and sonicated overnight. The solvent was removed under vacuum to afford a white solid of  $\text{LnCl}_3(\text{THF})_2$  ( $\text{Ln} = \text{Yb}, \text{Sm}$ ) which was confirmed by lanthanoid analysis.

*iii)* To a solution of **D** (0.21 g, 1.0 mmol) in MeCN (15  $\text{cm}^3$ ) was added  $\text{LnCl}_3$  (1.0 mmol,  $\text{Ln} = \text{Yb}$ , 0.28 g or  $\text{Ln} = \text{Sm}$  0.26 g). The reaction mixture was stirred and heated at  $60^\circ\text{C}$  for 12h and the mixture was evaporated to dryness and washed with pentane (10  $\text{cm}^3$ ) to yield a white solid. Lanthanoid analysis identified the product to be  $\text{LnCl}_3$ .

8.8.3.2 Lanthanoid Trichloride Complexes Containing L<sup>1</sup>H6f)  $\text{YbCl}_3(\text{L}^1\text{H})_{2/3}(\text{MeCN})_2$ 

To a solution of L<sup>1</sup>H (0.16 g, 1.0 mmol) in MeCN (15 cm<sup>3</sup>) was added YbCl<sub>3</sub> (0.28 g, 1.0 mmol). The reaction mixture was stirred and heated at 50°C for 12h and then the mixture was reduced under vacuum to yield a white solid (yield 0.45 g, 96%). (Found: Yb, 37.37; Cl, 22.79. C<sub>26/3</sub>H<sub>56/3</sub>Cl<sub>3</sub>N<sub>10/3</sub>YbSi<sub>2/3</sub> requires Yb, 37.00; Cl, 22.74 %) Infrared (KBr v/cm<sup>-1</sup>): 3465 br m, 3252 br m, 3126 br m, 3014 br w, 2962 br w, 2922 br w, 2250 s, 1682 s, 1595 s, 1466 vs, 1401 vs, 1290 s, 1255w, 1187 s, 1127w, 1067 s, 1003 br s, 926 s, 894 vs, 778 s, 758 s, 685 s, 602 w. Far Infrared (Polyethylene, v/cm<sup>-1</sup>): 575 br w, 541 m, 420w, 354 w, 244 br s, 116 w, 73 s, 56 w.

6g)  $\text{SmCl}_3(\text{L}^1\text{H})_{1/2}$ 

A similar preparation method to that used for compound 6f a white solid of the title complex was obtained (yield 0.32g, 95%). (Found: Sm, 44.20; Cl, 31.81. C<sub>7/2</sub>H<sub>19/2</sub>Cl<sub>3</sub>NSi<sub>1/2</sub>Sm requires Sm, 44.71; Cl, 31.61 %) Infrared (KBr v/cm<sup>-1</sup>): 3407 br m, 3317 s, 3260 vs, 3115 w, 3005 br w, 2967 br w, 2918 br w, 2839 s, 2797 w, 1605 vs, 1479 sh w, 1463 vs, 1407 s, 1327 s, 1290 s, 1239 s, 1189 w, 1176 s, 1133 s, 1111 s, 1095 s, 1069 s, 1055 s, 1034 s, 1015 s, 1004 br s, 924 s, 881 vs, 799 s, 590 s, 487 s, 450 s. Far Infrared (Polyethylene, v/cm<sup>-1</sup>): 590 s, 572 br m, 541 m, 488 br s, 466 br w, 451 br m, 395 s, 230 br s, 184 m, 122 s, 107 s, 86w, 72 s, 116 w, 73 s, 56 w.



8.8.3.3 Lanthanoid Trichloride Complexes Containing  $[\text{HN}(\text{SiMe}_3)\text{CH}_2]_2$  (C)6h)  $\text{YbCl}_3(\text{C})_{1/2}(\text{MeCN})_2$ 

To a solution of C (0.20 g, 1.0 mmol) in MeCN (15 cm<sup>3</sup>) was added YbCl<sub>3</sub> (0.28 g, 1.0 mmol). The reaction mixture was stirred and heated at 60°C for 12h and the mixture was reduced under vacuum to yield a white solid (yield 0.42g, 91%). (Found: Yb, 36.42; Cl, 22.25 C<sub>8</sub>H<sub>17</sub>Cl<sub>3</sub>N<sub>3</sub>YbSi requires Yb, 37.31; Cl, 22.94 %) Infrared (KBr v/cm<sup>-1</sup>): 3153 br m, 2295 s, 2308 s, 2280 s, 1632 s, 1581 s, 1453 w, 1402 s, 1252 s, 1051 w, 976 s, 926 s, 841 vs, 756 w, 680 w, 619w, 482 m. Far Infrared (Polyethylene, v/cm<sup>-1</sup>): 541 m, 504 br w, 406 br m, 352 w, 240 br s, 73 vs.

6i)  $\text{SmCl}_3(\text{C})_{1/3}$ 

A similar preparation method to that used for compound 6h gave a white solid of 6i (yield 0.30g, 93%). (Found: Sm, 45.89; Cl, 32.47 C<sub>8/3</sub>H<sub>22/3</sub>Cl<sub>3</sub>N<sub>2/3</sub>Si<sub>2/3</sub>Sm requires Sm, 46.29; Cl, 32.73 %) Infrared (KBr v/cm<sup>-1</sup>): 3429 br m, 3338 s, 3320 s, 3306 s, 3263 vs, 2956 s, 2922 w, 2881 s, 1582 vs, 1484 s, 1450 w, 1401m, 1253 s, 1183 w, 1059 w, 1043 s, 1020 s, 1011 s, 963 vs, 603 s, 583 sh w, 499sh w, 459 vs. Far Infrared (Polyethylene, v/cm<sup>-1</sup>): 458 br s, 384 br m, 282 m, 205 br s, 122 s, 107 br m, 87 m, 73 vs.

## 8.9 Experimental Procedures of Chapter 7

### 8.9.1 Reaction of $L^2H$ with $LiBu^n$

#### 7a) $[Li(L^2)(DME)_{0.5}]$

To a stirred solution of  $L^2H$  (0.72 g, 3.7 mmol) in DME (30 cm<sup>3</sup>) at 0°C was added dropwise  $LiBu^n$  (2.30 cm<sup>3</sup>, 3.7 mmol) and the resulting solution was warmed to room temperature *ca.* 1 h. The solvent volume was reduced until a solid began to form. The mixture was heated until dissolution and allowed to stand whereupon colourless crystals formed (yield 0.78 g, 86 %). (Found: C, 58.61; H, 8.96; N, 5.76.  $C_{24}H_{42}Li_2N_2O_4Si_2$  requires C, 58.51; H, 8.59; N, 5.69 %). Infrared (Nujol,  $\nu/cm^{-1}$ ): 1586 vs, 1560 w, 1482 s, 1404 s, 1377 vs, 1308 w, 1279 s, 1237 s, 1211 vs, 1173 vs, 1117 vs, 1076 s, 1050 s, 1030 vs, 937 s, 919 sh s, 843 sh m, 772 s, 741 s, 661 s, 615 w, 597 w. Mass Spectrum  $m/z$  402 (60%)  $[Li_2(L^2)_2]^+$ , 387 (20)  $[Li_2(L^2)_2 - Me]^+$ , 201 (100)  $[LiL^2]^+$ , 195 (25)  $[L^2H]^+$ , 165 (60)  $[L^2H - 2Me]^+$ , 150 (25)  $[L^2H - 2Me]^+$ , 135 (20)  $[C_6H_5ONSi]^+$ , 73 (40)  $[SiMe_3]^+$ , 58 (20)  $[SiMe_2]^+$ . NMR (300 MHz,  $C_6D_6$ , 298 K)  $^1H$ ,  $\delta$  0.26 (9 H, s,  $SiMe_3$ ), 2.69 (3 H, s, OMe), 2.75 (2 H, s,  $CH_2$  (DME)), 3.39 (3 H, s, OMe (DME)), 6.59-6.71 (2 H, m, H5, H6), 6.90-7.05 (1 H, ddd,  $^3J$  7.3,  $^4J$  1.8 Hz, H4), 7.06-7.13 (1 H, dd,  $^3J$  7.9,  $^4J$  1.7 Hz, H3);  $^7Li$  NMR (117.37 MHz),  $\delta$  -0.97.

7b)  $[\text{Li}(\text{L}^2)(\text{OEt}_2)]_2$ 

To a stirred solution of  $\text{L}^2\text{H}$  (0.05 mol, 10 g) in  $\text{Et}_2\text{O}$  (80  $\text{cm}^3$ ) at  $0^\circ\text{C}$  was added dropwise  $\text{LiBu}^n$  (32  $\text{cm}^3$ , 0.05 mol), and the resulting solution was warmed to room temperature over *ca.* 1 h. The resulting white precipitate was cooled to  $-78^\circ\text{C}$ , washed with hexane (40  $\text{cm}^3$ ) and dried under vacuum (yield 11.9 g, 86 %). A small amount of  $[\text{Li}(\text{L}^2)\text{OEt}_2]_2$  was redissolved in  $\text{Et}_2\text{O}$  where upon light-sensitive colourless crystals of good X-ray quality formed. (Found: C, 58.92, 59.08; H, 8.84, 8.67; N, 5.82, 6.01.  $\text{C}_{28}\text{H}_{52}\text{Li}_2\text{N}_2\text{O}_4\text{Si}_2$  requires C, 61.06; H, 9.52; N, 5.09;  $\text{C}_{10}\text{H}_{16}\text{LiNOSi}$  requires C, 59.68; H, 8.01; N, 6.96 %) Infrared (Nujol,  $\text{v}/\text{cm}^{-1}$ ): 1585vs, 1558s, 1280s, 1239s, 1212s, 1171s, 1117vs, 1052s, 1029vs, 934s, 840s, 821s, 734vs, 660s, 594s. Mass Spectrum  $m/z$  201 (100%)  $[\text{LiL}^2]^+$ , 195 (25)  $[\text{L}^2\text{H}]^+$ , 165 (60)  $[\text{L}^2\text{H} - 2\text{Me}]^+$ , 150 (25)  $[\text{L}^2\text{H} - 3\text{Me}]^+$ , 135 (20)  $[\text{C}_6\text{H}_5\text{ONSi}]^+$ , 73 (40)  $[\text{SiMe}_3]^+$ , 58 (20)  $[\text{SiMe}_2]^+$ . NMR (300 MHz,  $\text{C}_7\text{D}_8$ , 298 K):  $^1\text{H}$ ,  $\delta$  0.11 (18 H, s,  $\text{SiMe}_3$ ), 1.04 (12 H, t,  $^3\text{J}$  7.0 Hz, Me ( $\text{OEt}_2$ )), 3.26 (8H, q,  $^3\text{J}$  7.0 Hz,  $\text{CH}_2$  ( $\text{OEt}_2$ )), 3.35 (6 H, s, OMe), 6.50-6.57 (2 H, dd,  $^3\text{J}$  7.2,  $^4\text{J}$  1.6 Hz, H6), 6.62-6.68 (2 H, ddd,  $^3\text{J}$  7.0,  $^4\text{J}$  1.5 Hz, H5), 6.85-6.95 (2 H, ddd,  $^3\text{J}$  7.0,  $^4\text{J}$  1.6 Hz, H4), 6.96-7.04 (2 H, dd,  $^3\text{J}$  7.2,  $^4\text{J}$  1.7 Hz, H3);  $^7\text{Li}$  NMR (155.51 MHz,  $\text{C}_7\text{D}_8$ , 298 K):  $\delta$  1.85.

## 8.9.2 Reaction of $L^3H$ with $LiBu^n$

### 7c) $[Li(L^3)(THF)]$

$LiBu^n$  (1.63 cm<sup>3</sup>, 2.60 mmol) was added dropwise to a solution of  $L^3H$  (0.63 g, 2.45 mmol) in THF (30 cm<sup>3</sup>) at 0°C and stirred until it had warmed to room temperature (*ca.* 1 h) whereupon a white solid formed. This was washed with hexane (30 cm<sup>3</sup>) and dried under vacuum giving the title compound (yield 0.76 g, 87 %). (Found: C, 67.22; H, 7.98; N, 4.42.  $C_{19}H_{26}LiNO_2Si$  requires C, 68.03; H, 7.81; N, 4.18 %) Infrared (Nujol,  $\nu/cm^{-1}$ ): 1592 s, 1582 s, 1489 s, 1279 s, 1239 s, 1211 vs, 1170 s, 1102 vs, 1072 w, 1046 s, 947 vs, 868 s, 844 w, 824 vs, 769 m, 734 s, 694 vs, 663 w. NMR (400 MHz,  $C_7D_8$ , 298 K):  $^1H$ ,  $\delta$  0.35 (9 H, s,  $SiMe_3$ ), 1.20 (4 H, br m,  $\beta$ -H (THF)), 3.46 (4 H, br m,  $\alpha$ -H (THF)), 6.46 – 6.50 (1H, ddd,  $^3J$  7.2,  $^4J$  1.6 Hz, H4), 6.60 – 6.63 (1H, dd,  $^3J$  8.0,  $^4J$  1.6 Hz, H3), 6.67 – 6.69 (2H, br d,  $^3J$  7.8 Hz, H2',6'), 6.73 – 6.78 (1H, tt,  $^3J$  7.4,  $^4J$  1.1 Hz, H4'), 6.84 – 6.88 (2H, br t,  $^3J$  7.4 Hz, H3',5'), 6.96 – 7.03 (1H, ddd,  $^3J$  7.2,  $^4J$  1.7 Hz, H5), 7.15 – 7.20 (1H, dd,  $^3J$  8.0,  $^4J$  1.6 Hz, H6);  $^7Li$  (155.51 MHz, 298K),  $\delta$  1.68. The same compound (yield 0.68 g, 60 %) was obtained from a reaction of  $L^3H$  (0.63 g, 2.45 mmol) with two equivalents of  $LiBu^n$  (3.30 cm<sup>3</sup>, 5.25 mmol) in THF (30 cm<sup>3</sup>) followed by the same work up procedure.

7d)  $[Li(L^3)(DME)]$ 

LiBu<sup>n</sup> (2.44 cm<sup>3</sup>, 3.90 mmol) was added dropwise to a solution of L<sup>3</sup>H (0.94 g, 3.66 mmol) in DME (30 cm<sup>3</sup>) at 0°C. The resulting mixture was then stirred until it had warmed to room temperature (ca. 1 h) whereupon a white solid formed. The solid was washed with hexane (30 cm<sup>3</sup>) and dried under vacuum giving the title compound (yield 1.24 g, 96 %). Suitable single crystals for an X-ray analysis were obtained by recrystallisation from hot hexane. (Found: C, 63.69; H, 7.90; N, 4.23. C<sub>19</sub>H<sub>28</sub>LiNO<sub>3</sub>Si requires C, 64.56; H, 7.98; N, 3.96 %) Infrared (Nujol, v/cm<sup>-1</sup>): 1594 s, 1585 s, 1458 s, 1444 s, 1366 s, 1332 vs, 1309 s, 1238 s, 1206 vs, 1168 vs, 1150 w, 1117 s, 1099 m, 1082 vs, 1037 m, 1025 w, 955 vs, 907 w, 892 w, 872 m, 825 s, 768 w, 734 s, 690 s, 665 s, 624 w, 596 w. NMR (400 MHz, C<sub>7</sub>D<sub>8</sub>, 298 K): <sup>1</sup>H, δ 0.41 (9 H, s, SiMe<sub>3</sub>), 2.79 (6 H, s, Me (DME)), 2.80 (4 H, s, CH<sub>2</sub>(DME)), 6.33 – 6.37 (1H, ddd, <sup>3</sup>J 7.2, <sup>4</sup>J 1.8 Hz, H4), 6.63 – 6.66 (1H, dd, <sup>3</sup>J 7.8, <sup>4</sup>J 1.6 Hz, H3), 6.75 – 6.79 (1H, br t, <sup>3</sup>J 6.6 Hz, H4'), 6.88 – 6.92 (4H, br m H2',3',5',6'), 6.96 – 7.02 (1H, ddd, <sup>3</sup>J 7.1, <sup>4</sup>J 1.6 Hz, H5), 7.14 – 7.16 (1H, dd, <sup>3</sup>J 8.0, <sup>4</sup>J 1.6 Hz, H6); <sup>7</sup>Li (155.51 MHz, 298K), δ 1.43. An identical product (yield 1.12 g, 70 %) was obtained from a reaction of L<sup>3</sup>H (0.94 g, 3.66 mmol) with two equivalents of LiBu<sup>n</sup> (4.88 cm<sup>3</sup>, 7.80 mmol) in DME (30 cm<sup>3</sup>) followed by the same work up procedure.

7e)  $[Li(L^3)]_n$ 

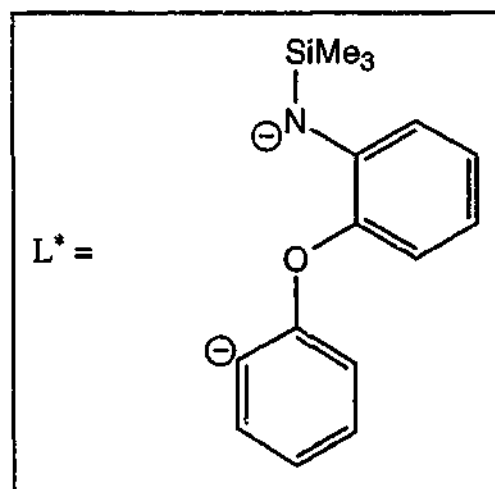
a) LiBu<sup>n</sup> (1.20 cm<sup>3</sup>, 1.90 mmol) was added slowly to a stirring solution of L<sup>3</sup>H (0.39 g, 1.52 mmol) in hexane (40 cm<sup>3</sup>) at 0°C. The resulting mixture was stirred at room temperature for 6 h, and then heated until dissolution of the white precipitate occurred. On cooling, colourless crystals of the title complex formed (0.36 g, 89 %) with identical IR and <sup>1</sup>H NMR data to the product obtained from the 2:1 preparation below.

b) A similar procedure using  $\text{LiBu}^n$  (2.30 cm<sup>3</sup>, 3.70 mmol) and  $\text{L}^3\text{H}$  (0.39 g, 1.52 mmol) in hexane (40 cm<sup>3</sup>) afforded a white precipitate (yield 0.34 g, 84%) (Found: C, 68.46; H, 7.20; N, 5.24.  $\text{C}_{15}\text{H}_{18}\text{LiNOSi}$  requires C, 68.42; H, 6.89; N, 5.32 %) Infrared (Nujol,  $\nu/\text{cm}^{-1}$ ): 1586 s, 1560 s, 1490 s, 1444 s, 1267 s, 1230 br s, 1203 s, 1167 vs, 1100 vs, 1067 w, 1040 s, 1022 w, 1004 w, 931 vs, 914 s, 867 vs, 851 s, 825 vs, 803 s, 780 s, 741 s, 694 vs, 620 w, 600 w, 556 w. NMR (400 MHz,  $\text{C}_7\text{D}_8$ , 288 K):  $^1\text{H}$ ,  $\delta$  0.12 (9H, s,  $\text{SiMe}_3$ ), 6.48-6.52 (1H, br dd,  $^3\text{J}$  7.9 Hz, H4), 6.57-6.59 (1H, br d,  $^3\text{J}$  7.9 Hz, H3), 6.65-7.00 (7H, vbr m, H5,6,2'-6'); (183 K; assignment based on two  $\text{L}^3$  environments in the ratio of 1:3; major component  $^*$ ) 0.23-0.26 (36H, br d,  $\text{SiMe}_3^*$ ), 6.45-6.52 (1H, br t, H4), 6.55-6.59 (3H, br t, H4 $^*$ ), 6.62-6.73 (15H, br m, H3 $^*$ , Ph), 6.79-6.90 (9H, br m, H3, Ph), 6.96-7.00 (1H, br d, H6), 7.00-7.04 (3H br m, H6 $^*$ ), 7.05-7.09 (3H, br d, H5 $^*$ ), 7.35-7.40 (1H br t, H5);  $^7\text{Li}$  (155.51 MHz, 303K),  $\delta$  1.65; (183 K) -1.77, 2.60, 2.96.

### 8.9.3 Reaction of $\text{L}^3\text{H}$ with excess $\text{LiBu}^n$

7f)  $[\{\text{Li}(\text{L}^3)(\text{OEt}_2)\text{Li}_2(\text{L}^*)\}_2(\text{diglyme})]$  ( $\text{L}^* = \text{N}(\text{C}_6\text{H}_4(2\text{-OC}_6\text{H}_4))(\text{SiMe}_3)$ )

To a solution of  $\text{L}^3\text{H}$  (1.02 g, 3.90 mmol) in  $\text{Et}_2\text{O}$  (30 cm<sup>3</sup>) was slowly added  $\text{LiBu}^n$  (2.70 cm<sup>3</sup>, 4.30 mmol), and the mixture was stirred until it had warmed to room temperature (*ca.* 1 h). The solvent was removed under vacuum, and hexane (20 cm<sup>3</sup>) was added. The volume was reduced to 10 cm<sup>3</sup> under vacuum and after standing for 3 days undisturbed, colourless crystals (suitable for X-ray analysis) of the title compound formed (yield 0.09 g, 8 %).



Infrared (Nujol,  $\nu/\text{cm}^{-1}$ ) 1585 vs, 1562 w, 1404 s, 1286 vs, 1242 s, 1208 vs, 1166 vs, 1095 vs, 1065 s, 1044 s, 1028 s, 937 vs, 827 s, 802 s, 769 s, 748 s, 730 vs, 694 vs, 668 w. NMR (400 MHz,  $\text{C}_7\text{D}_8$ , 303 K):  $^1\text{H}$ ,  $\delta$  0.17 (18H, br s,  $\text{SiMe}_3$ ), 0.24 (18H, s,  $\text{SiMe}_3$ ), 1.00 (12H, t,  $^3\text{J}$  7.0 Hz,  $\text{CH}_3$  ( $\text{OEt}_2$ )), 2.68 (6H, br s,  $\text{CH}_3$  (diglyme)), 2.74 (8H, br s,  $\text{CH}_2$  (diglyme)), 3.23 (8H, q,  $^3\text{J}$  7.0 Hz,  $\text{CH}_2$  ( $\text{OEt}_2$ )), 6.46 (4H, br t, Ar), 6.60 (2H, d,  $^3\text{J}$  7.9 Hz, Ar), 6.73 (2H, br m, Ar), 6.85 (12H, vbr s, Ar), 6.96 (4H, t,  $^3\text{J}$  7.9 Hz), 7.05 (4H, vbr s, Ar), 7.12 (4H, br m, Ar), 7.80 (2H, vbr s, Ar);  $^7\text{Li}$  (155.51 MHz, 303K),  $\delta$  1.67; (183 K) 0.83, 1.50, 2.08, 3.50.

7g)  $[Li_2(L^*)(OEt_2)Li(Bu^n)]_2$ 

To a solution of  $L^3H$  (0.77 g, 3.0 mmol,) in  $Et_2O$  ( $30\text{ cm}^3$ ) was slowly added  $LiBu^n$  ( $3.75\text{ cm}^3$ , 6.0 mmol), and the mixture was stirred until it had warmed to room temperature (*ca.* 1 h). The solvent was removed under vacuum, and hexane ( $20\text{ cm}^3$ ) added. Upon standing for 2 h undisturbed, colourless crystals (suitable for X-ray analysis) of the title compound formed (yield 0.23 g, 19%). (Found: C, 67.03; H, 8.83; N, 3.71.  $C_{46}H_{72}Li_6N_2O_4Si_2$  requires C, 67.80; H, 8.91; N, 3.44 %). Infrared (Nujol,  $\nu/\text{cm}^{-1}$ ): 1583 s, 1572 s, 1545 m, 1408 s, 1311 w, 1288 s, 1244 vs, 1182 s, 1148 vs, 1105 vs, 1068 m, 1039 w, 994 w, 939 vs, 829 s, 769 w, 734 w, 668 s, 619 w. NMR (400 MHz,  $C_7D_8$ , 303 K):  $^1H$ ,  $\delta$  -1.10 (4H, br s,  $\alpha$ - $CH_2$  ( $Bu^n$ )), 0.11 (18H, vbr s,  $SiMe_3$ ), 0.85 (16H, br m,  $CH_3$  ( $OEt_2$ ),  $\gamma$ - $CH_2$  ( $Bu^n$ )), 0.91 (6H, br m,  $CH_3$  ( $Bu^n$ )), 1.35 (4H, br s,  $\beta$ - $CH_2$  ( $Bu^n$ )), 3.12 (8H, br m,  $CH_2$  ( $OEt_2$ )), 6.40 (2H, br s, Ar), 7.05 (6H, br s, Ar), 7.16 (6H, br s, Ar), 7.88 (2H, br s, Ar); (183 K) -1.16 (2H, br m,  $\alpha$ - $CH_2$  ( $Bu^n$ )), -1.02 (2H, br m,  $\alpha$ - $CH_2$  ( $Bu^n$ )), 0.56 (12H, br t,  $CH_3$  ( $OEt_2$ )), 0.62 (18H, s,  $SiMe_3$ ), 0.90 (4H, br m,  $\gamma$ - $CH_2$  ( $Bu^n$ )), 1.05 (6H, br t,  $CH_3$  ( $Bu^n$ )), 1.50 (4H, br m,  $\beta$ - $CH_2$  ( $Bu^n$ )), 2.75 (4H, br m,  $CH_2$  ( $OEt_2$ )), 2.89 (4H, br m,  $CH_2$  ( $OEt_2$ )), 6.61 (2H, t,  $^3J$  7.4 Hz, Ar), 6.90 (2H, d,  $^3J$  8.0 Hz, Ar), 6.92 (2H, t,  $^3J$  7.5 Hz, Ar), 6.97 (2H, d,  $^3J$  7.9 Hz, Ar), 7.16 (2H, t, Ar), 7.35 (2H, d,  $^3J$  6.9 Hz, Ar), 7.38 (2H, d,  $^3J$  8.3 Hz, Ar), 7.88 (2H br s, Ar);  $^7Li$  (155.51 MHz, 303 K),  $\delta$  1.54 (183 K) 1.58, 1.71, 2.24.

7h)  $[Li_2(L^*)(DME)]_2$  (3I)

To a solution of  $L^3H$  (0.39 g, 1.52 mmol) in  $Et_2O$  ( $30\text{ cm}^3$ ) was slowly added  $LiBu^a$  ( $1.90\text{ cm}^3$ , 3.04 mmol), and the mixture was stirred until it had warmed to room temperature (*ca.* 1 h). The solvent was removed under vacuum and hexane ( $20\text{ cm}^3$ ) and DME ( $0.16\text{ cm}^3$ , 1.52 mmol) were then added and the resulting mixture was heated until dissolution of all the solid occurred. After standing overnight, colourless crystals suitable for X-ray analysis of the title compound were obtained (0.26 g, yield 47%). (Found: C, 63.67; H, 7.72; N, 4.05.  $C_{38}H_{54}Li_4N_2O_6Si_2$  requires C, 63.50; H, 7.57; N, 3.90 %). Infrared (Nujol,  $\nu/\text{cm}^{-1}$ ): 1585 s, 1565 w, 1550 w, 1409 s, 1284 s, 1243 m, 1191 w, 1172 vs, 1130 vs, 1097 s, 1077 vs, 1034 w, 941 vs, 869 s, 826 vs, 797 s, 749 s, 722 w, 667 w. NMR (400 MHz,  $C_7D_8$ , 303 K):  $^1H$ ,  $\delta$  0.41 (18H, s,  $SiMe_3$ ), 2.80 (12H, s,  $CH_3(DME)$ ), 2.81 (8H, s,  $CH_2(DME)$ ), 6.35 (2H, t,  $^3J$  7.0 Hz, Ar), 6.65 (2H, dd,  $^3J$  7.8 Hz,  $^4J$  1.6 Hz, Ar), 6.76 (2H, br t, Ar), 6.91 (6H, br m, Ar), 7.01 (2H, t,  $^3J$  7.6 Hz, Ar), 7.15 (2H, dd,  $^3J$  8.0 Hz,  $^4J$  1.5 Hz, Ar); (183 K) 0.72 (18H, s,  $SiMe_3$ ), 2.27 (8H, s,  $CH_2(DME)$ ), 2.54 (12H, s,  $CH_3(DME)$ ), 6.55 (2H, t,  $^3J$  8.0 Hz, Ar), 6.76 (2H, t,  $^3J$  7.0 Hz, Ar), 6.86 (2H, dd,  $^3J$  7.8 Hz,  $^4J$  1.3 Hz, Ar), 6.94 (6H, m, Ar), 7.30 (2H, t,  $^3J$  8.0 Hz, Ar), 7.43 (2H, d  $^3J$  8.0 Hz, Ar);  $^7Li$  (155.51 MHz, 303K),  $\delta$  1.42;(183 K) 1.48.



### 8.9.4 Reaction of $\text{Li}_2(\text{L}^*)$ with $\text{LnCl}_3$

#### *Unsuccessful reactions of $\text{Li}(\text{L}^*)$ with $\text{LnCl}_3$ ( $\text{Ln} = \text{Nd}, \text{Yb}$ )*

i)  $\text{LiBu}^n$  (2.90 cm<sup>3</sup>, 4.60 mmol) was added slowly to a solution of  $\text{L}^3\text{H}$  (0.59 g, 2.30 mmol) in  $\text{Et}_2\text{O}$  (40 cm<sup>3</sup>) at 0°C. The resulting mixture was stirred and warmed to room temperature (ca. 1 h) and  $\text{NdCl}_3(\text{THF})_2$  added (0.91 g, 2.30 mmol). The mixture was stirred and gently refluxed for 12 h with no reaction observed i.e. no colour change of the solution occurred.

ii)  $\text{LiBu}^n$  (2.90 cm<sup>3</sup>, 4.60 mmol) was added slowly to a solution of  $\text{L}^3\text{H}$  (0.59 g, 2.30 mmol) in  $\text{Et}_2\text{O}$  (40 cm<sup>3</sup>) at 0°C. The resulting mixture was stirred and warmed to room temperature (ca. 1 h) and  $\text{YbCl}_3$  added (0.64 g, 2.30 mmol). The mixture was stirred and gently refluxed for 12 h with no reaction observed i.e. no colour change of the solution occurred.

7i)  $[\text{Li}_4(\text{L}^*)_2\text{LiOEt}(\text{Et}_2\text{O})]_2(\text{hexane})$ 

To a solution of  $\text{L}^3\text{H}$  (0.63 g, 2.45 mmol) in  $\text{Et}_2\text{O}$  (40  $\text{cm}^3$ ) was slowly added  $\text{LiBu}^n$  (3.10  $\text{cm}^3$ , 4.90 mmol), and the mixture was stirred and warmed to room temperature (ca. 1 h).  $\text{LaCl}_3$  (0.60 g, 2.45 mmol) was added and the reaction mixture was then stirred overnight. After the solvent was removed under vacuum and hexane (25  $\text{cm}^3$ ) was added a white precipitate formed. The reaction mixture was filtered at  $-78^\circ\text{C}$  and the filtrate was reduced under vacuum (ca. 15  $\text{cm}^3$ ) where upon colourless crystals (suitable for X-ray crystallography) of 1.hexane deposited (yield 0.15 g, 18 %). M.p.  $180\text{-}184^\circ\text{C}$  (dec); (Found: C, 62.98; H, 7.74; N, 4.44.  $\text{C}_{78}\text{H}_{112}\text{Li}_{10}\text{N}_4\text{O}_8\text{Si}_4$  (7i.hexane) requires C, 66.19; H, 7.98; N, 3.96;  $\text{C}_{72}\text{H}_{98}\text{Li}_{10}\text{N}_4\text{O}_8\text{Si}_4$  (3i) requires C, 65.06; H, 7.43; N, 4.21 %). Infrared (Nujol,  $\text{v}/\text{cm}^{-1}$ ): 1589 s, 1561 w, 1544 w, 1408 vs, 1281 br s, 1244 s, 1147 vs, 1105 vs, 1162 m, 1044 s, 999 w, 945 s, 929 s, 886 w, 864 w, 828 s, 768 w, 768 s, 749 vs, 727 w, 668 w, 617 w  $\text{cm}^{-1}$ . NMR (400 MHz,  $[\text{C}_7\text{D}_8]$ , 303K):  $^1\text{H}$   $\delta$  0.02 (vbr s, 18H,  $\text{SiMe}_3$ ), 0.24 (s, 18H,  $\text{SiMe}_3$ ), 0.78 (t,  $^3\text{J}$  7.0Hz, 12H,  $\text{CH}_3$  ( $\text{OEt}_2$ )), 0.81-0.98 (m, 12H,  $\text{CH}_3$  (hexane)  $\text{CH}_3$  ( $\text{OEt}$ )), 1.23 (br m, 8H,  $\text{CH}_2$  (hexane)), 3.03 (q,  $^3\text{J}$  7.0 Hz, 8H,  $\text{CH}_2$  ( $\text{OEt}_2$ )), 3.39 (br q, 4H,  $\text{CH}_2$  ( $\text{OEt}$ )), 5.70 (br s, 2H, Ar), 6.08 (br s, 4H, Ar), 6.29 (br s, 2H, Ar), 6.45 (br t, 4H, Ar), 6.66 (br s, 2H, Ar), 6.80-7.10 (br m, 12H, Ar), 7.29 (br s, 2H, Ar), 7.82 (br dd, 4H, Ar); (213K) 0.35 (s, 18H,  $\text{SiMe}_3$ ), 0.37 (s, 18H,  $\text{SiMe}_3$ ), 0.86-0.99 (m, 18H,  $\text{CH}_3$  ( $\text{OEt}_2$ )  $\text{CH}_3$  (hexane)), 1.00-1.15 (br m, 6H,  $\text{CH}_3$  ( $\text{OEt}$ )), 1.17-1.38 (br m, 8H,  $\text{CH}_2$  (hexane)), 2.65 (br m, 4H,  $\text{CH}_2$  ( $\text{OEt}_2$ )), 2.82 (br m, 4H,  $\text{CH}_2$  ( $\text{OEt}_2$ )), 3.32 (br m, 2H,  $\text{CH}_2$  ( $\text{OEt}$ )), 3.47 (br m, 2H,  $\text{CH}_2$  ( $\text{OEt}$ )), 5.71 (d,  $^3\text{J}$  7.3Hz, 2H, Ar), 6.05 (d,  $^3\text{J}$  7.7Hz, 2H, Ar), 6.22 (t,  $^3\text{J}$  7.0Hz, 2H, Ar), 6.38-6.57 (m, 4H, Ar), 6.64 (d,  $^3\text{J}$  8.2Hz, 2H, Ar), 6.70-6.88 (m, 4H, Ar), 6.93-7.17 (m, 12H, Ar), 7.20 (br d, 2H, Ar), 7.37 (d,  $^3\text{J}$  7.5Hz, 2H, Ar); (183K) 0.35 (br s, 18H,  $\text{SiMe}_3$ ), 0.37 (br s, 18H,  $\text{SiMe}_3$ ), 0.86-0.99 (m, 18H,  $\text{CH}_3$  ( $\text{OEt}_2$ )  $\text{CH}_3$  (hexane)), 1.00-1.15 (br m, 6H,  $\text{CH}_3$  ( $\text{OEt}$ )), 1.17-1.40 (br m, 8H,  $\text{CH}_2$  (hexane)), 2.52 (vbr m, 4H,  $\text{CH}_2$  ( $\text{OEt}_2$ )), 2.85 (vbr m, 4H,  $\text{CH}_2$  ( $\text{OEt}_2$ )), 3.28 (vbr m, 2H,  $\text{CH}_2$  ( $\text{OEt}$ )), 3.47 (vbr m, 2H,  $\text{CH}_2$  ( $\text{OEt}$ )), 5.71 (br m, 2H, Ar), 6.05 (br m, 2H, Ar), 6.28 (br m, 2H, Ar), 6.42-6.57 (br m, 4H, Ar), 6.64 (br m, 2H, Ar), 6.70-6.88 (br m, 4H, Ar), 6.94-7.16 (br m, 12H, Ar), 7.20 (br m, 2H, Ar), 7.35 (m, 2H, Ar);  $^7\text{Li}$  NMR (155.51 MHz,  $[\text{D}_8]$ toluene, 303K):  $\delta$  = -2.57, 0.68, 1.16, 2.27; (273 K) -2.73, 0.66, 1.12, 1.67, 2.35; (243 K) -2.83, 0.68, 1.71, 2.45; (213 K) -2.98, 0.68, 1.70, 1.97; (183K) 3.11, 0.67, 1.72, 1.95, 3.14.

### 8.9.5 Attempted Reactions of $\text{Li}_2(\text{L}^*)$ with $[\text{Yb}(\text{C}_5\text{Me}_5)_2\text{Cl}(\text{THF})]$

7j) To a solution of  $\text{L}^3\text{H}$  (0.20 g, 0.78 mmol) in  $\text{Et}_2\text{O}$  (30  $\text{cm}^3$ ) was slowly added  $\text{LiBu}^n$  (1.00  $\text{cm}^3$ , 1.60 mmol), and the mixture was stirred until it had warmed to room temperature (ca. 1 h).  $[\text{Yb}(\text{C}_5\text{Me}_5)_2\text{Cl}(\text{THF})]$  (0.43 g, 0.78 mmol) was added resulting in rapid deposition of  $\text{LiCl}$  and the formation of a bright red solution. The reaction mixture was stirred for 30 minutes whereupon decomposition to a brown product was observed.

7k) To a stirring purple solution of  $[\text{Yb}(\text{C}_5\text{Me}_5)_2\text{Cl}(\text{THF})]$  (0.17 g, 0.03 mmol) in hexane (15  $\text{cm}^3$ ) at  $78^\circ\text{C}$  was added a solution of  $[\text{Li}_2(\text{L}^*)(\text{DME})]_2$  (0.11 g, 0.015 mmol) in hexane (10  $\text{cm}^3$ ). The reaction mixture was warmed to room temperature and gently refluxed ( $45^\circ\text{C}$ ) for 20 minutes. The solvent was evaporated to dryness and  $\text{THF}$  (25  $\text{cm}^3$ ) added. The resulting mixture was stirred and heated under gentle reflux for 20 minutes.  $\text{THF}$  was then removed under vacuum and  $\text{DME}$  (30  $\text{cm}^3$ ) added and the resulting solution was heated ( $60^\circ\text{C}$ ) for 2 h. The reaction mixture was filtered and the filtrate was evaporated to dryness and toluene added (10  $\text{cm}^3$ ). The toluene solution was reduced in volume under vacuum to ca. 5  $\text{cm}^3$  and on standing for 12 h at  $-20^\circ\text{C}$  purple crystals (suitable for X-ray analysis) of  $[\text{Yb}(\text{C}_5\text{Me}_5)_2\text{Cl}(\text{THF})]$  were deposited (0.15 g, 88 % recovery). Unit Cell data –  $\text{C}_{24}\text{H}_{38}\text{ClOYb}$ ,  $M$  551.2, triclinic,  $a$  16.779(1),  $b$  8.447(1),  $c$  18.041(1) Å;  $\alpha = 87.99(1)$ ,  $\beta = 116.58(1)$ ,  $\gamma = 87.51(1)^\circ$ ;  $V$  2284.2 Å<sup>3</sup>,  $T \sim 123$  K. ( $[\text{Yb}(\text{C}_5\text{Me}_5)_2(\text{Cl})(\text{THF})]$ )<sup>[13]</sup> Unit Cell data -  $\text{C}_{24}\text{H}_{38}\text{ClOYb}$ ,  $M$  551.2, triclinic,  $a$  17.138,  $b$  8.527,  $c$  18.570 Å;  $\alpha = 90.42$ ,  $\beta = 118.65$ ,  $\gamma = 88.01^\circ$ ;  $V$  2380 Å<sup>3</sup>,  $T \sim 295$  K.)

## 8.10 References

- 1 J. L. Atwood, W. E. Hunter, A. L. Wayda, and W. J. Evans, *Inorg. Chem.*, 1981, **20**, 4115.
- 2 G. B. Deacon, T. Feng, C. M. Forsyth, A. Gitlits, D. C. R. Hockless, Q. Shen, B. W. Skelton, and A. H. White, *J. Chem. Soc., Dalton Trans.*, 2000, 961.
- 3 G. B. Deacon, T. Feng, P. C. Junk, B. W. Skelton, A. N. Sobolev, and A. H. White, *Aust. J. Chem.*, 1998, **51**, 75.
- 4 G. Meyer, *Binary Lanthanoid(III) Halides, MX<sub>3</sub> (X = Cl, Br, I)*, in *Syntheses of Lanthanoid and Actinide Compounds*, eds. G. Meyer and L. R. Morss, Kluwer, Dordrecht, 1991.
- 5 G. B. Deacon, C. M. Forsyth, P. C. Junk, B. W. Skelton, and A. H. White, *J. Chem. Soc., Dalton Trans.*, 1998, 1381.
- 6 F. T. Edelmann, Lanthanoids and Actinides, in *Synthetic Methods of Organometallic and Inorganic Chemistry*, ed. W. A. Hermann, Thieme Medical, New York, 1997., vol. 6, p. 40.
- 7 G. B. Deacon, G. D. Fallon, C. M. Forsyth, H. Schumann, and R. Weimann, *Chem. Ber.*, 1997, **130**, 409.
- 8 T. D. Tilley, R. A. Anderson, and A. Zalkin, *Inorg. Chem.*, 1984, **23**, 2271.
- 9 T. D. Tilley, A. Zalkin, R. A. Anderson, and D. H. Templeton, *Inorg. Chem.*, 1981, **20**, 551.
- 10 C. C. Hunt and J. R. Doyle, *Inorg. Nucl. Chem. Lett.*, 1966, **2**, 283.
- 11 G. B. Deacon, *unpublished work*, 2001.
- 12 R. West, M. Ishikawa, and S. Murai, *J. Am. Chem. Soc.*, 1968, 727.
- 13 H. Yasuda, H. Yamamoto, K. Yokota, and A. Nakamura, *Chem. Lett.*, 1989, 1309.
- 14 T. J. Marks and R. D. Ernst, in *Comprehensive Organometallic Chemistry*, eds. G. Wilkinson, F. G. A. Stone, and E. W. Abel, Pergamon, Oxford, 1982, vol. 3, ch. 21, p. 173.

## *Publications*

(i) **Aryl Ether C—O Activation by Organoamidolanthanoid(II) Complexes.**

G.B. Deacon, C.M. Forsyth and N.M. Scott, *Eur. J. Inorg. Chem.*, 2000, 2501.

(ii) **Structural Diversity of Solvated Lanthanoid(III) Halide Complexes.**

G.B. Deacon, T. Feng, P.C. Junk, G. Meyer, N.M. Scott, B.W. Skelton and A.H. White, *Aust. J. Chem.*, 2000, 53, 853.

(iii) **A Striking, Multi-faceted, Decalithium Aggregate with Carbanion, Organoamide, and Alkoxide Functionalities.**

P.C. Andrews, G.B. Deacon, C.M. Forsyth and N.M. Scott, *Angew. Chem. Int. Ed. Engl.*, 2001, 2108.

(iv) **Unexpected Organoamido-, Organometallic-Lithium Aggregates from Reactions of *N*-(2-Phenoxyphenyl)-*N*-(trimethylsilyl)amine with LiBu<sup>n</sup>.**

G.B. Deacon, C.M. Forsyth and N.M. Scott, *J. Chem. Soc., Dalton Trans.*, 2001, 2494.

Organoamido- and Aryloxo-Lanthanoids, 23<sup>[1]</sup>

## Aryl Ether C–O Bond Activation by Organoamidolanthanoid(II) Complexes

Glen B. Deacon,<sup>\*[a]</sup> Craig M. Forsyth,<sup>[a]</sup> and Natalie M. Scott<sup>[a]</sup>*Dedicated to Prof. Dr. Herbert Schumann on the occasion of his 65th birthday*

Keywords: N ligands / Ytterbium / C–O activation / O ligands / Lanthanoids

The reaction of ytterbium metal, HgPh<sub>2</sub> and *N*-(2-methoxyphenyl)-*N*-(trimethylsilyl)amine (L<sup>1</sup>H) or *N*-(2-phenoxyphenyl)-*N*-(trimethylsilyl)amine (L<sup>2</sup>H) in tetrahydrofuran (thf) unexpectedly yielded the ytterbium(III) complexes [Yb(L<sup>1</sup>)<sub>2</sub>(μ-OMe)]<sub>2</sub> (1) and [Yb(L<sup>2</sup>)<sub>2</sub>(OPh)(thf)] (2), the structures of which were established by X-ray crystallography.

These are considered to be derived from C–O bond cleavage of the ligand aryl ether moiety by an initially formed Yb<sup>III</sup> species, e.g. the thermally unstable, but crystallographically authenticated [Yb(L<sup>1</sup>)<sub>2</sub>(thf)<sub>2</sub>] (3), which was independently prepared from [Yb{N(SiMe<sub>3</sub>)<sub>2</sub>}(thf)<sub>2</sub>] and L<sup>1</sup>H.

## Introduction

Divalent lanthanoid complexes react with a number of oxygen-containing substrates due to the oxophilicity of these metals and the large Ln<sup>3+</sup> → Ln<sup>2+</sup> reduction potentials (Ln = Yb, Sm).<sup>[2]</sup> For example, tetrahydrofuran (thf) solutions of SmI<sub>2</sub> have found extensive applications in organic synthesis as a selective reducing agent for ketones.<sup>[2–4]</sup> Other LnL<sub>2</sub> species are capable of stoichiometric reactions with ketones, forming metal-bound ketyl radical anions,<sup>[5,6]</sup> and the reductive coupling of carbon dioxide by Sm(C<sub>5</sub>Me<sub>5</sub>)<sub>2</sub> complexes has been reported.<sup>[7]</sup> Whilst Sm(C<sub>5</sub>Me<sub>5</sub>)<sub>2</sub>-induced deoxygenation of epoxides is facile, yielding [Ln(C<sub>5</sub>Me<sub>5</sub>)<sub>2</sub>(μ-O)]<sub>2</sub>,<sup>[8]</sup> transformations of unstrained carbon–oxygen single bonds occur only under unusual circumstances. For example, thermolytic cleavage of diethyl ether by very low coordinate ytterbium(II) complexes has been reported<sup>[9,10]</sup> and photolysis of 1,2-dimethoxyethane (dme) solutions of YbI<sub>2</sub> gives the methoxide complex [YbI<sub>2</sub>(μ-OMe)(dme)]<sub>2</sub>.<sup>[11]</sup> Furthermore, cleavage of dme by highly novel La<sup>III</sup> or Ce<sup>III</sup> organometallic complexes was recently reported.<sup>[12–14]</sup> These few examples of C–O cleavage of alkyl ethers contrast the numerous stable coordination complexes of divalent lanthanoids with these ligands.<sup>[15,16]</sup>

In this contribution, we report the unexpected cleavage of the aryl ether C–O single bond of the anionic bidentate N,O-ligands L<sup>1</sup>, L<sup>2</sup> [L<sup>1</sup> = N(SiMe<sub>3</sub>)C<sub>6</sub>H<sub>4</sub>-2-OMe, L<sup>2</sup> = N(SiMe<sub>3</sub>)C<sub>6</sub>H<sub>4</sub>-2-OPh] by a ytterbium(II) centre and the characterisation of the lanthanoid(III) products [Yb(L<sup>1</sup>)<sub>2</sub>(μ-OMe)]<sub>2</sub> (1) and [Yb(L<sup>2</sup>)<sub>2</sub>(OPh)(thf)] (2). The latter is the first structurally authenticated lanthanoid complex with an

unsubstituted phenoxide ligand; surprisingly, for a sterically undemanding ligand, it is nonbridging. The synthesis and characterisation of the thermally unstable, proposed ytterbium(II) precursor [Yb(L<sup>1</sup>)<sub>2</sub>(thf)<sub>2</sub>] (3) are also described.

## Results and Discussion

We initially attempted to prepare novel ytterbium(II) complexes of the bidentate N,O-ligands L<sup>1</sup> and L<sup>2</sup> (for preparations and the X-ray crystal structure of L<sup>1</sup>H see Experimental Section) by a redox transmetallation/ligand exchange reaction (Equation 1).



This route has previously been utilised for the preparation of Ln(NRR')<sub>2</sub> species including [Ln{N(SiMe<sub>3</sub>)Ar}<sub>2</sub>(thf)<sub>2</sub>] (Ar = C<sub>6</sub>H<sub>3</sub>-2,6-*i*Pr<sub>2</sub>, Ln = Sm, Yb).<sup>[17]</sup> The current reactions afford moderate to low yields of red-orange crystals after workup. The presence of L<sup>1</sup> or L<sup>2</sup> was evident from the infrared spectra, but the products were shown to contain Yb<sup>III</sup> by the observation of *f*–*f* transitions near 1060 nm<sup>[18]</sup> in the electronic spectra. Furthermore, the analytical data did not fit the compositions Yb(L<sup>1</sup>)<sub>3</sub> or Yb(L<sup>2</sup>)<sub>3</sub> and thus the formation of heteroleptic Yb<sup>III</sup> species was indicated. X-ray crystallography subsequently revealed that the products were the alkoxide and aryloxo complexes [Yb(L<sup>1</sup>)<sub>2</sub>(μ-OMe)]<sub>2</sub> (1) and [Yb(L<sup>2</sup>)<sub>2</sub>(OPh)(thf)] (2) (Figure 1 and 2).

Complex 1 crystallises as two virtually identical, but independent, dimers each having two bridging methoxide ligands, chelating L<sup>1</sup> coordination and hexacoordinate ytterbium atoms of an irregular geometry. Both molecules are sited on crystallographic twofold axes through the methox-

[1] Part 22: Ref.[1]

[a] School of Chemistry, Monash University, Victoria 3800, Australia

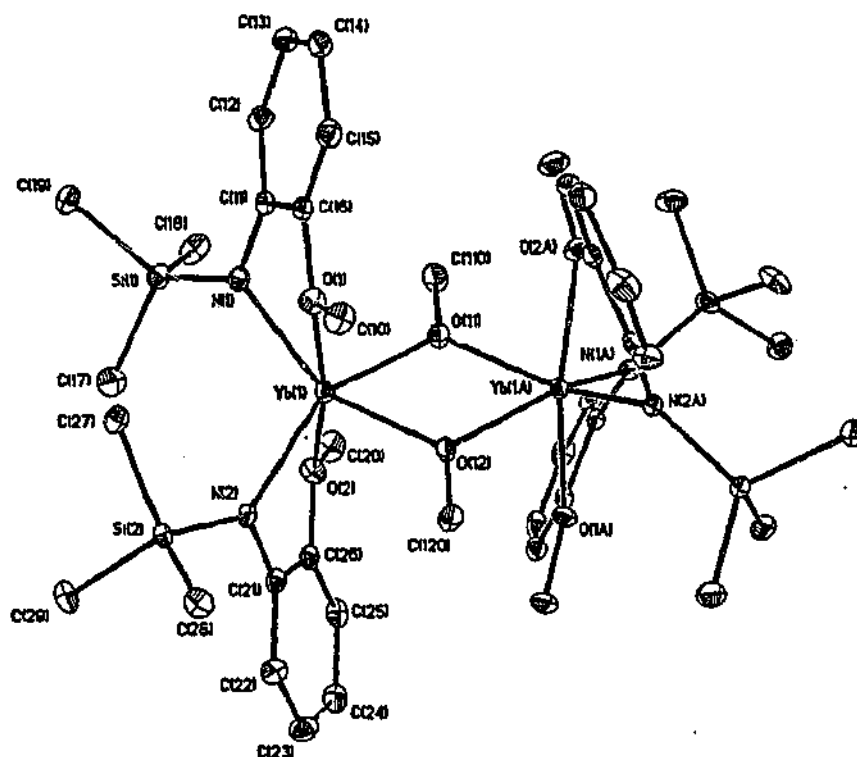


Figure 1. ORTEP view of one molecule of  $[\text{Yb}(\text{L}^1)_2(\mu\text{-OMe})_2]$  (**1**) drawn with 30% thermal ellipsoids; hydrogen atoms have been omitted for clarity; selected bond lengths (Å) and angles ( $^\circ$ ): Yb(1)–O(1) 2.346(2), Yb(1)–O(2) 2.355(2), Yb(1)–N(1) 2.250(3), Yb(1)–N(2) 2.245(3), Yb(1)–O(11) 2.221(2), Yb(1)–O(12) 2.217(2); O(1)–Yb(1)–O(2) 171.09(8), N(1)–Yb(1)–N(2) 112.7(1), N(2)–Yb(1)–O(1) 106.24(9), N(1)–Yb(1)–O(2) 102.03(9), N(2)–Yb(1)–O(2) 71.16(9), N(1)–Yb(1)–O(1) 70.80(9), O(12)–Yb(1)–O(11) 72.5(1), O(12)–Yb(1)–N(2) 91.12(9), O(11)–Yb(1)–N(2) 147.90(7), O(12)–Yb(1)–N(1) 149.79(8), O(11)–Yb(1)–N(1) 93.2(1), O(12)–Yb(1)–O(1) 85.27(6), O(11)–Yb(1)–O(1) 99.85(7), O(12)–Yb(1)–O(2) 103.17(6), O(11)–Yb(1)–O(2) 85.60(6), Yb(1)–O(11)–Yb(1A) 107.4(1), Yb(1)–O(12)–Yb(1A) 107.6(1); symmetry transformation:  $-x, y, -z + 3/2$

ide ligands, hence the four-membered  $\text{Yb}_2\text{O}_2$  rings are planar. The geometry of the methoxide bridges, with larger O–Yb–O than Yb–O–Yb angles is virtually identical to that of  $[\text{CeCp}^*\text{}_2(\mu\text{-OMe})_2]$  [ $\text{Cp}^* = \eta\text{-C}_5\text{H}_5\text{-1,3-(SiMe}_3)_2$ ].<sup>[12]</sup> The near equal Yb–OMe distances are comparable with the longer of the two Yb–OMe distances 2.210(6), 2.152(4) Å,<sup>[11]</sup> in  $[\text{YbI}_2(\mu\text{-OMe})(\text{dme})_2]$ , where the Yb–OMe bond lengthening was attributed to the *trans* influence of the iodide ligand.<sup>[11]</sup> In **1**, the two methoxide ligands have the same relative dispositions to the amide nitrogens. One nitrogen is *transoid* to each methoxide and hence exerts a *trans* influence. However, the present lengthening may also be attributed to steric crowding, since the Yb–O(ether) distances approach values expected for crowded systems.<sup>[19]</sup> The ether oxygen atoms of the  $\text{L}^1$  ligands are approximately *trans*, with Yb–O bond lengths somewhat larger than those of the dme ligands in  $[\{\text{YbI}_2(\mu\text{-OMe})(\text{dme})_2\}_2]$ , 2.317(6) and 2.308(5) Å.<sup>[11]</sup> Surprisingly, the angle between the nitrogens of the bulky aryl(trimethylsilyl)amide groups is *cisoid* [c.f. *transoid* O(ether)–Yb–O(ether)], although this is consistent with the *fac*-coordination of the alkyl(trimethylsilyl)amide groups in tris(*N,N*-dimethyl-*N'*-trimethylsilyl)ethane-1,2-diaminato)lanthanoid(III) complexes.<sup>[20]</sup> In a similar manner, the bulky carbazolate (cbz) ligands are *cisoid* in six coordinate  $[\text{Ln}(\text{cbz})_2(\text{thf})_4]$  (Ln = Yb and Sm).<sup>[21,22]</sup> The

Yb–N distances are nearly identical with those of six coordinate  $[\text{YbL}_2(\mu\text{-Cl})_2\text{Li}(\text{thf})_2]$  [L =  $\text{Me}_2\text{Si}(\text{O}i\text{Bu})(\text{N}i\text{Bu})$ ], 2.247(5) and 2.225(5) Å,<sup>[23]</sup> implying a similar steric congestion.

In contrast to **1**, complex **2** crystallises as discrete monomers with two independent, but similar, molecules comprising the asymmetric unit, one being displayed in Figure 2. The ytterbium atoms are hexacoordinate, each with an irregular coordination sphere provided by two chelating  $\text{L}^2$  ligands, a terminal phenoxide and a coordinated thf. The relative orientation of the  $\text{L}^2$  ligands, with the ether–OPh groups coordinated in an approximately *cis* arrangement, is different from that of  $\text{L}^1$  in **1**. One of the Yb–O(ether) bond lengths is significantly longer than the other, attributable to its *trans* disposition relative to the phenoxide oxygen. A meaningful *trans*-influence for aryloxide ligands in lanthanoid complexes has been reported.<sup>[19]</sup> Both the shorter Yb–O(ether) and the Yb–O(thf) bond lengths are of a similar magnitude to the mutually *trans* Yb–O(ether) distances in **1**. As with **1**, the bulky silylamide groups are *cisoid*, and whilst the N–Yb–N angle is marginally smaller than in **1**, there is no significant change in the Yb–N distances. The Yb–OPh distance is comparable to, albeit marginally smaller than, those of terminal 2,6-disubstituted aryloxide ligands bound to six coordinate ytterbium(III) (e.g.

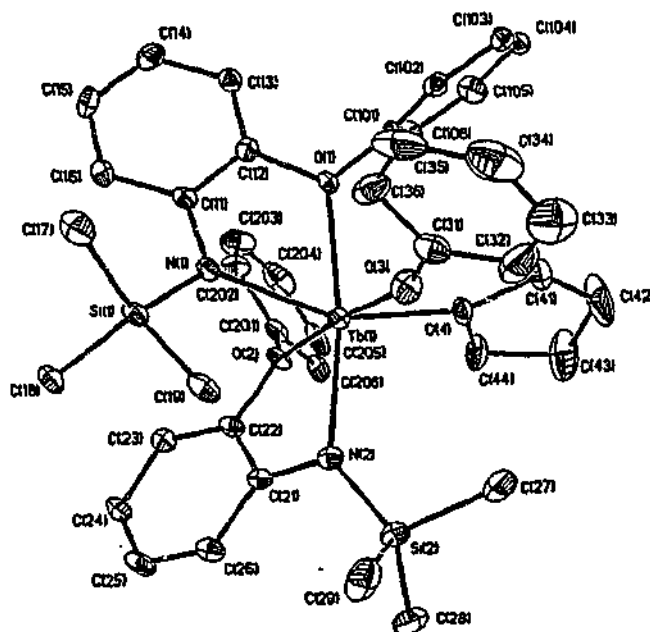


Figure 2. ORTEP view of one molecule of  $[\text{Yb}(\text{L}^2)_2(\text{OPh})(\text{thf})]$  (**2**) drawn with 30% thermal ellipsoids; hydrogen atoms have been omitted for clarity; selected bond lengths (Å) and angles ( $^\circ$ ): Yb(1)–O(1) 2.380(4), Yb(1)–O(2) 2.459(5), Yb(1)–O(3) 2.023(6), Yb(1)–O(4) 2.357(4), Yb(1)–N(1) 2.250(3), Yb(1)–N(2) 2.247(5), O(3)–Yb(1)–N(2) 108.4(2), O(3)–Yb(1)–N(1) 104.3(2), N(2)–Yb(1)–N(1) 107.0(2), O(3)–Yb(1)–O(4) 86.1(2), N(2)–Yb(1)–O(4) 95.6(2), N(1)–Yb(1)–O(4) 150.3(2), O(3)–Yb(1)–O(1) 95.9(2), N(2)–Yb(1)–O(1) 155.2(2), N(1)–Yb(1)–O(1) 70.7(2), O(4)–Yb(1)–O(1) 80.7(2), O(3)–Yb(1)–O(2) 173.2(2), N(2)–Yb(1)–O(2) 69.9(2), N(1)–Yb(1)–O(2) 82.5(2), O(4)–Yb(1)–O(2) 87.5(2), O(1)–Yb(1)–O(2) 85.4(2)

in  $[\text{Yb}(\text{MeC}_2\text{H}_4)(\text{OAr})_2(\text{thf})]$ , 2.040(4) and 2.078(4) Å<sup>[24]</sup> and  $[\text{Yb}(\text{OAr})\text{Cl}_2(\text{thf})_3]$ , 2.083(5) Å.<sup>[25]</sup> Ar = C<sub>6</sub>H<sub>2</sub>-2,6-*i*Bu<sub>2</sub>-4-Me), consistent with reduced crowding in **2**. The structure of **2** is novel as the first authenticated example of an unsubstituted phenoxide bound to a lanthanoid centre.<sup>[16,26]</sup> There must be a fine balance between formation of a six coordinate  $\mu$ -OPh (thf-free) species and the observed thf-coordinated structure **2**, since OPh is only marginally bulkier than thf.<sup>[27]</sup>

The methoxide and phenoxide groups in **1** and **2** are derived from the ligands L<sup>1</sup> and L<sup>2</sup>, respectively. There was some ambiguity arising from the use of dme as a recrystallisation solvent in our initial isolation of **1**, since dme could be a OMe source.<sup>[11–14]</sup> However, the same product is formed in similar yield in the absence of dme (Experimental Section), i.e. where the crude product of the redox transmetallation/ligand exchange was treated with diethyl ether and recrystallised from hexane. We propose that the formation of **1** and **2** occurs by a one-electron transfer from Yb<sup>II</sup> to an L<sup>1</sup> or L<sup>2</sup> ligand, Ar–O bond cleavage, formation of a Yb<sup>III</sup>–OR (R = Me or Ph) bond, and then protolysis of the intermediate **5** by L<sup>1</sup>H or L<sup>2</sup>H (Scheme 1) present as reactants (Equation 1). In confirmation, we have shown that  $[\text{Yb}(\text{L}^1)_2(\text{thf})_2]$  (**3**) (see below) is converted into **1** in the presence of an excess of L<sup>1</sup>H in hexane (see Experimental Section). A GC-MS analysis of the hydrolysed filtrate after the isolation of **2** showed the presence of phenol, *o*-phenoxylaniline and aniline, the last consistent with hydrolysis of

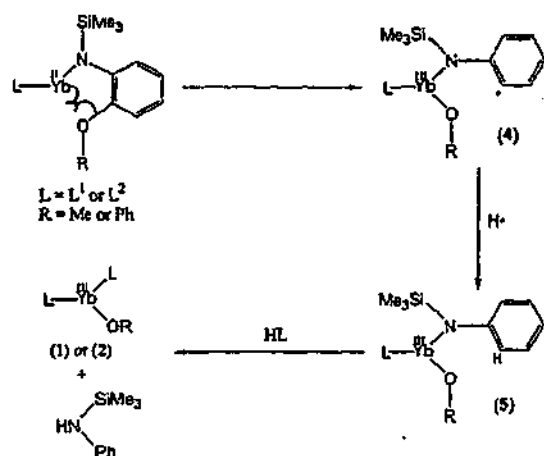
the proposed product HNPh(SiMe<sub>3</sub>) and hence with prior proton abstraction (probably from the solvent<sup>[28]</sup>) by the aryl radical **4** (Scheme 1). The first two are the expected products of hydrolysis of the isolated  $[\text{Yb}(\text{L}^2)_2(\text{OPh})(\text{thf})]$  (**2**). Instability of *N*-trimethylsilylamines to hydrolysis in the present systems was established by partial conversion of L<sup>1</sup>H into *o*-methoxyaniline on exposure to air. Whilst a mechanism involving reduction of the aryl ether by ytterbium metal (analogous to alkali metal cleavage of ethers)<sup>[29]</sup> may also be plausible, it would seem less likely since, under similar conditions, we have previously utilised methoxy-substituted aryloxo ligands in the presence of Yb metal without detection of ether cleavage.<sup>[30]</sup>

We have also prepared the thermally unstable divalent ytterbium complex  $[\text{Yb}(\text{L}^1)_2(\text{thf})_2]$  (**3**), by a ligand exchange reaction of  $[\text{Yb}\{\text{N}(\text{SiMe}_3)_2\}_2(\text{thf})_2]$ <sup>[17]</sup> with L<sup>1</sup>H in toluene at –78 °C (Equation 2).



The divalent complex **3** was characterised by spectroscopic methods and a single crystal structure determination. Satisfactory elemental analyses were not obtained, even for single crystals, presumably due to the instability of the complex, but the <sup>1</sup>H NMR spectrum is consistent with the proposed composition. The structure of **3** (Figure 3), determined at 123 K, shows a monomeric complex with the ytterbium atom situated on a twofold axis and surrounded





Scheme 1

by two chelating L<sup>1</sup> ligands and two *cis* thf molecules with an irregular six-coordinate geometry. The orientation of the L<sup>1</sup> ligands is similar to that found in 1 above, with comparable *transoid* O(ether)-Yb-O(ether) and *cisoid* N-Yb-N angles (Figure 3). The Yb-N distance of 3 is comparable with or shorter than those of [Yb(cbz)<sub>2</sub>(thf)<sub>2</sub>(dme)] [2.43(3), 2.45(2) Å]<sup>[30]</sup> and 3 has a similar N-Yb-N angle to that of the unidentate carbazolyl ligands (107.3(7)°).<sup>[31]</sup> The Yb-O(thf) distance is longer than <Yb-O(thf)> of the six coordinate complex [Yb(PhC(NSiMe<sub>3</sub>)<sub>2</sub>)(thf)<sub>2</sub>] (2.415 Å)<sup>[32]</sup> which has *trans* thf ligands since each thf oxygen of 3 is *transoid* to an amide nitrogen. Further, the *cis* thf coordination geometry in 3 is similar to that of [Yb(cbz)<sub>2</sub>(thf)<sub>2</sub>(dme)] [Yb-O(thf) 2.41(2), 2.48(2) Å; O(thf)-Yb-O(thf) 87.6(6)°].<sup>[31]</sup> It is noteworthy that there are only a few examples of bidentate, ether supported, amide ligands attached to a divalent lanthanoid, e.g. deprotonated 4,13-diaza-18-crown-6<sup>[33]</sup> and Me<sub>2</sub>Si(Oi-Bu)(NtBu).<sup>[23]</sup>

Compounds 1 and 2 are unique examples of the products of O-C(Ar) bond activation by a lanthanoid(II) centre. The ligands L<sup>1</sup> and L<sup>2</sup> also show the ability to stabilise heteroleptic lanthanoid(III) complexes with sterically undemanding co-ligands e.g. OMe, OPh.

## Experimental Section

All reactions were carried out under dry nitrogen using dry box and standard Schlenk techniques. Solvents were dried by distillation from sodium wire/benzophenone. IR data (4000–650 cm<sup>-1</sup>) were recorded for Nujol mulls sandwiched between NaCl plates with a Perkin-Elmer 1600 FTIR spectrometer. NMR spectra were obtained with a Bruker AC 300 MHz (1 H) spectrometer. The ytterbium(III) complexes gave unresolvable, uninterpretable, broadened spectra. Mass spectra were recorded with a VG Trio-1 GC mass spectrometer. Each listed *m/z* value for Yb-containing ions is the most intense peak of a cluster pattern in good agreement with the calculated pattern. GC-MS measurements were carried out using helium as a carrier gas and run on a Hewlett-Packard 5890A instrument interfaced to a VG Trio-1 GC mass spectrometer using

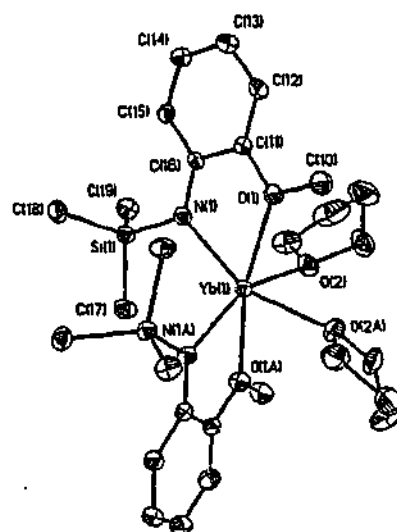


Figure 3. ORTEP view of [Yb(L<sup>1</sup>)<sub>2</sub>(thf)<sub>2</sub>] (3) drawn with 30% thermal ellipsoids; hydrogen atoms have been omitted for clarity; selected bond lengths (Å) and angles (°): Yb(1)-O(1) 2.458(2), Yb(1)-O(2) 2.494(2); Yb(1)-N(1) 2.316(2), N(1A)-Yb(1)-N(1) 108.81(12), N(1A)-Yb(1)-O(1) 121.79(8), N(1)-Yb(1)-O(1) 67.71(8), N(1)-Yb(1)-O(1A) 121.79(8), O(1)-Yb(1)-O(1A) 165.43(11), N(1A)-Yb(1)-O(2) 154.33(9), N(1)-Yb(1)-O(2) 89.45(9), O(1)-Yb(1)-O(2) 81.36(9), O(1A)-Yb(1)-O(2) 87.48(8), N(1A)-Yb(1)-O(2A) 89.48(8), O(1A)-Yb(1)-O(2A) 81.35(9), O(2)-Yb(1)-O(2A) 80.01(14); symmetry transformation:  $-x + 1, y, -z + 3/2$

a XT1-5 column (30m, 0.32 mm id) (bonded 5% phenyl - 95% dimethylpolysiloxane). The temperature program started at 50 °C (2 min) and then was increased by 10 °C/min to 280 °C. Retention times are measured in minutes from injection. Elemental analyses (C,H,N) were determined by the Campbell Microanalytical Service, University of Otago, New Zealand. Ytterbium analyses of digested samples were by complexometric titration with [Na<sub>2</sub>EDTA].<sup>[1,34]</sup> [Yb{N(SiMe<sub>3</sub>)<sub>2</sub>}(thf)<sub>2</sub>] was prepared according to a reported procedure.<sup>[17]</sup> Commercial HgPh<sub>2</sub> (Aldrich) and lanthanoid powders (Rhône-Poulenc) were used as received.

[L<sup>1</sup>H]: To a stirred solution of *o*-methoxyaniline (18 mL, 0.16 mol) in ether (100 mL) at 0 °C was slowly added *n*BuLi (100 mL, 0.16 mol). After complete addition a white solid was obtained which was stirred and warmed to room temperature (ca. 1 h). Following cooling to 0 °C, Me<sub>2</sub>SiCl<sub>2</sub> (18.5 mL, 0.16 mol) was slowly added and the reaction mixture was allowed to warm to room temperature (ca. 1 h). The solvent volume was then reduced in vacuo until a residual oil remained which was vacuum distilled and upon cooling formed a colourless moisture-sensitive (see below) crystalline solid (26.7 g, 85%). - m.p. 25–27 °C - IR:  $\bar{\nu}$  = 3401 vs, 3043 s, 2956 vs, 2901 s, 2884 s, 1599 vs, 1504 vs, 1460 s, 1446 s, 1386 vs, 1322 vs, 1289 vs, 1238 vs, 1215 vs, 1174 s, 1113 vs, 1050 s, 1031 vs, 902 vs, 842 vs, 776 s, 735 vs, 689 s, 620 w, 590 w cm<sup>-1</sup>. - MS: *m/z* (%) = 195 (80) [M<sup>+</sup>], 180 (50) [(L<sup>1</sup>)<sup>+</sup> - Me], 165 (100) [(L<sup>1</sup>)<sup>+</sup> - 2Me], 150 (60) [(L<sup>1</sup>)<sup>+</sup> - 3Me], 135 (45) [C<sub>6</sub>H<sub>5</sub>ONSi<sup>+</sup>], 108 (19) [C<sub>6</sub>H<sub>4</sub>OMe<sup>+</sup>], 73 (75) [SiMe<sub>3</sub><sup>+</sup>], 58 [SiMe<sub>2</sub><sup>+</sup>]. - <sup>1</sup>H NMR (300 MHz, C<sub>6</sub>D<sub>6</sub>, 298 K):  $\delta$  = 0.16 [s, 9 H, Si(CH<sub>3</sub>)<sub>3</sub>], 3.31 [s, 3 H, OCH<sub>3</sub>], 4.26 [br s, 1 H, NH], 6.57 [dd, <sup>3</sup>J = 7.4 Hz, <sup>4</sup>J = 1.1 Hz, 1 H, H-6], 6.74 [ddd, 1 H, H-5], 6.88 [m, 2 H, H-3, H-4]. - C<sub>10</sub>H<sub>17</sub>NOSi, (195.34): calcd. C 61.49, H 8.77, N 7.17; found C 61.66, H 8.89, N 7.29.

A sample of L<sup>1</sup>H was exposed to air for 5 h, diluted with CHCl<sub>3</sub>, and analysed by GC-MS: *R*, (rel. int.) = 9.73 (100), *m/z* (%) = 123

(90)  $[\text{CH}_3\text{OC}_6\text{H}_4\text{NH}_2^+]$ ;  $R_1 = 12.51$  (25),  $m/z$  (%) = 195 (20)  $[\text{L}^1\text{H}^+]$ ; no  $\text{SiMe}_3$ -containing decomposition products, e.g.  $\text{Me}_3\text{SiOH}$ , were observed.

$[\text{L}^2\text{H}]$ : As for  $\text{L}^1\text{H}$  above, 16.9 mL of a solution of  $n\text{BuLi}$  (1.6 M in hexanes) was added dropwise to a stirred solution of *o*-phenoxyaniline (5 g, 27 mmol) in ether (50 mL) at 0 °C. After complete addition a white solid was obtained which was stirred and warmed to room temperature (ca. 1 h) and  $\text{Me}_3\text{SiCl}$  (3.5 mL, 27 mmol) was slowly added. The reaction mixture was stirred for another 5 h. The reaction solution was decanted from the  $\text{LiCl}$  formed and the solvent volume was then reduced in vacuo until a residual oil remained. This was vacuum distilled and upon cooling formed a colourless moisture-sensitive crystalline solid (5.3 g, 76%). – m.p. 33–35 °C – IR:  $\tilde{\nu} = 3401$  vs, 1606 vs, 1589 s, 1583 s, 1499 s, 1307 vs, 1253 vs, 1240 vs, 1217 s, 1161 s, 1099 vs, 1072 s, 1038 s, 912 vs, 841 s, 750 vs, 689 vs.  $\text{cm}^{-1}$ . – MS:  $m/z$  (%) = 257 (60)  $[\text{M}^+]$ , 242 (61)  $[(\text{L}^2)^+ - \text{Me}]$ , 226 (15)  $[(\text{L}^2)^+ - \text{Me}_2\text{H}]$ , 211 (5)  $[(\text{L}^2)^+ - \text{Me}_2\text{H}]$ , 165 (100)  $[\text{OC}_6\text{H}_4\text{NHSiMe}_2^+]$ , 150 (40)  $[\text{C}_6\text{H}_4\text{ONHSiMe}_2^+]$ , 135 (30)  $[\text{C}_6\text{H}_4\text{OSiNH}^+]$ , 73 (35)  $[\text{SiMe}_2^+]$ , 58 (10)  $[\text{SiMe}_2^+]$ . –  $^1\text{H}$  NMR (300 MHz,  $\text{C}_6\text{D}_6$ , 298 K):  $\delta = 0.07$  [s, 9 H,  $\text{Si}(\text{CH}_3)_3$ ], 4.14 [br s, 1 H, NH], 6.57–6.63 [ddd, 1 H, H-4], 6.76–6.80 [tt, 1 H, H-5], 6.82–6.88 [dd, 1 H, H-3], 6.90–7.02 [m, 6 H, H-6, H-2', H-3', H-4', H-5', H-6'] –  $\text{C}_{15}\text{H}_{19}\text{NOSi}$  (257.41): calcd. C 69.99, H 7.44, N 5.44; found C 69.98, H 7.57, N 5.60.

$[\text{Yb}(\text{L}^1)_2(\mu\text{-OMe})_2]$  (1): Method 1. A mixture of ytterbium powder (0.69 g, 4.0 mmol),  $\text{HgPh}_2$  (0.71 g, 2.0 mmol) and  $\text{L}^1\text{H}$  (0.82 g, 4.0 mmol) in  $\text{thf}$  (60 mL) was stirred and heated at 60 °C for 24 h. Evaporation to dryness of the filtered reaction mixture gave a red oil. Treatment of the residue with  $\text{dme}$  (20 mL), evaporation to dryness, and then treatment with hexane (15 mL) afforded red/orange crystals of 1 on standing (0.45 g, 19%). – IR (Nujol):  $\tilde{\nu} = 1590$  vs, 1560 vs, 1314 w, 1287 s, 1242 s, 1204 vs, 1160 vs, 1115 vs, 1050 vs, 1033 vs, 1005 vs, 916 br s, 843 s, 832 s, 782 vs, 768 vs, 723 s, 670 s, 642 vs, 596 vs.  $\text{cm}^{-1}$ . – Vis/near IR ( $\text{dme}$ ):  $\lambda_{\text{max}}$  ( $\epsilon$ ) = 431 (304), 911 (22), 978 (63) nm ( $\text{dm}^3\text{mol}^{-1}$ ). – MS:  $m/z$  (%) = 990 (<1)  $[\text{M}^+ - \text{L}^1]$ , 368 (<1)  $[(\text{YbL}^1)^+]$ . –  $\text{C}_{42}\text{H}_{76}\text{N}_4\text{O}_6\text{Si}_4\text{Yb}_2$  (1185.47): calcd. C 42.55, H 5.95, N 4.73; found C 42.55, H 5.68, N 4.91.

Method 2: From a similar reaction [with  $\text{Yb}$  (0.30 g, 1.7 mmol),  $\text{HgPh}_2$  (0.35 g, 1.0 mmol) and  $\text{L}^1\text{H}$  (0.41 g, 2.0 mmol)], the resulting red oil was treated with diethyl ether instead of  $\text{dme}$ . Evaporation and recrystallisation of the residue from hexane (20 mL) gave 1 (0.22 g, 23%). The spectroscopic and X-ray properties were identical with those of the product from Method 1.

$[\text{Yb}(\text{L}^2)_2(\text{OPh})(\text{thf})]$  (2): A mixture of ytterbium powder (0.17 g, 1.0 mmol),  $\text{HgPh}_2$  (0.35 g, 1.0 mmol) and  $\text{L}^2\text{H}$  (0.51 g, 2.0 mmol) in  $\text{thf}$  (40 mL) was stirred and heated at 60 °C for 24 h. The resulting mixture was filtered and the dark red filtrate evaporated to dryness. Recrystallisation from toluene (20 mL) and standing overnight gave orange crystals (0.18 g, 21%). – IR (Nujol):  $\tilde{\nu} = 1718$  w, 1621 s, 1588 vs, 1554 s, 1307 vs, 1288 s, 1241 s, 1190 vs, 1158 vs, 1101 vs, 1070 vs, 1045 vs, 863 m, 830 br m, 807 m, 786 m, 756 s, 736 s, 706 s, 695 vs, 630 vs, 602 s, 594 s.  $\text{cm}^{-1}$ . – Vis/near IR ( $\text{dme}$ ):  $\lambda_{\text{max}}$  ( $\epsilon$ ) = 416 (401), 919 (31), 982 (73) nm ( $\text{dm}^3\text{mol}^{-1}$ ). – MS:  $m/z$  (%) = 779 (<1)  $[\text{M}^+ - \text{thf}]$ , 686 (<1)  $[(\text{YbL}^2)^+]$ , 613 (<1)  $[(\text{YbL}^2)^+ - \text{SiMe}_3]$ , 430 (<1)  $[(\text{YbL}^2)^+]$ . –  $\text{C}_{40}\text{H}_{49}\text{N}_2\text{O}_4\text{Si}_2\text{Yb}$  (851.03): calcd. C 56.45, H 5.80, N 3.29; found C 56.41, H 5.77, N 3.59. The reaction filtrate of 2 was hydrolysed with  $\text{H}_2\text{O}$  (15 mL) and this mixture extracted with  $\text{CHCl}_3$  (30 mL) which was then reduced under vacuum to 5 mL and analysed by GC-MS. – GC-MS:  $R_f$  (rel. int.) = 2.62 (80),  $m/z$  (%) = 93 (10)  $[\text{C}_6\text{H}_5\text{NH}_2^+]$ ;  $R_f = 7.12$  (5),  $m/z$  (%) = 94 (100)  $[\text{C}_6\text{H}_5\text{OH}^+]$ ;  $R_f = 17.35$  (95),  $m/z$  (%) = 185 (100)  $[\text{C}_6\text{H}_5\text{OC}_6\text{H}_4\text{NH}_2^+]$ .

$[\text{Yb}(\text{L}^1)_2(\text{thf})_2]$  (3): A toluene solution (5 mL) of  $\text{L}^1\text{H}$  (0.31 g, 2.0 mmol) was added to a toluene solution (40 mL) of  $[\text{Yb}(\text{N}(\text{SiMe}_3)_2)_2(\text{thf})_2]$  (0.65 g, 1.0 mmol) at –78 °C. The reaction mixture was warmed to –20 °C and dark red crystals formed overnight (0.54 g, 76%). – IR (Nujol):  $\tilde{\nu} = 1584$  vs, 1552 vs, 1320 sh s, 1296 br s, 1251 s, 1203 vs, 1162 vs, 1116 vs, 1054 vs, 1010 vs, 934 br s, 831 br s, 765 s, 723 s, 668 s, 617 vs, 593 vs.  $\text{cm}^{-1}$ . – Vis/near IR ( $\text{dme}$ ):  $\lambda_{\text{max}}$  ( $\epsilon$ ) = 487 sh (201) nm ( $\text{dm}^3\text{mol}^{-1}$ ). –  $^1\text{H}$  NMR (300 MHz,  $\text{C}_6\text{D}_6$ , 298 K):  $\delta = 0.44$  [s, 18 H,  $\text{Si}(\text{CH}_3)_2$ ], 1.19 [br s, 8 H,  $\beta\text{-H}$  (thf)], 3.35 [s, 8 H,  $\alpha\text{-H}$  (thf)], 3.47 [s, 6 H,  $\text{OCH}_3$ ], 6.54–6.59 [m (br), 4 H, Ar], 7.03 [s (br), 4 H, Ar]. –  $\text{C}_{28}\text{H}_{48}\text{N}_2\text{O}_4\text{Si}_2\text{Yb}$  (705.90): calcd. C 47.64, H 6.85, N 3.97, Yb, 24.51; found C 47.75, H 5.90, N 4.63, Yb, 25.59. A sample of diamagnetic 3 in

Table 1. Crystal data and refinement parameters

Compound	$\text{L}^1\text{H}^{[a]}$	1	2	3
Formula	$\text{C}_{16}\text{H}_{17}\text{NOSi}$	$\text{C}_{42}\text{H}_{76}\text{N}_4\text{O}_6\text{Si}_4\text{Yb}_2$	$\text{C}_{40}\text{H}_{49}\text{N}_2\text{O}_4\text{Si}_2\text{Yb}$	$\text{C}_{28}\text{H}_{48}\text{N}_2\text{O}_4\text{Si}_2\text{Yb}$
<i>M</i>	195.34	1185.47	851.03	705.90
Crystal system	tetragonal	monoclinic	monoclinic	monoclinic
Space group	$P4/n$	$C2/c$	$P2(1)/n$	$C2/c$
<i>a</i> (Å)	25.5964(5)	24.1340(4)	24.3109(3)	15.5139(2)
<i>b</i> (Å)		19.1294(3)	15.0605(2)	11.3411(2)
<i>c</i> (Å)	7.0684(2)	23.6252(4)	24.5560(2)	19.2898(3)
$\beta$ (°)		112.150(1)	118.833(1)	112.368(1)
<i>V</i> (Å <sup>3</sup> )	4631.0(13)	10102.1(3)	7876(3)	3138.6(11)
<i>Z</i>	16	4	8	4
$\rho_{\text{calcd}}$ ( $\text{g cm}^{-3}$ )	1.121	1.559	1.435	1.494
$\mu$ ( $\text{cm}^{-1}$ )	1.69	38.20	24.76	30.89
<i>F</i> (000)	1696	4752	3464	1440
$2\theta_{\text{max}}$ (°)	55.8	60.06	55.8	60.04
<i>N</i> <sub>total</sub>	18145	35621	97744	22197
<i>N</i> <sub>o</sub>	5497, 4209	14634, 12012	17146, 12246	4212, 3947
<i>R</i> <sub>int</sub> , <i>R</i> <sub>w</sub> [ <i>I</i> > 2 $\sigma$ ( <i>I</i> )]	0.039, 0.090	0.024, 0.074	0.054, 0.122	0.029, 0.083
<i>R</i> <sub>int</sub> , <i>R</i> <sub>w</sub> (all data)	0.060, 0.098	0.044, 0.089	0.100, 0.165	0.033, 0.084
Goodness of Fit	1.037	1.151	1.118	1.039

<sup>[a]</sup> The asymmetric unit comprises two independent, similar, well separated (no H-bonding), molecules. Bond lengths and angles were as expected,<sup>[36]</sup> and the details are available in the supplementary data.

$C_6D_6$  was shown to convert into a paramagnetic species upon heating at 60 °C for 24h by  $^1H$  NMR spectroscopy.

To 3 (0.47 g, 0.66 mmol) in hexane (30 mL) was added  $L^1H$  (0.13 g, 0.66 mmol). The resulting mixture was heated to 60 °C for 12h. The reaction mixture was then allowed to stand for 3 weeks at room temperature and the solvent volume was reduced to 3 mL under vacuum giving crystals of 1 which was identified by a unit cell determination and an IR spectrum.

**X-ray Crystal Structure Analysis:** Crystals were mounted under viscous oil onto a glass fibre. Low temperature ( $\approx 123$  K) data were collected on an Enraf-Nonius CCD area-detector diffractometer (Mo- $K_\alpha$  radiation,  $\lambda = 0.71073$  Å, frames comprised  $1.0^\circ$  increments in  $\phi$  and  $\omega$  yielding a sphere of data) using proprietary software (Nonius B.V., 1998). Each data set was merged ( $R_{int}$  as quoted) to  $N$  unique reflections and the structures were solved by conventional methods and refined, with anisotropic thermal parameter forms for the non-hydrogen atoms, by full-matrix least-squares on all  $F^2$  data using the SHELX 97 software package.<sup>[32]</sup> Hydrogen atoms were included in calculated positions and allowed to ride on the parent carbon atom with isotropic thermal parameters. For 1, the methoxide carbon atoms lie on crystallographic twofold axes and therefore two sets of hydrogens atoms, each with occupancies of 0.5, were placed on each carbon, disordered about the axes. Crystal and refinement data are listed in Table 1.

Crystallographic data (excluding structure factors) for the structures reported in this paper have been deposited with the Cambridge Crystallographic Data Centre as supplementary publication nos. CCDC-146332 (L<sup>1</sup>H), -143939 (1), -143940 (2), -143941 (3). Copies of the data can be obtained free of charge on application to CCDC, 12 Union Road, Cambridge CB2 1EZ, UK [Fax: (internat.) + 44-1223/336-033; E-mail: deposit@ccdc.cam.ac.uk].

### Acknowledgments

We acknowledge the financial support of the Australian Research Council and an Australian Postgraduate Award to N. M. S.

- [1] G. B. Deacon, T. Feng, C. M. Forsyth, A. Gitlits, D. C. R. Hockless, Q. Shen, B. W. Skelton, A. H. White, *J. Chem. Soc., Dalton Trans.* 2000, 961–966.
- [2] H. B. Kagan, J. L. Namy, *Handbook on the Physics and Chemistry of Rare Earths*, (Eds: K. A. Gschneidner, L. Eyring), North-Holland Amsterdam, 1984, vol. 6, chapter 50.
- [3] G. A. Molander, C. R. Harris, *Chem. Rev.* 1996, 96, 307–338; G. A. Molander, *Chem. Rev.* 1992, 92, 29–68.
- [4] T. Imamoto, *Lanthanides in Organic Synthesis*, Academic Press, 1994.
- [5] W. Clegg, C. Eaborn, K. Izod, P. O'Shaughnessy, J. D. Smith, *Angew. Chem. Int. Ed. Engl.* 1997, 36, 2815–2817.
- [6] Z. Hou, A. Fujita, Y. Zhang, T. Miyano, H. Yamazaki, Y. Wakatsuki, *J. Am. Chem. Soc.* 1998, 120, 754–766.
- [7] W. J. Evans, C. A. Seibel, J. W. Ziller, *Inorg. Chem.* 1998, 37, 770–776.
- [8] W. J. Evans, J. W. Grate, I. Bloom, W. E. Hunter, J. L. Atwood, *J. Am. Chem. Soc.* 1985, 107, 405–409.
- [9] I. R. van den Hende, P. A. Hitchcock, S. A. Holmes, M. F. Lappert, W.-P. Leung, T. C. W. Mak, S. Prashar, *J. Chem. Soc., Dalton Trans.* 1995, 1427–1433.
- [10] C. Eaborn, P. B. Hitchcock, K. Izod, Z.-G. Lu, J. D. Smith, *Organometallics* 1996, 15, 4783–4790.
- [11] D. J. Duncalf, P. B. Hitchcock, G. A. Lawless, *Chem. Commun.* 1996, 269–271.
- [12] Yu. K. Gun'ko, P. B. Hitchcock, M. F. Lappert, *J. Organomet. Chem.* 1995, 499, 213–219.
- [13] M. C. Cassani, M. F. Lappert, F. Laschi, *Chem. Commun.* 1997, 1563–1564.
- [14] M. C. Cassani, D. J. Duncalf, M. F. Lappert, *J. Am. Chem. Soc.* 1998, 120, 12958–12959.
- [15] F. T. Edelmann, in *Comprehensive Organometallic Chemistry II*, (Eds: G. Wilkinson, F. G. A. Stone, E. W. Abel), Pergamon, Oxford, 1995, vol. 3, chapter 2.
- [16] M. N. Bochkarev, L. N. Zacharov, G. S. Kalinina, *Organoderivatives of the Rare Earth Elements*, Kluwer Academic, Dordrecht, 1995.
- [17] G. B. Deacon, G. D. Fallon, C. M. Forsyth, H. Schumann, R. Weimann, *Chem. Ber.* 1997, 130, 409–415.
- [18] F. Calderazzo, R. Pappalardo, S. Losi, *J. Inorg. Nucl. Chem.* 1966, 28, 987–999.
- [19] G. B. Deacon, T. Feng, B. W. Skelton, A. H. White, *Aust. J. Chem.* 1995, 48, 741–756.
- [20] G. B. Deacon, C. M. Forsyth, P. C. Junk, B. W. Skelton, A. H. White, *J. Chem. Soc., Dalton Trans.* 1998, 1381–1387.
- [21] G. B. Deacon, C. M. Forsyth, B. M. Gatehouse, P. A. White, *Aust. J. Chem.* 1990, 43, 795–806.
- [22] W. J. Evans, G. W. Rabo, J. W. Ziller, *Organometallics* 1994, 13, 1641–1645.
- [23] A. Recknagel, A. Steiner, S. Brooker, D. Stalke, F. T. Edelmann, *J. Organomet. Chem.* 1991, 415, 315–326.
- [24] Y. Yao, Q. Shen, J. Sun, F. Xue, *Acta Crystallogr., Sect. C*, 1998, 54, 625–627.
- [25] Y. Yao, Q. Shen, J. Sun, *Polyhedron*, 1998, 17, 519–522.
- [26] R. C. Mehrotra, A. Singh, U. M. Tripathi, *Chem. Rev.* 1991, 91, 1287–1303.
- [27] J. Marcalo, A. P. De Matos, *Polyhedron*, 1989, 8, 2431–2437.
- [28] G. B. Deacon, P. I. MacKinnon, T. D. Tuong, *Aust. J. Chem.* 1983, 36, 43–53.
- [29] A. Maercker, *Angew. Chem. Int. Ed. Engl.* 1987, 26, 972–989.
- [30] S. C. Harris, *PhD Thesis*, Monash University, 1999; G. Zelesny, *Dr der Math.-Natur. Fakultät Thesis*, Universität zu Köln, 1998.
- [31] C. T. Abrahams, G. B. Deacon, B. M. Gatehouse, G. N. Ward, *Acta Crystallogr., Sect. C*, 1994, 50, 504–507.
- [32] M. Wedler, M. Notlemeyer, U. Pieper, H.-G. Schmidt, D. Stalke, F. T. Edelmann, *Angew. Chem. Int. Ed. Engl.* 1990, 29, 894–896.
- [33] L. Lee, D. J. Berg, G. W. Bushnell, *Inorg. Chem.* 1994, 33, 5302–5308.
- [34] J. L. Atwood, W. E. Hunter, A. L. Wayda, W. J. Evans, *Inorg. Chem.* 1981, 20, 4115–4118.
- [35] G. M. Sheldrick, *SHELX97, Program for Crystal Structure Determination*, Universität Göttingen, 1997.
- [36] *Interatomic Distances*, Special Publication II, The Chemical Society, London, 1958.

Received May 3, 2000  
[100174]

## Structural Variety in Solvated Lanthanoid(III) Halide Complexes

Glen B. Deacon,<sup>A,B</sup> Tiecheng Feng,<sup>A</sup> Peter C. Junk,<sup>A,C</sup> Gerd Meyer,<sup>D</sup> Natalie M. Scott,<sup>A</sup> Brian W. Skelton<sup>E</sup> and Allan H. White<sup>E</sup>

<sup>A</sup> School of Chemistry, Monash University, Vic. 3800.

<sup>B</sup> To whom correspondence should be addressed (e-mail: glen.deacon@sci.monash.edu.au)

<sup>C</sup> Department of Chemistry, James Cook University, Townsville, Qld 4811.

<sup>D</sup> Institut für Anorganische Chemie, Universität zu Köln, Greinstrasse 6, 50939 Köln, Germany.

<sup>E</sup> Department of Chemistry, University of Western Australia, Nedlands, W.A. 6907.

Treatment of lanthanum metal with  $\text{CH}_2\text{Br}_2$  or  $\text{CH}_2\text{I}_2$  in tetrahydrofuran (thf) under ultrasound conditions yields the corresponding  $[\text{LaX}_3(\text{thf})_4]$  ( $X = \text{Br}, \text{I}$ ) complexes in good yield. Recrystallization of  $[\text{LaBr}_3(\text{thf})_4]$  from 1,2-dimethoxyethane (dme) or bis(2-methoxyethyl) ether (diglyme) generates  $[\text{LaBr}_2(\mu\text{-Br})(\text{dme})_2]_2$  and  $[\text{LaBr}_2(\text{diglyme})_2][\text{LaBr}_4(\text{diglyme})]$ . Treatment of lanthanoid metals with hexachloroethane in dme yields  $[\text{LnCl}_3(\text{dme})_2]$  ( $\text{Ln} = \text{La}, \text{Nd}, \text{Er}$  or  $\text{Yb}$ ) and in acetonitrile  $[\text{YbCl}_2(\text{MeCN})_5]_2[\text{YbCl}_3(\text{MeCN})(\mu\text{-Cl})_2\text{YbCl}_3(\text{MeCN})]$ . The reaction of Yb metal pieces with 1,2-dibromoethane in thf and dme gave single crystals of  $[\text{YbBr}_3(\text{thf})_3]$  and  $[\text{YbBr}_3(\text{dme})_2]$ , respectively. The X-ray determined structure of  $[\text{LaBr}_3(\text{thf})_4]$  shows a seven-coordinate monomer with pentagonal-bipyramidal stereochemistry and apical bromide ligands. For  $[\text{YbBr}_3(\text{thf})_3]$ , a monomeric structure with *mer*-octahedral stereochemistry is observed. In  $[\text{LaBr}_2(\mu\text{-Br})(\text{dme})_2]_2$ , two eight-coordinate La centres are linked by two bridging bromides. The dme ligands have a *trans* relationship to each other, and *cis* terminal bromides are *transoid* to the bridging bromides with dodecahedral stereochemistry for La. By contrast, the 1:1.5 diglyme adduct is found to be ionic  $[\text{LaBr}_2(\text{diglyme})_2][\text{LaBr}_4(\text{diglyme})]$ , with an eight-coordinate bicapped trigonal-prismatic lanthanum cation and a seven-coordinate pentagonal-bipyramidal lanthanum anion. In the cation, the bromide ligands are *cis* to each other, and in the anion, two bromides are equatorial and two are axial. In  $[\text{YbBr}_3(\text{dme})_2]$ ,  $[\text{YbCl}_3(\text{dme})_2]$  and  $[\text{ErCl}_3(\text{dme})_2]$ , a seven-coordinate pentagonal-bipyramidal arrangement exists with apical halogen ligands. Far-infrared data, and in particular the absence of absorptions attributable to  $\nu(\text{La-Cl}_{\text{ter}})$ , suggest that  $[\text{LaCl}_3(\text{dme})]$  is polymeric with six bridging chlorides per lanthanum. For  $[\text{YbCl}_2(\text{MeCN})_5]_2[\text{YbCl}_3(\text{MeCN})(\mu\text{-Cl})_2\text{YbCl}_3(\text{MeCN})]$ , a remarkable ionic structure, with pentagonal-bipyramidal  $[\text{YbCl}_2(\text{MeCN})_5]^+$  cations and octahedral dinuclear  $[\text{YbCl}_3(\text{MeCN})(\mu\text{-Cl})_2\text{YbCl}_3(\text{MeCN})]^{2-}$  counter ions, is observed. In the former, chloride ligands are apical, while the MeCN ligands of the latter are *transoid*.

**Keywords:** Lanthanoid halides, lanthanum, ytterbium.

### Introduction

Anhydrous lanthanoid halide compounds are convenient precursors for the synthesis of many types of amido-, alkoxo-, aryloxo- and organo-lanthanoid complexes.<sup>1–3</sup> Preparing pure anhydrous lanthanoid halides is not a trivial exercise. Several methods for dehydration of  $\text{LnX}_3(\text{H}_2\text{O})_n$  have been reported, but inherent problems exist with them.<sup>4–6</sup> For many purposes, tetrahydrofuran (thf) or 1,2-dimethoxyethane (dme) complexes provide effective alternatives to the anhydrous halides, and several new syntheses of these compounds have been reported. Thus,  $[\text{LnCl}_3(\text{thf})_n]$  complexes have been obtained from Sc and Ln metals and  $\text{HgCl}_2$  in thf,<sup>7,8</sup> and from Ln metal,  $\text{Me}_3\text{SiCl}$  and  $\text{MeOH}$ .<sup>9</sup> Two dme complexes have been prepared from  $\text{Ln}_2\text{O}_3$  and  $\text{HCl}$  (from

$\text{Me}_3\text{SiCl}$  and  $\text{H}_2\text{O}$ ) in dme,<sup>10</sup> and some thf and dme complexes were prepared from  $\text{Ln}_2\text{O}_3$  or  $\text{Ln}_2(\text{CO}_3)_3$ ,  $\text{SOCl}_2$  and limited water in dme,<sup>11</sup> though the last method has considerable limitations.<sup>12</sup> We have developed an elegant high-yielding synthesis for  $\text{LnCl}_3(\text{thf})_n$  whereby a lanthanoid metal is treated with excess hexachloroethane in thf,<sup>12,13</sup> and we now extend metal-based syntheses to the bromides and iodides, and the use of  $\text{C}_2\text{Cl}_6$  to other solvents, namely, dme and MeCN. Hitherto, syntheses of lanthanoid bromides and iodides have generally been achieved either from dehydration of the hydrated lanthanoid halides, by reaction of  $\text{Ln}_2\text{O}_3$  with  $\text{NH}_4\text{Br}$  or  $\text{NH}_4\text{I}$ ,<sup>14</sup> or by treatment of the metal with elemental  $\text{Br}_2$  or  $\text{I}_2$  in a suitable solvent. The last was the method of choice for recent syntheses of  $[\text{La}_3(\text{thf})_4]^{15}$  and of several isopropanol adducts of  $\text{LnI}_3$  ( $\text{Ln} = \text{La}, \text{Ce}$  or  $\text{Nd}$ ).<sup>16</sup>

The far-infrared spectra of  $[\text{LaX}_3(\text{thf})_4]$  have bands attributable to  $\nu(\text{La-X})$  at 178 ( $X = \text{Br}$ ) and 156  $\text{cm}^{-1}$  ( $X = \text{I}$ ). These values are close to those of the corresponding modes reported for eight-coordinate  $[\text{YbCp}_2\text{X}(\text{thf})]$ , namely, 178 and 136  $\text{cm}^{-1}$  for  $X = \text{Br}$  and  $\text{I}$ , respectively.<sup>43</sup> Moreover, the values are consistent with  $\nu(\text{Ln-Cl}_{\text{ter}})$  (c. 270 and 240  $\text{cm}^{-1}$ ) reported for a range of  $\text{LnCl}_3(\text{thf})_n$  complexes,<sup>12,18</sup> including seven-coordinate  $[\text{GdCl}_3(\text{thf})_4]$ .<sup>18</sup>

The far-infrared spectrum of eight-coordinate  $[\text{LaBr}_3(\text{dme})_2]$ , which has both terminal and bridging  $\text{La-Br}$  bonds, has bands at 175 and 150  $\text{cm}^{-1}$  attributable to  $\nu(\text{La-Br}_{\text{ter}})$  and at 138  $\text{cm}^{-1}$  (and possibly 112  $\text{cm}^{-1}$ ) attributable to  $\nu(\text{La-Br}_{\text{br}})$ . For  $[\text{LaBr}_2(\text{diglyme})][\text{LaBr}_4(\text{diglyme})]$ , which has no bridging  $\text{La-Br}$  bonds, absorptions at 177  $\text{cm}^{-1}$  (and perhaps 135  $\text{cm}^{-1}$ ) can be assigned to  $\nu(\text{La-Br})$ . These are appropriately lowered from  $\nu(\text{Ln-Cl}_{\text{ter}})$  (280–240  $\text{cm}^{-1}$ ) and  $\nu(\text{Ln-Cl}_{\text{br}})$  (205–175  $\text{cm}^{-1}$ ) reported for  $[\text{LnCl}_3(\text{thf})_n]$  complexes.<sup>12</sup> For  $[\text{LaCl}_3(\text{dme})]$ , no bands  $\geq 240 \text{ cm}^{-1}$  attributable to  $\nu(\text{La-Cl}_{\text{ter}})$  (see above) are observed. Absorptions at 215 and 182  $\text{cm}^{-1}$  are assigned to  $\nu(\text{La-Cl}_{\text{br}})$  and correspond to  $\nu(\text{La-Cl}_{\text{br}})$  of  $[\text{LaCl}_3(\text{thf})_2]_n$ .<sup>12</sup> This implies lanthanum is associated with six bridging chloride ligands as in  $[\text{LaCl}_3(\text{thf})_2]_n$ . Thus,  $[\text{LaCl}_3(\text{dme})]$  is considered to have a similar structure to that of  $[\text{LaCl}_3(\text{thf})_2]_n$  but with a chelating  $\text{dme}$  replacing the  $\text{cis-thf}$  ligands of the latter. As the steric demands of  $\text{dme}$  are less than those of two  $\text{thf}$  ligands,<sup>44</sup> the current structure is less crowded. For  $[\text{NdCl}_3(\text{dme})_2]$ , which is probably a seven-coordinate monomer in view of the structures of  $[\text{LnCl}_3(\text{dme})_2]$  ( $\text{Ln} = \text{Y},^{29} \text{Eu},^{11} \text{Gd},^{30} \text{Dy},^{25} \text{Er},^2$  or  $\text{Yb}$  (below)), and for  $[\text{YbCl}_3(\text{dme})_2]$ , satisfactory far-infrared spectra could not be obtained. However, significant absorption was evident well above 200  $\text{cm}^{-1}$ , consistent with  $\text{Ln-Cl}_{\text{ter}}$  bonding.

#### X-Ray Structure Determinations

For the eight molecular structures determined by room-temperature single-crystal studies, a summary of crystal and refinement parameters is provided in the Experimental section, and pertinent bond distances and angles are shown in Tables 1–11. The structures are displayed in Figs 1–6.

#### $[\text{LaBr}_3(\text{thf})_4]$

The molecular structure of seven-coordinate, monomeric  $[\text{LaBr}_3(\text{thf})_4]$ , is shown in Fig. 1, and represents the first structurally authenticated example of a  $\text{thf}$ -solvated

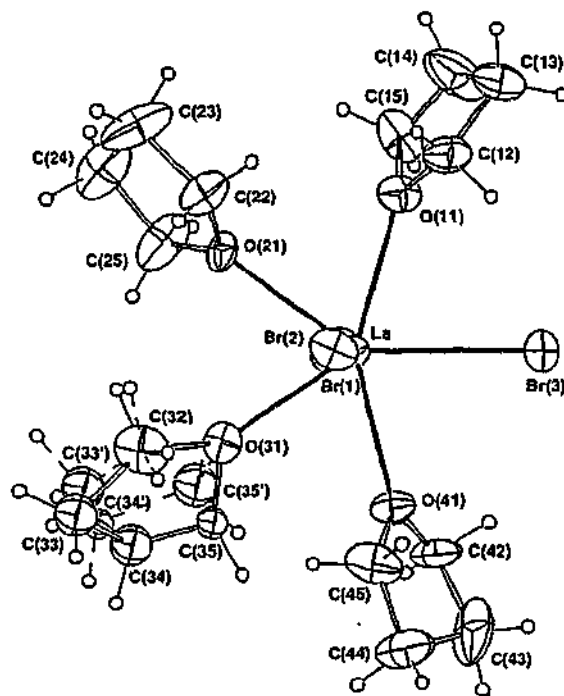


Fig. 1. The seven-coordinate mononuclear array of  $[\text{LaBr}_3(\text{thf})_4]$ .

lanthanoid tribromide complex. One molecule, devoid of crystallographic symmetry, comprises the asymmetric unit of the structure. The geometry about the  $\text{La}$  centre is best described as a distorted pentagonal bipyramid with  $\text{Br}$  ligands in the apical sites and a  $\text{Br}$  and four  $\text{thf}$  ligands in the five equatorial sites, putative symmetry  $C_{2v}$  being broken by the  $\text{thf}$  ring dispositions. This type of geometry has previously been identified in a number of solvated lanthanoid halides, for example,  $[\text{SmBr}_3(\text{Pr}^i\text{OH})_4]$ ,<sup>32</sup>  $[\text{LaI}_3(\text{Pr}^i\text{OH})_4]$ ,<sup>16</sup> and  $[\text{LnCl}_3(\text{thf})_4]$  ( $\text{Ln} = \text{Nd}, \text{Sm}, \text{Eu}$  and  $\text{Gd}$ )<sup>18–21</sup> and  $[\text{LaI}_3(\text{thf})_4]$ .<sup>15</sup> It is pertinent that  $\text{LaX}_3$  ( $X = \text{Br}$  (below) or  $\text{I}$ <sup>15</sup>) give compounds which are solvates with similar compositions and structures, namely, seven-coordinate  $[\text{LaX}_3(\text{thf})_4]$ , while the chloride is an eight-coordinate, polymeric species isolated as a bis( $\text{thf}$ ) complex,  $[\text{La}(\mu\text{-Cl})_3(\text{thf})_2]_n$ .<sup>12</sup>

The present  $\text{La-Br}$  distances (2.888(4)–2.909(4),  $\langle \rangle$  2.90(1) Å) (Table 1) are similar to the  $\text{La-Cl}$  distances found

Table 1. The lanthanum environment in  $[\text{LaBr}_3(\text{thf})_4]$   
 $r$  is the lanthanum–ligand atom distance. Other entries in the matrix are the angles (degrees) subtended by the relevant atoms at the head of the row and column. Also:  $\text{La-O}(n1)\text{-C}(n2)$ ;  $\text{La-O}(n1)\text{-C}(n5)$  ( $n = 1\text{--}4$ ) are 130(2), 123(2), 132(2), 122(2); 122(2), 126(2), 125(3)/121(4), 127(2)°

Atom	$r$ (Å)	Br(2)	Br(3)	O(11)	O(21)	O(31)	O(41)
Br(1)	2.909(4)	166.8(1)	91.2(1)	95.9(5)	84.6(5)	81.5(5)	97.2(5)
Br(2)	2.888(4)		102.0(1)	86.9(5)	34.3(5)	83.2(5)	86.8(5)
Br(3)	2.899(4)			74.6(5)	143.4(5)	144.6(5)	77.1(5)
O(11)	2.52(2)				69.8(7)	140.5(7)	148.9(6)
O(21)	2.58(2)					70.7(7)	139.6(7)
O(31)	2.52(2)						69.6(7)
O(41)	2.51(2)						

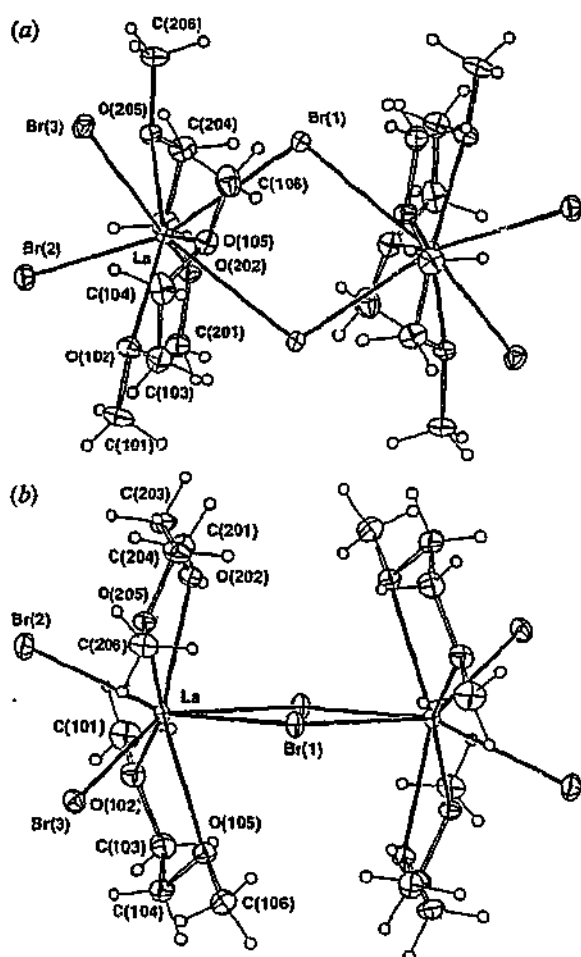


Fig. 2. Molecular structure of the binuclear  $[\text{La}(\text{dme})_2\text{Br}_2(\mu\text{-Br})_2\text{LaBr}_2(\text{dme})_2]$  (a) normal to and (b) through the  $\text{La}(\mu\text{-Br})_2\text{La}$  core.

in  $[\text{La}(\mu\text{-Cl})_3(\text{thf})_2]_n$  (2.882(3)–2.968(3),  $< >$  2.91(4) Å)<sup>12</sup> and are longer than Sm–Br in  $[\text{SmBr}_3(\text{Pr}^i\text{OH})_4]$  (2.805(3)–2.849(2),  $< >$  2.83(2) Å)<sup>32</sup> by an amount corresponding to the difference in size of the respective seven-coordinate  $\text{Ln}^{3+}$  ions (c. 0.08 Å).<sup>45</sup> A Cambridge Data Base search shows few compounds with La–Br connectivities, the most relevant being eight-coordinate  $[\text{LaBr}_3(12\text{-crown-4})(\text{Me}_2\text{CO})]$  with La–Br (2.944(1)–2.986(1),  $< >$  2.97(2) Å),<sup>46</sup> longer than <

La–Br  $>$  of  $[\text{LaBr}_3(\text{thf})_4]$  by the ionic radius change for the coordination number difference.<sup>45</sup> The mean of the La–O(thf) distances (2.51(2)–2.58(2),  $< >$  2.53(3) Å) (Table 1) is perhaps slightly shorter than in the eight-coordinate  $[\text{La}(\mu\text{-Cl})_3(\text{thf})_2]_n$  (2.549(2)–2.595(2),  $< >$  2.57(2) Å).<sup>12</sup> The axial Br–La–Br unit deviates quite significantly from linearity (166.8(1)°), this angle being at the lower end of values for related complexes, e.g. 176.8(1)° in  $[\text{SmBr}_3(\text{Pr}^i\text{OH})_4]$ ,<sup>32</sup> 166.4(1)° in  $[\text{NdCl}_3(\text{thf})_4]$ ,<sup>19</sup> 171.1(1)° in  $[\text{EuCl}_3(\text{thf})_4]$ ,<sup>21</sup> and 175.2(8)° in  $[\text{GdCl}_3(\text{thf})_4]$ .<sup>18</sup> The sum of the interligand angles of the equatorial pentagonal plane (361.8°) is close to that expected for pentagonal planar geometry.

#### $[\text{LaBr}_2(\mu\text{-Br})(\text{dme})_2]_2$

The X-ray structure of this complex (Fig. 2) shows a dimeric molecule with a pair of bridging bromide ions and is the first dme-solvated lanthanoid tribromide to be characterized by an X-ray study (but see also a lanthanoid(a) iodide complex  $[\text{SmI}_2(\text{dme})_3]$ <sup>38</sup>). A  $[\text{LaBr}_2(\mu\text{-Br})_2\text{LaBr}_2]$  unit is complexed by *trans* dme ligands, with one-half of the centrosymmetric dimer comprising the asymmetric unit of the structure. The coordination array about the eight-coordinate lanthanum centre is best described as a dodecahedron.<sup>47</sup> The overall structure has similarities to that of  $[\text{YbCl}_3(\text{thf})_2]_2$ ,<sup>13</sup> with chelating *trans* dme ligands in place of the *trans*-thf groups. In the present complex, the four Br ligands about each La atom deviate markedly from coplanarity, the angle between the least-squares planes defined by La, Br(2), Br(3) and by La, Br(1), Br(1') being 41.77(3)°, cf. the Yb atom of  $[\text{YbCl}_3(\text{thf})_2]_2$  where the four equatorial chloride ligands are coplanar about the metal.<sup>13</sup> The larger size of La compared to Yb not only enables a higher coordination number, but also accommodates the larger halogen. If the centre of the O··O vector of the dme ligand is taken as a coordination site, then the geometry about La is closer to a trigonal prism<sup>47</sup> than the octahedron of the Yb complex.<sup>13</sup>

The bridging La–Br distances (3.053(2), 3.115(2),  $< >$  3.08(3) Å) (Table 2) are much longer than the La–Br<sub>ter</sub> distances in  $[\text{LaBr}_3(\text{thf})_4]$  ( $< >$  2.90(1) Å (see above)), whereas the terminal distances ( $< >$  2.94(3) Å; Table 2) are similar. Further, the La–O distances (2.583(7)–2.677(7),  $< >$  2.63(3) Å) are longer than those in  $[\text{LaBr}_3(\text{thf})_4]$  ( $< >$  2.53(3) Å (see above)), as expected for the differences in

Table 2. The lanthanum environment in  $[\text{LaBr}_3(\text{dme})_2]_2$

Presentation is as in Table 1; primed atoms are related by the transformation (1–x, 1–y, 1–z). La···La' is 4.944(2), Br(1)···Br(1') is 3.683(2) Å. La–Br(1)–La' is 106.56(3)°; La–O(n02)–C(n01) are 123.5(6), 119.0(6)°; La–O(n02)–C(n03) are 118.4(4), 117.6(5)°; La–O(n05)–C(n04) are 112.1(7), 116.7(6)°; La–O(n05)–C(n06) are 125.6(7), 122.6(6)° (n = 1, 2)

Atom	r (Å)	Br(2)	Br(3)	O(102)	O(105)	O(202)	O(205)	Br(1')
Br(1)	3.053(2)	152.07(4)	93.17(4)	132.6(2)	77.7(2)	89.9(1)	71.3(1)	73.44(3)
Br(2)	2.972(2)		84.77(5)	75.1(2)	127.3(2)	74.3(2)	80.9(1)	121.04(4)
Br(3)	2.910(2)			98.9(1)	72.2(1)	139.2(2)	80.1(1)	146.93(4)
O(102)	2.583(7)				63.1(2)	108.6(2)	155.9(2)	71.7(2)
O(105)	2.677(7)					147.5(2)	136.8(2)	75.4(1)
O(202)	2.618(6)						62.5(2)	72.2(2)
O(205)	2.624(7)							121.3(1)
Br(1')	3.115(2)							

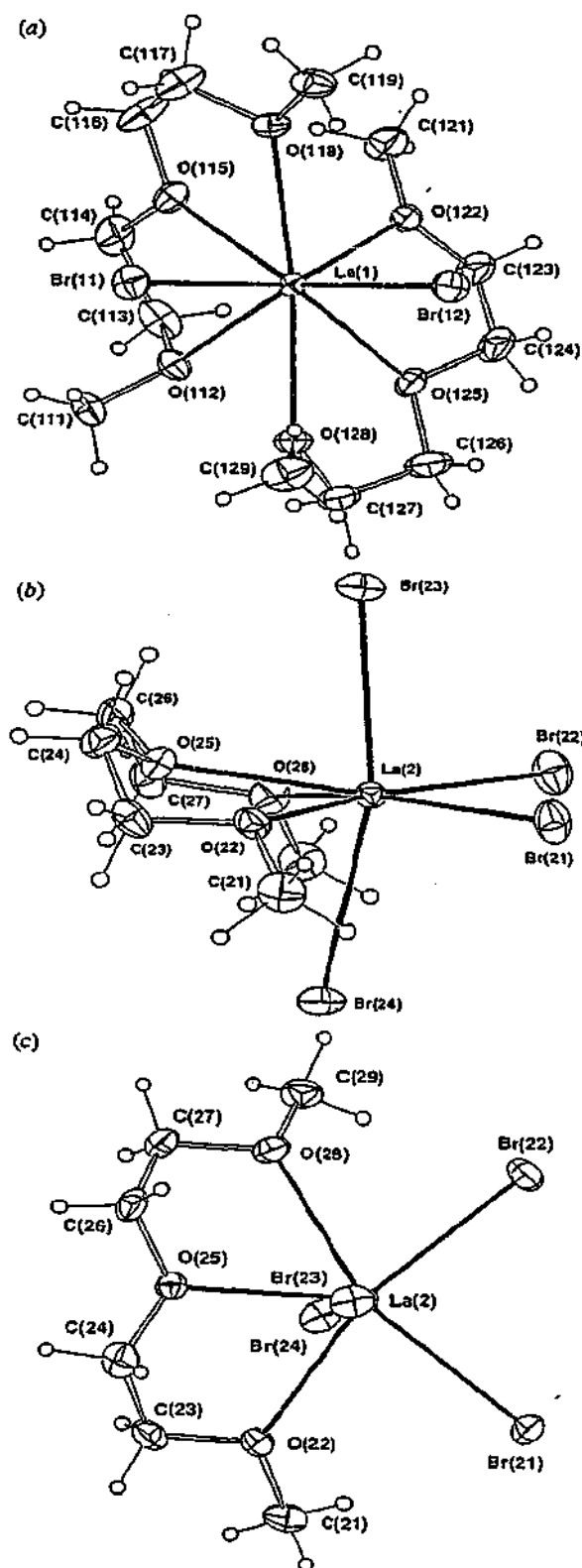


Fig. 3. Molecular structure of  $[\text{LaBr}_2(\text{diglyme})_2][\text{LaBr}_4(\text{diglyme})]$ . (a) The eight-coordinate cation showing the quasi square-antiprismatic geometry. (b) and (c) Two views of the seven-coordinate anion.

coordination numbers and the significant lengthening of Ln-O(dme) over Ln-O(thf).<sup>48</sup> In the only other lanthanum complexes with dme ligands, La-O (2.580(8), 2.673(9),  $\langle \rangle$  2.62(4) Å) in nine-coordinate  $[\text{Cp}''_2\text{La}(\text{dme})(\text{MeCN})][\text{BPh}_4](\text{dme})_{0.5}$  ( $\text{Cp}'' = 1,3\text{-bis}(\text{trimethylsilyl})\text{cyclopentadienyl}$ ),<sup>49</sup> and (2.589(4)-2.638(3),  $\langle \rangle$  2.61(2) Å) in eight-coordinate  $[\text{LaCl}(\text{dme})(\mu_2\text{-Cl})_2(\mu_3\text{-Cl})\text{La}(\text{dme})\text{Li}(\text{thf})_2]$ ,<sup>50</sup> are both similar to the present  $\langle \text{La-O} \rangle$  distance.

#### $[\text{LaBr}_2(\text{diglyme})_2][\text{LaBr}_4(\text{diglyme})]$

The X-ray structure of this complex shows an eight-coordinate cation  $[\text{LaBr}_2(\text{diglyme})_2]^+$  (Fig. 3a) and a seven-coordinate anion  $[\text{LaBr}_4(\text{diglyme})]^-$  (Fig. 3b,c); one formula unit, devoid of crystallographic symmetry comprises the asymmetric unit of the structure, the cation with quasi-2 symmetry and the anion *m* (the metal environments quasi- $\text{C}_{2v}$ ). The geometry about the eight-coordinate cation (Fig. 3a) is best described<sup>47</sup> as a 4,4-bicapped trigonal prism, while the anion is close to a pentagonal bipyramid with apical bromides and the equatorial pentagonal plane defined by two bromide ligands and the three oxygen atoms of diglyme (Fig. 3b,c). The sum of the interligand angles ( $363.2^\circ$ ) of the equatorial pentagonal plane in the anion (made up of Br(21), Br(22), O(22), O(25) and O(28)) is close to  $360^\circ$ , as expected for this geometry.

The La-Br distances (2.885(2), 2.902(2),  $\langle \rangle$  2.89(1) Å for the cation (Table 3), and 2.913(2)-2.933(2),  $\langle \rangle$  2.924(8) Å for the anion (Table 4) differ somewhat less than expected for the difference in coordination number.<sup>45</sup> The latter is similar to  $\langle \text{La-Br} \rangle$  of seven-coordinate  $[\text{LaBr}_3(\text{thf})_4]$  (2.90(1) Å; see above) and the former somewhat shorter than the terminal La-Br distances in eight-coordinate  $[\text{LaBr}_3(\text{dme})_2]_2$  (2.94(7) Å; see above) and those ( $\langle \rangle$  2.97(2) Å; see above) of eight-coordinate  $[\text{LaBr}_3(12\text{-crown-4})(\text{Me}_2\text{CO})]$ .<sup>46</sup>

The La-O distances (2.562(7)-2.615(9),  $\langle \rangle$  2.58(2) Å) in the cation, and 2.543(7)-2.669(7),  $\langle \rangle$  2.61(5) Å in the anion (Tables 3, 4) do not correlate with coordination number, since they are surprisingly longer than those for the same ligand (2.475(5)-2.642(6),  $\langle \rangle$  2.55(6) Å) in nine-coordinate  $[\text{La}(\text{hfa})_3(\text{diglyme})]$  (hfaH = hexafluoroacetylacetonate),<sup>51</sup> the only other X-ray characterized complex of lanthanum with diglyme. Subtraction of the ionic radius for the appropriate coordination number  $\text{La}^{3+}$  ion from  $\langle \text{La-O} \rangle$  gives 1.42 Å for the cation, 1.51 Å for the anion and 1.33 Å for  $[\text{La}(\text{hfa})_3(\text{diglyme})]$ .<sup>51</sup> For  $[\text{LaX}_3(\text{thf})_4]$  and  $[\text{LaBr}_3(\text{dme})_2]_2$ , corresponding values cover the narrower range 1.42-1.47 Å. Moreover, the most crowded structure,<sup>44</sup> namely  $[\text{La}(\text{hfa})_3(\text{diglyme})]$ , has the shortest La-O bonds. A possible explanation is that the bromide ligands exert some repulsive *trans* influence, which is greatest the nearer the O-La-Br angles approach  $180^\circ$ . The elongation of  $\langle \text{La-O} \rangle$  in the  $[\text{LaBr}_4(\text{diglyme})]^-$  anion arises from the long La-O bonds to the terminal oxygens (2.624(7) and 2.669(7) Å, cf. 2.543(7) Å to the other oxygen). Thus individual subtraction values are 1.52, 1.56 and (normal for  $\text{LaBr}_3$ -ether complexes) 1.44 Å. The terminal oxygens have O-La-Br angles of  $157.9(2)$  and  $165.0(2)^\circ$ , which are larger than any O-La-Br angles in the cation,

Table 3. The lanthanum environment of the cation  $[\text{LaBr}_2(\text{diglyme})_2]^+$  (La(1)) in  $[\text{LaBr}_2(\text{diglyme})_2][\text{LaBr}_4(\text{diglyme})]$

Presentation is as in Table 1. La(1)-O(1n2)-C(1n1) are 124.9(7), 126.8(7); La(1)-O(1n2)-C(1n3) are 108.8(9), 121.4(9) $^\circ$ ; La(1)-O(1n5)-C(1n4) are 121.1(8), 116.3(9) $^\circ$ ; La(1)-O(1n5)-C(1n6) are 123.1(9), 118.2(9) $^\circ$ ; La(1)-O(1n8)-C(1n7) are 119(1), 114.5(8) $^\circ$ ; La(1)-O(1n8)-C(1n9) are 124.2(7), 127(1) $^\circ$  (n = 1, 2)

Atom	r (Å)	Br(12)	O(112)	O(115)	O(118)	O(122)	O(125)	O(128)
Br(11)	2.902(2)	96.37(3)	86.4(2)	84.2(2)	77.9(2)	154.5(2)	143.2(2)	80.2(2)
Br(12)	2.885(2)		148.9(2)	147.9(2)	87.6(2)	90.5(2)	83.2(2)	79.7(2)
O(112)	2.566(9)			63.1(3)	123.1(2)	100.2(3)	76.6(3)	70.3(3)
O(115)	2.562(7)				61.0(3)	77.2(2)	115.1(3)	131.5(3)
O(118)	2.58(1)					77.8(3)	138.5(3)	153.2(3)
O(122)	2.572(8)						61.9(3)	125.3(3)
O(125)	2.599(8)							63.5(3)
O(128)	2.615(9)							

Table 4. The lanthanum environment of the anion  $[\text{LaBr}_4(\text{diglyme})]^-$  (La(2)) in  $[\text{LaBr}_2(\text{diglyme})_2][\text{LaBr}_4(\text{diglyme})]$

Presentation is as in Table 1. La(2)-O(22)-C(21,23) are 123.5(7), 117.6(6) $^\circ$ ; La(2)-O(25)-C(24,26) are 117.8(6), 118.0(7) $^\circ$ ; La(2)-O(28)-C(27,29) are 118.5(6), 122.0(6) $^\circ$

Atom	r (Å)	Br(22)	Br(23)	Br(24)	O(22)	O(25)	O(28)
Br(21)	2.921(2)	85.39(3)	91.82(5)	94.78(5)	79.6(2)	140.9(2)	157.9(2)
Br(22)	2.913(2)		92.53(5)	101.70(6)	165.0(2)	132.3(1)	74.9(2)
Br(23)	2.929(2)			164.74(5)	88.7(2)	78.6(2)	98.8(2)
Br(24)	2.933(2)				79.0(2)	87.6(2)	79.9(2)
O(22)	2.624(7)					62.5(2)	119.7(2)
O(25)	2.543(7)						60.8(2)
O(28)	2.669(7)						

which has relatively shorter La-O bonds. The structure of  $[\text{YbBr}_3(\text{thf})_3]$  (below) also shows evidence of a *trans* influence for bromide. Evidence of *trans* influences in lanthanoid complexes has been previously reported.<sup>52</sup> As the most crowded La/diglyme complex,<sup>44</sup>  $[\text{La}(\text{hfa})_3(\text{diglyme})]$ ,<sup>51</sup> has the shortest La-O bonds, the electron-withdrawing  $\text{CF}_3$  groups may stabilize La-O ligations.

It is interesting to note that, by variation of the solvent identity from unidentate (thf) to bidentate (dme) and then to tridentate (diglyme), major structural variations occur from monomeric to dimeric to ionic species for the same metal. Ionic structures  $[\text{LnCl}_2(\text{thf})_5][\text{LnCl}_4(\text{thf})_2]$  have previously been established for  $\text{LnCl}_3(\text{thf})_{3.5}$  species where  $\text{Ln} = \text{Gd} \rightarrow \text{Tm}$ .<sup>12,17,23,24</sup>

#### $[\text{YbBr}_3(\text{thf})_3]$

The complex comprises monomeric neutral molecules with six-coordinate ytterbium, which has *mer*-octahedral stereochemistry (Fig. 4). This is similar to the arrangement in  $[\text{YbCl}_3(\text{thf})_3]$ ,<sup>12</sup> but the complexes have different space groups. Here, the molecule is disposed about a crystallographic 2-axis, passing through the metal and the *trans* Br/O ligand atom array, so that one-half of the molecule comprises the asymmetric unit of the structure. The Yb-Br bond length for the mutually *trans* bromide ligands (Table 5) is closely comparable with those (2.719(2) and 2.747(2) Å) found in the *trans*- $[\text{YbBr}_4(\text{thf})_2]^-$  anion.<sup>22</sup> The Yb-Br *trans* to thf is marginally shorter. For the mutually *trans* oxygens, the Yb-O distance is similar to that (2.280(4) Å) of the thf ligands in *trans*- $[\text{YbBr}_4(\text{thf})_2]^-$ ,<sup>22</sup> but Yb-O *trans* to bromide is significantly longer (Table 5),

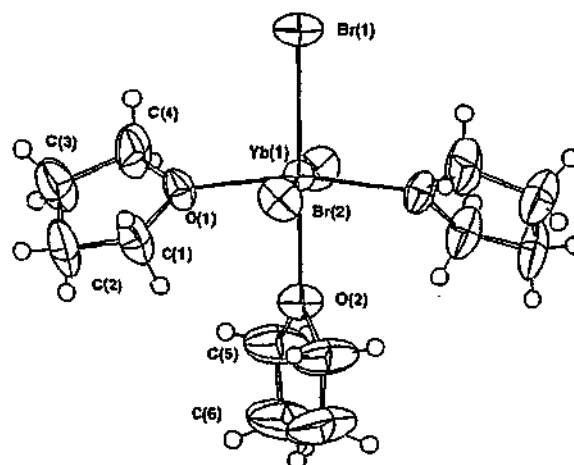


Fig. 4. Molecular structure of the six-coordinate *mer*- $[\text{YbBr}_3(\text{thf})_3]$ .

consistent with a detectable *trans* influence for bromide of the chloride.<sup>12</sup>

#### $[\text{ErCl}_3(\text{dme})_2]$ , $[\text{YbCl}_3(\text{dme})_2]$ and $[\text{YbBr}_3(\text{dme})_2]$

Our structural data for the first complex (Table 6) are consistent with those reported<sup>22</sup> for this compound while our study was in progress. The stereochemistry approximates pentagonal bipyramidal<sup>47</sup> with axial halides (Fig. 5), similar structures having been established for  $[\text{LnCl}_3(\text{dme})_2]$  ( $\text{Ln} = \text{Y}$ ,<sup>29</sup>  $\text{Eu}$ ,<sup>11</sup>  $\text{Gd}$ ,<sup>30</sup>  $\text{Dy}$ <sup>25</sup> or  $\text{Er}$ <sup>22</sup>), all isomorphous with the  $\text{Ln} = \text{Er}$  array. The current bond distances (Table 6) are entirely consistent with those of previous structures,<sup>11,22,25,29,30</sup> with



Table 5. The ytterbium environment in  $[\text{YbBr}_3(\text{thf})_3]$   
Presentation is as in Table 1; primed atoms are related by the transformation  $(x, y, \frac{1}{2}-z)$ .  $\text{Yb}-\text{O}(1)-\text{C}(1,4)$   
are  $123.2(6)$ ,  $125.6(6)^\circ$ ;  $\text{Yb}-\text{O}(2)-\text{C}(5)$   $127.6(5)^\circ$

Atom	$r(\text{\AA})$	Br(2)	O(1)	O(2)	Br(2')	O(1')
Br(1)	2.665(1)	93.39(3)	97.3(2)	180(-)	93.39(3)	97.3(2)
Br(2)	2.708(1)		89.4(2)	86.61(3)	173.22(4)	89.7(2)
C(1)	2.255(6)			82.7(2)	(89.7(2))	165.4(3)
O(2)	2.329(9)				(86.61(3))	(82.7(2))

Table 6. The lanthanoid environment in  $[\text{YbBr}_3(\text{dme})_2]$ ,  $[\text{YbCl}_3(\text{dme})_2]$  and  $[\text{ErCl}_3(\text{dme})_2]$   
Presentation is as in Table 1. Values are listed in order of  $[\text{YbBr}_3(\text{dme})_2]$ ,  $[\text{YbCl}_3(\text{dme})_2]$  and  $[\text{ErCl}_3(\text{dme})_2]$ .  $\text{Ln}-\text{O}(102)-\text{C}(101)$  are  $124.5(8)$ ,  $124.8(3)$ ,  $124.8(5)^\circ$ ;  $\text{Ln}-\text{O}(102)-\text{C}(103)$  are  $118.8(7)$ ,  $118.1(3)$ ,  $118.3(4)^\circ$ ;  $\text{Ln}-\text{O}(105)-\text{C}(104)$  are  $113.0(6)$ ,  $113.9(3)$ ,  $113.5(4)^\circ$ ;  $\text{Ln}-\text{O}(105)-\text{C}(106)$  are  $124.8(8)$ ,  $125.0(3)$ ,  $125.2(5)^\circ$ ;  $\text{Ln}-\text{O}(202)-\text{C}(201)$  are  $126.8(8)$ ,  $123.9(3)$ ,  $123.8(4)^\circ$ ;  $\text{Ln}-\text{O}(202)-\text{C}(203)$  are  $117.6(7)$ ,  $117.7(3)$ ,  $117.3(4)^\circ$ ;  $\text{Ln}-\text{O}(205)-\text{C}(204)$  are  $111.1(7)$ ,  $112.5(3)$ ,  $111.8(4)^\circ$ ;  $\text{Ln}-\text{O}(205)-\text{C}(206)$  are  $124.8(7)$ ,  $123.8(3)$ ,  $124.2(4)^\circ$

Atom	$r(\text{\AA})$	X(2)	X(3)	O(102)	O(105)	O(202)	O(205)
X(1)	2.707(1)	88.95(5)	171.32(4)	79.4(2)	106.2(2)	92.7(2)	85.9(2)
	2.556(1)	90.50(4)	170.10(4)	79.35(9)	106.31(8)	91.20(8)	85.4(1)
	2.585(2)	90.81(7)	169.61(6)	79.3(1)	106.6(1)	90.7(1)	85.3(1)
X(2)	2.729(1)		96.71(4)	140.7(2)	80.5(2)	147.1(2)	79.6(2)
	2.559(1)		97.08(4)	140.83(9)	80.25(8)	146.98(8)	79.76(9)
	2.582(2)		97.17(7)	140.6(1)	80.3(1)	147.0(1)	79.8(1)
X(3)	2.708(1)			100.0(2)	81.3(2)	79.0(2)	88.7(2)
	2.556(1)			98.45(9)	81.35(7)	78.98(8)	89.72(8)
	2.580(2)			98.4(1)	81.4(1)	79.0(1)	89.5(1)
O(102)	2.374(9)				67.3(3)	71.6(3)	135.8(3)
	2.403(3)				67.0(1)	71.6(1)	135.8(1)
	2.427(5)				66.7(2)	71.9(2)	136.1(2)
O(105)	2.403(8)					129.9(3)	156.5(3)
	2.403(3)					130.4(1)	156.9(1)
	2.423(4)					130.4(2)	156.9(2)
O(202)	2.422(7)						67.7(3)
	2.446(3)						67.5(1)
	2.462(4)						67.4(2)
O(205)	2.354(9)						
	2.347(3)						
	2.370(5)						

appropriate allowances for metal and halogen ionic radii. It should be noted that far-infrared data for  $[\text{LaCl}_3(\text{dme})]$  (above) have suggested that this complex has a different structure.

The  $\text{LnC}_2\text{O}_2$  dme five-membered rings of the isomorphous  $[\text{ErCl}_3(\text{dme})_2]$ ,  $[\text{YbCl}_3(\text{dme})_2]$  and  $[\text{YbBr}_3(\text{dme})_2]$  are set in the same common chirality. The rings have very similar conformations (Table 7) so that about the central metals, the metal ambience is chiral. All the complexes crystallize in the same centrosymmetric space group, so that the arrays in the crystal overall are racemic. The congruence in conformation in these  $[\text{LnX}_3(\text{dme})_2]$  complexes does not extend to all the pendant methyl groups. Here again, conformations are similar *except* in ligand 2 of the Er/Yb arrays (and of their isomorphous analogues  $[\text{LnCl}_3(\text{dme})_2]$  where  $\text{Ln} = \text{Y}^{29}$ ,  $\text{Eu}^{11}$ ,  $\text{Gd}^{30}$ ,  $\text{Dy}^{25}$  and  $\text{Er}^{22}$ ) where the putative 2-symmetry of the overall array is broken by the disposition of one of the methyl groups. The diglyme arrays, albeit restricted to one complex, nevertheless offer analogous examples within the one compound (Table 8). Within the anion, the single ligand is clearly close to *m* symmetry, and this also applies to the symmetry of the anion

overall (Fig. 3*b,c*). In the cation, ligand 2 is also close to *m* symmetry, but with a departure by one of the methyl groups, while in ligand 1, the symmetry is more akin to that of a twofold axis within the ligand, but again broken by terminal methyl group inconsistency. The conformations of the chelate rings of the ligands are given in overview in Tables 7 and 8.



This complex comprises seven-coordinate cations  $[\text{YbCl}_2(\text{MeCN})_5]^+$  (Fig. 6*a*) accompanied by a six-coordinate binuclear anion  $[\text{YbCl}_3(\mu\text{-Cl})(\text{MeCN})]_2^{2-}$  (Fig. 6*b, c*; geometric data: Tables 9 and 10). One-half of the full formula unit comprises the asymmetric unit of the structure, i.e. a complete cation, devoid of crystallographic symmetry, and half an anion, which is disposed about a crystallographic centre of symmetry. The stereochemistry of the cation is pentagonal-bipyramidal with apical chlorides, while the anion is distorted octahedral with two chlorides *trans* to the bridging chlorides, and the acetonitrile *cis* to the bridge. A dysprosium analogue of the anion has previously been observed in  $[\text{Dy}_2\text{Cl}_4(\text{dibenzo-18-crown-}$

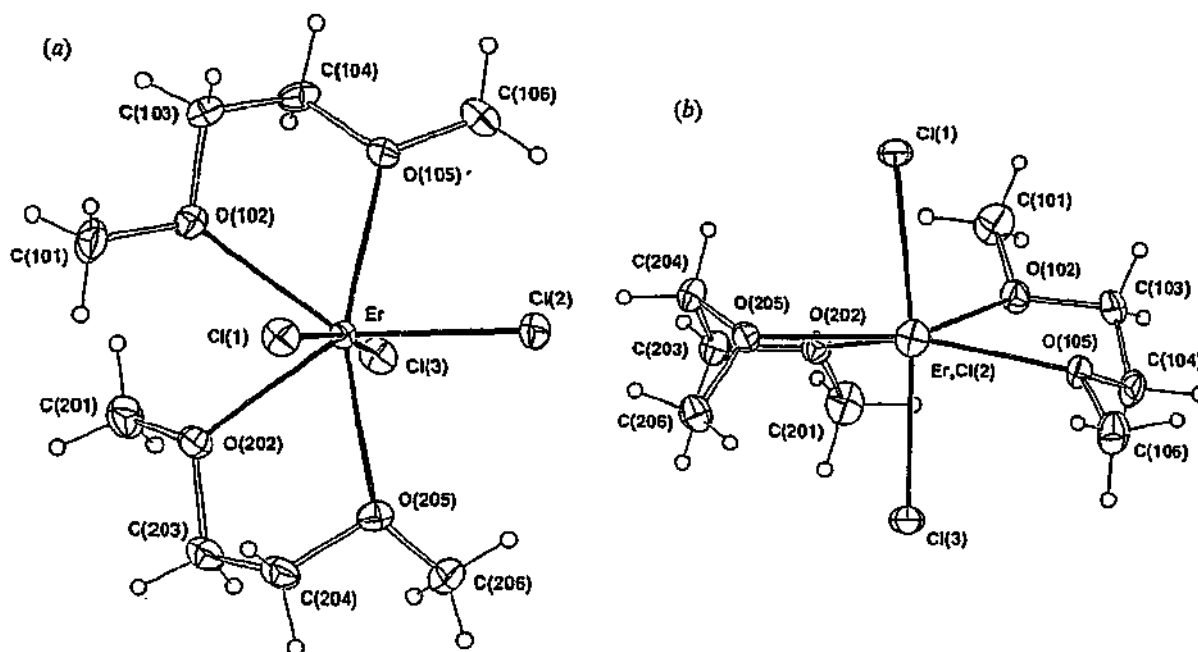


Fig. 5. (a), (b) Two views of the seven-coordinate  $[\text{ErCl}_3(\text{dme})_2]$ .  $[\text{YbCl}_3(\text{dme})_2]$  and  $[\text{YbBr}_3(\text{dme})_2]$  are isostructural.

Table 7. Cyclic ligand torsion angles (degrees) of *dme* ligands of  $[\text{LaBr}_3(\text{dme})_2]$ ,  $[\text{YbBr}_3(\text{dme})_2]$ ,  $[\text{YbCl}_3(\text{dme})_2]$  and  $[\text{ErCl}_3(\text{dme})_2]$

M/X/L	La/Br/1, 2	(Yb/Br), (Yb/Cl), (Er/Cl)/1	(Yb/Br), (Yb/Cl)(Er/Cl)2
C(1)-O(2)-C(3)-C(4)	-172(1), -176(1)	-172(1), -173.6(4), -173.9(7)	179(1), 176.2(4), 177.0(6)
Ln-O(2)-C(3)-C(4)	39(1), 44(1)	33(1), 34.0(5), 32.2(8)	29(1), 26.5(5), 28.1(7)
O(2)-C(3)-C(4)-O(5)	-60(1), -57(1)	-55, -54.1(5), -53.6(8)	-55(1), -52.1(5), -54.2(8)
C(3)-C(4)-O(5)-C(6)	-163(1), -168(1)	-162(1), -163.0(4), -162.7(6)	-89(1), -88.8(5), -87.8(8)
C(3)-C(4)-O(5)-Ln	53(1), 46(1)	53(1), 51.4(4), 51.2(7)	58(1), 56.0(4), 57.2(7)

$6)_2][\text{Dy}_2\text{Cl}_8(\text{MeCN})_2]$ .<sup>53</sup> In the present anion, the Yb-Cl distances (both shorter terminal and longer bridging) are shorter than the corresponding Dy-Cl distances by amounts in conformity with the differing ionic radii of  $\text{Dy}^{3+}$  and  $\text{Yb}^{3+}$ .<sup>45</sup> The same is true of the two Ln-N distances in the respective complex anions. The Yb-Cl and Yb-N distances of the seven-coordinate cation are surprisingly similar to Yb-Cl<sub>ter</sub> and Yb-N of the octahedral anion, although the ionic radii differ by 0.06 Å.<sup>45</sup> Moreover, the Yb-N distances are approximately the same as those<sup>40</sup> of eight-coordinate  $[\text{Yb}(\text{MeCN})_8]^{3+}$ . The sums of the steric coordination numbers<sup>44</sup> for the cation (6.0 Å) and the anion (5.8 Å) are essentially the same and close to that (6.4 Å) of  $[\text{Yb}(\text{MeCN})_8]^{3+}$ , and this may account for the similar bond distances.

#### Overview

For convenience, the structural assignments made in this work are summarized in Table 11. For three classes of compounds,  $[\text{LnCl}_3(\text{dme})_2]$ ,  $[\text{LnBr}_3(\text{dme})_2]$  and  $[\text{LnBr}_3(\text{thf})_2]$ , structural information is available for the largest lanthanoid

ion ( $\text{La}^{3+}$ ) and the second smallest ( $\text{Yb}^{3+}$ ). In all cases there is a decrease in coordination number with the decrease in ionic size. Thus, the far-infrared spectrum of  $[\text{LaCl}_3(\text{dme})_2]$  is consistent with an eight-coordinate structure (above), whereas  $[\text{YbCl}_3(\text{dme})_2]$  has seven-coordinate  $\text{Yb}^{3+}$ . With  $[\text{LnBr}_3(\text{thf})_2]$  complexes there is a gradation from seven-coordinate ( $\text{Ln} = \text{La}$ ,  $n = 4$ ) to six-coordinate ( $\text{Ln} = \text{Yb}$ ,  $n = 3$ ) in a mononuclear array, while for  $[\text{LnBr}_3(\text{dme})_2]$ , there is a change from eight-coordinate in the dimeric  $[\text{LaBr}_2(\mu\text{-Br})(\text{dme})_2]_2$  to seven-coordinate in monomeric  $[\text{YbBr}_3(\text{dme})_2]$  (Table 6). The lower coordination numbers found in the thf derivatives than in the corresponding *dme* complexes reflect the greater size of two thf ligands than one bidentate *dme*.<sup>44</sup> More structural data are needed to establish the transition point in each series. For the  $[\text{LnCl}_3(\text{dme})_2]$  series, seven-coordinate monomers are now known from Eu to Yb, leaving a need to explore further the lighter lanthanoids to find the point of transition to eight-coordinate. Indeed, there is a need to establish the higher coordination number crystallographically, but suitable crystals have not yet been grown. In the  $[\text{LnCl}_3(\text{thf})_2]$  series, the transition

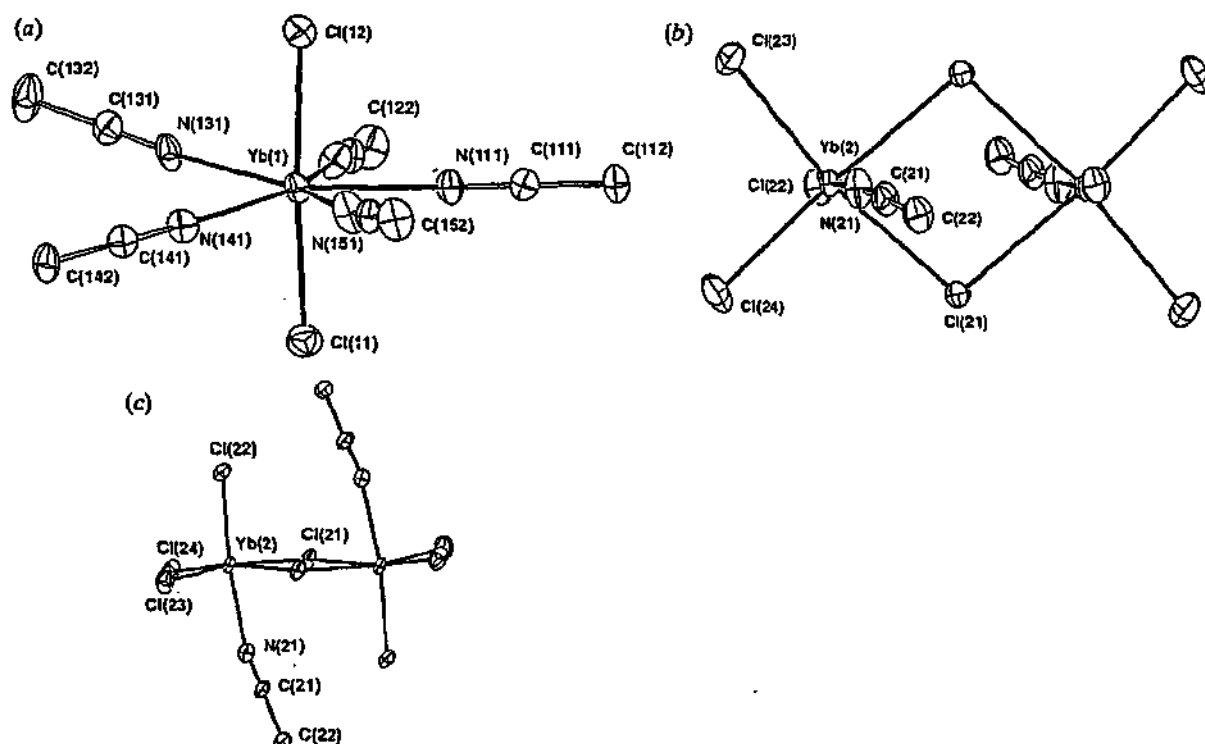


Fig. 6. Molecular structure of  $[\text{YbCl}_2(\text{MeCN})_5]_2[\text{Yb}(\text{MeCN})\text{Cl}_3(\mu\text{-Cl})_2\text{YbCl}_3(\text{NCMe})]$ . (a) The seven-coordinate cation. (b) and (c) Two views of the binuclear anion; normal to and through the  $\text{Yb}(\mu\text{-Cl})_2\text{Yb}$  core, respectively

Table 8. Cyclic ligand torsion angles (degrees) of diglyme ligands of  $[\text{LaBr}_2(\text{diglyme})_2][\text{LaBr}_4(\text{diglyme})]$

Ligand	Cation	Anion
C(1)-O(2)-C(3)-C(4)	84(2),	-177(1), -176(1)
La-O(2)-C(3)-C(4)	-61(1),	-22(2), 37(1)
O(2)-C(3)-C(4)-O(5)	49(2),	43(2), -56(2)
C(3)-C(4)-O(5)-La	-14(1),	-46(2), 52(1)
C(3)-C(4)-O(5)-C(6)	176(1),	172(2), -162(1)
C(4)-O(5)-C(6)-C(7)	166(1),	-179(1), 156(1)
La-O(5)-C(6)-C(7)	-4(2),	40(2), -58(1)
O(5)-C(6)-C(7)-O(8)	24(2),	-54(2), 52(1)
C(6)-C(7)-C(8)-C(9)	172(1),	-115(1), -175(1)
C(6)-C(7)-C(8)-La	-35(2)	44(1), -28(1)

from eight- to seven-coordination has been defined as La to Ce for single crystals, but far-infrared data have suggested bulk  $[\text{CeCl}_3(\text{thf})_2]$  is also eight-coordinate.<sup>12</sup> For the  $\text{LnBr}_3$  complexes with thf and dme, no structural data yet exist for complexes of metals lying between La and Yb. The possibility of ionic intermediate structures cannot be discounted in view of the numerous  $[\text{LnCl}_2(\text{thf})_5][\text{LnCl}_4(\text{thf})_2]$  ( $\text{Ln} = \text{Gd-Tm}$ )<sup>12,17,21,23-25</sup> and  $[\text{SmI}_2(\text{thf})_5][\text{SmI}_4(\text{thf})_2]$  ionic arrays.<sup>31</sup> In the  $[\text{LnCl}_3(\text{thf})_n]$  series, the maximally solvated Yb and Lu complexes ( $n = 3$ ) are mononuclear and isostructural, and the same is likely for their  $[\text{LuBr}_3(\text{thf})_n]$  counterpart since there is unlikely to be a reduction in coordination number from six (low coordinate for  $\text{Ln}^{3+}$ ) in  $[\text{YbBr}_3(\text{thf})_3]$ .

However, given that structural and/or coordination number discontinuities have been defined between Yb and Lu (e.g. for  $[\text{Ln}(\text{H}_2\text{O})_n(\text{NO}_3)_3]$ <sup>54</sup> or  $\text{LnCp}_3$ <sup>55</sup>), it may be premature to assume  $[\text{LuX}_3(\text{dme})_2]$  ( $\text{X} = \text{Br}, \text{Cl}$ ) complexes to be seven-coordinate. With diglyme, the ionic  $[\text{La}(\text{diglyme})_2\text{Br}_2]^+[\text{La}(\text{diglyme})\text{Br}_4]^-$  arrangement of overall composition  $\text{LaBr}_3(\text{diglyme})_{1.5}$  with an eight-coordinate cation and a seven-coordinate anion represents a compromise between a crowded nine-coordinate  $[\text{LaBr}_3(\text{diglyme})_2]$  and coordination-unsaturated six-coordinate  $[\text{LaBr}_3(\text{diglyme})]$ .

The correlation of decreasing coordination number with decreasing ion size observed for  $[\text{LnCl}_3(\text{dme})_n]$ ,  $[\text{LnBr}_3(\text{dme})_2]$  and  $[\text{LnBr}_3(\text{thf})_n]$  complexes (Table 11) is archetypically observed in the 'maximally hydrated' lanthanoid trihalides, where  $\text{H}_2\text{O}$  can be viewed as an ether prototype. The chlorides are obtained as two types of array. For the lighter rare earths, a triclinic  $P\bar{1}$  binuclear nine-coordinate heptahydrate cation,  $[(\text{H}_2\text{O})_7\text{Ln}(\mu\text{-Cl})_2\text{Ln}(\text{OH}_2)_7]^{4+}$ , incorporating bridging halides is found, while, for the heavier elements of the series, an ionic monoclinic  $P2_1/n$  eight-coordinate mononuclear hexahydrate  $[\text{LnCl}_2(\text{H}_2\text{O})_6]^{2+}\text{Cl}^-$  obtains, the former occurring for  $\text{Ln} = \text{La-Pr}$ , the latter for  $\text{Ln} = \text{Nd-Lu}$  and Y.<sup>56</sup> More recently, a similar study of the bromides shows the persistence of these same phases, the transition point between the two structural types displaced somewhat towards the lighter end, the triclinic  $P\bar{1}$  heptahydrate being found for La and Ce, and the monoclinic  $P2_1/m$  hexahydrate beyond.<sup>57</sup> Unlike the chlorides, the latter array does not per-

Table 9. The ytterbium environments of the seven-coordinate cation  $[\text{YbCl}_2(\text{MeCN})_5]^+$  ( $\text{Yb}(1)$ ) in  $[\text{YbCl}_3(\text{MeCN})_3]$   
Presentation is as in Table 1

Atom	$r$ (Å)	Cl(12)	N(111)	N(121)	N(131)	N(141)	N(151)
Cl(11)	2.527(4)	175.0(1)	87.2(3)	83.9(3)	97.0(3)	87.4(3)	95.1(3)
Cl(12)	2.505(4)		89.0(3)	91.9(3)	84.3(3)	97.6(3)	86.8(3)
N(111)	2.419(9)			73.6(3)	145.5(3)	142.2(3)	72.5(3)
N(121)	2.41(1)				72.9(3)	142.7(3)	146.1(3)
N(131)	2.42(1)					72.3(3)	140.3(4)
N(141)	2.391(9)						70.7(3)
N(151)	2.42(1)						

Table 10. The ytterbium environments of the six-coordinate dinuclear anion  $[\text{YbCl}_3(\mu\text{-Cl})(\text{MeCN})_2]^{2-}$   
( $\text{Yb}(2)$ ) in  $[\text{YbCl}_3(\text{MeCN})_3]$   
Presentation is as in Table 1. Symmetry operation  $(1-x, y, 1-z)$ :  $\text{Yb}(2)\text{-Cl}(21)\text{-Yb}(2')$  is 99.6(1) $^\circ$ ;  
 $\text{Yb}(2)\text{-Yb}(2')$  4.084(2);  $\text{Cl}(21)\text{-Cl}(21')$  3.453(4) Å

Atom	$r$ (Å)	Cl(22)	Cl(23)	Cl(24)	N(21)	Cl(21')
Cl(21)	2.663(3)	92.2(1)	167.4(1)	94.1(1)	80.9(3)	80.4(1)
Cl(22)	2.516(4)		96.1(1)	94.8(1)	172.8(3)	93.7(1)
Cl(23)	2.503(4)			94.7(1)	90.4(3)	89.6(1)
Cl(24)	2.516(3)				88.0(3)	170.1(1)
N(21)	2.42(1)					83.0(2)
Cl(21')	2.685(3)					

Table 11. Structures of some  $\text{LnX}_3(\text{L})_n$  complexes ( $X = \text{Cl}, \text{Br}$ ;  $L = \text{thf}, \text{dme}, \text{diglyme}, \text{MeCN}$ ) determined in the present study  
Determined by X-ray crystallography unless indicated otherwise. For structures of  $[\text{LnCl}_3(\text{thf})_n]$  complexes, see refs<sup>12,13</sup>

Coordination number	Structural type
8	$[\text{LaCl}_3(\text{dme})]_n^A, \text{LaBr}_2(\mu\text{-Br})(\text{dme})_2$
8/7	$[\text{LaBr}_2(\text{diglyme})_2][\text{LaBr}_4(\text{diglyme})]$
7	$[\text{LaBr}_3(\text{thf})_4], [\text{LnCl}_3(\text{dme})_2]$ ( $\text{Ln} = \text{Er},^B \text{Yb}^C$ ), $[\text{YbBr}_3(\text{dme})_2]$
7/6	$[\text{YbCl}_2(\text{MeCN})_5]_2[\text{Yb}_2\text{Cl}_6(\mu\text{-Cl})_2(\text{MeCN})_2]$
6	$[\text{YbBr}_3(\text{thf})_3]$

<sup>A</sup> From far-infrared spectroscopy.

<sup>B</sup> Also ref.<sup>22</sup>

<sup>C</sup> Similar structures reported for  $\text{Ln} = \text{Y},^{29} \text{Eu},^{11} \text{Gd},^{30} \text{Dy}.$ <sup>25</sup>

sist to the exhaustion of the series, a monoclinic  $P2_1/n$  mononuclear octahydrate form,  $[\text{Ln}(\text{OH}_2)_8]\text{Br}_3$ , being found for  $\text{Ln} = \text{Ho}$  and beyond, inclusive of  $\text{Y}$ , with the halide excluded from the coordination sphere for the first time,<sup>57</sup> the 'softer' anions becoming less competitive as ligands with the smaller metal ions, a trend which becomes dominant in the iodides.

In the 'maximally hydrated' iodides, complete iodide displacement is now observed throughout and there are two structural types.<sup>58</sup> For the lighter lanthanides,  $\text{La-Ho}$ , an orthorhombic  $Pm\bar{m}n$  nona-aqua complex is found,  $[\text{Ln}(\text{OH}_2)_9]\text{I}_3$ , and for the heavier, a monoclinic  $P2_1/n$  decahydrate but an octa-aqua complex,  $[\text{Ln}(\text{OH}_2)_8]\text{I}_3 \cdot 2\text{H}_2\text{O}$ . The position of ' $\text{Ln}$ ' =  $\text{Y}$  at this point is somewhat ambiguous. With such small differences in ionic radius between adjacent lanthanoids, it may be possible to influence transition points between phases by minor variations in the conditions of synthesis. Complete displacement of halides by ether ligands has not been observed in the present

complexes (above) or  $[\text{LnCl}_3(\text{thf})_n]$  species,<sup>12</sup> by contrast with the stronger hydrate donors. Some transitional ambiguity has been observed in the  $[\text{LnCl}_3(\text{thf})_n]$  series. Thus the seven-coordinate  $[\text{LnCl}(\mu\text{-Cl})_2(\text{thf})_2]_n$  structure is typical of the lighter rare earths,  $\text{Ce}, \text{Pr}$  and  $\text{Nd}$ , but has surprisingly also been observed for  $\text{Y},^{23b,29}$  which also has the ionic species  $[\text{YCl}_2(\text{thf})_5][\text{YCl}_4(\text{thf})_2]$  typically found for  $\text{Gd-Tm}.$ <sup>12,17,21-25</sup> With  $\text{Nd}$  both the seven-coordinate polymer and the seven-coordinate monomer  $[\text{NdCl}_3(\text{thf})_4]^{19}$  have been defined. Moreover, the  $[\text{CeCl}_3(\text{thf})_2]$  composition is observed with both eight-coordinate and seven-coordinate polymeric forms  $[\text{Ce}(\mu\text{-Cl})_3(\text{thf})_2]_n^{12}$  and  $[\text{CeCl}(\mu\text{-Cl})_2(\text{thf})_2]_n.$ <sup>17</sup>

#### Experimental

Hexachloroethane was sublimed before use, and dibromomethane and diiodomethane were used as received from Aldrich Chemical Company. Lanthanum and erbium metal powders were purchased from Rhone-

Poulenc, Phoenix, Arizona. 1,2-Dimethoxyethane, diglyme, pentane and thf were freshly distilled from sodium/benzophenone, and acetonitrile was distilled from  $\text{CaH}_2$  prior to use. The lanthanoid halide complexes are moisture-sensitive and all preparations were conducted under an inert atmosphere (purified  $\text{N}_2$  or Ar) involving conventional glovebox and Schlenk techniques. Infrared (Nujol mulls) and far-infrared (petroleum jelly mulls) spectra were obtained and halogen and lanthanoid analyses were effected as described previously.<sup>12</sup>

*Preparation of  $\text{LnX}_3(\text{L})_x$  Complexes ( $X = \text{Br}$  or  $\text{I}$ ;  $L = \text{thf}$ ,  $\text{dme}$  or  $\text{diglyme}$ )*

$[\text{LaBr}_3(\text{thf})_4]$ .—A mixture of La powder (0.50 g, 3.6 mmol) and dibromomethane (2.0 ml, 29 mmol) in thf (40 ml) was subjected to ultrasonic irradiation for 5 h, whereupon a white powder precipitated. The solvent was decanted and the solid washed with thf ( $3 \times 5$  ml), then dried *in vacuo*, yielding  $[\text{LaBr}_3(\text{thf})_4]$  (yield 1.60 g, 67%). Single crystals were obtained by recrystallization from thf (Found: Br, 46.0; La, 26.1.  $\text{C}_{16}\text{H}_{32}\text{Br}_3\text{LaO}_4$  requires Br, 45.9; La, 26.6%). I.r. absorption: 1346m, 1295w, 1248w, 1174w, 1019s, 954w, 915m, 859s, 669m  $\text{cm}^{-1}$ . Far-i.r. absorption: 578w, 551w, 432w, 385w, 295sh, 178s, 125w  $\text{cm}^{-1}$ .

$[\text{YbBr}_3(\text{thf})_3]$ .—From a similar preparation to that of  $[\text{LaBr}_3(\text{thf})_4]$ ,  $[\text{YbBr}_3(\text{thf})_3]$  was obtained (yield 77%) (Found: Yb, 28.1.  $\text{C}_{12}\text{H}_{24}\text{Br}_3\text{YbO}_4$  requires Yb, 27.5%). I.r. absorption: 1305w, 1260w, 1181w, 1040s, 1003s, 912w, 842s, 722s  $\text{cm}^{-1}$ .

$[\text{YbBr}_3(\text{dme})_2]$ .—Recrystallization of  $[\text{YbBr}_3(\text{thf})_3]$  (0.62 g, 1.0 mol) from dme (35 ml) yielded a white precipitate of the title complex (yield 0.45 g, 76%) (Found: Br, 38.8; Yb, 30.0.  $\text{C}_8\text{H}_{20}\text{Br}_3\text{YbO}_4$  requires Br, 40.4; Yb, 29.2%). I.r. absorption: 1458m, 1367m, 1184w, 1116w, 1077s, 1027s, 975w, 859s  $\text{cm}^{-1}$ . Far-i.r. absorption: 581w, 562w, 542w, 463w, 399m, 324w, 274w, 172s, 150m, 106m, 73w, 54w  $\text{cm}^{-1}$ .

$[\text{LaI}_3(\text{thf})_4]$ .—Diiodomethane (3.0 ml, 37.2 mmol) was added to a slurry of La powder (0.50 g, 3.6 mmol) in thf (40 ml), whereupon an exothermic reaction took place. After stirring for 1 h, the resulting white precipitate was collected and washed with thf ( $3 \times 5$  ml), then dried *in vacuo* (yield 2.50 g, 87%) (Found: I, 52.2; La, 18.9.  $\text{C}_{16}\text{H}_{32}\text{I}_3\text{LaO}_4$  requires I, 51.7; La, 18.9%). I.r. absorption: 1346m, 1293w, 1246w, 1172w, 1012s, 922m, 855s, 835sh, 668m  $\text{cm}^{-1}$ . Far-i.r. absorption: 574w, 553w, 484w, 433w, 388w, 307w, 229sh, 196sh, 156s  $\text{cm}^{-1}$ . Single crystals (from thf) had unit cell data (295 K; monoclinic, space group  $P2_1/c$ ,  $a$  8.783(6),  $b$  17.660(5),  $c$  16.741(7) Å,  $\beta$  93.75(5)°,  $V$  2591 Å<sup>3</sup>), harmonious with those of ref.<sup>15</sup>

$[\text{La}(\text{dme})_2\text{Br}_2(\mu\text{-Br})_2\text{LaBr}_2(\text{dme})_2]$ .—Recrystallization of  $[\text{LaBr}_3(\text{thf})_4]$  from dme yielded colourless crystals of the title complex. I.r. absorption: 1406w, 1289m, 1282m, 1241m, 1188s, 1158w, 1115s, 1094s, 1044s, 1024s, 1005w, 858s, 836s  $\text{cm}^{-1}$ . Far-i.r. absorption: 574m, 384s, 311s, 284s, 194w, 175m, 150w, 138m, 114s  $\text{cm}^{-1}$ .

$[\text{LaBr}_2(\text{diglyme})_2][\text{LaBr}_4(\text{diglyme})]$ .—Recrystallization of  $[\text{LaBr}_3(\text{thf})_4]$  from diglyme yielded colourless crystals of the title complex. I.r. absorption: 1352w, 1342w, 1283w, 1244m, 1199m, 1107s, 1096s, 1050w, 1023s, 1005sh, 991m, 962m, 938m, 870s, 857s, 828m, 818m  $\text{cm}^{-1}$ . Far-i.r. absorption: 558m, 447m, 394m, 347s, 309w, 295w, 268w, 177w, 135w, 112w  $\text{cm}^{-1}$ .

*Preparation of  $\text{LnCl}_3(\text{dme})_x$  Complexes*

In typical syntheses, lanthanoid metal powder or lump (0.50 g, 2.86–3.60 mmol or 1.0 g) and hexachloroethane (1.5 g, 6.34 mmol) in 1,2-dimethoxyethane (40 ml) were sonicated under  $\text{N}_2$  or Ar until all traces of metal disappeared and a milk-like suspension remained. Pentane (20 ml) was added to the reaction mixture, separating insoluble  $[\text{LnCl}_3(\text{dme})_x]$ . The supernatant liquid was decanted, and the residue was washed with pentane, and dried at room temperature under vacuum.

$[\text{LaCl}_3(\text{dme})_2]$ .—Sonication time 20 h; yield 1.23 g (81%) (Found: La, 41.9.  $\text{C}_8\text{H}_{16}\text{Cl}_3\text{LaO}_4$  requires La, 41.4%). I.r. absorption: 1343m, 1297w, 1244w, 1178w, 1020s, 956w, 925m, 865s, 835s, 722w, 667w  $\text{cm}^{-1}$ . Far-i.r. absorption: 589w, 545m, 491w, 387s, 320s, 215s, 182s, 145w, 115s  $\text{cm}^{-1}$ .

$[\text{NdCl}_3(\text{dme})_2]$ .—Sonication time 38 h; yield 1.11 g (74%) (Found: Cl, 24.8; Nd, 33.2.  $\text{C}_8\text{H}_{16}\text{Cl}_3\text{NdO}_4$  requires Cl, 24.7; Nd, 33.5%). I.r.

absorption: 1289w, 1251w, 1191w, 1119m, 1094m, 1040s, 986m, 858s, 722w, 550w  $\text{cm}^{-1}$ .

$[\text{ErCl}_3(\text{dme})_2]$ .—Sonication time 24 h; yield 1.06 g (78%). The product was obtained as high-quality crystals which were characterized by X-ray crystallography.

$[\text{YbCl}_3(\text{dme})_2]$ .—Sonication time 54 h; yield 1.12 g (84%) (Found: Cl, 23.1; Yb, 37.8.  $\text{C}_8\text{H}_{16}\text{Cl}_3\text{YbO}_4$  requires Cl, 23.1; Yb, 37.7%). I.r. absorption: 1352m, 1284w, 1240m, 1167w, 1154w, 1116m, 1032br s, 978m, 860s, 834s, 722w, 566w  $\text{cm}^{-1}$ .

$[\text{YbCl}_3(\text{MeCN})_2][\text{YbCl}_3(\text{MeCN})(\mu\text{-Cl})_2\text{YbCl}_3(\text{MeCN})]$ .—Ytterbium metal (0.20 g, 1.1 mmol), hexachloroethane (0.60 g, 2.5 mmol) and acetonitrile (30 ml) were sonicated under an inert atmosphere until all metal had been consumed (c. 12 h). The volume was then reduced *in vacuo* until traces of material began to precipitate. The solution was heated to dissolve the precipitate and then allowed to stand at room temperature, whereupon colourless crystals of the title compound deposited. These were collected and washed with cold acetonitrile (yield 0.32 g, 73%) (Found: C, 17.3; H, 2.1; N, 10.8.  $\text{C}_{24}\text{H}_{36}\text{Cl}_{12}\text{N}_{12}\text{Yb}_4$  requires C, 17.9; H, 2.3; N, 10.4%). I.r. absorption (AgCl plates): 2307s, 2279s, 1155w, 1034s, 938s, 785w  $\text{cm}^{-1}$ .

$[\text{YbBr}_3(\text{thf})_3]$  and  $[\text{YbBr}_3(\text{dme})_2]$ .—These compounds were grown as single crystals by treatment of Yb pieces with 1,2-dibromoethane in the appropriate ether. The single crystals grew from the surface of the metal chunks.

*Structure Determinations*

Unique room-temperature single-counter diffractometer data sets were measured (2 $\theta$ / $\theta$  scan mode, monochromatic Mo K $\alpha$  radiation,  $\lambda = 0.71073$  Å;  $T \sim 298$  K) on capillary-mounted specimens, yielding  $N$  independent reflections,  $N_o$  of these with  $I > 3\sigma(I)$  being considered 'observed' and used in the full-matrix least-squares refinements after analytical absorption correction. Anisotropic thermal parameters were refined for the non-hydrogen atoms, ( $x, y, z, U_{11}, U_{22}, U_{33}, U_{12}, U_{13}, U_{23}$ ) being constrained at estimated values. Conventional residuals on  $|F|$ ,  $R$ ,  $R_w$  (statistical weights) are quoted at convergence. Neutral atom complex scattering factors were employed, computation using the XTAL 3.4 system implemented by S. R. Hall.<sup>59</sup> Pertinent results are given in Figs 1–6 (20% thermal ellipsoids for the non-hydrogen atoms, 0.1 Å arbitrary radii for H) and Tables 1–11; material deposited comprises atomic coordinates and thermal parameters, full non-hydrogen geometries and structure factor amplitudes. Copies are available until 31 December 2005 on application to the Australian Journal of Chemistry, CSIRO Publishing, P.O. Box 1139, Collingwood, Vic., 3066.

*Crystal/Refinement Data*

$[\text{LaBr}_3(\text{thf})_4]$  =  $\text{C}_{16}\text{H}_{32}\text{Br}_3\text{LaO}_4$ ,  $M_r$  667.1. Triclinic, space group  $P\bar{1}$  ( $C_1$ , No. 2),  $a$  15.987(9),  $b$  9.458(5),  $c$  8.335(3) Å,  $\alpha$  74.99(4),  $\beta$  87.82(4),  $\gamma$  79.76(5)°,  $V$  1198 Å<sup>3</sup>.  $D_c$  ( $Z = 2$ ) 1.849 g  $\text{cm}^{-3}$ ;  $F(000)$  644.  $\mu_{\text{Mo}}$  68  $\text{cm}^{-1}$ ; specimen: 0.12  $\times$  0.10  $\times$  0.38 mm;  $T_{\text{min,max}}$  0.25, 0.54.  $2\theta_{\text{max}}$  50°;  $N$  4161,  $N_o$  1453;  $R$  0.069,  $R_w$  0.062.  $\nu_u$  169,  $|\Delta\rho_{\text{max}}|$  0.98 e Å<sup>-3</sup>.

*Variata*. C(33–35) of thf(3), with associated hydrogen atoms, were modelled as disordered over two sets of sites, occupancies set at 0.5 after trial refinement (isotropic thermal parameter forms).

$[\text{YbBr}_3(\text{thf})_3]$  =  $\text{C}_{12}\text{H}_{24}\text{Br}_3\text{YbO}_4$ ,  $M_r$  629.1. Orthorhombic, space group  $Pbcn$  ( $D_{2h}^8$ , No. 60),  $a$  9.125(1),  $b$  14.249(1),  $c$  14.270(1) Å,  $V$  1855 Å<sup>3</sup>.  $D_c$  ( $Z = 4$ ) 2.25 g  $\text{cm}^{-3}$ ;  $F(000)$  1180.  $\mu_{\text{Mo}}$  115  $\text{cm}^{-1}$ ; specimen: 0.36  $\times$  0.44  $\times$  0.46 mm;  $T_{\text{min,max}}$  0.28, 0.73.  $2\theta_{\text{max}}$  50°;  $N$  3149,  $N_o$  1634;  $R$ ,  $R_w$  0.032, 0.11 (all data).  $\nu_u$  89,  $|\Delta\rho_{\text{max}}|$  1.08 e Å<sup>-3</sup>.

*Variata*. For this complex and  $\text{YbX}_3 \cdot \text{dme}$  (1:2) below, full spheres of CCD area detector data were measured (JCNQ), multiscan absorption corrections being applied.

$[\text{La}(\text{dme})_2\text{Br}_2(\mu\text{-Br})_2\text{LaBr}_2(\text{dme})_2]$  =  $\text{C}_{16}\text{H}_{40}\text{Br}_6\text{La}_2\text{O}_8$ ,  $M_r$  1117.8. Monoclinic, space group  $P2_1/n$  ( $C_2^2$ , No. 14 (variant)),  $a$  11.369(7),  $b$  13.128(5),  $c$  11.383(4) Å,  $\beta$  101.20(4)°,  $V$  1666 Å<sup>3</sup>.  $D_c$  ( $Z = 2$  dimers) 2.227 g  $\text{cm}^{-3}$ ;  $F(000)$  1048.  $\mu_{\text{Mo}}$  98  $\text{cm}^{-1}$ ; specimen: 0.20  $\times$  0.32  $\times$  0.19 mm;  $T_{\text{min,max}}$  0.23, 0.38.  $2\theta_{\text{max}}$  55°;  $N$  3208,  $N_o$  2270;  $R$  0.043,  $R_w$  0.045;  $\nu_u$  147,  $|\Delta\rho_{\text{max}}|$  1.8 e Å<sup>-3</sup>.

*Variata.* 'Crystal decomposition' of c. 15% was compensated by appropriate scaling of the data.

$[LaBr_2(diglyme)_2][LaBr_3(diglyme)] = C_{12}H_{42}Br_5La_2O_9, M_r 1159.8$ . Triclinic, space group  $PT$ ,  $a$  16.143(3),  $b$  14.950(2),  $c$  8.134(5) Å,  $\alpha$  83.89(3),  $\beta$  83.60(3),  $\gamma$  64.16(1)°,  $V$  1752 Å<sup>3</sup>.  $D_c$  ( $Z = 2$  f.u.) 19.8 g cm<sup>-3</sup>;  $F(000)$  1092,  $\mu_{Mo}$  93 cm<sup>-1</sup>; specimen: 0.28 × 0.20 × 0.32 mm;  $T_{min,max}$  0.088, 0.21, 2θ<sub>max</sub> 50°;  $N$  5295,  $N_0$  3897;  $R$  0.044,  $R_w$  0.049;  $\nu_0$  318,  $|\Delta\rho_{max}|$  1.18 e Å<sup>-3</sup>.

$[LuX_3(dme)_2]$ ,  $Ln, X = Yb, Br, Er, Cl; Yb, Cl = C_8H_{20}X_3LnO_4$ . Monoclinic, space group  $P2_1/c$ ,  $Z = 4$ . (a)  $Ln = Yb, X = Br, M_r 593.0$ .  $a$  11.698(2),  $b$  8.947(2),  $c$  15.905(3) Å,  $\beta$  105.06(3)°,  $V$  1607 Å<sup>3</sup>.  $D_c$  2.45 g cm<sup>-3</sup>;  $F(000)$  1100,  $\mu_{Mo}$  133 cm<sup>-1</sup>; specimen: 0.3 × 0.2 × 0.4 mm;  $T_{min,max}$  0.17, 0.21, 2θ<sub>max</sub> 50°;  $N$  7128,  $N_0$  2313;  $R, R_w$  0.067, 0.072 (all data),  $\nu_0$  147,  $|\Delta\rho_{max}|$  2.53 e Å<sup>-3</sup>. (b)  $Ln = Er, X = Cl, M_r 453.9$ .  $a$  11.432(4),  $b$  8.931(2),  $c$  15.644(9) Å,  $\beta$  104.99(4)°,  $V$  1543 Å<sup>3</sup>.  $D_c$  1.954 g cm<sup>-3</sup>;  $F(000)$  876,  $\mu_{Mo}$  60 cm<sup>-1</sup>; specimen: 0.16 × 0.18 × 0.28 mm;  $T_{min,max}$  0.37, 0.48, 2θ<sub>max</sub> 55°;  $N$  3532,  $N_0$  2549;  $R$  0.034,  $R_w$  0.035.  $\nu_0$  146,  $|\Delta\rho_{max}|$  0.95 e Å<sup>-3</sup>. (c)  $Ln = Yb, X = Cl, M_r 459.6$ .  $a$  11.380(1),  $b$  8.993(1),  $c$  15.594(2) Å,  $\beta$  104.887(2)°,  $V$  1525 Å<sup>3</sup>.  $D_c$  2.002 g cm<sup>-3</sup>;  $F(000)$  884,  $\mu_{Mo}$  66 cm<sup>-1</sup>; specimen: 0.36 × 0.35 × 0.26 mm;  $T_{min,max}$  0.20, 0.28, 2θ<sub>max</sub> 46.6°;  $N$  6649,  $N_0$  2184;  $R$  0.034,  $R_w$  0.035.  $\nu_0$  150,  $|\Delta\rho_{max}|$  0.91 e Å<sup>-3</sup>.

*Variata.* 'Crystal deterioration' of c. 20% was compensated for by appropriate scaling of the data (Er adduct only). The Er adduct has been the subject of an independent contemporary study,<sup>22</sup> the results of which are consonant with the present. The cell and coordinate settings of these three adducts are the same as those of ref.<sup>22</sup>

$[YbCl_2(MeCN)_2]_2[YbCl_3(MeCN)](\mu-Cl)_2YbCl_3(MeCN)] = C_{24}H_{36}Cl_{12}N_{12}Yb_4, M_r 1610.2$ . Triclinic, space group  $PT$ ,  $a$  13.68(1),  $b$  10.295(7),  $c$  9.678(9) Å,  $\alpha$  78.59(7)°,  $\beta$  82.31(7)°,  $\gamma$  80.93(6)°,  $V$  1312 Å<sup>3</sup>.  $D_c$  ( $Z = 1$  f.u.) 2.03 g cm<sup>-3</sup>;  $F(000)$  748,  $\mu_{Mo}$  77 cm<sup>-1</sup>; specimen: 0.14 × 0.40 × 0.55 mm;  $T_{min,max}$  0.092, 0.55, 2θ<sub>max</sub> 55°;  $N$  6023,  $N_0$  4540;  $R$  0.053,  $R_w$  0.058.  $\nu_0$  238,  $|\Delta\rho_{max}|$  2.8 e Å<sup>-3</sup>.

*Variata.* Available material was twinned and data measured on a deconvoluted reciprocal lattice, 250 reflections apparently affected by overlap being refined with an independent scale factor. Hydrogen atoms were neither located nor included in the refinement.

#### Acknowledgments

We gratefully acknowledge support of the work by grants from the Australian Research Council, DAAD and an Australian Postgraduate Award to N.M.S.

#### References

- (a) Schumann, H., and Genthe, W., 'Organometallic Compounds of the Rare Earths' in 'Handbook on the Physics and Chemistry of Rare Earths' (Eds K. A. Gschneidner and L. Eyring) Vol. 7, Ch. 53 (Elsevier: Amsterdam 1984); (b) Bochkarev, M. N., Zakharov, L. N., and Kalinina, G. S., 'Organoderivatives of the Rare Earth Elements' (Kluwer Academic: Dordrecht 1995).
- (a) Hart, F. A., 'Scandium, Yttrium, and the Lanthanides' in 'Comprehensive Coordination Chemistry' (Eds G. Wilkinson, R. D. Gillard, J. A. McCleverty) Vol. 3, Ch. 39 (Pergamon Press: Oxford 1987); (b) Anwander, R., *Top. Curr. Chem.*, 1998, 179, 33.
- Mehrotra, R. C., Singh, A., and Tripathi, U. M., *Chem. Rev.*, 1991, 91, 1287.
- (a) Cotton F. A., and Wilkinson G., 'Advanced Inorganic Chemistry' 4th Edn, p. 990 (John Wiley: New York 1980). (b) Bradley, D. C., Mehrotra, R. C., Rothwell, I. P., and Singh, A., 'Alkoxo and Aryloxo Derivatives of Metals' 2001 (Academic Press: London).
- 'Gmelin Handbook of Inorganic Chemistry, Sc, Y, La-Lu' Vol. 4a 'Chlorides' pp. 51-73 (Springer Verlag: Berlin 1982); Meyer, G., 'Binary Lanthanide(III) Halides, MX<sub>3</sub> (X = Cl, Br, I) in 'Syntheses of Lanthanide and Actinide Compounds' (Eds G. Meyer and L. R. Morss) (Kluwer: Dordrecht 1991).
- (a) Deacon, G. B., and Koplick, A. J., *Inorg. Nucl. Chem. Lett.*, 1979, 15, 263; (b) Deacon, G. B., Tuong, T. D., and Wilkinson, D. L., *Inorg. Synth.*, 1990, 27, 136; (c) Deacon, G. B., Tuong, T. D., and Wilkinson, D. L., *Inorg. Synth.*, 1990, 28, 286.
- Evans, W. J., Feldmann, J. D., and Ziller, J. W., *J. Am. Chem. Soc.*, 1996, 118, 4581.
- Kravchenko, O. V., Kravchenko, S. E., Makhaev, V. D., Polyakova, V. B., Slobodenchuck, G. V., and Semenenko, K. N., *Koord. Khim.*, 1982, 8, 1356.
- Wu, S.-H., Ding, Z.-B., and Li, X.-J., *Polyhedron*, 1994, 13, 2679.
- Petricek, S., Demsar, A., and Golic, L., *Polyhedron*, 1999, 18, 529.
- Belli Dell'Amico, D., Calderazzo, F., della Porta, C., Merigo, A., Biagini, P., Lugli, G., and Wagner, T., *Inorg. Chim. Acta*, 1995, 240, 1.
- Deacon G. B., Feng, T., Junk, P. C., Skelton, B. W., Sobolev, A. N., and White, A. H., *Aust. J. Chem.*, 1998, 51, 75.
- Deacon, G. B., Feng, T., Nickel, S., Skelton, B. W., and White, A. H., *J. Chem. Soc., Chem. Commun.*, 1993, 1328.
- Taylor, M. D., and Carter, C. P., *J. Inorg. Nucl. Chem.*, 1962, 24, 387.
- Trifonov, A. A., Van de Weghe, P., Collin, J., Domingos, A., and Santos, I., *J. Organomet. Chem.*, 1997, 527, 225.
- Barnhart, D. M., Frankcom, T. M., Gordon, P. L., Sauer, N. N., Thompson, J. A., and Watkin, J. G., *Inorg. Chem.*, 1995, 34, 4662.
- Evans, W. J., Shreeve, J. L., Ziller, J. W., and Doedens, R. J., *Inorg. Chem.*, 1995, 34, 576.
- Willey, G. R., Woodman, T. J., and Drew, M. G. B., *Polyhedron*, 1997, 16, 3385.
- Weng, C., Zhongshen, J., Yan, X., Yuguo, F., and Guangdi, Y., *Inorg. Chim. Acta*, 1987, 130, 125.
- Lin, G.-Y., Wei, G.-C., Jin, Z.-S., and Chen, W.-Q., *Jiegou Huaxue (J. Struct. Chem.)*, 1992, 11, 200.
- (a) Lin, S.-H., Dong, Z.-C., Huang, J.-S., Zhang, Q. E., and Lu, J. X., *Acta Crystallogr., Sect. C*, 1991, 47, 426; (b) Kong, D.-Y., Wang, S.-W., Zhu, Q., Xie, Y.-Y., and Huang, X.-Y., *Jiegou Huaxue (J. Struct. Chem.)*, 1998, 17, 61.
- Anfang, S., Karl, M., Faza, N., Massa, W., Magull, J., and Dehnicke, K., *Z. Anorg. Allg. Chem.*, 1997, 623, 1425.
- (a) Xie, Z.-W., Qian, C.-T., Sun, J., and Jin, X.-L., *Jiegou Huaxue (J. Struct. Chem.)*, 1993, 12, 107; (b) Sobota, P., Utiko, J., and Szafert, S., *Inorg. Chem.*, 1994, 33, 5203.
- Willey, G. R., Meehan, P. R., Woodman, T. J., and Drew, M. G. B., *Polyhedron*, 1997, 16, 623.
- Anfang, S., Dehnicke, K., and Magull, J., *Z. Naturforsch.*, 1996, 51b, 531.
- Atwood, J. L., and Smith, K. D., *J. Chem. Soc., Dalton Trans.*, 1974, 921.
- Qian, C.-T., Wang, B., Deng, D.-L., Xu, C., Sun, X.-Y., and Ling, R.-G., *Jiegou Huaxue (J. Struct. Chem.)*, 1993, 12, 18.
- Magomedov, G. K.-I., Voskoboinikov, A. Z., Kirillova, N. I., Gusev, A. I., Parshina, I. N., and Beletskaya, I. P., *Metallorg. Khim. (Organometallic Chem. in U.S.S.R.)*, 1992, 5, 679.
- Evans, W. J., Boyle, T. J., and Ziller, J. W., *J. Am. Chem. Soc.*, 1993, 115, 5084.
- Gecheng, W., Hanrong, G., Zhongsheng, J., and Qi, S., *Jiegou Huaxue (J. Struct. Chem.)*, 1989, 8, 61.
- Xie, Z., Chui, K.-Y., Wu, B., and Mak, T. C. W., *Inorg. Chem.*, 1996, 35, 5957.
- Depero, L. E., Arienti, M. T., Zocchi, M., and Gallazzi, M. C., *Struct. Chem.*, 1991, 2, 595.
- Ye Sun Chun, H., Huang, H., Xian Xu, G., Sheng Ma, Z., and Shi, M.-C., *Chin. Chem. Lett.*, 1994, 5, 255.
- Hou, Z., and Wakatsuki Y., *J. Chem. Soc., Chem. Commun.*, 1994, 1205.
- Evans, W. J., Gummshaimer, T. S., and Ziller, J. W., *J. Am. Chem. Soc.*, 1995, 117, 8999.
- Van den Hende, J. R., Hitchcock, P. B., Holmes, S. A., Lappert, M. F., Leung, W.-P., Mak, T. C. W., and Prashar, S., *J. Chem. Soc., Dalton Trans.*, 1995, 1427.

- <sup>37</sup> Bochkarev, M. N., Fedushkin, I. L., Fagin, A. A., Petrovskaya, T. V., Ziller, J. W., Broomhall-Dillard, R. N. R., and Evans, W. J., *Angew. Chem., Int. Ed. Engl.*, 1997, 36, 133.
- <sup>38</sup> Håkansson, M., Vestergren, M., Gustafsson, B., and Hilmersson, G., *Angew. Chem., Int. Ed.*, 1999, 38, 2199.
- <sup>39</sup> Errington, W., Spry, M. P., and Willey, G. R., *Acta Crystallogr., Sect. C*, 1998, 54, 290.
- <sup>40</sup> Deacon, G. B., Görtler, B., Junk, P. C., Lórk, E., Mews, R., Petersen, J., and Zemva, B., *J. Chem. Soc., Dalton Trans.*, 1998, 3887.
- <sup>41</sup> (a) Clark, R. J. H., Lewis, J., Machin, D. J., and Nyholm, R. S., *J. Chem. Soc.*, 1963, 379; (b) Lewis, J., Miller, J. R., Richards, R. L., and Thompson, A., *J. Chem. Soc.*, 1965, 5850.
- <sup>42</sup> Walton, R. A., *Q. Rev. Chem. Soc.*, 1965, 19, 126.
- <sup>43</sup> Deacon, G. B., Harris, S. C., Meyer, G., Stellfeldt, D., Wilkinson, D. L., and Zelesny, G., *J. Organomet. Chem.*, 1996, 525, 247.
- <sup>44</sup> Marcalo, J., and De Matos, A. P., *Polyhedron*, 1989, 8, 2431.
- <sup>45</sup> Shannon, R. D., *Acta Crystallogr., Sect. A*, 1976, 32, 751.
- <sup>46</sup> Runschke, C., and Meyer, G., *Z. Anorg. Allg. Chem.*, 1997, 623, 1017.
- <sup>47</sup> Johnson, M., Taylor, J. C., and Cox, G. W., *J. Appl. Crystallogr.*, 1980, 13, 188.
- <sup>48</sup> Deacon, G. B., Delbridge, E. E., Skelton, B. W., and White, A. H., *Eur. J. Inorg. Chem.*, 1999, 751.
- <sup>49</sup> Hazin, P. N., Bruno, J. W., and Schulte, G. K., *Organometallics*, 1990, 9, 416.
- <sup>50</sup> Li, X., Liu, J., Hu, N., Jin, Z., and Liu, G., *Huaxue Xuebao*, 1989, 47, 1191.
- <sup>51</sup> Malandrino, G., Licata, R., Castelli, F., Fragala, I. L., and Benelli, C., *Inorg. Chem.*, 1995, 34, 6233.
- <sup>52</sup> Deacon, G. B., Feug, T., Skelton, B. W., and White, A. H., *Aust. J. Chem.*, 1995, 48, 741.
- <sup>53</sup> Crisco, G., and Meyer, G., *Z. Anorg. Allg. Chem.*, 1994, 620, 1023.
- <sup>54</sup> Junk, P. C., Kepert, D. L., Skelton, B. W., and White, A. H., *Aust. J. Chem.*, 1999, 52, 497.
- <sup>55</sup> Schumann, H., Meese-Marktscheffel, J. A., and Esser, L., *Chem. Rev.*, 1995, 95, 865.
- <sup>56</sup> Kepert, C. J., Skelton, B. W., and White, A. H., *Aust. J. Chem.*, 1994, 47, 385.
- <sup>57</sup> Junk, P. C., Semenova, L. I., Skelton, B. W., and White, A. H., *Aust. J. Chem.*, 1999, 52, 531; see also references therein.
- <sup>58</sup> Lim, K. C., Skelton, B. W., and White, A. H., *Aust. J. Chem.*, 2000, 53, paper CH00119.
- <sup>59</sup> Hall, S. R., Flack, H. D., and Stewart, J. M. (Eds), 'The XIAL 3.2 Reference Manual', Universities of Western Australia, Geneva and Maryland, 1992.

## COMMUNICATIONS

149.5 (py-C6), 139.4 (py-C4), 139.3 (py-C4), 136.5 (Ar-C2), 126.4 (q,  $J(\text{CB}) = 2.8 \text{ Hz}$ , BA-C3), 125.5 (py-C3), 125.4 (py-C3), 124.2 (py-C5), 122.6 (BA-C4), 121.9 (py-C5), 72.9 (NCH<sub>2</sub>-py<sub>2</sub>), 70.2 (NCH<sub>2</sub>-py<sub>2</sub> and RhCH<sub>2</sub>CH<sub>2</sub>O), 35.0 (d,  $J(\text{CRh}) = 25.0 \text{ Hz}$ , RhCH<sub>2</sub>CH<sub>2</sub>O); ESI-MS (CD<sub>3</sub>CN): 453 [M-BPh<sub>4</sub>]<sup>+</sup>, 425 [M-C<sub>2</sub>H<sub>5</sub>-BPh<sub>4</sub>]<sup>+</sup>, 409 [M-C<sub>2</sub>H<sub>4</sub>O-BPh<sub>4</sub>]<sup>+</sup>, 393 [M-C<sub>2</sub>H<sub>4</sub>O<sub>2</sub>-BPh<sub>4</sub>]<sup>+</sup>, 391 [M-C<sub>2</sub>H<sub>4</sub>O<sub>2</sub>-BPh<sub>4</sub>]<sup>+</sup>.

Received: December 15, 2000 [Z16283]

- [1] a) H. Mimoun, M. M. P. Machirant, I. S. de Roch, *J. Am. Chem. Soc.* 1978, 100, 5437; b) G. Read, *J. Mol. Catal.* 1988, 44, 15; c) M. Bressan, F. Morandini, A. Morvillo, P. Rigo, *J. Organomet. Chem.* 1985, 280, 139; d) R. A. Sheldon, J. A. van Doorn, *J. Organomet. Chem.* 1975, 94, 115.
- [2] a) B. de Bruin, M. J. Boerakker, J. A. W. Verhagen, R. de Gelder, J. M. M. Smits, A. W. Gal, *Chem. Eur. J.* 2000, 6, 298; b) B. de Bruin, M. J. Boerakker, J. J. M. Donners, B. E. C. Christiaans, P. P. J. Schlabos, R. de Gelder, J. M. M. Smits, A. L. Spek, A. W. Gal, *Angew. Chem.* 1997, 109, 2153; *Angew. Chem. Int. Ed. Engl.* 1997, 36, 2063; c) B. de Bruin, J. A. W. Verhagen, C. H. J. Schouten, A. W. Gal, D. Feichtinger, D. A. Plattner, *Chem. Eur. J.* 2001, 7, 416.
- [3] tpa = tri(2-pyridylmethyl)amine; Meopa = [(6-methyl-2-pyridyl)methyl]di(2-pyridylmethyl)amine.
- [4] a) G. Read, M. Urgelles, A. M. R. Galas, M. B. Hursthouse, *J. Chem. Soc. Dalton Trans.* 1983, 911; b) L. Pandolfo, G. Paiaro, G. Valle, P. Ganis, *Gazz. Chim. Ital.* 1985, 115, 59.
- [5] NaBPh<sub>4</sub> was used instead of KPF<sub>6</sub> to precipitate the ethene complex.
- [6] Transparent yellow crystals of 2bBPh<sub>4</sub> were obtained by slow diffusion of diethylether into a 1,2-dichloroethane/acetonitrile solution. The X-ray diffraction data were collected at 150(2) K on an Enraf-Nonius CAD4 diffractometer with rotating anode and CCD area detector using graphite monochromatized MoK $\alpha$  radiation ( $\lambda = 0.71073 \text{ \AA}$ ). The structure was solved by the PATTY<sup>[12]</sup> option of the DIRDIF<sup>[13]</sup> program system. Crystal data: C<sub>24</sub>H<sub>24</sub>O<sub>2</sub>B<sub>2</sub>Cl<sub>10</sub>Rh,  $M_r = 879.60$ , monoclinic, space group C2/c,  $a = 35.8999(8)$ ,  $b = 10.7567(3)$ ,  $c = 24.2379(5) \text{ \AA}$ ,  $\beta = 116.4699(12)$ ,  $V = 8378.6(3) \text{ \AA}^3$ ,  $Z = 8$ ,  $\rho_{\text{calc}} = 1.395 \text{ Mg m}^{-3}$ . All non-hydrogen atoms that could be located were refined with anisotropic temperature factors. The hydrogen atoms were placed at calculated positions and refined isotropically in riding mode. The 5-membered dioxolane ring has the envelope form and occurs in two conformations. As expected there is considerable positional overlap for some of the atoms (C1A and C1B, C2A and C2B, O1A and O1B). Therefore some geometrical constraints had to be applied: the two conformations were "SAMED" and the anisotropic thermal displacement parameters were tied. Calculations (PLATON, Spek 1995)<sup>[14]</sup> showed two distinct voids, one of 228 Å<sup>3</sup>, containing 68 electrons, around a two-fold axis (position 4e, 0,  $y$ , 1/4;  $z = -0.037$ ), and one of 151 Å<sup>3</sup>, containing 51 electrons, around an inversion center (position 4b: 1/2, 0, 0). Based on the synthetic route and evidence from NMR spectroscopy it is assumed that these electron densities possibly stand for one molecule diethylether (C<sub>4</sub>H<sub>10</sub>O, 42 electrons) plus one molecule acetonitrile (CH<sub>3</sub>CN, 22 electrons) in the first void (64 electrons, 28.5 Å<sup>3</sup>/atom), and one molecule dichloroethane (C<sub>2</sub>H<sub>4</sub>Cl<sub>2</sub>, 50 electrons) in the second void (30.2 Å<sup>3</sup>/atom). It was not possible to assign any physically meaningful parameters to the electron densities found in the difference fourier map. Therefore the SQUEEZE procedure was applied to account for these electron densities. Crystallographic data (excluding structure factors) for the structure reported in this paper have been deposited with the Cambridge Crystallographic Data Centre as supplementary publication no. CCDC-157414. Copies of the data can be obtained free of charge on application to CCDC, 12 Union Road, Cambridge CB2 1EZ, UK (fax: (+44)1223-336-033; e-mail: deposit@ccdc.cam.ac.uk).
- [7] O<sub>2</sub> and C<sub>2</sub> (O2 and C2) are positioned above and below the O1-M-Cl plane: the displacement of O2 from this plane is +0.51 Å in 2bA<sup>+</sup> and -0.46 Å in 2bB<sup>+</sup>, compared to +0.49 Å in the 3-platina-1,2-dioxolane. The displacement of C2 is -0.21 Å in 2bA<sup>+</sup> and +0.27 Å in 2bB<sup>+</sup>, compared to -0.29 in the 3-platinadioxolane.
- [8] This range is based on O-O bonds in 48 crystal structures containing a M-O-O-C fragment (M = any metal); 4 outliers were not taken into account.

- [9] This range is based on O-C bonds in 48 crystal structures containing a M-O-O-C fragment (M = any metal); 9 outliers were not taken into account.
- [10] R. Cramer, *Inorg. Chem.* 1990, 28, 86.
- [11] G. Anderegg, F. Wenk, *Helv. Chim. Acta* 1967, 50, 2330.
- [12] P. T. Beurskens, G. Beurskens, M. Strumpel, C. E. Nordman in *Patterson and Pattersons* (Eds.: J. P. Glusker, B. K. Patterson, M. Rossi) Clarendon Press, Oxford, 1987, p. 356.
- [13] DIRDIF-96. A computer program system for crystal structure determination by Patterson methods and direct methods applied to difference structure factors: P. T. Beurskens, G. Beurskens, W. P. Bosman, R. de Gelder, S. Garcia-Granda, R. O. Gould, R. Israël, J. M. M. Smits, Crystallography Laboratory, University of Nijmegen, The Netherlands, 1996.
- [14] PLATON-93. Program for display and analysis of crystal and molecular structures: A. L. Spek, University of Utrecht, The Netherlands, 1995.

### A Striking, Multifaceted, Decalithium Aggregate with Carbanion, Organoamide, and Alkoxide Functionalities\*\*

Philip C. Andrews, Glen B. Deacon,\* Craig M. Forsyth, and Natalie M. Scott

Mixed-anion alkali metal complexes are of significant interest because of their ability to act as superbases.<sup>[1]</sup> Normally superbase aggregates are composed of two anions and two differing metals, [R'M·M'OR]<sub>n</sub> (R' = alkyl, aryl, amide; R = alkyl; M = Li; M' = Na, K), and it is these complexes that display greatest reactivity and have the widest application in synthetic processes.<sup>[1d-e]</sup> Solid-state structural information on mixed-anion systems is of vital importance to provide a more complete understanding of the reasons behind their differing reactivity. However, such complexes have historically proved extremely difficult to crystallize,<sup>[1a-2]</sup> hence solid-state structures are scarce despite the emergence of some data for each class of mixed-anion alkali metal complexes.<sup>[3]</sup>

Unimetallic mixed-anion aggregates (M = M'), though usually less effective, are also of significant synthetic importance since, with suitable anions and metal, they can also show increased reactivity over that of the two separate starting reagents, for example [*n*BuLi·LiO(CH<sub>2</sub>)<sub>2</sub>NMe<sub>2</sub>].<sup>[4]</sup>

Herein, we report the crystallization and structure determination of the remarkable multifaceted unimetallic complex [(N(SiMe<sub>3</sub>)(2-(2'-C<sub>6</sub>H<sub>4</sub>O)C<sub>6</sub>H<sub>4</sub>))<sub>2</sub>Li·LiOEt·(Et<sub>2</sub>O)<sub>2</sub>]·hexane, 1·hexane, which contains three different superbase anionic components, amide, carbanion, and alkoxide. The presence of *ethoxide* is particularly striking since Lochmann has indicated that the most stable mixed-anion aggregates are

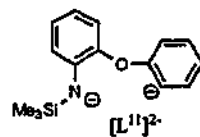
[\*] Prof. Dr. G. B. Deacon, Dr. P. C. Andrews, Dr. C. M. Forsyth, N. M. Scott  
School of Chemistry  
Monash University  
Victoria, 3800 (Australia)  
Fax: (+613)9905-4597  
E-mail: Glen.Deacon@sci.monash.edu.au

[\*\*] This work was supported by the Australian Research Council, an ARC QE11 Research Fellowship to P.C.A. and an Australian Postgraduate Award to N.M.S.



formed with bulky alkoxides, as exemplified by the presence of  $t\text{BuO}^-$  in many known alkoxo solid-state structures.<sup>[14]</sup>

Deprotonation of *N*-(2-phenoxyphenyl)-*N*-(trimethylsilyl)-amine generates a highly useful lithium organoamide  $\text{Li}(\text{L}^1)$  ( $\text{L}^1 = \text{N}(\text{SiMe}_3)(2\text{-PhOC}_6\text{H}_4)$ )<sup>[5]</sup> which reacts further with  $n\text{BuLi}$  to form  $\text{Li}_2(\text{L}^1)$  ( $\text{L}^1 = \text{N}(\text{SiMe}_3)(2\text{-}(2\text{-C}_6\text{H}_4\text{O})\text{C}_6\text{H}_4)$ ),



containing a Li-carbanion derived from abstraction of the proton from the *ortho* position of the phenyl substituent.<sup>[6]</sup> Remarkably, on attempted reaction of  $\text{Li}_2(\text{L}^1)$  with  $\text{LaCl}_3$  in diethyl ether, a decalithium

assembly, 1·hexane, comprising four  $\text{Li}_2(\text{L}^1)$  units and two  $\text{LiOEt}$  groups (Figure 1) was serendipitously crystallized. The lithium ethoxide is presumably derived from ether cleavage, and is dependent upon the presence of the lanthanoid halide. In the absence of  $\text{LaCl}_3$ , the formation of a product that incorporated a lithium alkoxide unit was not observed.<sup>[6]</sup> We have previously observed aryl ether cleavage with formation of  $[\text{Yb}(\text{L}^1)_2\text{OPh}(\text{thf})]$  on decomposition of  $[\text{Yb}(\text{L}^1)_2(\text{thf})_2]$ , hence an intermediate unstable La complex is implicated in the present system.

Determination of the structure of 1·hexane by X-ray crystallography<sup>[6]</sup> revealed a centrosymmetric decalithium aggregate (Figure 1) located at each of the eight unit cell

vertices, with a molecule of hexane positioned in a channel parallel to the *a* axis in the center of the unit cell. The asymmetric unit encompasses five unique Li atoms, two  $\text{L}^1$  ligands and an ethoxide group. Each of the chelating  $\text{L}^1$  ligands binds through bridging amide and aryl ether moieties. One ligand is coordinated by both to Li1 and Li3, whilst the other has the amide nitrogen (N2) bridging Li2 and Li4 and the aryl ether oxygen (O2) bridging Li4 and Li5A. The Li–N(amide) distances (av 2.05 Å) are typical of these structural features, whilst the less common bridging aryl ether oxygen atoms have one long (av 2.42 Å) and one shorter (av 2.08 Å) Li–O(ether) bond length.<sup>[7a]</sup> Characteristic of lithium amides,<sup>[7]</sup> Li1 is also coordinated by a molecule of diethyl ether which presumably inhibits further agglomeration of the aggregate. The ethoxide group is bound to three lithium atoms, Li1, Li2, and Li3 with one shorter (Li2–O3 1.839(5) Å) and two longer (Li1–O3 1.918(5), Li3–O3 1.890(5) Å) Li–O distances, though all are in the reported RO–Li range.<sup>[8]</sup> A  $\mu_3$ -alkoxide–Li<sub>3</sub> arrangement is characteristic of lithium clusters with bulky alkoxides,  $[\text{Li}(\text{OR})_n]_n$  ( $n=4,6$ )<sup>[9, 7a]</sup> and presumably the rare incorporation of the much smaller OEt anion in the current structure is facilitated by the steric protection provided by the two nearby bulky  $\text{SiMe}_3$  groups (Figure 1). The third anionic component is derived from the phenyl carbanion that bridges three lithium atoms in different modes. One phenyl group binds to Li2, Li4, and Li5 through a single

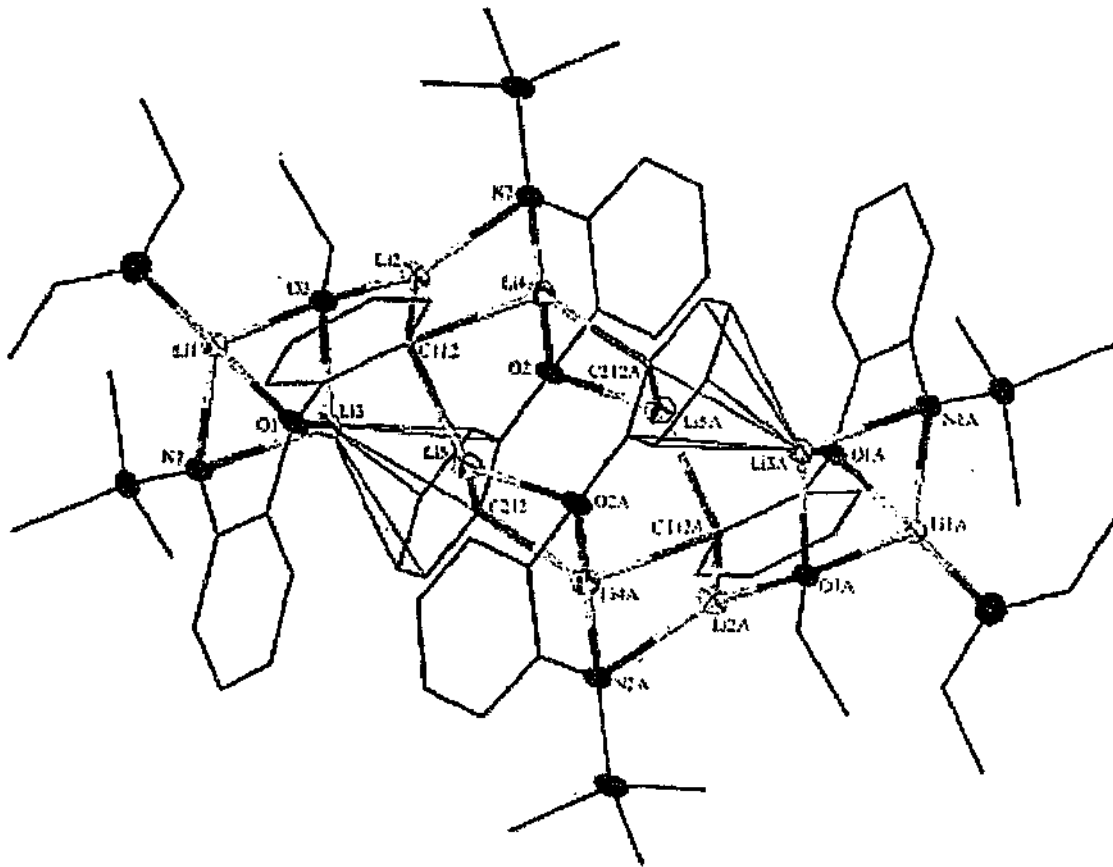


Figure 1. Molecular structure of 1·hexane with the thermal ellipsoids shown at 30% probability level for the non-carbon atoms. For clarity, the molecule of hexane and the hydrogen atoms have been omitted and the carbon atoms are represented by lines.

## COMMUNICATIONS

carbon atom (C112), whilst the other has a  $\mu_2$ -C (C212) interaction to Li5 and Li4A but also coordinates more weakly with Li3 by means of an  $\eta^6$ - $\pi$ -Ph interaction. The range of the shorter carbon–lithium bond lengths (2.128(5)–2.567(5) Å) has some longer than those observed in aryllithium clusters which similarly contain a  $\mu_2$ -aryl-Li<sub>2</sub> arrangement (e.g.  $\{[Li(3,5\text{-}t\text{-Bu}_2\text{C}_6\text{H}_3)]_2\}$ : Li–C 2.119(7)–2.247(7) Å<sup>[9]</sup>). The relative positions of the lithium atoms Li2, Li4, and Li5 (Figure 2a) and Li4A and Li5 (Figure 2b) and of the

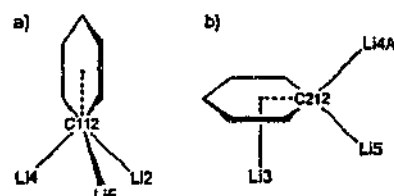


Figure 2. Schematic representation of Li–aryl bonding in 1-hexane. a) Relative positions of Li2, Li4, and Li5 (a) and Li4A and Li5 (b) to the associated phenyl ring.

associated phenyl rings in **1** (Li–C to C<sub>6</sub> ring plane angles 0.4–59.2°) suggest predominantly  $\sigma$ -Li–C bonding. The  $\pi$ -Ph coordination to Li3 (Li–C<sub>6</sub> centroid to C<sub>6</sub> ring plane angle 84.3°) occupies a vacant tetrahedral coordination site on this lithium atom. The average Li–C separation (av Li–C 2.62 Å) is at the longer extreme of the range (2.28–2.77 Å)<sup>[10–12]</sup> previously observed for Li complexation by a neutral arene. Presumably a closer approach to Li3 is prevented by the bonding of the phenyl ring to Li2A and Li5 as well as being fixed to the L<sup>11</sup> backbone through the aryl ether oxygen O2. All Li–C( $\pi$ -phenyl) distances are much less than the sum (3.30 Å) of the metallic radius for Li<sup>[10]</sup> and the van der Waals radius of an arene ring.<sup>[10c]</sup>

The above bonding arrangements give five distinct lithium environments: Li1 four-coordinate (distorted tetrahedral), Li2 three-coordinate (trigonal planar  $\Sigma^*$  359.9), Li3 three-coordinate (pyramidal) augmented by the  $\eta^6$ - $\pi$ -Ph interaction to become pseudo-tetrahedral, Li4 four-coordinate (the donor atoms at the vertices of a triangular pyramid), and Li5 three-coordinate (near trigonal-planar  $\Sigma^*$  351.0). The Li2 environment is unique in lithium coordination chemistry being ligated by three “superbase” anions, amide, alkoxide, and carbanion with three different donor atoms (see also a Li/Na bimetallic complex with Li coordinated by hydroxide, alkoxide, and amide<sup>[11]</sup>). The <sup>7</sup>Li NMR spectrum of a [D<sub>6</sub>]toluene solution of **1**·hexane showed only four separate broad peaks at room temperature, but on cooling, these resolved into the expected five sharp resonance signals. Similarly, variable-temperature <sup>1</sup>H NMR spectroscopy indicated some fluxional behavior that could be frozen at low temperature (see Experimental Section). However, two distinct L<sup>11</sup> environments were detected (even at room temperature) which suggests that the gross structure may remain largely intact in solution as was also observed in the unimetallic mixed-anion complex  $\{(\text{iPr})_2\text{NLi} \cdot (\text{Me}_2\text{NCH}_2)_2\text{CHOLi}\}_2$ .<sup>[12]</sup> The unexpected stability may be attributed to the integrity of  $[\text{Li}_2(\text{L}^{11})]_2$  units, which under appropriate

conditions can sequester small LiX entities in solution, and appears to support the observations of Schleyer et al. on the conformational stability of mixed aggregates in “superbase” mixtures.<sup>[12]</sup> Indeed we have also isolated a *n*BuLi adduct from these systems.<sup>[13]</sup> Although it is premature to speculate on the possible behavior of triple anion aggregates as superbases, the successful isolation of **1**·hexane should encourage their more deliberate synthesis and hence investigation of their superbase role. The presence of chelation in **1** may be, but is not necessarily, a deterrent to superbase behavior (see ref. [4a]), especially since coordination fluxionality has been detected at room temperature.

### Experimental Section

**1**: *n*BuLi (3.1 mL, 4.9 mmol) was slowly added to a stirring solution of *N*-(2-phenoxyphenyl)-*N*-(trimethylsilyl)amine (0.63 g, 2.45 mmol) in Et<sub>2</sub>O (40 mL), and the mixture was stirred until it had warmed to room temperature (ca. 1 h). LaCl<sub>3</sub> (0.60 g, 2.45 mmol) was added and the reaction mixture was then stirred overnight. After the solvent had been removed under vacuum, hexane (25 mL) was added which gave a white precipitate. The reaction mixture was filtered at –78 °C and the filtrate was reduced under vacuum (ca. 15 mL) whereupon colorless crystals of **1**·hexane deposited (0.15 g, 18%). M.p. 180–184 °C (decomp); IR (Nujol):  $\nu$  = 1589 s, 1561 w, 1544 w, 1408 vs, 1281 brs, 1244 s, 1147 vs, 1105 vs, 1162 m, 1044 s, 999 w, 945 s, 929 s, 886 w, 864 w, 828 s, 786 w, 768 s, 749 vs, 727 w, 668 w, 617 w cm<sup>-1</sup>; <sup>1</sup>H NMR (400 MHz, [D<sub>6</sub>]toluene, 303 K):  $\delta$  = 0.02 (vbrs, 18H; Si(CH<sub>3</sub>)<sub>3</sub>), 0.24 (s, 18H; Si(CH<sub>3</sub>)<sub>3</sub>), 0.78 (t, <sup>3</sup>J = 7.0 Hz, 12H; CH<sub>2</sub>(OEt<sub>2</sub>)), 0.81–0.98 (m, 12H; CH<sub>2</sub>(hexane) CH<sub>2</sub>(OEt)), 1.23 (brm, 8H; CH<sub>2</sub>(hexane)), 3.03 (q, <sup>3</sup>J = 7.0 Hz, 8H; CH<sub>2</sub>(OEt<sub>2</sub>)), 3.39 (brq, 4H; CH<sub>2</sub>(OEt)), 5.70 (brs, 2H; Ar), 6.08 (brs, 4H; Ar), 6.29 (brs, 2H; Ar), 6.45 (brt, 4H; Ar), 6.66 (brs, 2H; Ar), 6.80–7.10 (brm, 12H; Ar), 7.29 (brs, 2H; Ar), 7.82 (brdd, 4H; Ar); <sup>1</sup>H NMR (400 MHz, [D<sub>6</sub>]toluene, 213 K):  $\delta$  = 0.35 (s, 18H; Si(CH<sub>3</sub>)<sub>3</sub>), 0.37 (s, 18H; Si(CH<sub>3</sub>)<sub>3</sub>), 0.86–0.99 (m, 18H; CH<sub>2</sub>(OEt<sub>2</sub>)), 1.00–1.15 (brm, 6H; CH<sub>2</sub>(OEt)), 1.17–1.38 (brm, 8H; CH<sub>2</sub>(hexane)), 2.65 (brm, 4H; CH<sub>2</sub>(OEt)), 2.82 (brm, 4H; CH<sub>2</sub>(OEt)), 3.32 (brm, 2H; CH<sub>2</sub>(OEt)), 3.47 (brm, 2H; CH<sub>2</sub>(OEt)), 5.71 (d, <sup>3</sup>J = 7.3 Hz, 2H; Ar), 6.05 (d, <sup>3</sup>J = 7.7 Hz, 2H; Ar), 6.22 (t, <sup>3</sup>J = 7.0 Hz, 2H; Ar), 6.38–6.57 (m, 4H; Ar), 6.64 (d, <sup>3</sup>J = 8.2 Hz, 2H; Ar), 6.70–6.88 (m, 4H; Ar), 6.93–7.17 (m, 12H; Ar), 7.20 (brd, 2H; Ar), 7.37 (d, <sup>3</sup>J = 7.5 Hz, 2H; Ar); <sup>7</sup>Li NMR (155.51 MHz, [D<sub>6</sub>]toluene, 303 K):  $\delta$  = –2.57, 0.68, 1.16, 2.27; (183 K) –3.11, 0.67, 1.72, 1.95, 3.14: A satisfactory C analysis could not be obtained presumably owing to decomposition.<sup>[14]</sup>

Received: February 1, 2001 [Z16540]

- [1] a) L. Lochmann, *Eur. J. Inorg. Chem.* 2000, 1115–1126; R. E. Mulvey, *Chem. Soc. Rev.* 1998, 27, 339; b) R. S. Snaith, D. S. Wright in *Lithium Chemistry: A Theoretical and Experimental Overview* (Eds.: A.-M. Sapse, P. von R. Schleyer), Wiley, New York, 1995, chap. 8, p. 227; c) W. Bauer, L. Lochmann, *J. Am. Chem. Soc.* 1992, 114, 7482; d) A. Mordini in *Advances in Carbanion Chemistry, Vol. 1* (Ed.: V. Snieckus), JAI, London, 1992, p. 1; e) M. Schlosser in *Organometallics in Synthesis* (Ed.: M. Schlosser), Wiley, Chichester, 1994, chap. 7.
- [2] R. Pi, W. Bauer, P. von R. Schleyer, *J. Organomet. Chem.* 1986, 306, C1; L. Lochmann, D. Lim, *J. Organomet. Chem.* 1971, 28, 153.
- [3] Alkyl/alkoxide: a) S. Harder, A. Streitwieser, *Angew. Chem.* 1993, 105, 1108; *Angew. Chem. Int. Ed. Engl.* 1993, 32, 1066; b) M. Marsch, K. Harms, L. Lochmann, G. Boche, *Angew. Chem.* 1990, 102, 334; *Angew. Chem. Int. Ed. Engl.* 1990, 29, 308; amide/alkoxide: c) P. C. Andrews, G. D. Fallon, M. Maguire, A. C. Peatt, *Angew. Chem.* 2000, 112, 4690; *Angew. Chem. Int. Ed.* 2000, 39, 4516; d) R. Holland, J. C. Jeffrey, C. A. Russell, *J. Chem. Soc. Dalton Trans.* 1999, 3331; e) K. W. Henderson, D. S. Walther, P. G. Williard, *J. Am. Chem. Soc.* 1995, 117, 8680.
- [4] a) P. Gros, Y. Fort, P. Caubere, *J. Chem. Soc. Perkin Trans. 1* 1997, 3071; b) P. Caubere, *Chem. Rev.* 1993, 93, 2317.
- [5] a) G. B. Deacon, C. M. Forsyth, N. M. Scott, *Eur. J. Inorg. Chem.* 2000, 2501; b) G. B. Deacon, C. M. Forsyth, N. M. Scott, unpublished results.

- [6] Crystal data for 1-hexane: colorless crystal,  $0.18 \times 0.23 \times 0.38$  mm, triclinic,  $P\bar{1}$ ,  $a = 10.7828(3)$ ,  $b = 13.1998(5)$ ,  $c = 16.1826(7)$  Å,  $\alpha = 105.724(2)$ ,  $\beta = 103.774(2)$ ,  $\gamma = 92.199(3)^\circ$ ,  $V = 2140.2(7)$  Å<sup>3</sup>,  $Z = 1$ ,  $\rho_{\text{calc}} = 1.098$  g cm<sup>-3</sup>,  $\mu = 0.120$  mm<sup>-1</sup>,  $2\theta_{\text{max}} = 56.5^\circ$ . A total of 10232 ( $R_{\text{int}} = 0.033$ ) unique reflections were collected (Enraf Nonius CCD, MoK $\alpha$  radiation ( $\lambda = 0.71073$  Å),  $T = 123$  K) and used in least-squares refinement on  $F^2$ , 469 refined parameters, GOF = 1.030 (based on  $F^2$ ),  $R1 = 0.073$ ,  $wR2 = 0.169$  ( $I > 2\sigma(I)$ ),  $R1 = 0.134$ ,  $wR2 = 0.198$  (all data), residual electron density  $-0.366/0.523$  e Å<sup>-3</sup>. The hydrogen atoms were placed in calculated positions using a riding model. Crystallographic data (excluding structure factors) for the structure reported in this paper have been deposited with the Cambridge Crystallographic Data Centre as supplementary publication no. CCDC-157276. Copies of the data can be obtained free of charge on application to CCDC, 12 Union Road, Cambridge CB21EZ, UK (fax: (+44) 1223-336-033; e-mail: deposit@ccdc.cam.ac.uk).
- [7] a) F. Pauer, P. P. Power in *Lithium Chemistry: A Theoretical and Experimental Overview* (Eds.: A.-M. Sapse, P. von R. Schleyer), Wiley, New York, 1995, chap. 9; b) M. F. Lappert, P. P. Power, A. R. Sanger, R. C. Srivastava, *Metal and Metalloid Amides*, Ellis Horwood, Chichester, 1980, chap. 2.
- [8] D. C. Bradley, R. C. Mehrotra, I. P. Rothwell, A. Singh, *Alkoxo and Aryloxo Derivatives of Metals*, Academic Press, London, 2001.
- [9] R. J. Wehmschulte, P. P. Power, *J. Am. Chem. Soc.* 1997, 119, 2847.
- [10] a) K. Ruhlandt-Senge, J. J. Ellison, R. J. Wehmschulte, F. Pauer, P. P. Power, *J. Am. Chem. Soc.* 1993, 115, 11353; b) B. Schiemenz, P. P. Power, *Angew. Chem.* 1996, 108, 2288; *Angew. Chem. Int. Ed. Engl.* 1996, 35, 2150; c) M. Niemeyer, P. P. Power, *Inorg. Chem.* 1996, 35, 7264; d) A. F. Wells, *Structural Inorganic Chemistry*, 5th ed., Clarendon, Oxford, 1984, p. 1288; e) L. C. Pauling, *The Nature of the Chemical Bond*, Cornell University Press, Ithaca, 1960.
- [11] A. R. Kennedy, J. G. MacLellan, R. E. Mulvey, A. Robertson, *J. Chem. Soc. Dalton Trans.* 2000, 4112.
- [12] T. Kremer, S. Harder, M. Junge, P. von R. Schleyer, *Organometallics* 1996, 15, 585.
- [13] Typical elemental analyses calcd for 1 C<sub>77</sub>H<sub>10</sub>Li<sub>10</sub>N<sub>4</sub>O<sub>8</sub>Si<sub>4</sub> (%): C 65.06, H 7.43, N 4.21 (1-hexane C<sub>77</sub>H<sub>112</sub>Li<sub>10</sub>N<sub>4</sub>O<sub>8</sub>Si<sub>4</sub>: C 66.19, H 7.98, N 3.96); found: C 62.98, H 7.74, N 4.44.

### Self-Assembly of Nanometer-Scale Secondary Building Units into an Undulating Two-Dimensional Network with Two Types of Hydrophobic Cavity\*\*

Susan A. Bourne, Jianjiang Lu, Arunendu Mondal, Brian Moulton, and Michael J. Zaworotko\*

By using some of the recently enunciated principles of crystal engineering<sup>[1-3]</sup> and self-assembly it has become possible to design and construct new classes of crystalline compounds from molecular components that possess useful

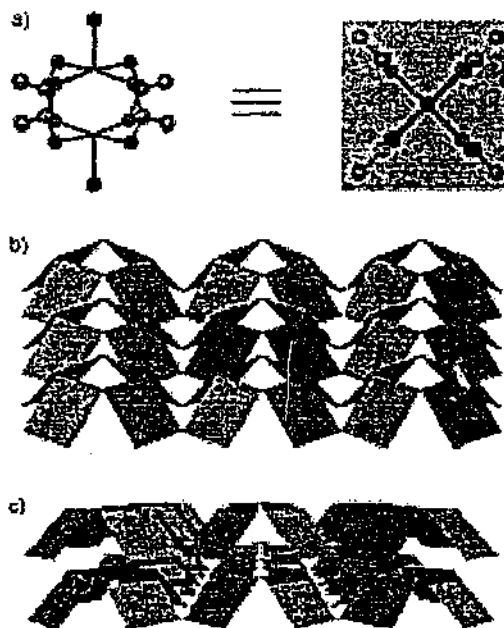
[\*] Prof. M. J. Zaworotko, J. Lu, Dr. A. Mondal, B. Moulton  
Department of Chemistry  
University of South Florida  
4202 E. Fowler Avenue, SCA 400, Tampa, FL 33620 (USA)  
Fax: (+1) 813-974-1733  
E-mail: zaworo@chuma1.cas.usf.edu

Dr. S. A. Bourne  
Department of Chemistry  
University of Cape Town  
Rondebosch 7701 (South Africa)

[\*\*] M.J.Z. gratefully acknowledges the financial support of the NSF (DMR 0101641).

physical properties including bulk magnetism,<sup>[4]</sup> nonlinear optical properties,<sup>[5]</sup> and porosity.<sup>[6-9]</sup> Open-framework structures can be assembled by using metals or metal clusters as nodes and multifunctional organic ligands to link these nodes. This approach has afforded structures that exhibit high surface areas, affinity for a wide range of organic guest molecules,<sup>[10]</sup> and some show potential for catalysis.<sup>[9]</sup> Herein we illustrate how the use of metal-organic secondary building units (SBUs) that are linked by angular ligands can generate nanoscale SBUs (nSBUs) with curvature.

The use of carboxylate-bridged metal clusters as metal-organic SBUs to build extended self-assembled structures has been delineated by Yaghi et al.<sup>[9]</sup> Scheme 1 illustrates such a



Scheme 1. Schematic illustrations of a) the square SBU (green) based on metal ions bridged by carboxylate anions, b) how the square SBUs can self-assemble at their vertices to generate nanosized bowls (purple) which in turn form curved sheets, and c) how the curved sheets pack because of shape considerations.

cluster—in this case two metal ions are bridged by four carboxylate anions and each metal is bonded to one axial pyridine ligand. When viewed along the axial direction the extension of the carboxylate ligands forms a “square SBU”. Such clusters are ubiquitous in the Cambridge Structural Database,<sup>[11]</sup> but most contain monofunctional carboxylates and, therefore, they will not generate extended structures. However, the use of bifunctional carboxylate ligands such as 1,4-benzenedicarboxylate allows the formation of self-assembled infinite structures that contain channels capable of incorporating a variety of guest molecules.<sup>[12-15]</sup> 1,3-Benzenedicarboxylate is suitable for the linking of square SBUs at 120° and Scheme 1b shows one of the ways in which square SBUs can pack when there is a 120° angle at their vertices: a two-dimensional (2D) infinite metal-organic framework resembling a layer of upended bowls. In such a structure one bowl

# Structurally diverse organoamides and organoamido-, organo-metallic-lithium aggregates from reactions of *N*-(2-phenoxyphenyl)-*N*-(trimethylsilyl)amine with LiBu<sup>+</sup>†

Glen B. Deacon,\* Craig M. Forsyth and Natalie M. Scott

School of Chemistry, Monash University, Victoria 3800, Australia.  
E-mail: g.deacon@scL.monash.edu.au

Received 24th April 2001, Accepted 28th June 2001  
First published as an Advance Article on the web ??????

Deprotonation of *N*-(2-phenoxyphenyl)-*N*-(trimethylsilyl)amine (L<sup>1</sup>H) with a slight excess of LiBu<sup>+</sup> in tetrahydrofuran (thf) or 1,2-dimethoxyethane (dme) yielded the solvated lithium organoamide complexes [Li(L<sup>1</sup>)(thf)]<sub>n</sub> (1) and [Li(L<sup>1</sup>)(dme)]<sub>2</sub> (2) (L<sup>1</sup> = N(C<sub>6</sub>H<sub>4</sub>OPh-2)(SiMe<sub>3</sub>)), respectively. Reaction of L<sup>1</sup>H with LiBu<sup>+</sup> in hexane gave the solvent free lithium organoamide [Li(L<sup>1</sup>)]<sub>n</sub> (3). Monomeric 2 was shown to have a four-coordinate lithium centre surrounded by chelating L<sup>1</sup> and dme ligands in a distorted tetrahedral environment. Utilisation of diethyl ether as the reaction solvent, followed by work up in hexane containing a trace of bis(2-methoxyethyl) ether (diglyme), gave a low yield of colourless crystals, shown by X-ray crystallography to be {[Li(OEt<sub>2</sub>)(L<sup>1</sup>)Li<sub>2</sub>(L<sup>1</sup>)<sub>2</sub>(O, O, O, O-diglyme)]} (4) (L<sup>1</sup> = N(C<sub>6</sub>H<sub>4</sub>(OC<sub>2</sub>H<sub>5</sub>-2')(SiMe<sub>3</sub>)), a hexalithium cluster having both singly deprotonated (L<sup>1</sup>) and doubly deprotonated (L<sup>1</sup>) ligands. In L<sup>1</sup>, the proton of the phenyl substituent *ortho* to the oxygen has been removed in addition to the amine hydrogen. Deliberate attempts to prepare a pure double lithiated product by reaction of L<sup>1</sup>H with 2 equivalents of LiBu<sup>+</sup> in diethyl ether yielded two different Li<sub>2</sub>(L<sup>1</sup>) complexes depending upon the crystallisation solvent. From hexane, a hexalithium aggregate [Li<sub>2</sub>(L<sup>1</sup>)(OEt<sub>2</sub>)Li(Bu<sup>+</sup>)<sub>2</sub>] (5) was obtained. The structure of 5 showed the presence of two doubly deprotonated Li<sub>2</sub>(L<sup>1</sup>) units but, surprisingly, also incorporation of two molecules of LiBu<sup>+</sup>. Alternatively, a Li<sub>2</sub>(L<sup>1</sup>) complex free of LiBu<sup>+</sup>, [Li<sub>2</sub>(L<sup>1</sup>)(dme)]<sub>2</sub> (6) was obtained by crystallisation of the product, prepared in diethyl ether, from a hexane/dme mixture. Variable temperature solution NMR (<sup>1</sup>H, <sup>7</sup>Li) data for 4–6 indicated the occurrence of dynamic exchange processes at room temperature, but 4 and 5 have the same number of lithium environments at –90 °C as in the solid state structures.

↑ μ-η<sup>3</sup>  
↑ O', O''

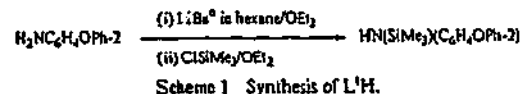
## Introduction

Lithium organoamides are of major intrinsic interest because of their structural variety, as strong bases in organic synthesis, and as precursors of organoamidometallics of other elements.<sup>1–4</sup> On transfer to lanthanoid elements, diorganoamide groups provide an alternative to cyclopentadienyls as ligands for compound stabilisation and catalysis.<sup>1,7–9</sup> Bulky chelation supported amide ligands are of particular interest as they can eliminate coordination of ancillary solvent molecules leading to six-coordination which is low for lanthanoids.<sup>10–13</sup> As a prelude to the use of lithium derivatives of the recently prepared *N*-(2-phenoxyphenyl)-*N*-(trimethylsilyl)amine<sup>14</sup> in metathesis reactions, we have studied the lithiation of this compound and discovered a rich synthetic and structural chemistry, which is now reported.

## Results and discussion

### Syntheses and crystal structures

*N*-(2-Phenoxyphenyl)-*N*-(trimethylsilyl)amine (L<sup>1</sup>H), obtained by reaction of LiNH(C<sub>6</sub>H<sub>4</sub>OPh-2) with ClSiMe<sub>3</sub> in diethyl ether (Scheme 1), is a colourless, moisture sensitive, low melting solid, which has been characterised by elemental analyses, IR and <sup>1</sup>H NMR spectroscopy.<sup>14</sup> Subsequently, single crystals have been obtained and the crystal structure determined (see ESI†).



Delocalisation of the nitrogen lone pair into the aromatic ring is indicated by the partial double bond character of the N–C bonds (1.389(2) Å) and is consistent with the near planar environment (Σ(°) 357°) of the nitrogen atom. The diaryl ether moiety has the phenyl substituent bent away from the arene backbone plane (torsion angle C(3)–C(2)–O(1)–C(11) 78.5°) and rotated near perpendicular to it (interplanar angle 76.64(4)°).

Lithium derivatives of L<sup>1</sup>H are readily prepared by reaction of a slight excess of LiBu<sup>+</sup> in hexane with L<sup>1</sup>H in tetrahydrofuran (thf), 1,2-dimethoxyethane (dme), or hexane yielding [Li(L<sup>1</sup>)(thf)]<sub>n</sub> (1), [Li(L<sup>1</sup>)(dme)]<sub>2</sub> (2) and [Li(L<sup>1</sup>)]<sub>n</sub> (3) respectively (Scheme 2), in high yield (>80%). The compositions of the colourless, crystalline products were established by elemental analyses (C, H, N). For 1 and 2, a 1 : 1 ratio of coordinated thf or dme to the L<sup>1</sup> ligand, distinct <sup>1</sup>H NMR resonances for each of the backbone aromatic protons (H3–H6) and a typical phenyl pattern were evident in the room temperature <sup>1</sup>H NMR spectra for C<sub>7</sub>D<sub>8</sub> solutions. In contrast, the room temperature <sup>1</sup>H NMR spectrum of 3 was poorly resolved, but at –90 °C, two unique ligand (L<sup>1</sup>) environments at a ratio of ca. 1 : 3 were detected (see Experimental). The <sup>7</sup>Li NMR spectra of 1 and 2 in C<sub>7</sub>D<sub>8</sub> solution showed narrow (Δν<sub>1/2</sub> 10–30 Hz) single peaks at 1.68 and 1.43 ppm, respectively, consistent with the single Li environment in the structure of 2 (see below). For 3, the comparable <sup>7</sup>Li resonance (1.65 ppm) is somewhat broader (Δν<sub>1/2</sub> 50

† Electronic supplementary information (ESI) available: Table of selected bond distances and angles for L<sup>1</sup>H. See <http://www.rsc.org/suppdata/dt/b1/b103642b/>

Hz) but is resolved into two broad peaks at 0 °C and three sharp resonances at -90 °C (Fig. 1). The NMR behaviour of solutions

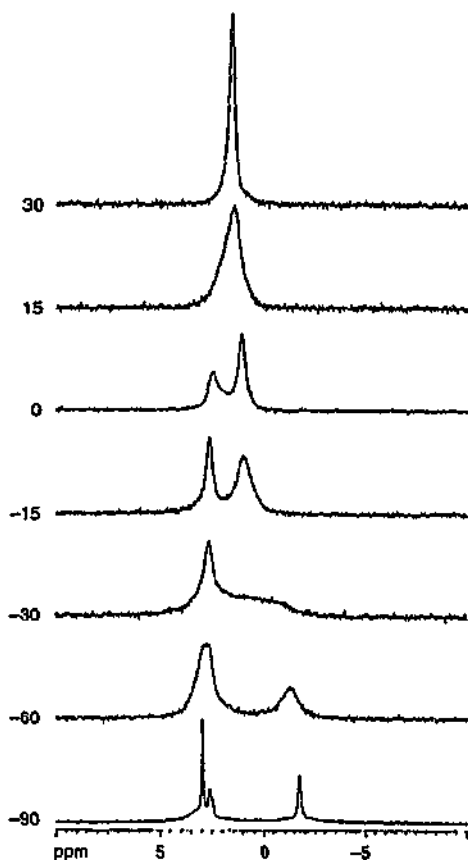


Fig. 1  $^7\text{Li}$  NMR spectra of  $[\text{Li}(\text{L}^1)]_n$  in  $\text{C}_6\text{H}_6$  at 30 to  $-90^\circ\text{C}$ .

of 2 is typical of the presence of rapidly exchanging species at room temperature and of one or more aggregates with different

Li environments at  $-90^\circ\text{C}$  (see below). Comparable data for the recently prepared  $[\text{LiNPh}(\text{SiMe}_3)]_n$  showed two  $^7\text{Li}$  resonances (0.9 and  $-4.6$  ppm) at  $-110^\circ\text{C}$ , the low frequency peak being assigned to a terminal Li nucleus with an intramolecular  $\eta^6$ - $\pi$ -phenyl interaction.<sup>15</sup>

The molecular structure of 2 (Fig. 2) shows a monomeric

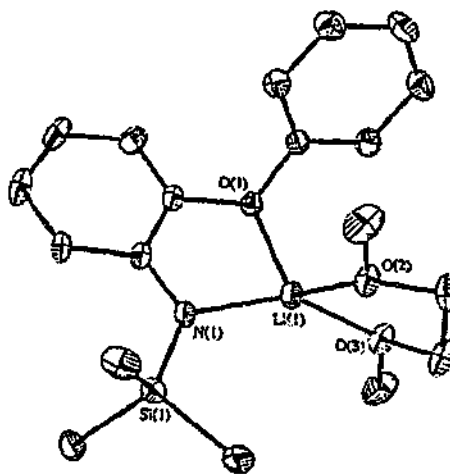


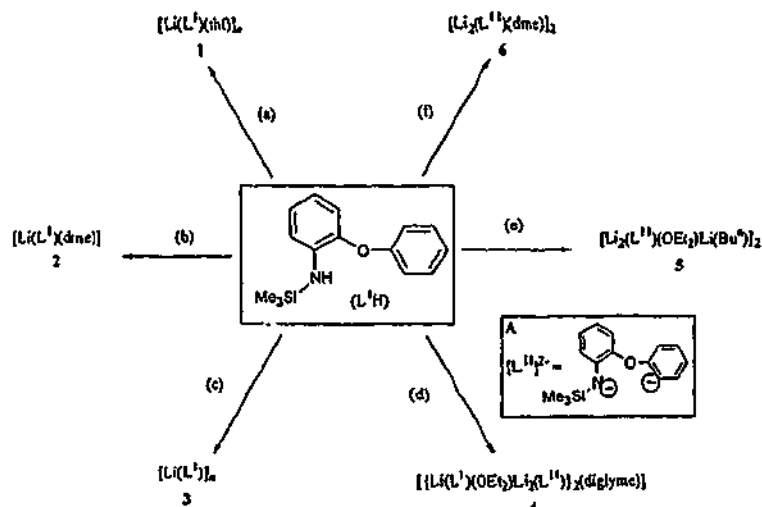
Fig. 2 The molecular structure of  $[\text{Li}(\text{L}^1)(\text{dme})]_2$ .

complex with lithium surrounded by chelating  $\text{L}^1$  and dme ligands in a highly distorted tetrahedral arrangement (Table 1).

Table 1 The lithium environment in  $[\text{Li}(\text{L}^1)(\text{dme})]_2$

$\text{Li}(1)-\text{N}(1)$	1.930(3)	$\text{N}(1)-\text{Li}(1)-\text{O}(2)$	117.2(1)
$\text{Li}(1)-\text{O}(2)$	1.963(3)	$\text{N}(1)-\text{Li}(1)-\text{O}(3)$	144.2(2)
$\text{Li}(1)-\text{O}(3)$	1.986(3)	$\text{O}(2)-\text{Li}(1)-\text{O}(3)$	83.4(1)
$\text{Li}(1)-\text{O}(1)$	2.062(3)	$\text{N}(1)-\text{Li}(1)-\text{O}(1)$	85.2(1)
		$\text{O}(2)-\text{Li}(1)-\text{O}(1)$	119.6(1)
		$\text{O}(3)-\text{Li}(1)-\text{O}(1)$	111.0(1)

The irregular geometry is presumably due to the narrow bite angles of the  $\text{L}^1$  ( $85.2(1)^\circ$ ) and dme ( $83.4(1)^\circ$ ) ligands and to repulsion between the bulky  $\text{SiMe}_3$  and  $\text{OPh}$  substituents. The Li-N distance (Table 1) is marginally smaller than that of



Scheme 2 Reagents and conditions: (a)  $\text{L}^1\text{H}$ ,  $\text{LiBu}^+$  (1.6 M in hexane) (1 : 1 or 1 : 2), thf; (b)  $\text{L}^1\text{H}$ ,  $\text{LiBu}^+$  (1.6 M in hexane) (1 : 1 or 1 : 2), dme; (c)  $\text{L}^1\text{H}$ ,  $\text{LiBu}^+$  (1.6 M in hexane) (1 : 1 or 1 : 2), hexane; (d)  $\text{L}^1\text{H}$ ,  $\text{LiBu}^+$  (1.6 M in hexane) (1 : 1.1),  $\text{Et}_3\text{O}$ , ii) diglyme (trace) hexane; (e)  $\text{L}^1\text{H}$ ,  $\text{LiBu}^+$  (1.6 M in hexane) (1 : 2),  $\text{Et}_3\text{O}$ , ii) hexane; (f) i) as for (e), ii) hexane, dme.

monomeric and four-coordinate  $[\text{Li}(\text{N}(\text{SiMe}_3)_2)(\text{pmdeta})]$  (pmdeta = *N,N,N',N',N'*-pentamethyldiethylenetriamine) ( $\text{Li}-\text{N}(\text{amide})$  1.988(6) Å).<sup>14</sup> The  $\text{Li}-\text{O}(\text{OPh})$  bond length in 2 is significantly longer than  $\text{Li}-\text{O}(\text{dme})$  owing to the bulkiness and the electron withdrawing character of the aryl groups. The relative disposition of the two arene rings is similar to that of  $\text{L}^1\text{H}$  (torsion angle  $\text{C}(3)-\text{C}(2)-\text{O}(1)-\text{C}(1)$  55.5°; interplanar angle 67.6(5)°). Possible structures for 1 are a three-coordinate monomer (Fig. 3a) or a four-coordinate dimer (Fig. 3b). A

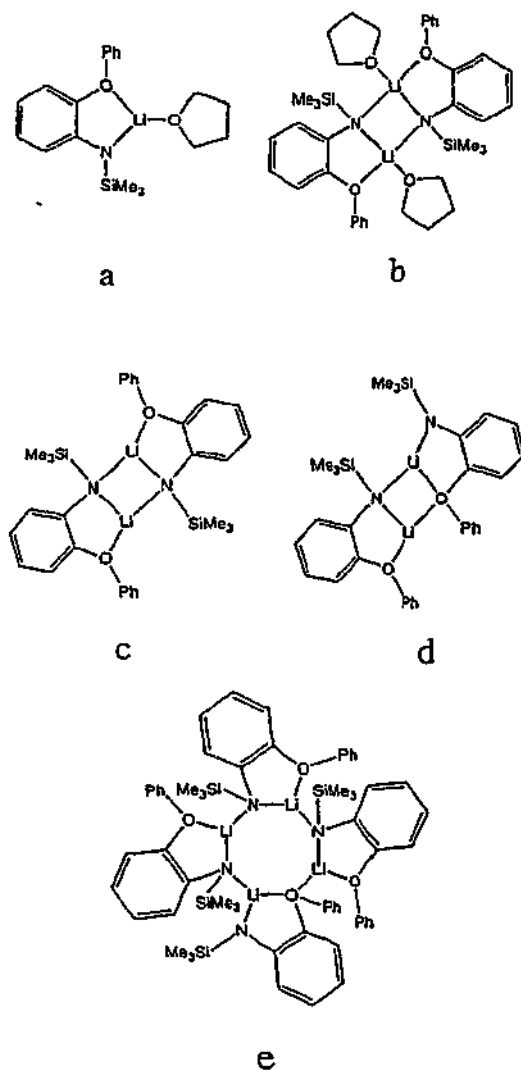


Fig. 3 Possible structures of 1 (a, b) and 3 (c-e).

dimeric  $[\text{Li}(\text{L}(\text{S}))_2]$  arrangement has precedents for Li complexes of bidentate amides, e.g.  $\text{L} = 8$ -quinolinyl(trimethylsilyl)amide,  $\text{S} = \text{OEt}_2$ ,<sup>17</sup> but more sterically hindered systems display an unsymmetrical dinuclear  $[\text{Li}(\text{L})_2\text{Li}(\text{OEt}_2)]$  structure e.g.  $\text{L} = \text{N,N}$ -dimethyl-*N'*-trimethylsilyl ethane-1,2-diamine.<sup>10</sup> Given the bulky diaryl ether moiety present in  $\text{L}^1$ , a dimeric structure would seem less probable than the monomer.

The structure of 3 is, reasonably, at least dimeric (Fig. 3c or d). The related complex  $[\text{Li}(\text{L})_2]$  ( $\text{L} = 8$ -quinolinyl(trimethylsilyl)amide) is a symmetrical dimer with three-coordinate Li centres bridged by two amido nitrogen atoms.<sup>17</sup> However, this

arrangement has only a single Li environment in contrast to the three suggested by the low temperature NMR spectrum of 3 (Fig. 1). A mixture of the two possible dimeric structures (Fig. 3c and d) would show three Li environments (one from the symmetrical dimer 'c' and two from the unsymmetrical dimer 'd'). A higher aggregate is also possible and a tetramer (Fig. 3e) derived from combining 'c' and 'd' would approximate the number of Li and  $\text{L}^1$  environments suggested by the NMR spectra. A tetranuclear structure was recently observed for unsolvated  $[\text{LiNPh}(\text{SiMe}_3)]_4$ .<sup>18</sup>

In an attempt to generate a crystalline lithium salt of  $\text{L}^1$  without co-ligands,  $\text{L}^1\text{H}$  was reacted with an excess of  $\text{LiBu}^n$  in diethyl ether (Scheme 2). Work up of the product in hexane that contained a trace of adventitious bis(2-methoxyethyl) ether (diglyme) gave a very low yield of colourless crystals which were subsequently shown to be the novel lithium aggregate  $\{[\text{Li}(\text{L}^1)(\text{OEt}_2)\text{Li}_2(\text{L}^1)]_2(\text{diglyme})\}$  (4) ( $\text{L}^1 = \text{N}(\text{C}_6\text{H}_4(\text{OC}_2\text{H}_5)_2)_2(\text{SiMe}_3)$ ), by X-ray crystallography (Fig. 4). There are two trillithium units, one comprising the asymmetric unit. Each contains the expected  $\text{Li}(\text{L}^1)(\text{OEt}_2)$  moiety but, remarkably, each is bridging to an  $\text{Li}_2(\text{L}^1)$  fragment with a doubly deprotonated ligand ( $\text{L}^{11}$ ) (A, Scheme 2). The two  $\text{Li}(\text{L}^1)(\text{OEt}_2)\text{Li}_2(\text{L}^1)$  units are linked by a diglyme, coordinated by two oxygen atoms to one lithium ( $\text{Li}(3)$ ) and by one oxygen to the corresponding lithium atom ( $\text{Li}(3\text{A})$ ) of the neighbouring, symmetry generated, trillithium unit. The diglyme is disordered over the symmetry site with the ligation to the two lithium atoms ( $\text{Li}(3)$  and  $\text{Li}(3\text{A})$ ) reversed in the other component of the disorder. The lithium atom  $\text{Li}(1)$  of the  $\text{Li}(\text{L}^1)(\text{OEt}_2)$  fragment is four-coordinate and is terminally bound by the  $\text{Et}_2\text{O}$  and  $\text{L}^1$  oxygen atoms and bridges to  $\text{Li}(2)$  through the amide nitrogen ( $\text{N}(1)$ ) of  $\text{L}^1$  and the phenoxy oxygen ( $\text{O}(2)$ ) of  $\text{L}^{11}$ . A diaryl ether bridging two lithium centres has previously been observed only once in lithium organoamides<sup>19</sup> and, as in 4, was supported by further donor groups located on the aryl ether unit. Four-coordinate of the central lithium atom  $\text{Li}(2)$  is completed by the amide nitrogen,  $\text{N}(2)$ , and the *ortho* carbon  $\text{C}(212)$  of the phenoxy substituent of the  $\text{L}^{11}$  ligand. Both  $\text{N}(2)$  and  $\text{C}(212)$  also bridge to  $\text{Li}(3)$ . The disordered diglyme coordinates to  $\text{Li}(3)$  which is thus four- and three-coordinate in the respective disordered components. The  $\text{Li}-\text{N}$  distances in 4 (Table 2) are

Table 2 The lithium environments in  $\{[\text{Li}(\text{L}^1)(\text{OEt}_2)\text{Li}_2(\text{L}^{11})]_2(\text{diglyme})\}$  (4)

$\text{Li}(1)-\text{O}(1)$	1.980(5)	$\text{O}(1)-\text{Li}(1)-\text{O}(3)$	106.1(2)
$\text{Li}(1)-\text{O}(3)$	1.979(5)	$\text{O}(1)-\text{Li}(1)-\text{N}(1)$	83.5(2)
$\text{Li}(1)-\text{N}(1)$	2.009(5)	$\text{O}(3)-\text{Li}(1)-\text{N}(1)$	139.4(3)
$\text{Li}(1)-\text{O}(2)$	2.033(5)	$\text{O}(1)-\text{Li}(1)-\text{O}(2)$	108.0(2)
		$\text{O}(3)-\text{Li}(1)-\text{O}(2)$	112.7(2)
		$\text{N}(1)-\text{Li}(1)-\text{O}(2)$	100.8(2)
$\text{Li}(2)-\text{N}(1)$	2.073(5)	$\text{N}(1)-\text{Li}(2)-\text{N}(2)$	139.7(2)
$\text{Li}(2)-\text{N}(2)$	2.020(5)	$\text{N}(1)-\text{Li}(2)-\text{O}(2)$	96.2(2)
$\text{Li}(2)-\text{O}(2)$	2.110(5)	$\text{N}(1)-\text{Li}(2)-\text{C}(212)$	120.3(2)
$\text{Li}(2)-\text{C}(212)$	2.254(5)	$\text{N}(2)-\text{Li}(2)-\text{O}(2)$	86.4(2)
$\text{Li}(2)-\text{C}(211)$	2.509(5)	$\text{N}(2)-\text{Li}(2)-\text{C}(212)$	97.9(2)
		$\text{O}(2)-\text{Li}(2)-\text{C}(212)$	67.4(2)
$\text{Li}(3)-\text{N}(2)$	2.060(6)	$\text{N}(2)-\text{Li}(3)-\text{C}(212)$	100.6(2)
$\text{Li}(3)-\text{C}(212)$	2.133(6)	$\text{N}(2)-\text{Li}(3)-\text{O}(51)$	121.7(3)
$\text{Li}(3)-\text{O}(51)$	2.032(7)	$\text{N}(2)-\text{Li}(3)-\text{O}(53)$	121.6(3)
$\text{Li}(3)-\text{O}(52)$	1.835(7)	$\text{C}(212)-\text{Li}(3)-\text{O}(51)$	117.9(3)
$\text{Li}(3)-\text{O}(53)$	2.181(7)	$\text{C}(212)-\text{Li}(3)-\text{O}(53)$	116.7(3)
		$\text{O}(51)-\text{Li}(3)-\text{O}(53)$	79.2(2)
		$\text{N}(2)-\text{Li}(3)-\text{O}(52)$	123.9(3)
		$\text{C}(212)-\text{Li}(3)-\text{O}(52)$	133.3(3)

longer than the corresponding terminal distance in 2 above, as expected for bridging atoms, and are comparable with the  $\text{Li}-\text{N}_w$  bond length in  $[\text{Li}(\text{N}(\text{SiMe}_3)_2)(\text{OEt}_2)_2]$  (2.055(5) Å).<sup>20,21</sup> The terminal  $\text{Li}(1)-\text{O}$  distances in 4 (to  $\text{OAr}_2$ ,  $\text{OEt}_2$ ) are virtually identical, whilst the bonding of the diglyme to  $\text{Li}(3)/\text{Li}(3\text{A})$

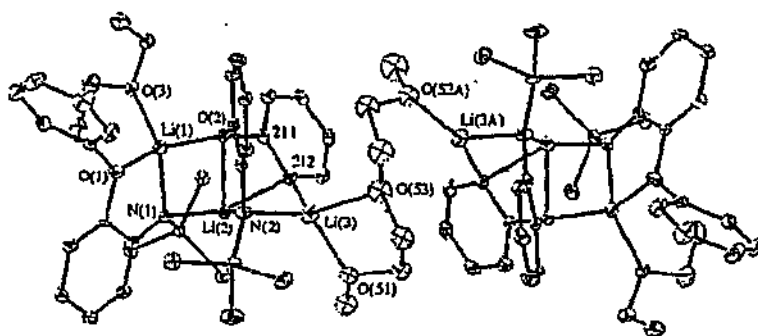


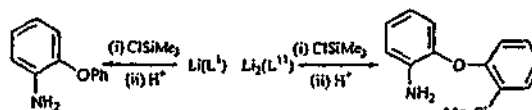
Fig. 4 The molecular structure of  $[(\text{Li}(\text{L}^1)(\text{OEt}_2)\text{Li}_2(\text{L}^1))_2(\text{diglyme})]_4$ .

is highly unsymmetrical (Table 2) due to the presence of both four- and three-coordinate lithium atoms. Not only is the terminal  $\text{Li}(1)-\text{O}(1)(\text{OAr}_2)$  bond (Table 2) shorter than the bridging  $\text{Li}-\text{O}(2)(\text{OAr}_2)$  distances, it is also shorter (by 0.08 Å) than the corresponding bond length in 2 (Table 1), possibly owing to weaker binding of the bridging amide nitrogen in 4 than the terminal nitrogen of 2. A major feature of the structure of 4 is the presence of the  $\text{Li}_2(\mu-\eta^1: \eta^1\text{-Ph})$  unit resulting from deprotonation of the phenoxy substituent in  $\text{L}^1$  (Scheme 2). The  $\text{Li}-\text{C}(212)$  bonds are not equivalent. The shorter,  $\text{Li}(3)-\text{C}(212)$ , is comparable with  $\text{Li}-\text{C}$  bond lengths previously reported for  $[\text{Li}(\mu-\eta^1: \eta^1\text{-Ar})_2]$  ( $\text{Ar} = \text{C}_6\text{H}_3(\text{OBu}^t)_2, 2.6$  2.139(5)–2.160(6) Å)<sup>22</sup> whilst the longer,  $\text{Li}(2)-\text{C}(212)$ , is in the range for dimeric  $[\text{Li}(\mu-\eta^1: \eta^1\text{-Ar})_2]$  ( $\text{Ar} = \text{C}_6\text{H}_3(\text{CH}(\text{Me})\text{NMe}_2)_2, 2.6$  2.21(1)–2.26(2) Å).<sup>22</sup> Severe distortion of the  $\text{Li}(2)$  coordination geometry from tetrahedral, as evidenced by the narrow  $\text{O}(2)-\text{Li}(2)-\text{C}(212)$  angle (Table 2), results from attachment of the nitrogen, oxygen and *ortho*-carbon from the  $\text{L}^1$  ligand to the same lithium atom. To accommodate this configuration, the phenyl ring of the  $\text{L}^1$  ligand is pulled further out from the plane of the arene backbone (torsion angle  $\text{C}(23)-\text{C}(22)-\text{O}(21)-\text{C}(211)$  89.7°; interplanar angle 53.04(9)°) than in  $\text{L}^1\text{H}$  (see above). In contrast, the  $\text{L}^1$  ligand in 4 has the phenoxy group in line with the backbone (torsion angle  $\text{C}(3)-\text{C}(2)-\text{O}(1)-\text{C}(11) -2.8^\circ$ ) but the ring plane is rotated by 84.18(9)°. As a result of  $\text{O}(2), \text{C}(212)$  chelation of the phenoxy ring to  $\text{Li}(2)$ , the *ipso* carbon  $\text{C}(211)$  is close (2.509(5) Å) to  $\text{Li}(2)$ , but is probably not bonding.

An attempted deliberate preparation of a lithium derivative of the  $\text{L}^1$  ligand by reaction of 2 equivalents of  $\text{LiBu}^t$  in hexane with  $\text{L}^1\text{H}$  in diethyl ether, followed by work up in hexane (free of donor impurities) generated a low yield of  $[\text{Li}_2(\text{L}^1)(\text{OEt}_2)\text{Li}(\text{Bu}^t)]_2$  (5) (Scheme 2), with the desired  $\text{Li}_2(\text{L}^1)$  unit unexpectedly accompanied by a molecule of  $\text{LiBu}^t$ . Repeating this preparation followed by crystallisation from hexane containing a little *dme* eliminated residual  $\text{LiBu}^t$  and gave pure  $[\text{Li}_2(\text{L}^1)(\text{dme})]_2$  (6) in moderate yield (Scheme 2). Both 5 and 6 gave satisfactory elemental analyses and their compositions were further confirmed by single crystal X-ray studies (see below). The incorporation of organolithium reagents in the structures of lithiated products is novel and unusual but has occasionally been observed previously, the most closely related system being formation of  $[(\text{Ph}_2\text{NLi})(\text{Ph}(\text{C}_6\text{H}_4\text{Li})\text{NLi})_2(\text{LiBu}^t)_2(\text{Et}_2\text{O})_4]$ , on lithiation of diphenylamine.<sup>24</sup>

In contrast to the preparations of  $\text{Li}_2(\text{L}^1)$  complexes in diethyl ether, reaction of two equivalents of  $\text{LiBu}^t$  with  $\text{L}^1\text{H}$  in either the more polar *thf* or *dme* or in the less polar hexane gave only complexes of the mono-deprotonated ligand, 1–3. The presence of solely the  $\text{L}^1$  ligand in the sample of 3 from the  $\text{L}^1\text{H}/\text{LiBu}^t$  (mole ratio 1 : 2) reaction in hexane was proven by treatment of the product with  $\text{ClSiMe}_3$ , followed by hydrolysis. Only  $\text{H}_2\text{N}(\text{C}_6\text{H}_4\text{OPh}-2)$ , derived from  $\text{L}^1$ , and no

$\text{H}_2\text{N}(\text{C}_6\text{H}_4(\text{OC}_6\text{H}_4\text{SiMe}_2-2')-2)$ , the product expected<sup>24,26</sup> from  $\text{L}^1$ , was detected (Scheme 3).



Scheme 3 Hydrolysis outcomes for  $\text{Li}(\text{L}^1)$  and  $\text{Li}_2(\text{L}^1)$ .

The structure of 5 (Fig. 5) shows a hexalithium aggregate

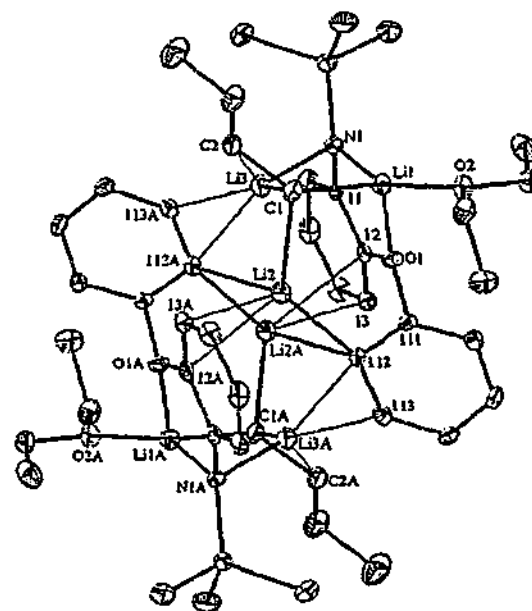


Fig. 5 The molecular structure of  $[\text{Li}_2(\text{L}^1)(\text{OEt}_2)\text{Li}(\text{Bu}^t)]_2$ , 5.

derived from two  $\text{Li}_2(\text{L}^1)(\text{OEt}_2)$  units and two molecules of  $\text{LiBu}^t$ . A distinctive feature of the structure is the central organolithium array (comprising  $\text{Li}(3), \text{C}(1), \text{Li}(2), \text{C}(112), \text{C}(112A), \text{Li}(2A), \text{C}(1A)$  and  $\text{Li}(3A)$ ) which is sandwiched between two organoamidolithium units. The overall core can be described as an 'S' shaped ladder of  $\text{Li}, \text{N}$  and  $\text{C}$  atoms (Fig. 6) and the central  $\text{Li}_2\text{C}_2$  unit is situated on a crystallographic inversion centre.

There are three unique lithium atoms, with four-coordinate  $\text{Li}(1)$  surrounded by the phenoxy and diethyl ether oxygen atoms ( $\text{O}(1)$  and  $\text{O}(2)$ ), the amide nitrogen atom ( $\text{N}(1)$ ) and the  $\alpha$ -carbon atom ( $\text{C}(1)$ ) of the  $\text{Bu}^t$  group in an approximately tetrahedral geometry. The amide nitrogen is bridging to  $\text{Li}(3)$

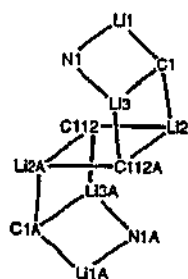


Fig. 6 The S-shaped ladder in 5.

whilst the  $\alpha$ -carbon atom C(1) bridges all three lithium atoms. Surprisingly, the second lithium atom, Li(2), is coordinated solely by carbon atoms (Fig. 5) with the shortest interactions being to the  $\alpha$ -carbon atom of the Bu<sup>o</sup> group and the *ortho* carbon atom (C(112)) of L<sup>11</sup>. The phenyl carbon C(112) and its symmetry equivalent C(112A) are bridging between Li(2) and Li(2A) (Fig. 5), as in 4 above, but in 5 the bridging is highly unsymmetrical. The Li(2)–C(112) distance (Table 3) is similar

Table 3 The lithium environments in [Li<sub>2</sub>(L<sup>11</sup>)(OEt<sub>2</sub>)Li(Bu<sup>o</sup>)]<sub>2</sub> (5)

Li(1)–O(1)	1.948(4)	O(1)–Li(1)–O(2)	102.7(2)
Li(1)–O(2)	1.973(4)	O(1)–Li(1)–N(1)	82.8(1)
Li(1)–N(1)	2.057(4)	O(2)–Li(1)–N(1)	147.5(2)
Li(1)–C(1)	2.350(4)	O(1)–Li(1)–C(1)	116.1(2)
		O(2)–Li(1)–C(1)	105.3(2)
		N(1)–Li(1)–C(1)	100.5(2)
Li(2)–C(112)	2.189(4)	C(112)–Li(2)–C(112A) <sup>a</sup>	109.8(2)
Li(2)–C(112A) <sup>a</sup>	2.660(4)	C(1)–Li(2)–C(112)	128.9(2)
Li(2)–C(1)	2.226(4)	C(1)–Li(2)–C(112A) <sup>a</sup>	97.1(2)
Li(2)–C(12A) <sup>a</sup>	2.596(4)	C(112)–Li(2)–C(1C) <sup>a</sup>	115.7(5)
Li(2)–C(13A) <sup>a</sup>	2.583(4)	C(112A)–Li(2)–C(1C) <sup>a</sup>	79.9(5)
		C(1)–Li(2)–C(1C) <sup>a</sup>	111.1(5)
Li(3)–N(1)	2.016(4)	N(1)–Li(3)–C(1)	109.3(2)
Li(3)–C(1)	2.143(4)	N(1)–Li(3)–C(11C) <sup>a</sup>	121.8(5)
Li(3)–C(2)	2.419(4)	C(1)–Li(3)–C(11C) <sup>a</sup>	127.1(5)
Li(3)–C(112A) <sup>a</sup>	2.241(4)		
Li(3)–C(113A) <sup>a</sup>	2.304(4)		

Symmetry transformations used to generate equivalent atoms: <sup>a</sup>–x, –y + 1, –z. <sup>b</sup>C(1C) = centre of C(12A) and C(13A). <sup>c</sup>C(11C) = centre of C(112A) and C(113A).

to those of 4 (Table 2), but Li(2)–C(112A) (Table 3) is exceptionally long for an Li–C  $\sigma$ -bond<sup>23</sup> and it even approaches the longer extreme of the range of neutral  $\pi$ -arene–Li interactions (see below).<sup>27–29</sup> Supporting the two primary C(1) and C(112) bonds to Li(2), there are also longer, similar length Li(2)–C interactions with the two of the carbon atoms C(12A) and C(13A) from the symmetry generated L<sup>11</sup> ligand (L<sup>11</sup>A) (Table 3). Ligand is best described as a neutral  $\pi$ - $\eta^2$ -arene–Li interaction since Li(2) is side on to the C(12A)–C(13A) bond (the angle defined by Li(2)–centre of the C(12A) and C(13A) bond–centre of the arene ring (C(11A)–C(15A)) is 98.7°). The Li(2)–C(12A, 13A) lengths are in the range (2.28–2.77 Å) for this type of bonding,<sup>27–29</sup> and are shorter than Li(2)–C(112A).

The remaining lithium atom Li(3) is coordinated by the bridging amide nitrogen and the  $\alpha$ -carbon atom of the Bu<sup>o</sup> group. The amide bridge to Li(1) and Li(3) has near equivalent Li–N distances but Li(3)–C(1) is 0.207 Å shorter than Li(1)–C(1) (Table 3). As with Li(2) above, Li(3) further interacts with two arene carbon atoms (C(112A) and C(113A)), in this case from the phenyl substituent of L<sup>11</sup>A. Thus C(112) and C(112A) each bridge three lithium atoms (Fig. 5). The Li(3)–C(112A)/C(113A) bond lengths are considerably shorter than  $\pi$ -bonded Li(2)–C(112A)/C(113A) (Table 3) and are close to the  $\sigma$ -bonded Li(2)–C(1) and Li(1)–C(1) distances. Significant  $\sigma$ -bond char-

acter in the Li(3)–C(112A)/C(113A) bonding may also be indicated by the Li(3)–centre C(112A)–C(113A) bond–centre of the phenyl ring (C(111A)–C(116A)) angle (131.9°) which is much larger than the expected 90° for a  $\pi$ -phenyl–Li interaction. A possible Li(3)–C(2) ( $\beta$ -C of the butyl chain) interaction (Table 3) is longer than in the parent [Li(Bu<sup>o</sup>)<sub>2</sub>(Li- $\beta$ -C 2.287 Å)<sup>24</sup> but is presumably shorter than in the related aggregate [(Ph<sub>2</sub>N–Li)(Ph(C<sub>6</sub>H<sub>4</sub>Li)NLi)<sub>2</sub>(LiBu<sup>o</sup>)<sub>2</sub>(OEt<sub>2</sub>)<sub>2</sub>]<sub>2</sub><sup>24</sup> for which no Li- $\beta$ -C interaction was suggested. Whilst 5 and [Li(Bu<sup>o</sup>)<sub>2</sub>]<sub>2</sub> both have a  $\mu$ - $\alpha$ -C arrangement, the parent has two shorter (2.137(3)–2.175(3) Å) and one longer Li- $\alpha$ -C distances (2.727(3)–2.262(3) Å), whereas 5 has one in each of these ranges as well as one much longer.

Despite problems with the data collection for 6 (see Experimental), sufficient data were obtained to establish unambiguously the atom connectivity of the complex (Fig. 7), which was the ultimate synthetic target. Thus, 6 consists of a [Li<sub>2</sub>(L<sup>11</sup>)(dme)]<sub>2</sub> dimer with the Li<sub>2</sub>(L<sup>11</sup>)<sub>2</sub> unit capped at each end by a chelated dme. The core consists of a four-rung ladder of Li, N, and C atoms. The dme ligand chelates to Li(1) and L<sup>11</sup> binds in a tridentate manner (N, O, C) to Li(2), whilst the amide nitrogen is bridging between Li(2) and Li(1). The deprotonated phenyl substituents bridge three lithium atoms Li(1), Li(2) and Li(3) through C(112) and three Li(2), Li(3) and Li(4) through C(212). Thus each lithium atom is four-coordinate, consistent with coordinative saturation resulting from the presence of the strongly basic dme. Within the errors of the structure determination, the bond distances and lithium geometries (Table 4) are

Table 4 Selected bond distances and angles for [Li<sub>2</sub>(L<sup>11</sup>)(dme)]<sub>2</sub> (6)<sup>a</sup>

Li(1)–N(1)	2.04(1)	N(1)–Li(1)–C(112)	103.0(7)
Li(1)–C(112)	2.25(1)	N(1)–Li(1)–O(31)	115.0(5)
Li(1)–O(31)	1.96(1)	N(1)–Li(1)–O(32)	131.0(6)
Li(1)–O(32)	1.98(2)	C(112)–Li(1)–O(31)	114.7(5)
Li(2)–N(1)	2.01(1)	C(112)–Li(1)–O(32)	109.3(5)
Li(2)–O(1)	2.015(9)	O(31)–Li(1)–O(32)	83.7(6)
Li(2)–C(112)	2.30(1)	N(1)–Li(2)–O(1)	86.9(4)
Li(2)–C(212)	2.18(1)	N(1)–Li(2)–C(112)	102.3(5)
		N(1)–Li(2)–C(212)	130.0(5)
		O(1)–Li(2)–C(112)	67.7(3)
		O(1)–Li(2)–C(212)	139.5(7)
		C(112)–Li(2)–C(212)	111.3(4)

<sup>a</sup>For one of the independent molecules only (data for the remaining molecules are similar and are listed in the deposited CIF data. See <http://www.rsc.org/suppdata/dub1/b103642b/>

unexceptional. Furthermore, the tridentate L<sup>11</sup> ligands display similar features to those of the L<sup>11</sup> ligand in 4 (above), in contrast to 5, with severe bending of the phenoxy substituent out of the plane of the arene backbone (torsion angles C(X3)–C(X2)–O(X)–C(X1) (X = 1, 2, 5, 6, 9) 93.7–98.4°; interplanar angles 58.2(2)–65.3(2), *cf.* –18.5/88.51(6) for 5) as a result of *ortho* carbon/oxygen bonding with the same lithium atom.

#### Solution NMR studies of 4–6

Room temperature solution NMR (<sup>1</sup>H, <sup>7</sup>Li) data obtained for 4–6 in toluene-*d*<sub>6</sub> clearly indicated the occurrence of dynamic exchange phenomena. A single <sup>7</sup>Li resonance was observed for all, despite several unique lithium environments in the solid-state structures. Although the room temperature <sup>1</sup>H NMR spectrum of 4 exhibited many broad features, two distinct SiMe<sub>3</sub> resonances were observed, one from each of the amide ligands, L<sup>1</sup> and L<sup>11</sup>. Cooling to –90 °C produced only a limited increase in resolution of the <sup>1</sup>H NMR spectrum, but the <sup>7</sup>Li resonance resolved into four separate peaks (see Experimental), consistent with the four unique lithium atoms observed in the

<sup>†</sup> These numbers refer to the unique torsion angles derived from the 2.5 dimers which comprise the asymmetric unit of the structure of 6.



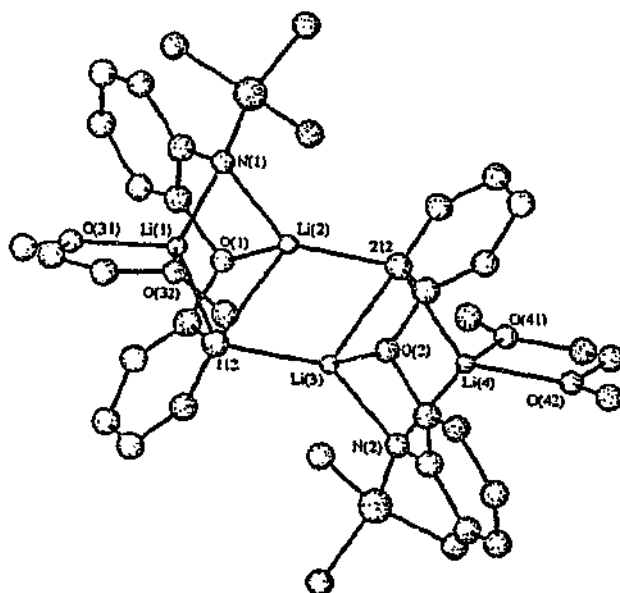


Fig. 7 The molecular structure of  $[\text{Li}(\text{L}'')(\text{dme})]_2$ , 6.

solid state structure of 4 (Fig. 4). For the butyllithium cluster 5, the room temperature  $^1\text{H}$  spectrum was broadened but at  $-90^\circ\text{C}$  was well resolved showing a single set of  $\text{L}'$  resonances in line with one type of  $\text{L}'$  ligand in the solid state. The protons of the  $\alpha$ -C of the butyl group were evident as two broad multiplets at  $-1.16$  and  $-1.02$  ppm, close to the values observed for  $\text{LiBu}^*$ .<sup>21</sup> Whilst this is consistent with reversion of 5 into separate  $\text{Li}_2(\text{L}')$  and  $\text{LiBu}^*$  species in solution, the variable temperature  $^7\text{Li}$  NMR spectra (Fig. 8) ultimately resolved into three

peaks at  $-90^\circ\text{C}$  as expected for the three unique Li environments in the solid state structure of 5 (Fig. 5). The room temperature  $^1\text{H}$  NMR spectrum of the dme complex 6 showed the expected  $\text{L}'$  and dme resonances in a 1 : 1 ratio. Only a single  $^7\text{Li}$  NMR resonance was observed at room temperature and also at  $-90^\circ\text{C}$ . Since two distinct lithium atoms are observed in the X-ray structure (Fig. 7), these data suggest either a very rapid exchange process or accidental coincidence of the two lithium resonances.

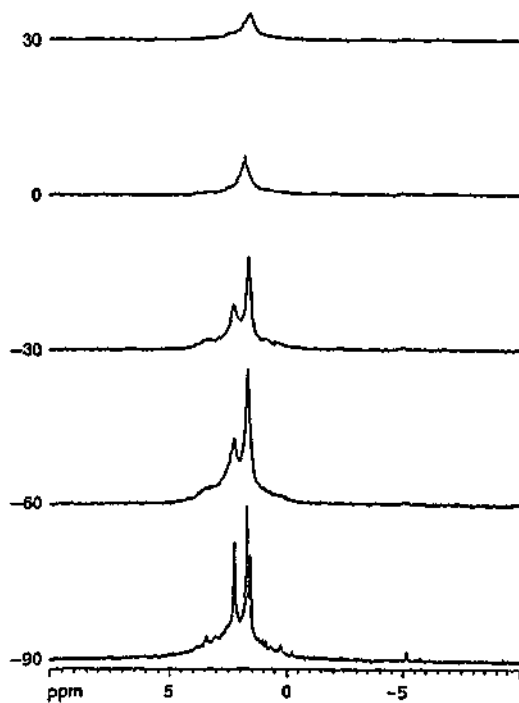


Fig. 8  $^7\text{Li}$  NMR spectra of  $[\text{Li}_2(\text{L}')(\text{OEt}_2)\text{Li}(\text{Bu}^*)]_2$  in  $\text{C}_7\text{H}_8$  at 30 to  $-90^\circ\text{C}$ .

### Conclusions

Lithiation of *N*-(2-phenoxyphenyl)-*N*-(trimethylsilyl)amine is strongly solvent dependent with both the highly polar thf and dme and the non-polar hexane giving complexes (1-3) of the monodeprotonated ligand,  $\text{L}'$ , whereas the intermediate polarity  $\text{Et}_2\text{O}$  allows formation of the doubly deprotonated  $\text{L}''$ , as in 4 and 5 (Scheme 2). However in  $\text{Et}_2\text{O}$ ,  $\text{LiBu}^*$  can compete with the solvent for coordination sites on  $\text{Li}_2\text{L}''$  giving 5. Although dme is unsuitable for the generation of  $\text{L}''$ , it removes coordinated  $\text{LiBu}^*$  from 5 enabling isolation of  $[\text{Li}_2\text{L}''(\text{dme})]_2$ , 6 in a conveniently accessible form (Scheme 2). Still greater lithium coordination versatility can be demonstrated by this system, since double deprotonation in  $\text{Et}_2\text{O}$  (now established as leading to isolation of 5) followed by addition of  $\text{LaCl}_3$  led to crystallisation of the remarkable, decalithium cage,  $[\text{La}(\text{LiOEt})(\text{OEt}_2)]_2$ , hexane with carbanion, organoamide and alkoxide functionalities.<sup>22</sup>

Full formula  $[\{\text{Li}_2(\text{L}'')\}_2(\text{LiOEt})(\text{OEt}_2)]_2$   $\downarrow (\text{L}'')$

### Experimental

- hexane  
All operations were performed under dry nitrogen using dry box and standard Schlenk techniques. Solvents were dried by distillation from sodium wire/benzophenone. IR data ( $4000$ – $650$   $\text{cm}^{-1}$ ) were recorded for Nujol mulls sandwiched between NaCl plates with a Perkin-Elmer 1600 FTIR spectrometer. NMR spectra were obtained either on a Bruker AC 200 MHz ( $^1\text{H}$ ) or a Bruker AC 400 MHz spectrometer ( $^7\text{Li}$  and  $^1\text{H}$ ) as indicated. Deuterated solvents were degassed and distilled from Na/K alloy prior to use.  $^1\text{H}$  NMR spectra were referenced to the solvent (toluene- $d_6$  ~~signals~~) signals; chemical shifts for  $^7\text{Li}$  spectra are given relative to external 0.1 M  $\text{LiCl}$  in  $\text{D}_2\text{O}$  X

Table 5 Crystal and refinement parameters\*

compound	1 <sup>†</sup>	2	4	5	6
formula	C <sub>11</sub> H <sub>10</sub> NOSi	C <sub>11</sub> H <sub>10</sub> LiNO <sub>2</sub> Si	C <sub>10</sub> H <sub>10</sub> Li <sub>2</sub> N <sub>2</sub> O <sub>2</sub> Si <sub>2</sub>	C <sub>10</sub> H <sub>10</sub> Li <sub>2</sub> N <sub>2</sub> O <sub>2</sub> Si <sub>2</sub>	C <sub>10</sub> H <sub>10</sub> Li <sub>2</sub> N <sub>2</sub> O <sub>2</sub> Si <sub>2</sub>
<i>M</i>	257.41	353.45	1347.62	810.84	718.78
crystal system	orthorhombic	monoclinic	monoclinic	monoclinic	monoclinic
space group	<i>Pbcn</i>	<i>P2<sub>1</sub>/c</i>		<i>C2/c</i>	<i>P2<sub>1</sub>/n</i>
<i>a</i> /Å	21.4777(4)	10.1225(2)	40.3040(11)	12.9117(2)	22.1749(10)
<i>b</i> /Å	7.9215(2)	12.8885(2)	10.5611(3)	11.5166(3)	14.3421(6)
<i>c</i> /Å	16.9555(2)	16.4847(3)	18.7239(3)	16.9667(5)	34.5285(11)
$\beta$ /°		107.395(1)	99.263(1)	100.243(2)	105.890(3)
<i>V</i> /Å <sup>3</sup>	2884.7(2)	2052.3(7)	7866(3)	2482.7(9)	10562(4)
<i>Z</i>	8	4	4	2 (dimers)	10 (dimers)
$\mu$ (MoK $\alpha$ )/mm <sup>-1</sup>	0.151	0.130	0.129	0.111	0.126
<i>N</i> ( <i>R</i> <sub>int</sub> )	3414 (0.058)	5063 (0.050)	9451 (0.047)	5851 (0.073)	14985 (0.069)
<i>R</i> , <i>R</i> <sub>w</sub> [ <i>I</i> > 2 $\sigma$ ( <i>I</i> )]	0.045, 0.090	0.046, 0.100	0.070, 0.139	0.056, 0.125	0.110, 0.273
<i>R</i> , <i>R</i> <sub>w</sub> (all data)	0.060, 0.095	0.082, 0.113	0.122, 0.162	0.100, 0.143	0.228, 0.343

\* Measured at 123 K.

7.01 (2H, t, <sup>1</sup>J 7.6 Hz, Ar), 7.15 (2H, dd, <sup>3</sup>J 8.0 Hz, <sup>4</sup>J 1.5 Hz, Ar); (183 K) 0.72 (18H, s, SiMe<sub>3</sub>), 2.27 (8H, s, CH<sub>2</sub>(dme)), 2.54 (12H, s, CH<sub>2</sub>(dme)), 6.55 (2H, t, <sup>3</sup>J 8.0 Hz, Ar), 6.76 (2H, t, <sup>3</sup>J 7.0 Hz, Ar), 6.86 (2H, dd, <sup>3</sup>J 7.8 Hz, <sup>4</sup>J 1.3 Hz, Ar), 6.94 (6H, m, Ar), 7.30 (2H, t, <sup>3</sup>J 8.0 Hz, Ar), 7.43 (2H, d, <sup>3</sup>J 8.0 Hz, Ar); <sup>7</sup>Li (155.51 MHz, 303 K),  $\delta$  1.42; (183 K) 1.48.

## X-Ray crystallography

Under an inert atmosphere the air and moisture sensitive crystals were covered by viscous oil and mounted onto a glass fibre. Low temperature (=123 K) data were collected on an Enraf-Nonius CCD area-detector diffractometer (Mo-K $\alpha$  radiation,  $\lambda$  0.7107 Å, frames comprised 1.0° increments in  $\phi$  and  $\omega$  yielding a sphere of data) using proprietary software (Nonius B.V., 1998). For 6, loss of crystal integrity occurred after approximately 1 h exposure of the crystal to the X-ray beam (unexposed crystals from the same batch remained intact). Consequently data were collected from several specimens and the resulting data sets combined yielding an adequate but still limited amount of data. Each data set was merged (*R*<sub>int</sub> as quoted) to *N* unique reflections and the structures were solved by conventional methods and refined with anisotropic thermal parameter forms for the non-hydrogen atoms by full matrix least-squares on all *F*<sup>2</sup> data using the SHELX97 software package.<sup>21</sup> Hydrogen atoms were included in calculated positions and allowed to ride on the parent carbon atom with isotropic thermal parameters. Crystal and refinement details for each compound are listed in Table 5.

CCDC reference numbers 163622–163626.

See <http://www.rsc.org/suppdata/dub1/b103642b/> for crystallographic data in CIF or other electronic format.

## Acknowledgements

We are grateful to the Australian Research Council for support and for an Australian Postgraduate Award to N.M.S., and to Dr P. C. Andrews for helpful discussions.

## References

- M. F. Lappert, P. P. Power, A. R. Sanger and R. C. Srivastava, *Metal and Metalloid Arildes*, Ellis Horwood, Chichester, 1980.
- A. M. Sapsa and P. v. R. Schleyer, *Lithium Chemistry: A Theoretical and Experimental Overview*, Wiley-Interscience, New York, 1995.
- M. Gray, M. Tinkl and V. Snieckus in *Comprehensive Organometallic Chemistry*, ed. E. W. Abel, F. G. A. Stone and G. Wilkinson, Pergamon, Oxford, 2nd edn., 1995, vol. 11, ch. 1, p. 1.
- K. Gregov, P. v. R. Schleyer and R. Snaith, *Adv. Inorg. Chem.*, 1991, 37, 47.
- R. E. Mulvey, *Chem. Soc. Rev.*, 1991, 20, 176.
- D. S. Wright and M. A. Beswick, in *Comprehensive Organometallic Chemistry*, ed. E. W. Abel, F. G. A. Stone and G. Wilkinson, Pergamon, Oxford, 2nd edn., 1995, vol. 1, ch. 1, p. 1.
- R. Kempe, *Angew. Chem., Int. Ed.*, 2000, 39, 468.
- R. Anwander, *Top. Curr. Chem.*, 1996, 179, 33.
- R. Anwander, *Top. Organomet. Chem.*, 1999, 2, 1.
- G. B. Deacon, C. M. Forsyth, P. C. Junk, B. W. Skelton and A. H. White, *J. Chem. Soc., Dalton Trans.*, 1998, 1381.
- P. W. Roesky, *Chem. Ber./Rec.*, 1997, 130, 859.
- F. T. Edelmann, *Coord. Chem. Rev.*, 1995, 137, 403.
- R. Duchateau, T. Tunstra, E. A. C. Brussee, A. Meestma, P. Th. van Duijn and J. H. Teuben, *Organometallics*, 1997, 16, 3511.
- G. B. Deacon, C. M. Forsyth and N. M. Scott, *Eur. J. Inorg. Chem.*, 2000, 2501.
- J. P. Pecombes, P. B. Hitchcock, M. F. Lappert and P. G. Merle, *J. Chem. Soc., Dalton Trans.*, 2001, 816.
- X. W. Henderson, A. A. Dorigo, Q.-Y. Liu and P. G. Williard, *J. Am. Chem. Soc.*, 1997, 119, 11 855.
- L. M. Engelhardt, G. E. Jacobsen, P. C. Junk, C. L. Raston, B. W. Skelton and A. H. White, *J. Chem. Soc., Dalton Trans.*, 1988, 1011.
- F. Antolini, P. B. Hitchcock, M. F. Lappert and P. Merle, *Chem. Commun.*, 2000, 1301.
- I. Cragg-Hine, M. G. Davidson, O. Kocian, F. S. Mair, E. Pohl, P. R. Raithby, R. Snaith, N. Spencer and J. F. Stoddart, *Angew. Chem., Int. Ed. Engl.*, 1993, 32, 1182.
- M. F. Lappert, M. J. Slade, A. Singh, J. L. Atwood, R. D. Rogers and R. Shaki, *J. Am. Chem. Soc.*, 1983, 105, 302.
- L. M. Engelhardt, A. S. May, C. L. Raston and A. H. White, *J. Chem. Soc., Dalton Trans.*, 1983, 1671.
- S. Harder, J. Boesma, L. Brandsma, J. A. Kanters, A. J. M. Duisenberg and J. H. van Lenthe, *Organometallics*, 1991, 10, 1623.
- J. G. Donkersvoort, J. L. Vicaño, E. Rijnberg, J. T. B. H. Jastrzebski, H. Kooijman, A. L. Spek and G. van Koten, *J. Organomet. Chem.*, 1998, 463, 463.
- P. Davies, P. R. Raithby and R. Snaith, *Angew. Chem., Int. Ed. Engl.*, 1997, 36, 1215.
- N. N. Greenwood and A. Earnshaw, *Chemistry of the Elements*, Butterworth and Heinemann, Oxford, 2nd edn., 1997, ch. 9, p. 328.
- E. A. V. Ebsworth, *Volatile Silicon Compounds*, Pergamon, Oxford, 1963, ch. 5, p. 101.
- K. Rühlant-Senge, J. I. Ellison, R. I. Wehmschulte, F. Pauer and P. Power, *J. Am. Chem. Soc.*, 1993, 115, 11 353.
- B. Schiemenz and P. P. Power, *Angew. Chem., Int. Ed. Engl.*, 1996, 35, 2150.
- M. Niemeyer and P. P. Power, *Inorg. Chem.*, 1996, 35, 7264.
- T. Kottke and D. Stalke, *Angew. Chem., Int. Ed. Engl.*, 1993, 32, 580.
- J. F. McGarrihy and C. A. Ogle, *J. Am. Chem. Soc.*, 1984, 107, 1805.
- P. C. Andrews, G. B. Deacon, C. M. Forsyth and N. M. Scott, *Angew. Chem., Int. Ed.*, 2001, ~~39~~, 468.
- G. M. Sheldrick, in *SHELX97, Program for Crystal Structure Determination*, Universität Göttingen, 1997.

† 40, 2108

to Dr. J. Weigold for assistance  
with NMR spectroscopy,

at room temperature. Elemental analyses (C, H, N) were determined by the Campbell Microanalytical Service, University of Otago, New Zealand. Commercial LiBu<sup>a</sup> in hexanes (1.6 M) and SiMe<sub>3</sub>Cl (Aldrich) were used as received. *N*-(2-Phenoxyphenyl)-*N*-(trimethylsilyl)amine was prepared as previously reported.<sup>14</sup>

**Li(L<sup>1</sup>)(thf) (1)**

LiBu<sup>a</sup> (1.63 cm<sup>3</sup>, 2.60 mmol) was added dropwise to a stirring solution of L<sup>1</sup>H (0.63 g, 2.45 mmol) in thf (30 cm<sup>3</sup>) at 0 °C. The resulting mixture was then stirred until it had warmed to room temperature (ca. 1 h) whereupon a white solid formed. This was washed with hexane (30 cm<sup>3</sup>) and dried under vacuum giving the title compound (0.76 g, 87%) (Found: C, 67.2; H, 8.0; N, 4.4. C<sub>19</sub>H<sub>24</sub>LiNO<sub>2</sub>Si requires C, 68.0; H, 7.8; N, 4.2) Infrared (Nujol, w/cm<sup>-1</sup>): 1592 s, 1582 s, 1489 s, 1279 s, 1239 s, 1211 vs, 1170 s, 1102 vs, 1072 w, 1046 s, 947 vs, 868 s, 844 w, 824 vs, 769 m, 734 s, 694 vs, 663 w. NMR (400 MHz, C<sub>7</sub>D<sub>8</sub>, 298 K): <sup>1</sup>H, δ 0.35 (9 H, s, SiMe<sub>3</sub>), 1.20 (4 H, br m, β-H (thf)), 3.46 (4 H, br m, α-H (thf)), 6.46–6.50 (1H, ddd, <sup>3</sup>J 7.2, <sup>4</sup>J 1.6 Hz, H4), 6.60–6.63 (1H, dd, <sup>2</sup>J 8.0, <sup>4</sup>J 1.6 Hz, H3), 6.67–6.69 (2H, br d, <sup>2</sup>J 7.8 Hz, H2',6'), 6.73–6.78 (1H, t, <sup>3</sup>J 7.4, <sup>4</sup>J 1.1 Hz, H4'), 6.84–6.88 (2H, br t, <sup>3</sup>J 7.4 Hz, H3',5'), 6.96–7.03 (1H, ddd, <sup>2</sup>J 7.2, <sup>4</sup>J 1.7 Hz, H5), 7.15–7.20 (1H, dd, <sup>2</sup>J 8.0, <sup>4</sup>J 1.6 Hz, H6); <sup>7</sup>Li (155.51 MHz, 298 K), δ 1.65. An identical product (0.68 g, 60%) was obtained from a reaction of L<sup>1</sup>H (0.63 g, 2.45 mmol) with two equiv. of LiBu<sup>a</sup> (3.30 cm<sup>3</sup>, 5.25 mmol) in thf (30 cm<sup>3</sup>) followed by the same work up procedure.

**Li(L<sup>1</sup>)(dme) (2)**

LiBu<sup>a</sup> (2.44 cm<sup>3</sup>, 3.90 mmol) was added dropwise to a stirring solution of L<sup>1</sup>H (0.94 g, 3.66 mmol) in dme (30 cm<sup>3</sup>) at 0 °C. The resulting mixture was then stirred until it had warmed to room temperature (ca. 1 h) whereupon a white solid formed. The solid was washed with hexane (30 cm<sup>3</sup>) and dried under vacuum giving the title compound (1.24 g, 96%) (Found: C, 63.7; H, 7.7; N, 4.0. C<sub>19</sub>H<sub>22</sub>LiNO<sub>2</sub>Si requires C, 64.6; H, 8.0; N, 4.0) Infrared (Nujol, w/cm<sup>-1</sup>): 1594 s, 1585 s, 1458 s, 1444 s, 1366 s, 1332 vs, 1309 s, 1238 s, 1206 vs, 1168 vs, 1150 w, 1117 s, 1099 m, 1082 vs, 1037 m, 1025 w, 955 vs, 907 w, 892 w, 872 m, 825 s, 768 w, 734 s, 690 s, 665 s, 624 w, 596 w. NMR (400 MHz, C<sub>7</sub>D<sub>8</sub>, 298 K): <sup>1</sup>H, δ 0.41 (9 H, s, SiMe<sub>3</sub>), 2.79 (6 H, s, Me(dme)), 2.80 (4 H, s, CH<sub>2</sub>(dme)), 6.33–6.37 (1H, ddd, <sup>2</sup>J 7.2, <sup>4</sup>J 1.8 Hz, H4), 6.63–6.66 (1H, dd, <sup>2</sup>J 7.8, <sup>4</sup>J 1.6 Hz, H3), 6.75–6.79 (1H, br t, <sup>2</sup>J 6.6 Hz, H4'), 6.88–6.92 (4H, br m, H2',3',5',6'), 6.96–7.02 (1H, ddd, <sup>2</sup>J 7.1, <sup>4</sup>J 1.6 Hz, H5), 7.14–7.16 (1H, dd, <sup>2</sup>J 8.0, <sup>4</sup>J 1.6 Hz, H6); <sup>7</sup>Li (155.51 MHz, 298 K), δ 1.43. An identical product (1.12 g, 70%) was obtained from a reaction of L<sup>1</sup>H (0.94 g, 3.66 mmol) with two equiv. of LiBu<sup>a</sup> (4.88 cm<sup>3</sup>, 7.80 mmol) in dme (30 cm<sup>3</sup>) followed by the same work up procedure.

**Li(L<sup>1</sup>)<sub>2</sub> (3)**

a) LiBu<sup>a</sup> (1.2 cm<sup>3</sup>, 1.9 mmol) was added slowly to a stirring solution of L<sup>1</sup>H (0.39 g, 1.52 mmol) in hexane (40 cm<sup>3</sup>) at 0 °C. The resulting mixture was stirred at room temperature for 6 h, and then heated until dissolution of the white precipitate occurred. On cooling colourless crystals of the title complex formed (0.36 g, 89%) with identical IR and <sup>1</sup>H NMR data to the product obtained from the 2 : 1 preparation below.

b) A similar procedure using LiBu<sup>a</sup> (2.3 cm<sup>3</sup>, 3.7 mmol) and L<sup>1</sup>H (0.39 g, 1.52 mmol) in hexane afforded a white precipitate (0.34 g, 84%) (Found: C, 68.5; H, 7.2; N, 5.2. C<sub>19</sub>H<sub>22</sub>LiNO<sub>2</sub>Si requires C, 68.4; H, 6.9; N, 5.3) Infrared (Nujol, w/cm<sup>-1</sup>): 1586 s, 1560 s, 1490 s, 1444 s, 1267 s, 1230 br s, 1203 s, 1167 vs, 1100 vs, 1067 w, 1040 s, 1022 w, 1004 w, 931 vs, 914 s, 867 vs, 851 s, 825 vs, 803 s, 780 s, 741 s, 694 vs, 620 w, 600 w, 556 w. NMR (400 MHz, C<sub>7</sub>D<sub>8</sub>, 288 K): <sup>1</sup>H, δ 0.12 (9H, s, SiMe<sub>3</sub>), 6.48–6.52 (1H, br dd, <sup>2</sup>J 7.9 Hz, H4), 6.57–6.59 (1H, br d, <sup>2</sup>J 7.9 Hz, H3), 6.65–

within the bracket → ; major component \*

7.00 (7H, vbr m, H5,6,2'-6'); (183 K; assignment based on two L<sup>1</sup> environments in the ratio of 1 : 3) 0.23–0.26 (36H, br d, SiMe<sub>3</sub>), 6.45–6.52 (1H, br t, H4'), 6.55–6.59 (3H, br t, H4\*), 6.62–6.73 (15H, br m, Ph), 6.79–6.90 (9H, br m, Ph), 6.96–7.00 (1H, br d, H6'), 7.00–7.04 (3H br m, H6\*), 7.05–7.09 (3H, br m, H5\*), 7.35–7.40 (1H br t, H5'); <sup>7</sup>Li (155.51 MHz, 303 K), δ 1.65; (183 K) -1.77, 2.60, 2.96.

H3\*,  
H3,

**Li(L<sup>1</sup>)(OEt)<sub>2</sub>Li(L<sup>1</sup>)<sub>2</sub>(diglyme) (4)**

To a solution of L<sup>1</sup>H (1.02 g, 3.9 mmol) in Et<sub>2</sub>O (30 cm<sup>3</sup>) was slowly added LiBu<sup>a</sup> (2.7 cm<sup>3</sup>, 4.3 mmol), and the mixture was stirred until it had warmed to room temperature (ca. 1 h). The solvent was removed under vacuum, and hexane (20 cm<sup>3</sup>) was added. The volume was reduced to 10 cm<sup>3</sup> under vacuum and, after standing for 3 days undisturbed, colourless crystals of the title compound formed (0.09 g, yield 8%). Infrared (Nujol, w/cm<sup>-1</sup>): 1585 vs, 1562 w, 1404 s, 1286 vs, 1242 s, 1208 vs, 1166 vs, 1095 vs, 1065 s, 1044 s, 1028 s, 937 vs, 827 s, 802 s, 769 s, 748 s, 730 vs, 694 vs, 668 w. NMR (400 MHz, C<sub>7</sub>D<sub>8</sub>, 303 K): <sup>1</sup>H, δ 0.17 (18H, br s, SiMe<sub>3</sub>), 0.24 (18H, s, SiMe<sub>3</sub>), 1.00 (12H, t, <sup>3</sup>J 7.0 Hz, CH<sub>2</sub>(OEt)), 2.68 (6H, br s, CH<sub>2</sub>(diglyme)), 2.74 (8H, br s, CH<sub>2</sub>(diglyme)), 3.23 (8H, q, <sup>3</sup>J 7.0 Hz, CH<sub>2</sub>(OEt)), 6.46 (4H, br t, Ar), 6.60 (2H, d, <sup>2</sup>J 7.9 Hz, Ar), 6.73 (2H, br m, Ar), 6.85 (12H, vbr s, Ar), 6.96 (4H, t, <sup>2</sup>J 7.9 Hz), 7.05 (4H, vbr s, Ar), 7.12 (4H, br m, Ar), 7.80 (2H, vbr s, Ar); <sup>7</sup>Li (155.51 MHz, 303 K), δ 1.67; (183 K) 0.83, 1.50, 2.08, 3.50.

**Li<sub>2</sub>(L<sup>1</sup>)(OEt)<sub>2</sub>Li(Bu<sup>a</sup>)<sub>2</sub> (5)**

To a solution of L<sup>1</sup>H (0.77 g, 3.0 mmol), in Et<sub>2</sub>O (30 cm<sup>3</sup>) was slowly added LiBu<sup>a</sup> (3.75 cm<sup>3</sup>, 6.0 mmol), and the mixture was stirred until it had warmed to room temperature (ca. 1 h). The solvent was removed under vacuum, and hexane (20 cm<sup>3</sup>) added. Upon standing for 2 h undisturbed, colourless crystals of the title compound formed (0.23 g, yield 19%) (Found: C, 67.0; H, 8.8; N, 3.7. C<sub>24</sub>H<sub>27</sub>Li<sub>2</sub>N<sub>2</sub>O<sub>4</sub>Si<sub>2</sub> requires C, 67.8; H, 8.9; N, 3.4) Infrared (Nujol, w/cm<sup>-1</sup>): 1583 s, 1572 s, 1540 m, 1408 s, 1311 w, 1288 s, 1244 vs, 1182 s, 1148 vs, 1105 vs, 1068 m, 1039 w, 994 w, 939 vs, 829 s, 769 w, 734 w, 668 s, 619 w. NMR (400 MHz, C<sub>7</sub>D<sub>8</sub>, 303 K): <sup>1</sup>H, δ -1.10 (4H, br s, α-CH<sub>2</sub>(Bu<sup>a</sup>)), 0.11 (18H, vbr s, SiMe<sub>3</sub>), 0.85 (16H, br m, CH<sub>2</sub>(OEt), γ-CH<sub>2</sub>(Bu<sup>a</sup>)), 0.91 (6H, br m, CH<sub>2</sub>(Bu<sup>a</sup>)), 1.35 (4H, br s, β-CH<sub>2</sub>(Bu<sup>a</sup>)), 3.12 (8H, br m, CH<sub>2</sub>(OEt)), 6.40 (2H, br s, Ar), 7.05 (6H, br s, Ar), 7.16 (6H, br s, Ar), 7.88 (2H, br s, Ar); (183 K) -1.16 (2H, br m, α-CH<sub>2</sub>(Bu<sup>a</sup>)), -1.02 (2H, br m, α-CH<sub>2</sub>(Bu<sup>a</sup>)), 0.56 (12H, br t, CH<sub>2</sub>(OEt)), 0.62 (18H, s, SiMe<sub>3</sub>), 0.90 (4H, br m, γ-CH<sub>2</sub>(Bu<sup>a</sup>)), 1.05 (6H, br t, CH<sub>2</sub>(Bu<sup>a</sup>)), 1.50 (4H, br m, β-CH<sub>2</sub>(Bu<sup>a</sup>)), 2.75 (4H, br m, CH<sub>2</sub>(OEt)), 2.89 (4H, br m, CH<sub>2</sub>(OEt)), 6.61 (2H, t, <sup>2</sup>J 7.4 Hz, Ar), 6.90 (2H, d, <sup>2</sup>J 8.0 Hz, Ar), 6.92 (2H, t, <sup>2</sup>J 7.5 Hz, Ar), 6.97 (2H, d, <sup>2</sup>J 7.9 Hz, Ar), 7.16 (2H, t, Ar), 7.35 (2H, d, <sup>2</sup>J 6.9 Hz, Ar), 7.38 (2H, d, <sup>2</sup>J 8.3 Hz, Ar), 7.88 (2H, d, Ar); <sup>7</sup>Li (155.51 MHz, 303 K), δ 1.54; (183 K) 1.58, 1.71, 2.24.

**Li<sub>2</sub>(L<sup>1</sup>)(dme)<sub>2</sub> (6)**

To a solution of L<sup>1</sup>H (0.39 g, 1.52 mmol) in Et<sub>2</sub>O (30 cm<sup>3</sup>) was slowly added LiBu<sup>a</sup> (1.90 cm<sup>3</sup>, 3.04 mmol), and the mixture was stirred until it had warmed to room temperature (ca. 1 h). The solvent was removed under vacuum and hexane (20 cm<sup>3</sup>) and dme (0.16 cm<sup>3</sup>, 1.52 mmol) were then added and the resulting mixture was heated until dissolution of all the solid occurred. After standing overnight, colourless crystals of the title compound formed (0.26 g, yield 47%) (Found: C, 63.7; H, 7.7; N, 4.1. C<sub>19</sub>H<sub>22</sub>Li<sub>2</sub>N<sub>2</sub>O<sub>4</sub>Si<sub>2</sub> requires C, 63.5; H, 7.6; N, 3.9) Infrared (Nujol, w/cm<sup>-1</sup>): 1585 s, 1565 w, 1550 w, 1409 s, 1284 s, 1243 m, 1191 w, 1172 vs, 1130 vs, 1097 s, 1077 vs, 1034 w, 941 vs, 869 s, 826 vs, 797 s, 749 s, 722 w, 667 w. NMR (400 MHz, C<sub>7</sub>D<sub>8</sub>, 303 K): <sup>1</sup>H, δ 0.41 (18H, s, SiMe<sub>3</sub>), 2.80 (12H, s, CH<sub>2</sub>(dme)), 2.81 (8H, s, CH<sub>2</sub>(dme)), 6.35 (2H, t, <sup>2</sup>J 7.0 Hz, Ar), 6.65 (2H, dd, <sup>2</sup>J 7.8 Hz, <sup>4</sup>J 1.6 Hz, Ar), 6.76 (2H, br t, Ar), 6.91 (6H, br m, Ar),